

**Alma Mater Studiorum – Università di Bologna**

**DOTTORATO DI RICERCA IN**

**Scienze della Terra, della Vita e dell'Ambiente**

**Ciclo XXIX**

**Settore Concorsuale di afferenza: A04/02**

**Settore Scientifico disciplinare: GEO 01**

**Integration of Morphological and Stratigraphic Information in  
Phylogenetics and Applications in Palaeontology**

**Presentata da: Andrea Cau**

**Coordinatore Dottorato**

**Prof.ssa Barbara Mantovani**

**Relatore**

**Prof. Federico Fanti**

**Esame finale anno 2017**

# Integration of Morphological and Stratigraphic Information in Phylogenetics and Applications in Palaeontology

Page left blank

## CONTENTS

<b>ABSTRACT</b>	6
<b>RIASSUNTO</b>	9
<b>INTRODUCTION</b>	14
<b>MATERIAL AND METHODS</b>	20
<b>GENERAL AIMS OF THIS THESIS</b>	29
<b>CHAPTER 1 - Integrating palaeoecology and morphology in theropod diversity estimation: a case from the Aptian-Albian of Tunisia</b>	35
<b>CHAPTER 2 - Why so many dipnoans? A multidisciplinary approach on the Lower Cretaceous lungfish record from Tunisia</b>	88
<b>CHAPTER 3 - Evidence of iguanodontian dinosaurs from the Lower Cretaceous of Tunisia</b>	132
<b>CHAPTER 4 - Sustained miniaturization and anatomical innovation in the dinosaurian ancestors of birds</b>	158
<b>CHAPTER 5 - New large-clawed theropod (Dinosauria: Tetanurae) from the Lower Cretaceous of Australia and the Gondwanan origin of megaraptorid theropods</b>	196
<b>CHAPTER 6 - High evolutionary rates and the origin of the Rosso Ammonitico Veronese Formation (Middle-Upper Jurassic of Italy) reptiles</b>	243
<b>CHAPTER 7 - New information on <i>Tataouinea hannibalis</i> from the Early Cretaceous of Tunisia and implications for the <i>tempo</i> and mode of rebbachisaurid sauropod evolution</b>	270
<b>CHAPTER 8 - The largest thalattosuchian (Crocodylomorpha) supports teleosaurid survival across the Jurassic-Cretaceous boundary</b>	337
<b>CHAPTER 9 - Specimen-level phylogenetics in palaeontology using the Fossilized Birth-Death model with Sampled Ancestors</b>	370
<b>GENERAL CONCLUSIONS</b>	394
<b>ACKNOWLEDGMENTS</b>	405
<b>APPENDIX - Peer-reviewed studies published during this Ph.D. project but not included in this thesis</b>	407

Page left blank

## ABSTRACT

The role of the fossil record in Natural Sciences and its relevance in the investigation of the *tempo* and mode of evolution have been commonly split between a stratigraphic approach, focusing on the occurrence of the fossil forms along the geological series, and a phylogenetic approach, focusing on the systematic hierarchy inferred from the analysis of the biological diversity. A recently introduced methodology, derived from applications of the Bayesian inference in molecular phylogenetics, aims to integrate the stratigraphic and morphological information in phylogenetic analysis of fossil clades. In this thesis, a modified version of this new methodology is introduced and applied to the analysis of extinct clades of marine and terrestrial vertebrates. This approach has been compared to non-integrative methodologies, in particular, to *a posteriori* combination of cladistic analyses with the stratigraphic distribution of the recovered clades. Furthermore, novel applications of this phylogenetic method beyond the mere reconstruction of ultrametric topologies have been explored and discussed.

This thesis is subdivided into two main research lines (named “Project 1” and “Project 2” below) that partially overlap in their contents and aims:

- Project 1 introduces and describes in detail the Bayesian inference method applied in all analyses included in this thesis, and explores possible fields of application for this methodology beyond the mere reconstruction of ultrametric topologies. In the first study of this Project, the distribution of 1549 morphological features among 121 Mesozoic birds and their closest relatives was analyzed to produce an ultrametric framework for the investigation of size trends and evolutionary rates. The second study of this Project describes a new theropod dinosaur from the Lower Cretaceous of New South Wales (Australia) and explores palaeogeographic applications of the novel Bayesian method. A time-calibrated phylogeny of theropods, based on Bayesian inference of a data set of both morphological and stratigraphic data, was elaborated and used as ultrametric framework for palaeobiogeographic analyses at the continental scale. The third study of this Project explores the application of the novel Bayesian phylogenetic method in palaeoecological inference. In this study, the phylogenetic affinities and the evolutionary rates of the two marine reptiles cur-

rently known from the Rosso Ammonitico Veronese Formation (RAVF) of Northern Italy were inferred using Bayesian phylogenetics. This study also introduces a new pliosaurid taxon, *Anguanax zignoi* Cau and Fanti, 2015. The evolutionary patterns (rate of phenotypic change and timing of cladogenesis) shared by these two Italian reptiles were compared with the palaeogeographic and tectonic evolution of the RAVF to infer the environmental conditions that drove the evolution of these reptiles.

- In Project 2, the morphological approach was combined with taphonomic and stratigraphic analyses to estimate the vertebrate diversity in several Lower Cretaceous fossil localities from southern Tunisia. In fact, a significant part of this Thesis focuses on the results of field activities led in Southern Tunisia in November-December 2014 by an Italian-Tunisian palaeontological team that prospected a number of Lower Cretaceous fossil localities. One aim of this Project is to test whether and how much the collected disparity in the sample was due to non-phylogenetic phenomena (in particular, taphonomic, ontogenetic and palaeoecological factors). The first case study focuses on predatory dinosaur disparity and concludes that the analysis of morphological diversity alone may lead to taxonomic inflation when not associated to accurate taphonomic analysis. In addition, the Tunisian record of the clade Ornithischia is analysed for the first time. The third research pertaining to this Project focuses on the taxonomy of the dipnoan sarcopterygians: as in the study on the theropod material, data support that the taxonomic composition of the sample may be inflated when phylogenetic and morphological analyses are not integrated with taphonomic and stratigraphic investigations. The fourth research study of this Project focuses on the osteology and affinities of the Tunisian sauropod dinosaur *Tataouinea hannibalis* Fanti et al., 2013, including new material collected from the type locality. A time-calibrated phylogeny of sauropods based on Bayesian inference on a data set of both morphological and stratigraphic data was produced and used as framework for palaeobiogeographic analyses at a continental scale. The most significant specimen collected from southern Tunisia is the holotype of a new species of marine crocodylomorph, *Machimosaurus rex* Fanti et al., 2016: this taxon

is described and its evolutionary affinities reconstructed in the fifth part of this Project.

This novel Bayesian phylogenetic method focusing on fossil taxa represents an innovative and useful tool in the following research areas, all of which expand the original aims of application for the method (i.e., the reconstruction of phylogenetic relationships among fossil taxa and a quantitative and testable inference of cladogenetic timing):

1. Quantitative estimation of the rates of phenotypic evolution among fossil lineages. The identification of heterogeneity in morphological transitions, and the estimation of “hot spots” of phenotype evolution, provide a testable framework for the investigation of the *tempo* and mode of Life history in the geological past.
2. Realization of ultrametric frameworks for palaeobiogeographic inference, in particular for analyses requiring branch lengths in ancestral area reconstruction. This method provides a quantitatively-defined base for the integration of palaeogeographic models in the reconstruction of clade history.
3. Comparison between the phylogenetic patterns among distinct lineages sharing palaeogeographic and stratigraphic ranges. This approach allows for testing whether environmental evolution constrained the biological evolution along shared trajectories.
4. Inference on the taxonomic diversity among a sample of individuals collected from the same stratigraphic unit. This application of Bayesian phylogenetic methods uses, as terminal units, individual specimens instead of clades. This approach allows for testing taxonomic hypotheses in the fossil record.
5. Auxiliary and independent test of stratigraphic relationships among fossil localities sharing the same fossil groups. This application stems from the previous approach, and provides testable hypotheses on the relative stratigraphic relationships among a series of fossil-bearing localities.

Page left blank

## RIASSUNTO

Il ruolo del *record* fossile nelle Scienze Naturali e la sua rilevanza nell'indagine del tempo e modo dell'evoluzione sono generalmente distinti tra un approccio stratigrafico, che si focalizza sulla sequenza delle forme fossili lungo la serie geologica, e un approccio filogenetico, che si focalizza sulla gerarchia sistematica derivante dall'analisi della diversità biologica.

Una metodologia introdotta recentemente, derivata dall'applicazione della inferenza Bayesiana nella filogenetica molecolare, si propone di integrare simultaneamente l'informazione stratigrafica e morfologica nell'analisi dei cladi fossili. In questa tesi, è introdotta una versione modificata di questa nuova metodologia ed è applicata all'analisi di cladi estinti di vertebrati marini e terrestri. Questo approccio integrativo è stato confrontato con metodologie non-integrative, in particolare con la combinazione *a posteriori* dei risultati delle analisi filogenetiche con la distribuzione stratigrafica dei cladi ottenuti. Inoltre, questa tesi ha esplorato nuove applicazioni di questo metodo filogenetico al di là della mera ricostruzione di topologie calibrate stratigraficamente (ultrametriche).

Nello specifico, sono state sviluppate analisi filogenetiche nell'ambito di due linee di ricerca principali, i cui obiettivi e ambiti in parte si sovrappongono:

- Il Progetto 1 introduce e descrive in dettaglio il metodo di inferenza Bayesiana seguito dalle successive analisi applicate ai casi studio presentati in questa tesi. Nel primo studio di questo progetto, il metodo è applicato per l'analisi della distribuzione di 1549 caratteri morfologici in un campione di 121 *taxa* tra uccelli mesozoici e loro parenti prossimi, per determinare tendenze nella variazione della taglia corporea, e per determinare i tassi evolutivi lungo una filogenesi calibrata sul tempo. Il secondo studio incluso in questo Progetto applica la nuova metodologia filogenetica nell'inferenza di *pattern* paleogeografici. Questo approccio è stato applicato nello studio di un nuovo dinosauro teropode dal Cretacico Inferiore del Nuovo Galles del Sud (Australia). Una filogenesi calibrata cronologicamente dei teropodi, basata sull'inferenza Bayesiana applicata ad un insieme di dati sia morfologici che stratigrafici, è

stata elaborata ed utilizzata come base per una analisi paleobiogeografica alla scala continentale. Infine, il terzo studio esplora l'applicazione di questa nuova metodologia nell'inferenza di *pattern* paleoecologici. Nello studio, sono ricostruite le affinità filogenetiche ed i tassi evolutivi dei due rettili marini attualmente noti dalla Formazione del Rosso Ammonitico Veronese (RAVF) dell'Italia settentrionale. Questo studio inoltre introduce un nuovo *taxon* di pliosauride: *Anguanax zignoi* Cau e Fanti, 2015. I *pattern* evolutivi (tasso di cambiamento fenotipico e datazione degli eventi cladogenetici) condivisi da questi due rettili italiani sono confrontati con l'evoluzione paleogeografica e tettonica della RAVF per ricostruire le condizioni ambientali che influenzarono l'evoluzione di questi due *taxa*.

- Nel Progetto 2, l'approccio morfologico è stato integrato alle analisi tafonomiche e stratigrafiche per stimare la diversità a vertebrati da una serie di località fossilifere del Cretacico Inferiore della Tunisia. Una parte significativa di questa tesi è stata dedicata ai risultati delle attività sul campo nella Tunisia meridionale, in particolare, quelle svolte tra il novembre ed il dicembre 2014, da parte di una ricerca italo-tunisina che ha prospettato numerose località fossilifere risalenti al Cretacico Inferiore. Uno degli obiettivi della serie di studi inclusi in questo Progetto è stato di testare se e come la disparità campionata fosse dovuta a fenomeni non-filogenetici (in particolare, fattori tafonomici, ontogenetici e paleoecologici). Il primo studio di questo Progetto si è focalizzato sulla disparità nei dinosauri predatori, ed ha mostrato che le analisi morfologiche, se usate senza l'integrazione dell'analisi tafonomica, tendono a sovrastimare la diversità tassonomica nel campione. Sempre nell'ambito di questo progetto, il record fossile tunisino del clade Ornithischia è stata analizzato e discusso. Nella terza parte di questo Progetto, è stata analizzata la diversità tassonomica dei pesci dipnoi rinvenuti nelle varie località del Cretacico Inferiore tunisino. In analogia con i risultati dello studio sui resti di teropodi, questo studio conclude che la diversità dei dipnoi è sovrastimata qualora le indagini morfologiche e filogenetiche non siano integrate con l'approccio stratigrafico e tafonomico. Una quarta ricerca di questo Progetto si è focalizzata sulla osteologia e affinità del dinosauro sauropode tunisino *Tataouinea hannibalis* Fanti et al., 2013, con l'aggiunta di nuovo materiale raccolto di recente dalla località tipo. Una filogenesi

dei sauropodi calibrata cronologicamente è stata elaborata ed utilizzata come base per analisi paleobiogeografiche alla scala continentale. L'esemplare più significativo raccolto nelle campagne scavo in Tunisia del 2014 rappresenta l'olotipo di una nuova specie di crocodilomorfo marino, *Machimosaurus rex* Fanti et al., 2016: in questa tesi, il taxon è descritto e le sue affinità filogenetiche ricostruite nella quinta parte del Progetto.

Questo nuovo metodo di inferenza Bayesiana focalizzato sui *taxa* fossili rappresenta un innovativo strumento la cui utilità può essere estesa ai seguenti filoni di ricerca, posti oltre gli obiettivi originali del metodo (ovvero, la ricostruzione di relazioni filogenetiche tra i *taxa* fossili e l'introduzione di un metodo quantitativo e testabile per stimare i momenti di cladogenesi):

1. Stima quantitativa dei tassi di evoluzione fenotipica lungo le linee fossili. L'identificazione di eterogeneità nelle transizioni morfologiche, e la stima di "punti caldi" nell'evoluzione fenotipica, può produrre dei *framework* testabili per l'investigazione dei tempi e modi dell'evoluzione biologica nel passato geologico.
2. La creazione di basi ultrametriche per l'inferenza paleobiogeografica, in particolare per quelle analisi (che utilizzano l'inferenza Bayesiana) che richiedono la lunghezza dei rami per la ricostruzione delle aree ancestrali. Questo metodo fornisce quindi basi quantitative per l'integrazione dei modelli paleogeografici nella ricostruzione della storia dei cladi.
3. Comparazione tra i pattern filogenetici tra linee distinte che condividono la medesima distribuzione paleogeografia e stratigrafica. Questo approccio permette di testare se l'evoluzione ambientale vincoli la traiettoria dell'evoluzione biologica.
4. Stima della diversità tassonomica in un campione di individui fossili raccolti da una medesima unità stratigrafica. Questo approccio introduce un nuovo metodo per testare ipotesi tassonomiche nel registro fossilifero.
5. Test ausiliario ed indipendente per le relazioni stratigrafiche tra località che condividono il medesimo gruppo fossile.

Page left blank

## INTRODUCTION

“By itself, a genealogy is a very incomplete statement of evolution; and a purely cladistic statement of descent is therefore even more incomplete” Szalay (1977)

Founded in 2008, the International Standard Text Code (ISTC) system is a global identification system for textual works. Among all possible candidates to be honoured with the first registration code, the ISTC developers have chosen “On the Origin of Species by Means of Natural Selection” by C.R. Darwin. In his most famous and influential work, Darwin (1859: p. 117) included only one single figure, a schematic representation of the branching pattern that leads origin to new species from one or more ancestral forms, according to the processes that he discussed as the natural drivers of biological diversity. As explained by Darwin (1859: pp. 116-126), the diagram shows a series of successive sampling moments, regularly spaced along the geological time. At each sampling moment, the biological diversity is represented by the species distinct at that moment, shown as the intersections between the phyletic tree and the time horizon. The position and distribution of the species at each moment reflected two main factors: the morphological diversification from the ancestors, and the rate of extinction occurred between two consecutive sampling moments. This branching diagram, illustrating at the same time a biological pattern and a chronological succession along the geological past, is the first modern depiction of a phylogeny. Since Darwin’s work (1859), phylogenetic diagrams have been represented as branching patterns in an abstract space, the latter defined by two or more axes, describing morphological variation (or, in general, variation among intrinsic features of taxa) and time (usually, the geological time). According to the Darwinian paradigm, phylogenetic hypotheses are thus testable models on the causes of biological diversity along the geological time.

### Phylogenetic Systematics

The advent of the phylogenetic systematics (Hennig 1965, 1975) as the standard methodology for evolutionary inference marks a division from the traditional approach

(e.g., Simpson 1944) that, since Darwin's work, had been integrating morphological and stratigraphic information in phyletic hypotheses. The aim of the phylogenetic systematics (often, improperly named as "cladistics") is to provide a testable scenario on the relationships among a set of taxa, a scenario that describes and explains causally the distribution of derived features shared by selected taxa. This method thus stems directly from the Darwinian concept of evolution as "descent with modification". Nevertheless, no information from the stratigraphic occurrence of analysed taxa is included in the "cladistic" approach (Hennig 1965, Farris 1976). Accordingly, any assumption on taxonomic relationships based on stratigraphic distribution is *a priori* excluded from the analyses, as it may be biased by the incompleteness of the fossil record. Stratigraphic data are therefore coupled and compared with the phyletic pattern after interpretation of morphological information alone. Although such strictly morphological approach is adequate in phylogenetic analysis of living forms (that can be considered as coeval, thus having a null amount of stratigraphic diachrony), it results problematic when fossil forms are included (or are the solely analysed taxa). Stratigraphic diachrony among the taxa may in fact provide information on their phylogenetic relationships. It may indicate for instance that one or more forms are ancestral to others, a condition *a priori* excluded by analyses using exclusively contemporary taxa. Furthermore, since the branches leading to sister taxa with different stratigraphic positions must have different lengths, this implies that the relative morphological disparity among sister taxa is also a by-product of their different chronological distance (which means, anagenetic divergence) from their last common ancestor. This has significant implications for any method trying to infer ancestral states at nodes from the diversity among the terminal taxa analysed.

In phylogenetic systematics, the ancestor-descendant relationships is considered as a non-testable hypothesis (Farris 1976), as it cannot be distinguished from unresolved (soft) polytomies due to absence of information (Gould 2002). Nevertheless, if direct ancestor-descendant couples cannot be affirmed by phylogenetic systematic method, they can be falsified by character analysis. Furthermore, even if a taxon cannot be considered unambiguously as ancestral to others included in the same analysis, it may show a combination of plesiomorphic features recalling the hypothetical common ancestor. The hypothesis that some taxa may provide information on the ancestral condition of others,

even if not representing their direct ancestors, may be either supported or challenged by integrating the stratigraphic distribution of analysed forms. Thus, stratigraphic distribution can be used as discriminant parameter among competing phyletic scenarios when introduced with defined criteria (Szalay 1977).

To summarise, although the omission of hypotheses on relationships based on stratigraphic information is justified in the analysis of morphological diversity, it represents a relevant loss of information once this morphological pattern aims to provide an estimation of the *tempo* and mode of the phyletic phenomenon, in particular in palaeontology.

### ***A posteriori* stratigraphic calibration of cladograms**

Although stratigraphic data are not taken into account during the tree search strategy used to infer evolutionary patterns in phylogenetic systematics, they are commonly incorporated *a posteriori* in order to integrate the cladogenetic diagram with the geological record (in particular, the chronostratigraphic distribution of the fossil forms). Stratigraphic calibration of a phylogenetic diagram, the latter based on analysis of morphological features (cladogram), is a common practice in recent palaeontological literature. The method follows two steps (discussed by Lee et al. 2014a):

1. Given a phylogenetic diagram inferred by phylogenetic analysis of a set of taxa (most commonly, the strict consensus of the most parsimonious topologies found using parsimony as tree search strategy), the oldest known age of the members of each recovered branch is used as “hard” minimum age for each lineage.
2. Divergence times are then either: (i) enforced onto the rest of tree in order to minimize ghost lineages, or (ii) calibrated on an older stratigraphic position inferred according to non-phylogenetic criteria.

As outlined by Lee et al. (2014a), the most significant shortcoming of *a posteriori* stratigraphic calibration of cladograms is the arbitrariness and subjectivity in the estimation

of ghost lineage extents and durations. From an epistemological point of view, such arbitrariness results in several challenges in both reproduction and falsification of historical scenarios based on such integration of the phylogenetic and stratigraphic information.

### **Quantitative integration of morphological and stratigraphic data using Bayesian inference**

The application of Maximum Likelihood and Bayesian inference methods in phylogenetic analysis has been increasingly and widely used over the last two decades (see review by Lee and Palci 2015). Most of these analytical methods have focused on molecular data and thus are used in neontological phylogenetics (e.g., Yang and Rannala 1997). With minor remarkable exceptions, fossils lack soft tissue remains and moreover lack remnant of genetic material. This preservational bias implies that phylogenetic analyses focusing exclusively on fossil taxa must refer to the morphological information, and thus cannot be directly integrated with analyses that used exclusively the genetic/molecular data. Furthermore, phylogenetic inference based on genetic/molecular information cannot be applied to an extinct speciose clade (e.g., Conodonts), or when the clade is represented by a single pauci- or monospecific crown group and a more diversified and speciose stem group (e.g., Rynchocephalia).

Lewis (2001) introduced a model for the phylogenetic analysis of the morphological information following the Maximum Likelihood approach consequently extended to the Bayesian framework. The original intent of this method was to apply a probabilistic approach to the reconstruction of undated phylogenies (not incorporating stratigraphic information in the tree-search inference), thus representing an alternative to the widely-used approach based on parsimony. During the last decade, this approach has been progressively used in “total evidence” analyses which integrate molecular and morphological data combining extant and extinct forms. Furthermore, age-related information for taxa have been integrated to set age constraints for the duration of extant lineages inferred mostly from genetic information (see Ronquist et al. 2012b). More recently, this approach has been extended to the study of the phylogenetic relationships among sets of exclusively extinct taxa, thus using exclusively the morphological data (Lee

et al. 2014a). As noted above, in the maximum parsimony methods, geochronological information can only be used *a posteriori*, by comparing the congruence of alternative topologies (inferred from morphological data) and the stratigraphic record. In contrast, geological dates can be used simultaneously with morphological data in the Bayesian framework, as age priors that inform on the amount of changes leading to dated taxa, thus discriminating among alternative topologies according to their congruence with the stratigraphic sequence of taxa (Ronquist et al. 2012b, Lee et al. 2014a).

As the Bayesian phylogenetic approach outperforms maximum parsimony when applied to discrete characters that are evolving at a high rate and when there are missing data (Wright and Hillis 2014, O'Reilly et al. 2016), it is expected to produce more reliable hypotheses of relationships for the fossil record than the maximum parsimony analysis (Dembo et al. 2016).

Page left blank

## **MATERIAL AND METHODS**

For this Ph. D. research project, taxonomic identification criteria and phylogenetic methodologies have been applied to different case studies. Most of these studies included phylogenetic analysis as the main investigation methodology, or included phylogenetics as one of the analytical tools, integrated with other methodologies. Both parsimony (excluding non-morphological information) and Bayesian methods (integrating morphological information with other non-biological data, in particular, stratigraphic data) were used as phylogenetic inference strategies, and the alternative results of analyses using these methods were compared and discussed. In particular, a Bayesian phylogenetic methodology, modified from the method described by Lee et al. (2014a), has been introduced here and applied to the analysis of a series of extinct clades of vertebrates. In order to explore the alternative applications of this phylogenetic methodology, the thesis has also tested a series of case studies focusing on the vertebrate fossil assemblages from several Lower Cretaceous localities from Southern Tunisia.

### **Taxon sampling**

Although often not explicitly stated, any phylogenetic analysis is a test on the congruence between observed data and a series of systematic hypotheses. These hypotheses refer to the taxonomic units included (and, implicitly, those excluded) and the homology among sets of features present in the taxonomic sample. The taxonomic sampling is the subset of systematic hypotheses that defines the taxonomic axis explored by any phylogenetic analysis. I define two main forms of taxon sampling in phylogenetic analyses. The first is the assumption on the monophyly of the analysed ingroup (i.e., the set of taxa object of the analysis) relative to the outgroup (i.e., those included taxa, assumed as not belonging to the ingroup and used as root for character polarity inference). Although ingroup monophyly is usually one of the most explicitly discussed among the taxon sampling hypotheses, the possible exclusion of some members of that monophyletic clade from the ingroup is rarely discussed. The second main set of hypotheses on taxon sampling is relative to the monophyly and composition of each terminal taxon itself. This second set of hypotheses is rarely discussed in depth. It is noteworthy that only in analyses using exclusively single

individuals/specimens as terminal taxa (e.g., Tschopp et al. 2015) the latter are equivalent to proper taxonomic “data”.

### **Protocol of the phylogenetic and palaeobiogeographic analyses using the Bayesian inference**

This approach is based on the method originally developed by Yang and Rannala (1997) for the analysis of molecular data, then extended to discrete morphological characters by Lewis (2001). See a more detailed procedure description in Dembo et al. (2016), here briefly summarised. Within the Bayesian framework, obtaining the posterior probability of a phylogenetic topology involves solving the equation:

$$P(T, \theta | X) = P(X | T, \theta) P(T, \theta) / P(X).$$

The term  $P(T, \theta | X)$  represents the posterior probability of a particular topology  $T$  and the prior parameters  $\theta$  given the data  $X$ . The likelihood function,  $P(X | T, \theta)$ , is the probability of observing the data given the candidate topology  $T$  and the prior parameters  $\theta$ . The second term,  $P(T, \theta)$ , is the prior probability of the tree and the prior parameters.  $P(X)$  is the probability of the data across all possible topologies and parameter values. Since available information on the priors represented by the second term in the numerator -  $P(T, \theta)$  - is often not available, it is assumed that most topologies and parameter values are given equal prior probabilities. The denominator  $P(X)$  indicates that a Bayesian phylogenetic analysis returns a point probability for each topology and set of parameter values, which means that, theoretically, the sum of these point probabilities across all possible trees and parameter values must be 1. It should be noted that the overall prior probability value of the data needed to calculate the posterior probabilities cannot be determined directly, because the number of possible combinations of trees and parameter values approaches infinity. Therefore, the posterior probabilities needed to evaluate the topologies are approximated using the sampling “Markov chain Monte Carlo (MCMC)” method (Yang and Rannala 1997) that estimates the posterior probability of a topology according to its frequency in a distribution of sampled topologies. The sampled topologies are evaluated and retained in this distribution following an iterative process: each time a new topology and/or set of parameter values is proposed, the resulting likelihood is multiplied by the

prior probability of the topology and associated parameter values. Then, that product is compared to the corresponding value of the previously retained topology. If the product is higher than that of the previous topology, the new topology and/or set of parameter values is retained. If it is worse, it is retained proportionally to its similarity with the values of the previous topology. Every time a topology is retained, the process produces a “generation” in a “chain” and the retained topology becomes the reference for comparison in the subsequent step. This procedure is usually iterated over millions of steps, with best combinations of topologies and parameter values being retained at higher frequencies in the sample, suboptimal ones retained at lower frequency, and very poor ones ignored. Being the starting topology of each analysis usually defined randomly, those trees sampled early in a chain tend to poorly fit the data: these early generations are usually discarded as “burn-in”. Visual representations of the posterior probability values obtained progressively by the chain allow to estimate the extent of the burn-in, the latter usually corresponding to a wide initial excursion of the values that precedes the stabilization of the results along a narrower “plateau” region reached toward the end of the analysis. Several millions of trees are produced and evaluated during the sampling procedure. From this large sample, a subset is retained, sampling periodically from the whole distribution, to obtain a “posterior MCMC distribution”. This final distribution is analysed to infer parameter values, prior probabilities and likelihoods estimations for all elements of the clades recovered. The robustness of a phylogenetic hypothesis is thus estimated according to the amount and frequency of topologies present in the final distribution and supporting that hypothesis.

Bayesian analyses integrating the morphological data and stratigraphic data were performed with BEAST (Bayesian Evolutionary Analysis Sampling Trees, Drummond et al. 2012) following the method described in the Supplementary Material of Chapter 4 of this thesis. Stratigraphic data and age constraints for each terminal were obtained primarily from the Paleobiology Database (<http://paleobiodb.org/>) and from the literature, using known geochronological age ranges for the stratigraphic stages in which the taxa were found, or the mean age value of the stages associated with those formations. In all analyses, rate variation across traits was modelled using the gamma parameter, and rate variation across branches was modelled using an uncorrelated relaxed clock (following

Lee et al. 2014a). The analyses used four replicate runs of usually 10/40 million generations each (values depending on the size of the data set and the computation time involved), with sampling every 1000/4000 generations. Burnin was set at initial 20% of the sampled topologies, and the Maximum Clade Credibility Tree (MCCT) of the post-burnin samples was used as framework for phyletic reconstructions.

In a subset of the analyses included in this thesis, the topologies recovered by the Bayesian analyses were used as frameworks for palaeobiogeographic reconstruction, inferring ancestral geographic placement at the nodes of the topologies using RASP (Reconstruct Ancestral State in Phylogenies, Yan et al. 2011). The distribution range of the included taxa was *a priori* divided into discrete areas. Each terminal taxon was scored for the area character state(s) according to the geographic area(s) where it was recovered. Biogeographic inferences on the phylogenetic frameworks were obtained by utilising two models included in RASP: Statistical Dispersal-Vicariance analysis (S-DIVA) and Bayesian Binary Markov Chain Monte Carlo (BBM) analysis. S-DIVA and BBM methods suggest possible ancestral ranges at each node and also calculate probabilities of each ancestral range at nodes. The S-DIVA and BBM analyses performed ten Markov Chain Monte Carlo analyses of 50 million generations, sampling every 100 trees. State frequencies were set as fixed and among-site rate variation was set using the gamma parameter. The initial 20% of the recovered trees were discarded (analogous to the burn-in in the tree-search analyses in BEAST, described above) and the remaining trees were used to infer ancestral range distribution at nodes. In the S-DIVA analyses, direct range dispersal constraints were enforced, excluding those routes considered as not plausible based on published literature on tectonic and palaeogeographic reconstructions.

### **Data sets assembled or modified for this thesis**

The character-taxon matrices for the phylogenetic analyses were modified from previously published matrices or were assembled and published for the first time, as follows:

In Chapter 1, isolated theropod teeth from the Tataouine basin (Tunisia) were categorized in eight distinct morphotypes: accordingly, eight taxonomic units were entered into a modified version of the data set of Hendrickx and Mateus (2014). The original data set was

modified removing the four OTUs based on the Portuguese teeth (see details in Hendrickx and Mateus 2014).

In Chapter 1, two theropod specimens collected from the Tataouine basin were scored in the data set of Cau et al. (2013).

Data set in Chapter 2 was assembled by Gabriele Larocca Conte and myself by scoring data from both published literature and direct examination of the Ain el Guettar Formation material housed in the Museo Geologico "G. Capellini" in Bologna. This data set was then modified and used in the analysis performed in Chapter 9.

No quantitative analyses were used in Chapter 3: this study followed an identification approach (i.e., referral to clades based on identification of synapomorphies) as taxonomic criterion.

The data set in the main analysis used in Chapter 4 was assembled by myself and is currently stored in the digital repository *Dryad* (see details in Chapter 4).

One of the data sets used in Chapter 5 was modified from Zanno and Makovicky (2013) by including the scores of the new Australian theropod described in the study.

The second data set used in Chapter 5 was modified from Novas et al. (2013) including the new Australian specimen, two Jurassic coelurosaurians (*Archaeopteryx* and *Zuolong*), and the recently named megaraptoran *Siats* (Zanno and Makovicky, 2013). In the character list, modifications involved the addition of 26 new morphological characters relevant in resolving the positions of the listed taxa. Characters 255, 271 and 285 were *a priori* set with weight = 0 as they became redundant with other included characters, respectively, characters 35, 78 and 108 (as outlined by Porfiri et al. 2014). In both datasets used in Chapter 7, character scores for *Megaraptor* were updated following Porfiri et al. (2014).

One of the data sets used in Chapter 6 is based on the data set of Cau (2014), which had been modified from the data in Young (2014). Modifications included: 1) merging the type and referred specimens of *Neptunidraco* into a single taxonomic unit, and 2) *a priori* exclusion of all non-thalattosuchian crocodyliforms, as the analysis focused on thalattosuchians. As this study was submitted before the study presented in Chapter 6 (the

latter focused on teleosaurid evolution), the data set in Chapter 8 does not include the two teleosaurid taxa included in the version used in Chapter 6.

The second data set used in Chapter 6 is modified from Benson et al. (2013), as follows: 1) most non-pliosauroids not relevant for the aims of the analysis were removed *a priori*, and 2) the Italian pliosaurid *Anguanax zignoi* was added and scored after direct examination of the holotype specimen.

The data set used in Chapter 7 was modified from Carballido et al. (2012) by *a priori* removal of most of the non-diplodocoid taxa from the original data set, as the analysis focused on rebbachisaurids. The taxon *Tataouinea* was added to the data set based on direct examination of the specimen. The taxon *Rebbachisaurus* was re-scored based on Wilson and Allain (2015). The taxon *Katepensaurus* was added based on published literature. In the character list, five additional characters were added and all taxa were scored for such characters based on published literature.

One of the data sets used in Chapter 8 was implemented from Cau (2014), which had been modified from Young (2014), by: 1) merging the type and referred specimens of *Neptunidraco* into a single taxonomic unit, 2) including *Machimosaurus buffetauti*, based on the published literature, 3) including *Machimosaurus rex*, scored after examination of the holotype specimen, and 4) *a priori* exclusion of most of the non-thalattosuchian crocodylomorphs, as the analysis focused on thalattosuchians.

The data set in Chapter 9 is a modified version of the data set assembled in Chapter 2.

### **Institutional abbreviations**

*MGGC*, Museo Geologico “Giovanni Capellini”, Bologna; *MGP*, Museo Geologico di Padova, Padova; *MPPL*, Museo Paleontologico e della Preistoria “Leonardi”, Ferrara; *ONM*, Office National des Mines, Tunis.

### **Fossil material analysed**

The following fossil material was examined first-hand during the realisation of this thesis:

Isolated crocodylomorph material from the Ain el Guettar Formation: MGGC TUN2, MGGC TUN4, MGGC TUN6, MGGC TUN7, MGGC TUN8, MGGC TUN11, MGGC TUN12, MGGC TUN18, MGGC TUN20, MGGC TUN21, MGGC TUN22, MGGC TUN23, MGGC TUN24, MGGC TUN25, MGGC TUN29, MGGC TUN34, MGGC TUN35, MGGC TUN48, MGGC TUN49, MGGC TUN50, MGGC TUN51, MGGC TUN52, MGGC TUN53, MGGC TUN54, MGGC TUN56, MGGC TUN57, MGGC TUN59, MGGC TUN60, MGGC TUN61, MGGC TUN62, MGGC TUN63, MGGC TUN65, MGGC TUN66, MGGC TUN71, MGGC TUN73, MGGC TUN74, MGGC TUN81 , MGGC TUN83, MGGC TUN84, MGGC TUN85, MGGC TUN88, MGGC TUN89, MGGC TUN90, MGGC TUN91, MGGC TUN92 , MGGC TUN93, MGGC TUN94, MGGC TUN96, MGGC TUN97, MGGC TUN98, MGGC TUN99, MGGC TUN100, MGGC TUN110, MGGC TUN115, MGGC TUN117, MGGC TUN118, MGGC TUN119, MGGC TUN120, MGGC TUN121, MGGC TUN122, MGGC TUN123, MGGC TUN124, MGGC TUN125, MGGC TUN128, MGGC TUN129, MGGC TUN130, MGGC TUN131, MGGC TUN133, MGGC TUN135, MGGC TUN136, MGGC TUN138, MGGC TUN139, MGGC TUN140, MGGC TUN141, MGGC TUN142, MGGC TUN144, MGGC TUN145, MGGC TUN146, MGGC TUN147, MGGC TUN148, MGGC TUN150, MGGC TUN152.

Isolated dipnoan material from the Ain el Guettar Formation: MGGC 21912, MGGC 21913, MGGC 21914, MGGC 21915, MGGC 21916, MGGC 21917, MGGC 21918, MGGC 21919, MGGC 21920, MGGC 21921, MGGC 21922, MGGC 21923, MGGC 21924, MGGC 21925, MGGC 21926, MGGC 21927, MGGC 21928, MGGC 2129, MGGC 21930.

Isolated iguanodontian material from the Ain el Guettar Formation: ONM NG OR1, MGGC TUN 153, MGGC TUN 154, MGGC TUN 155.

Isolated theropod material from the Ain el Guettar Formation: MGGC TUN1, MGGC TUN10, MGGC TUN101, MGGC TUN102, MGGC TUN103, MGGC TUN104, MGGC TUN105, MGGC TUN106, MGGC TUN107, MGGC TUN108, MGGC TUN109, MGGC TUN111, MGGC TUN112, MGGC TUN113, MGGC TUN114, MGGC TUN116, MGGC TUN126, MGGC TUN127, MGGC TUN13, MGGC TUN134, MGGC TUN137, MGGC TUN14, MGGC TUN143, MGGC TUN149, MGGC TUN15, MGGC TUN151, MGGC

TUN153, MGGC TUN16, MGGC TUN17, MGGC TUN19, MGGC TUN26, MGGC TUN27, MGGC TUN28, MGGC TUN3, MGGC TUN30, MGGC TUN31, MGGC TUN32, MGGC TUN33, MGGC TUN36, MGGC TUN37, MGGC TUN38, MGGC TUN39, MGGC TUN40, MGGC TUN41, MGGC TUN42, MGGC TUN43, MGGC TUN44, MGGC TUN45, MGGC TUN46, MGGC TUN47, MGGC TUN5, MGGC TUN55, MGGC TUN67, MGGC TUN68, MGGC TUN69, MGGC TUN70, MGGC TUN72, MGGC TUN75, MGGC TUN76, MGGC TUN77, MGGC TUN78, MGGC TUN79, MGGC TUN80, MGGC TUN82, MGGC TUN86, MGGC TUN87, MGGC TUN9, MGGC TUN95.

Type material of *Anguanax zignoi*: MGP 18797.

Type material of *Machimosaurus rex*: ONM NG 1-25, ONM NG 80, ONM NG 81, ONM NG 83-87.

Type and referred material of *Neptunidraco ammoniticus*: MGGC 8846/1UCC123b, MGGC 8846/1UCC123a, MPPPL 35, MPPPL 39, MGP 6552.

High-resolution 3D-photogrammetric images of the type material of *Tataouinea hannibalis* were also used in the analyses (specimen housed in ONM).

Page left blank

## GENERAL AIMS OF THIS THESIS

“The present analysis is the first attempt to evaluate morphological-palaeontological evidence with quantitative phylogenetic dating methods analogous to those used in molecular studies, and it is hoped will spur further empirical analyses —especially among palaeobiologists —which will help answer these questions”. Lee et al. (2014a)

This thesis aims to apply a multidisciplinary approach to the investigation of palaeontological phenomena involving both phylogenetic and stratigraphic information, and introduces a modified version of the phylogenetic method based on Bayesian inference recently published by Lee et al. (2014a). In particular, the thesis explores novel areas of application for this method, beyond the mere reconstruction of ultrametric frameworks. The thesis describes two main lines of research which partially intersect each other. The first project (Project 1) focuses on the novel phylogenetic method based on Bayesian inference, and explores novel fields of application among a series of distinct case studies from the Vertebrate Palaeontology. The second project (Project 2) used a multidisciplinary approach in the analysis of fossil localities from southern Tunisia: the novel phylogenetic method based on Bayesian inference was among the methodologies used in these studies.

This thesis includes nine studies (listed below, Figure 1). In these studies, the descriptive approaches of morphological palaeontology and stratigraphy were associated to well-established phylogenetic methods (i.e., “cladistic” analysis based on parsimony) and recently-introduced analytical tools (i.e., Bayesian phylogenetics). The Bayesian phylogenetic approach, integrating morphological and stratigraphic data, is here named the “integrative” approach. The other methods are thus named “non-integrative” approaches. Not all methods and approaches have been included in each of these publications. A subset of the studies (Chapters 4-9) form the bulk of this thesis introducing and testing the integrative approach (Project 1). Although the remaining studies (Chapters

1-3) used non-integrative methods, they focused on some of the methodological and theoretical elements of the integrative approach. They, therefore, form an auxiliary context for the main studies into which the integrative approach can properly be understood and appreciated.

Note that a subset of the chapters (i.e., Chapters 7 to 9) pertains to both Projects 1 and 2.

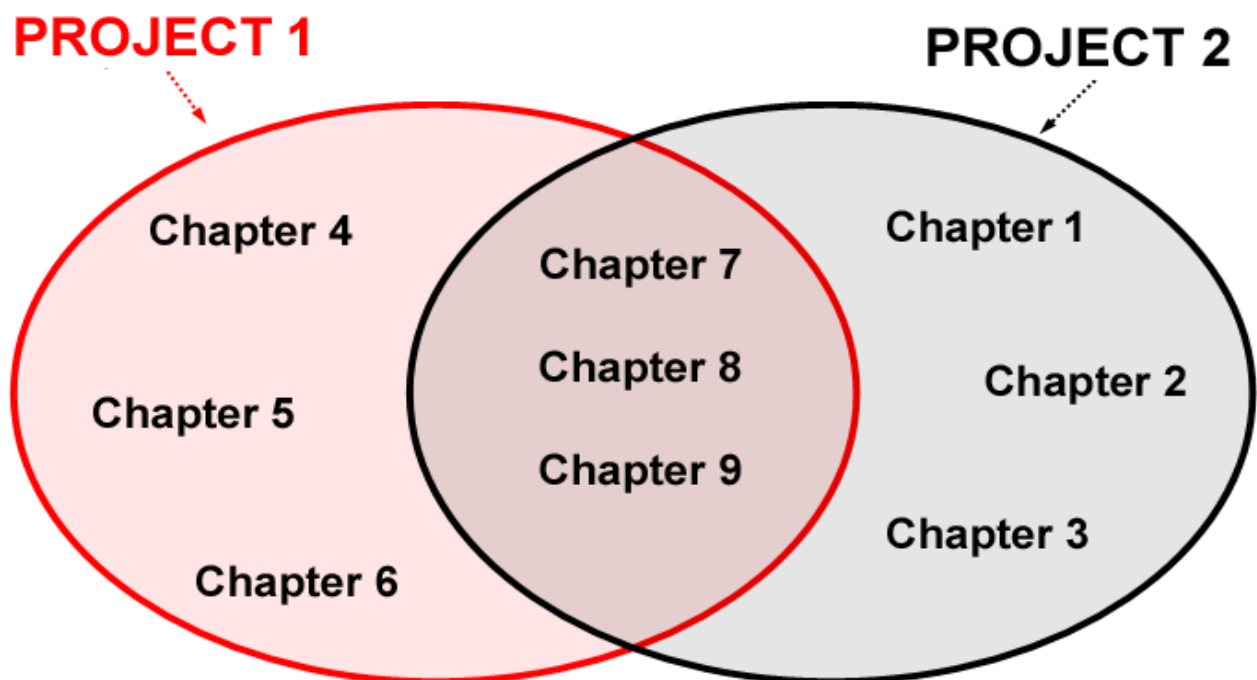


Figure 1 - Relationships among the Chapters and the Projects in this Thesis

Below, the nine publications are listed in chronological order of submission.

1. Lee, Cau, Naish and Dyke (2014b). Submitted: 14<sup>th</sup> February 2014. Published: 1<sup>st</sup> August 2014 in *Science* vol. 345:562-566. (Chapter 4). This study forms the basis for Project 1: it describes in detail the integrative approach used in the other studies of the thesis.
2. Fanti, Cau, Martinelli and Contessi (2014). Submitted: 6<sup>th</sup> March 2014. Published: 02<sup>nd</sup> June 2014 in *Palaeogeography, Palaeoclimatology, Palaeoecology* vol. 410:39–57. (Chapter 1). Project 2, does not include the integrative approach.

3. Fanti, Cau, Cantelli, Hassine and Auditore (2015). Submitted: 21<sup>st</sup> October 2014. Published: 29<sup>th</sup> April 2015 in *PLoS ONE* vol.10, issue4:e0123475. (Chapter 7). This study refers to both Project 1 and Project 2, using both integrative and non-integrative approaches in the investigation of the first sauropod taxon from the Lower Cretaceous of Tunisia.
4. Bell, Cau, Fanti and Smith (2016). Submitted: 29<sup>th</sup> October 2014. Published online: 02<sup>nd</sup> October 2015 and in formatted version in August 2016 in *Gondwana Research* 36:473–487. (Chapter 5). Project 1, exploring palaeobiogeographic applications of the integrative approach.
5. Cau and Fanti (2015). Submitted: 25<sup>th</sup> March 2015. Published: 1<sup>st</sup> August 2016 in *Historical Biology* vol. 28:952-962. (Chapter 6). Project 1, testing palaeoecological applications of the integrative approach.
6. Fanti, Miyashita, Cantelli, Mnasri, Dridi, Contessi and Cau (2016). Submitted: 18<sup>th</sup> July 2015. Published: 10<sup>th</sup> January 2016 in *Cretaceous Research* vol. 61:263-274. (Chapter 8). This study refers to both Project 1 and Project 2, as it used both approaches in the investigation of the first crocodylomorph taxon from the Lower Cretaceous of Tunisia.
7. Fanti, Cau, Panzarin and Cantelli (2016). Submitted: 27<sup>th</sup> November 2015. Published: 12<sup>th</sup> January 2016 in *Cretaceous Research* vol. 60:267-274. (Chapter 3). Project 2, does not include the integrative approach.
8. Fanti, Larocca Conte, Angelicola and Cau (2016). Submitted: 15<sup>th</sup> December 2015. Published: 18<sup>th</sup> February 2016 in *Palaeogeography, Palaeoclimatology, Palaeoecology* vol. 449:255-265. (Chapter 2). Project 2, does not include the integrative approach.
9. Cau (2017). Submitted: 14<sup>th</sup> September 2016. Published: 1<sup>st</sup> March 2017 in *PeerJ* vol. 5:e3055:1-19 (Chapter 9). This study belongs to both Projects 1 and 2, as it re-analyses the material studied in Chapter 2 using the integrative approach.

Chapter 1 (*"Integrating palaeoecology and morphology in theropod diversity estimation: a case from the Aptian-Albian of Tunisia"*), Chapter 2 (*"Why so many dipnoans? A multidisciplinary approach on the Lower Cretaceous lungfish record from Tunisia"*) and Chapter 3 (*"Evidence of iguanodontian dinosaurs from the Lower Cretaceous of Tunisia"*) investigate the taxonomic diversity of multiple fossil localities from the Lower Cretaceous of Southern Tunisia focusing on the isolated vertebrate remains referable to, respectively, theropod and ornithomimid dinosaurs (Chapters 1 and 3) and dipnoan sarcopterygians (Chapter 2). In these studies, results of systematic analyses using a qualitative approach (taxonomic identification based on synapomorphies discussed in literature, Chapter 3) and quantitative parsimony analyses (Chapters 1 and 2) are integrated *a posteriori* with stratigraphic and taphonomic information of localities in order to infer the number of taxa represented by the samples.

Chapter 4 (*"Sustained miniaturization and anatomical innovation in the dinosaurian ancestors of birds"*) describes a novel version of the Bayesian inference method in palaeontological phylogenetics introduced by Lee et al. (2014a). In the study, body size evolution among the early birds and their closest relatives is inferred for the first time using a phylogenetic framework resulted by the integration of morphological diversity and stratigraphic distribution of analysed taxa.

Chapter 5 (*"New large-clawed theropod (Dinosauria: Tetanurae) from the Lower Cretaceous of Australia and the Gondwanan origin of megaraptorid theropods"*) describes a fragmentary theropod dinosaur from Australia. The Bayesian phylogenetic method introduced in Chapter 4 and the palaeobiogeographic application using RASP are integrated to test alternative scenarios on the origin and dispersal patterns across the Southern continents of this clades of predatory dinosaurs.

Chapter 6 (*"High evolutionary rates and the origin of the Rosso Ammonitico Veronese Formation (Middle-Upper Jurassic of Italy) reptiles"*) reviews the plesiosaurian fossil record from the Rosso Ammonitico Veronese Formation (RAVF) of Northern Italy. A new genus and species of plesiosaurian is officially erected. The Bayesian phylogenetic method introduced in Chapter 4 is used to infer the phylogenetic relationships and the rate of evolutionary divergence for the new plesiosaurian and for the other named marine reptile from the RAVF, the crocodylomorph *Neptunidraco ammoniticus*. The evolutionary patterns

resulted by the analyses of the clades including the two Italian taxa are compared and discussed.

Chapter 7 (*“New information on *Tataouinea hannibalis* from the Early Cretaceous of Tunisia and implications for the tempo and mode of rebbachisaurid sauropod evolution”*) describes the osteology, stratigraphic occurrence and taphonomy of the holotype of the sauropod dinosaur *Tataouinea hannibalis*. The phylogenetic method introduced in Chapter 4 is used here to investigate affinities of this taxon and the cladogenetic timing of its clade. The resulted phyletic scenario is consequently used as “ultrametric” framework for additional analyses based on Bayesian inference using RASP to investigate the palaeogeographic patterns among rebbachisaurid dinosaurs.

Chapter 8 (*“The largest thalattosuchian (*Crocodylomorpha*) supports teleosaurid survival across the Jurassic-Cretaceous boundary”*) describes a new marine crocodylomorph discovered in Southern Tunisia by a team including the author of this thesis. The Bayesian method introduced in Chapter 4 is applied to infer the duration of this African lineage and the divergence from its European relatives.

Chapter 9 (*“Specimen-level phylogenetics in palaeontology using the Fossilized Birth-Death model with Sampled Ancestors”*) re-analyses the dipnoan data set used in Chapter 2 using a novel phylogenetic model that is an implementation of the Bayesian inference method introduced in Chapter 4. The differences in the results and interpretations obtained using alternatively the parsimony and Bayesian methods are discussed.

Page left blank

## **CHAPTER 1 - Integrating palaeoecology and morphology in theropod diversity estimation: a case from the Aptian-Albian of Tunisia**

Submitted: 6<sup>th</sup> March 2014. Published: 02<sup>nd</sup> June 2014 in *Palaeogeography, Palaeoclimatology, Palaeoecology* vol. 410:39–57.

Federico Fanti, Andrea Cau, Agnese Martinelli, Michela Contessi

### Abstract

Current knowledge of theropod dinosaurs of northern Africa and their diversity during the Early Cretaceous is deceptively fragmentary and commonly associated with inadequate stratigraphic and palaeoecological data. Thereby, confused taxonomic affinities of theropod remains, represented primarily by isolated teeth and fragmentary skeletal remains, resulted in speculations on the number of genera and their stratigraphic, geographic and ecological distribution. In this study, we introduce a discussion on the theropod diversity in the Aptian–Albian of southern Tunisia based on a multidisciplinary approach that combines detailed sedimentological analyses with canonical morphological and phylogenetic analyses. This study indicates the presence of three theropod clades, Spinosauridae, Abelisauroida, and Carcharodontosauridae. Relevant for the identification of isolated specimens from the Saharan regions, carcharodontosaurids are not represented in the Aptian-Albian teeth record and thus relatively less abundant than spinosaurids and abelisauroids. Five ziphodont tooth morphotypes are referred to ontogenetic and/or positional differences among a single abelisauroid taxon. The other three teeth morphotypes most likely represent two distinct spinosaurid taxa. Finally, the calibrated stratigraphic distribution of discussed elements indicates a clear ecological partition between theropod taxa. In particular, abelisauroids and carcharodontosaurids are commonly found in inland, fluvial deposits together with titanosauriform and rebbachisaurid sauropods, and rare crocodylians. Conversely, spinosaurids are limited to estuarine to coastal deposits dominated by a rich and diverse crocodylian fauna along with actinopterygians and sarcopterygians, including large-sized coelacanthiforms.

**Keywords:** Aptian-Albian; Morphology; Palaeoecology; theropod diversity; Tunisia

## 1. Introduction

Fossil vertebrates from the deposits marking the Aptian-Albian in the Saharan region play a fundamental role in understanding the stratigraphic and geographic distribution of several dinosaur lineages in continental Africa and neighbouring regions. Although a number of different dinosaur clades are now recognized in the fossil record, fragmentary and isolated skeletal remains combined with largely understudied stratigraphic sections commonly limit the potential of such discoveries to a regional meaning. In the last decade, detailed revisions of both stratigraphic and palaeontological data from the well-known successions of southern Tunisia have yielded evidences of a diverse, late Early Cretaceous ecosystem composed of bony fish, sharks, turtles, crocodiles, pterosaurs, as well as several vertebrate tracksite (Bouaziz et al., 1988; Benton, 2000; Buffetaut and Ouaja, 2002; Cuny et al., 2004; Srarfi et al., 2004; Srarfi, 2006; Contessi and Fanti 2012a, b, Fanti et al., 2012; Contessi, 2013a, b, and references therein). Dinosaurs are represented by skeletal remains of titanosauriforms and rebbachisaurid sauropods, whereas ornithopods and theropods are to date represented by isolated teeth, with the exception of fragmentary and poorly preserved cranial and post-cranial material (Lapparent, 1951; Buffetaut and Ouaja, 2002; Fanti et al., 2013, 2014; F.F., pers. obs.). In this study, we discuss the taxonomic potential of isolated theropod teeth and fragmentary, non-dental materials collected from the Dahar escarpment of southern Tunisia and extend taxonomic analyses and comparisons to a rich collection of isolated theropod teeth from other Saharan localities (Fig. 1). As tooth assemblages give important insights into faunal constituents otherwise poorly represented by skeletal remains, a detailed analysis of isolated theropod teeth offers the opportunity to 1. evaluate theropod taxonomical diversity in the Aptian-Albian of southern Tunisia, and 2. compare the data from Tunisia with currently known theropod diversity in coeval deposits of northern Africa. As such, the results of this research improve general understanding of the Lower Cretaceous Tunisian ecosystems and have important implications for Gondwanan and peri-Mediterranean palaeobiogeography.

## 2. Geological setting

A recent revision of stratigraphic correlations and fossil occurrence in the Tataouine basin (Fig. 1) revealed that the strata exposed in the area preserve multiple fossil-bearing levels: all identifiable dinosaur remains, however, occur within the Oum ed Dhiab Member of the Ain el Guettar Formation (upper Aptian–Albian) (Fanti et al., 2012). Relevant to this study, theropod remains historically referred to the fluvial deposits of the Chenini Member (Benton et al., 2000) are instead representative of transgressive lag deposits on transgressive, erosional surface which mark the base of the overlying Oum ed Diab Member (Fanti et al., 2012, 2014). Therefore, the faunal assemblage in these coarse-grained beds preserves taxa that may originally pertained to the underlying Chenini Member deposits as well as taxa that relate to the Oum ed Diab Member. The coarse-grained Chenini beds are representative of high-energy fluvial deposits that accumulated on a low-gradient, distal alluvial plain similar to modern *wadi*-like drainage systems (Benton et al., 2000; Fanti et al., 2012). Differently, fine-grained, sandy deposits of the Oum ed Diab Member overlying the basal transgressive lag preserve estuarine to shoreface and tidal flat deposits interpreted as deposited in a vast embayment (Fanti et al., 2012, 2013). Although at the time of writing it is not possible to constrain the temporal gap represented by the unconformity that separates the Chenini and the Oum ed Diab members, the Chenini Member is referred to the uppermost Aptian-lowermost Albian, whereas the Oum ed Diab Member to the middle Albian (Ben Youssef et al., 1985; Bodin et al., 2010; Pons et al., 2010; Fanti et al., 2012, and references therein). Specimens described in this study were surface collected from the two above-mentioned lithostratigraphic intervals within the Oum ed Diab Member. From a taphonomic perspective, specimens collected from the basal, lag deposits are partly or completely covered with a solid, diagenetic crust and present clear evidences of abrasion on both enamel surface and serrations, indicative of intense pre-burial transportation within the coarse-grained sediments (i.e. coarse quartzarenite with centimetre- to decimetre-sized pebbles). Conversely, specimens collected from the juxtaposing, unconsolidated sandy deposits are in good preservation conditions although they were likely shed teeth, being found isolated and rootless. Significant differences in the taphonomic conditions and

matrix associated with collected teeth allowed a robust stratigraphic discrimination of morphotypes discussed herein.

### 3. Material and methods

The relative paucity of well-preserved material from the Tataouine region and the lack of detailed classification of Saharan isolated teeth in the literature challenged the possibility for detailed study. Historically, all isolated elements, including teeth, have been referred to a 'typical' northern-Africa theropod fauna based on the very few skeletal material collected in these regions. This fauna includes three mid-Cretaceous theropod clades represented by a restricted number of taxa: carcharodontosaurids (*Carcharodontosaurus saharicus*, *C. iguidensis*, *Eocarcaria dinops*, *Sauroniops pachytholus*, Depéret and Savornin, 1925; Stromer, 1931; Lavocat, 1954; Russell, 1996; Sereno et al., 1996; Amiot et al., 2004; Brusatte and Sereno, 2007; Sereno and Brusatte, 2008; Cau et al., 2012, 2013), spinosaurids (*S. aegyptiacus* and its possible synonym *S. maroccanus*, *Cristatusaurus lapparenti*, and its possible synonym *Suchomimus tenerensis*, Stromer, 1915; Russell, 1996; Taquet and Russell, 1998; Smith et al., 2006; Sereno et al., 1998), and abelisaurids (*Rugops primus*, *Kryptos palaios*, Sereno et al., 2004; Sereno and Brusatte, 2008). A fourth lineage is represented by *Deltadromeus* (Sereno et al., 1996), a taxon lacking cranial and dental remains and with a controversial phylogenetic placement among Ceratosauria (see Carrano and Sampson, 2008). Recently, Amiot et al. (2004) and Richter et al. (2013) claimed the possible presence of dromaeosaurids in the Cenomanian of Morocco, the second report in continental Africa after the discovery of isolated teeth in the Wadi Milk Formation of Sudan (Rauhut and Werner, 1995). In continental Africa, Aptian–Cenomanian theropods are known primarily from the peri-Saharan regions (Fig. 1), thus the role of Tunisian taxa is pivotal in the comprehension of evolutionary and biogeographic patterns within African theropods in the mid-Cretaceous. Therefore, additional data on theropod tooth variability in the fossil record of key localities - i.e. Algeria (Taquet and Russell, 1998), Egypt (Smith and Lamanna, 2006; Smith et al., 2006), Libya (Smith and Dalla Vecchia, 2006; Le Loeuff et al., 2010), Morocco (Amiot et al., 2004; Richter et al., 2013), Niger (Sereno et al., 2004; Brusatte and Sereno, 2007; Sereno and Brusatte, 2008), Sudan (Rauhut and Werner, 1995), and Saudi Arabia (Kear et al., 2013) - were included in this study. Furthermore, a large collection of unstudied specimens

collected from several well-known localities of the Saharan region (i.e. Gadoufaoua, Niger; Tabroumit and Gara Sbaa, Morocco; Djoua, Algeria) housed in the collection of the Muséum National d'Histoire Naturelle in Paris provided a solid database for a proper definition and comparison of northern Africa morphotypes. In total, approximately 500 specimens were studied at both macro- and microscopic scale: optical microscopes were used to observe general morphological characters. In addition, on the light of morphological similarities between isolated spinosaurid and crocodylian teeth (see also Sereno and Larsson, 2009, for a revision of Saharan crocodyliforms) that are ordinarily found in the same fossil association, a total of 160 crocodylian teeth (including complete and partial dental series) of *Sarcosuchus* sp., *Araripesuchus* sp., *Hamadasuchus* sp., and *Elosuchus* sp. were measured and included in the comparative morphometric analyses (Lapparent, 2002; Sereno et al., 2001; Larsson and Sues, 2007; Sereno and Larsson, 2009; Cuny et al., 2010; Fanti et al., 2012; FF, MC, pers. obs. 2014). SEM secondary electron images of selected tooth characters were acquired using a Scanning Electron Microscope Philips 515b (operating voltage 3kV) on uncoated specimens at the Dipartimento di Scienze Biologiche, Geologiche e Ambientali in Bologna. Morphometric parameters were taken with standard calliper with the precision to the nearest mm.

### 3.1 Tooth nomenclature

Theropod dentition has been the subject of a number of studies and several authors proposed a number of both quantitative and qualitative parameters to diagnose taxa; in particular, multivariate analyses have proven to be useful in the determination of theropod taxa based on isolated material (Larson and Currie, 2013; Hendrickx and Mateus, 2014; Hendrickx et al., *in press*; Torices et al., *in press*). Principal Component Analyses (PCA) were performed using Past 3.x01 software on Tunisian teeth to discriminate specimens according to the variance of the height, FABL, basal width, and presence/absence of denticles, enamel ridges, blood grooves, and enamel wrinkles. Data were log-transformed for the analyses. Tooth terminology used herein follows that of Currie et al. (1990), Farlow et al. (1991), Fanti and Therrien (2007), and Hendrickx and Mateus (2014). Additional parameters for the description of serrations include denticle morphology, cellae (*sensu* Buscalioni et al., 1997), and blood grooves description (*sensu* Buscalioni et al., 1997 and

Fanti and Therrien, 2007). Crown ornamentation are described following the nomenclature proposed by Brusatte et al. (2007). The term *enamel wrinkles* refers herein to parallel ridges or grooves that flank the serrations and do not extend on the crown surface. *Band* indicates herein continuous wrinkles that extend across the entire labial or lingual surfaces commonly limited to the basal section of the crown: these laminations, commonly displaying alternation of dark/light colouring, reflect dentine growth and have been used to infer tooth development and replacement rates (Erickson, 1996; Straight et al., 2004; Cillari, 2011). *Ridges* refer to either regular and irregular apicobasal enamel rises located on both lingual and labial crown surfaces (Buffetaut, 2008; Buffetaut et al., 2008; Richter et al., 2013).

Institution abbreviation: GZG, Geowissenschaftliches Zentrum der Universität Göttingen Museum; MGGC, Museo Geologico Giovanni Capellini (Bologna, Italy); MNHN, Muséum National d'Historie Naturelle, Institut de Paléontologie, (Paris, France); ONM, Office National des Mines (Tunis, Tunisia).

Other abbreviations: BW, tooth basal width; FABL, fore-aft basal length; FABL/BW, basal compression ratio; FABL/TCH, elongation ratio; NDPM, number of denticles per millimetre on both mesial and distal carinae (measured at mid-crown); OTU, Operational Taxonomic Unit; TCH, tooth crown height.

### 3.2 Phylogenetic analyses

For this research, the phylogenetic affinities of the theropod material described herein were tested entering operational taxonomic units – based on the main tooth morphotypes present in the Oum ed Diab Member and on the most informative isolated, non-dental material – into two previously published data-sets focusing on, respectively, 1. theropod tooth morphology and 2. African theropods.

1. Isolated theropod teeth from the Tataouine basin are categorized in eight distinct morphotypes: we accordingly entered eight OTUs into a modified version of the 'second analysis' (i.e., the 'supermatrix') of Hendrickx and Mateus (2014); the data set was modified by the removal of the four OTUs based on the Portuguese teeth (see details in Hendrickx and Mateus 2014). Analytical protocol and nodal support

calculation followed the procedure outlined by Hendrickx and Mateus (2014). See Supplementary Material for character score for the Tunisian OTUs.

2. Two OTUs based on a fragmentary dentary (MGGC 21889) and an isolated caudal vertebra (MGGC 21891) collected from the Oum ed Diab Member were entered in the data set of Cau et al. (2013). Analytical protocol and nodal support calculation followed the procedure outlined by Cau et al. (2012, 2013). See Supplementary Material for character score for the Tunisian OTUs.

All phylogenetic analyses were employed with the Hennig Society version of TNT vers. 1.1 (Goloboff et al., 2008). With both data set, the matrix was analysed under performing a 'New Technology Search' with the 'driven search' option (TreeDrift, Tree Fusing, Ratchet, and Sectorial Searches selected with default parameters; addition sequence replicates set at 100); followed by a 'Traditional Search' of the tree islands saved from the 'New Technology Search' analyses. Nodal support (Decay Index) values were calculated performing 1000 'Traditional Search' analyses set with default parameter, and saving all trees up to ten steps longer than the shortest topologies.

#### **4. Description of theropod teeth**

##### *Morphotype 1* (Fig. 2A-D; Tab. 1)

Although several specimens are fragmentary (either shed teeth or teeth with unpreserved root) the preservation quality of the crown and denticles is good. These mesial teeth are generally bigger than other collected from the same levels (TCH 30–70 mm), have an almost conical crown only slightly laterally compressed (FABL-BW ratio <1.5) and have a nearly symmetrical, oval to lanceolate basal cross section. The crown is slightly curved distally so that the tooth apex forms a distal concavity but never extends beyond the distal end of the crown base. Both labial and lingual surfaces are convex and the carinae are strongly developed; the mesial carina is straight whereas the distal one shifts labially toward the base of the tooth. Denticles are present on the entire length of both carinae and are generally rounded in overall shape, as long as they are wide, and oriented perpendicularly to the edge of the tooth, with 2.5 denticles per millimetre being found on the mesial carina and 2 in the distal carina. On both carinae, however, denticles

decrease in size toward the base of the tooth: as measured teeth do not preserve the root, the absence of denticles in the most basal section of the carinae cannot be excluded. U-shaped cellae with no blood grooves are present in the interdenticular region. Faint, parallel bands that extend from the carinae over the labial and lingual surfaces of the crown are observed in a restrict number of specimens and are limited to the basal region of the tooth. Marginal enamel wrinkles become less distinct and progressively disappear as they approach both the mesial and distal carinae.

#### *Morphotype 2* (Fig. 2E-H; Tab. 1)

Isolated teeth pertaining to this morphotype are rare in the Tataouine basin, representing only the 2% of collected specimens. The overall tooth morphology is blade-like, having a slender and elongated crown, a strongly labio-lingually compressed (FABL-BW ratio  $>2$ ), lanceolate basal section and both labial and lingual surfaces are slightly convex. The apical margin of the tooth is straight, whereas the mesial margin curves gently apically. Both carinae are serrated with rounded denticles, and – in apical view – they lie on the same plane without twisting: the mesial carina bears 3 denticles per millimetre whereas 2.5 are counted on the distal carina. Denticles on the mesial carina are as tall as they are wide with shallow blood grooves either absent or limited to the interdenticular base. The distal denticles are more developed and higher than the mesial ones with deep blood grooves inclined toward the base of the tooth (comma-shaped grooves), and a moderately hooked distal margin. In addition, these teeth do not display the parallel bands observed in Morphotype 1 but have marginal enamel wrinkles on the labial and lingual surfaces of both distal and mesial carinae (more pronounced in the latter), extending along the entire length of the serrated carina.

#### *Morphotype 3* (Fig. 3A-E; Tab. 1)

Straight, often elongated crowns and overall triangular-conical shape in longitudinal section characterize teeth pertaining to Morphotype 3. In addition, the apex of teeth is particularly pointed. Serrations are absent and replaced by two, symmetrical, well-developed carinae that extend for the entire crown height and clearly visible in the basal section. Enamel ridges are absent and a smooth, enamel surface characterizes this morphotype; SEM images of the tooth enamel indicate that the lack of a textured enamel is

not imputable to a taphonomic artefact. Only a few tooth crowns display shallow wear facets and irregular enamel ridges. Marginal enamel wrinkles are present adjacent to the distal carina in some teeth. The marginal wrinkles are slightly developed and faint, closely spaced and inclined basally for a short distance mesially to the carina. Where preserved, the tooth root is hollow with a well-developed pulpar cavity: in cross-section, the enamel delimiting the pulpar cavity is relatively thick. The basal cross-section is sub-circular to elliptical, whereas it becomes extremely narrow, labio-lingually compressed, and leaf-shaped apically. Teeth included in this morphotype do not display major morphometric variation.

*Morphotype 4* (Fig. 3F-N; Tab. 1)

Teeth pertaining to this morphotype are common in the Tataouine basin as well as in the collection representative of different Saharan localities. Overall, teeth are slender with an elongated, conical crown that curves distally forming a distal concavity with the tooth apex extending beyond the distal end of the crown base. Labio-lingual compression is moderate, no wrinkles nor band are observed. The mesial and distal carinae are characterized by heavily worn, shallow and irregular denticles (up to 6 per millimetre). In addition, regular ridges characterize each tooth: these ornamentations extend longitudinally along the entire crown, with the enamel smoothing out toward both the carinae and along the apicobasal axis of the tooth. The number of these ridges is quite conservative, being 8 on both labial and lingual sides in the 90% of measured specimens, and 10, 12 or 14 in the remnant 10%. The number of ridges is inversely proportional to the size of the tooth (small teeth have higher – and more variable number of ridges, whereas the larger specimens commonly display 8 ridges). The basal cross section is sub-oval, having in approximately 40% of observed specimens a central, labio-lingual compression that confers an overall 'eight' shape to the section. The root is hollow with a well-developed, oval pulpar cavity: alike teeth included in Morphotype 3, in cross-section, the enamel delimiting the pulpar cavity is thin.

*Morphotype 5* (Fig. 3O-Q; Tab. 1)

All specimens assigned to this morphotype display enamel ornamentation in having shallow apicobasal crenulation. These enamel structures differ from typical enamel ridges

in being: 1. faint and shallow, 2. nor straight nor parallel along the crown height, and 3. extending discontinuously along the tooth crown. In addition, they commonly differ in number between the lingual and labial surfaces. The number of these ornamentations on each surface varies greatly on observed specimens, ranging from 6 to 32. SEM images also revealed that the entire enamel surface is ornamented with irregular, apicobasal crenulations. As observed in Morphotype 3, teeth have a sub-circular basal section, whereas they become labio-lingually compressed toward the apex of the crown.

#### *Morphotype 6* (Fig. 4A-B; Tab. 1)

Teeth included in this morphotype are relatively small with a low crown with an overall triangular shape and both mesial and distal sides curved. In particular, the mesial profile is strongly curved in labio-lingual view having a typical deflection point near the midpoint of the crown; on the contrary, the distal curvature profile shows either moderate curvature or a straight profile, so that the tooth apex does not extend beyond the distal end of the crown base. Teeth are laterally compressed with a symmetrical, lanceolate cross section. Denticles are present on the entire length of the mesial and distal carinae, and they are smaller and shorter (3-3.5 denticles per mm) on the mesial carina than on the distal carina (2-2.5 per mm) and display a rounded distal morphology. In addition, denticles on the distal carina become smaller and shorter toward the tooth apex. Blood grooves are clearly visible to the naked eye and are deep and inclined toward the basal end of the tooth. A restricted number of teeth included in this morphotype shows enamel banding extending between the two carinae on both labial and lingual surfaces.

#### *Morphotype 7* (Fig. 4C-E; Tab. 1)

Teeth included in this morphotype are small lateral teeth characterized by a very slender and elongated crown (TCH is three times FABL). The crown is sub-triangular in overall shape, is pointed apically, and has the distal side straight and the mesial carina gently curved. The basal cross section is strongly labio-lingually compressed (FABL/BW ratio between 2 and 3.2) and teardrop-shaped. Rounded denticles extend along the entire length of both carinae, are slightly smaller in the basal section, with an average serration density of 3.5-4 denticles per mm in the mesial carina and 3 in the posterior one. Blood

grooves are absent, with shallow, rounded cellae located at the base of the denticles. Neither surface undulations nor colour bands are observed.

#### *Morphotype 8* (Fig. 4F-H; Tab. 1)

Teeth included in this morphotype are the smallest collected from the Tataouine region (TCH < 1cm); none, however, has a preserved root. Overall, these primarily lateral teeth display a strongly curved mesial carina and a nearly straight distal carina so that tooth apex forms a shallow distal concavity extending as posteriorly as the distal end of the crown base. The crown is not elongated (TCH/FABL between 1 and 1.5) and the basal cross section is strongly labio-lingually compressed. Both carinae are serrated with rounded denticles (4.5 per mm in the mesial carina, 4 per mm in the distal carina) that extend along the entire crown length. Blood grooves are deep and inclined toward the basal end of the tooth. No enamel banding or wrinkles are observed.

### 5. Theropod teeth analyses

Morphometrics parameters of isolated teeth were compared statistically to those of Tunisian crocodylians as well as to selected well-known theropods from continental Africa, Madagascar, India and other continents. Tooth parameters for *Carcharodontosaurus* sp., *Majungasaurus crenatissimus*, *Indosuchus raptorius*, *Masiakasaurus knopfleri*, *Spinosaurus* sp., *Deinonychus anthirropus*, *Dromaeosaurus albertensis*, *Saurornitholestes langstoni*, as well as undetermined abelisaurid teeth were either acquired from the literature or measured by the senior author (see Table 1). Standard bivariate plots of TCH-FABL/BW ratio discriminate large clusters (i.e. spinosaurids, carcharodontosaurids, abelisaurids, and small theropods) but do not suggest clear affinities for included Tunisian morphotypes (Fig. 5). Principal Components Analysis of the log-transformed data of the Tunisian specimens (Fig. 6) indicates that two components explain the variance of the data. PC1 shows a heavy loading in the tooth size parameters: height (loading value 0.91), FABL (l.v. 0.33), and basal width (0.26), whereas PC2 shows heavier loading in the presence/absence of enamel wrinkles (l.v. 0.72). Graphically, the PCA analysis: 1. clearly separates teeth pertaining to morphotypes 1 and 2 from all other samples; 2. gathers with some overlap morphotypes 3, 4 and 5; and 3. places morphotypes 5, 6, and 7 in a cluster that does not overlap with other measured theropod teeth. Finally, the PCA discriminates

crocodilian and theropod teeth. Furthermore, in order to properly discuss the taxonomic affinities of isolated theropod teeth from the Tataouine region and correlatives from other localities of the Saharan region, results of morphological and statistical analyses were also compared with teeth already described in the literature and consequently included in phylogenetic analyses (Fig. 7). The result of updated analysis based on the data set of Hendrickx and Mateus (2014, Fig. 7A) provided a phylogenetic framework for interpreting the affinities of the Tunisian tooth morphotypes, to infer a minimum number of taxa represented and to estimate abundance and diversity. A first comparison based on standard morphometric and morphologic parameters resulted in a preliminary taxonomic assignment of all morphotypes as follows:

Morphotype 1: based on available data in the literature, the assignment of teeth included in this morphotype is problematic as canonical diagnostic parameters considered of this group are not directly referable to the dentition of any northern African theropod. However, teeth referable to this morphotype have been found not only in southern Tunisia, but also in other Saharan localities (i.e. Gadoufaoua, Sereno and Brusatte 2008, fig. 8; MNHN GRD553a, GRD553b, GAD600, this study), thus supporting the institution of a distinct morphotype. The overall morphology is similar to the one described for several anterior and lateral isolated teeth assigned to large-bodied tetanurans, such as *Megalosaurus* and *Neovenator* (Cillari, 2011; Han et al., 2011; Cobos et al., 2014). The large and almost conical crown, the labial migration of the distal carina, and the leaf-shaped basal cross section clearly distinguish Morphotype 1 from typical, blade-like carcharodontosaurid teeth (e.g., Coria and Currie, 2006). However, high TCH values falls within average carcharodontosaurid teeth, as well as characteristics of serrations along the mesial and distal carinae. The enlarged basal cross section as well as the position of the carinae (not aligned on the antero-posterior axis of the tooth) most likely place these teeth in the anterior part of the dentition. Currie and Azuma (2006) describe in detail an almost complete dental series of *Fukuiraptor*, including anterior maxillary teeth (their fig. 4) which interestingly display a strong labiolingual compression and an almost teardrop basal cross-section. Similarly, we refrain from referring Morphotype 1 to as premaxillary teeth of a tetanuran, as the former does not display a U-shaped cross-section nor a lingual migration of the anterior carina as commonly observed in large tetanurans (including *Fukuiraptor*, Currie and Azuma, 2006, fig. 1), and disparity in the denticles density between the carinae.

This morphotype was scored as a 'mesialmost tooth' OTU in the data set of Hendrickx and Mateus (2014).

Morphotype 2: all typical morphological features of carcharodontosaurid teeth are identifiable in teeth included in Morphotype 2, including large and moderately curved crowns, strong labiolingual compression of the basal cross-section, and enamel wrinkles flanking both serrated carinae. Within the northern Saharan context teeth of *Carcharodontosaurus saharicus* and *Eocarcharia dinops* (Stromer, 1931; Brusatte and Sereno, 2008; Brusatte et al., 2007, 2008) represent the better documented basis for comparison. However, similar characteristics are observed in the teeth of the abelisaurid *Skorpiovenator bustingorryi* (Canale et al., 2008, fig. 2), including deep and arcuate marginal ornamentation, as well as in a single isolated abelisaurid tooth from Morocco (Buffetaut et al., 2005). Therefore, Morphotype 2 is assigned to either a carcharodontosaurid or abelisaurid theropod. This morphotype was scored as a 'lateral tooth' OTU in the data set of Hendrickx and Mateus (2014).

Morphotype 3 and 5: teeth included in these morphotypes display all characteristic features of spinosaurine teeth. Teeth are relatively large, conical in overall shape with rounded cross-sections, and both mesial and distal carinae are well-developed and unserrated. Teeth associated with the holotype of *Siamosaurus suteethorni* of Thailand and other isolated spinosaurid teeth from eastern Asia (Buffetaut and Ingevat, 1986; Buffetaut et al., 2008; Bertin, 2010, fig. 2) are virtually indistinguishable from teeth included in Morphotype 5. As spinosaurine theropods from Africa that display similar dentition are represented solely by *Spinosaurus aegyptiacus* and other isolated elements referred to as *Spinosaurus* sp. (Stromer, 1915; Buffetaut, 1989; Bouaziz et al., 1988; Buffetaut and Ouaja, 2002; Bertin, 2010; Richter et al., 2013), Morphotype 3 and 5 are tentatively assigned to cf. *Spinosaurus* sp.. Differences in the enamel ornamentation are here inferred to either variability in the dentition (although such condition is not supported by any known specimen of *Spinosaurus*) or most likely to the presence of different spinosaurine species in the region. These morphotypes were scored as a 'lateral tooth' OTUs in the data set of Hendrickx and Mateus (2014).

Morphotype 4: although teeth included in this morphotype are not significantly different in overall morphology from those assigned to *Spinosaurus*, the curved crown, the peculiar apicobasal enamel ridges, and the presence of small, irregular serration in the

mesial and distal carinae (as in *Baryonyx*, *Cristatusaurus*, and *Suchomimus*; Charig and Milner, 1996; Taquet and Russell, 1998; Sereno et al., 1998; Buffetaut, 2007; Buffetaut et al., 2008, FF, pers. obs., 2014) are all consistent with a baryonychine spinosaurid. This morphotype was scored as a 'lateral tooth' OTU in the data set of Hendrickx and Mateus (2014).

Morphotype 6: diagnostic features of abelisaurid teeth are observed in this Morphotype. In particular, the crown displaying a sub-triangular shape with the mesial side curved (with a typical inflexion point near the midlength of the crown) and the distal one almost straight, 2.5-3 denticles per mm, and well developed blood grooves (Mahler, 2005; Fanti and Therrien, 2007; Smith and Dalla Vecchia, 2006; Smith and Lamanna, 2006; Smith, 2007; Sereno and Brusatte, 2008). This morphotype was scored as a 'lateral tooth' OTU in the data set of Hendrickx and Mateus (2014).

Morphotype 7: the specimens of this morphotype exhibit small and relatively flat tooth crowns that curve distally toward the apex of the tooth, strong labiolingual compression and serrated carinae. Overall morphology resembles that of Morphotype 2, including the shape and diagnostic characteristics of denticles (even though they are denser in Morphotype 7). On the light of the documented variability along the dental series of carcharodontosaurids and abelisaurids, characterized by tiny distal maxillary and dentary teeth (Smith, 2007; Sereno and Brusatte, 2008; FF, pers. obs. on the *Majungasaurus crenatissimus* specimen FMNH PR2100), a possible assignment is to this clades, either considering Morphotype 7 as posterior lateral teeth or possibly juvenile lateral teeth. This morphotype was scored as a 'lateral tooth' OTU in the data set of Hendrickx and Mateus (2014).

Morphotype 8: teeth pertaining to this morphotype are generally small with a teardrop-shaped basal cross-section. The posterior carina also displays an inflection point where the curvature becomes more pronounced distally, and blood grooves are pronounced, both characters typically observed in abelisaurid teeth. The relatively dense serrations (4.5 denticles per mm in the mesial carina and 4 per mm in the distal one) are comparable with those of posteriormost lateral teeth of abelisaurids, as in the case of *Majungasaurus* (3.5-4 denticles per millimetre, FF., pers. obs.) and *Kryptos* (up to 3 serrations per millimetre, Sereno and Brusatte, 2008, fig. 5). Morphometric and morphological analyses suggest that Morphotype 8 includes abelisaur posterior lateral

teeth or possibly juvenile lateral teeth. This morphotype was scored as a 'lateral tooth' OTU in the data set of Hendrickx and Mateus (2014).

The phylogenetic analysis of the tooth morphotypes resulted in 60 shortest trees of 3623 steps each (Consistency Index =0.5620, Retention Index =0.6348). The strict consensus of the shortest trees found is well resolved and in overall topology agrees with the original result of Hendrickx and Mateus (2014, Fig. 7A). Morphotype 1 resulted among a basal branch of Abelisauroidea, sister taxon of the 'Noasauridae + Abelisauridae' node. This placement is relatively poorly supported (Decay Index = 1) and based on a single character state reversal (char. 38.1, a proportional character relative to baso-apical crown elongation). Morphotypes 2, 6 and 8 formed a clade nested in Abelisauridae. Character support for this node is relatively robust (Decay Index = 4) and supported by four unambiguous synapomorphies (chars. 70.1, presence of flattened labial surface of crown; 71.1, presence of a labial concavity adjacent to distal carina; 98.1, presence of a lower number of denticles apically than a mid-crown; 109.1, presence of tenuous transversal undulations on crown). Morphotypes 6 and 8 resulted closer to each other than to Morphotype 2 since they share a weak crown elongation (char. 67.0) and distal denticles that are asymmetrical and lack an uncinated distal margin (char. 88.1). The latter node is moderately robust (Decay Index = 4). Morphotype 7 resulted among the same abelisaurid polytomy including the above-mentioned three morphotypes, although this result is poorly supported (Decay Index = 1) and based on a single unambiguous synapomorphy (char. 92.1, presence of mid-crown denticles on distal carina mesiodistally wider than apicobasally long). The remaining morphotypes (i.e., Morphotypes 3, 4, 5) formed an unresolved polytomy with *Irritator/Angaturama*, *Spinosaurus* and the Baryonychinae node. The nodal support of this polytomy is low (Decay Index = 1) since it is based on three unambiguous synapomorphies (chars. 85.1, presence of a high denticle density; 93.1, presence of irregularly-sized denticles; 107.2, presence of flutes on both labial and lingual surfaces of crown), two of them scored as 'inapplicable' in the spinosaurine taxa (lacking marginal denticles). It is noteworthy that nodal support values for the clades Megalosaurinae, Neovenatoridae and Baryonychinae (the '*Baryonyx* + *Suchomimus*' node) are relatively robust (Decay Indices >3), suggesting that actual data do not support the referral of the Tunisian morphotypes to the latter three clades.

## 6. Description of theropod non-dental remains

### Systematic Palaeontology

Dinosauria

Theropoda

Ceratosauria

Abelisauridae

Abelisauridae gen. et sp. indet.

Specimens: MGGC 21889 (Fig. 8A-G), ONM TM 02

Description. Both specimens are fragments of the dentigerous part of dentary rami, including, respectively, five and four alveoli. In both occlusal and lateral view, the dentigerous margin is straight. The lateral surface (Fig. 5B) is divided dorsoventrally into two areas: a dorsoventrally convex dorsal part, forming the lateral surface of the alveoli, and a slightly concave and smooth ventral sulcus, running anteroposteriorly and parallel to the dentigerous margin. The dorsal part is devoid of ornamentation and neurovascular foramina, and we hypothesise that the latter were housed along the now-lost central surface of the ventral sulcus. The alveolar part of the lateral surface (dorsal to the sulcus) becomes slightly more convex toward the anterior end. In ventral view (Fig. 8G), the posterior end of the ventral sulcus is overhung by the ventral margin of the alveolar margin, whereas in the distal end of the bone the sulcus is relatively shallower and is not overhung by the ventral margin of the alveolar margin. The alveoli are ovoid-quadrangular in occlusal view (Fig. 8A). The interalveolar spaces are very narrow lips of bone. In medial view, the paradental plates are fused, forming a continuous paradental lamina that apically does not reach the level of the dorsal margin of the lateral surface (Figs. 8C, E). The medial surface of the paradental lamina is ornamented by a continuous series of low ridges and sulci inclined posterodorsally at 45 degrees (Fig. 8E). The lingual bar is preserved posterior to the anteriormost alveolus. Although the lingual bar is tightly connected with the medial surface of the alveolar surface, a discontinuous sulcus is visible along their contact in occlusal view. The dorsoventral depth of the lingual bar decreases toward the anterior end. The palatal surface of the lingual bar is slightly convex mediolaterally and concave ventrally. The ventral surface of the lingual bar and the medial

surface of the bone, ventral to the alveoli, form the smooth lateral margin of the Meckelian fossa. The basal part of erupting tooth crowns are preserved inside the alveoli. The cross section of the crowns is elliptical to drop-shaped, more convex labially. The mesiodistal axis of the teeth is directed anterolaterally relative to the anteroposterior axis of the tooth row.

## Tetanurae

### Carcharodontosauridae

#### Carcharodontosauridae gen. et sp. indet.

Specimen: MGGC 21891 (Fig. 8H-L).

Description. The specimen is an incomplete middle caudal vertebra. Most of the centrum is preserved, whereas the neural arch is mostly lost with the exception of the neural canal floor, the zygapophyseal pedicels and the proximal end of the ribs. The neural arch is fused to the centrum and no neurocentral suture is visible. The centrum is amphicoelous, with both intercentral facets that are elliptical, and taller than wide. The anterior intercentral facet is taller than the posterior, due to the presence of prominent centroprezygapophyseal laminae that dorsally roof the centrum margin (Figs. 8I, J). The centrum is mediolaterally compressed at mid-length and hourglass-shaped in ventral view. The narrow ventral surface of the centrum bears a shallow depression bounded laterally at both anterior and posterior ends by the chevron facets. The chevron facets are significantly worn, although the preserved surfaces show that the posterior chevron facets were slightly longer than the anterior. The lateral surfaces of the centrum are slightly concave anteroposteriorly. No pleurocoels are present. The neural arch is extended along the anterior six seventh of the dorsal surface of the centrum. The broken margins of the neural arch show a camellate internal structure (several small chambers separated by narrow septa; Fig. 8L). The bases of the prominent centroprezygapophyseal laminae are preserved, and indicate that the latter funnelled the anterior end of the neural canal (Figs 8H, I). The prezygapophyses are lost, except for their bases, in the point where the centroprezygapophyseal laminae and the anterior end of the ribs merge. The proximal base of the ribs is preserved: it is extended along the central half of the ventral margin of the neural arch. The rib bases are dorsally concave in lateral view (Fig. 8H). The

preserved ventral part of the neural canal is narrow. The bases of the centropostzygapophyseal laminae are preserved. They are less prominent than the corresponding prezygapophyseal laminae, and do not form a funnel-like extension of the neural canal (Fig. 8J).

cf. Spinosauridae

Specimen: MGGC 21892 (Fig. 8M-P)

**Description.** The specimen is a partial ungual phalanx. The articular end, flexor tubercle and distal tip are missing. In proximal view, the ungual is elliptical, about twice taller than wide at mid-height (58 mm vs 31 mm; Fig. 8N). The internal texture of the bone is exposed in proximal view. The dorsal half of the internal of the bone appears spongy. In the centre, an elliptical pit is present. The pit is one-third the depth of the bone and may represent the distal end of a hollow chamber. The ventral fourth of the bone is formed by compact bone with no vascularisation. In lateral view, the bone is ventrally concave and dorsally convex. The preserved dorsal curvature of the ungual is about 80 mm long proximodistally, the ventral margin is 50 mm long. The curvature along the ventral margin is more marked than along the dorsal margin. Along the middle of both lateral sides a shallow collateral sulcus runs proximodistally (Fig. 8M). The two collateral sulci are sub-parallel. The dorsal surface of the phalanx is uniformly convex transversely. The ventral surface of the phalanx is transversely convex, lacking both sulcus and keel.

## 7. Taxonomy of theropod non-dental remains

Based on the combination of distal paradental laminae that are fused and ornamented by lingual furrows and rugosities, MGGC 21889 is referred to Abelisauridae (Sampson and Witmer, 2007; Carrano and Sampson 2008). In overall shape and relevant features, the specimen is comparable to the posterior end of the buccal margin of the dentary of *Majungasaurus* (Sampson and Witmer, 2007). This interpretation is confirmed by the result of the phylogenetic analysis, placing the specimen among an unresolved polytomy with the abelisaurid OTUs included (Fig. 7B). Unambiguous synapomorphies supporting this placement are the presence of sculptured and furrowed medial surface of

the parodontal laminae (char. 376.1), and presence of quadrangular alveoli (char. 490.1). Therefore, the specimen is referred to an indeterminate abelisaurid taxon.

The presence of camellate pneumatization in the neural arch restricts the referral of MGGC 21891 to three theropod clades: Abelisauroidae, Carcharodontosauria, and Coelurosauria (Benson et al., 2011). The presence of prominent centroprezygapophyseal laminae funnelling the neural canal was reported by Rauhut (2011) as a synapomorphy of Carcharodontosauridae. In overall shape and proportions, the specimen is comparable to the middle caudal vertebrae of carcharodontosaurids (e.g., Coria and Currie, 2006). This interpretation is confirmed by the result of the phylogenetic analysis, that placed MGGC 21891 among the carcharodontosaurids (Fig. 7B) based on two unambiguous synapomorphies: presence of camellate pneumatization (char. 189.2), and presence of dorsally concave caudal ribs (char. 675.1). Therefore, we refer MGGC 21891 to the latter clade.

Based on overall shape, size, curvature and mediolateral compression, the phalanx MGGC 21892 is interpreted as the manual ungual of a large-bodied theropod. Among Theropoda, the evident ventrodorsal curvature of the bone (suggesting a falciform shape) and the presence of collateral sulci in MGGC 21892 exclude its referral to Abelisauridae, the latter bearing atrophied manual phalanges lacking unguals (Carrano and Sampson 2008). The absence of a keeled ventral margin, the significant distal tapering of the ventral outline, and the symmetrical placement of the collateral sulci exclude the referral of the specimen to Megaraptora (Benson et al. 2012). Although lacking unambiguous synapomorphies of Spinosauridae, in overall size, shape and proportions, MGGC 21892 is comparable to manual ungual I of the spinosaurid *Suchomimus* (see Benson et al. 2012, fig. 15 G-H). We therefore refer this specimen to cf. Spinosauridae.

## 8. Discussion

The phylogenetic analysis on discussed theropod teeth recovered them into two clades: Abelisauroidae and Spinosauridae. Both clades are also represented in the non-tooth material (Bouaziz et al., 1988; Buffetaut and Ouaja, 2002, this study). A third clade, Carcharodontosauridae, is represented by an isolated caudal vertebra. These results indicate an early Albian 'basal theropod association' lacking coelurosaurs, in agreement with previous studies on North African theropod faunas (e.g., Sereno and Brusatte, 2008).

However, the exact number of species present in the association is unclear although a minimum of three species is inferred based on the three recovered clades. The absence of carcharodontosaurids in the tooth material supports the hypothesis that the latter were relatively less abundant than spinosaurids and abelisauroids, which are represented by, respectively, three and five tooth morphotypes. Morphotypes 1 and 2 include the largest recovered teeth in the Tunisian beds. Although overall size, denticle morphology and distribution, and enamel characteristics are consistent between Morphotype 1 and 2, there are significant differences in the basal cross-section as well as in the position of the carinae, which are here interpreted as a reflection of positional differences (see Smith, 2007). Thus, being referable to distinct positions along the tooth row (i.e., more mesial dentition for Morphotype 1, more distal dentition for Morphotype 2), their differences can be explained, at least in part, as the result of heterodonty along the same tooth row, and do not necessarily imply a taxonomic distinction. Phylogenetic analysis indicates that Tunisian teeth included in Morphotype 1 as well as specimens MNHN GRD553a, GRD553b and GAD600 may be interpreted as anterior teeth of large-bodied abelisauroids characterized by a leaf-shaped basal cross section and a migration of the distal carina toward the labial side.

Teeth pertaining to Morphotype 2 have a symmetrical, strongly labio-lingually compressed basal cross-section with no displacement of the carinae along the tooth crown. These primarily lateral teeth are the relatively more common in the examined database in comparison with those included in Morphotype 1, a numerical disparity that could reflect abundance difference between lateral (more abundant) and mesial (less abundant) teeth in typical theropod oral series (e.g., Smith, 2007). Enamel wrinkles are very prominent and deeper near the serrated carinae in Morphotype 2, a parameter that has been considered as diagnostic for carcharodontosaurids, including *Carcharodontosaurus saharicus* (e.g., Sereno et al., 1996; Coria and Currie, 2006; Cillari, 2011; Richter et al., 2013), although it is also present in some abelisaurids (Canale et al., 2009; Hendrickx and Mateus, 2014). We consider Morphotypes 1 and 2 as mesial and lateral teeth referable to adult individuals of the same large-bodied abelisauroid taxon. Alternatively, these morphotypes represent two distinct large-bodied abelisauroid taxa that are at the time of writing represented by teeth from distinct positions along the oral margin: an interpretation that we consider as less parsimonious and more unlikely.

The Morphotypes 6, 7 and 8 resulted among Abelisauroidea, with Morphotypes 6 and 8 closely related to Morphotype 2. The most macroscopic difference of these morphotypes from Morphotypes 1 and 2 teeth is in overall smaller size. Furthermore, Morphotypes 6 and 8 differ from Morphotype 2 in lacking marginal ornamentation and in lacking hooked denticles. The latter combination is a reversal to the plesiomorphic conditions shared by non-abelisaurid ceratosaurians (based on character state distribution in the analyses of Hendrickx and Mateus, 2014). Although no data are known on the ontogenetic modification in abelisauroid dentition, ontogenetic changes in tooth morphology comparable to the differences between Morphotypes 6/8 and Morphotype 2 are reported in other large-bodied theropods (e.g., Carr, 1999). For example, in tyrannosaurids, the juvenile dentition retains symplesiomorphic features shared by most non-tyrannosaurid coelurosaurs (Carr, 1999). Assuming a similar phenomenon among abelisaurids, the features in Morphotypes 6 and 8 could be explained as an ontogenetically immature stage of development instead of a genuine plesiomorphic condition. Although we cannot exclude that Morphotypes 6 and 8 (and eventually, Morphotype 7) represent a second abelisauroid taxon with adult body size smaller than the taxon represented by Morphotypes 2 (and eventually, Morphotype 1), we suggest to consider the former morphotypes as belonging to immature individuals of the same taxon represented by larger specimens. It is noteworthy that large-bodied abelisauroids are reported from lower Aptian levels of western Libya, less than 50 km from the Tunisian border (Smith et al., 2010).

The Morphotypes 3, 4 and 5 are referred to Spinosauridae. Although Morphotype 3 shares a serration pattern with members of Baryonychinae (Charig and Milner, 1997; Sereno et al., 1998), the former OTU was not recovered as a member of the '*Baryonyx* + *Suchomimus*' node. In particular, the Morphotype 3 teeth lack the braided enamel texture characteristic of the mentioned baryonychine genera (Hendrickx and Mateus, 2014), suggesting that the Tunisian teeth belonged to a spinosaurid taxon distinct from *Baryonyx* and *Suchomimus*. Buffetaut and Ouaja (2002) reported presence of spinosaurine spinosaurids in the Lower Cretaceous of Tunisia. Although Morphotypes 4 and 5 share derived features with spinosaurine teeth (e.g., Sues et al., 2002), the phylogenetic analyses did not recover a Spinosaurinae clade including any of the Tunisian morphotypes.

## 8. Stratigraphic and palaeoecological occurrence of theropod material

The deposition of the Chenini fluvial unit marks a major variation in the environmental condition in southern Tunisia during the late Aptian. The Chenini Member preserves high-energy fluvial deposits that accumulated under arid to strongly seasonal conditions, as indicated by indurated and cemented grains, the abundance of iron oxides and phosphatized organic remains (including dinosaur teeth and bones) and the absence of megaplants (Fanti et al., 2012 and references therein). A vast, palaeo-drainage system characterized by periods of very low net sediment accumulation and channel incision as well as high rates of sediment reworking is also consistent with the absence of well-preserved, articulated or associated fossil remains. The basal deposits of the overlying Oum ed Diab Member, interpreted as a transgressive lag, also include reworked elements originally within the Chenini Member. As such, theropod teeth described here pertains also to the Chenini deposits. Previous studies also reported isolated and poorly preserved sauropod bone and teeth (titanosauriforms and rebbachisaurids), teeth and scales of actinopterygian fishes, and rare crocodylian teeth and turtle carapace fragments from this interval (Bouaziz et al., 1988; Benton, 2000; Fanti et al., 2012, 2014). The fossil assemblage referred to the Chenini Member preserves teeth representative of all discussed morphotypes although with significant variations in their relative abundance. Morphotypes 1, 2, 6, 7, and 8 represent approximately the 90% of all theropod teeth referable to this unit, whereas Morphotypes 3 and 5 amount to the 8% and Morphotype 4 only to the 2% (Fig. 9).

The overlying deposits of the Oum ed Diab Member are interpreted as a vast estuarine to embayment environment characterized by freshwater and marine fishes such as elasmobranchs, actinopterygians, and sarcopterygians, including large-sized coelacanthiforms (*Mawsonia* sp.) and dipnoans (*Ceratodus* sp. and *Neoceratodus* sp.). Crocodyliforms are the dominant tetrapod fauna, represented by approximately 85% of all identifiable elements collected from this unit (Fig. 9). Known taxa range from small-bodied forms comparable to *Araripesuchus* to large-bodied taxa related to *Hamadasuchus* and *Sarcosuchus* (Fanti et al., 2012). Dinosaur remains are rare and represented by scattered postcranial elements, the articulated remains of the rebbachisaurid sauropod *Tataouinea hannibalis*, and isolated theropod remains (Fanti et al., 2012, 2013, 2014). Isolated

theropod teeth from the Oum ed Diab deposits pertains almost exclusively to Morphotypes 3, 4 and 5 (96% of collected specimens), with rare teeth referred to Morphotypes 2 and 6 (Fig. 9).

Thus, available data support a robust correlation between the stratigraphic occurrence of theropod taxa and a major variation in the palaeoecological conditions inferred from the sedimentological data. Abelisauroids and the rare carcharodontosaurids (together with titanosauriforms and rare rebbachisaurids) are confined in the *wadi*-like, arid alluvial plain deposits of the Chenini Member. Conversely, spinosaurids (including baryonychine taxa) become predominant in the estuarine and embayment deposits of the Oum ed Diamb Member, characterized by rich and diverse crocodylian and fish fauna (Fig. 9). Spinosaurids have been interpreted as piscivorous animals, based on direct evidence of fish remains associated with spinosaurids and on the morphology of both skull and dentition (Charig and Milner, 1997; Dal Sasso et al., 2005). Furthermore, isotopic analyses on spinosaurid teeth support a more aquatic lifestyle for these theropods, compared to other predatory dinosaurs (Amiot et al., 2010). The environmental segregations between the estuarine-based spinosaurids and the arid/alluvial-based non-spinosaurid theropods documented in the Chenini and Oum ed Diamb members, is coherent with these hypotheses, and support the interpretation of the spinosaurid peculiarities as the result of adaptive evolution to a 'crocodile-like' ecology in these basal tetanurans (Holtz, 1998). Although the phylogenetic analysis of discussed tooth morphotypes does not clearly discriminate the placement of the spinosaurid Morphotypes 3 to 5 between Spinosaurinae or Baryonychinae, the overall morphologies of these teeth supports the co-occurrence of a baryonychine-like taxon and a spinosaurine-like taxon in the estuarine ecosystems of the Albian of Tunisia. The numerical abundance and co-occurrence of diverse spinosaurid lineages in the same palaeoenvironment has not been reported before (see Bertin, 2010), and further supports the hypothesis that spinosaurids were not only ecologically segregate from other large-bodied theropods, but also well adapted to specific environmental conditions not exploited by other dinosaurs (Hone, 2010). Following these arguments, the morphological differences in both snout and dentition between baryonychines and spinosaurines (Charig and Milner, 1996; Sereno et al., 1998; Sues et al., 2002; Dal Sasso et al., 2005) may be explained as the result of adaptive divergence in order to reduce source competition among sympatric spinosaurids.

## 9. Conclusions

A revision of theropod material from the mid-Cretaceous deposits of southern Tunisia provides important insight into the taxonomic diversity of important theropod clades in the Saharan region. Pending the discovery of more complete and diagnostic skeletal material, results presented in this study indicate the presence of three clades, Spinosauridae, Abelisauroida, and Carcharodontosauridae. In particular, parsimony analysis suggests that the eight tooth morphotypes are referable to two clades. Several lines of evidence provided here concur in interpreting the five ziphodont tooth morphotypes recovered (i.e., Morphotypes 1, 2, 6, 7, 8) as representing ontogenetic and positional differences among the dental series of a single abelisauroid taxon, instead of several species of different size. The interpretation of the three morphotypes referred to Spinosauridae is more problematic, and we cannot exclude that they may represent two distinct clades (i.e., Baryonychinae and Spinosaurinae). Relevant for the identification of Saharan isolated specimens, carcharodontosaurids are not represented in the teeth record but by isolated postcranial material only, thus relatively less abundant than spinosaurids and abelisauroids. In addition, the stratigraphic occurrence of theropod material supports an accentuate partition of abelisauroids –and rare carcharodontosaurids– in the fluvial deposits of the Chenini Member, and spinosaurids in the overlying estuarine to coastal deposits of the Oum ed Diab Member.

## Acknowledgements

We thank C. Hendrickx, A. Torices and Editor F. Surlyk for their detailed reviews of this manuscript. The authors are grateful to L. Cantelli, A. Bacchetta, M. Hassine, and H. Aljane for their valuable support in the field. We also thank G. Gasparotto for SEM analyses. Images of specimens hosted at the Muséum National d'Histoire Naturelle in Paris in figures 2, 3, and 4, were taken by FF and MC under kind permission of R. Allain. A special acknowledgment to R. Allain (Muséum National d'Histoire Naturelle, Paris), the Office National des Mines (Tunis, Tunisia), and the Musée de l'Association des Amis de la Mémoire de la Terre in Tataouine for access to specimens in their care. Finally, we would like to thank D. Bonadonna for the silhouettes in Fig. 9. This research was conducted in collaboration with the Office National Des Mines, Tunis, and the Integrated Geoscience

Research Group (Dipartimento di Scienze Biologiche, Geologiche e Ambientali, Università di Bologna), and was financially supported by Fondazione Alma Mater, Professor G. Gabbianelli, and the Museo Geologico Giovanni Capellini (Bologna, Italy). The program TNT was made available with the sponsorship of the Willi Hennig Society.

## References

- Amiot, R., Buffetaut, E., Lécuyer, C., Wang, X., Boudad, L., Ding, Z., Fourel, F., Hutt, S., Martineau, F., Medeiros, A., Mo, J., Simon, L., Suteethorn, V., Sweetman, S., Tong, H., Zhang, F., Zhou, Z. 2010. Oxygen isotope evidence for semi-aquatic habits among spinosaurid theropods. *Geology* 38, 139–142.
- Amiot, R., Buffetaut, E., Tong, H., Boudad, L., Kabiri, L., 2004. Isolated theropod teeth from the Cenomanian of Morocco and their palaeobiogeographical significance. *Revue de Paléobiologie* 9, 143–149.
- Ben Youssef, M., Biely, A., Kamoun, Y., Zouari, M., 1985. L'Albien moyen supérieur à *Knemiceras* forme la base de la grande transgression crétacée au Tebaga de Medenine (Tunisie meridionale). *Comptes Rendus de l'Académie des Sciences, Paris, Serie II* 300, 965–968.
- Benson R., Butler, R., Carrano, M., O'Connor, P., 2011. Air-filled postcranial bones in theropod dinosaurs: physiological implications and the 'reptile'–bird transition. *Biological Reviews* 87, 168–193.
- Benson R., Rich, T., Vickers-Rich, P., Hall, M., 2012. Theropod fauna from Southern Australia indicates high polar diversity and climate-driven dinosaur provinciality. *PLoS ONE* 7(5): e37122. doi:10.1371/journal.pone.0037122.
- Benton, M.J., Bouaziz, S., Buffetaut, E., Martill, D., Ouaja, M., Soussi, M., Trueman, C., 2000. Dinosaurs and other fossil vertebrates from fluvial deposits in the Lower Cretaceous of southern Tunisia. *Palaeogeography, Palaeoclimatology, Palaeoecology* 157, 227–246.
- Bertin, T., 2010. A catalogue of material and review of the Spinosauridae. *PalArch's Journal of Vertebrate Paleontology* 7, 1–39.
- Bodin, S., Petitpierre, L., Wood, J., Elkanouni, I., Redfern, J., 2010. Timing of early to mid-cretaceous tectonic phases along North Africa: new insights from the

- Jeffara escarpment (Libya–Tunisia). *Journal of African Earth Sciences* 58, 489–506.
- Bouaziz, S., Buffetaut, E., Ghanmi, M., Jaeger, J.J., Martin, M., Mazin, J.M., Tong, H., 1988. Nouvelles découvertes de vertèbres fossiles dans l'Albien du Sud tunisien. *Bulletin de la Société Géologique de France* 4, 335–339.
- Brusatte, S., Sereno, P., 2007. A new species of *Carcharodontosaurus* (Dinosauria: Theropoda) from the Cenomanian of Niger and a revision of the genus. *Journal of Vertebrate Paleontology*, 27(4), 902-916.
- Brusatte S.L., Benson R.J., Carr T.D., Williamson T.E., Sereno P.C. 2007. The systematic utility of theropod enamel wrinkles. *Journal of Vertebrate Paleontology* 27(4), 1052-1056.
- Brusatte S., Benson R.B.J., Hutt S. 2008. Osteology of *Neovenator salerii* (Dinosauria: Theropoda) from the Wealden Group (Barremian) of the Isle of Wight. *Monograph of the Paleontographical Society*, London, 75 pp.
- Buffetaut, E., 2007. The spinosaurid dinosaur *Baryonyx* (Saurischia, Theropoda) in the Early Cretaceous of Portugal. *Geol. Mag.* 144 (6), 1021–1025.
- Buffetaut, E., 2008. Spinosaurid teeth from the Late Jurassic of Tendaguru, Tanzania, with remarks on the evolutionary and biogeographical history of the Spinosauridae. *Mid-Mesozoic Life and Environments*, Cognac (France), June 2008.
- Buffetaut, E., Ingevat, R., 1986. Unusual theropod dinosaur teeth from the Upper Jurassic of Phu Wiang, northeastern Thailand. *Rev. Paléobiol.* 5, 217-220.
- Buffetaut, E., Escuillié, F., Pohl, B., 2005. First theropod dinosaur from the Maastrichtian phosphates of Morocco. *Kaupia* 14, 3–8.
- Buffetaut E., Suteethorn V., Tong H., Amiot R., 2008. An Early Cretaceous spinosaurid theropod from southern China. *Geological Magazine* 145 (5), 745–748.
- Buffetaut, E., Ouaja, M., 2002. A new specimen of *Spinosaurus* (Dinosauria, Theropoda) from the Lower Cretaceous of Tunisia, with remarks on the evolutionary history of the Spinosauridae. *Bulletin de la Société Géologique de France* 173, 415–421.
- Buscalioni A.D., Gasparini Z., Perez-Moreno B., Sanz J.L., 1997. Argentinean theropods: first morphological analysis on isolated teeth. *Proceedings from the first European workshop on Vertebrate Paleontology*, Geological Museum, Copenhagen University, 1-4 May 1996.

- Canale, J.I., Scanferla, C.A., Agnolin, F., and Novas, F.E., 2009. New carnivorous dinosaur from the Late Cretaceous of NW Patagonia and the evolution of abelisaurid theropods. *Naturwissenschaften* 96 (3), 409–414.
- Carr, T. D. 1999. Craniofacial ontogeny in Tyrannosauridae (Dinosauria, Coelurosauria). *Journal of Vertebrate Paleontology* 19, 497–520.
- Carrano, M. T., Sampson, S. D., 2007. The phylogeny of Ceratosauria (Dinosauria: Theropoda). *Journal of Systematic Palaeontology* 6 (2), 183-236.
- Cau, A., Dalla Vecchia, F. M., Fabbri, M., 2012. Evidence of a new carcharodontosaurid from the Upper Cretaceous of Morocco. *Acta Palaeontologica Polonica* 57(3), 661-665.
- Cau, A., Dalla Vecchia, F. M., Fabbri, M., 2013. A thick-skulled theropod (Dinosauria, Saurischia) from the Upper Cretaceous of Morocco with implications for carcharodontosaurid cranial evolution. *Cretaceous Research* 40, 251-260.
- Charig, A.J., Milner, A.C., 1997. *Baryonyx walkeri*, a fish-eating dinosaur from the Wealden of Surrey. *Bulletin of the Natural History Museum of London* 53, 11–70.
- Cillari, A., 2011. Teeth of theropoda (Dinosauria: Saurischia): morphology, function and classification. Ph. D. thesis, Università Sapienza, Roma, 235 pp.
- Cobos, A., Lockley, M., Gascò, F., Royo-Torres, R., Alcalà, L., 2014. Megatheropods as apex predators in the typically Jurassic ecosystems of the Villar del Arzobispo Formation (Iberian Range, Spain). *Palaeogeography, Palaeoclimatology, Palaeoecology* 399, 31–41.
- Contessi, M., Fanti, F., 2012a. First record of bird tracks in the Late Cretaceous (Cenomanian) of Tunisia. *Palaios* 27, 455-464.
- Contessi, M., Fanti, F., 2012b: Vertebrate tracksites assemblages in the Middle Jurassic-Upper Cretaceous of South Tunisia. *Ichnos* 19, 227-227.
- Contessi, M., 2013a. A new dinosaur ichnofauna from Tunisia: Implications for the palaeobiogeography of peri-Adriatic carbonate platforms in the mid-Cretaceous. *Palaeogeography, Palaeoclimatology, Palaeoecology* 392, 302-311.
- Contessi, M., 2013b. First report of mammal-like tracks from the Cretaceous of North Africa (Tunisia). *Cretaceous Research* 42, 48-54.
- Coria R. A., Currie P. J., 2006. A new carcharodontosaurid (Dinosauria, Theropoda) from the Upper Cretaceous of Argentina. *Geodiversitas* 28(1), 71-118.

- Cuny, G., Ouaja, M., Sraf, D., Schmitz, L., Buffetaut, E., Benton, M.J., 2004. Fossil sharks from the Early Cretaceous of Tunisia. *Revue de Paléobiologie* 9, 127–142.
- Cuny, G., Cobbett, A., Meunier, F., Benton, M., 2010. Vertebrate microremains from the Early Cretaceous of southern Tunisia. *Geobios* 43, 615–628.
- Currie, P., Rigby, J., Sloan, R., 1990. Theropod teeth from the Judith River Formation of southern Alberta, Canada, in: Carpenter, K., Currie, P.J. (Eds.), *Dinosaur Systematics. Approaches and Perspectives*. Cambridge University Press, Cambridge, Massachusetts, pp. 107–125.
- Dal Sasso, C., Maganuco, S., Buffetaut, E., Mendez, M.A. 2005, New information on the skull of the enigmatic theropod *Spinosaurus*, with remarks on its sizes and affinities. *Journal of Vertebrate Paleontology* 25, 888–896.
- Erickson G.M. 1996. Incremental lines of von Ebner in dinosaurs and the assessment of tooth replacement rates using growth line counts. *Proceedings of the National Academy of Sciences* 93, 14623–14627.
- Fanti, F., Therrien, F., 2007. Theropod tooth assemblages from the Late Cretaceous Maevarano Formation and the possible presence of dromaeosaurids in Madagascar. *Acta Palaeontologica Polonica* 52, 155–166.
- Fanti, F., Contessi, M., Franchi, F., 2012. The “*Continental Intercalaire*” of southern Tunisia: stratigraphy, paleontology, and paleoecology. *Journal of African Earth Sciences* 73-74, 1-23.
- Fanti, F., Cau, A., Hassine, M., Contessi, M., 2013. A new sauropod dinosaur from the Early Cretaceous of Tunisia with extreme avian-like pneumatization. *Nature Communications* 4:2080, DOI: 10.1038/ncomms3080
- Fanti, F., Cau, A., Hassine, M., 2014. Evidence of titanosauriforms and rebbachisaurids (Dinosauria: Sauropoda) from the Early Cretaceous of Tunisia. *Journal of African Earth Sciences* 90, 1-8.
- Farlow, J., Brinkman, D., Abler, W., Currie, P., 1991. Size, shape and serration density of theropod dinosaur lateral teeth. *Modern Geology* 16, 161–198.
- Goloboff, P., Farris, J., Nixon, K., 2008. TNT, a free program for phylogenetic analysis. *Cladistics* 24, 774-786.

- Han, F., Clark, J., Sullivan, C., Choiniere, J., Hone, D., 2011. Theropod teeth from the middle-upper Jurassic Shishugou Formation of Northwest Xinjiang, China. *Journal of Vertebrate Paleontology* 31(1), 111–126.
- Hendrickx, C., Mateus, O., 2014. Abelisauridae (Dinosauria: Theropoda) from the Late Jurassic of Portugal and dentition-based phylogeny as a contribution for the identification of isolated theropod teeth. *Zootaxa* 3759 (1), 1-174.
- Hendrickx, C., Mateus, O., Araujo, R., *in press*. The dentition of megalosaurid theropods. *Acta Palaeontologica Polonica*, DOI: 10.4202/app.00056.2013.
- Holtz, T.R., Jr. 1998. Spinosaurids as crocodile mimics. *Science* 282, 1276–1277.
- Hone, D.W.E., Xu, X., Wang, D.-Y. 2010. A probable baryonychine (Theropoda: Spinosauridae) tooth from the Upper Cretaceous of Henan Province, China. *Vertebrata Palasiatica* 48, 19–26.
- Kear, B., Rich, T., Vickers-Rich, P., Ali, M., Al-Mufarreh, Y., Matari, A., Al-Massari, A., Nasser, A., Attia, Y., Halawani, M., 2013. First Dinosaurs from Saudi Arabia. *PLoS ONE* 8(12): e84041. doi:10.1371/journal.pone.0084041
- Lapparent, A.F.de, 1951. Découverte de dinosauriens, associés à une faune de reptiles et de poissons, dans le Crétacé inférieur de l'Extrême Sud tunisien. *Comptes Rendus de l'Académie des Sciences* 232, 1430.
- Lapparent, A.F.de Broin, 2002. *Elosuchus*, a new genus of crocodile from the Cretaceous of the North of Africa. *Comptes Rendus Palevol.* 1 (5), 275-285.
- Larson, D.W., Currie, P.J., 2013. Multivariate analyses of small theropod dinosaur teeth and implications for paleoecological turnover through time. *PLoS ONE* 8(1): e54329. doi:10.1371/journal.pone.0054329
- Larsson, H., Sues, H-D., 2007. Cranial osteology and phylogenetic relationships of *Hamadasuchus rebouli* (Crocodyliformes: Mesoeucrocodylia) from the Cretaceous of Morocco. *Zoological Journal of the Linnean Society* 149, 533–567.
- Lavocat, R., 1954. Sur les dinosauriens du Continental Intercalaire des Kem-Kem de la Daoura. *Comptes Rendus de la 19<sup>ème</sup> session du Congrès Géologique International (1952)*, section 13, Questions diverses de géologie générale, 3<sup>ème</sup> partie paléontologie stratigraphique, quaternaire et pétrographie, 15: 65-68.
- Le Loeuff, J., Metais, E., Dutheil, D., Rubinos, J., Buffetaut, E., Lafont, F., Cavin, L., Moreau, F., Tong, H., Blanpied, C., Sbeta, A., 2010. An Early Cretaceous vertebrate

- assemblage from the Cabao Formation of NW Libya. *Geological Magazine* 147, 750–759.
- Mahler, L., 2005 Record of Abelisauridae (Dinosauria: Theropoda) from Cenomanian Morocco. *Journal of Vertebrate Paleontology* 25, 236–239.
- Pons, E., Chikhi-Aouimeur, F., Abdallah, H., 2010. Albian *Eoradiolites* (Bivalvia: Radiolitidae) from Jabal Naïmia, Gafsa Region, Tunisia, with revisional studies on the Albian forms of the genus. *Journal of Paleontology* 84, 321–331.
- Rauhut, O.W.M., 2011. Theropod dinosaurs from the Late Jurassic of Tendaguru (Tanzania). *Special Papers in Palaeontology* 86, 195–239.
- Rauhut O.W.M., Werner C., 1995. First record of the family Dromaeosauridae (Dinosauria: Theropoda) in the Cretaceous of Gondwana (Wadi Milk Formation, northern Sudan). *Paläontologische Zeitschrift* 69, 475-489.
- Richter, U., Mudroch, A., Buckley, L., 2013. Isolated theropod teeth from the Kem Kem Beds (Early Cenomanian) near Taouz, Morocco. *Paläontologische Zeitschrift* 87, 291–309.
- Russell, D.A., 1996. Isolated dinosaur bones from the Middle Cretaceous of the Tafilalt, Morocco. *Bulletin du Muséum national d'Histoire naturelle, Paris, série 4*, 18, section C, 349-352.
- Sampson, S., Witmer, L., 2007. Craniofacial anatomy of *Majungasaurus crenatissimus* (Theropoda: Abelisauridae) from the Late Cretaceous of Madagascar, in: Sampson, S., Krause, D. (Eds.). *Majungasaurus crenatissimus* (Theropoda: Abelisauridae) from the Late Cretaceous of Madagascar. *Society of Vertebrate Paleontology Memoir* 8. pp. 32–102.
- Sereno, P., Larsson, H., 2009. Cretaceous Crocodyliforms from the Sahara. *ZooKeys* 28, 1–143.
- Sereno, P., Larsson, H., Sidor, C., Gado, B., 2001. The giant crocodyliform *Sarchosuchus* from the Cretaceous of Africa. *Science* 294, 1516-1519.
- Sereno, P., Brusatte, S. 2008. Basal abelisaurid and carcharodontosaurid theropods from the Lower Cretaceous Elrhaz Formation of Niger. *Acta Palaeontologica Polonica* 53 (1), 15–46.

- Sereno, P., Dutheil, D.B., Iarochene, M., Larsson, H.C.E., Lyon, G.H., Magwene, P.M., Sidor, C.A., Varricchio, D.J., Wilson, J.A., 1996. Predatory dinosaurs from the Sahara and Late Cretaceous faunal differentiation. *Science* 272, 986-991.
- Sereno, P., Wilson, J., Conrad, J., 2004. New dinosaurs link southern landmasses in the mid-Cretaceous. *Proceedings of the Royal Society of London B* 271, 1325–1330.
- Sereno, P., Beck, A.L., Dutheil, D.B., Gado, B., Larsson, H.C.E., Lyon, G.H., Marcot, J.D., Rauhut, O.W.M., Sadleir, R.W., Sidor, C.A., Varricchio, D.D., Wilson, G.P., Wilson, J.A., 1998. A long-snouted predatory dinosaur from Africa and the evolution of spinosaurids. *Science* 282, 1298–1302.
- Smith, J., 2007. Dental morphology and variation in *Majungasaurus crenatissimus* (Theropoda: Abelisauridae) from the Late Cretaceous of Madagascar, in: Sampson, S., Krause, D., (Eds.). *Majungasaurus crenatissimus* (Theropoda: Abelisauridae) from the Late Cretaceous of Madagascar. Society of Vertebrate Paleontology Memoir 8. pp. 103–126.
- Smith, J., Dalla Vecchia, F., 2006. An abelisaurid (Dinosauria: Theropoda) tooth from the Lower Cretaceous Chicla formation of Libya. *Journal of African Earth Sciences* 46, 240–244.
- Smith, J., Lamanna, M., 2006. An abelisaurid from the Late Cretaceous of Egypt: implications for theropod biogeography. *Naturwissenschaften* 93, 242-245.
- Smith, J., Vann, D., Dodson, P., 2005. Dental morphology and variation in theropod dinosaurs: implications for the taxonomic identification of isolated teeth. *The Anatomical Record Part A* 285: 699–736.
- Smith, J., Lamanna, M.C., Mayr, H., Lacovara, K.J., 2006. New information regarding the holotype of *Spinosaurus aegyptiacus* Stromer, 1915. *Journal of Paleontology* 80, 400–406.
- Smith, J., Lamanna, M., Askar, A.S., Bergig, K.A., Tshakreen, S.O., Abugares, M.M., Rasmussen, D.T. 2010. A large abelisauroid theropod dinosaur from the Early Cretaceous of Libya. *Journal of Paleontology* 84, 927–934.
- Srarfi, D., 2006. Biostratigraphie, biodiversité, taphonomie and paléoenvironnement des niveaux à vertébrés du Jurassique–Crétacé du Sud-Est de la Tunisie. Implications paléobiogéographiques. PhD Thesis, Université Claude Bernard Lyon 1.

- Srarfi, D., Ouaja, M., Buffetaut, E., Cuny, G., Barale, G., Ferry, S., Fara, E., 2004. Position stratigraphique des niveaux à vertébrés du Mésozoïque du Sud-Est de la Tunisie. Notes du Service Géologique de Tunisie 72, 5–16.
- Straight W.H., Barrick R.E., Eberth D.A., 2004. Reflections of surface water, seasonality and climate in stable oxygen isotopes from tyrannosaurid tooth enamel. *Palaeogeography, Palaeoclimatology, Palaeoecology* 206, 239–256.
- Stromer, E., 1915. Ergebnisse der Forschungsreisen Prof. E. Stromers in den Wüsten Ägyptens. II. Wirbeltier-Reste der Baharije-Stufe (unterstes Cenoman). 3. Das Original des Theropoden *Spinosaurus aegyptiacus* nov. gen., nov. spec. *Abhandlungen der Königlich Bayerischen Akademie der Wissenschaften, Mathematisch-physikalische Classe*, 28(3) Abhandlung:1–32.
- Stromer, E., 1931. Wirbeltiere-Reste der Baharijestufe (unterstes Cenoman). Ein Skelett-Rest von *Carcharodontosaurus* nov. gen. *Abhandlungen der Bayerischen Akademie der Wissenschaften, Mathematisch-naturwissenschaftliche Abteilung*, 9 (Neue Folge): 1–23.
- Sues, H. D., Frey, E., Martill, D. M., Scott, D.M., 2002. *Irritator challengeri*, a Spinosaurid (Dinosauria: Theropoda) from the Lower Cretaceous of Brazil. *Journal of Vertebrate Paleontology* 22 (3), 535-547.
- Taquet, P., Russell, D., 1998. A massively-constructed iguanodont from Gadoufaoua, Lower Cretaceous of Niger. *Annals de Paleontologie* 85, 85–96.
- Torices, A., Currie, P.J., Canudo, J., Pereda-Suberbiola, X., in press. Theropod dinosaurs from the Upper Cretaceous of the South Pyrenees Basin of Spain. *Acta Palaeontologica Polonica*, <http://dx.doi.org/10.4202/app.2012.0121>

## Figures

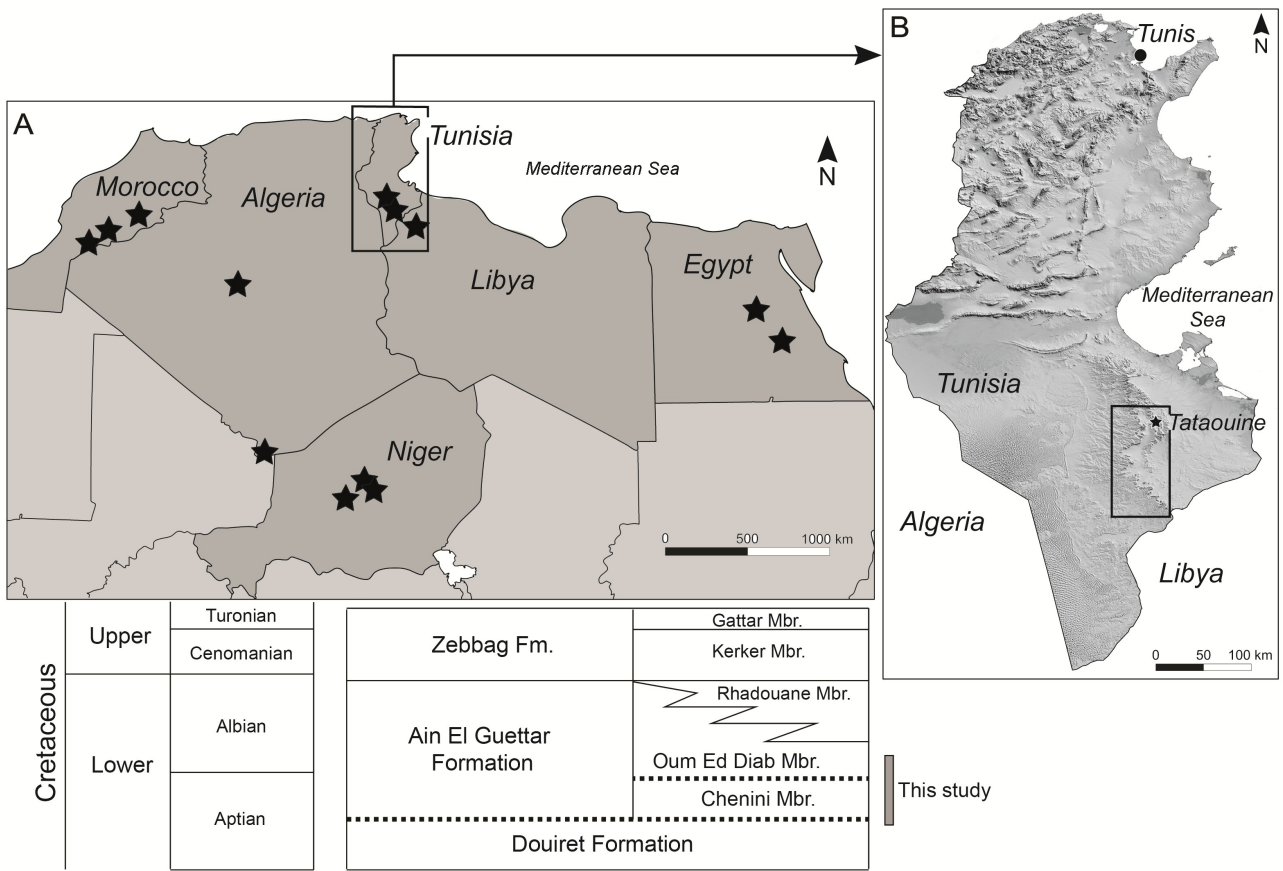


Fig. 1: A. Present day map of Africa showing the mid-Cretaceous localities from which isolate theropod teeth included in this study have been discovered. B. Reference map of Tunisia showing the position of the Tataouine Basin: the study area is located along the prominent Jeffara escarpment. C. Stratigraphic nomenclature for the mid-Cretaceous of southern Tunisia (after Fanti et al., 2012). Dashed lines indicate major unconformities.

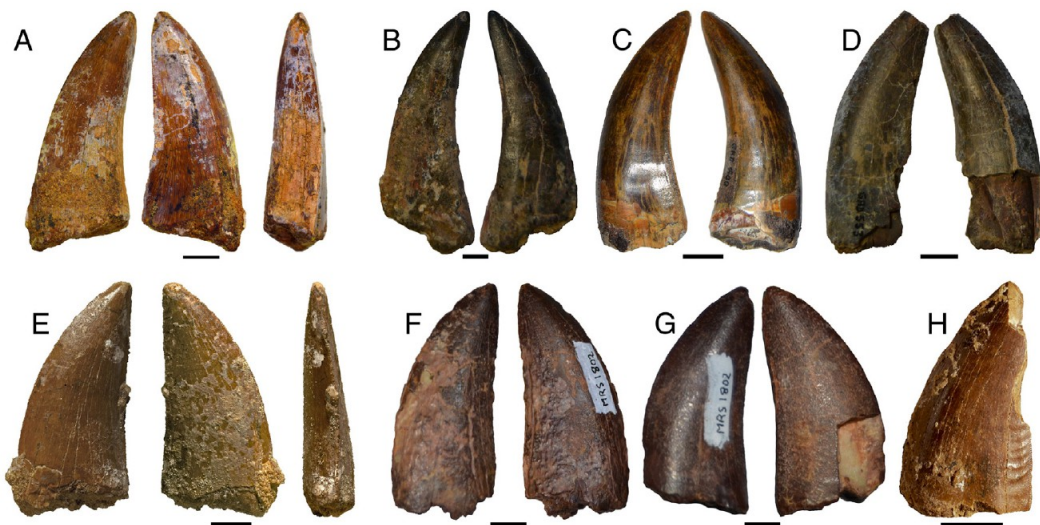


Fig. 2: Morphotype 1. A, MGGC TUN33; B, MNHN GRD553; C, MNHN GAD600; D, MNHN GRD553a. Morphotype 2. E, MGGC TUN86; F, MNHN MRS1802a; G, MNHN MRS1802b; H, MGGC TUN9 (note the marginal wrinkles near the distal carina). Scale bar 1cm.



Fig. 3: Morphotype 3. A, MGGC TUN86 and B, SEM image of the mesial carina (scale bar 0.5 mm); C, MNHN MRS654; D, MNHN GRD514; E, MNHN MRS1593. Morphotype 4. F, MGGC TUN107 and G, SEM image of the apical margin of the distal carina (scale bar 0.2

mm); H, MGGC TUN143; I, MNHN GAD570; J, MNHN GAD544; K, MNHN GAD161; L, MNHN GAD1966; M, MNHN GAD507; N, MNHN GRD520. Morphotype 5. O, MGGC TUN153 and P, SEM images of the ornamented enamel surface and mesial carina (scale bar 1mm); Q, MNHN MRS656. Scale bar 1 cm.

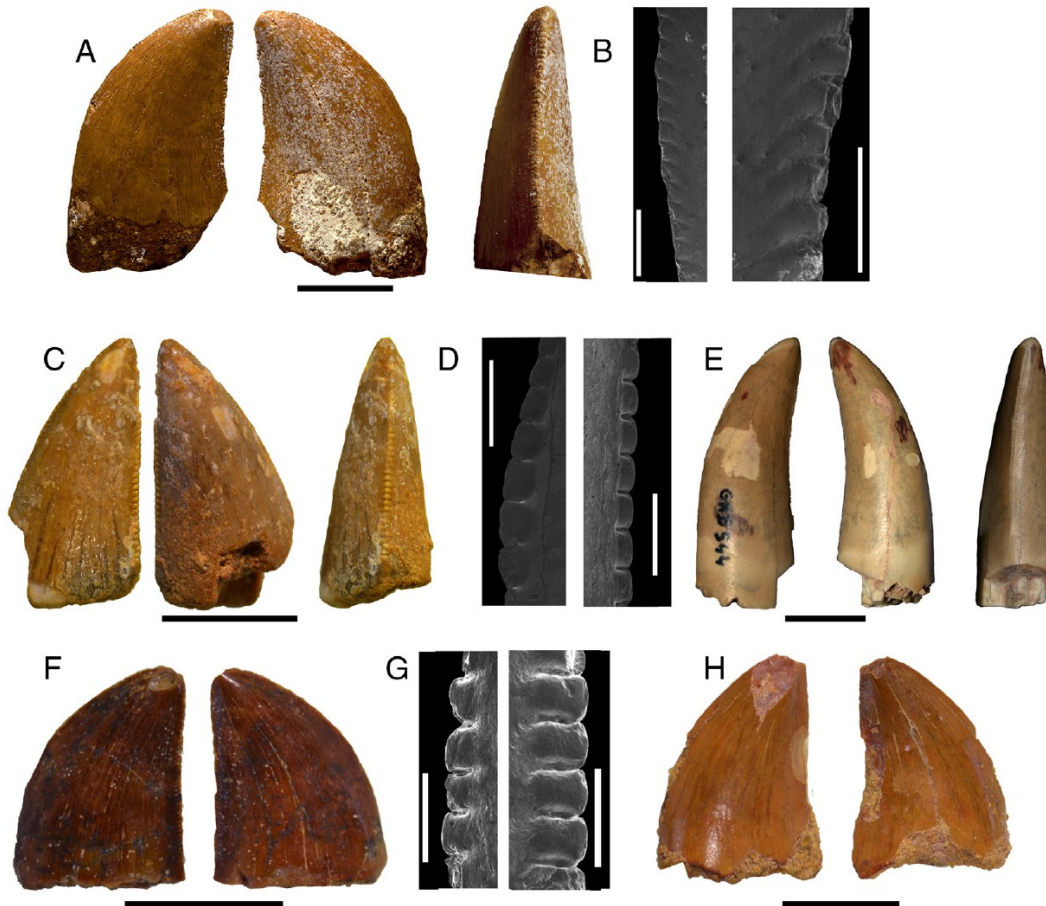


Fig. 4. Morphotype 6. A, MGGC TUN47 and B, SEM images of the distal and mesial carinae (scale bar 1mm). Morphotype 7. C, MGGC TUN26 and D, SEM images of the distal and mesial carinae (scale bar 1mm); E, MNHN GAD544. Morphotype 8. F, MGGC TUN45 and G, SEM images of the distal and mesial carinae (scale bar 0.5 mm); H, MGGC TUN78. Scale bar 1 cm.

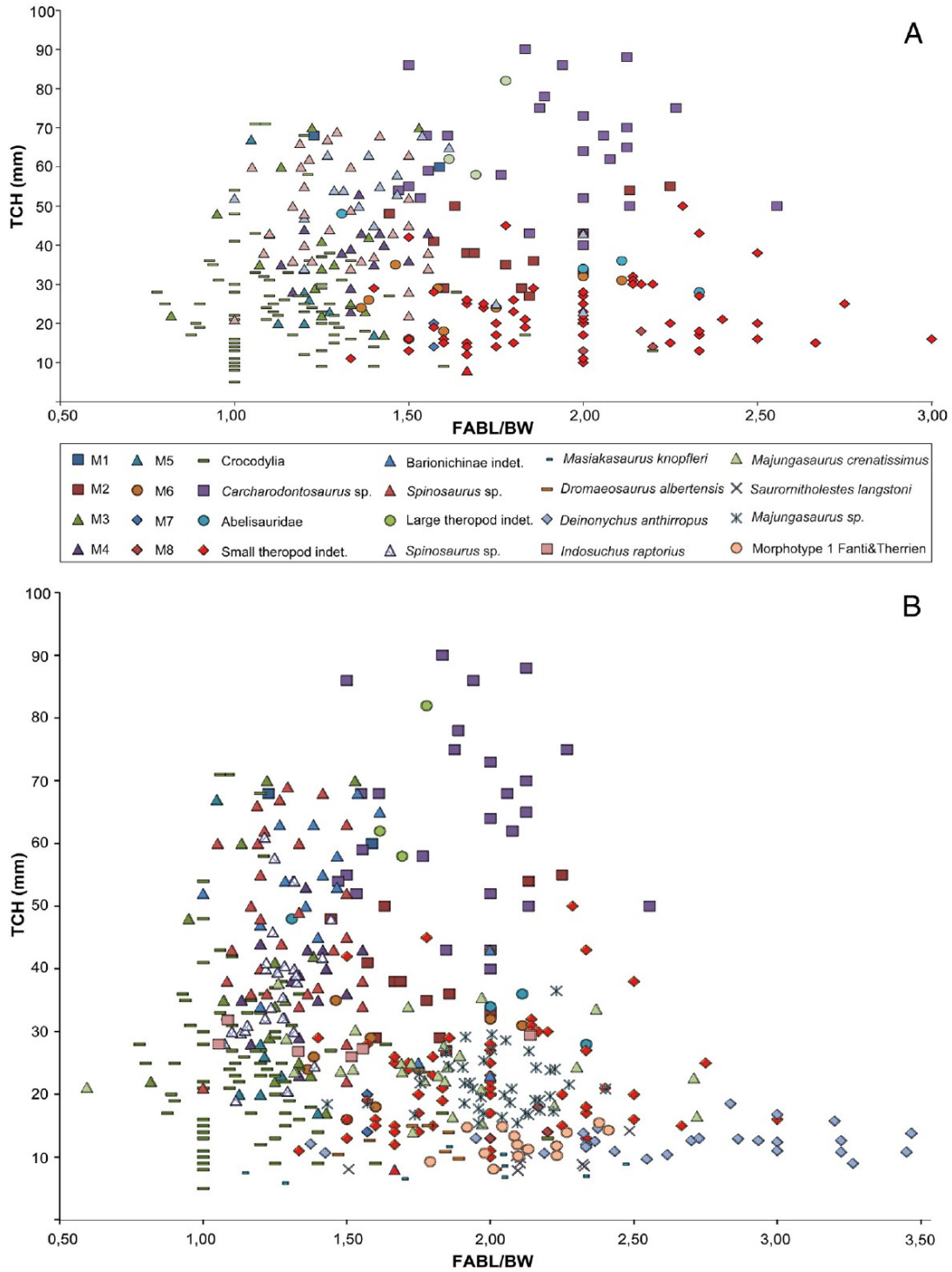


Fig. 5. Bivariate plots of theropod tooth parameters. A. TCH versus FABL/BW ratio of specimens collected in Southern Tunisia and those hosted in the MNHN collections. B. bivariate plot including all discussed specimen and other selected theropod taxa from Africa and North America.

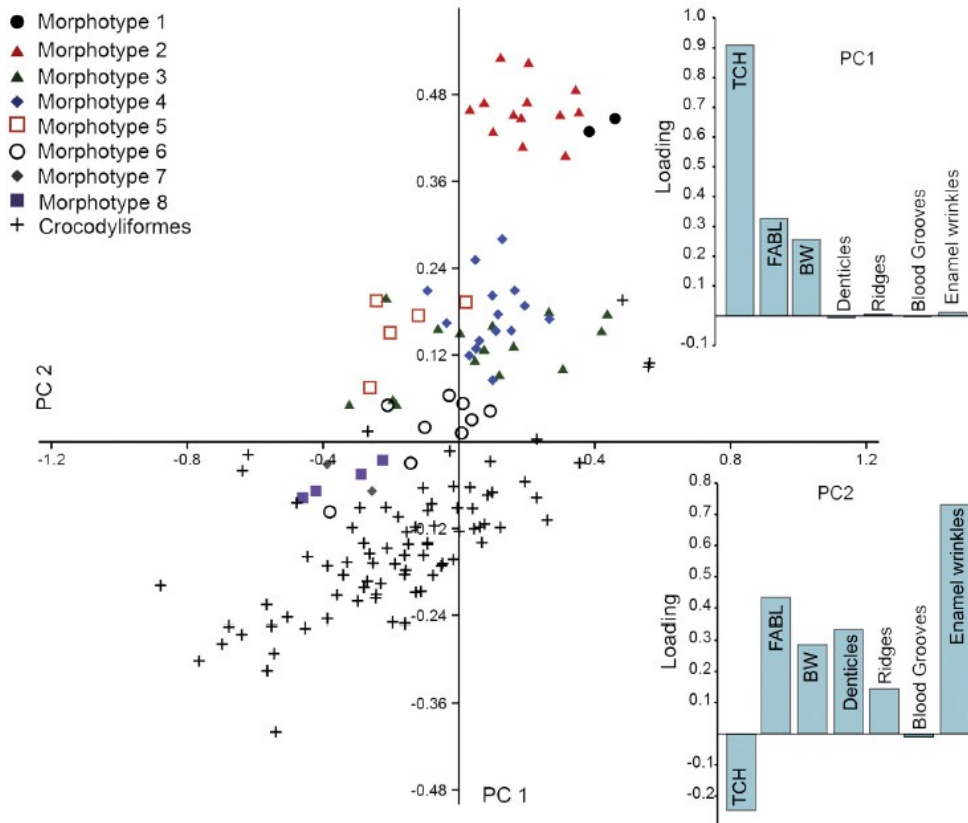


Fig. 6. Principal Component Analysis of the Tunisian samples according to the first two principal components (PC1 and PC2). Column plots show relative loading of variables included in the PCA.

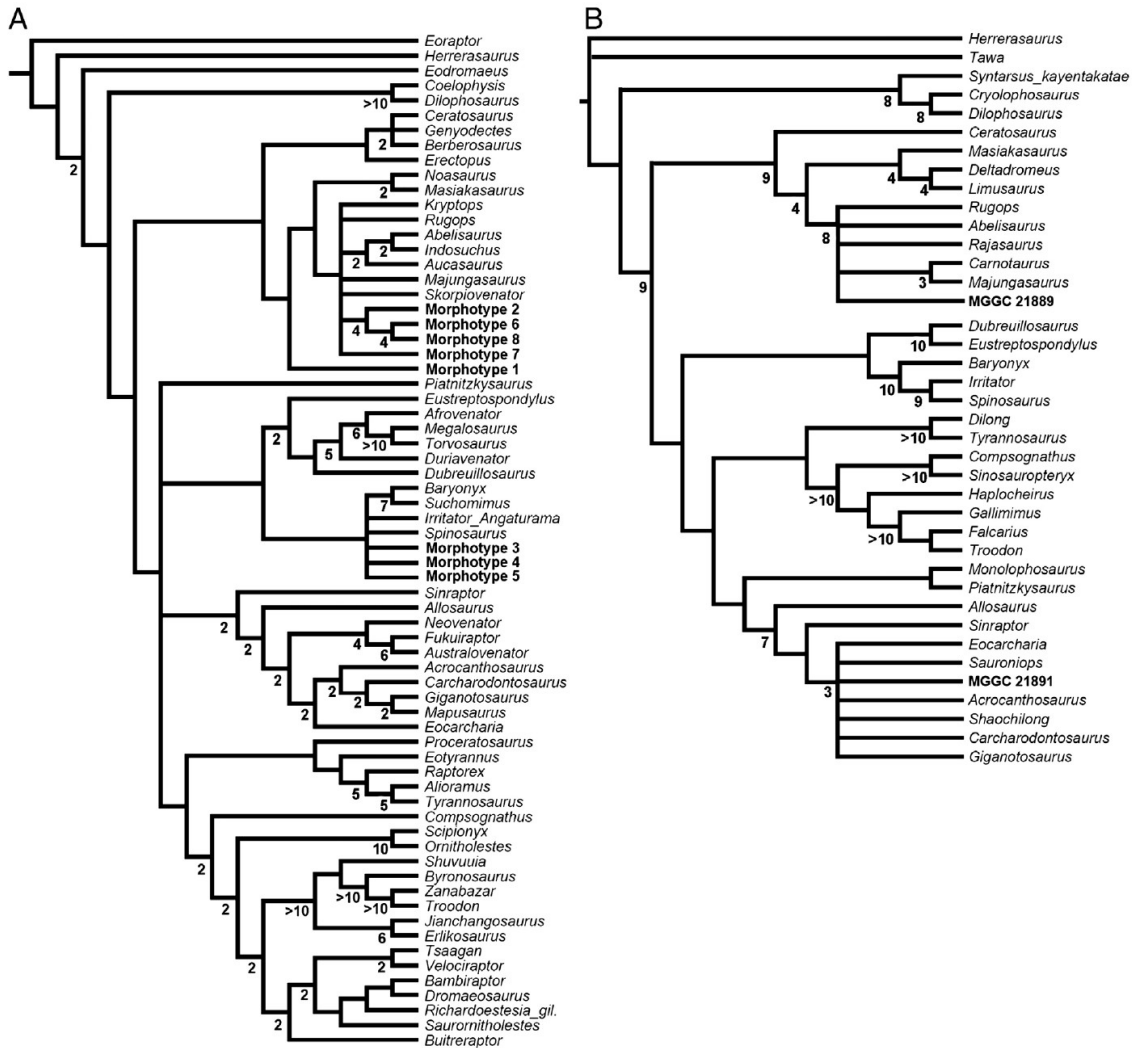


Fig. 7. A, strict consensus topology of the shortest trees found by the analysis of the data set updated from Hendrickx and Mateus (2014). Tunisian morphotypes in bold. B, strict consensus topology of the 82 shortest trees found (length =2463, Consistency Index =0.3886, Retention Index =0.5201) by the analysis of the data set updated from Cau et al. (2013). Tunisian specimens in bold. In both diagrams, numbers adjacent to nodes indicate Decay Index values >1.

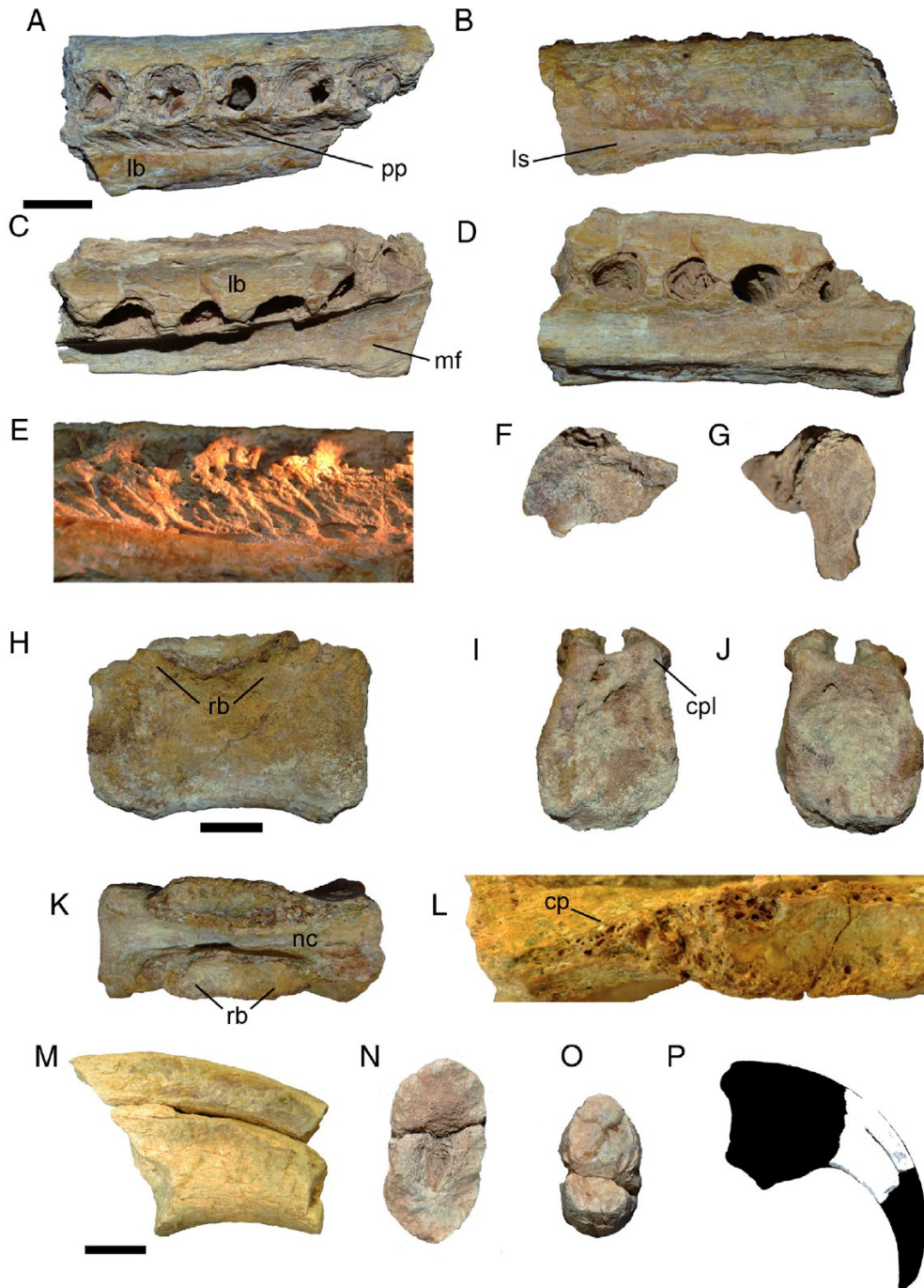


Fig. 8. Isolated theropod remains from the Aptian-Albian of Southern Tunisia. A-G, fragment of abelisaurid left dentary (MGGC 21889) in dorsal (A), lateral (B), medial (C), ventral (D), anterior (F), posterior (H) views. E, detail of the parodontal laminae in medial view, showing gornamentation pattern. H-L, charcharodontosaurid middle caudal vertebra 21891 in right lateral (H), anterior (I), posterior (J), dorsal (K) views. L, detail of neural arch in dorsal views showing camellate pneumatisation. M-P, spinosaurid manual ungual in right lateral (M), proximal (N) and distal (O) views. Reconstruction of the complete ungual, with black parts based on *Suchomimus tenerensis* (Benson et al., 2012, fig. 15). Abbreviations: cp, camellate pneumatisation; cpl, centroprezygapophyseal lamina; lb,

lingual bar; ls, lateral sulcus; mf, Meckelian fossa; nc, neural canal; pp, parodontal plates; rb, rib base.

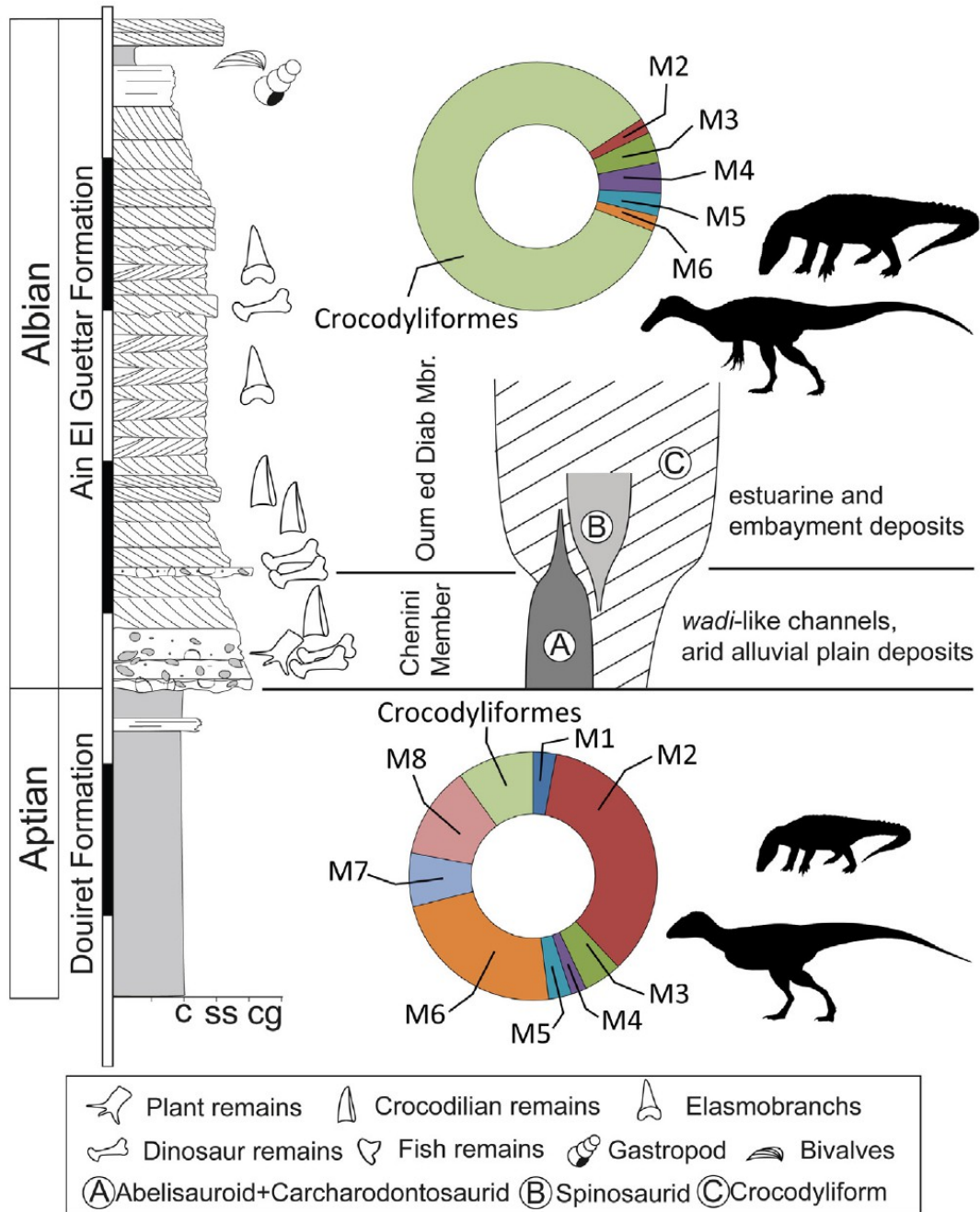


Fig. 9. Simplified and comprehensive stratigraphic log of the Early Cretaceous continental beds exposed in the study area and relative palaeoenvironmental interpretation. The different fossil assemblages found in the Chenini and Oum ed Diab members allows to refer vertebrate remains to a specific chronostratigraphic framework and also support a robust correlation between the stratigraphic occurrence of theropods and crocodyliforms and major variation in the palaeoecological conditions.

**Table 1. Parameters of isolated Saharan theropod and crocodyliformes teeth discussed in the text and comparative taxadental measurements.**

	TCH (mm)	FABL (mm)	BW (mm)
<b>Tunisian Material</b>			
<b>Specimen</b>			
<b>Morphotype 1</b>			
MGGCTUN33	60	27	17
MGGCTUN112	68	27	22
<b>Morphotype 2</b>			
MGGCTUN9	41	22	14
MGGCTUN14	50	31	19
MGGCTUN19	38	25	15
MGGCTUN39	38	27	16
MGGCTUN41	33	24	12
MGGCTUN42	36	26	14
MGGCTUN46	35	32	18
MGGCTUN72	29	31	17
MGGCTUN86	55	27	12
MGGCTUN87	54	32	15
MGGCTUN111	29	24	15
MGGCTUN113	27	24	13
MGGCTUN114	48	26	18
<b>Morphotype 3</b>			
MGGCTUN3	29	16	13
MGGCTUN5	42	18	13
MGGCTUN10	48	19	20
MGGCTUN17	35	15	14
MGGCTUN31	23	11	8
MGGCTUN40	17	10	7
MGGCTUN43	60	17	15
MGGCTUN44	35	18	14
MGGCTUN82	22	10	8
MGGCTUN101	70	22	18
MGGCTUN102	35	15	14
MGGCTUN104	22	9	11
MGGCTUN105	34	15	12
MGGCTUN127	41	15	12
MGGCTUN134	25	16	12
MGGCTUN106	70	26	17
<b>Morphotype 4</b>			
MGGCTUN1	40	20	14
MGGCTUN13	28	14	12

MGGCTUN36	39	16	12
MGGCTUN37	43	14	9
MGGCTUN38	35	14	10
MGGCTUN55	43	17	12
MGGCTUN68	36	15	11
MGGCTUN69	36	15	10
MGGCTUN70	23	16	12
MGGCTUN95	43	15	11
MGGCTUN107	44	18	15
MGGCTUN108	38	17	13
MGGCTUN143	53	19	14
MGGCTUN149	29	20	15
MGGCTUN126	35	17	15
<b>Morphotype 5</b>			
MGGCTUN116	28	18	15
MGGCTUN153	67	22	21
MGGCTUN67	20	9	8
MGGCTUN103	23	14	11
MGGCTUN109	20	12	10
MGGCTUN137	17	14	10
MGGCTUN151	26	17	14
<b>Morphotype 6</b>			
MGGCTUN27	32	20	10
MGGCTUN30	31	19	9
MGGCTUN32	35	19	13
MGGCTUN45	18	16	10
MGGCTUN47	29	19	12
MGGCTUN76	24	14	8
MGGCTUN79	26	18	13
MGGCTUN80	16	9	6
MGGCTUN15	24	15	11
<b>Morphotype 7</b>			
MGGCTUN26	20	11	7
MGGCTUN77	14	11	7
<b>Morphotype 8</b>			
MGGCTUN16	18	13	6
MGGCTUN28	14	11	5
MGGCTUN75	13	10	5
MGGCTUN78	20	14	7
<b>Crocodyliformes</b>			
MGGCTUN2	36	16	12
MGGCTUN4	35	14	12
MGGCTUN6	9	8	5
MGGCTUN7	9	5	4

MGGCTUN8	15	9	7
MGGCTUN11	13	11	5
MGGCTUN12	38	14	11
MGGCTUN18	27	12	10
MGGCTUN20	68	30	25
MGGCTUN21	20	10	5
MGGCTUN22	19	13	10
MGGCTUN23	28	9	9
MGGCTUN24	58	23	19
MGGCTUN25	14	7	5
MGGCTUN29	17	11	6
MGGCTUN34	5	5	5
MGGCTUN35	15	6	6
MGGCTUN48	13	5	5
MGGCTUN49	33	15	13
MGGCTUN50	19	9	10
MGGCTUN51	30	10	10
MGGCTUN52	28	7	9
MGGCTUN53	17	7	8
MGGCTUN54	23	12	10
MGGCTUN56	36	13	14
MGGCTUN57	48	17	17
MGGCTUN59	25	10	9
MGGCTUN60	20	8	9
MGGCTUN61	22	8	8
MGGCTUN62	25	12	15
MGGCTUN63	25	9	10
MGGCTUN65	35	15	16
MGGCTUN66	14	15	15
MGGCTUN71	24	12	9
MGGCTUN73	18	11	8
MGGCTUN74	25	18	15
MGGCTUN81	17	9	7
MGGCTUN83	11	6	6
MGGCTUN84	71	37	34
MGGCTUN85	71	36	34
MGGCTUN88	31	10,5	11
MGGCTUN89	43	18	17
MGGCTUN90	54	16	16
MGGCTUN91	42	22	20
MGGCTUN92	27	13	11
MGGCTUN93	21	10	10
MGGCTUN94	17	7	6
MGGCTUN96	27	11	10

MGGCTUN97	16	10	10
MGGCTUN98	41	14	14
MGGCTUN99	9	7	5
MGGCTUN100	13	6	6
MGGCTUN110	22	9	8
MGGCTUN115	26	8	7
MGGCTUN117	8	4	4
MGGCTUN118	24	11	9
MGGCTUN119	36	17	14
MGGCTUN120	10	5	5
MGGCTUN121	16	4	3
MGGCTUN122	33	12	10
MGGCTUN123	25	14	11
MGGCTUN124	37	15	12
MGGCTUN125	22	9	7
MGGCTUN128	33	18	17
MGGCTUN129	12	6	5
MGGCTUN130	13	5	4
MGGCTUN131	31	11	10
MGGCTUN133	29	10	8
MGGCTUN135	20	9	7
MGGCTUN136	24	12	11
MGGCTUN138	20	10	8
MGGCTUN139	32	13	12
MGGCTUN140	23	10	9
MGGCTUN141	9	5	5
MGGCTUN142	28	18	11
MGGCTUN144	27	13	9
MGGCTUN145	21	12	11
MGGCTUN146	31	17	13
MGGCTUN147	23	15	12
MGGCTUN148	30	15	12
MGGCTUN150	16	11	11
MGGCTUN152	13	5	4

**Specimen hosted at the MNHN in Paris**

***Carcharodontosaurus* sp.**

MRS 1532a	68	31	20
MRS 1532b	50	32	15
MRS 1532c	59	28	18
MRS 1802a	50	23	9
MRS 1802b	75	30	16
MRS 1802c	62	27	13
MRS 1802d	68	29	18

MRS 1802e	43	16	8
MRS1458a	86	36	24
MRS1458b	58	30	17
MRS1458c	75	34	15
MRS1458d	73	32	16
MRS1458e	78	34	18
MRS1458f	64	28	14
MRS1458g	52	23	15
MRS1458i	52	28	14
MRS1234	70	34	16
MRS1235	55	24	16
MRS1237	88	34	16
MRS1236	68	35	17
MRS1238	54	25	17
MRS1239	65	34	16
MRS1521	43	24	13
MRS1438	40	22	11
GADSTELLA	86	33	17
MRS1458h	90	33	18
<b>Abelisauridae indet.</b>			
MRS1266	34	14	7
MRS 348	48	17	13
MRS 1838	36	19	9
MRS783	28	14	6
<b>Small theropod indet.</b>			
GAD587	25	11	4
GAD568	30	11	5
GAD571	25	10	5
GAD557	50	16	7
GAD573	30	13	6
GAD627	32	15	7
GAD575	21	8	4
GAD208	29	13	7
GAD369	27	14	6
GAD601	17	7	3
GAD583	38	15	6
GAD595	22	8	4
GAD610	14	7	4
GAD597	16	8	5
GAD592	26	9	5
GAD602	18	7	3
GAD591	23	9	5
GAD588	25	10	6
GAD559	20	14	8

GAD562	15	10	6
GAD608	15	8	3
GAD574	20	9	4
GAD596	16	10	4
GAD616	10	6	3
GAD565	13	6	4
GAD613	11	4	3
GAD606	14	5	3
GAD614	12	5	3
GAD577	29	7	5
GAD612	13	7	3
GAD620	11	6	3
Loc. Tahroumit a	42	15	10
Loc. Tahroumit b	45	16	9
Loc. Tahroumit c	27	12	6
Loc. Tahroumit d	31	15	7
Loc. Tahroumit e	30	15	7
Loc. Tahroumit f	16	9	6
Loc. Tahroumit g	17	7	4
Loc. Tahroumit h	21	11	6
Loc. Tahroumit i	15	9	5
Loc. Tahroumit l	28	11	7
Loc. Tahroumit m	21	11	6
Loc. Tahroumit n	23	10	5
Loc. Tahroumit o	15	8	5
Loc. Tahroumit p	19	11	6
GAD505	43	10	5
GAD596	43	14	6
DSC9680a	17	6	3
DSC9680b	15	9	4
DSC9680c	20	10	4
DSC9680d	16	9	3
DSC9680e	21	12	5
DSC9680f	16	9	3
DSC9693a	19	11	7
DSC9693b	24	12	7
DSC9693c	28	12	6
DSC9693d	26	15	9
MRS1619	21	12	6
MRS1620	20	10	5
MRS1255	21	12	6
MRS1123	22	12	6
MRS1264	25	12	7

**Baryonichinae indet.**

GAD1966	55	17	12
GAD544	34	12	10
GAD1966 a	47	18	15
GAD1966 b	52	17	17
GAD1966 c	63	19	15
GAD210	25	14	8
GAD570	23	14	7
GAD582	8	5	3
GAD625	43	20	10
GAD520	58	22	15
GAD154	50	19	14
GAD504	63	18	13
GAD507	54	21	16
GAD166	54	18	14
GAD161	68	20	13
GAD518	45	14	10
GAD151	53	22	15
GAD374	65	21	13
<b><i>Spinosaurus</i> sp.</b>			
MRS 1104a	62	17	14
MRS 1104b	43	11	10
MRS 514	63	21	14
MRS 516	69	22	17
MRS 525	67	19	15
MRS 530	36	14	12
MRS 588	34	12	9
MRS 595	28	12	8
MRS 343	60	25	21
MRS 345	66	19	16
MRS 352	48	18	15
MRS 349	52	21	14
MRS 355	60	16	12
MRS 359	38	13	12
MRS ?1593?	36	15	11
MRS 347	37	14	10
MRS 1103	60	21	20
MRS 656	40	18	15
MRS 1593	68	17	12
MRS1240	55	18	15
Denti cassetto 1	36	11	9
Denti cassetto 2	50	14	12
Denti cassetto 3	43	16	11
Denti cassetto 4	49	16	12
Denti cassetto 5	43	16	11

Denti cassetto 6	45	15	10
Denti cassetto 7	21	7	7
Denti cassetto 8	22	12	8
Denti cassetto 9	44	14	11
Denti cassetto 10	38	14	9
Denti cassetto 11	34	14	9
<b>Large theropod indet.</b>			
GRD553 a	62	21	13
GRD553 b	82	32	18
GAD600	58	22	13
<b>Crocodyliformes</b>			
MRS 573	30	9	9
MRS 524	55	25	21
MRS 527	42	15	11
MRS 589	54	14	13
MRS 342	96	35	29
<b>Data from Richter et al., 2013</b>			
<b><i>Spinosaurus?</i></b>			
GZG.V.19990	29,8	13,0	11,5
GZG.V.19991	41,8	15,0	10,6
GZG.V.19992	28,1	12,9	12,0
GZG.V.19993	33,9	13,6	11,0
GZG.V.19994	30,2	11,0	9,6
GZG.V.20000	40,0	14,5	11,9
GZG.V.20001	32,2	14,1	11,0
GZG.V.20003	19,0	7,8	7,0
GZG.V.20007	32,1	13,5	11,1
GZG.V.20010	30,0	12,5	9,5
GZG.V.20011	37,9	13,4	10,1
GZG.V.20015	40,5	15,4	12,0
GZG.V.20017	40,0	15,8	12,0
GZG.V.20018	30,0	11,0	10,0
GZG.V.20019	39,5	17,0	13,5
GZG.V.20020	39,0	13,9	10,5
GZG.V.20022	32,2	11,5	9,0
GZG.V.20024	35,5	13,8	10,8
GZG.V.20026	41,0	12,2	10,0
GZG.V.20028	31,0	10,5	9,1
GZG.V.20029	24,5	11,1	8,0
GZG.V.20030	20,5	11,9	9,2
GZG.V.20032	45,9	15,9	12,8
GZG.V.20033	54,0	22,4	17,0
GZG.V.20034	48,0	17,5	12,1

GZG.V.20035	61,0	21,0	17,3
GZG.V.20036	57,7	21,6	17,3

Comparative taxa dental parameter from Fanti and Therrien 2007

<i>Masiakasaurus knopfleri</i>	7,5	4,5	3,9
<i>Masiakasaurus knopfleri</i>	7,0	5,3	2,3
<i>Masiakasaurus knopfleri</i>	14,3	6,2	3,0
<i>Masiakasaurus knopfleri</i>	5,9	2,8	2,2
<i>Masiakasaurus knopfleri</i>	6,5	3,3	1,9
<i>Masiakasaurus knopfleri</i>	10,4	7,1	3,5
<i>Masiakasaurus knopfleri</i>	11,6	4,6	2,5
<i>Masiakasaurus knopfleri</i>	8,6	4,9	2,4
<i>Masiakasaurus knopfleri</i>	6,8	4,9	2,4
<i>Masiakasaurus knopfleri</i>	8,9	5,5	2,2
<i>Indosuchus raptorius</i>	29,4	19,5	9,1
<i>Indosuchus raptorius</i>	26,9	17,3	13,0
<i>Indosuchus raptorius</i>	27,3	16,6	10,7
<i>Indosuchus raptorius</i>	28,0	13,6	12,9
<i>Indosuchus raptorius</i>	26,0	16,0	10,5
<i>Indosuchus raptorius</i>	31,9	13,0	12,0
<i>Majungasaurus crenatissimus</i>	23,5	11,1	8,4
<i>Majungasaurus crenatissimus</i>	24,9	14,2	8,4
<i>Majungasaurus crenatissimus</i>	22,2	13,1	7,4
<i>Majungasaurus crenatissimus</i>	23,0	14,0	7,7
<i>Majungasaurus crenatissimus</i>	24,0	13,6	8,9
<i>Majungasaurus crenatissimus</i>	23,6	14,6	8,6
<i>Majungasaurus crenatissimus</i>	24,9	14,5	8,4
<i>Majungasaurus crenatissimus</i>	23,7	12,7	8,6
<i>Majungasaurus crenatissimus</i>	30,3	12,7	8,3
<i>Majungasaurus crenatissimus</i>	21,1	13,4	22,5
<i>Majungasaurus crenatissimus</i>	14,0	11,6	6,7
<i>Majungasaurus crenatissimus</i>	28,9	16,0	12,4
<i>Majungasaurus crenatissimus</i>	34,0	18,0	10,5
<i>Majungasaurus crenatissimus</i>	15,3	14,2	7,2
<i>Majungasaurus crenatissimus</i>	35,4	19,7	10,0
<i>Majungasaurus crenatissimus</i>	24,4	16,1	8,7
<i>Majungasaurus crenatissimus</i>	24,4	16,8	7,3
<i>Majungasaurus crenatissimus</i>	16,5	13,6	5,0
<i>Majungasaurus crenatissimus</i>	20,8	12,8	6,5
<i>Majungasaurus crenatissimus</i>	22,1	14,0	7,6
<i>Majungasaurus crenatissimus</i>	26,2	16,1	8,5
<i>Majungasaurus crenatissimus</i>	27,7	16,0	8,7
<i>Majungasaurus crenatissimus</i>	16,4	12,9	6,9

<i>Majungasaurus crenatissimus</i>	33,6	19,9	8,4
<i>Majungasaurus crenatissimus</i>	37,7	18,3	14,5
<i>Majungasaurus crenatissimus</i>	18,2	14,9	6,7
<i>Majungasaurus crenatissimus</i>	22,6	16,8	6,2
<i>Morphotype 3 - Majungasaurus</i>	20,9	12,0	5,8
<i>Morphotype 3 - Majungasaurus</i>	26,9	12,4	5,8
<i>Morphotype 3 - Majungasaurus</i>	21,9	11,9	6,2
<i>Morphotype 3 - Majungasaurus</i>	19,7	10,8	4,9
<i>Morphotype 3 - Majungasaurus</i>	15,4	10,0	4,8
<i>Morphotype 3 - Majungasaurus</i>	16,7	8,8	5,1
<i>Morphotype 3 - Majungasaurus</i>	24,5	12,6	6,8
<i>Morphotype 3 - Majungasaurus</i>	19,5	12,5	6,4
<i>Morphotype 3 - Majungasaurus</i>	21,8	12,9	7,4
<i>Morphotype 3 - Majungasaurus</i>	17,4	13,8	6,4
<i>Morphotype 3 - Majungasaurus</i>	15,4	11,2	5,7
<i>Morphotype 3 - Majungasaurus</i>	16,7	10,8	5,0
<i>Morphotype 3 - Majungasaurus</i>	18,6	8,5	5,4
<i>Morphotype 3 - Majungasaurus</i>	18,7	12,7	6,1
<i>Morphotype 3 - Majungasaurus</i>	18,6	11,7	6,1
<i>Morphotype 3 - Majungasaurus</i>	18,5	10,3	7,2
<i>Morphotype 3 - Majungasaurus</i>	21,6	13,9	6,1
<i>Morphotype 3 - Majungasaurus</i>	20,9	13,3	5,5
<i>Morphotype 3 - Majungasaurus</i>	24,0	16,1	7,3
<i>Morphotype 3 - Majungasaurus</i>	17,0	10,4	4,9
<i>Morphotype 3 - Majungasaurus</i>	17,7	10,0	5,1
<i>Morphotype 3 - Majungasaurus</i>	26,7	12,3	6,7
<i>Morphotype 3 - Majungasaurus</i>	23,3	12,3	7,0
<i>Morphotype 3 - Majungasaurus</i>	19,1	11,4	5,3
<i>Morphotype 3 - Majungasaurus</i>	24,3	11,4	5,3
<i>Morphotype 3 - Majungasaurus</i>	29,1	14,6	7,6
<i>Morphotype 3 - Majungasaurus</i>	17,3	11,0	5,0
<i>Morphotype 3 - Majungasaurus</i>	16,4	13,2	6,5
<i>Morphotype 3 - Majungasaurus</i>	27,1	15,1	7,5
<i>Morphotype 3 - Majungasaurus</i>	29,6	16,6	8,3
<i>Morphotype 3 - Majungasaurus</i>	21,8	12,6	6,6
<i>Morphotype 3 - Majungasaurus</i>	25,4	12,5	6,3
<i>Morphotype 3 - Majungasaurus</i>	23,8	13,6	6,2
<i>Morphotype 3 - Majungasaurus</i>	36,5	16,7	7,5
<i>Morphotype 3 - Majungasaurus</i>	28,6	14,1	6,9
<i>Morphotype 3 - Majungasaurus</i>	21,0	13,0	6,7
<i>Morphotype 3 - Majungasaurus</i>	19,9	11,4	5,6
<i>Morphotype 3 - Majungasaurus</i>	19,1	9,6	4,4
<i>Morphotype 3 - Majungasaurus</i>	17,0	10,1	5,1
<i>Morphotype 3 - Majungasaurus</i>	24,3	10,3	5,4

<i>Morphotype 1 - Dromeosaurid?</i>	14,0	8,9	3,9
<i>Morphotype 1 - Dromeosaurid?</i>	15,5	8,5	3,6
<i>Morphotype 1 - Dromeosaurid?</i>	14,3	7,6	3,2
<i>Morphotype 1 - Dromeosaurid?</i>	10,6	5,8	3,0
<i>Morphotype 1 - Dromeosaurid?</i>	14,8	7,8	4,1
<i>Morphotype 1 - Dromeosaurid?</i>	12,0	7,6	3,6
<i>Morphotype 1 - Dromeosaurid?</i>	10,2	6,5	3,1
<i>Morphotype 1 - Dromeosaurid?</i>	11,8	8,8	3,9
<i>Morphotype 1 - Dromeosaurid?</i>	8,1	5,5	2,8
<i>Morphotype 1 - Dromeosaurid?</i>	13,4	8,8	4,2
<i>Morphotype 1 - Dromeosaurid?</i>	10,3	7,4	3,3
<i>Morphotype 1 - Dromeosaurid?</i>	9,3	6,8	3,8
<i>Morphotype 1 - Dromeosaurid?</i>	14,9	9,3	4,6
<i>Morphotype 1 - Dromeosaurid?</i>	11,3	8,3	3,9
<i>Sauromitholestes langstoni</i>	8,5	5,0	2,1
<i>Sauromitholestes langstoni</i>	7,9	4,8	2,3
<i>Sauromitholestes langstoni</i>	8,9	5,2	2,2
<i>Sauromitholestes langstoni</i>	8,1	2,3	1,5
<i>Sauromitholestes langstoni</i>	9,9	4,6	2,2
<i>Sauromitholestes langstoni</i>	14,2	8,1	3,2
<i>Sauromitholestes langstoni</i>	10,5	4,9	2,3
<i>Sauromitholestes langstoni</i>	7,9	3,9	1,9
<i>Sauromitholestes langstoni</i>	9,1	4,1	1,9
<i>Sauromitholestes langstoni</i>	10,2	4,4	2,1
<i>Sauromitholestes langstoni</i>	10,6	4,9	2,3
<i>Dromaeosaurus albertensis</i>	15,0	7,8	4,4
<i>Dromaeosaurus albertensis</i>	10,4	4,0	2,7
<i>Dromaeosaurus albertensis</i>	15,0	7,3	4,2
<i>Dromaeosaurus albertensis</i>	12,7	5,2	3,3
<i>Dromaeosaurus albertensis</i>	13,9	7,8	4,2
<i>Dromaeosaurus albertensis</i>	23,6	8,9	5,0
<i>Dromaeosaurus albertensis</i>	8,1	5,3	2,6
<i>Dromaeosaurus albertensis</i>	10,9	5,9	3,2
<i>Dromaeosaurus albertensis</i>	9,8	5,9	3,1
<i>Deinonychus antirrhopus</i>	18,5	7,8	2,8
<i>Deinonychus antirrhopus</i>	12,6	8,8	3,0
<i>Deinonychus antirrhopus</i>	9,7	7,0	2,8
<i>Deinonychus antirrhopus</i>	12,4	9,8	2,0
<i>Deinonychus antirrhopus</i>	10,9	7,3	3,0
<i>Deinonychus antirrhopus</i>	13,8	10,4	3,0
<i>Deinonychus antirrhopus</i>	12,0	7,0	3,0
<i>Deinonychus antirrhopus</i>	10,4	7,9	3,0
<i>Deinonychus antirrhopus</i>	10,6	7,0	3,2
<i>Deinonychus antirrhopus</i>	16,8	10,8	3,6

<i>Deinonychus antirrhopus</i>	14,6	9,5	4,0
<i>Deinonychus antirrhopus</i>	15,8	9,6	3,0
<i>Deinonychus antirrhopus</i>	13,0	7,8	4,0
<i>Deinonychus antirrhopus</i>	9,0	6,2	1,9
<i>Deinonychus antirrhopus</i>	12,5	7,8	3,3
<i>Deinonychus antirrhopus</i>	12,6	8,7	2,7
<i>Deinonychus antirrhopus</i>	10,8	8,7	2,7
<i>Deinonychus antirrhopus</i>	10,8	6,9	2,0
<i>Deinonychus antirrhopus</i>	12,6	8,1	3,0
<i>Deinonychus antirrhopus</i>	13,8	8,6	3,7
<i>Deinonychus antirrhopus</i>	10,7	5,7	4,0
<i>Deinonychus antirrhopus</i>	12,1	5,5	4,0
<i>Deinonychus antirrhopus</i>	12,4	8,7	2,2
<i>Deinonychus antirrhopus</i>	12,9	6,3	2,2
<i>Deinonychus antirrhopus</i>	12,4	8,7	2,9
<i>Deinonychus antirrhopus</i>	13,0	6,0	2,2
<i>Deinonychus antirrhopus</i>	11,0	6,0	2,0
<i>Deinonychus antirrhopus</i>	11,6	7,0	3,0

Page left blank

## **CHAPTER 2 - Why so many dipnoans? A multidisciplinary approach on the Lower Cretaceous lungfish record from Tunisia.**

Submitted: 15<sup>th</sup> December 2015. Published: 18<sup>th</sup> February 2016 in *Palaeogeography, Palaeoclimatology, Palaeoecology* vol. 449:255-265.

Federico Fanti, Gabriele Larocca Conte, Luana Angelicola, Andrea Cau

### **Abstract**

The Lower Cretaceous record of vertebrates from Africa is problematic as the majority of fossil localities lack adequate stratigraphic and paleoecological data when compared with coeval Laurasian deposits. Thereby, our comprehension of paleocommunities and paleobiogeographic patterns may be affected by the lack of multidisciplinary approach. Among taxonomically and paleoecological significant clades, lungfishes (Sarcopterygii, Dipnoi) are commonly found in the Cretaceous fresh water, brackish and marginal-marine deposits of Gondwana, although identifiable elements are limited to isolated tooth plates. We provide the first taxonomic identification of dipnoans from the Ain el Guettar Formation of southern Tunisia (Oum ed Diab Member, Albian). Identification of tooth plates based on morphological parameters and phylogenetic analyses indicate the co-occurrence in a discrete stratigraphic unit of at least five lineages referable to *Equinoxiodus*, *Neoceratodus*, *Asiatoceratodus* and/or *Ferganoceratodus*, *Ceratodus*, and *Lavocatodus*. This unusually high diversity is unparalleled in the fossil record and is also challenged by an actualistic comparison with extant taxa. We suggest that a series of taphonomic factors significantly inflated observed lungfish diversity in the

estuarine and marginal-marine deposits of the Oum ed Diab Member. Therefore, we recognize the fossil fauna as representative of a larger, inland paleo-hydrographic system. This study confirms the paleoecological scenario resulted from the analyses on terrestrial reptiles from the Oum ed Diab Member.

## 1. Introduction

Despite the extensive record of lungfish taxa throughout the Paleozoic, Mesozoic and Cenozoic, the record of Cretaceous Gondwanan dipnoans is both stratigraphically and geographically incomplete being primarily represented by isolated tooth plates, rarely associated to more complete remains (Agnolin, 2010; Soto and Perea, 2010; Clack et al., 2011; Claeson et al., 2014). Recent studies based on a widely accepted set of diagnostic morphologic parameters have constrained known taxa to five lineages, corresponding to Linnean-rank families (i.e. Asiatoceratodontidae, Ceratodontidae, Lepidosirenidae, Neoceratodontidae, and Ptychoceratodontidae), the paleogeographic distribution of which is largely discussed (Agnolin, 2010; Soto and Perea, 2010, and references therein). Conversely, only a few studies have discussed the taphonomic and paleoecologic implication of the co-occurrence in discrete units, or even in single fossil localities, of multiple dipnoan taxa, primarily limiting the discussion to extant species.

In this study, we describe surface-collected dipnoan tooth plates from the Lower Cretaceous deposits of the Tataouine basin of southern Tunisia (Fig. 1).

The Tunisian material offers the opportunity to evaluate a diverse non-tetrapod sarcopterygian community including both coelacanthid and dipnoans, the latter

represented by several genera and species. Based on comparison with both the fossil record and present day ecology of lungfish species, such high diversity is unexpected within a single formation. The aim of this study is twofold: first, provide taxonomic information on the “mid-Cretaceous” dipnoans of southern Tunisia, and second, discuss this unique assemblage as a proxy for taphonomic and paleoecological implications. The combination of new parameters for the description of dipnoan tooth plates, high-resolution stratigraphic and sedimentological information, and phylogenetic analyses, provide new tools to interpret unusual assemblages in several Saharan and other Gondwanan localities.

## **2. Material and methods**

Dipnoan tooth plates discussed here (n=42) were surface collected from the Albian Oum ed Diab Member of the Ain el Guettar Formation beds exposed in the Tataouine region of southern Tunisia. Isolated plates are representative of four localities covering more than 80 km of the sedimentary basin: from North to South, El Hmima, El Mra, Oum ed Dhiab, and El Kambout (Figs. 1 and 2).

To properly identify isolated tooth plates, Tunisian specimens were first compared to other Gondwanan taxa described in the literature, and specifically from South America (Castro et al., 2004; Soto and Perea, 2010; Sousa et al. 2015), continental Africa (Martin, 1984a; Churcher and De Iuliis, 2001), Asia (Nessov and Kaznyshkin, 1985), Australia (Kemp, 1997b), and Europe (Skrzycki, 2015) (Supplementary Material). The description of isolated dipnoan tooth plates resulted over the years in a variety of parameters considered as phylogenetically informative, although the majority of authors focused on the following

parameters: 1. morphology and ratios comparison of margin length; 2. number, morphology and arrangement of crests; 3. broadness and position (anterior or mesial) of the mesiointernal angle; 4. presence of occlusal pits; 5. presence of ornamentation of the enamel. Agnolin (2010) remarked the inadequacy of several standard parameters in phylogenetic analyses (i.e. ornamentation and the presence of tubercles on the occlusal surface, the morphology of the intracrestal clefts, labial cusps, posterior heel at the end of the tooth plate, and the biometric parameters based on angles between crest) as they most likely reflect ontogenetic and individual variations.

We formally re-defined most of the characters used by previous authors (Supplementary Material) and analyzed the distribution of these features among our sample using a phylogenetic approach, clustering the individual specimens according to shared derived features resulted by a phyletic framework minimizing the number of evolutionary events necessary to describe the observed variability. Morphometric and morphologic parameters of Tunisian specimens were consequently compared with plate parameters available in the literature for specimens of *Equinoxiodus schultzei* (Sousa et al., 2015), *Ceratodus humei* (Churcher and De Iuliis, 2001), *Asiatoceratodus* cf. *tiguidiensis* (Castro et al., 2004), *Arganodus tiguidiensis*, *Neoceratodus africanus* (Martin, 1984a), *Ferganoceratodus jurassicus* (Nessov and Kaznyshkin, 1985), and *Ceratodus africanus* (Soto and Perea, 2010). The data set includes 45 morphological characters, scored for 53 operational taxonomic units (OTUs). Among the OTUs, the Australian ceratodontid *Metaceratodus wollastoni* (Kemp, 1997b) was used as outgroup, following the phylogenetic framework of Schultze (2004). The ingroup includes 35 OTUs based on Tunisian specimens collected by us, and nine additional dipnoan OTUs based on specimens referred to, respectively, *Asiatoceratodus tiguidiensis* (two OTUs), *Ceratodus*

*africanus* (one OTU), *Equinoxiodus schultzei* (two OTUs), *Ferganoceratodus jurassicus* (one OTU), *Lavocatodus humei* (two OTUs), *Neoceratodus africanus* (two OTUs), and *Ptychoceratodus roemeri* (one OTU). The data set was analyzed using TNT (Goloboff et al., 2008). We performed 100 Heuristic Search replicates, saving all shortest trees found. To reduce computation time, no more than 50000 trees were saved. Exploration of results setting a larger number of saved trees did not produce significant differences from the analysis with tree space set to 50000.

In this study, we primarily follow the terminology of Churcher and De Iuliis (2001). We also consider ‘inner angle’ as synonymous for the mesiointernal angle (Fig. 3). Finally, in our positional identification, the distinction between upper and lower dental plates follows Martin (1984a), as inferior tooth plates commonly display a slightly concave lingual margin near the inner angle and a convex one toward distal edge.

Measurements were made with digital calipers with a precision to the nearest mm. Specimens are currently deposited at the Museo Geologico Giovanni Capellini (Bologna, Italy) under accession number 21912- 21931, whereas specimens ONM NG EMD 1-22 are housed at the Musée de l’Office National des Mines in Tunis.

## 2.1 Institutional abbreviations

**CPHNAMA**, Centro de Pesquisa de História Natural e Arqueologia do Maranhão, Praia Grande, São Luís, Brazil; **MGGC**, Museo Geologico Giovanni Capellini, Bologna, Italy; **MGCT**, Museo de Geociencias, Tacuarembó, Uruguay; **MNHNP HGS**, Museum National d’Histoire Naturelle, Paris, Sud du Hoggar; **MNHNP HGN**, Museum National

d'Histoire Naturelle, Paris, Nord du Hoggar; **ONM**, Office National des Mines, Tunis; **QM**, Queensland Museum, Brisbane, Australia; **ROM**, Royal Ontario Museum, Toronto, Canada; **UFMA**, Coleção Paleontológica da Universidade Federal do Maranhão, Bacanga, São Luís, Brazil; **ZPAL**, Institute of Paleobiology, Polish Academy of Sciences, Warsaw, Poland.

### 3. Geological and paleoenvironmental setting

The late Aptian–Albian Aïn El Guettar Formation crops out extensively along a 120 km long section of the prominent cliff separating the Dahar Plateau from the Jeffara Plain in the Tataouine region of southern Tunisia (Bouaziz et al., 1988, 1999; Ben Ismaïl, 1991; Benton et al., 2000; Barale and Ouaja, 2002; Bodin et al., 2010; Fanti et al., 2012, 2015). In ascending order, the Aïn El Guettar Formation consists of the Chenini, Oum ed Diab and Rhadouane members representative of fluvial, coastal and shallow-marine deposits respectively (Fig. 2) (Fanti et al., 2012). Specimens described in this study were collected from the sandy deposits of the Oum ed Diab Member (Fanti et al., 2014, 2015, 2016). The lower beds of this unit are interpreted as fluvial sand bars that deposited in a vast estuarine system, whereas the overlying deposits gradually shift to shoreface, tidal flat, and foreshore deposits. The occurrence of frequent *in situ* tubules, rhizcretions and hematitic hard grounds interbedded in the sandy deposits support arid to xeric environments. Recent paleontological and stratigraphic studies on this Member in the Tataouine region revealed a rich and diverse vertebrate fauna representative of both fluvial and coastal environments (Fanti et al., 2014, 2015). With rare exceptions, all vertebrate remains are found as disarticulated elements, although their preservation is good. Based

on the stratigraphic occurrence of dipnoan tooth plates in the lower deposits of the Oum ed Diab Member, the age of discussed taxa is considered as Albian (Fig. 2). The base of the Oum ed Diab Member is marked by a conglomeratic, fossil-rich transgressive lag: vertebrate remains from this marker bed may therefore be representative of both Chenini and Oum ed Diab deposits. Specimens from the El Mra locality represent the stratigraphically lowermost occurrence of isolated dipnoan plates discussed in this study: however, they were collected approximately 1.5 meters above the basal conglomerate of the Oum ed Diab and in lower energy, finer deposits. Therefore, we consider that the discussed association is not a result of reworking factors.

#### **4. Taxonomic history of problematic taxa**

##### *4.1 Asiatoceratodus and Arganodus*

*Asiatoceratodus* and *Arganodus* are considered as synonymous by Kemp (1998), Castro et al., (2004) and Agnolin, 2010, whereas Cavin et al., (2007), Soto and Perea (2010) do not fully recognize the synonymy. Based also on descriptions and discussion provided by Tabaste (1963), Vorobiyeva (1967), Martin (1982, 1984a), as well as on the light of direct observations on the Tunisian material, in this study we consider the two genera as synonymous.

##### *4.2 Neoceratodus and Ceratodus*

*Ceratodus africanus* was erected by Haug in 1905 to describe tooth plates from the Cretaceous of Niger and consequently transferred to the genus *Neoceratodus* by Martin

(1982, 1984a). Several authors challenged this interpretation, as neoceratodontid are restricted to the Cretaceous and Cenozoic deposits of Australia, as well as to the present day *Neoceratodus forsteri* (Cavin et al., 2007; Soto and Perea, 2010). Agnolin (2010) suggested a Late Cretaceous distribution limited to Gondwana for both Ceratodontidae and Neoceratodontidae although with biases related to the fossil record of Argentina. In this study, *Ceratodus* and *Neoceratodus* are considered as two valid and distinct taxa (see below).

#### 4.3 *Ceratodus humei* and *Lavocatodus humei*

Martin (1982) referred several tooth plates to *Ceratodus humei* but in his later publications (1984a, b) he transferred the genus to *Protopterus*. Churcher and De Iuliis (2001) have challenged this hypothesis recognizing both genera as valid. Cleason et al. (2014) referred *C. humei* to *Lavocatodus humei* based on newly collected Egyptian specimens and on a revision of plates described by Martin (1995) and Churcher and De Iuliis (2001). In this study, we agree with the taxonomic interpretation of Cleason et al. (2014) considering *Lavocatodus humei* as a valid taxon.

## 5. Results

### 5.1 Systematic paleontology

Dipnoi Müller, 1844

Ceratodontiformes Berg, 1940

Lepidosirenidae Bonaparte, 1841

*Lavocatodus* Martin, 1995

*L. humei* Priem, 1914

**Referred material:** MGGC 21920; MGGC 21922 (Fig. 4)

**Locality:** El Hmaima; Oum Dhiab.

**Description:** these plates are sub-triangular, bearing five denticulations, with a distinct step between the buccal and occlusal margins. MGGC 21920, a left lower tooth plate, shows a series of crests on both buccal and occlusal sides that are strongly rounded and flat. The last denticulation is flatter than the other is, and joined to the distal edge. The occlusal surface is smooth and undulating. The last feature may be due to wearing during life and thus expresses some ontogenetic-biased variation in the sample. The inner angle is strongly obtuse (about 145°). A few thick ridges are visible occlusally. They do not converge to the mesiointernal angle. The first ridge does not correspond to the mesiobuccal margin, such as in other species (e.g., *Neoceratodus africanus*, Martin, 1984a), but bisects the first denticulation (Tabaste, 1964; Martin, 1984a; Churcher and De Iuliis, 2001). The sulci are “U”-shaped, wide and shallow, decreasing in size distally. The distal sulcus is more “V”-shaped (Churcher and De Iuliis, 2001). The occlusal surface display a ‘dotted’ surface formed by several pits. MGGC 21920 is a left lower tooth plate. In ventral view, it retains part of the pre-articular, showing a “V”-shaped groove. This is the first specimen referred to *L. humei* that preserves that bony support, in agreement with

Cleason et al. (2014) that reported a prearticular fragment referred to *L. protopteroides* with a preserved symphyseal facet. An anterior process shows a linear symphysis along which the two hemimandibles joined together.

MGGC 21922 is a fragmentary left upper tooth plate but shows more acute crests than the other specimens show. Observed difference between lower and upper tooth plates concurs with the description by Churcher and De Iuliis (2001).

**Stratigraphic Distribution:** plates referred to *Lavocatodus humei* are reported from the Upper Cretaceous Quseir Formation of Egypt, which includes nearshore to fluvial deposits (Cleason et al., 2014). The Quseir Formation yielded three species of *Lavocatodus*, *L. humei*, *L. protopteroides* and *L. giganteus*, as well as *Protopterus nigeriensis* (Cleason et al., 2014). Cleason et al. (2014) also assigned *Ceratodus humei* to *Lavocatodus humei*: therefore, the distribution of this species should be extended to the Alcântara Formation of Brazil (Medeiros and Schultz 2001, 2002; Castro et al., 2004; Toledo and Bertini, 2005) where this taxon is recovered in association with *Ceratodus africanus* and *Asiatoceratodus tiguidiensis* (Toledo et al., 2011).

?Neoceratodontidae Miles, 1977

*Equinoxiodus* Toledo et al., 2011

*Equinoxiodus* sp.

**Referred material:** MGGC 21913; ONM NG EMD 13 (Fig. 5)

**Locality:** Oum Dhiab; El Mra.

**Description:** MGGC 21913 (right lower tooth plate) and ONM NG EMD 14 are partially preserved, being broken, respectively, near the third and the fourth crests. We infer that originally both had a trapezoidal shape; unfortunately, the total number of crests remains unknown. In both specimens, the mesial margin is rounded. The mesiointernal angle is obtuse and opposes to the second crest. The ridges are not particularly thick and do not converge to the mesiointernal angle. The sulci are “V”-shaped, with a rounded cleft. The occlusal surface shows a network of anastomosed pulp canals, which cross the whole plate lingually–buccally. The punctuations are parallel to the pulpar canals and extend along the entire surface. Both specimens are interpreted as lower tooth plates, as they show a well preserved prearticular with one “V”-shaped groove. In basal view, the latter feature starts approximately between the first and the second crests. According to Sousa et al. (2015) they may belong to juvenile individuals since the mesiobuccal margin gradually merges to the interdental margin. Our referral of three Tunisian specimens to *Equinoxiodus* is based on the shared presence of an overall flattened shape of the tooth, and undulated occlusal surface (Toledo et al., 2011; Sousa et al., 2015).

**Distribution:** The genus *Equinoxiodus* is represented by two species (*E. alcantarensis* and *E. schultzei*) in the Cenomanian Alcântara Formation of Brasil; specimens were collected in deposits interpreted as tide-dominated estuarine environments within an incised valley setting (Toledo et al., 2011; Sousa et al., 2015). This genus also includes specimens described by Schultze (1991) from the Paleocene Santa Lucia Formation of Bolivia

(Toledo et al., 2011; Sousa et al., 2015) thus its temporal range extends from the lower Cenomanian to Paleocene.

*Asiatoceratodontidae* Vorobiyeva, 1967

*Asiatoceratodus* Vorobiyeva, 1967

*A. cf. tiguidiensis* Tabaste, 1963

**Referred material:** MGGC 21915-19, 21923; ONM NG EMD 1, 3-9, 11, 12, 16, 17, 19, 20, 22 (Fig. 6).

**Locality:** Oum Dhiab, El Hmaima and El Mra. El Kambout

**Description:** This genus can be distinguished from all other dipnoan tooth plates by very short crests in proportion and distinctive acute anterior crests (Vorobiyeva, 1967; Agnolin, 2010; Alves et al, 2013). Tunisian teeth are small to medium in size. The elements are triangular in shape, bearing six to eight acute crests and showing the mesial angle close to 90° or slightly obtuse. Only MGGC 21916 shows the inner angle that is strongly obtuse (122°). The apical termination of the ridges is rather keeled in lateral view (Churcher and De Iuliis, 2001; Soto and Perea, 2010). The furrows are deep and narrow, and the sulci are “V”-shaped. The ridges are straight and narrow, directed progressively to the distal edge. The occlusal surface is ornamented by coarse punctuations, arranged without a definite pattern. MGGC 21917 is interpreted as a lower right tooth plate of a probable juvenile

individual. This is the only specimen among the Tunisian material referred to this species preserving the pre-articular bearing two dips.

**Distribution:** *Asiatoceratodus* is reported from the Cenomanian coastal beds of the Alcântara Formation of Brazil in association with a continental faunal assemblage that includes bony fish, crocodylians and dinosaurs (Pedrão et al. 1993; Rosseti et al., 1997; Rosseti, 2001; Castro et al., 2004; Dutra et al., 2001; Sousa, de, 2006). In South America, this genus is also known from the Cenomanian-Turonian Adamantina Formation of Brazil (Alves et al., 2013), and from the fluvio-lacustrine beds of the Kimmeridgian-Tithonian Tacuarembò Formation in Uruguay (Soto and Perea, 2008; Perea et al., 2009). *Asiatoceratodus* is reported from the Tithonian Mughher Mudstone Formation of Ethiopia (Goodwin et al., 1999). Martin (1984a) described *Arganodus (Asiatoceratodus) tiguidiensis* from Niger extending its stratigraphic range from the Upper Jurassic to the Cenomanian. Finally, Martin et al., (1981a) reported *Arganodus (Asiatoceratodus) atlantis* from the Late Triassic of Morocco.

Neoceratodontidae Miles, 1977

*Neoceratodus* De Castelnau, 1876

*N. africanus* Haug, 1905

**Referred material:** MGGC 21921, 21925; ONM NG EMD 10 (Fig. 7).

**Locality:** Oum Dhiab; El Mra

**Description:** Both MGGC 21925, MGGC 21921 are incomplete tooth plates, whereas ONM NG EMD 10 is well preserved. The latter shows a trapezoidal shape bearing six acute crests. The mesial margin shows a distinct mesial angle that marks the boundary between the mesiobuccal and interdental margins. The mesiointernal angle is obtuse: in MGGC 21921, it measures  $108^\circ$  whereas in ONM NG EMD 10 it is approximately  $125^\circ$ . In MGGC 21925, only the second, third and fourth crests are preserved, and thus it is impossible to estimate the gradation of the mesiointernal angle along the crests. The ridges are straight and thick, but do not converge to the mesiointernal angle. In MGGC 21921, the apex of the second and third crests is slightly bent. In all specimens, the furrows are “U”-shaped, relatively deep and large. The occlusal surface displays small circular pits.

**Distribution:** the genus *Neoceratodus* is relatively common in the Cretaceous fossil record of the Saharan regions, with isolated tooth plates reported from a variety of localities in Niger, Tunisia, Morocco, Algeria, Egypt and Libya (Peyer, 1925; Arambourg and Soleaud, 1943; Tabaste, 1963; Taquet, 1976; Wenz, 1980; Martin, 1981a, 1984a; Bouaziz et al., 1988; Murray, 2000; Churcher and De Iuliis, 2001; López-Arbarelo, 2004; Churcher et al., 2006; Soto and Perea, 2010). However, Plates from the Early Cretaceous of Ethiopia (Werner, 1995; Schmidt et al., 1998; Soto and Perea, 2010) were later assigned to *Asiatoceratodus tiguidiensis* and the age of fossiliferous bed pre-dated to the Tithonian (Goodwin et al 1999; Soto and Perea, 2010).

Ceratodontidae Gill, 1872

*Ceratodus* Agassiz, 1838

*C. sp.*

**Referred material:** MGGC 21912, 21914, 21924; ONM NG EMD 14, 18 (Fig. 8).

**Locality:** El Mira

**Description:** specimens are triangular in overall shape, bearing six ridges with acute crests and stepped bucco-lingual margin. The ridges converge to the inner angle; the second, third and fourth ridges being paralleling each other, and the last one slightly diverging distally from the others. The mesial margin is curved and the inner angle is obtuse: it is about 130°-132° in MGGC 21912, and 120° in MGGC 21914. Furrows are rounded: they decrease both in width and in depth distally. In MGGC 21930, the thickness of the enamel is visible in buccal view between the crests. The latter specimen is recognized as a lower right tooth plate due to the presence of a well-preserved pre-articular bone bearing a “V”-shaped groove. In mesial view, there is no evidence of the anterior process as the edge of the bone is rounded and houses a circular facet. The latter is interpreted as the symphyseal facet for the contralateral element. The upper tooth plates show a triangular isosceles shape. In ONM NG EMD 18, part of the pterigo-palatine bone is preserved, with one distinct process between the third and fourth crests visible in basal view.

**Distribution:** *C. africanus* is the most common dipnoan species from the ‘*Contiental Intercalaire*’ deposits of northern Africa, but it also occur in the middle Cretaceous deposits of

Brazil (Soto and Perea, 2010, and references therein). Soto and Perea (2010) also reported *Ceratodus africanus* from the continental deposits of the Tacuarembò Formation of Uruguay (Batovì Member, Kimmeridgian-Lower Cretaceous), in co-occurrence with *Asiatoceratodus tiguidiensis* and *Ceratodus humei*, as previously documented in the Cenomanian Alcântara Formation of Brazil (De Sousa Carvalho, 2006).

Ptychoceratodontidae Martin, 1982

*Ferganoceratodus* Nesson and Kaznyshkin, 1985

*Ferganoceratodus* sp.

**Referred material:** MGGC 21926-21930; ONM NG EMD 2, 10, 15 (Fig. 9).

**Locality:** El Mra.

**Horizon:** Ain el Guettar Formation, Oum Dhiab member, (Albian).

**Description:** These elements are small- to medium-sized, with a triangular shape. The crests are acute and strongly keeled in buccal view. The second crest is slightly more elongated than the others are. The ridges are straight, radiating gradually to the distal edge. The first furrow is deeper and wider than the others are. The remaining furrows are “V”-shaped, deep, narrow and strongly sliced. The inner angle is in anteriorly set and is close to 90° or slightly obtuse. In lateral view, the crests are strongly keeled. The occlusal surface is dotted. These tooth plates are of the cutting type (Agnolin, 2010). MGGC 21926 and ONM NG EMD 15 differ from the other specimens of our sample in being the only

ones bearing five radiating ridges. Our referral to *Ferganoceratodus* is based on limited number of cusps (i.e., five) in the upper teeth, on the beveled mesiointernal angle, and on the 'cutting type' morphology of the occlusal surface (Nessov and Kaznyshkin, 1985; Agnolin, 2010). Nevertheless, we acknowledge that some of these features are similar in specimens referred to *Asiatoceratodus* (see Castro et al., 2004).

**Distribution:** *Ferganoceratodus* tooth plates are reported primarily from central Asia and Thailand (Nessov and Kaznyshkin, 1985; Cavin et al., 2007, 2009) and the paleogeographic distribution of this genus has been related to a terrestrial connection between southern Thailand and Central Asia in the Jurassic (Buffetaut et al., 2006; Cavin et al., 2009). In addition, different species have been named based on isolated plates: *F. concinnus*, from the Triassic of Germany; *F. sharategensis*, from the Upper Jurassic of Mongolia; and *F. madagascariensis* from the Late Cretaceous of Madagascar (Martin et al, 1997, 1999). Therefore, the stratigraphic record of this genus possibly extends from the late Triassic to the late Cretaceous.

## 5.2 Phylogenetic analysis

The analysis of the data set found 50000 shortest trees of 173 steps each (Consistency Index: 0.2659; Retention Index: 0.6492) (Fig. 10). Although the number of characters analyzed is relatively low compared to the number of OTUs, the length of the shortest trees found is significantly lower than the lengths of the trees sampled after permuting the relationships randomly (number of replications: 1000,  $p = 0.01$ ). This test suggests that the recovered shortest topologies are not significantly affected by error sampling due to the limited morphological information. The strict consensus topology of all

shortest trees found placed the Tunisian OTUs in two main lineages: one including seven Tunisian specimens and specifically those referred to *Equinoxiodus* sp., *Lavocatodus humei* and *Neoceratodus africanus*; the other lineage includes 34 Tunisian tooth plates and specimens referred to *Asiatoceratodus* cf. *tiguidiensis*, *Ceratodus africanus*, *Ferganoceratodus* sp. and *Ptychoceratodus roemeri*. The relationships among the first lineage are well resolved: two Tunisian OTUs cluster at the base of that lineage, three specimens result closer to *N. africanus*, and the remaining two result closer to *L. humei*. No Tunisian specimen results closer to *E. schultzei*. The relationships among the second lineage are less resolved than in the first. Two Tunisian OTUs result the basalmost members of this group. The remaining specimens form a large unresolved polytomy with the specimens referred to *Asiatoceratodus tiguidiensis*, *Ceratodus africanus*, *Ferganoceratodus jurassicus* and *Ptychoceratodus roemeri*. Among this large unresolved cluster, the analysis found three groups including a subset of the Tunisian specimens (Fig. 10). Nevertheless, the data set lacks information allowing to discriminate whether these three clusters are closer to some of the included species relative to the rest of the sample. Comparison between our preliminary identification of the Tunisian specimens based on published description and their placement based on the phylogenetic analysis indicates that:

1. two specimens are referred to an *Equinoxiodus*-like form. It is unclear whether the latter taxon is actually represented in our sample or if these specimens represent a new taxon.
2. two specimens are referred to *Lavocatodus humei*.

3. two specimens are referred to *Neoceratodus africanus*. A third specimen, initially identified as *Ferganoceratodus jurassicus*, may represent an additional specimen of *N. africanus*.
4. two specimens may represent a *Ceratodus*-like form. It is unclear whether the latter taxon is represented in our sample, or if these specimens represent a new taxon.
5. the vast majority of specimens may represent individuals of *Asiatoceratodus tiguiddiensis*, *F. jurassicus* or a new, unidentified species related to *A. tiguiddiensis* or *F. jurassicus*.

## 6. Comparison with extant Dipnoi

Dipnoans are primarily non-marine animals that generally share fresh and brackish water environments with a variety of taxa. However, based on different adaptation strategies of living dipnoans as well as taphonomic and paleoecological data for the Tunisian specimens, it is possible to discuss such diversity and the co-existence of different genera in a - supposed to be - single ecosystem.

First, the lower beds of the Oum ed Diab Member are interpreted to represent estuarine and marginal-marine deposition characterized by high sediment supply and arid to xeric climatic conditions (Fanti et al., 2012, 2015). The occurrence of rare *in situ* plant roots possibly indicates a patchy, mangrove-like vegetation and are consistent with sub-aerial to low water depth conditions. Therefore, such ecological conditions may have represented a major limitation for fish and other vertebrate diversity. Studies on the living African lungfish *Protopterus annectus* revealed that this potamodromous fish aestivates during drought seasons, tolerates seawater up to a maximum of 30%, and requires a tem-

perature range between 29°- 37°C (Smith, 1931; Okafor, 2004; Okafor and Chukwu, 2005; Snoeks et al., 2009). Similar adaptations are documented for the South American species *Lepidosiren paradoxa*, although this taxon is less tolerant to high temperatures and brackish environments (Hochachka and Helbert, 1978; Fink and Fink, 1979; Planquette et al., 1996; Mesquita-Saad et al., 2002; Bemis et al., 2003). The endemic Australian species *Neoceratodus forsteri* lives in highly vegetated areas, does not aestivate, requires temperatures between 13° to 25°, and overall inhabits less strenuous environments than *Lepidosiren* and *Protopterus* as it does not tolerate seawater (Pusey et al., 2004; Arthington, 2009; Glass and Wood, 2009; DSITIA, 2013). Furthermore, both *Protopterus* and *Lepidosiren* are obligate air breathers, whereas *Neoceratodus* is not (Johansen, 1986). As such, although as a group extant dipnoans are indeed found in fluvial, brackish, and swampy-coastal ecosystems, occurring in both netic and lotic habitats of major rivers, individual lineages display more accentuated ecological preferences and adaptations in present day and, most likely, extinct taxa (McAllister et al., 1988; Cloutier and Ahlberg, 1996; Ahlberg, et al., 2003; Okafor, 2005). Otero (2011) provided an excellent case study on extinct and extant representatives of the genus *Protopterus*. The Late Cretaceous record of the genus is restricted to continental Africa and specifically in narrowed central (Niger, and Mali) and north-eastern (Egypt and Sudan) regions. Conversely, seven extant species and subspecies of *Protopterus* inhabit the central Africa's vast river systems, where they occasionally overlap large hydrographic basins, extending from piedmont to coastal areas (Paugy et al., 2008; Froese and Pauly, 2009; Otero, 2011, and references therein). However, even within the same genus, species and subspecies display a clear ecologic partitioning (proximal-distal section of the river, lacustrine areas, coastal swamps, etc.).

Although present day lungfish diversity and distribution is a fraction compared to the Cretaceous fossil record, such data clash with the dipnoan record in Gondwanan deposits and specifically with the Aptian-Albian Tunisian faunal assemblage, where six genera have been identified. In addition to the six genera of dipnoans, the faunal assemblage is represented by a diverse array of species that includes marine elasmobranchs, bony fish taxa (including the coelacanthid *Mawsonia*), crocodyliforms, and dinosaurs (Fanti et al., 2013, 2015). Such biodiversity dramatically unfits with paleoecological reconstructions proposed for the Oum ed Diab Member. From a taphonomic perspective, macro- and micro-vertebrate remains from the Oum ed Diab Member are nicely preserved but systematically disarticulated. These marginal-marine deposits most likely represent the downstream section of a much wider and complex drainage system capable to transfer and accumulate sediments and vertebrate remains from the mainland into the coastal areas. To support this interpretation, coeval deposits of Niger and other sub-Saharan regions with dipnoan remains have been interpreted as a more diversified, inland floodplains habitat rich in plant resources and characterized by recurrent lacustrine areas (Buffetaut and Taquet, 1977; Lefranc and Guiraud, 1990; Benton et al., 2000; Sereno et al., 2001, 2007; Sereno and Brusatte, 2008; Sereno and Larsson, 2009). As the dipnoan diversity observed in Tunisia share many similarities with coeval lungfishes faunas of Brazil, results presented here may further support the postulated faunal partitioning between northern and southern South America during the mid-Cretaceous (Apesteguia et al., 2007; Agnolin et al., 2010; Candeiro et al., 2011; Novas et al., 2013).

## **7. Conclusions**

Data presented in this study indicate a remarkable lungfish diversity in the mid-Cretaceous Oum ed Diab Member of southern Tunisia. In fact, dipnoans are represented by the neoceratodontid *Equinoxiodus* (or a related form) and *Neoceratodus*, the asiaticeratodontid *Asiatoceratodus*, the ceratodontid *Ceratodus* (or a related form), the lepidosirenid *Lavocatodus*, and the ptychoceratodontid *Ferganoceratodus*. The integration of systematic methodologies and phylogenetic analysis supports this taxonomic interpretation. In particular, this study indicates that *Ceratodus* and *Neoceratodus* are two valid and distinct taxa, as well as the taxonomic validity of *Lavocatodus humei*. As such, all recognized Mesozoic lungfish families are surprisingly represented within a discrete stratigraphic unit. This assumption conflicts with the paleoecological interpretation of the Oum ed Diab deposits, and also infers a degree of sympatry and ecologic partitioning not seen in present day lungfishes. However, detailed facies analyses and taphonomic interpretations suggest a different scenario. The fossil assemblage pertaining to the Oum ed Diab Member most likely represent a taphonomic artifact and therefore is representative not only of the estuarine-coastal environments in which they are collected, but also of a wider arrays of brackish and freshwater ecosystems that extended to the African inlands during the mid-Cretaceous. As the vast majority of isolated dipnoan tooth plates from Gondwana come from paleo-environments comparable with the marginal-marine Oum ed Diab Member, this multidisciplinary approach may indicate that our comprehension of Mesozoic Gondwanan dipnoans diversity and ecologic distribution is biased by the lack of detailed information on the geology and taphonomy of discrete localities. This approach can provide new tools to refine the study on the stratigraphic-chronostratigraphic occurrence of vertebrates but also to better estimate the geographic distribution of both single taxon and selected faunal assemblages.

## 8. Acknowledgements

This research was supported by the National Geographic Society (grant 9586-14), Museo Geologico Giovanni Capellini (Bologna, Italy), and Office National des Mines (Tunis, Tunisia). We are indebted with the members of the 2010-2014 Italian-Tunisian paleontological expedition in the Tataouine Governorate, in particular L. Cantelli, F. Mnasri, J. Dridi, A. Bacchetta, M. Contessi, J. Carlet, G. Mignani, and H. Aljane. P. Ferrieri (MGGC) photographed all specimens.

## References

Agassiz (1838) Agassiz L. Recherches Sur Les Poissons Fossiles. Tome III (livr.

11) Neuchatel: Imprimerie de Petitpierre; 1838. pp. 73–140.

Agnolin, F., 2010. A new species of the genus *Atlantoceratodus* (Dipnoiformes:

Ceratodontidei) from the uppermost Cretaceous of Patagonia and brief overview of fossil dipnoans from the Cretaceous and Paleogene of South America. Brazilian Geographical Journal: Geosciences and Humanities Research Medium 1(2), 162–210.

Ahlberg, P.E., Johansen, Z., Zerina, J., Daeschler, E.B., 2003. The late Devonian lungfish,

*Soederberghia* (Sarcopterygii, Dipnoi) from Australia and North America and its biogeographical implications. Journal of Vertebrate Palaeontology 21(1), 1–12.

- Alves Y. M, Machado L. P., Bergqvist L.P., Paulo M. Brito P. M., 2013. Redescription of two lungfish (Sarcopterygii: Dipnoi) tooth plates from the Late Cretaceous Bauru Group, Brazil. *Cretaceous Research* 40, 243–250.
- Arambourg, C., Joleaud, L., 1943. Vertébrés fossiles du bassin du Niger. *Bulletin de la Service des Mines, Gouvernement Général de l'Afrique Occidentale Française* 7, 27–84.
- Arthington, A.H., 2009. Australian lungfish, *Neoceratodus forsteri*, threatened by a new dam. *Environmental Biology of Fish* 84, 211–221.
- Bemis, W., Fernandes C., Castro R., Zuanon, J., Py-Daniel, L., Alves-Gomes, J., Machado, F., Malabarba L., 2003. Notes on the Systematics, Distribution and Natural History of the South American Lungfishes in the genus *Lepidosiren* Fitzinger 1837 (Dipnoi: Lepidosirenidae). On-line pdf, [www.bio.umass.edu/biology/bemis/Lungfish\\_ms.pdf](http://www.bio.umass.edu/biology/bemis/Lungfish_ms.pdf)
- Ben Ismail, M.H., 1991. Les bassins mésozoïques (Trias a Aptien) du sud de la Tunisie: stratigraphie intégrée, caractéristiques géophysiques et évolution géodynamique. Ph.D. Thesis, Université de Tunis II, 446 pp.
- Benton, M.J., Bouaziz, S., Buffetaut, E., Martill, D., Ouaja, M., Soussi, M., Trueman, C., 2000. Dinosaurs and other fossil vertebrates from fluvial deposits in the Lower Cretaceous of Southern Tunisia. *Palaeogeogr. Palaeoclimatol. Palaeoecol.* 157, 227–246.

- Bodin, S., Petitpierre, L., Wood, J., Elkanouni, I., Redfern, J., 2010. Timing of early to mid-Cretaceous tectonic phases along North Africa: new insights from the Jeffara escarpment (Libya–Tunisia). *Journal of African Earth Sciences* 58, 489–506.
- Bonaparte, C. L., 1841. A new systematic arrangement of vertebrate animals. *Transactions of the Linnean Society* 18, 247–303.
- Bouaziz, S., Buffetaut, E., Ghanmi, M., Jaeger, J.-J., Martin, M., Mazin, J.-M., Tong, H., 1988. Nouvelles découvertes de vertébrés fossiles dans l'Albien du sud tunisien. *Bulletin de la Société géologique de France* 4, 335–339.
- Bouaziz S., Donze P., Ghanmi, M. e Zarbout, M., 1989. La série à dominante continentale (Oxfordien à Cénomanién) de la falaise du Dahar (Sud tunisien) ; son évolution du Tebaga de Médenine à la frontière tripolitaine. *Géologie Méditerranéenne* 15, 67-76.
- Buffetaut, E., Taquet, P., 1977. The giant crocodylian *Sarcosuchus* in the Early Cretaceous of Brazil and Niger. *Palaeontology* 20, 203-208.
- Buffetaut, E., Suteethorn, V., Thong, H., 2006. Dinosaur assemblages from Thailand: a comparison with Chinese faunas. In: Lu, J., Kobayashi, Y., Huang, D., Lee, Y. (Eds.), *Papers from the 2005 International Dinosaur Symposium*. Geological Publishing House. Beijing, pp. 19-37.
- Busson G., 1967. Le Mésozoïque saharien. 1ère partie: L'Extrême Sud tunisien. C.N.R.S. Edit., Paris, Centre Rech. Zones Arides, Géol., 8, 194.
- Candeiro, C.R., Fanti, F., Therrien, F., Lamanna, M., 2011. Continental fossil vertebrates from the mid-Cretaceous (Albian-Cenomanian) Alcantara Formation, Brazil, and their

relationship with contemporaneous faunas from North Africa. *Journal of African Earth Sciences* 60, 79-92.

Carroll, R.L., 1988. *Vertebrate Palaeontology and Evolution*. W. H. Freeman and Company, New York. 1996 pp.

Castro, D.F., Toledo, C.E.V., De Sousa, E.P., Medeiros, M.A., 2004. Nova ocorrência de *Asiatoceratodus* (Osteichthyes, Dipnoiformes) na Formação Alcântara , Eocenomaniano da Bacia de Sao Luis, MA, Brasil. *Revista Brasileira de Paleontologia* 7(2), 245-248.

Cavin, L., Suteethorn, V., Buffetaut, E., Tong, H., 2007. A new Thai Mesozoic lungfish (Sarcopterygii, Dipnoi) with an insight into post-Palaeozoic dipnoan evolution. *Zoological Journal of the Linnean Society* 149, 141–177.

Churcher, C.S., De Iuliis, G., 2001. A new species of *Protopterus* and a revision of *Ceratodus humei* (Dipnoi: Ceratodontiformes) from the Late Cretaceous Mut Formation of eastern Dakhleh Oasis, Western Desert of Egypt. *Palaeontology* 44(2), 305-323.

Churcher, C.S., De Iuliis, G., Kleindienst, M.R., 2006. A new genus for the dipnoan species *Ceratodus tuberculatus* Tabaste, 1963. *Geodiversitas* 28, 635–647.

Clack, J.A., E.L. Sharp, and J. A. Long. 2011. The fossil record of lungfishes. In: Jorgensen, J.M., Joss, J. (Eds.) *The Biology of Lungfishes*. CRC Press, Boca Raton, Florida, pp. 1–42.

- Cleason, K.M., Sallam, H.M., O'Connor P.M., Sertich, J.J. W., 2014. A Revision of the Upper Cretaceous Lepidosirenid Lungfishes from the Quseir Formation, Western Desert, Central Egypt. *Journal of Vertebrate Paleontology* 34(4), 760–766.
- Cloutier R., Ahlberg P.E., 1996. Morphology, characters and the interrelationships of basal sarcopterygians. In: Stiassny, M., Parenti, L., Johnson, J. (Eds.) *Interrelationships of Fishes*. Academic Press, London, pp. 445–479.
- De Castelnau, 1876. Mémoire sur les poissons appelés barramundi par les aborigènes du nord-est de l'Australie. *Journ. Zool. (Gervais)*, V, 129-136.
- DSITIA, 2013. Review of Water Resource (Burnett Basin) Plan 2000 and Resource Operations Plan: Appendix A– Assessment of critical water requirements for selected ecological assets. Department of Science, Information Technology, Innovation and the Arts, Brisbane.
- Fanti, F., Contessi, M., Franchi, F., 2012: The '*Continental Intercalaire*' of southern Tunisia: stratigraphy, palaeontology, and palaeoecology. *Journal of African Earth Sciences*, 73-74, 1-23.
- Fanti, F., Cau, A., Martinelli, A., Contessi, M., 2014. Integrating palaeoecology and morphology in theropod diversity estimation: a case study from the Aptian-Albian of Tunisia. *Palaeogeography, Palaeoclimatology, Palaeoecology* 410, 39-57.
- Fanti, F., Cau, A., Cantelli, L., Hassine, M., Auditore, M., 2015. New information on *Tataouinea hannibalis* from the early Cretaceous of Tunisia and implications for the tempo and mode of Rebbachisaurid sauropod evolution. *PLoS ONE* 10 (4): e0123475. doi:10.1371/journal.pone.0123475

- Fanti, F., Cau, A., Panzarin, L., Cantelli, L., 2016. Evidence of iguanodontian dinosaurs from the Lower Cretaceous of Tunisia. *Cretaceous Research* 60, 267-274.
- Fink, W.L., Fink, S.V., 1979, Central Amazonia and its fishes. *Comp. Biochem. Physiol.* 62A, 13-29.
- Fitzinger, L.J., 1837. Vorläufiger Bericht über eine höchst interessante Entdeckung Dr. Natterer in Brasil. *Isis (Oken)* 30, 379 – 380.
- Froese, R., Pauly, D., 2009. FishBase. World Wide Web electronic publication, <http://www.fishbase.org>, version (06/2009).
- Gill, T., 1872. Arrangement of the families of fishes, or classes Pisces, Marsipobranchii and Leptocardii. *Smithsonian Miscellaneous Collections* 247, 1–49.
- Glass, M.L., Wood, S.C., 2009. Cardio-respiratory control in vertebrates: Comparative and evolutionary aspects. Dordrecht: Springer, 546 pp.
- Goloboff, P.A., Carpenter, J.M., Arias, J.S., Esquivel, D.F.M., 2008. Weighting against homoplasy improves phylogenetic analysis of morphological datasets. *Cladistics* 24, 758–773.
- Haug, E., 1905. Documents de la mission saharienne: mission Foureau – Lamy: Paléontologie. *Soc. geog. Paris* 1905, 751–832.
- Hochachka, P.W., Hulbert, W.C., 1978. Glycogen seas, glycogen bodies, and glycogen granules in heart and skeletal muscle of two air-breathing, burrowing fishes. *Can. J. Zool.* 56, 774-786.

- Johansen, K., Lenfant, C., 1967. Respiratory functions in South American lungfish, *Lepidosiren paradoxa*. *Journal of Experimental Biology* 46, 205-218.
- Kemp, A., 1997a. Four species of *Metaceratodus* (Osteichthyes: Dipnoi: family Ceratodontidae) from Australian Mesozoic and Cenozoic deposits. *Journal of Vertebrate Paleontology* 17, 26–33.
- Kemp, A., 1997b. A revision of Australian Mesozoic and Cenozoic lungfish of the family Neoceratodontidae (Osteichthyes: Dipnoi), with a description of four new species. *Journal of Paleontology* 71, 713–733.
- Kemp, A., 1998. Skull structure in post-paleozoic lungfish. *Journal of Vertebrate Paleontology*, 18(1), 43-63.
- Lefranc, J.P., Guiraud, R., 1990. The *Continental Intercalaire* of northwestern Sahara and its equivalents in the neighboring regions. *Journal of African Earth Sciences* 10, 27–77.
- López-Arbarello, A., 2004. The record of Mesozoic fishes from Gondwana (excluding India and Madagascar). In: Arratia, G., Tintori, A. (Eds.) *Mesozoic Fishes 3- Systematics, Paleoenvironments and Biodiversity*. Verlag Dr. Friedrich Pfeil, München, 597–612 pp.
- Martin, M., 1979. *Arganodus atlantis* et *Ceratodus arganensis*, deux nouveaux dipneustes du Trias supérieur continental marocain. *Compte Rendu de l'Académie de Sciences Paris* 289, 89-92.
- Martin, M., 1981a. Les Ceratodontiformes (Dipnoi) de Gadoufaoua (Aptien supérieur, Niger). *Bulletin du Musée national d'Histoire naturelle (Paris)*, 4e sér. 3(C), 267–282.

- Martin, M., 1981b. Über drei Zahnplatten von *Ceratodus* aus der ägyptischen Kreid. Mitteilungen der Bayerischen Staatssammlung für Paläontologie und Geologie 21, 73-80.
- Martin, M., 1982. Nouvelles données sur la phylogénie et la systématique des Dipneustes postpaléozoïques, conséquences stratigraphiques et paléogéographiques. Geobios Mémoires Spéciales 6, 53-64.
- Martin, M., 1984a. Révision des Arganodontidés et des Néocératodontidés (Dipnoi, Ceratodontiformes) du Crétacé africain. Neues Jahrbuch für Geologie und Paläontologie. Abhandlungen 169, 225-260.
- Martin, M., 1984b. Deux Lepidosirenidae (Dipnoi) du Crétacé du Sahara *Protopterus humei* (Priem) et *Protopterus protopteroïdes* (Tabaste). Paläontologische Zeitschrift 58, 265–277.
- Martin, M., 1995. Nouveaux lepidosirenides (Dipnoi) du Tertiaire africain. Geobios 19:245–280.
- Martin M., Barbieri L., Cuny G., 1999. The Madagascan Ptychoceratodontids (Dipnoi). Systematic relationships and paleobiogeographical significance. Oryctos 2, 3–16.
- McAllister, J.A., Dubiel R.F., Blodgett R.H., Brown T.M., 1988. Lungfish burrows in the Upper Triassic Chinle and Dolores formations, Colorado Plateau – comments on the recognition criteria of fossil lungfish burrows. Journal of Sedimentary Petrology 58, 365–367.

- Medeiros, M.A., Schultz, C.L. 2001. Uma paleocomunidade de vertebrados do Cretáceo médio, Bacia de São Luís. In: Rossetti, D.F., Góes, A.M., Truckenbrodt, W. (Eds.) O Cretáceo na Bacia de São Luís - Grajaú, MPGE Editoração, 209-221 pp.
- Medeiros M. A., Schultz C.L., 2002. A fauna dinossauriana da *Laje do Coringa*, Cretáceo Médio do Nordeste do Brasil. Arq. Mus. Nac. 60(3), 155–162.
- Mesquita-Saad, L.S., Leitao, M.A., Paula-Silva, M.N., Chippari-Gomes, A.R., Almeida-Val, V.M., 2002. Specialized metabolism and biochemical suppression during aestivation of the extant South American lungfish *Lepidosiren paradoxa*. Brazilian Journal of Biology 62, 495-501.
- Miles, R.S., 1977. Dipnoan (lungfish) skulls and the relationships of the group: a study based on new species from the Devonian of Australia. Zoological Journal of the Linnean Society 61, 1–328.
- Müller, J., 1844. Ueber den Bau und die Grenzen der Ganoiden und über das natürliche System der Fische. Abhandlungen der Königlichen Preussischen Akademie der Wissenschaften, Berlin, 117 – 126.
- Nessov L.A., Kaznyshkin M.N., 1985. A lungfish and turtles from Upper Jurassic of Northern Fergana, Kirghiz SSR. Vestnik Zoologii 1, 33–39.
- Novas, F., Agnolin, F., Ezcurra, M., Porfiri, J., Canale, J., 2013. Evolution of carnivorous dinosaurs during the Cretaceous: the evidence from Patagonia. Cretaceous Research 45, 174-215.
- Okafor A.I., 2004. Salinity tolerance of the African lungfish, *Protopterus annectens* (Owen). African Journal of Science, 5(1), 1073–1083.

- Okafor A. I., Chukwu L. O., 2005. The effect of salinity stress on buccal ventilatory rate in the African lungfish, *Protopterus annectens* (Owen). *Animal Research International* 2(1), 252–254.
- Otero O., 2011. Current knowledge and new assumptions on the evolutionary history of the African lungfish, *Protopterus*, based on a review of its fossil record. *Fish and Fisheries* 12, 235–255.
- Ouaja M., 2003. Etude sédimentologique et paléobotanique du Jurassique moyen-Crétacé inférieur du bassin de Tataouine (Sud-Est de la Tunisie). Ph.D. thesis, Université Claude-Bernard, Lione.
- Owen R., 1839. On a new species of the genus *Lepidosiren* of Fitzinger and Natterer. *Proc. Linn. Soc. Lond.* 1, 27-32.
- Pedrão E., Arai M., Carvalho I.S., Santos M.H.B., 1993. Palinomorfos da Formação Itapecurú – análise palinológica de uma amostra de superfície da Ponta do Farol, São Luís - MA. Petrobrás, Cenpes, 10 p. (Relatório técnico).
- Peyer B., 1925. Die Ceratodus-Funde. II. Wirbeltier-Reste der Baharije-Stufe (unterstes Cenoman). *Ergebnisse der Forschungsreisen Prof. E. Stromer in den Wüsten Ägyptens. Abhandlungen der Bayerischen Akademie der Wissenschaften, Mathematisch-naturwissenschaftliche* 30, 5–32.
- Planquette P., Keith P., Le Bail P.-Y., 1996. Atlas des Poissons d'Eau Douce de Guyane, Tome 1. Collection du Patrimoine Naturel, vol. 22. Paris, IEGB - M.N.H.N., INRA, CSP, Ministère de l'Environnement.

- Priem F., 1914. Sur des vertébrés du Crétacé et de l'Éocène de l'Égypte. Bulletin de la Société Géologique de France, Série 4, 14, 366 – 382.
- Pusey B.J., Kennard M.J., Arthington A.H., 2004. Freshwater fishes of North-Eastern Australia. CSIRO, Collingwood, Victoria. 684 pp.
- Schultze, H.P., 1991. Lungfish from the El Molino (Late Cretaceous) and Santa Lucia (Early Paleocene) formations in southcentral Bolivia. Rev. Tec. YPF 12, 441-448.
- Schultze, H.P., 2004. Mesozoic sarcopterygians. In: Arratia, G., Tintori, A. (Eds.) Mesozoic Fishes 3—Systematics, paleoenvironments and biodiversity. Verlag Dr. Freidrich Pfeil, Munchen, pp- 463-492.
- Sereno, P.C., Brusatte, S., 2008. Basal abelisaurid and carcharodontosaurid theropods from the Lower Cretaceous Elrhaz Formation of Niger. Acta Palaeontologica Polonica 53(1), 15–46.
- Sereno, P.C., Larsson, H.C.E., Sidor, C.A., Gado, B., 2001. The giant crocodyliform *Sarcosuchus* from the Cretaceous of Africa. Science 294, 1516–1519.
- Sereno, P.C., Wilson, J., Witmer, L., Whitlock, J., Maga, A., Ide, O., Rowe, T., 2007. Structural extremes in a Cretaceous dinosaur. PLoS ONE 2(11): e1230.  
doi:10.1371/journal.pone.0001230
- Sereno, P.C., Larsson, H.C.E., 2009. Cretaceous Crocodyliforms from the Sahara. ZooKeys 28: 1–143.
- Smith H. W., 1931. Observations on the African Lung-Fish, *Protopterus aethiopicus*, and on Evolution from Water to Land Environments. Ecology 12, 164-181.

- Skrzycki P., 2015. New species of lungfish (Sarcopterygii, Dipnoi) from the Late Triassic Krasiejów site in Poland, with remarks on the ontogeny of Triassic dipnoan tooth plates. *Journal of Vertebrate Paleontology*, DOI:[10.1080/02724634.2015.964357](https://doi.org/10.1080/02724634.2015.964357)
- Snoeks J., Laleye P., Contreras-MacBeath T., 2009. *Protopterus annectens*. The IUCN Red List of Threatened Species
- Soto M., Perea D., 2010. Late Jurassic Lungfishes (Dipnoi) from Uruguay, with Comments on the Systematics of Gondwanan Ceratodontiforms. *Journal of Vertebrate Paleontology* 30(4), 1049–1058
- Sousa, de, E.P., 2006. Os Dipnoiformes da Formação Alcântara (Albo-Cenomaniano), Ilha do Cajual, Maranhão. Ph.D. thesis, Universidade Estadual Paulista "Júlio de Mesquita Filho" Instituto de Geociencias e Ciencias Exatas.
- Sousa E.P., Medeiros M. A., Toledo C. E. V., Bertini R. J., Pereira A. A., Lindoso R. M., 2015. A new species of *Equinoxiodus* (Dipnoi: ?Neoceratodontidae) from the Late Cretaceous of Brazil. *Zootaxa*, 3905(3), 397-406.
- Stuhlmann F., 1889. Zitzberich. Kbnligl. P)-euss. Akad. Wiss., p. 645. Tabaste, N., 1963. Étude des restes de poissons du Crétacé Saharien. *Memoire IFAN, Mélanges Ichthyologiques*, Dakar, 437–481.
- Taquet P., 1976. Géologie et Paléontologie du gisement de Gadoufaoua (Aptien du Niger). *Cahiers de Paléontologie*, 1–191.
- Toledo C.E.V., Bertini R.J., 2005. Occurrences of the fossil Dipnoiformes in Brazil and its stratigraphic and chronological. *Revista Brasileira de Paleontologia* 8(1), 47-56.

Toledo C.E.V., Sousa E.P., Medeiros M.A., Bertini R.J., 2011. A new genus of Dipnoiformes from the Cretaceous of Brazil. *Anais da Academia Brasileira de Ciências* 83, 1181–1192.

Vorobiyeva E.I., 1967. Triassic ceratod from South Fergana and remarks on the systematics and phylogeny of ceratodontids. *Paleontological Journal* 4, 1–87.

## **Figures**

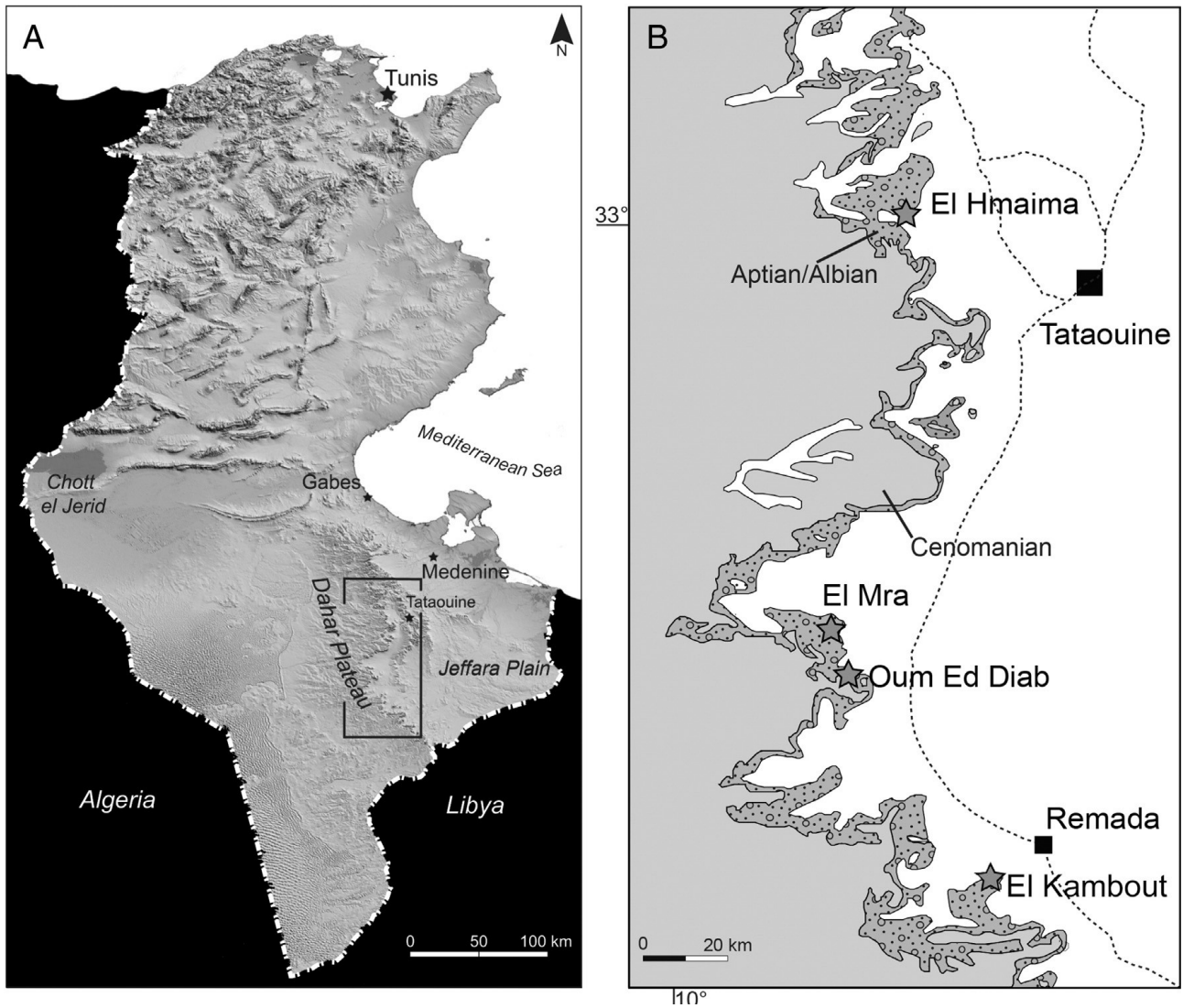


**Figure 1.** (A) reference map of Tunisia showing the study area in the Tataouine region. (B) simplified geological map of the Dahar Escarpment indicating the El Hmaima, El Mra, Oum ed Diab, and El Kambout localities.

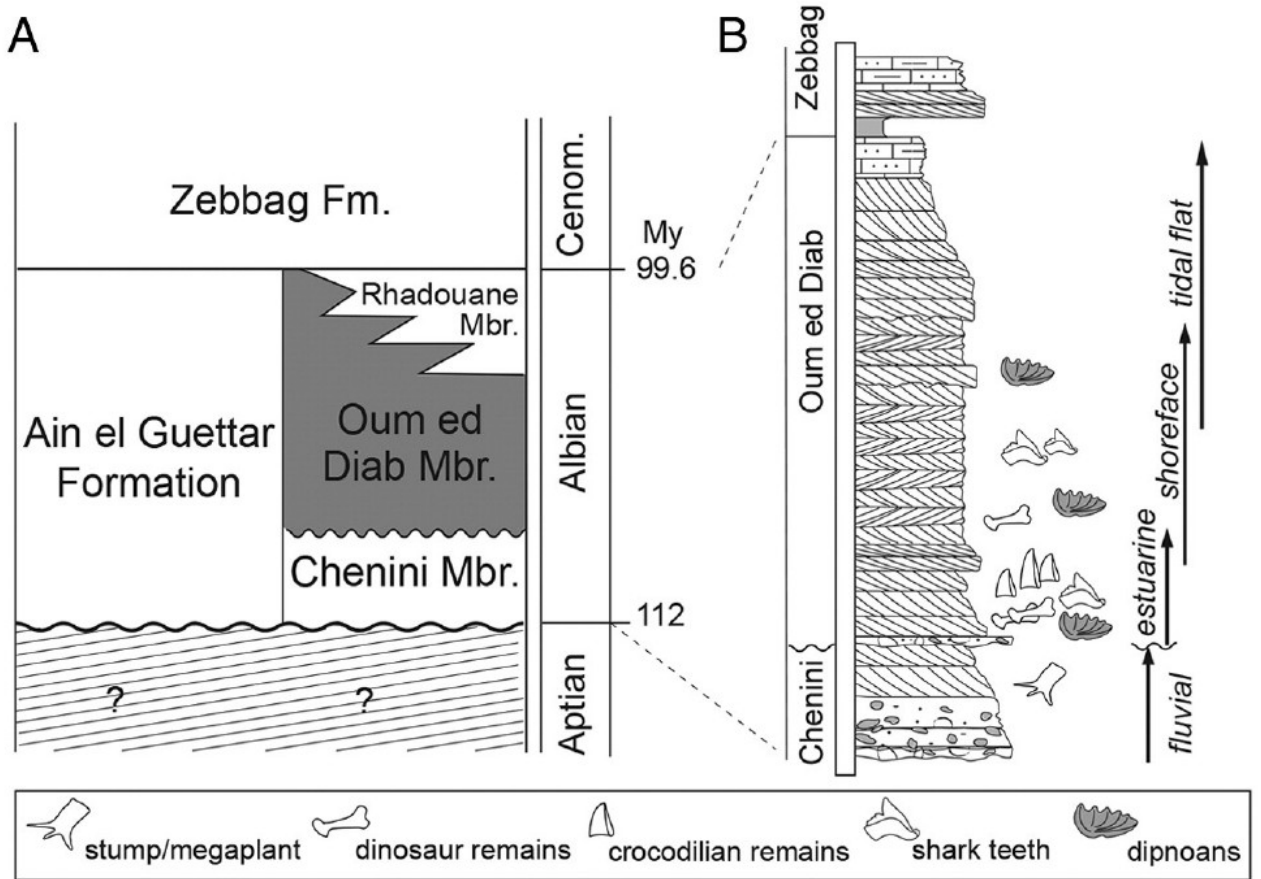


**Figure 2.** (A) stratigraphic nomenclature for the Aptian-Cenomanian deposits of southern Tunisia. Specimens discussed in this study were surface collected from the Albian beds Oum ed Diab Member of the Ain el Guettar Formation. (B) simplified field log showing facies interpretation and the stratigraphic occurrence of vertebrate remains and lungfish in the Oum ed Diab Member.

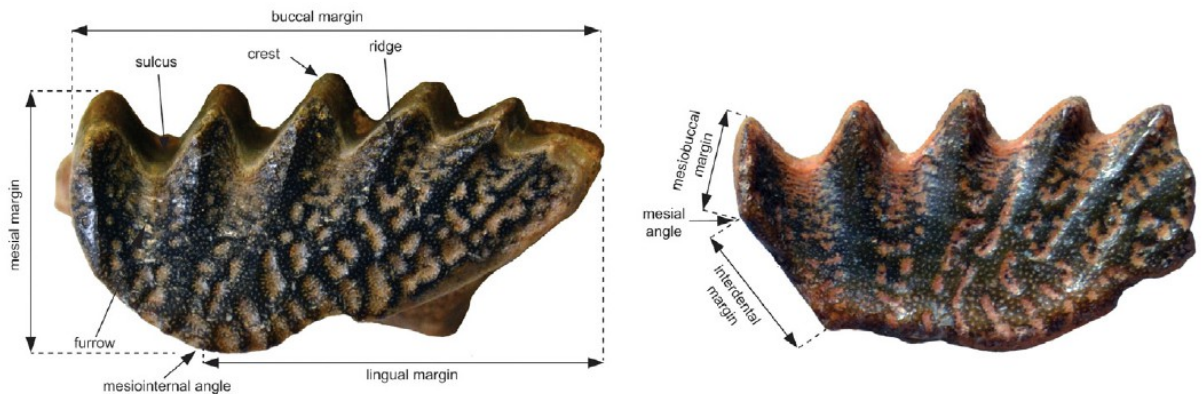


**Figure 3.** Plan of occlusal surface of lower right tooth plate with features named as in text, based on MGGC 21930 (left) and ONM NG EMD 10 (right). In this study we follow the terminology of Churcher and De Iuliis (2001) and we also consider 'inner angle' as synonymous for the mesiointernal angle.



**Figure 4.** *Lavocatodus humei* (MGGC 21920), lower left plate, from the El Hmaima locality in (A) occlusal, (B) lingual, and (C) ventral views. Scale bar, 2 cm.

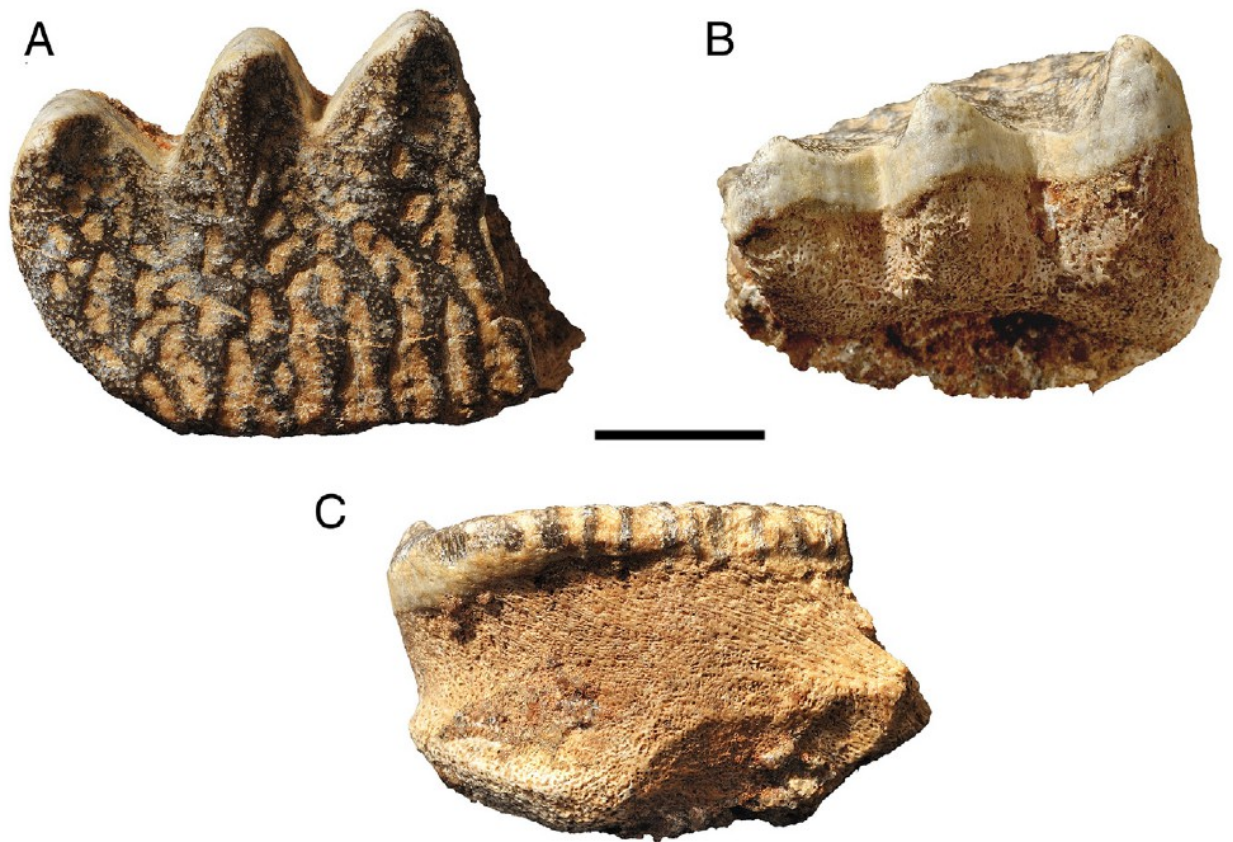


**Figure 5.** *Equinoxiodus* sp. (MGGC 21913), lower right plate, surface collected at the Oumed Diab locality in (A) occlusal, (B) buccal, and (C) lingual views. Scale bar, 1 cm.

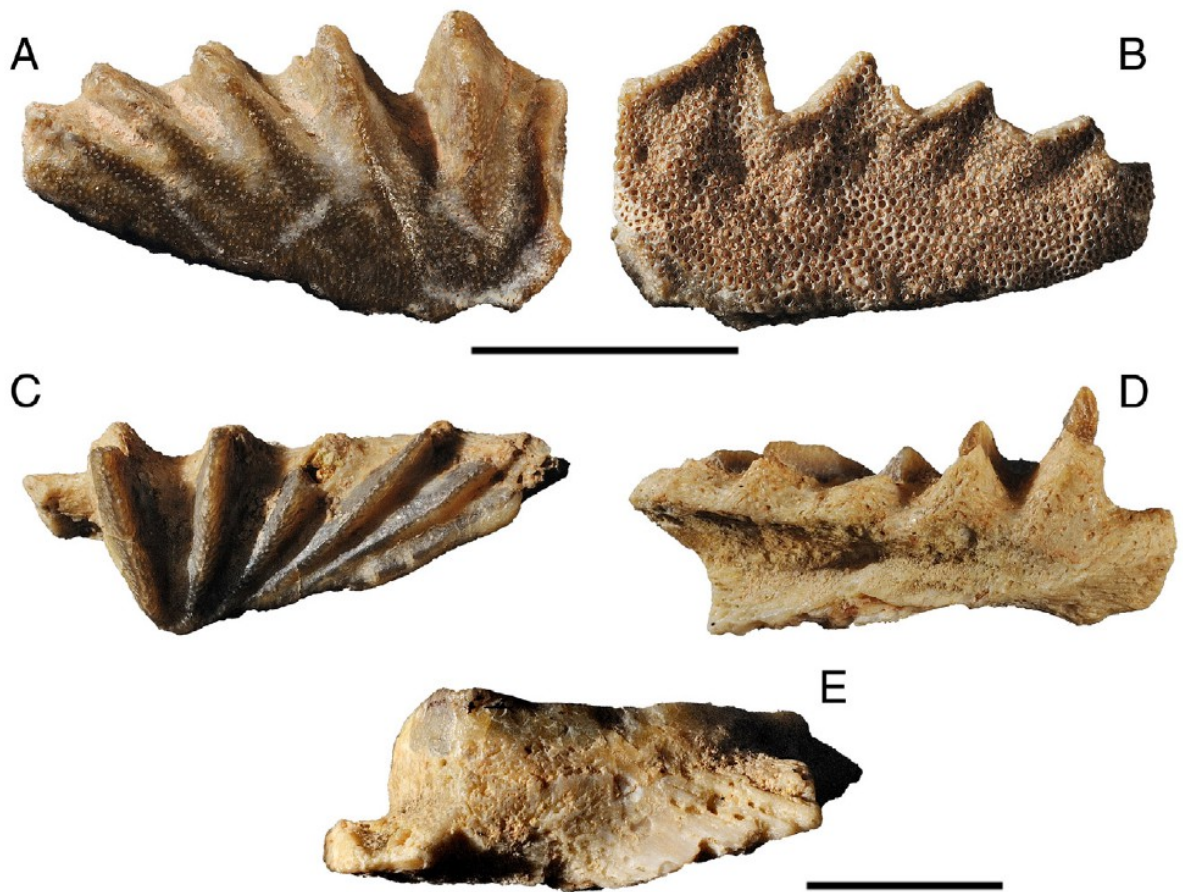


**Figure 6.** *Asiatoceratodus cf. tiguidiensis*. A-B, MGGC 21915, upper right plate from the Oum ed Diab locality in occlusal and ventral views. Scale bar, 1 cm. C-E, MGGC 21917, lower right plate, Oum ed Diab locality in occlusal, buccal, and lingual views. Scale bar, 5 mm.



**Figure 7.** *Neoceratodus africanus*. A-B, MGGC 21925, lower right plate from the El Mira locality in occlusal and ventral views. C-D, MGGC 21921, upper right plate from the Oum ed Diab locality in occlusal and ventral views. Scale bars, 1 cm.

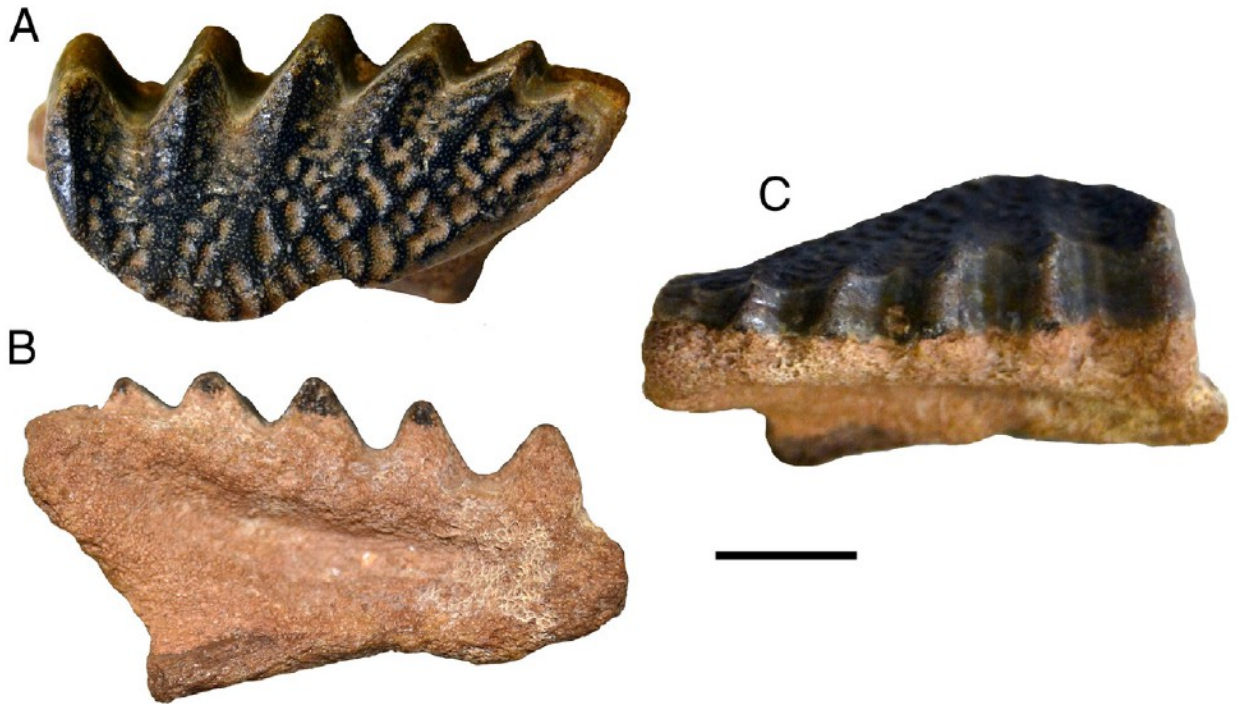


**Figure 8.** *Ceratodus* sp. (MGGC 21930), lower right plate from the El Mra locality in (A) occlusal, (B), ventral, and (C) buccal views. Scale bar, 1 cm.

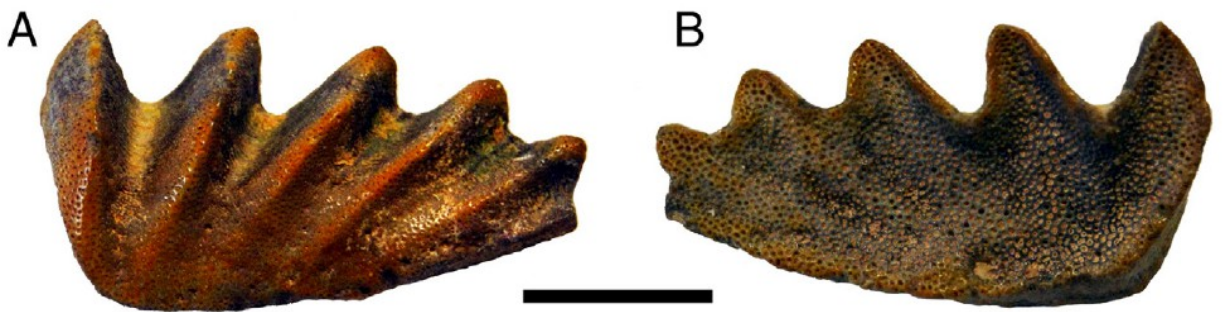


**Figure 9.** *Ferganoceratodus* sp. (MGGC 21926), upper left plate collected at the El Mra locality in (A) occlusal, and (B), ventral views. Scale bar, 1 cm.

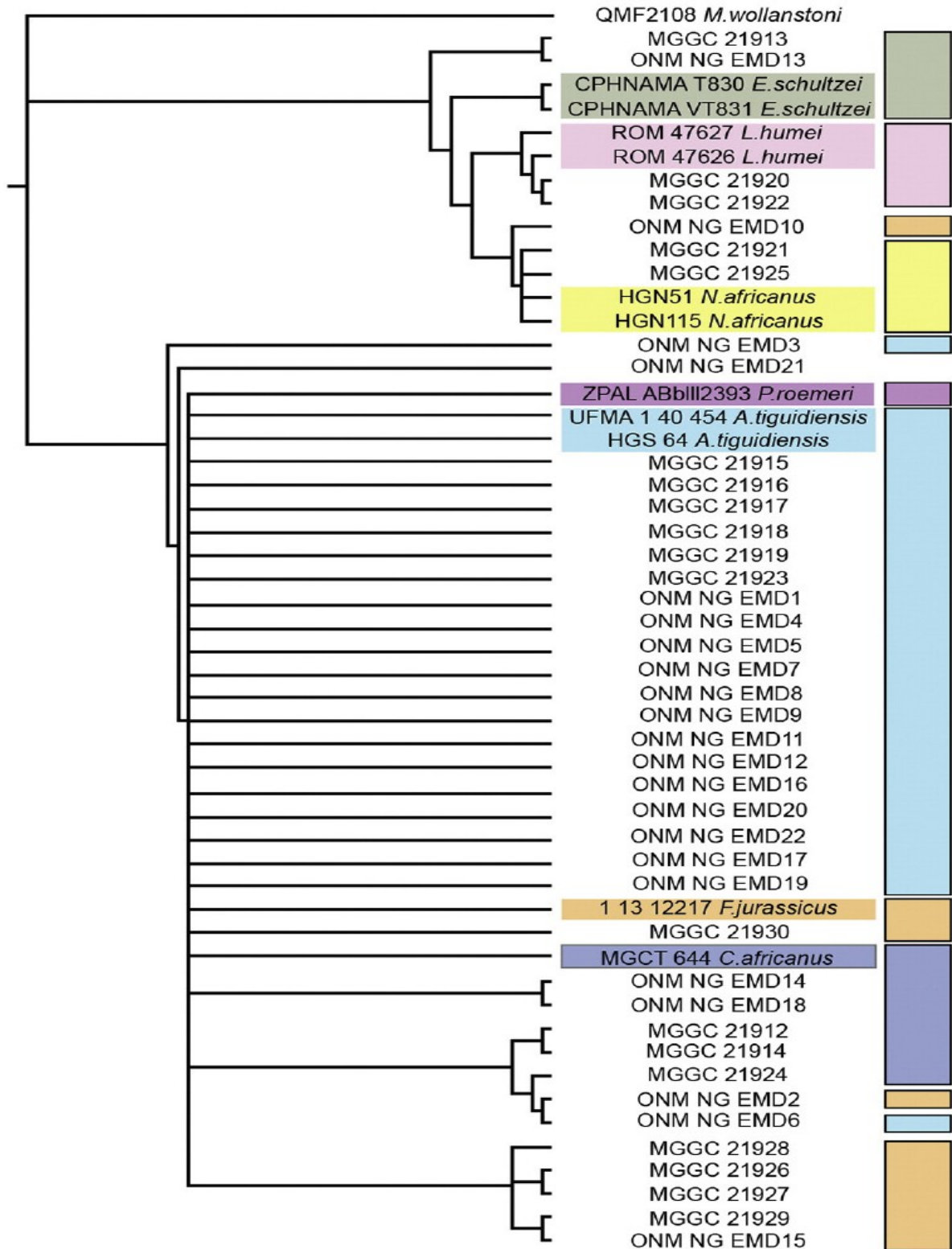


**Figure 10.** Strict consensus topology of the shortest trees found by the phylogenetic analysis of the morphological data set. Colored areas indicate the taxonomic identification of the Tunisian specimens prior to the phylogenetic analysis, according to the diagnostic

features of the non-Tunisian taxa included (Supplementary Material). Note the overall overlap between the taxonomic identification and the phylogenetic analysis.

## **CHAPTER 3 - Evidence of iguanodontian dinosaurs from the Lower Cretaceous of Tunisia.**

Submitted: 27<sup>th</sup> November 2015. Published: 12<sup>th</sup> January 2016 in *Cretaceous Research* vol. 60:267-274.

Federico Fanti, Andrea Cau, Lukas Panzarin, Luigi Cantelli

### **Abstract**

The fossil record of ornithischian dinosaurs from Africa is particularly scarce and limited to a few historic localities. In this study we describe new ornithischian remains from the Albian deposits of southern Tunisia (Tataouine Governorate), represented by isolated teeth of large-bodied iguanodontians. Teeth display a wide, diamond-shaped crown with a primary ridge dividing the occlusal surface in two unequal parts and two or more secondary ridges. Hook-like denticles are present on both mesial and distal crown margins and do not display mammillae. In overall morphology, specimens are comparable to those of many Early Cretaceous basal hadrosauriforms, including isolated ornithopodan teeth from comparably-aged levels of Niger. Transversal sections of the crowns permitted identification of dental tissues, which include a thick enamel, and well developed longitudinal and transverse giant tubules. Their relative extents appear to be related to the size, thus developmental age, of the tooth. Teeth are representative of the Oum ed Diab Member, a unit characterized by coastal deposits accumulated under arid to xeric climatic conditions and dominated by fish, crocodylians, and hydraulically transported rebbachisaurid and spinosaurid remains. Sedimentological data and preservation bias

strongly support selective taphonomic causes for the fossil distribution of ornithischians in southern Tunisia questioning the purported geographic and paleoecologic distribution of isolated Saharan dinosaurs.

**Key words:** Dinosauria, Early Cretaceous, Ornithopoda, teeth, Tunisia

## Introduction

The Cretaceous fossil record of the dinosaurian clade Ornithischia underlines remarkable disproportion between Northern and Southern hemispheres: such bias is related to a number of factors, including historical collections and major differences in ecosystems and associated taphonomic parameters. Within Gondwanan landmasses, South America bears the richest diversity of ornithischian taxa, whereas they are surprisingly scarce in Africa (Taquet, 1976; Cooper, 1985; Taquet and Russell, 1999; Weishampel et al. 2004; Maidment et al., 2008; Galton, 2009; Contessi, 2013). Specifically, the mid-Cretaceous record of ornithischian dinosaurs from northern Africa is limited to three taxa discovered in the Echkar Formation of Niger: the dryosaurid *Elhrazosaurus nigeriensis* (Galton, 2009), the large-bodied ankylopollexians *Lurdusaurus arenatus* (Taquet and Russell, 1999), and *Ouranosaurus nigeriensis* (Taquet, 1976). Here, we describe new iguanodontian teeth from the Lower Cretaceous of the Tataouine Governorate (Fig. 1), adding further information on the diversity and distribution of North African ornithischians. The integration of detailed stratigraphic and sedimentological data

for the mid-Cretaceous of Tunisia provide pivotal tools to discuss the paleoecological significance of isolated remains in the Saharan regions.

### **Comparative Material**

Isolated ornithopod teeth and jaw fragments are relatively common in the Lower Cretaceous beds of Gadaofaoua, Niger, although the literature lacks detailed and comprehensive analyses on the dentition of the recovered taxa. Furthermore, as the vast majority of these specimens were surface collected, pivotal information as detailed stratigraphic occurrence, taphonomy of localities, and co-occurrence of other taxa, is missing. The sole specimens of *Elhrazosaurus nigeriensis* and *Lurdusaurus* are devoid of complete skull and teeth (Taquet and Russell, 1999; Galton, 2009), and those of *Ouranosaurus* lack detailed information on teeth and variability along the dental series (Taquet, 1976). For this study, we compared the Tunisian material to 14 isolated teeth as well as several lower jaw fragments with *in situ* teeth hosted at the National History Museum in Paris and four isolated teeth housed in the Natural History Museum in Venice collected at the Gadaofaoua locality.

In 1960, De Lapparent reported on an isolated tooth from the Jebel Kambout locality near the town of Remada in the Tataouine Governorate of southern Tunisia (named *Gara Kanboute* in the manuscript) and referred it to *Iguanodon*. The Jebel Kambout locality, located approximately 75 km to the south of Tataouine, has been lately the subject of detailed stratigraphic and paleontological studies (Fanti et al., 2012) allowing the referral of the specimen described by De Lapparent to a specific stratigraphic unit. In fact, De Lapparent (1960, p. 13) states that the tooth was collected '*at the top of the continental*

*series, only several meters under the marine Cenomanian* [English translation from the original French manuscript]: based on measured field sections at the Jebel Kambout locality, we refer the tooth to the upper deposits of the Albian Oum ed Diab Member (Fanti et al., 2012, 2015). Unfortunately, the author provided only a brief description supported by a single photograph of the specimen in lingual view (De Lapparent, 1960, Plate V, fig. 23). The tooth, currently housed in the National History Museum in Paris (MNHN.F.HGN167) has a preserved crown approximately 40 mm long apicobasally and 20 mm wide mesio-distally.

*Institutional abbreviations:* **GAD**, Gadaofaoua locality (Niger) as in the collections of the National History Museum in Paris; **MGGC**, Museo Geologico Giovanni Capellini, Bologna, Italy; **ONM**, Office National des Mines, Tunis, Tunisia.

### **The Oum Ed Diab Member**

Specimens described in this study are representative of five different localities covering latitudinally more than 100 km in the Tataouine Basin of southern Tunisia (Fig. 1). In the Tataouine Basin, the Albian Aïn el Guettar Formation displays variation in terms of facies and overall thickness from north to south (Fanti et al., 2012). Major stratigraphic gaps are represented at the base of both the Chenini and the Oum ed Diab members: the former represents a regional, angular, erosive unconformity, whereas the latter has been interpreted as a transgressive surface responsible for a mixed faunal assemblage representative of both units. The deposition of the Oum ed Diab estuarine/coastal deposits on top of the coarse, *wadi*-like, alluvial plain beds of the Chenini Member marks a major

variation in the paleoecologic – and consequently taphonomic – conditions in the Aptian of Tunisia. With the exception of one tooth possibly representative of the Chenini Member (*sensu* Fanti et al., 2012), they pertain to the sandy deposits of the Oum ed Diab Member of the Aïn el Guettar Formation. Stratigraphic and biostratigraphic data from the study area allowed referral of the Oum ed Diab Member and coeval lateral units to the Albian. The deposition of this unit is interpreted as the result of high-rate accumulation of siliciclastic deposits in a vast estuarine to embayment environment dominated by arid to xeric climatic conditions (Fanti et al., 2014a, b, 2015). This unit is remarkably rich in well-preserved vertebrate remains and it is bounded at the base by a transgressive lag deposit that yielded a diverse fauna that includes elasmobranchs, bony fish taxa, crocodyliforms, and dinosaurs, including carcharodontosaurids, spinosaurids, abelisaurids, and titanosauriforms (Bouaziz et al., 1988; Benton et al., 2000; Cuny et al., 2004, 2010; Srarfi, 2006; Bodin et al., 2010; Fanti et al., 2014a, b). The overlying finer facies are dominated by crocodylian remains, spinosaurid theropods, and rebbachisaurids (i.e. *Tataouinea hannibal*s, Fanti et al., 2013, 2015, and isolated remains referable to the latter). Vertebrate fossils are almost exclusively disarticulated or isolated, although the fine preservation of microvertebrates as well as larger elements is not consistent with prolonged pre-burial transport of elements.

### **Systematic Palaeontology**

Dinosauria Owen, 1842

Ornithischia Seeley, 1888

Ornithopoda Marsh, 1881

Iguanodontia Dollo, 1888

Hadrosauroidea Cope, 1869

Gen. et sp. indet.

### **ONM NG OR1**

**Locality and Horizon:** ONM NG OR1 was surface collected during prospecting activities south-west of the El Mra locality, approximately 50 km south of the city of Tataouine (Fig. 1B). The tooth was recovered approximately 10 meters above the Chenini/Oum ed Diab contact. In addition to the ornithopod tooth, the locality yielded skull elements referred to the actinistian *Mawsonia* sp., isolated crocodylian teeth and osteoderms, and a large sauropod humerus about 90 cm long.

**Description:** ONM NG OR1 is an isolated dentary tooth missing most of the root and the distal margin of the crown apex (Fig. 2A-D). The preserved crown is 40 mm apicobasally high (the total height of the tooth is 51 mm) and 26 mm mesiodistally wide, giving a height-to-width ratio of 1.6. The diamond-shaped crown is mesiodistally expanded with a wide, flattened lingual surface. Enamel is limited to the lingual side of the crown and to the marginal denticles. Both mesial and distal surfaces of the labial face are slightly concave. A primary ridge runs along the entire height of the crown, displaced slightly distally relative to the center of the lingual surface, demarcating two relatively deep sulci and dividing the surface in two unequal parts. Four shallow, secondary ridges, one located distally and three mesially relative to the primary ridge, extend parallel to the primary one along the enameled surface. Denticles are present on both mesial and distal crown margins, with 19 present along the distal margin and 11 along the mesial margin. Denticles are almost hook-like, recurved toward the apex of the crown, and oriented at approximately 25° to the

apicobasal axis of the crown. They are also graded in size, being smaller toward the base of the crown. Marginal denticles do not display mammillae, although a restricted number show a faint apical bifurcation. Although incomplete, it is possible to distinguish a mammillated apical margin with no clear denticle development. The basal end of the distal margin of the labial surface is thickened by a distinct lip that is ornamented by very slight tubercle only on its apical end. The lingual surface of the tooth is broad and smooth. Overall, cross-sections measured at different levels of the crown (Fig. 3) are asymmetrically concave (D-shaped), whereas the basal cross-section is sub-circular becoming almost circular with a prominent concavity in the mesial margin, possibly related to the position of a replacement tooth.

## **ONM NG OK 29**

**Locality and Horizon:** ONM NG OK 29 was originally reported by Srarfi (2006) as representative of the rich vertebrate diversity of the Oued El Khil locality (see also Benton et al., 2000; Fanti et al., 2012; Fig. 1B). The tooth was surface collected from the coarse-grained deposits historically interpreted as the Chenini Member (Srarfi, 2006); however, such beds have been reassigned to the Oum ed Diab Member and specifically to a transgressive lag that marks the base of the unit on a basin scale (Fanti et al., 2012). Lacking detailed information on the stratigraphic occurrence of ONM NG OK 29, it is not possible to discriminate if the tooth was collected from the basal lag, thus the possibility that the specimen pertains to the underlying, lower Albian, fluvial deposits of the Chenini Member cannot be dismissed.

**Description:** Isolated dentary tooth lacking entirely the root, with enamel limited to the lingual side of the crown and to the marginal denticles (Fig. 2E-H). The crown is 51 mm high and 29 mm wide, giving a height-to-width ratio of 1.75. The enameled crown is broad and diamond-shaped. Both mesial and distal surfaces of the labial face are slightly concave in lateral view. A primary ridge and three, secondary ridges run along almost the entire length of the crown. Small denticles are present on both mesial and distal crown margins, with eight present along the distal margin and three along the mesial margin.

### **MGGC TUN 153, 154 and 155**

**Locality and Horizon:** MGGC TUN 153, 154 and 155 (Fig. 4) were collected at the El Mra locality, approximately 50 km to the south of Tataouine and 5 km to the south of the Bir Amir village (Fanti et al., 2012, 2015) in the lower deposits of the Oum ed Diab Member, approximately five meters above the base of the unit (Fig. 1).

**Description:** MGGC TUN 154 (Fig. 4A, B) is a broken tooth missing the apical portion (Fig. 4). A broad and relatively flattened primary ridge runs along the entire length of the crown dividing the surface in two slightly asymmetric parts. The preserved crown is 14 mm long and 12 mm wide. Denticles are prominent and extend lingually forming a sharp wedge with the smooth and concave lingual surface. As in ONM NG OR1, the basal end of the distal margin of the labial surface is characterized by a prominent lip ornamented by small tubercles apically. MGGC TUN 155 is a relatively large, broken tooth with the primary ridge preserved (Fig. 4C). MGGC TUN 153 (Fig. 4E) is a partial crown of a relatively large tooth, comparable in size with ONM NG OR1. A total of 11 denticles are present on the preserved right crown margin showing a decrease in size toward the base

of the tooth. The apical portion of the denticles is worn, thus it is not possible to identify the presence of mammillae nor apical bifurcation.

### **MGGC TUN 156 and 157**

**Locality and Horizon:** MGGC TUN 156 and 157 were surface collected at the Oum Ed Diab section (Fig. 1B), located 60 km to the south of Tataouine (Fanti et al., 2012). Teeth were collected 26 meters above the Chenini/Oum ed Diab contact, and roughly 30 meters below the Cenomanian marls.

**Description:** both teeth are broken but show two well-developed ridges on the lingual surface (Fig. 4). Despite the fact that MGGC TUN 156 and 157 do not allow informative analyses on the overall morphology of the crown, they provide the opportunity to describe inner histological features.

### **Tooth histology features**

Erickson et al. (2012) and Erickson and Zelenitzky (2014), documented dental organization and tissue distribution in *Edmontosaurus* sp. and *Hypacrosaurus stebingeri* teeth from North America, providing useful tools to describe histological and topographical features in hadrosaurid dinosaurs (see also Erickson and Druckenmiller, 2011). As comparable data are not available in the literature for more basal forms, the Tunisian material offers the opportunity to document such features in African iguanodontians (Fig. 5). Although the sample is limited and partial, thus precluding analyses on individual or ontogenetic variability, it is possible to document variations in the relative development of

tissues within the discussed teeth. Following the terminology of Erickson et al. (2012), all teeth display a thick enamel and well developed longitudinal (lgt) and transverse (tgt) giant tubules, the latter commonly forming a curtain-like structure of juxtaposed tubules. MGGC TUN 154 is the smallest among the discussed samples and displays a combination of large, longitudinal giant tubules in the central region delimited by a relative thick enamel (Fig. 5A). MGGC TUN 157 displays a predominance of lgt although faint, tgt develop marginally toward the buccal surface (Fig. 5B). MGGC TUN 155 and 156 have a thick enameled margin and minor lgt confined in the central region of the tooth, whereas tgt are easily identifiable forming well developed, curtain-like structures on the buccal margin. Finally, MGGC TUN 153 lacks lgt, with the tooth characterized by transverse and curtain-like tubules extending radially to the enamel (Fig. 5E). The relative distribution of tgt and lgt seems to reflect size-related variations, with a predominance of longitudinal giant tubules in smaller teeth and inversely well-developed transverse tissues in larger specimens. Although intra- and inter-specific variations cannot be excluded, this trend most likely reflects ontogenetic modification in the tooth structure in order to support variations in feeding habits.

## **Discussion**

Both ONM NG OR1 and ONM NG OK 29 are referred to the dentary series of large-bodied ornithopods, due to the broad diamond shape of the lingual surface, differing from the relatively slender, lozenge-shaped outline present in maxillary crowns of these dinosaurs. The robust, primary ridge slightly displaced distally relative to the crown apicobasal axis is a derived feature of Iguanodontia among ornithopods (Norman, 2004;

McDonald et al., 2010; McDonald, 2011). The relatively high crown, the not markedly robust primary ridge and the absence of several secondary ridges all oriented apicobasally exclude a referral to a “rhabdodontid-grade” form such as *Tenontosaurus* (Thomas, 2015) and *Zalmoxes* (Weishampel et al., 2003). Among iguanodontians, the mammillate shape of the marginal denticles is a synapomorphy of taxa closer to hadrosaurids than *Camptosaurus* and *Dakotadon* (McDonald, 2011; Boyd and Pagnac, 2015). We exclude the referral to the subclade of Hadrosauroidea including hadrosaurids and *Probactrosaurus* due to the relatively broad proportion of the crowns, the latter being more slender in derived taxa with more numerous and closely spaced teeth (Norman, 2002). In overall shape and proportions, these teeth are comparable to those of many iguanodontid-grade forms, in particular *Ouranosaurus*, *Iguanodon*, and *Altirhinus* (e.g., Norman, 1980, 1996). Not surprisingly, a comparison with a nicely preserved tooth referred to *Ouranosaurus nigeriensis* from Gadaofaoua (GAD301; Taquet, 1976) reveals relevant similarities between the latter and the Tunisian specimens (Fig. 6). The best-preserved tooth, ONM NG OR1 shows a combination of features intermediate between basal ankylopollexians and taxa closer to hadrosaurids. In particular, both secondary and tertiary ridges are poorly marked, contrasting with more basal “iguanodontid-like” taxa that bear a more robust set of accessory ridges (Norman, 1980). Furthermore, the distal basal lip on the crown is only weakly denticulated, being almost completely devoid of tubercles: this combination of features is intermediate between basal ankylopollexians, bearing a more extensive serration of the lip, and the “hadrosaurid-like” forms that lack any denticulation of the lip (Wu and Godefroit, 2012).

The paucity of the material prevents us for discussing variation along both the same tooth series and among the individual sample, thus, we have not tested quantitatively (i.e.,

using a numerical cladistics analysis) the affinities of the specimens, which are provisionally referred to large bodied non-hadrosaurid hadrosauriforms.

### **Stratigraphic and paleoecologic occurrence**

Previous studies in southern Tunisia documented direct correlations between paleoecological variations and occurrence of dinosaur and crocodyliform taxa in the Aïn el Guettar Formation (Fanti et al., 2013). Specifically, abelisauroids, carcharodontosaurids, titanosauriforms and rare rebbachisaurids are confined to the Chenini Member, whereas spinosaurids, rebbachisaurids and crocodylians are predominant in the Oum ed Diab Member, where fish remains also represent a major component of the fauna (Fanti et al., 2014b). Although fragmentary and represented solely by teeth, ornithopod remains from Tunisia, with the sole possible exception of ONM NG OK 29, are strictly representative of the Oum ed Diab Member. Of note, specimens described in this study are representative of localities that cover approximately 100 km along the Tataouine basin, but also occur in discrete beds stratigraphically spanning the entire Member. Therefore, ornithopods are here considered as part of the Albian Oum ed Diab Member, in association with rebbachisaurids (i.e. *Tataouinea hannibalis*), spinosaurids (including both Baryonychinae and Spinosaurinae), and crocodyliforms, including the large-bodied *Sarcosuchus* (Fanti et al., 2013, 2014b). The Aptian beds of the renowned Gadaofaoua locality in Niger represent the best basis for comparison with the Tunisian material. A postulated inland floodplains habitat rich in plant resources associated with both lacustrine and sandy, high-energy river systems for Gadaofaoua (Serenio et al., 2001, 2007) contrasts with paleoecological reconstructions proposed for the Aïn el Guettar Formation. The fluvial Chenini beds are

representative of a *wadi*-like, high-energy river systems: the lack of fossilized vertebrates and plants within this member may therefore reflect unfavorable taphonomic conditions. Conversely, the marginal marine deposits of the Oum ed Diab Member indicate deposition under arid to xeric climatic conditions, thus inadequate to support a megaherbivore fauna. From a taphonomic perspective, specimens recovered in the Oum ed Diab Member, with the sole exception of the exquisitely preserved skeleton of the rebbachisaurid *Tataouinea hannibalis* collected at the El Mra locality (Fanti et al., 2015), are systematically disarticulated. However, all bony elements display negligible wearing and the preservation of micro- and macro-fossils is remarkable. For instance, teeth described here commonly display clean and recent breakage surfaces but no evidence of wearing nor abrasion on the external surfaces. Ornithopod teeth, however, are relatively large, stocky, and most likely less affected by transportation-related abrasion. The Oum ed Diab, marginal-marine facies represent the downstream section of most likely a much wider drainage system that transferred sediments and vertebrate remains from the Saharan regions into the peri-Mediterranean coastal area. Consequently, the faunal assemblage recorded in the Oum ed Diab Member most likely gather taxa that originally pertained to more discrete and ecologically confined areas. As such, isolated elements historically collected from the Saharan regions may be affected by this taphonomic bias, thus limiting or diverting our comprehension of their paleogeographic and paleoecologic distribution.

Based on observations on the Chenini deposits in the northern section of the Tataouine Basin, Benton et al. (2000) hypothesized the development of giant fluvial systems in northern Africa during the Early Cretaceous responsible for the transportation over hundreds of kilometers of terrestrial remains from the south in present-day southernmost Algeria. However, data provided in Fanti et al. (2012) challenged this

interpretation: paleoflows from the Chenini and Oum ed Diab members indicate a predominant north-west flows direction and a depocenter located westerly to the present day Jeffara Escarpment, suggesting a possible source area for both sediment and taxa in central and southern Libya (Fanti et al., 2012).

## **Conclusions**

The fossil record of ornithischian dinosaurs from Tunisia is particularly scarce, compared to the richer record of other archosaurian clades (e.g., saurischians and crocodylomorphs; Fanti et al., 2012, 2013, 2014a, b, *in press*), and reflects a general paucity of members of this clade from Africa (Weishampel et al., 2004). All known material pertains to isolated teeth of large-bodied iguanodontid-grade iguanodontians. From these units, no material pertaining to other ornithischian clades, to non-dental elements or to small-bodied individuals has been reported so far. Although distributed over 100 km along the Tataouine region, ornithischian remains appear constrained to the Oum ed Diab Member. This peculiar preservational bias indicates a set of selective taphonomic causes for the fossil distribution of ornithischians in southern Tunisia.

## **Acknowledgements**

This research was supported by the National Geographic Society (grant 9586-14), Museo Geologico G. Capellini (Bologna) and Office National des Mines (Tunis). This manuscript benefited from discussion with D. Evans (Royal Ontario Museum, Toronto). ONM NG OR1 was recovered by J. Carlet during prospecting activities in 2014. We thank

the other members of the 2014 Italian-Tunisian palaeontological expedition in the Tataouine Governorate, in particular, J. Dridi, F. Mnasri, H. Aljane, M. Hassine, L. Angelicola, A. Bacchetta, S. Cafaggi, J. Carlet and G. Mignani. We thank R. Allain (Muséum national d'Histoire naturelle, Paris), B. Favaretto and M. Bon (Museo di Storia Naturale, Venice) and M. Casarin (Centro Studi e Ricerche Ligabue, Venice) for the access to specimens in their care. Photos of specimens were taken by F.F. and P. Ferrieri.

## References

- Benton MJ, Bouaziz S, Buffetaut E, Martill D, Ouaja M, Soussi M, et al. (2000). Dinosaurs and other fossil vertebrates from fluvial deposits in the Lower Cretaceous of southern Tunisia. *Palaeogeography, Palaeoclimatology, Palaeoecology* 157: 227–246.
- Bodin, S., Petitpierre, L., Wood, J., Elkanouni, I., & Redfern, J. (2010). Timing of early to mid-cretaceous tectonic phases along North Africa: new insights from the Jeffara escarpment (Libya–Tunisia). *Journal of African Earth Sciences* 58, 489–506.
- Bouaziz, S., Buffetaut, E., Ghanmi, M., Jaeger, J.J., Martin, M., Mazin, J., & Tong, H. (1988). Nouvelles découvertes de vertébrées fossiles dans l'Albien du Sud-Tunisien. *Bulletin Société Géologique de France* 8, IV, 335-339.
- Boyd, C.A., & Pagnac, D.C. (2015). Insight on the anatomy, systematic relationships and age of the Early Cretaceous ankylopollexian dinosaur *Dakotadon lakotensis*. *PeerJ* 3:e1263.[doi.org/10.7717/peerj.1263](https://doi.org/10.7717/peerj.1263).
- Contessi, M., (2013). A new dinosaur ichnofauna from Tunisia: Implications for the

palaeobiogeography of peri-Adriatic carbonate platforms in the mid-Cretaceous.

Palaeogeography, Palaeoclimatology, Palaeoecology 392, 302-311.

Cooper, M.R. (1985). A revision of the ornithischian dinosaur *Kangnasaurus*

*coetzeei* Haughton, with a classification of the Ornithischia. Annals of the South African Museum 95: 281–317.

Cuny, G., Ouaja, M., Sraf, D., Schmitz, L., Buffetaut, E., & Benton, M.J. (2004). Fossil sharks from the Early Cretaceous of Tunisia. *Revue de Paleobiologie* 9, 127–142.

Cuny, G., Cobbett, A., Meunier, F., & Benton, M. (2010). Vertebrate microremains from the Early Cretaceous of southern Tunisia. *Geobios* 43, 615–628.

De Lapparent, A.F. (1960). The Dinosaurs of the '*Continental Intercalaire*' of the Central Sahara. *Memoirs of the Geological Society of France*, Vol XXXIX, 60 pp.

Erickson, G., & Druckenmiller, P. (2011). Longevity and growth rate estimates for a polar dinosaur: a *Pachyrhinosaurus* (Dinosauria: Neoceratopsia) specimen from the North Slope of Alaska showing a complete developmental record. *Historical Biology* 2011, 9 pp. DOI: 10.1080/08912963.2010.546856

Erickson, G., & Zelenitsky, D. (2004). Osteohistology and occlusal morphology of *Hypacrosaurus stebingeri* teeth throughout ontogeny with comments on wear-induced form and function. In D. Eberth, D. Evans (Eds.), *Hadrosaurs*. Indiana University Press, Bloomington & Indianapolis, pp. 422-432.

Erickson, G., Krick, B., Hamilton, M., Bourne, G., Norell, M., Lilleodden, E., & Sawyer, G. (2012). Complex dental structure and wear biomechanics in hadrosaurid dinosaurs. *Science Reports* 338, 98-101.

Fanti F, Cau A, Hassine M, & Contessi M. (2013). A new sauropod dinosaur from the Early

Cretaceous of Tunisia with extreme avian-like pneumatization. *Nature Communications* 4:2028, 7 pp. doi: 10.1038/ncomms3028

Fanti F, Contessi M, & Franchi F. (2012). The '*Continental Intercalaire*' of southern Tunisia: stratigraphy, paleontology, and paleoecology. *Journal of African Earth Sciences* 73–74:123.

Fanti F, Cau A, & Hassine M. (2014a). Evidence of titanosauriforms and rebbachisaurids (Dinosauria: Sauropoda) from the Early Cretaceous of Tunisia. *Journal of African Earth Sciences* 90: 1–8.

Fanti F, Cau A, Martinelli A, & Contessi M. (2014b). Integrating palaeoecology and morphology in theropod diversity estimation: A case from the Aptian-Albian of Tunisia. *Palaeogeography, Palaeoclimatology, Palaeoecology* 410: 39–57.

Fanti F, Cau A, Cantelli L, Hassine M, & Auditore M. (2015). New Information on *Tataouinea hannibalis* from the Early Cretaceous of Tunisia and Implications for the Tempo and Mode of Rebbachisaurid Sauropod Evolution. *PLoS ONE* 10 (4): e0123475. doi:10.1371/journal.pone.0123475.

Fanti F., Miyashita T., Cantelli L., Mnasri F., Dridi J., Contessi M. & Cau A. *in press*. The largest Thalattosuchian (Crocodylomorpha) supports Teleosaurid survival across the Jurassic-Cretaceous boundary. *Cretaceous Research* doi:10.1016/j.cretres.2015.11.011.

Galton, P.M. (2009). Notes on Neocomian (Late Cretaceous) ornithomimid dinosaurs from England – *Hypsilophodon*, *Valdosaurus*, "*Camptosaurus*", "*Iguanodon*" – and referred specimens from Romania and elsewhere. *Revue de Paléobiologie* 28 (1): 211–273.

- Maidment, S.C., Norman, D.B., Barrett, P.M., & Upchurch, P. (2008). Systematics and phylogeny of Stegosauria (Dinosauria: Ornithischia). *Journal of Systematic Palaeontology* 6: 367-407.
- McDonald, A. T. (2011). The taxonomy of species assigned to *Camptosaurus* (Dinosauria: Ornithopoda). *Zootaxa* 2783: 52–68.
- McDonald, A.T., Kirkland, J.I., DeBlieux, D.D., Madsen, S.K., Cavin, J., Milner, A.R.C., Panzarin, L. (2010). New Basal Iguanodontians from the Cedar Mountain Formation of Utah and the Evolution of Thumb-Spiked Dinosaurs. *PLoS ONE* 5 (11): e14075.
- Norman, D. B. (1980). On the ornithischian dinosaur *Iguanodon bernissartensis* of Bernissart (Belgium). *Mémoires de l'Institut Royal des Sciences Naturelles de Belgique* 178: 1–105.
- Norman, D.B. (1996). On Asian ornithopods (Dinosauria, Ornithischia). 1. *Iguanodon orientalis* Rozhdestvensky, 1952. *Zoological Journal of the Linnean Society*. 116: 303-315.
- Norman D.B. (2002). On Asian ornithopods (Dinosauria: Ornithischia). 4. *Probactrosaurus* Rozhdestvensky, 1966. *Zoological Journal of the Linnean Society* 136(1): 113-144.
- Norman, D. B. (2004). Basal Iguanodontia. In Weishampel, D.B., Dodson, P., and Osmólska, H. (eds.). *The Dinosauria* (2nd ed.). Berkeley: University of California Press. pp. 413–437.
- Sereno, P.C., Larsson, H.C., Sidor, C.A., & Gado, B. (2001). The giant crocodyliform *Sarcosuchus* from the Cretaceous of Africa. *Science* 294: 1516-1519.
- Sereno, P.C., Wilson, J., Witmer, L., Whitlock, J., Maga, A., Ide, O., & Rowe, T. (2007). Structural extremes in a Cretaceous dinosaur. *PLoS ONE* 2(11): e1230.  
doi:10.1371/journal.pone.0001230

- Srarfi, D. (2006). Biostratigraphie, biodiversité, taphonomie and paleoenvironnement des niveaux a vertébrées du Jurassique-Crétacé du Sud-Est de la Tunisie. Implications paleobiogeographiques. PhD Thèses, Université Claude Bernard Lyon 1.
- Taquet, P. (1976). Géologie et Paléontologie du Gisement de Gadoufaoua (Aptien du Niger). Cahiers de paléontologie. Editions du Centre National de la Recherche Scientifique, Paris, France, 191 pp.
- Taquet, P., & Russell, D.A. (1999). A massively-constructed iguanodont from Gadoufaoua, Lower Cretaceous of Niger. *Annales de Paléontologie* 85 (1): 85–96.
- Thomas, D. A. (2015). The cranial anatomy of *Tenontosaurus tilletti* Ostrom, 1970 (Dinosauria, Ornithopoda). *Palaeontologia Electronica* 18.2.37A: 1-99.
- Weishampel, D.B., Barrett, P.M., Coria, R.A., Le Loeuff, J., Xu, X., Zhao, X., Sahni, A., Gomani, E.M.P., & Noto, C. (2004). Dinosaur distribution. In: Weishampel, David B.; Dodson, Peter; and Osmólska, Halszka (eds.): *The Dinosauria*, 2nd, Berkeley: University of California Press. Pp. 517-606.
- Weishampel, D.B., Jianu, C.-M., Csiki, Z., & Norman, D.B. (2003). Osteology and phylogeny of *Zalmoxes* (n. g.), an unusual euornithopod dinosaur from the Latest Cretaceous of Romania. *Journal of Systematic Palaeontology* 1 (2): 65-123.
- Wu, W., & Godefroit, P. (2012). Anatomy and relationships of *Bolong yixianensis*, an Early Cretaceous iguanodontoid dinosaur from western Liaoning, China. In: P. Godefroit (ed.): *Bernissart dinosaurs and Early Cretaceous terrestrial ecosystems*. Bloomington: Indiana University Press. 293–333.

Figures

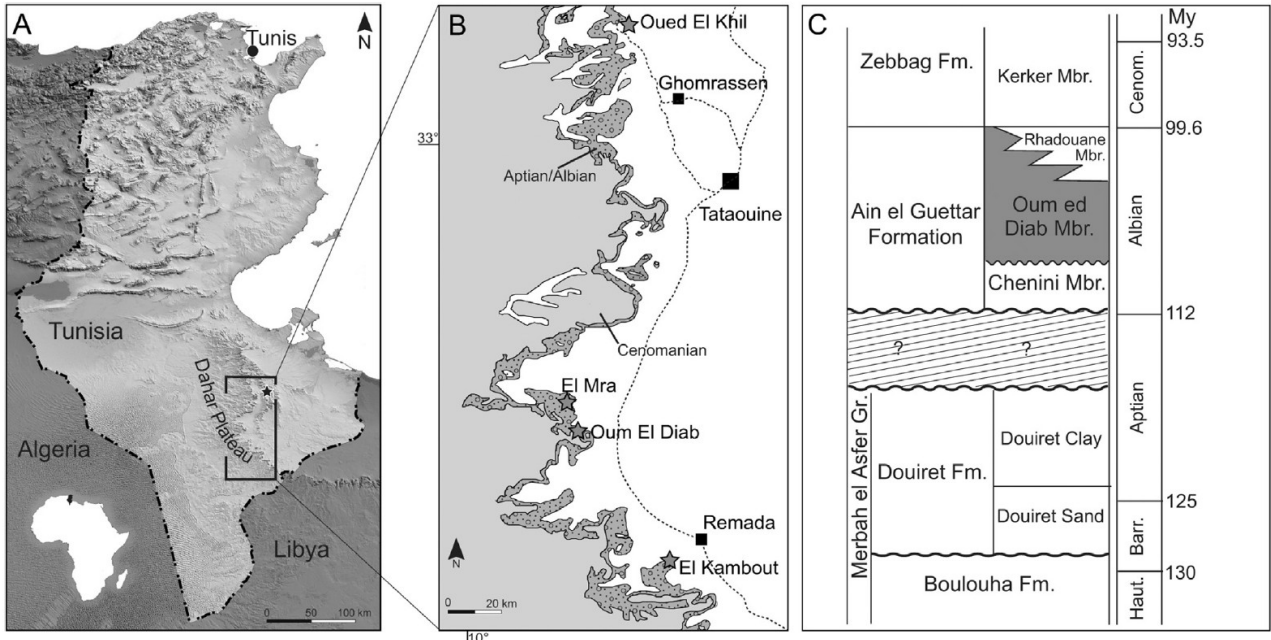


**Figure 1:** A, present day reference map of Tunisia showing the location of the Tataouine Basin. B, locality map showing the mid-Cretaceous outcrops located along the prominent Jeffara Escarpment. Stars indicate localities discussed in the text. C, stratigraphic nomenclature and chrono-stratigraphic subdivision for the Cretaceous beds in the study area. Specimens described here were collected from the Albian Oum ed Diab Member.

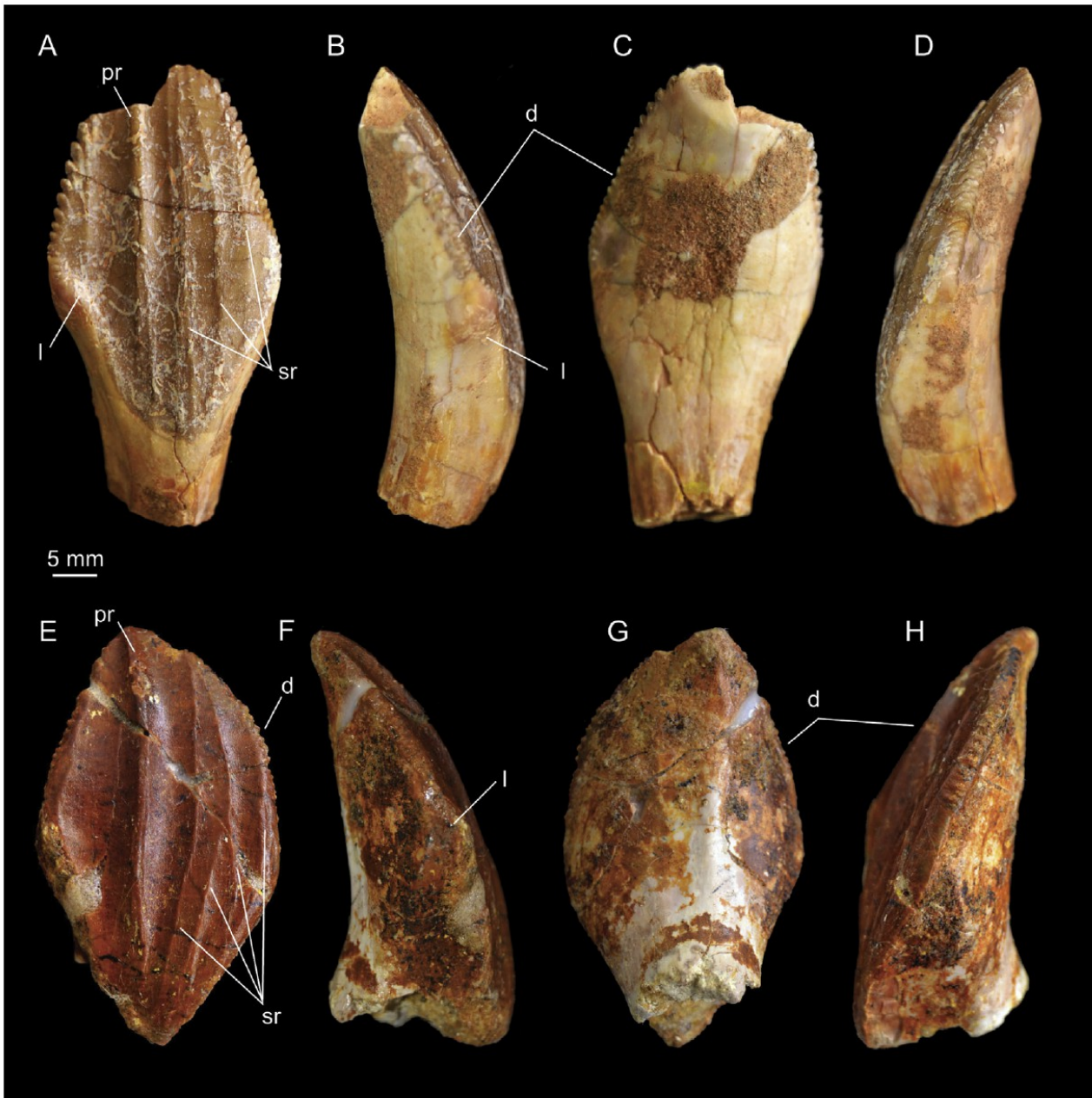


**Figure 2:** ONM NG OR1 in lingual (A), distal (B), labial (C) and mesial (D) views. ONM NG OK 29 in lingual (E), distal (F), labial (G) and mesial (H) views. Abbreviations: d, denticles; l, baso-distal lip; pr, primary ridge; sr, secondary ridge.

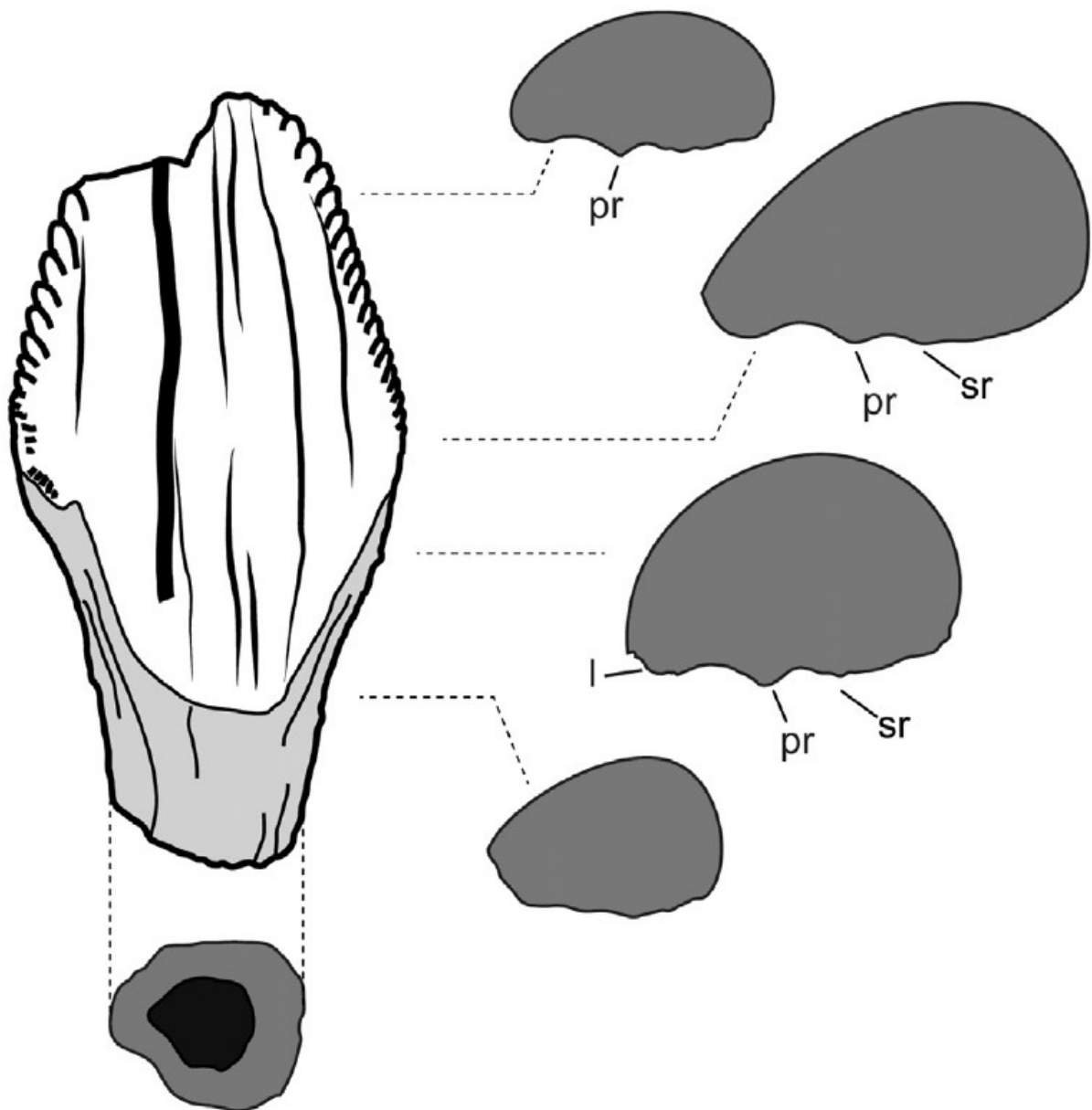


**Figure 3:** Schematic drawing of ONM NG OR1 showing variation in cross-section along the apico-basal axis. Abbreviations: l, baso-distal lip; pr, primary ridge; sr, secondary ridge.

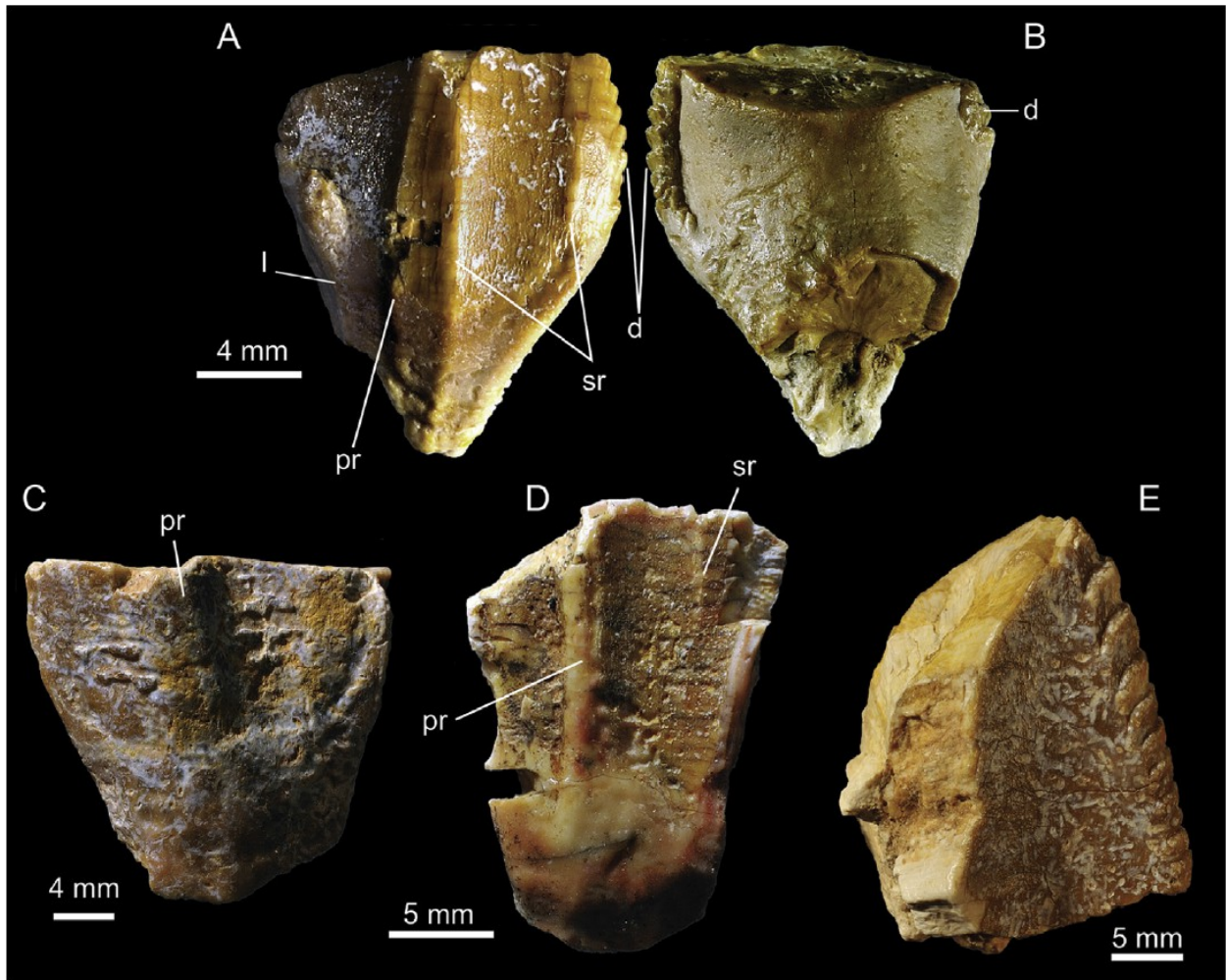


**Figure 4:** MGGC TUN 154 in lingual (A) and labial (B) views. C, MGGC TUN 155 in lingual view. D, MGGC TUN 157 in lingual view. E, MGGC TUN 153 in lingual view. Abbreviations: d, denticles; l, baso-distal lip; pr, primary ridge; sr, secondary ridge.

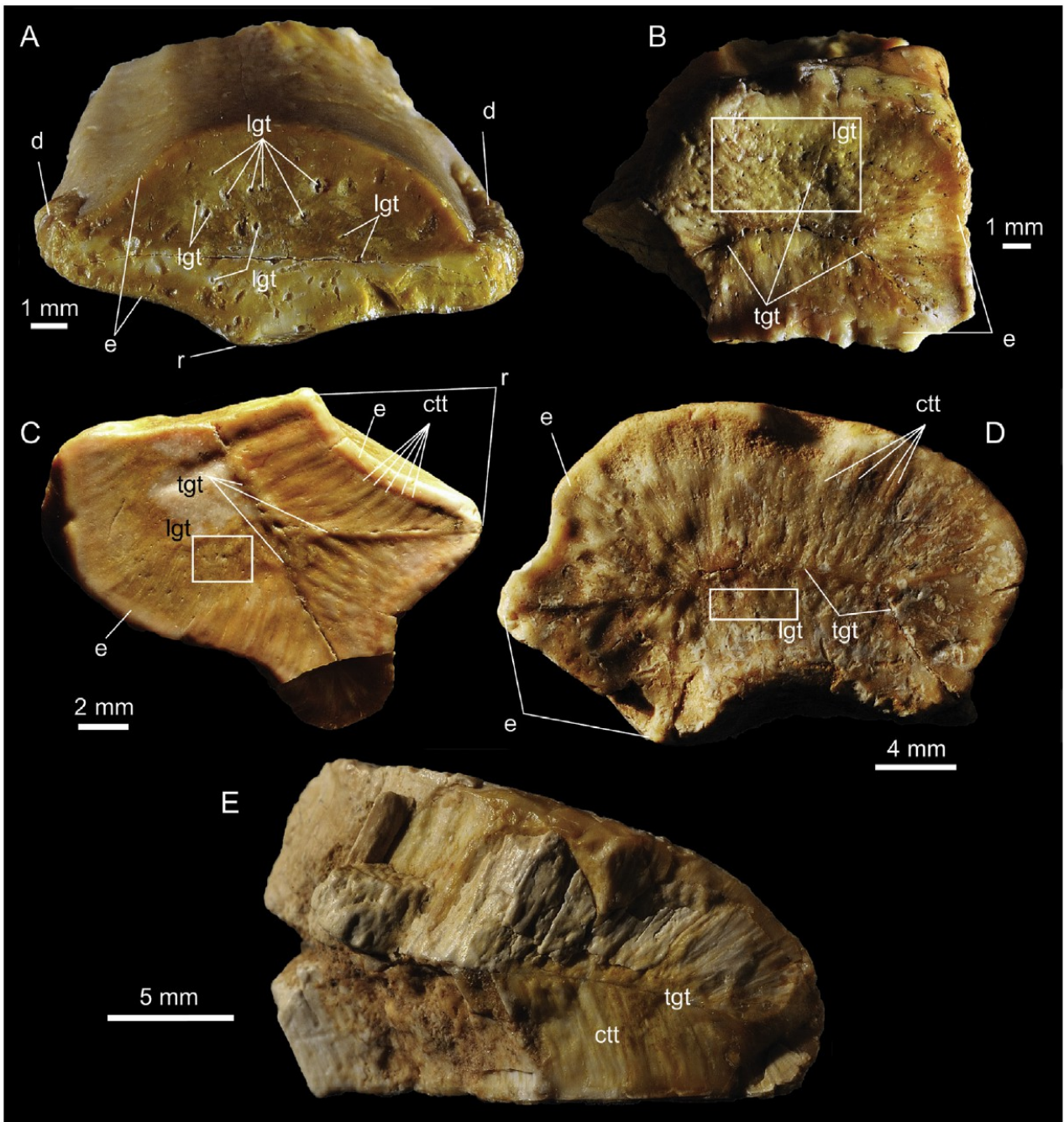


**Figure 5:** Transversal sections of iguanodontian teeth from Tunisia showing different pattern of dental organization. A, MGGC TUN 154; B, MGGC TUN 157; C, MGGC TUN 156; D, MGGC TUN 155; E, MGGC TUN 153. Abbreviations: ctt, curtain transverse tubules; d, denticles; e, enamel; lgt, longitudinal transversal tubules; r, ridge; tgt, transverse giant tubules.

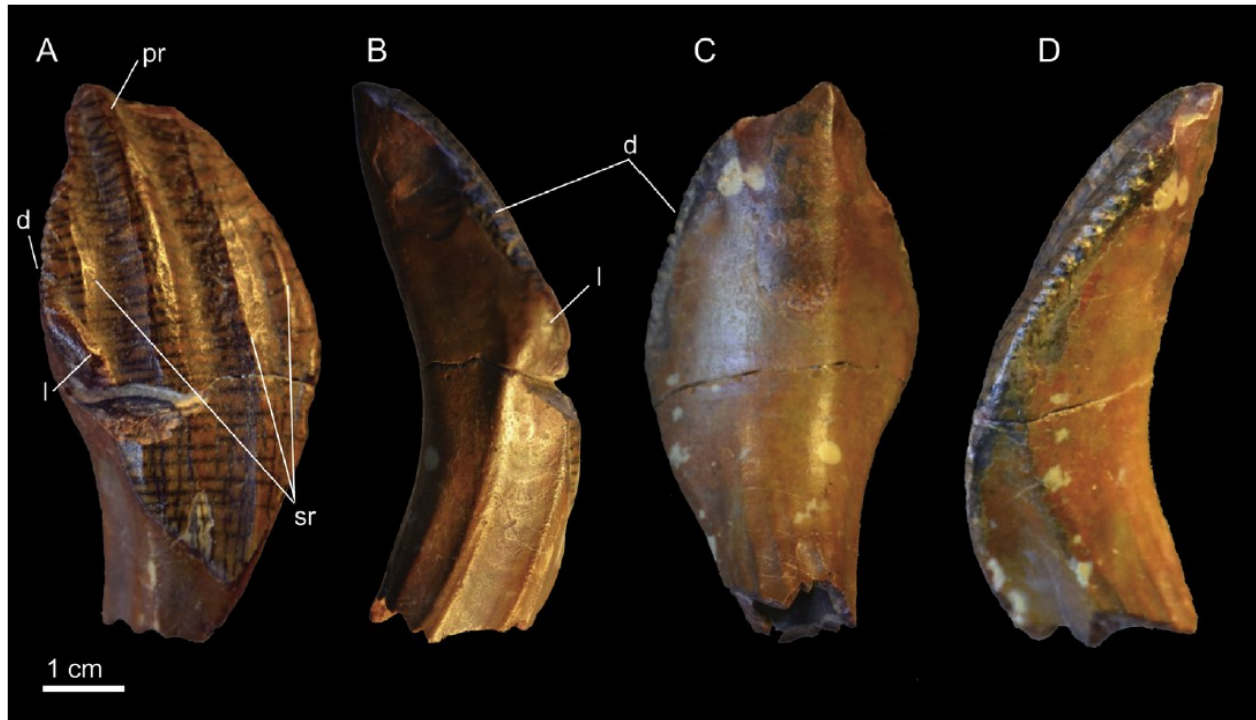


**Figure 6:** GDF301, left dentary tooth referred to *Ouranosaurus nigeriensis* from Gadofaoua (Taquet, 1976, plate XX, Fig. 2a). Abbreviations: d, denticles; l, baso-distal lip; pr, primary ridge; sr, secondary ridge.

Page left blank

## **CHAPTER 4 - Sustained miniaturization and anatomical innovation in the dinosaurian ancestors of birds**

Submitted: 14<sup>th</sup> February 2014. Published: 01<sup>st</sup> August 2014 in *Science* vol. 345:562-566.

Michael S.Y. Lee, Andrea Cau, Darren Naish, Gareth Dyke

**Recent discoveries have highlighted the dramatic evolutionary transformation of massive, ground-dwelling theropod dinosaurs into light, volant birds. Here we apply Bayesian approaches (developed for inferring geographic spread and rates of molecular evolution in viruses) in a novel context: to infer size changes and rates of anatomical innovation (across up to 1549 skeletal characters) in fossils. These approaches identify two drivers underlying the dinosaur-bird transition. The theropod lineage directly ancestral to birds undergoes sustained miniaturisation across 50 million years and at least 12 consecutive branches (internodes), and evolves novel skeletal adaptations four times faster than seen in other dinosaurs. The unique, prolonged phase of miniaturization along the bird stem would have facilitated the evolution of many novel adaptations associated with small body size, such as reorientation of body mass, increased aerial ability, and pedomorphic skulls with enlarged eyes and brains but reduced snouts.**

The evolution of birds from bipedal carnivorous dinosaurs is now one of the most compelling examples of macroevolution (1-7). The cumulative evolution of avian characteristics along the ~160my lineage from large Triassic theropods (oldest widely-accepted records *Herrerasaurus* and *Eodromaeus* ca. 230myo) leading to modern birds (Neornithes; oldest widely-accepted record *Vegavis* ca. 67myo) has been extensively documented (1-18). However, there remain many intriguing questions regarding size evolution and anatomical innovation along the bird stem lineage. Theropods were typically large to gigantic, but small body size characterized all taxa near the origin of forewing-powered flight in birds (*Avialae sensu* 1-3, *Aves sensu* 15). It has been both proposed (4-8) and contested (9-11) that sustained trends of size reduction occurred within theropod

evolution. However, nearly all previous studies of size evolution along the bird stem lineage identified trends anecdotally, and employed undated cladograms or supertrees, along with parsimony-based character reconstructions (e.g. 4-9,14), which ignore vital temporal (branch length) information, potentially compromising accuracy (19). The only studies to use quantitative likelihood approaches in an explicitly temporal framework (15, 16) focused on identifying individual branches undergoing fast changes (e.g. Coelurosauria and Paraves: 6-8, 15-16) and thus did not evaluate directional trends (sustained miniaturization or gigantism) across consecutive branches. Furthermore, rates of anatomical innovation along the bird stem lineage remains vastly underexplored. Previous studies have evaluated evolutionary rates of a few continuous characters, such as limb proportions or body size (6,11,15,16,19). However, evolutionary innovation is arguably much better represented by the hundreds of discrete anatomical traits (from across the entire phenotype) that typically comprise large phylogenetic datasets. Surprisingly, no previous study of bird origins has quantified rates of evolution in these character-rich datasets.

Here, we identify unique evolutionary dynamics (sustained miniaturization and accelerated skeletal innovation) in the bird stem lineage, using the largest anatomical character set for dinosaurs compiled to date (120 taxa, 1549 characters including autapomorphies: Dataset 1, expanded from 20). We also analyzed a second matrix (Dataset 2: 100 taxa, 421 characters) which employs a smaller number of characters that has been heavily scrutinized by numerous workers (21, based on 8,22). Stratigraphic age and femur length was recorded for all adequately known taxa (Appendix 6). The femur is frequently preserved and scales more tightly with inferred body mass than any other measurement (23:  $r > 0.995$ ), exhibiting homogenous allometry at least within non-avian theropods (6). It is thus often used as a size proxy (e.g. 9,11,15,23), yielding estimates highly consistent with volumetric (14) and composite (16) estimates. Accordingly, we use femur length as a size proxy up to Avialae (but not beyond [6]: see SM part B); use of multi-measurement proxies would greatly reduce taxon sampling.

The anatomic, stratigraphic, and size data were simultaneously analyzed using novel implementations of Bayesian methods. BEAST (24) modules originally developed for inferring patterns of DNA evolution and geographic spread in "real time" virus samples

were adapted to infer patterns of anatomic evolution and size changes in the "deep time" fossil record. Bayesian Markov Chain Monte Carlo (MCMC) methods were then used to reconstruct – with confidence intervals – phylogenetic relationships, divergence dates, temporal duration of lineages, evolutionary rates across all 1549/421 morphological characters, and body size at every ancestral node. Our approach explicitly considers the temporal (stratigraphic) distribution of taxa when estimating all of these variables. Furthermore, all parameters were simultaneously estimated and thus jointly optimized. Such an approach has been argued to be better at finding global optima and estimating uncertainty (24,25), and is thus preferable to the sequential inference typical of earlier approaches (e.g. 4-10: inferring topology first, then sometimes inferring divergence dates, and then mapping size or some other trait:). A stochastic Markov model was then applied to the discrete character data, with Bayes factors favouring inclusion of parameters for among-trait ( $\gamma$ ) and among-lineage (relaxed clock) rate variation. An undirected Brownian motion model was applied to the continuous (size) data. Tests for directionality using PGLS as implemented in Bayestraits (26) (SM part D) confirmed no significant trends towards size increase or decrease across Theropoda as a whole (9,10,27: Fig. S7), while rate-heterogeneous diffusion models proved overparameterized (SM part C). The significance and robustness of retrieved patterns was corroborated using both: (1) Traditional parsimony methods for inferring phylogeny and ancestral body sizes (which have been argued to entail fewer assumptions but are consequently less powerful, and do not adequately measure uncertainty); and, (2) Parametric simulations (SM part E).

Body size, as proxied by  $\log_{10}$  femur length ( $FL_{10}$ ), is highly phylogenetically conserved across theropods (Fig. 1), and there is a prolonged, directional trend in size reduction within the clade that spans at least 50 Ma and encompasses the entire bird stem lineage from the very base of Theropoda, with rapid decreases in 12 consecutive branches from Tetanurae onwards (Fig. 2). The ancestral tetanuran is inferred to be ~198myo and ~163kg, and size then decreases along subsequent nodes as follows; neotetanurans / avetheropods (~174Ma, ~46kg), coelurosaurians (~173Ma, ~27kg), maniraptorans (~170Ma, ~10kg), paravians (~167.5Ma, ~3kg) and birds (~163Ma, ~0.8kg). A similar trend is found for Dataset 2:  $FL_{10}$  again continuously decreases across all bird stem nodes from Tetanurae onwards, and there are similar estimated ancestral sizes and divergence

dates for each of the above clades (Fig. S5). Simulations demonstrate that this trend is much greater than that expected given a null model of non-directionality across the entire tree ( $P < 0.05$ ; SM part E).

This pervasive trend towards smaller body size along the avian stem lineage is the result of a previously unnoticed pattern; the oldest representatives of successively closer outgroups to birds tend to be progressively smaller. In both datasets used here (Figs 1, S5), major tetanuran clades branch off the avian stem in this approximate order (e.g. 3-9, 16, 20, 21, 20); megalosauroids, allosauroids, tyrannosauroids, ornithomimosaur, alvarezsauroids, oviraptorosaurs, dromaeosaurids and troodontids. Among the taxa sampled here, the oldest megalosauroid (*Afrovenator*) and allosauroid (*Sinraptor*) with preserved femora are inferred to be ~900-1600kg, the oldest tyrannosauroid (*Guanlong*) and ornithomimosaur (*Harpymimus*) are ~100kg, the oldest alvarezsauroid (*Haplocheirus*) is ~17kg, the oldest oviraptorosaur (*Caudipteryx*) is ~5kg, the oldest troodontid (*Jinfengopteryx*) and other taxa near the base of birds (Avialae), such as *Archaeopteryx* and *Aurornis*, are consistently ~0.5kg. This size trend closely mirrors the phylogenetic arrangement of these clades along the bird stem, and is the primary pattern responsible for driving the trend of progressive size reduction in bird ancestors: the oldest taxon in each outgroup clade tends to be basal and exerts the strongest influence on the reconstructed body size in that part of the bird stem lineage, either because it is separated from the stem by chronologically short branch lengths (Bayesian Brownian motion model) or by few intervening nodes (parsimony reconstruction). Within most outgroup clades, there is concordance between phylogeny and stratigraphy (oldest taxa are generally basal: Fig. 1); this increases confidence in the phylogenetic results as well as body size reconstructions. Both datasets reveal uncertainty in basal paravian relationships (e.g. 20); notably, however, Bayesian MCMC methods, unlike most other methods (e.g. supertrees), fully integrate over such topological uncertainty (24,25).

Our study is the first comprehensive analysis of rates of evolutionary innovation in dinosaurs, using 1549/421 anatomical (mainly skeletal) traits distributed across the entire body. A clear pattern emerges: branches along the bird stem undergo substantially faster morphological evolution than do others. In Dataset 1, every branch along the avian stem between Neotetanurae and birds (Fig. 3) evolves at least twice as fast as the average

theropod "background" rate: their average rate of change is 0.0319, which equates to 3.19% divergence per lineage per Ma (range 1.96-5.33%), approximately four times as fast as the unweighted average branch rate across the entire tree (0.88% per lineage per Ma). In both datasets, rates are fastest in the middle region of the bird stem lineage, between the most recent common ancestors of Neotetanurae and Paraves; these peak rates are consistent with the near-simultaneous stratigraphic appearance (~160my) of several lineages in this part of the tree, notably Allosauroidea, Tyrannosauroidea, Compsognathidae, Alvarezsauroidea and Paraves. The same patterns are found in Dataset 2 (Fig. S6). They are also not artefacts of internal node age constraints, persisting in both datasets even if no age constraints (besides root age) are employed (SM part C). However, in such analyses the peak rates "spread out" onto more basal branches of the bird stem lineage.

Accelerated rates of innovation along the bird stem are potentially inflated by oversampling (by bird-centric researchers) of characters changing along the avian stem. However, there are three reasons suggesting that the strong rate patterns found here are at least partly real. First, our primary dataset (Dataset 1) attempted to avoid ascertainment bias by explicitly sampling characters across all branches of the theropod tree (including autapomorphies – not sampled in any previous studies). Second, Dataset 2 was largely constructed to infer relationships among alvarezsaurs (22) and thus likely over-sampled characters (and overestimated rates) within that relatively minor "side" clade: yet, nearly all the fastest branches in Dataset 2 are on the bird stem. Third, Bayesian approaches "dampen" perceived rate heterogeneity by considering these patterns when (co)sampling topologies and branch lengths, and are thus more conservative in this respect than traditional sequential approaches. Ultimately, the potential effects of character oversampling will best be addressed by studies from independent investigators all aiming to explicitly sample all characters – including autapomorphies and, ideally, also invariant characters – in similar fashion to the collection of molecular sequence data.

These results reconcile contradictory studies identifying presence (4-8) or absence (9-11) of a trend towards size reduction in theropods. While there is no overall theropod-wide trend (Fig. S7; SM part D), there is an exceptional trend within the single lineage that comprises the avian stem. This prolonged miniaturization is consistent with many aspects

of bird origins. Many traits that evolve along the shrinking bird stem lineage are potentially related to developmental truncation which often accompanies size reduction, regardless of which trait is under primary selection (28), including short snouts, large brains and eyes (12), and smaller teeth with reduced serrations (29). Also, progressive elaboration of feathers along the bird stem, permitting more efficient insulation along with other functions, might have facilitated the evolution of smaller body sizes. Sauropodomorphs (the closest outgroup to theropods) and adequately known basal theropods were entirely or largely featherless, basal-most coelurosaurs possessed only simple hair-like filaments, while ornithomimosaur and maniraptorans possessed a range of more complex feather types (13,17,18,20). Finally, the evolution of many bird innovations along the avian stem would have been facilitated by smaller body size, including the reorganisation of body mass balance, the increasingly horizontal (and biomechanically demanding) orientation of the femur, a stiffened tail, greater agility and cursoriality, and arboreal and aerial habits (1-8,12-18). Because size reduction, feather elaboration, paedomorphism, and other anatomical novelties permitted by small size all evolved cumulatively along the bird stem, identifying the primary driver of this trend is probably impossible. It is likely that all traits influenced and provided the context for the evolution of others (30).

## References and Notes

1. J. Gauthier, L.F. Gall (eds) *New Perspectives on the Origin and Early Evolution of Birds*. (Peabody Museum of Natural History, New Haven, 2001).
2. G. Dyke, G. Kaiser (eds) *Living Dinosaurs: the Evolutionary History of Modern Birds* (Wiley, Chichester, 2011).
3. J. Gauthier, *Mem. Calif. Acad. Sci.* **8**, 1 (1986).
4. P.C. Sereno, *Annu. Rev. of Earth Planet. Sci.* **25**, 435 (1997).
5. K. Padian, K., A.J. de Ricqlès, J.R. Horner, *Nature* **412**, 405 (2001).
6. T.A. Dececchi, H.C.E. Larsson, *Evolution* **67**, 2741 (2013).

7. F.E. Novas, M.D. Ezcurra, F.L. Agnolín, D. Pol, R. Ortíz, *Rev. Museo Argentino de Ciencias Naturales, n.s.*, **14**, 57 (2012).
8. A.H. Turner, D. Pol, J.A. Clarke, G.M. Erickson, M.A. Norell, *Science* **317**, 1378 (2007).
9. M.T. Carrano, Ch 8 in *Amniote Paleobiology* (eds M.T. Carrano, T.J. Gaudin, R.W. Blob, J.R. Wible) (University of Chicago Press, Chicago, 2006).
10. D.W.E. Hone, T.M. Keeseey, D. Pisani, A. Purvis, *J. Evol. Biol.* **18**, 587 (2005).
11. R.B. Sookias, R.J. Butler, R.B.J. Benson, *Proc. R. Soc. Lond. B* **279**, 2180 (2012).
12. B.-A.S. Bhullar, *et al. Nature* **487**, 223 (2012).
13. A.M. Heers, K.P. Dial, *Trend Ecol. Evol.* **27**, 296 (2012).
14. V.A. Allen, K.T. Bates, Z. Li, J.R. Hutchinson, *Nature* **497**, 104 (2013).
15. M.N. Puttick, G.H. Thomas, M.J. Benton, *Evolution* doi: 10.1111/evo.12363 (2014).
16. R.B.J. Benson, *et al. Plos Biology* **2**(5), e1001853 (2014).
17. D.K. Zelenitsky, *et al. Science* **338**, 510 (2012).
18. X. Zheng, *et al. Science* **339**, 1309 (2013).
19. R.B.J. Benson, J. Choiniere, 2012. *Proc. R. Soc. Lond. B* **280**, 1471 (2013).
20. P. Godefroit, *et al. Nature* **498**, 359 (2013).
21. X. Xu, *et al. Nature* **484**, 92 (2012).
22. J.N. Choiniere, *et al. Science* **327**, 571 (2010).
23. P. Christiansen, R.A. Farina, *Hist. Biol.* **16**, 85 (2004).
24. A. Drummond, M.A. Suchard, D. Xie, A. Rambaut, *Mol. Biol. Evol.* **29**, 1969 (2012).
25. A. Drummond, S.Y.W. Ho, M. Phillips, A. Rambaut, *PLoS Biology* **4**(5), e88 (2006).
26. M. Pagel, M., A. Meade, *BayesTraits. Software and documentation.*  
<http://www.evolution.rdg.ac.uk/BayesTraitsV2Beta.html> (2013).

27. L.E. Zanno, P.J. Makovicky, *Proc. R. Soc. Lond. B* 280, 1471 (2013).
28. J. Hanken, D.B. Wake, *Ann. Rev. Ecol. Syst.* 24: 501 (1993).
29. O.W.M. Rauhut, C. Foth, H. Tischlinger, M.A. Norell, *PNAS* **109**, 11746 (2012).
30. T.S. Kemp, *Proc. R. Soc. Lond. B* **274**, 1667 (2007).

**Acknowledgements.** We thank e-research SA for use of grid computing facilities, and the Environment Institute (Univ. of Adelaide) for funding, and the University of Bologna for logistic support.

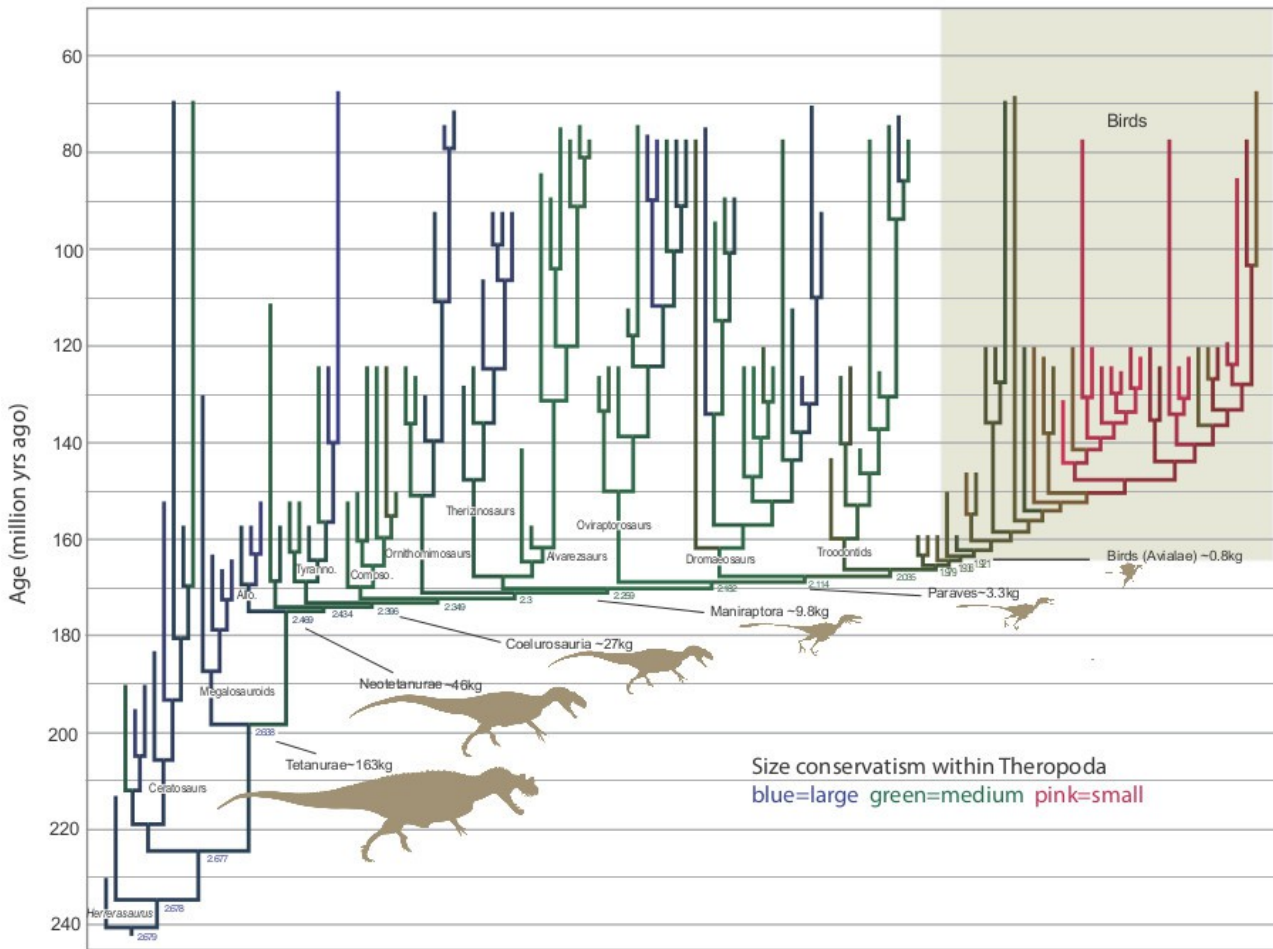


**Figure 1. Body size is highly conserved within theropod dinosaurs; birds and their closest relatives are consistently small.** Bayesian MPP consensus tree and size reconstructions from Dataset 1: branches are coloured according to inferred body size (indexed by log<sub>10</sub> femur length), with ancestral values for nodes along bird stem lineage shown. All taxon names and size values for all nodes and tips are in Fig. S1; posterior probabilities of all clades are in Fig. S2. Parsimony analysis and reconstructions reveal similar conservatism (Fig. S8), as did Bayesian and parsimony analysis of an alternative dataset (21,22: Fig. S5, S9). Abbreviations: Allo - Allosauroids, Tyranno - Tyrannosauroids, Compsa - Compsognathids.

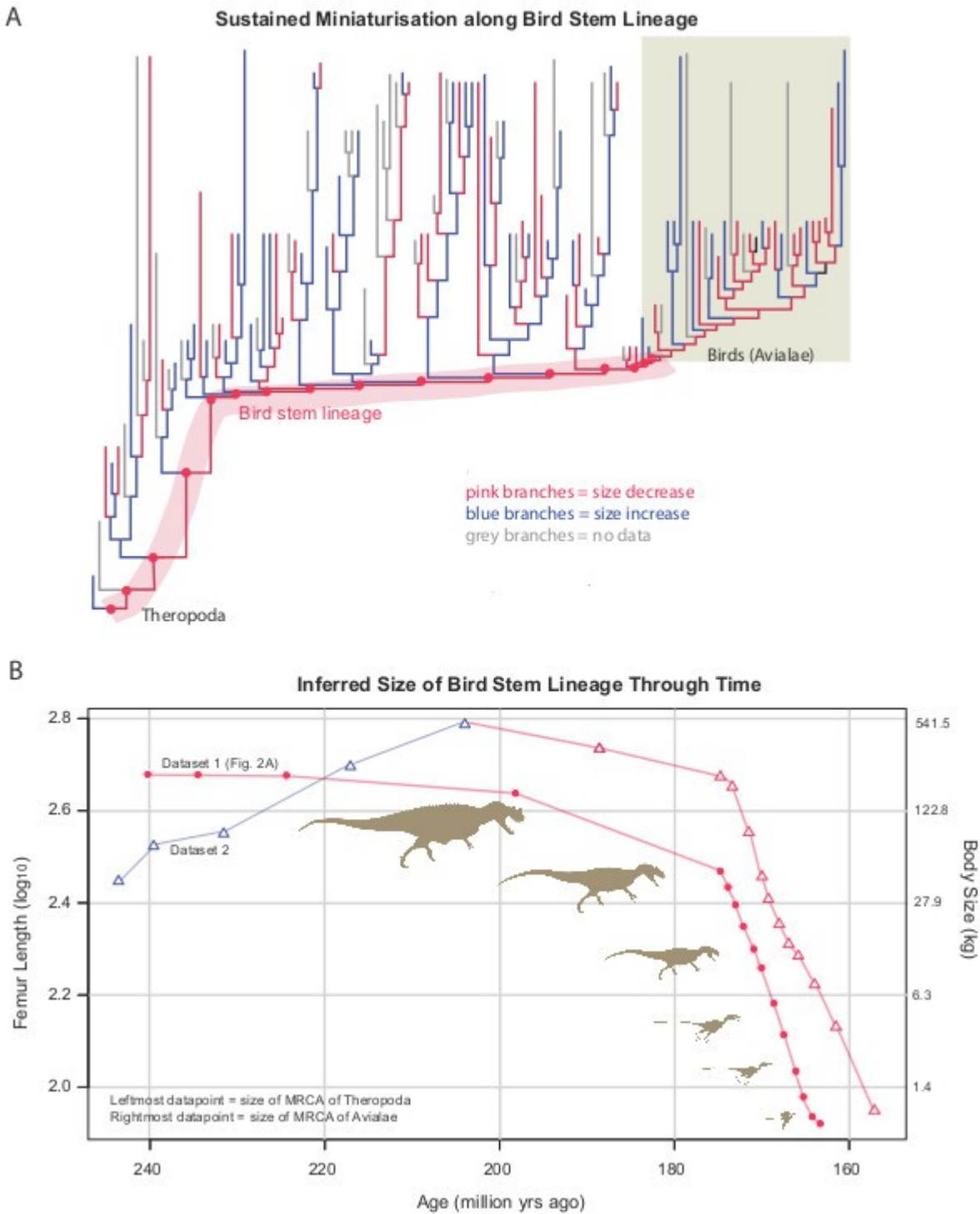


**Figure 2. Sustained miniaturization along the bird stem lineage is unique amongst theropod dinosaurs.** (a) Theropod tree from Dataset 1 (Fig. 1), with branches color-coded according to whether body size decreases (pink) or increases (blue). Pink branches span basal theropods to birds; in contrast, the rest of the tree shows no comparable “run” of decreases or increases. Parsimony analysis gives consistent results (Fig. S8), as do analyses of Dataset 2; (21,22: Figs S5, S9). (b) Evolution of body size through time along the bird stem lineage. Plot of body size versus age of successive nodes (‘ancestors’) along the bird stem lineage (from Fig. 1). Y axis (left) shows

femur length, Y axis (right) shows inferred body size (23). Curves represent results from Datasets 1 and 2; both indicate a sustained, unreversed size decrease commencing ~200mya, with the next 12 or more consecutive nodes each being smaller than the preceding.

## Elevated Rates of Anatomical Innovation on the Bird Stem Lineage

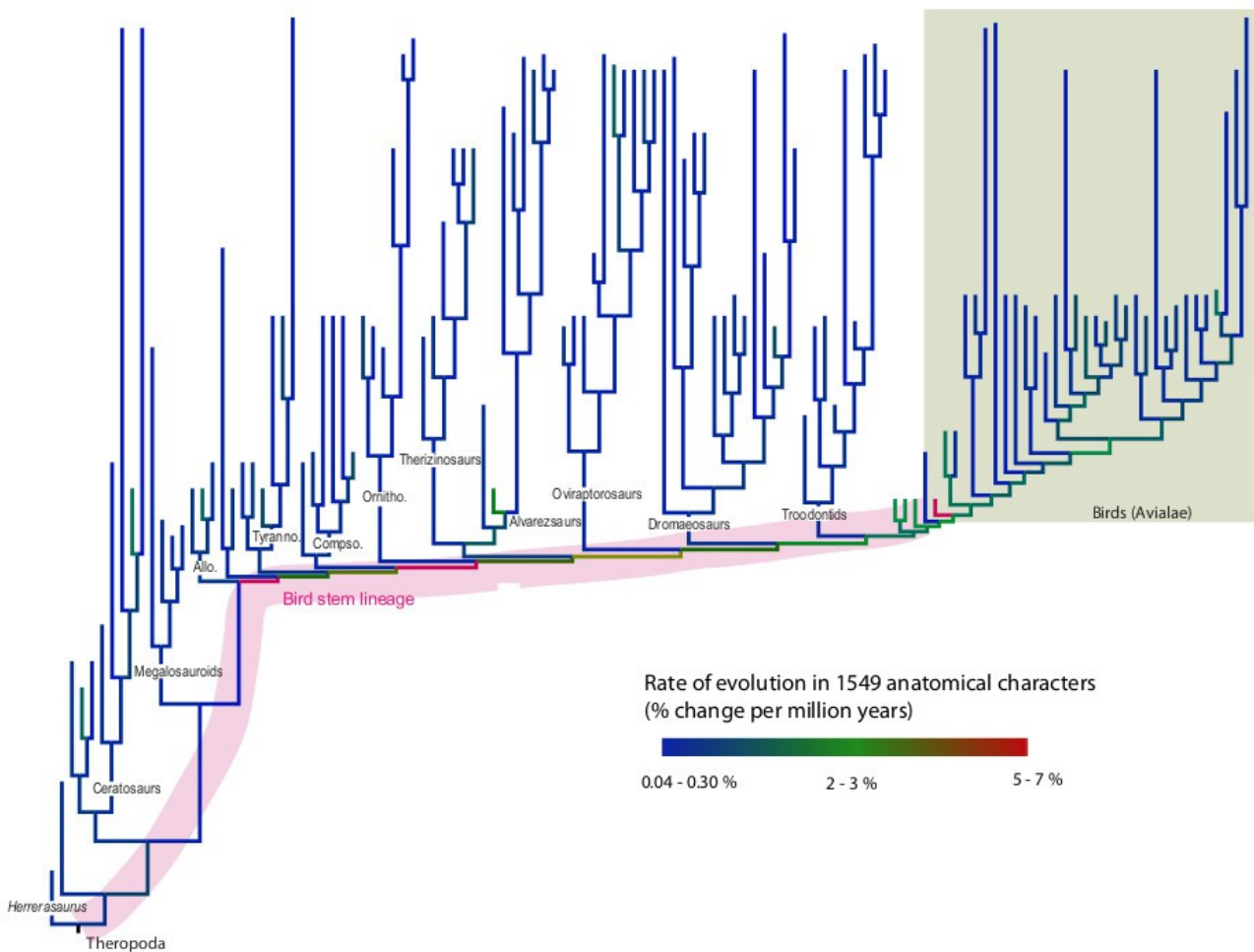


**Fig. 3. Elevated rates of anatomical (skeletal) innovation in the bird stem lineage.** Branches are color-coded according to the rate of morphological evolution across all 1549 discrete (mainly skeletal) characters in Dataset 1 (blue= up to ~0.5% per Ma, green= ~2-3% per Ma, pink= >4% per Ma; exact rates in Fig. S3). The fastest anatomical innovation occurs along the bird stem lineage, especially in basal tetanurans. Taxon names and timescale are shown in Fig. 1. The same pattern is found in Dataset 2 (21,22: Fig. S6).

## Supplementary Materials

### Materials and methods

- A. Phylogenetic Datasets
- B. Stratigraphic, Body Size and Body Mass Data
- C. Bayesian Analyses

D. Testing for Trends: PGLS

E. Testing for Trends: Parametric Simulations

F. Parsimony Analyses

G. List of Data Archived on Dryad Digital Repository:

Cau A., Dyke G.J., Lee M.S.Y., Naish D. 2014 - Data from: Sustained miniaturization and anatomical innovation in the dinosaurian ancestors of birds. *Science*

<http://dx.doi.org/10.5061/dryad.jm6pj>

Figures S1-S9

References (31-60)

## Materials and Methods

### A. Phylogenetic Datasets

Two of the largest current datasets encompassing all theropods, with very different taxon and character sets, were analysed: patterns found in both datasets are thus likely to be general across all theropods. (1) **Dataset 1** is new to this study and consisted of 120 theropod taxa and 1549 characters. It is the largest phylogenetic matrix for theropods ever compiled, expanded from (20) through the addition of 49 new characters and 28 taxa (with 9 fragmentary or immature taxa removed). Bayesian methods require sampling of all characters including those which are invariant (same across all taxa) and autapomorphic (unique specialisations of single taxal, typically excluded due to being parsimony-uninformative). This dataset is the only theropod data matrix to date which considers such characters: of the 1549 characters, 114 were invariant and 184 were autapomorphies. The character list, sources of anatomical information, and the character-by-taxon matrix are archived on Dryad (see below). (2) **Dataset 2** is a recent published dataset consisting of 100 theropod taxa and 421 parsimony-informative characters (21,22; expanded from 8). As with nearly previously published phylogenetic datasets, autapomorphies were not sampled.

## B. Stratigraphic, Body Size and Body Mass Data

Stratigraphic data for each taxon was obtained from the primary literature, with the most recently published, well-corroborated age used; all data are archived on Dryad. Where published ages were given in stratigraphic units (e.g. stage or epoch), the dates for the relevant unit were taken from the ICS/IUGS International Stratigraphic Chart ([www.stratigraphy.org/column.php?id=Chart/Time%20Scale](http://www.stratigraphy.org/column.php?id=Chart/Time%20Scale)).

Body size data for each taxon was obtained from the primary literature (Table S1). Femur length is the most commonly used proxy for body size in non-avian theropods (e.g. 11, 15, 27); it was the single measurement most predictive of body size ( $r=0.995$ : 23) and is also a commonly-preserved feature measurable in many taxa. It exhibits a relatively constant relationship across non-avian theropods including non-avian Paravians (6; see below). Only measurements from typical adult specimens were used; measurements from specimens which were identified as definitely or likely juvenile were not used (those taxa were scored as missing data if no other adult measurements were available). To reduce heteroscedasticity, all femur length measurements were  $\log_{10}$  transformed (23); thus, a doubling of femur length along a branch always results in the same increase in this quantitative trait ( $\log_{10} 2 = 0.301$ ), regardless of absolute ancestral and descendant size.  $\log_{10}$  Femur Length (hereafter  $FL_{10}$ ) for all ancestral nodes was co-estimated simultaneously with phylogeny (in the Bayesian analyses), or optimized on the most-parsimonious tree (in the parsimony analyses). Conversion of femur length to body size was based on the tight ( $r=0.995$ ) empirical relationship (23):

$$\log_{10} \text{BodyMass (kg)} = -6.288 + 3.222 \log_{10} \text{Femur length (mm)}$$

We apply this formula to infer ancestral body sizes within theropods only up to Avialae (Fig. 3), where it is highly predictive of "size", whether measured as mass (23) or snout-vent length (6). We do not use it to make any inferences about mass on branches *within* Avialan theropods, due to changes in femur morphology and allometry in these taxa due to adaptations for flight and/or diving, and femoral reorientation (e.g. 6, 13). Application of bird-specific regressions might produce accurate estimates. Hence, our discussion (e.g. Fig. 2) focuses on body size evolution in the avian stem lineage only up to Avialae, but not beyond.

It should be noted that use of this formula still returns reasonably reliable weights even for basal Avialans such as *Archaeopteryx*: its femur length and the above regression yields a weight of ~453g, consistent with most studies (e.g. 31, 32). However, it contradicts the anomalously low weight of 132g estimated in Table S4 in ref (14). This discrepancy might be related to some skeletal measurements of *Archaeopteryx* in Table S3 in ref (14) being considerably smaller than values published here (Appendix 5) and elsewhere (33).

### **C. Bayesian Analyses (simultaneous inference of phylogeny and character evolution)**

The BEAST package (24), which implements Markov-Chain Monte Carlo Bayesian methods for estimating phylogeny and associated traits, has 5 capabilities that make it uniquely applicable to this dataset. In particular, BEAST models for inferring dated phylogenies using DNA from viruses sampled across real-time are fundamentally analogous to models required for inferring dated phylogenies using morphological traits from fossils sampled across deep time. Similarly, "diffusion" models for inferring the geographic spread of viruses (in two dimensions) are broadly similar to Brownian motion models of body size evolution (in a single dimension). The only other potentially relevant package, MrBayes (34) cannot implement methods 1, 2 or 5 from the list below, and was consequently not used.

(1) It can simultaneously infer tree topology, divergence dates (lineage durations), and ancestral states for both discrete and continuous traits. All variables are co-estimated: for instance, all discrete and continuous traits directly contribute to the estimated phylogeny and divergence dates (continuous traits are not "mapped onto" a pre-determined phylogeny). However, in the current analysis, tree topology and branch lengths are largely determined by the discrete characters, due to the large number of discrete traits (1549 or 421), and the single continuous trait (body size).

(2) It can implement likelihood-based models of evolution for both discrete and continuous morphological traits. Discrete characters are modeled using the Lewis (35) Markov model which allows ordering of multistate characters (if desired), and also accommodates variability in rates of evolution among characters (using the gamma

distribution) and across lineages (using relaxed clocks, 25). Continuous traits are modeled using a Brownian motion process (36); as with discrete characters, the “rate” of Brownian motion can be constant throughout the tree (strict clock) or can vary across lineages (relaxed clock).

(3) It assesses uncertainty for each parameter, taking into account the uncertainties for every other estimated parameter. For instance, uncertainty in body size reconstruction takes into consideration not only uncertainty inherent in the chosen reconstruction model (e.g. rate-constant Brownian motion), but also uncertainty in tree topology and divergence dates.

(4) It can directly infer dated phylogenies where the terminal taxa differ in stratigraphic age, i.e. it estimates the optimal phylogeny and lineage durations that best explain the stratigraphic distribution and characters exhibited by the terminal taxa (34,37). Traditional phylogenetic methods only infer tree topology (branching sequence): lineage durations are often arbitrarily ascertained, e.g. to match the stratigraphic dates and minimise ghost lineages. In contrast, BEAST (and MrBayes) directly infers lineage durations and phylogeny which best fit the combined stratigraphic and character data (37)

(5) In addition to calibrating trees via tip ages (see 4), it can also enforce traditional node calibrations, where the ancestor of a particular set of taxa is constrained to be a certain age (or age distribution), without topological constraints. Unlike all other dating programs, BEAST does not require enforcing the monophyly of calibrated groups. Thus, it is possible to calibrate a tree yet leave phylogenetic relationships totally unconstrained (to determined by the character data); the calibration applies to the most recent common ancestor of a given set of taxa, regardless of whether or not they form an exclusive clade. In contrast, all other dating software (including MrBayes) enforces monophyly of calibrated taxon sets.

Simultaneous estimation of evolutionary rates, topology and divergence dates is now a standard practice in molecular phylogenetics and has been argued to superior at identifying global optima that best fit all relevant parameters (e.g. 25). In the current context, it should be noted that this approach yields conservative estimates of rate changes, by attempting to dampen extreme rates via changes in branch lengths or

topology. In particular, the need to infer implausibly fast rates could be removed either by minor stretching of very short branches (which barely affects overall tree shape), or by accepting a marginally less parsimonious tree that is much more stratigraphically consistent (and which cannot be rejected by topology tests). In contrast, fixing topology and divergence dates before calculating rates will often retrieve extremely short branches with implausibly fast rates (at an extreme, zero-length branches with infinitely fast rates: 38). Hence, simultaneous analysis of rates and tree shape results in lower (ie conservative) estimates of rate variability than sequential analysis (e.g. 39).

Each dataset was analysed in BEAST, using the Lewis (35) Markov model for the discrete characters; characters which formed morphoclines were ordered (see Appendix 3). All (ordered and unordered) discrete characters were treated as a single partition for estimating relevant parameters (e.g. mean rate, gamma). The most appropriate model for each dataset was chosen using Bayes Factors (BF) *sensu* Kass and Raftery (40), i.e. twice the difference in marginal  $\text{Log}_n$  likelihoods. The latter were estimated in Tracer (41), which implements the refinement by Suchard et al. (42). For both Datasets 1 and 2, BF strongly favoured inclusion of the gamma parameter for among-character rate heterogeneity (BF 1302 & 125 respectively), and a relaxed (uncorrelated lognormal) clock over a strict clock for among-lineage rate heterogeneity (BF 2928 & 920 respectively). The relaxed clock analysis employed (see below) also returned very high variation in evolutionary rates across branches, again inconsistent with a strict clock (uclid.stdev mean exceeding 1 and 95% HPD not abutting 0). The overall rate across the tree was given a very wide (conservative) uniform prior spanning 0 to 1000 changes per Ma (ie no change to extraordinarily fast rates). All characters were treated as independent. Character independence is a central assumption of all standard methods for phylogenetic inference (likelihood, parsimony, phenetics, and Bayesian). However, as organisms are integrated entities, this assumption is almost certainly violated in all real datasets (especially morphological ones), leading to potential errors such as over-confidence of related parameters, such as over-estimated clade probabilities.

The continuous trait ( $FL_{10}$ ) was analysed using a Brownian model, with the tree-wide evolutionary rate/variance empirically estimated from the data using BEAST, using the relatively uninformative default prior (36). Analyses with relaxed clocks (branch-specific

evolutionary rates) proved over-parameterized, with meaninglessly wide confidence intervals for rates on most branches. Additional (directed) models were tested with Bayestraits, which concluded the undirected model (as implemented in BEAST) was adequate.

Lineage durations (branch lengths) are integral to Brownian motion models, since large changes are less likely on short branches. Thus, the reconstructed ancestral value for a node will be most influenced by fossil taxa separated from that node by short branch lengths. For instance, the node representing the ancestral tyrannosauroid is reconstructed as small ( $FL_{10}=2.49$ , ~54kg; see Fig. 1), consistent with previous proposals (43-45). Even though two included taxa (*Yutyranus*, *Tyrannosaurus*) are huge, the small *Guanlong* ( $FL_{10}=2.54$ , ~81kg) is closest to the ancestral tyrannosauroid node in terms of branch lengths, and exerts the strongest influence on the reconstructed state.

Analyses were conducted using (1) only a single root age constraint, or with (2) two additional internal constraints; both yielded qualitatively similar size and rate trends. The age of each constrained clade was given a uniform prior, between the maximum age and 0 Ma. In practice, clade ages younger than the oldest included taxon are not sampled; however, as clade content is variable across MCMC samples (because monophyly is not enforced), this effective younger bound varies.

(1) The root age constraint consisted of the maximum age for Theropoda and was set at 246Ma, as this substantially pre-dates the earliest robust record of dinosaurs (~230Ma: 46-48), and even the earliest potential dinosaurs (~243Ma: 49). There is a rich global archosaur record in the Lower Triassic (~246-251Ma) which does not contain any unequivocal dinosaurs. (2) The first internal constraint consisted of a plausible upper limit (168.3 Ma) on the age of Paraves. This substantially pre-dates the earliest unequivocal paravians *Anchiornis*, *Aurornis* and *Xiaotingia* at ~159Ma (see Appendix 6), and is the same age as the oldest possible evidence for paravians, consisting of footprint evidence acknowledged to be of questionable stratigraphy and taxonomic affinity (50). The second internal constraint consisted of a plausible upper limit (175Ma) on the age of Neotetanurae. This substantially pre-dates the earliest unequivocal neotetanurans (the allosauroids *Xuanhanosaurus qilixiaensis*, *Yangchuanosaurus zigongensis* and *Shidaisaurus jinae*, all of undetermined age within the Middle Jurassic (51), and the

coelurosaur *Proceratosaurus bradleyi* from the Bathonian (52). There is a rich Lower Jurassic (175-200Ma) theropod fossil record that does not include any neotetanurans or even undisputed tetanurans. The oldest undisputed tetanurans are ~175Ma (53), though there are potential tetanurans at about 196Ma (e.g. *Eshanosaurus*: 54).

The character matrix (with age and size data) for Datasets 1 and 2 with BEAST commands for the analysis enforcing root and internal constraints is archived on Dryad. All analyses were performed in BEAST 1.7 and 1.8 (24), on the e-research SA (erSA) computer grid. Each BEAST analysis involved 6 replicate runs (with different random starting trees and random number seeds). Each of the 6 replicate runs involved 30 million steps with sampling every 5000 generations, with a burnin of 5 million steps. Convergence (stationarity) in numerical parameters was identified using Tracer (41): broadly overlapping, non-trending traces across all replicate runs for every parameter, with effective sample sizes (ESS) of every parameter exceeding 100. Convergence for both datasets was reached before the relevant burnin, and the post-burnin parameter and tree samples were retained for analysis and concatenated using LogCombiner in the BEAST package. Estimates (mean and 95% highest posterior density) for all numerical parameters were generated using Tracer (41). Convergence in topology was assessed using AWTY (55), with posterior probabilities of splits of post-burnin trees always highly correlated across the replicate runs. The maximum clade credibility (MCC) consensus tree using mean branch lengths was obtained using TreeAnnotator in the BEAST package, together with estimates (mean and 95% highest posterior density) of tree-based parameters, including posterior probabilities, divergence dates, lineage durations (branch lengths), rates of morphological evolution (discrete characters), and ancestral state reconstructions for femur length / inferred body size (continuous character). The final summary trees with node values were generated using TreeAnnotator and visualized via FigTree (56).

**Dataset 1.** The dated maximum clade credibility (MCC) tree (with branch lengths in Ma) is shown in Fig. 1 & S1 with inferred ancestral states for femur length/body size, in Fig. S2 with posterior probabilities for each clade, and in Fig. 3 & S3 with rates of evolution on each branch (numerical values, in % divergence per Ma). These results are discussed in the main text. The dated MCC with branch lengths in terms of amount of morphological

evolution is shown in Fig. S4; despite the elevated rates along the bird stem lineage, the absolute amounts of change along the branches near the origin of Avialae are rather small, emphasising the morphological continuum between birds and non-avian dinosaurs (e.g. 1,2,12,14.20).

**Dataset 2.** The dated MCC tree (with branch lengths in Ma) is shown in Fig. S5 branches coloured according to reconstructed body size; absolute values are also given. A pattern of consistent, unreversed size reduction along the avian stem (from Tetanurae upwards) is again found. Fig. S6 shows the tree branches coloured according to rates of change, along with rates for each branch. Because this dataset did not sample autapomorphies, rates on terminal branches are almost certainly underestimates. Even so, the pattern is similar to dataset 1: the Avian stem exhibits consistently faster rates of evolution than the rest of the tree, even when only internal (non-terminal) branches are considered.

#### **D. Testing for Trends: PGLS**

The presence or absence of an overall trend towards size decrease (or increase) in the dataset was determined using PGLS one of the most powerful methods for detecting temporal evolutionary trends (57). BayesTraits (26) can implement a range of models of continuous trait evolution, in a fully Bayesian framework integrating across different sampled tree topologies and branch lengths. An undirected Brownian motion model was tested against a model which also included a trend parameter (beta); in the latter model, the size of each descendant node is predicted jointly by the ancestral node, the estimated rate of Brownian motion ("variance"), and the trend parameter. Analyses employed 1000 primary (ie sampled) trees from each dataset, and default BayesTraits priors. Both datasets exhibited no significant overall trend towards larger or smaller body size across all theropods (Fig. S7AB). Adding the trend parameter did not improve model fit (Dataset 1 - BF =0.14; Dataset 2 - BF = 0.07), and the estimated trend parameter was insignificant (Figure S7AB), with the 95% HPD interval broadly encompassing 0 (Dataset 1, mean=0.0015, HPD = -0.0012 to +0.0042; Dataset 2, mean = 0.0011, HPD = -0.0017 to +0.0037). Thus, both datasets do not exhibit a trend towards body size increase or decrease with time, when the overall tree is considered. This is consistent with recent

results for three theropod subclades, which showed no directionality in these clades despite expected size trends due to herbivory (27).

To test for a significant trend on the bird stem lineage, we repeated the PGLS analysis (26) on the relevant subtree in each of the 1000 sampled trees. This subtree spanned the outgroup to the bird clade; all other taxa were pruned from each sampled tree (Fig. S7C). Only Dataset 1 sampled sufficient bird taxa to employ this test. This test is also conservative because the tested trend along the bird stem lineage will be diminished by any non-directionality on the other remaining branches (i.e. branches leading to the outgroup, and within birds). To reduce this effect, bird taxa on very long tip branches were also pruned (Fig. S7C). Despite the conservative nature of this test, addition of the trend parameter significantly improved model fit ( $BF = 18.6$ ) and accordingly the estimated trend parameter was significantly negative (mean =  $-0.0066$ , HPD =  $-0.0120$  to  $-0.0007$ ), indicating a significant trend of size reduction with time.

### **E. Testing for Trends: Parametric simulations**

Parametric simulations ("bootstraps") were performed to test if the observed consecutive run of size reductions along the bird stem lineage could have been generated stochastically, under a null model where size increases or decreases randomly across the entire phylogeny.

Missing tip data can inflate inferred trends, because inferred ancestors at certain nodes are directly inferred from nodes above and below (rather than via tip data). To remove this bias, the phylogeny in Fig. S1 was pruned down to the 87 taxa which all had size ( $FL_{10}$ ) information. We then inferred the evolution of size along this phylogeny using the Bayesian analyses discussed above, on this pruned, fixed topology. These analyses retrieved a pattern identical to that depicted in Figs 1 and 2: the longest "run" of consecutive size reductions in this 87-taxon tree was 27, and spanned all of the bird stem lineage.

We then simulated the evolution of size along this phylogeny, using an undirected Brownian motion model in Mesquite (58); the root value (2.679) and rate of change / variance (0.045 per Ma) matched that inferred by BEAST from the actual data (BEAST's retrieved rate of 7.7 scaled by tree height of 173). We also confirmed that the simulations

using a rate/variance of 0.045 yielded variation in tip values very similar to the actual values (e.g. similar range between largest and smallest sizes). Because the actual ancestral values for the real tree are not known (only tip values are known, ancestral values are inferred via the Bayesian analyses described above), we treated the simulated data in exactly the same way. We used the tip values at the simulations and inferred nodal values using the same methods used for the real data. Only 20 such simulations could be completed due to high computational burden. Across these 20 simulations, longest run of size increases was 14 (mean = 8.5), and longest run of decreases was 20 (mean = 10.7); the observed value of 27 decreases exceeds both these values substantially. These results suggest that the trend observed in the real data is too persistent to have been generated by chance, and is significant at least at  $P=0.05$  (the smallest value that can be retrieved given 20 simulations).

## **F. Parsimony Analyses and Character Optimisation**

Parsimony analysis and optimization was also employed, to test the robustness of the above trends to alternative methodologies. These methods are very different to the Bayesian likelihood methods above: for instance, in a parsimony framework, temporal duration (length) of branches is irrelevant to both phylogenetic inference or character optimization.

Each dataset was analysed in PAUP\* (59), using search settings aimed at sampling as many tree islands as possible [HSEARCH addseq=random nreps=1000 nchuck=1000 chuckscore=1]. Both Datasets 1 and 2 resulted in >100000 most parsimonious trees (MPTs); many more presumably exist but could not be retained due to memory constraints. However, the strict consensus tree obtained for Dataset 2 matched that from a previous parsimony analysis of the same data (21), suggesting the correct overall consensus topology was retrievable from the pools of sampled trees in both analyses. The strict consensus for both datasets contained large polytomies, and characters should not be optimized on such consensus trees, as they are not optimal trees, and imply much more homoplasy than any of the individual MPTs (e.g. 60). Hence, a majority-rule consensus was obtained from the sampled MPTs (Figs. S8, S9), which was fully resolved.

Body size was optimized onto the trees from Datasets 1 and 2 using both linear and square-change parsimony in Mesquite (58). Both methods produced similar results, so only linear parsimony results are presented (Figs. S8, S9). Both datasets 1 and 2 indicate that body size consistently decreased, or remained unchanged, along every branch of the bird stem lineage from neotetanurans upward. Similar results have been obtained with parsimony analysis of a dataset of tetanurans (7). Thus, the parsimony analyses are consistent with the more parameterized Bayesian models, and demonstrate that the trends observed here are robust to different models and assumptions.

**G. Data Archived on Dryad Digital Repository (<http://dx.doi.org/10.5061/dryad.jm6pj>)**

1. Character list for Dataset 1 in Word format (Dataset 2 is available from 21).
2. Taxon list and sources of anatomical information for Dataset 1 in Word format (Dataset 2 is available from 21).
3. Stratigraphic and size data for Datasets 1 and 2 in Excel format.
4. Nexus file for Dataset 1 as a plain text executable for PAUP (Dataset 2 is available from 21).
5. xml file for Dataset 1, a plain text executable for BEAST 1.7 or 1.8.
6. xml file

SUPPLEMENTARY FIGURES S1-S9

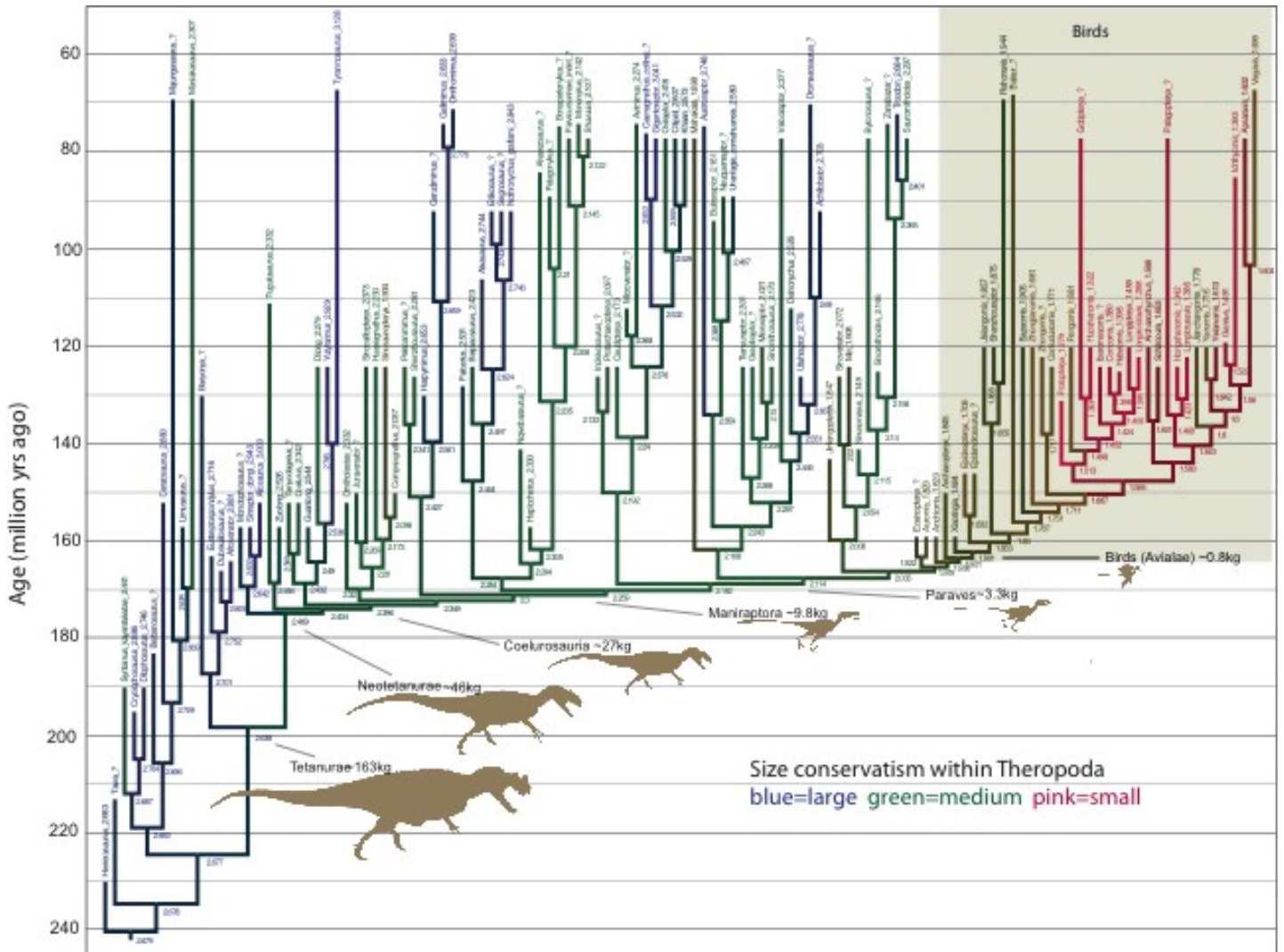


Fig. S1. **Size evolution across the theropod-bird transition.** This is more detailed version of Fig. 1, and represents the maximum clade credibility (MCC) tree from Dataset 1, with size information superimposed. All taxon names are shown, and size (indexed by  $\log_{10}$  femur length) is shown for all tip taxa (observed values) and all nodes (reconstructed values).

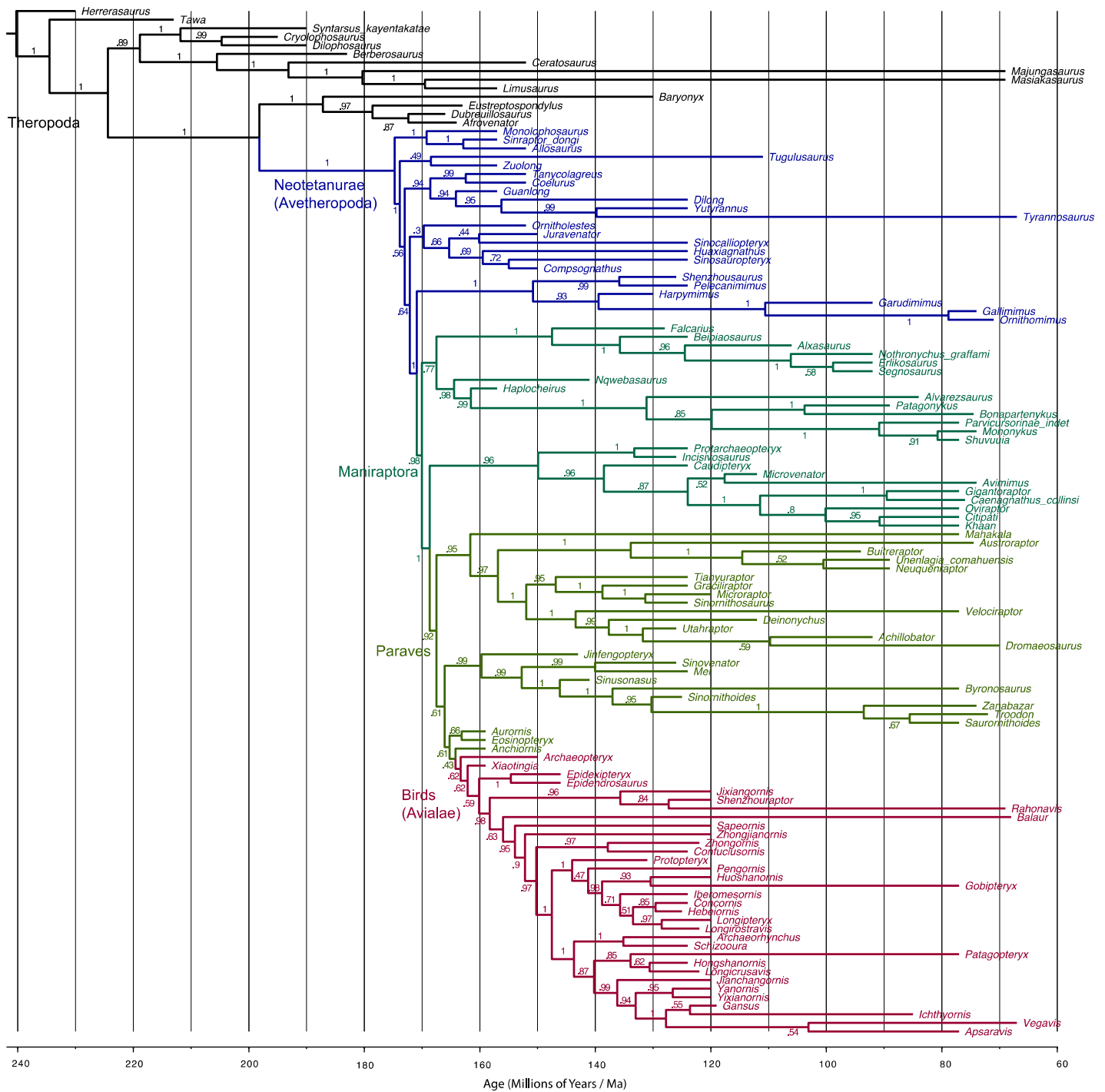


Fig. S2. **Theropod phylogeny, based on the new morphological data matrix (Dataset 1).** This tree is the Bayesian MCC tree with posterior probabilities shown at nodes. Taxon order is identical to that in Fig. 1. Tree is colour-coded by clade: Black (and upwards) = Theropoda, Blue (and upwards) = Neotetanurae, Green (and upwards) = Maniraptora, Olive (and upwards) = Paraves, Pink = Avialae / Aves.

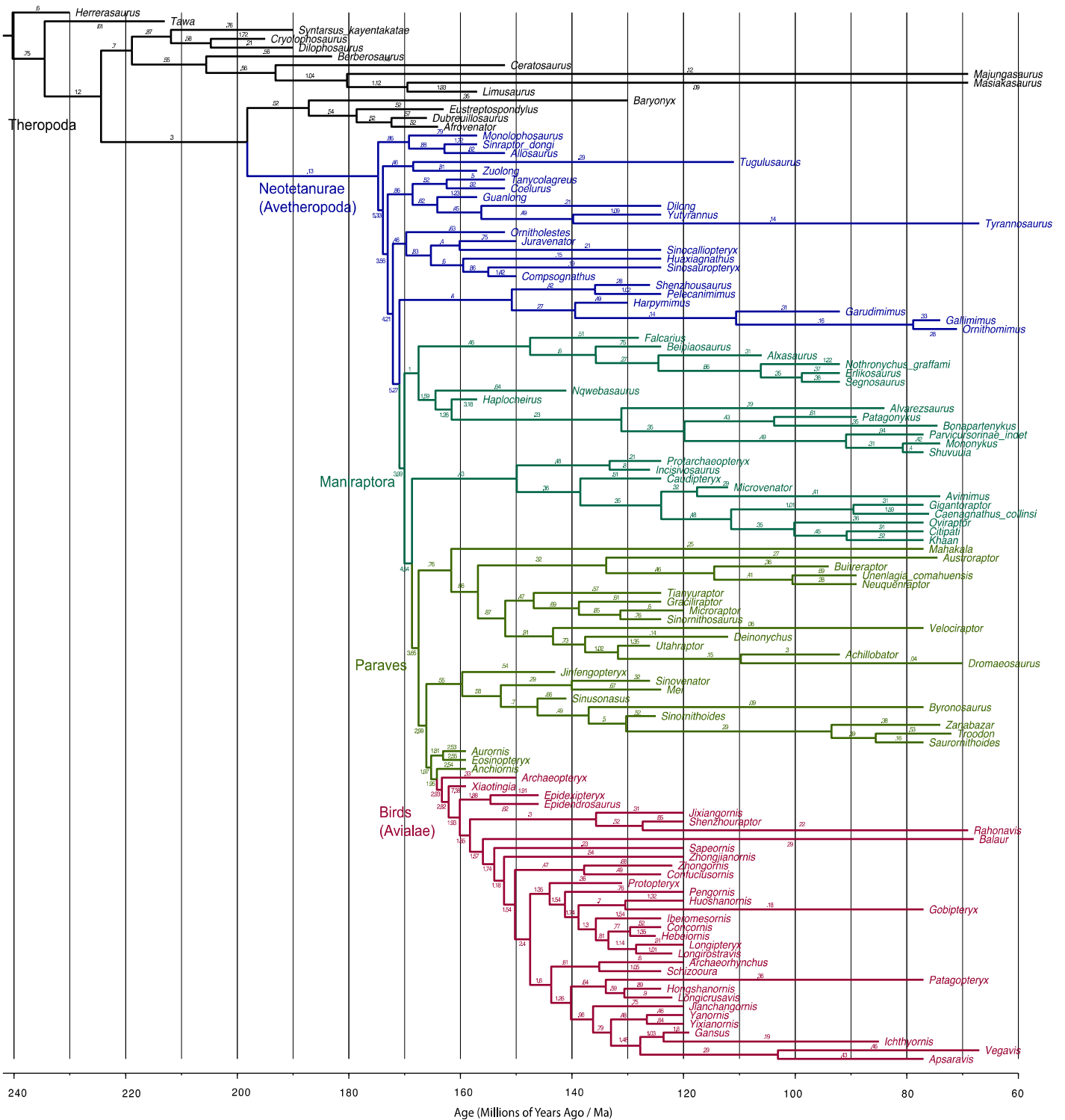


Fig. S3. Rates of morphological evolution in theropods, based on Dataset 1. Bayesian MCC tree with mean evolutionary rates shown on each branch (percentage divergence per million years, across all 1549 discrete characters. A rate of 1% equates to a 0.01 probability of change per character per lineage per Ma). The bird stem lineage is consistently faster than the rest of the tree, with the fastest

rates occurring between Neotetanurans and Paraves (see also Fig. 3, main text, where branches are colour-coded according to rate). Tree is colour-coded by clade (see Fig. S2).

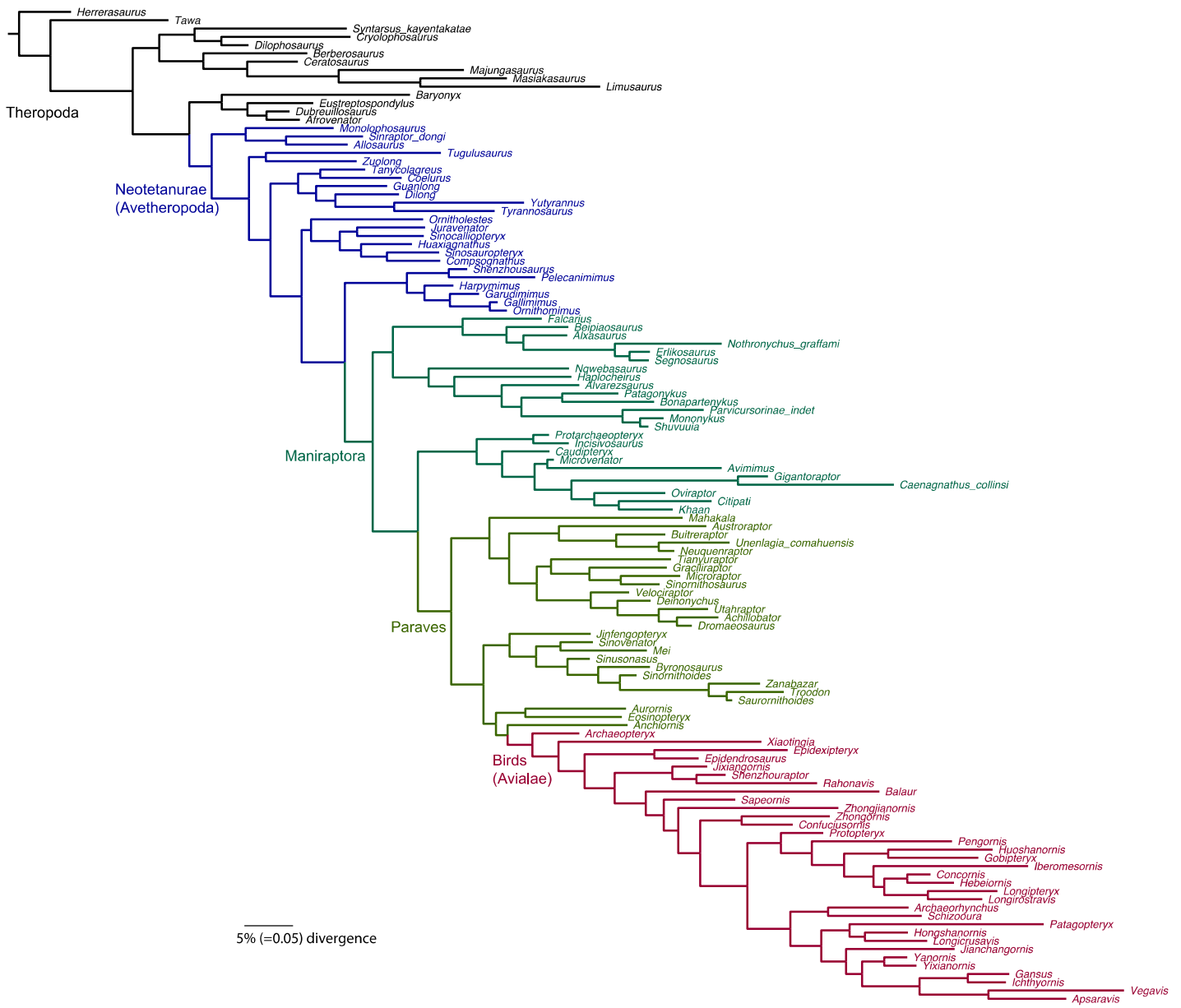


Fig. S4. **The dinosaur-bird continuum: Amounts of morphological evolution in theropods, based on Dataset 1.** Bayesian MCC tree, with branch lengths scaled to the absolute amount (rather than rate) of evolutionary divergence across all discrete characters. The branch leading to “birds” (Aviale, *Aves sensu lato*) does not undergo exceptional amounts of evolution. Tree is colour-coded by clade (see S2).

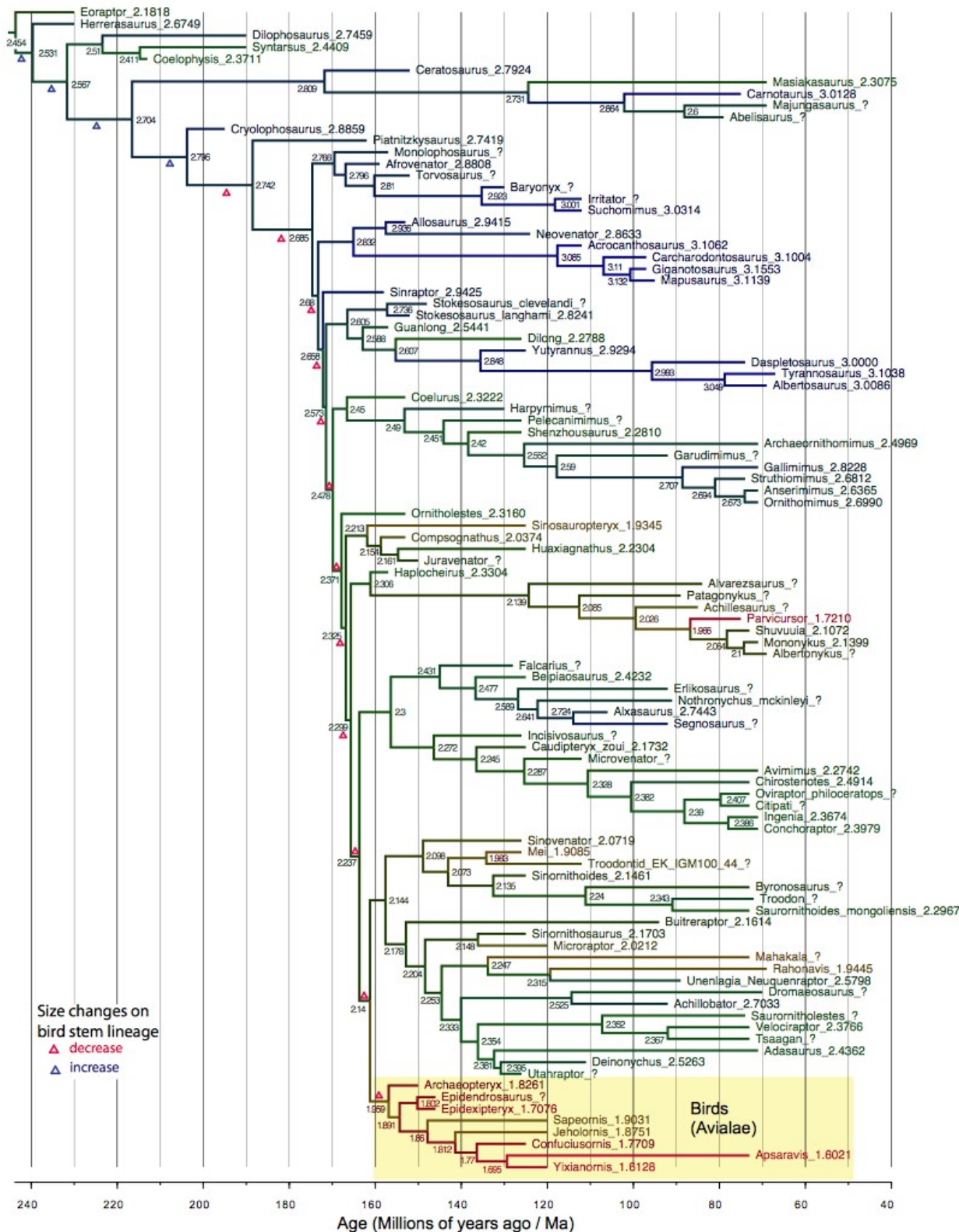


Fig. S5. **Theropod phylogeny and body size evolution, based on Dataset 2.** The same trend of continuous, unreversed size reduction along most of the bird stem lineage is found as in Dataset 1. Bayesian MCC tree with branches colour-coded according to body size as indexed by  $\log_{10}$  femur length (compare with Figs. 1 and S1); numbers denote observed values at tips, or inferred ancestral values at nodes. Triangles denote size increases or decreases along the bird stem lineage (compare with Fig 2a), and size trends in this lineage are plotted in Fig. 2b.

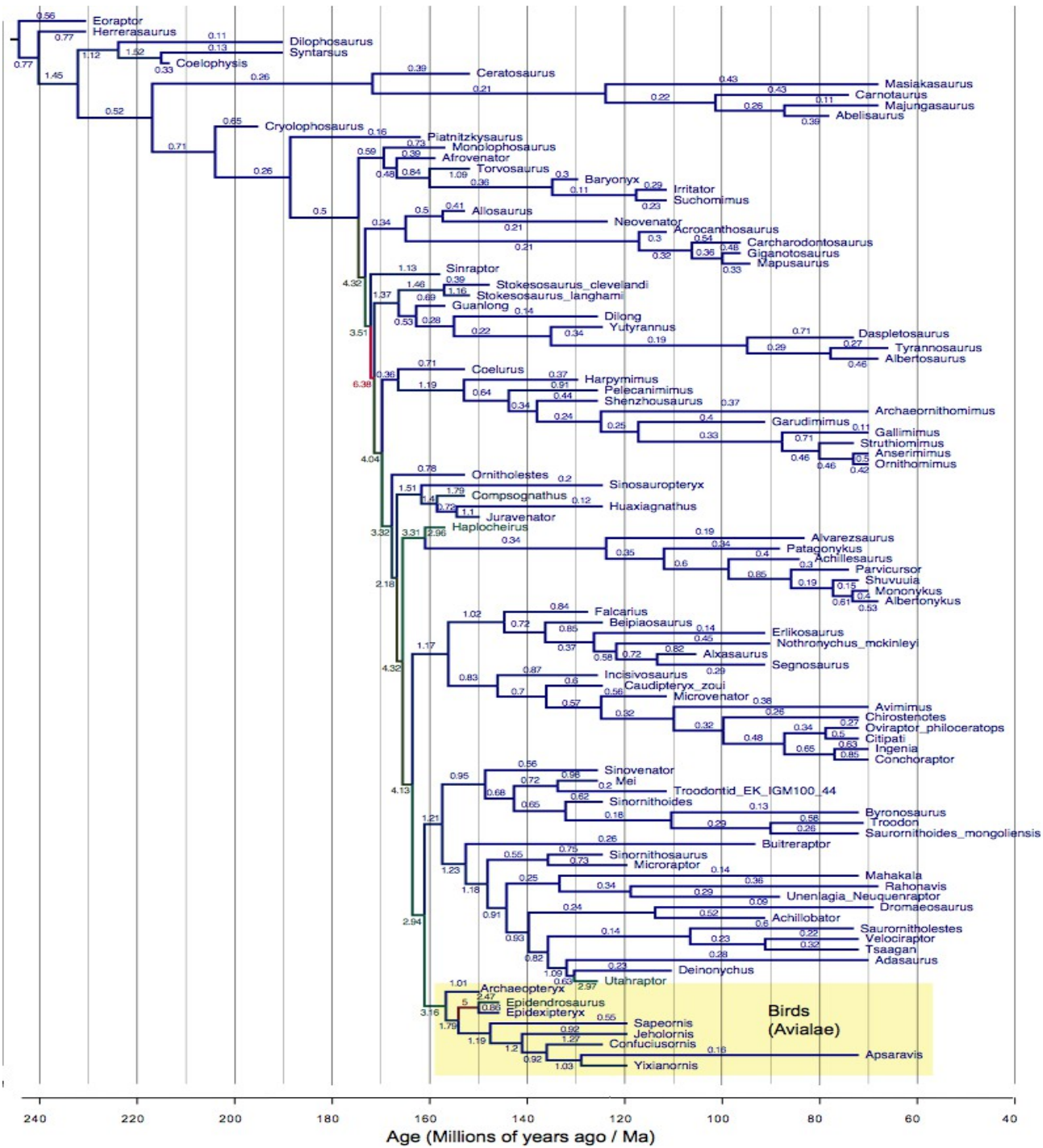


Fig. S6. **Theropod evolutionary rates, based on Dataset 2.** Fast rates characterise the bird stem lineage, as in Dataset 1 (compare with Fig. 3). Bayesian MCC tree with branches colour-coded according to inferred rate of evolution (percentage divergence per million years, across all 1549 discrete characters). A rate of 1% equates to a 0.01 probability of change per character per lineage per Ma).

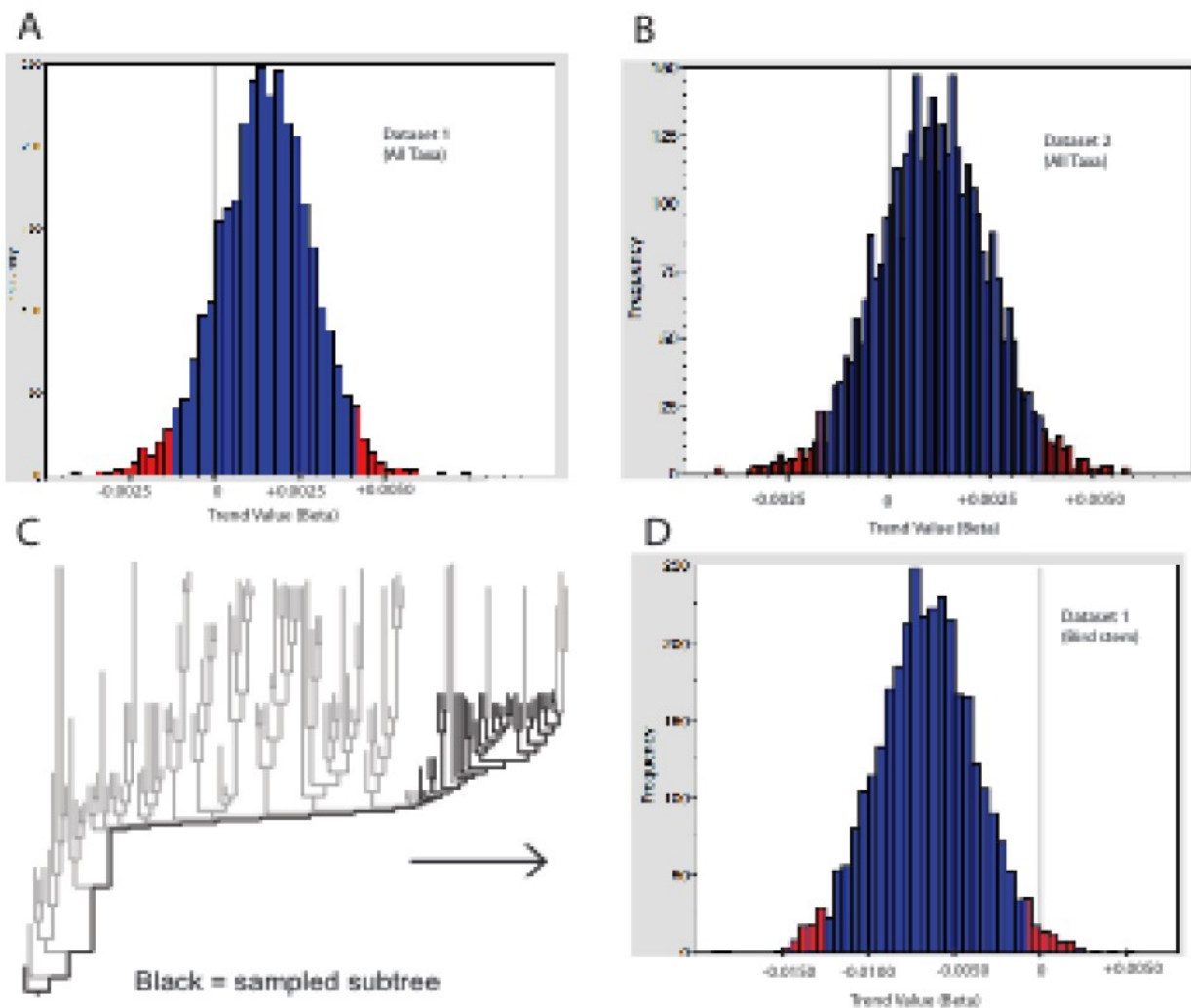


Fig. S7. **No overall trend in body size evolution across theropods, but a significant trend in the bird lineage.** The estimated trend parameter (beta) from a BayesTraits (26) analysis across 1000 sampled trees in (A) Dataset 1 and (B) Dataset 2. In both datasets, the mean estimate of the trend parameter is close to 0 ( $\sim 0.0012$ ) and the 95% highest posterior density (blue) encompasses 0. Adding this parameter also does not improve model fit (see S1\_D). (C) Pruned subtree retaining the outgroup and basal bird taxa; this is the maximum MCC consensus of the pruned subtrees (1000 sampled subtrees representing relationships among the retained taxa were used for actual analysis). (D) The estimated trend parameter (beta) from a BayesTraits analysis of the 1000 pruned subtrees; the mean estimate is  $\sim 5$ x times the absolute magnitude than that for the full tree ( $-0.0066$ ), and the 95% highest posterior density (blue) excludes zero.

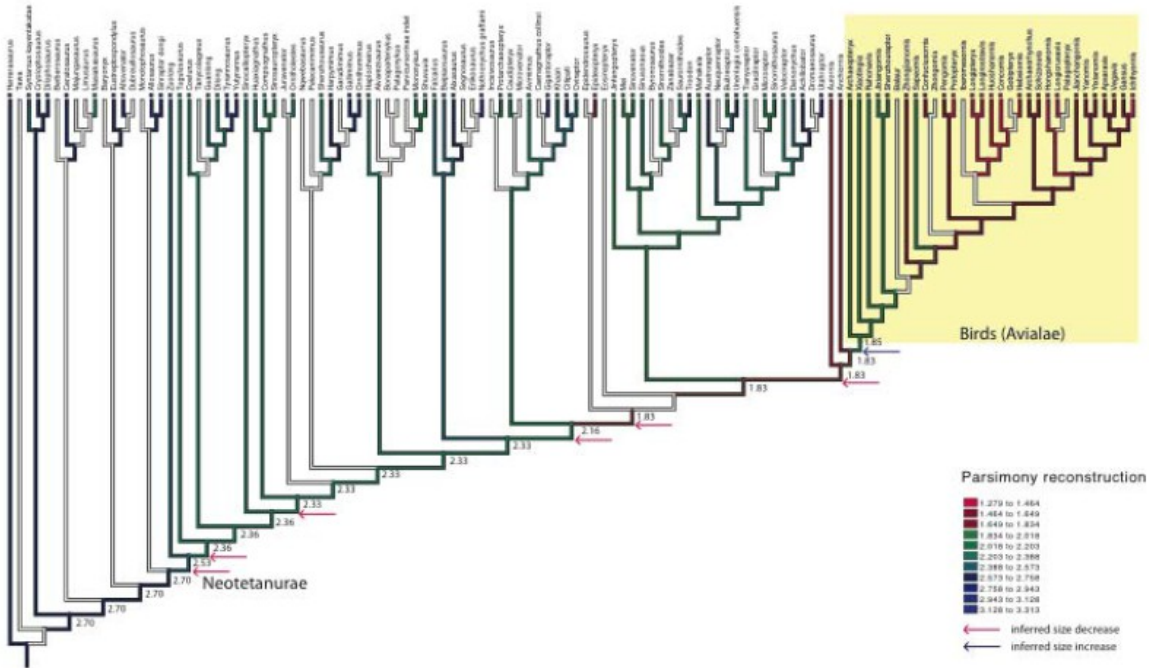


Fig. S8. **Theropod phylogeny and size evolution based on parsimony (cladistic) analysis of Dataset 1.** Majority-rule consensus of >100 000MPTs, with ancestral node reconstructions based on linear parsimony. Branches are colour-coded according to size, as indexed by log<sub>10</sub> femur length (blue=large, green=medium, pink=small); numbers at nodes are inferred values for size along the bird stem lineage. Where there is a range of equally-parsimonious values for a node, Mesquite (58) by default prints the lower value (shown here). Using the mean value or upper value does not change the retrieved pattern.

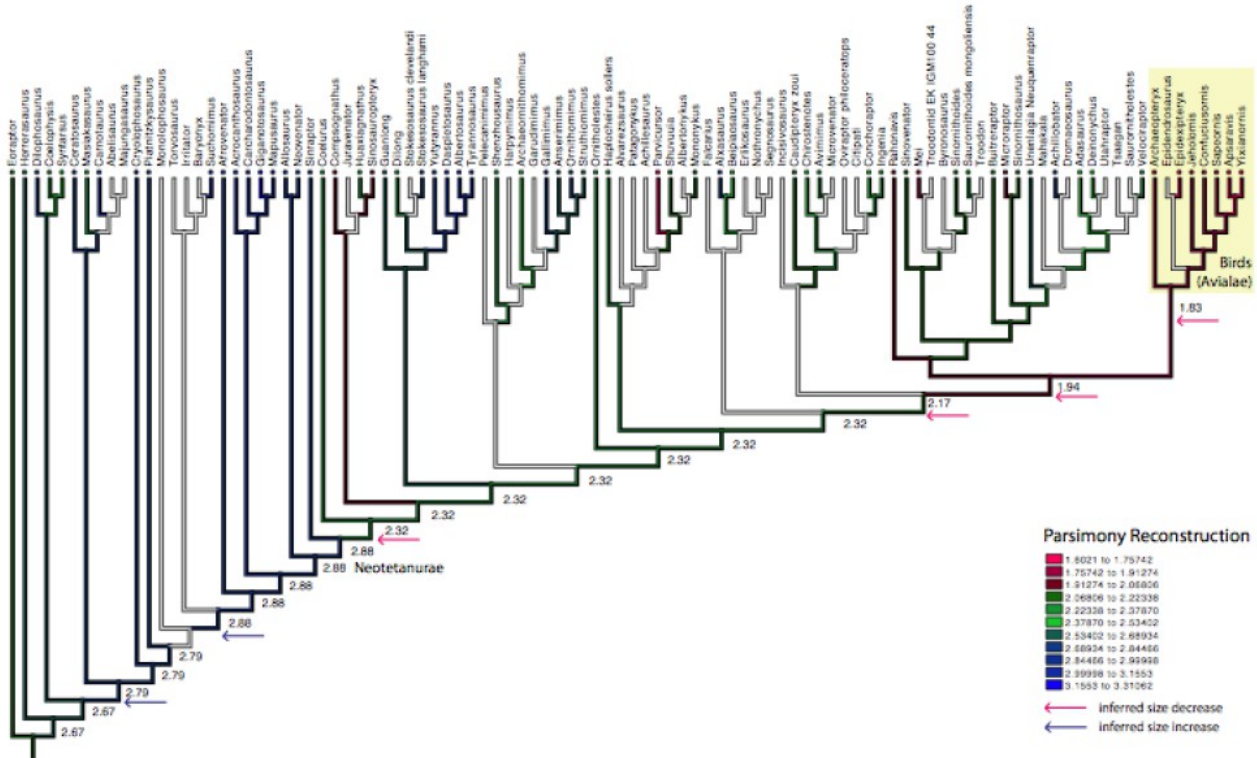


Fig. S9. **Theropod phylogeny and size evolution based on parsimony (cladistic) analysis of Dataset 2.** Majority-rule consensus of >100 000MPTs, with ancestral node reconstructions based on linear parsimony. Branches are colour-coded according to size, as indexed by log<sub>10</sub> femur length (blue=large, green=medium, pink=small); numbers at nodes are inferred values for size along the bird stem lineage. Where there is a range of equally-parsimonious values for a node, Mesquite (58) by default prints the lower value (shown here). Using the mean value or upper value does not change the retrieved pattern.

**References (31-60 are additional to main text )**

1. J. Gauthier, L.F. Gall (eds) *New Perspectives on the Origin and Early Evolution of Birds.* (Peabody Museum of Natural History, New Haven, 2001).
2. G. Dyke, G. Kaiser (eds) *Living Dinosaurs: the Evolutionary History of Modern Birds* (Wiley, Chichester, 2011).
3. J. Gauthier, Saurischian monophyly and the origin of birds. *Mem. Calif. Acad. Sci.* 8, 1 (1986).
4. P.C. Sereno, The origin and evolution of dinosaurs. *Annu. Rev. of Earth Planet. Sci.* 25, 435 (1997).

5. K. Padian, K., A.J. de Ricqlès, J.R. Horner, Dinosaurian growth rates and bird origins. *Nature* 412, 405 (2001).
6. T.A. Dececchi, T.A., H.C.E. Larsson, Body and limb size dissociation at the origin of birds: uncoupling allometric constraints across a macroevolutionary transition. *Evolution* 67, 2741 (2013).
7. F.E. Novas, M.D. Ezcurra, F.L. Agnolín, D. Pol, R. Ortíz, New Patagonian Cretaceous theropod sheds light about the early radiation of Coelurosauria. *Rev. Museo Argentino de Ciencias Naturales, n.s.*, 14, 57 (2012).
8. A.H. Turner, D. Pol, J.A. Clarke, G.M. Erickson, M.A. Norell, basal dromaeosaurid and size evolution preceding avian flight. *Science* 317, 1378 (2007).
9. M.T. Carrano, Ch 8 in *Amniote Paleobiology* (eds M.T. Carrano, T.J. Gaudin, R.W. Blob, J.R. Wible) Ch. 8 (University of Chicago Press, Chicago, 2006).
10. D.W.E. Hone, T.M. Keesey, D. Pisani, A. Purvis, Macroevolutionary trends in the Dinosauria: Cope's Rule. *J. Evol. Biol.* 18, 587 (2005).
11. R.B. Sookias, R.J. Butler, R.B.J. Benson, Rise of dinosaurs reveals major body size transitions are driven by passive processes of trait evolution. *Proc. R. Soc. Lond. B* 279, 2180 (2012).
12. B.-A.S. Bhullar, *et al.* Birds have paedomorphic dinosaur skulls. *Nature* 487, 223 (2012).
13. A.M. Heers, A.M., K.P. Dial, From extant to extinct: locomotor ontogeny and the evolution of avian flight. *Trend Ecol. Evol.* 27, 296 (2012).
14. V.A. Allen, K.T. Bates, Z. Li, J.R. Hutchinson, Linking the evolution of body shape and locomotor biomechanics in bird-line archosaurs. *Nature* 497, 104 (2013).
15. M.N. Puttick, G.H. Thomas, M.J. Benton, High rates of evolution preceded the origin of birds. *Evolution* doi: 10.1111/evo.12363 (2014).
16. R.B.J. Benson, *et al.* Rates of dinosaur body mass evolution indicate 170 Million years of sustained ecological innovation on the avian stem lineage. *Plos Biology* 2(5), e1001853 (2014).
17. D.K. Zelenitsky, *et al.* Feathered non-avian dinosaurs from North America provide insight into wing origins. *Science* 338, 510 (2012).
18. X. Zheng, *et al.* Hind wings in basal birds and the evolution of leg feathers. *Science* 339, 1309 (2013).
19. R.B.J. Benson, J. Choiniere, 2012. Rates of dinosaur limb evolution provide evidence for exceptional radiation in Mesozoic birds. *Proc. R. Soc. Lond. B* 280, 1471 (2013).
20. P. Godefroit, *et al.* A Jurassic avialan dinosaur from China resolves the early phylogenetic history of birds. *Nature* 498, 359 (2013).

21. X. Xu, *et al.* A gigantic feathered dinosaur from the Lower Cretaceous of China. *Nature* 484, 92 (2012).
22. J.N. Choiniere, *et al.* A basal alvarezsauroid theropod from the early Late Jurassic of Xinjiang, China. *Science* 327, 571 (2010).
23. P. Christiansen, P., R.A. Farina, Mass prediction in theropod dinosaurs. *Hist. Biol.* 16, 85 (2004).
24. A. Drummond, M.A. Suchard, D. Xie, A. Rambaut, Bayesian phylogenetics with BEAUti and the BEAST 1.7. *Mol. Biol. Evol.* 29, 1969 (2012).
25. A. Drummond, S.Y.W. Ho, M. Phillips, A. Rambaut, Relaxed phylogenetics and dating with confidence. *PLoS Biology* 4(5), e88 (2006).
26. M. Pagel, M., A. Meade, *BayesTraits. Software and documentation.* <http://www.evolution.rdg.ac.uk/BayesTraitsV2Beta.html> (2013).
27. L.E. Zanno, P.J. Makovicky, No evidence for directional evolution of body mass in herbivorous theropod dinosaurs. *Proc. R. Soc. Lond. B* 280, 1471 (2013).
28. J. Hanken, D.B. Wake. Miniaturization of body size: organismal consequences and evolutionary significance. *Ann. Rev. Ecol. Syst.* 24, 501 (1993).
29. O.W.M. Rauhut, C. Foth, H. Tischlinger, M.A. Norell, Exceptionally preserved juvenile megalosauroid theropod dinosaur with filamentous integument from the Late Jurassic of Germany. *PNAS* 109, 11746 (2012).
30. T.S. Kemp, The concept of correlated progression as the basis of a model for the evolutionary origin of major new taxa. *Proc. R. Soc. Lond. B* 274, 1667 (2007).
31. Hone, D.W.E., Dyke, G.J., Benton, M.J., Haden, M. (2008) Body size evolution in Mesozoic birds. *Journal of Evolutionary Biology* 21, 618-624.
32. A. Ekzanowski, A. Archaeopterygidae. In L. Chiappe, L. Witmer (eds.) *Mesozoic Birds: Above the Heads of Dinosaurs.* (University of California Press, Berkeley, 2002).
33. Wellnhofer, P. (2008) *Archaeopteryx: der Urvogel von Solnhofen.* Verlag Dr. Friedrich Pfeil.
34. Ronquist F., Teslenko M., van der Mark P., Ayres D.L., Darling A., Höhna S., Larget B., Liu L., Suchard M.A. & Huelsenbeck J.P. (2012) MrBayes 3.2: Efficient Bayesian phylogenetic inference and model choice across a large model space. *Systematic Biology* 61, 539-42.
35. Lewis, P.O. (2001). A likelihood approach to estimating phylogeny from discrete morphological character data. *Systematic Biology* 50, 913-925.
36. Lemey P., Rambaut A., Welch J.J. & Suchard M.A. (2010) Phylogeography takes a relaxed random walk in continuous space and time. *Molecular Biology and Evolution* 27, 1877-1886.

37. Lee, M.S.Y., Cau, A., Naish, D. & Dyke, G.J. (2014) Morphological clocks in palaeontology, and a Mid-Cretaceous origin of crown Aves. *Systematic Biology* (doi: 10.1093/sysbio/syt110).
38. Hunt, G. & Carrano, M.T. 2010. Models and methods for analyzing phenotypic evolution in lineages and clades. In: Alroy, J. Hunt, G. Editors, Short Course on Quantitative Methods in Paleobiology. Denver, CO: Paleontological Society, pp. 245–269.
39. Lee, M.S.Y., Soubrier, J., Edgecombe, G.D. 2013. Rates of phenotypic and genomic evolution during the Cambrian Explosion. *Curr. Biol.* 23: 1889-1895.
40. Kass, R. E. & Raftery, A. E. (1995) Bayes factors. *Journal of the American Statistical Association* 90, 773-795.
41. Rambaut, A. & Drummond, A. J. (2009). *Tracer: MCMC Trace Analysis Tool* v1.5. <http://beast.bio.ed.ac.uk/>
42. Suchard M.A., Weiss R.E., & Sinsheimer J.S. (2001) Bayesian selection of continuous-time Markov chain evolutionary models. *Molecular Biology and Evolution* 18, 1001-1013.
43. Holtz, T.R. Jr. (1994) The phylogenetic position of the Tyrannosauridae: implications for theropod systematics. *Journal of Palaeontology* 68, 1100-1117.
44. Rauhut, O.W.M. (2003) A tyrannosauroid dinosaur from the Upper Jurassic of Portugal. *Palaeontology* 46, 903-910.
45. Brusatte, S., Norell, M.A., Carr, T.D., Erickson, G.M., Hutchinson, J.R., Balanoff, A.M., Bever, G.S., Choiniere, J.N., Makovicky, P.J. & Xu, X. (2010). Tyrannosaur paleobiology: new research on ancient exemplar organisms. *Science* 329, 1481-1485.
46. Brusatte, S.L., Nesbitt, S.J., Irmis, R.B., Butler, R.J., Benton, M.J. & Norell, M.A. (2010). The origin and early radiation of dinosaurs. *Earth Science Reviews* 101, 68–100.
47. Ezcurra, M.D. (2010) A new early dinosaur (Saurischia: Sauropodomorpha) from the Late Triassic of Argentina: a reassessment of dinosaur origin and phylogeny. *J. Syst. Palaeontol.* 8, 371–425.
48. Langer, M.C., Ezcurra, M.D., Bittencourt, J.S. & Novas, F.E. (2010) The origin and early evolution of dinosaurs. *Biological Reviews* 85, 55–110.
49. S.J. Nesbitt *et al.* The oldest dinosaur? A Middle Triassic dinosauriform from Tanzania. *Biol. Lett.* 9, e20120949 (2013).
50. Mudroch, A., Richter, U., Joger, U., Kosma, R., Ide, O., Maga, A. 2011 Didactyl tracks of paravian theropods (Maniraptora) from the ?Middle Jurassic of Africa. *Plos ONE* 6: e14642. (doi:10.1371/journal.pone.0014642)

51. Carrano, M.T., Benson, R.B.J. & Sampson, S.D. (2012) The phylogeny of Tetanurae (Dinosauria: Theropoda). *Journal of Systematic Palaeontology* 10, 211-300
52. Rauhut, O.W.M., Milner, A.C. & Moore-Fay, S. (2010) Cranial osteology and phylogenetic position of the theropod dinosaur *Proceratosaurus bradleyi* (Woodward, 1910) from the Middle Jurassic of England. *Zoological Journal of the Linnean Society*, 158, 155–195.
53. Benson, R.B.J. 2010. A description of *Megalosaurus bucklandii* (Dinosauria: Theropoda) from the Bathonian of the UK and the relationships of Middle Jurassic theropods. *Zoological Journal of the Linnean Society*, 2010, 158, 882–935.
54. Barrett, P.M. (2009). The affinities of the enigmatic dinosaur *Eshanosaurus deguchii* from the Early Jurassic of Yunnan Province, People's Republic of China. *Palaeontology*, 52, 681-688.
55. Wilgenbusch J. C., Warren D. L. & Swofford D. L. (2004) AWTY: A system for graphical exploration of MCMC convergence in Bayesian phylogenetic inference. (<http://ceb.csit.fsu.edu/awty>) (2004).
56. Rambaut, A. (2006) *Figtree: Tree Figure Drawing Tool*. Institute of Evolutionary Biology, University of Edinburgh. <http://tree.bio.ed.ac.uk/software/figtree/>
57. Laurin, M. (2010) Assessment of the relative merits of a few methods to detect evolutionary trends. *Systematic Biology* 59, 789-704.
58. Maddison, W.P. & D.R. Maddison. (2011). *Mesquite: a modular system for evolutionary analysis*. Version 2.75 <http://mesquiteproject.org>
59. Swofford, D. L. PAUP\*. (2003) *Phylogenetic Analysis Using Parsimony (\*and Other Methods)*, Version 4.0. Sinauer Associates, Sunderland, Massachusetts (2003).
60. Carpenter, J.M. (1988) Choosing among multiple equally parsimonious cladograms. *Cladistics* 4, 291-296.

Page left blank

## **CHAPTER 5 - New large-clawed theropod (Dinosauria: Tetanurae) from the Lower Cretaceous of Australia and the Gondwanan origin of megaraptorid theropods.**

Submitted: 29<sup>th</sup> October 2014. Published online: 02<sup>nd</sup> October 2015, and in formatted version: 01<sup>st</sup> August 2016 in *Gondwana Research* 36:473–487.

Phil R. Bell, Andrea Cau, Federico Fanti, Elizabeth Smith

### **Abstract**

Megaraptoridae comprises a clade of enigmatic Gondwanan theropods with characteristic hypertrophied claws on the first and second manual digits. The majority of megaraptorids are known from South America, although a single genus (*Australovenator*) plus additional indeterminate material is also known from Australia. This clade has a controversial placement among theropods, and recently has been interpreted alternatively as a carcharodontosaurian or a tyrannosauroid lineage. We describe a new megaraptorid based on fragmentary but associated postcranial remains from the opal fields of Lightning Ridge (middle-Albian, Griman Creek Formation) in north-central New South Wales. The new taxon predates *Australovenator* by c.10 Ma; the oldest megaraptoran is cf. *Megaraptor* from the Eumeralla Formation of Victoria, which is minimally coeval with this new specimen, but potentially 6.1–9.5 Ma older. From an Australian perspective, the new megaraptorid is also notable as the largest predatory dinosaur and is only the second theropod known from more than a single element. A Bayesian phylogenetic approach integrating morphological, stratigraphic and palaeogeographic information tested both the carcharodontosaurian and tyrannosauroid placements for Megaraptora. Regardless of the preferred placement among Tetanurae, rigorous palaeobiogeographic analyses support an Asian origin of Megaraptora in the latest Jurassic (about 150–135 Ma), an Early Cretaceous (about 130–121 Ma) divergence of the Gondwanan lineage leading to Megaraptoridae, and an Australian root for megaraptorid radiation. These results indicate that Australia's Cretaceous dinosaur fauna did not comprise simply of immigrant taxa but

was a source for complex two-way interchange between Australia-Antarctica-South America leading to the evolution of at least one group of apex predatory dinosaurs in Gondwana.

**Keywords:** Megaraptoridae, Dinosauria, Grimán Creek Formation, palaeobiogeography, Gondwana

## 1) Introduction

Historically, Australia has been viewed as an evolutionary *cul-de-sac* with regards to its enigmatic dinosaur fauna (Molnar, 1992a, 1997). Two hypotheses currently dominate, which suggest Australia's dinosaurs were either an aberrant and relict fauna with North American and Asian affinities (e.g. Rich and Rich, 1989; Rich and Vickers-Rich, 1994, 2003; Rich, 1996; Rich et al., 2014), or alternatively show close affiliations with faunas from western Gondwana, namely South America and Africa (e.g. Smith et al., 2008; Agnolin et al., 2010; Novas et al., 2013; Poropat et al., 2014). These polarised interpretations stem from a lack of consensus regarding taxonomic identifications, which in turn are a result of the highly fragmentary preservation of many Australian dinosaur specimens (see Agnolin et al., 2010; Poropat et al., 2014). Nevertheless, a Gondwanan affiliation for Australia's dinosaur fauna appears most tenable and is bolstered by similar interpretations of contemporaneous vertebrate groups including crocodyliforms, chelids, and mammals (Luo et al., 2002; Salisbury et al., 2006; Sterli et al., 2013; Poropat et al., 2014). Regardless, there is no convincing evidence to suggest that any major dinosaur lineage originated in Australia. In a marked departure from most other Australian Cretaceous vertebrates, the crocodyliform *Isisfordia duncani* from the earliest Late Cretaceous of Queensland (Salisbury et al., 2006) suggests that the radiation of at least one major clade—the modern crocodyliforms, Eusuchia—originated in Australia.

Of relevance to the current interpretation of Gondwanan dinosaur dispersal is the fossil record of Australian theropods, which almost exclusively comprises isolated elements. Such an inherently limited record has frustrated attempts to properly compare taxa and limited their use in palaeobiogeographic analyses (see Agnolin et al., 2010; Poropat et al., 2014 for recent revisions of Australian dinosaurs). The only named theropod represented by more than a single element is the megaraptorid *Australovenator wintonensis* from the lowermost Upper Cretaceous of south-central Queensland (Hocknull et al., 2009; White et al., 2012, 2013a; Tucker et al., 2013). In addition to *Australovenator*, Megaraptoridae (*sensu* Novas et al., 2013) consists of three Argentinean genera *Aerosteon*, *Megaraptor*, and *Orkoraptor*, which are generally characterised by their elongate, gracile metatarsus and hypertrophied claws on the first manual digit. The closely

related Asian form, *Fukuiraptor* was recovered as the sister taxon to Megaraptoridae (Novas et al., 2013) making Megaraptoridae purely Gondwanan in distribution (Porfiri et al., 2014).

Despite their distinctive morphology, megaraptoran affinities are unclear having been posited as closely related to Carcharodontosauridae within Allosauroidea (Benson et al., 2010a; Carrano et al., 2012; Zanno and Makovicky, 2013) or as deeply nested within Coelurosauria possibly within Tyrannosauroidea (Novas et al., 2013; Porfiri et al., 2014). Here, we report on associated fragmentary remains of a new megaraptorid from the Lower Cretaceous Griman Creek Formation exposed at Lightning Ridge (New South Wales, Australia). The partial remains do not allow a unequivocal classification of the taxon and therefore we refrain from assigning a formal naming to it. However, it represents only the second theropod specimen from Australia that comprises more than a single element and, more importantly, provides the basis for revised discussions on the dispersal history of Megaraptora and Australia's role in faunal interchange within Gondwana.

*Abbreviations.* LRF, Australian Opal Centre, Lightning Ridge, New South Wales, Australia, Lightning Ridge Fossil; MIWG, Dinosaur Isle, Isle of Wight Museum Service (formerly Museum of Isle of Wight Geology), Sandown, UK; NHMUK, Natural History Museum, London, United Kingdom; NMV, National Museum of Victoria, Melbourne, Victoria, Australia, Palaeontological collections.

## 2. Locality and Geology

LRF 100–106 was excavated from an underground mine at the 'Carter's Rush' opal field, 30 km southwest of the town of Lightning Ridge, north-central New South Wales (Fig. 1). Although the precise stratigraphic provenance of LRF 100-106 is unknown due to the mining process during which the specimen was discovered and excavated (see Comments in Systematic Palaeontology below), opals and opalised fossils are routinely sourced from the top of the Finch Claystone near its contact with the overlying Wallangulla Sandstone (both pertaining to the Griman Creek Formation, Rolling Downs Group, Surat Basin; Green et al., 1997). Sediments of the Griman Creek Formation consist of primarily non-marine, thinly bedded and interlaminated fine- to medium-grained sandstone and mudstone. Both

freshwater and brackish molluscs occur in the lower part of the formation whereas coals seams and freshwater bivalves are found in the upper deposits, therefore, beds are interpreted as representing a variety of coastal fluvial to estuarine and lagoonal deposits that accumulated on the southern margin of the Eromanga Sea (Dettman et al., 1992; Haig and Lynch, 1993; Green et al., 1997). In particular, deposition is considered to have been initially regressive beach or nearshore marine, followed by paralic to deltaic and finally fluvial floodplain conditions in the upper sequences of the formation (Green et al., 1997). The Griman Creek Formation preserves a poorly known but diverse vertebrate fauna that includes titanosauriform sauropods (Molnar and Salisbury, 2005; Molnar, 2011), megaraptoran theropods (von Huene 1932; Molnar, 1980a; Agnolin et al., 2010; White et al., 2013b), basal ornithopods (von Huene, 1932; Molnar and Galton, 1986), iguanodontian-grade ornithopods (Molnar, 1992b), crocodylians (Etheridge, 1917; Molnar, 1980b; Molnar and Willis, 2001), birds (Molnar, 1999), plesiosaurs (Kear, 2006), dipnoans (Kemp and Molnar, 1981; Kemp, 1993, 1997a,b), chelids (Smith, 2010; Smith and Kear, 2013), monotremes (Archer et al., 1985; Rich et al., 1989; Flannery et al., 1995), as well as possible indeterminate synapsids (Clemens et al., 2003) and undescribed teleost and chondrichthyan remains (Dettman et al., 1992; PRB, ES pers. obs.).

Direct chronostratigraphic constraints for the Griman Creek Formation are limited to two fission-track analyses on core samples from the eastern margin of the Surat Basin. The first indicates a ~107 myr age, the second suggests that sedimentation ended at ca 99 myr (Raza et al., 2009) and was followed by a denudation phase responsible for a major unconformity in the area (Korsch and Totterdell, 2009; Totterdell et al., 2009). Similarly, palynofloras of reference unit APK5 are associated with the Griman Creek Formation deposits (*Coptospora paradoxa* spore-pollen zone; Burger, 1980; Dettmann et al., 1992; Price, 1997 and references therein), supporting a middle Albian age for this interval. Furthermore, basin-scale correlations between the Surat Basin and the Eromanga Basin deposits to the northwest indicate that the Griman Creek Formation is coeval to the Toolebuc and Allaru formations, both referred to the mid- and early-lower Albian, respectively (Haig and Lynch, 1993; Gray et al., 2002; Cook, 2012). These units are overlaid by the upper Albian Mackunda Formation and the upper Albian–lower Turonian Winton Formation (see Cook, 2012 and Tucker et al., 2013 for a detailed revision of

biostratigraphic data). Relevant to this study, detrital zircon ages for the Winton Formation (a pivotal unit preserving a rich and diverse vertebrate fauna which crops out widely across central-western Queensland, north of the study area) record a depositional history during the interval ~103–92 Ma (Tucker et al., 2013). More specifically, rocks containing Australia's only named megaraptorid, *Australovenator*, lie at or close to the Cenomanian-Turonian boundary (94.5–92.5 Ma; Tucker et al., 2013). Thus, *Australovenator* (and associated vertebrate fauna including dinosaurs, crocodyliforms, aquatic squamates, turtles, lungfish and teleost fishes), is roughly 12 million years younger than the deposits (and its constituent fauna) around Lightning Ridge.

### 3. Systematic Palaeontology

Dinosauria Owen 1842

Saurischia Seeley 1887

Theropoda Marsh 1881

Tetanurae Gauthier 1986

Megaraptora Benson, Carrano, et Brusatte 2010a

Megaraptoridae Novas, Agnolin, Ezcurra, Porfiri, et Canale 2013

Gen. et sp. indet.

*Remarks:* The associated but fragmentary postcranial skeleton (LRF 100–106) includes proximal parts of the right ulna and the left or right manual ungual I-2, possible fragments of the distal tibia, the left metatarsal III, the pubic peduncle of left ilium, numerous rib and gastral rib fragments, and many unidentified fragments. All the elements are preserved as natural casts (pseudomorphs) in bluish-grey potch opal, which in places shows flashes of reds and blues that are associated with precious opal. Unfortunately, this unusual mode of fossilisation generally results in the total loss of bone microstructure (Rey, 2013), which in this case obviates histological observation that may have provided clues as to the maturity

of the individual. The available material is referred to a medium-sized (approx. 6 m long) megaraptorid theropod characterised by proximal end of metatarsal III strongly asymmetrical (mediolateral aspect) with trapezoidal cranial process extending further distally along the shaft than the caudal process giving an overall ball-peen hammer-shaped profile; and contact for metatarsal II on metatarsal III divided into cranial and caudal halves by shallow, longitudinal groove. Although no formal taxon is erected, it differs from the other Australian megaraptorid, *Australovenator*, based on the following combination of features: 1. More robust cranial process on the ulna; 2. More gracile manual ungual I-2 with sharply defined median ridge on proximal articular surface; 3. Prominent, broad groove between the articular facet and the flexor tubercle on manual ungual I-2 (convergent in *Megaraptor*); 4. Metatarsal III with a well-developed lateral ridge on proximal shaft; and 5. Distal articular surface of metatarsal III as wide as it is long.

*Locality and horizon:* LRF 100–106 was excavated from an underground mine at the ‘Carter’s Rush’ opal field, 30 km southwest of the town of Lightning Ridge, north-central New South Wales. The specimen comes from the top of the Finch Claystone near its contact with the overlying Wallangulla Sandstone (both pertaining to the Griman Creek Formation, Rolling Downs Group, Surat Basin [Green et al., 1997]), and is middle Albian in age.

*Comments:* Opalised fossils at Lightning Ridge (and other opal-bearing regions such as Coober Pedy and Andamooka) are typically discovered following a protracted process of extraction, sieving, washing and sorting of bulk sediments. As a result, fossils discovered during this process are typically small, isolated, and abraded, and any association between specimens is lost. In contrast, LRF 100-106 was discovered *in situ* during excavation of an underground mine at the ‘Carter’s Rush’ opal field. Some of the bones were recognized and manually removed by miners and eventually donated to the Australian Opal Centre in 2005. Regrettably, an unknown number of bones were not recognized and presumably destroyed prior to or during excavation of what was almost certainly a more complete skeleton than is currently represented. Fresh breaks on most of the recovered bones (e.g. ulna, manual ungual) attest to the unfortunate damage done during excavation. Although the original (*in situ*) positions of the bones were not recorded during excavation, the overall paucity of dinosaur fossils and the extreme rarity of large

(>10 cm) bones in the Griman Creek Formation all suggest the elements come from a single individual. Moreover, the respective sizes of bones, lack of overlapping elements, and megaraptoran features present on many of the bones are all consistent with their assignment to a single individual. Thus, we reject the possibility that the specimen represents a chimera as has been argued for some other Australian dinosaurs (see Herne and Salisbury, 2009 and counterargument by Rich et al., 2010). No other fossil remains were found (or at least recognised by the miners) alongside the megaraptoran elements.

In 1932, a single metacarpal I (NHMUK R3718) also from the Griman Creek Formation at Lightning Ridge was used to erect a new theropod taxon, *Rapator ornitholestoides* (von Huene, 1932). Recent comparisons with *Australovenator* and *Megaraptor* suggest megaraptoran affinities of NHMUK R3718 although there is disagreement regarding the validity of *R. ornitholestoides* (Hocknull et al., 2009; Agnolin et al., 2010; White et al., 2013b). We follow Agnolin et al. (2010) in considering *R. ornitholestoides* as a *nomen dubium* and although NHMUK R3718 and LRF 100-106 may conceivably pertain to the same taxon, there are no overlapping elements to test this hypothesis. In addition to the questionable validity of *Rapator*, LRF 100-106 comprises more complete remains and is consequently more informative than NHMUK R3718, and; LRF 100-106 displays a suite of characters that provide higher resolution of its phylogenetic position.

## 4. Description

### 4.1. Ulna

The proximal end of the right ulna consists of the articular surface for the humerus and part of the olecranon process (Fig. 2). In lateral view, the bone is craniocaudally broadest between the cranial process and the caudal crest, tapering distally. The humeral articular surface is arcuate in mediolateral view and flattened across the articular surface to form a smooth contact with the distal humerus. A lateral ridge extends along the midline of the ulna for the full preserved length of the element (Fig. 2D). The ridge is low, symmetrical in section and becomes less prominent distally. Although broken, the crest is reminiscent of the lateral crest present in the megaraptorids *Australovenator*, *Megaraptor*,

and cf. *Megaraptor* from Victoria (Novas, 1998; Smith et al., 2008; White et al., 2012). As the proximal part of the crest is broken in LRF 100-106, it is unclear whether it also formed a prominent tuberosity as in *Australovenator* and *Megaraptor* (Fig. 2A, D). Several megalosauroids (*Baryonyx*, *Poikilopleuron*, *Suchomimus*, *Torvosaurus*) also possess a lateral tuberosity; however, they lack the proximodistally-orientated crest present in megaraptorids (Smith et al., 2008). Caudal to the lateral crest, the caudolateral surface forms a shallow but broad fossa, which Smith et al. (2008) posited as the insertion for the m. *triceps brachii* complex. Such a fossa is present in megaraptorids and some spinosaurids (*Baryonyx*, *Suchomimus*); however, the fossa is more caudally facing in the latter group (Smith et al., 2008). The forelimb osteology is not well known in allosauroids although a caudolateral fossa is absent in *Allosaurus* (Madsen, 1976), *Acrocanthosaurus* (Currie and Carpenter, 2000), and *Concavenator* (Ortega et al., 2010, fig. 4). Several small neurovascular foramina pierce the surface of this fossa in LRF 100-106. The medial surface is concave and comparatively featureless. The medial and lateral sides meet to form a sharply defined caudal margin, or crest; a feature peculiar to megaraptorids (Smith et al., 2008; Novas et al., 2013). Proximally, the sheared base of the olecranon process indicates that it was mediolaterally compressed and at least as craniocaudally long as the humerus-ulna articular surface (in proximal view). A mediolaterally compressed olecranon process is characteristic of megaraptorids (Novas et al., 2013). A similar condition is present in *Suchomimus* and *Baryonyx*; however, in these taxa the olecranon process (in proximal view) is distally expanded compared to the triangular process in megaraptorids. In addition, the olecranon process and cranial process of this taxon and megaraptorids are in the same craniocaudal plane when viewed proximally, whereas they form a comparatively acute angle in *Baryonyx* and *Suchomimus* (Smith et al., 2008). Separating the olecranon process and the proximal articular surface is a shallow, transverse sulcus visible in lateral aspect (Fig. 2C, F). This sulcus exposes the internal trabecular bone, therefore it is unclear whether this feature is real or an artefact; the latter may be more likely given its close proximity to other fractures (e.g. on the lateral crest and olecranon process). A small sulcus is present on the right ulna of *Australovenator* (absent on the left), where it too is associated with a break in the specimen (White et al., 2012; S. Salisbury pers. comm. 2014). No sulcus is evident in any specimen referred to *Megaraptor* (Novas,

1998, fig. 1; Agnolin et al., 2010, fig. 19) nor in an isolated megaraptoran ulna (NMV P186076) from the Aptian-Albian of Victoria (Smith et al., 2008; Fig. 3).

#### 4.2. Manual Ungual

The proximal end of a manual unguis is identified as belonging to digit I based on its large size, which compares more favourably to the unguis of digit I of *Australovenator* rather than to either digits II or III (Table 1). It preserves the proximal articular surface, flexor tubercle and part of the unguis blade (Fig. 4). Parts of the lateral and palmar surfaces are obscured by opal patch spicules (a product of diagenesis); however, enough can be discerned to tell that the unguis was strongly mediolaterally compressed and tapered to a sharp edge along its inner curvature (palmar margin). The proximal articular surface is dorsoventrally elongate (height to width ratio=2:1), ovoid, and strongly ginglymoid (Fig. 4A,E), typical of megaraptoran theropods (Novas, 1998; Novas et al. 2013). The lateral and medial margins of the articular surface extend as low ridges onto the dorsal part of the unguis continuing a short distance distally before converging at the midline. These ridges delineate a raised proximodorsal extensor tubercle, the dorsal portion of which is missing in this specimen. Immediately distal to this region, both lateral and medial sides of the unguis are ornamented by numerous, fine, axially-orientated striations. In both *Australovenator* (White et al., 2012) and *Megaraptor* (Novas, 1998; Calvo et al., 2004), the distal halves of the medial and lateral grooves are asymmetrically positioned so that the medial groove is positioned higher than the lateral one. Although both grooves are present in the new theropod, not enough of the claw is preserved to identify whether they were similarly asymmetrical. As a result, it is not currently possible to identify whether this element is from the left or right side. The flexor tubercle is low as in *Australovenator* (White et al., 2012) and *Megaraptor* (Novas, 1998), square in palmar view and separated from the proximal articular surface by a deep sulcus. This sulcus extends distally onto the lateral and medial surfaces of the unguis (Fig. 4E, F). A similar sulcus between the flexor tubercle and proximal articular surface is present in *Megaraptor* (Novas, 1998, fig. 3) but absent in *Australovenator* (White et al., 2012, fig. 16) where it is replaced by a shallow transverse groove (“ventral medio-lateral groove” of White et al., 2012). The flexor tubercle is subdivided into discrete regions in palmar view (Fig. 4H):

proximally, it forms a flattened, transverse rectangular platform. The platform is delineated distally by a low transverse ridge in front of which are two shallow depressions (medial and lateral flexor facets) separated by a median ridge.

### 4.3. Pubic peduncle of ilium

An incomplete, triangular bone is tentatively identified as the ventral end of the pubic peduncle of the ilium. This bone part is known in two megaraptorans, *Fukuiraptor* (Azuma and Currie, 2000; Benson et al., 2010a) and *Aerosteon* (Sereno et al., 2008; Novas et al., 2013). The bone is broken transversely exposing the highly pneumatic interior (Fig. 5C). Pneumatisation of the ilium is a derived feature shared by Megaraptora and *Neovenator* (Sereno et al., 2008; Benson et al., 2010a). In ventral aspect, the bone forms an asymmetrical triangle; the medial and lateral sides are caudally divergent, although the medial edge extends further caudally than the lateral edge forming a sharply attenuating caudal process in distal view (Fig. 5C). The medial and lateral caudal processes are separated by a broad concavity that forms the acetabular margin. This contrasts with the condition in other megaraptorans for which this element is preserved and most tetanurans in which the pubic peduncle is broadly U-shaped in distal view (e.g. Novas et al., 2013, fig. 15). It also differs from the heart-shaped outline of megalosauroids (*Eustreptospondylus*, Sadleir et al., 2008; *Megalosaurus*, Benson, 2009). The ventral articular surface is obscured by matrix but weakly convex in lateral view and tapers dorsally such that the articular surface is the longest and broadest part of the preserved element. The medial and lateral surfaces are ornamented by fine dorsoventrally-orientated striations (Fig. 5A, B), which are likely scars representing the attachment site for connective tissues between the pubic peduncle and the pubis (Hutchinson, 2001). The ventral surface is craniocaudally longer (17.5 cm) than mediolaterally wide (11.1 cm) at its caudal end, proportionally more elongate than in *Fukuiraptor* (the latter showing a ventral end of the pubic peduncle that is about as wide as long, Benson et al., 2010a), but not as elongate as *Aerosteon* in which the peduncle is more than twice longer than wide in ventral view (Sereno et al., 2008; Novas et al., 2013).

#### 4.4. Fibula

Based on comparisons with the holotype of *Australovenator* (Hocknull et al., 2009; White et al., 2013a), two incomplete bones are tentatively interpreted as parts of the shaft and distal end of the (?)left fibula. Despite uncertainty regarding the identification of these bones, they are briefly described here to supplement the description. The largest fragment, broken both proximally and distally, measures 9.5 cm long. Medially an elongate concavity extends the entire length of the bone (Fig. 6B), which may correspond to the longitudinal groove on the fibula of *Australovenator* (Hocknull et al., 2009). The lateral surface forms a convex V-shape in cross section. The second fragment appears to represent the distal tip of the fibula. In distal view, the lateral margin is convex, the apex of this convexity lying cranial of the midpoint. The medial margin is flat, where it presumably formed an articulating facet for the distal tibia (Fig. 6E).

#### 4.5. Metatarsal III

The left metatarsal III is the most complete element of LRF 100-106 (Fig. 7), roughly 9% longer than the equivalent element on the holotype of *Australovenator* (Table 1). In general, it is elongate and transversely narrow, typical of most coelurosaurs (including megaraptorans), *Mapusaurus*, but contrasting with the more stout proportions in *Neovenator* and basal tetanurans (Novas, 1998; Coria and Currie, 2006; Hocknull et al., 2009; Novas et al., 2013). It is straight in both mediolateral and craniocaudal views. In mediolateral view, the proximal end of the metatarsal is asymmetrically expanded craniocaudally (Fig. 7C); the cranial process is trapezoidal and extends farther distally than the roughly cuboidal-shaped caudal (palmar) process. This configuration gives the proximal metatarsal the overall appearance of a ball-peen hammer, which strongly contrasts with the fan-shaped profile that is otherwise widespread among Theropoda (e.g. Currie and Zhao, 1993; Azuma and Currie, 2000; Coria and Currie, 2006; Figs. 7L,M). The cranial process in *Neovenator* approaches the condition in the new taxon; however, *Neovenator* differs in that the cranial margin of the cranial process (when viewed medially) is parallel to the shaft of the metatarsal (Brusatte et al., 2008, pl. 42) whereas it is oblique in the new Australian specimen. The caudal process in *Neovenator* is broken; therefore a

full comparison cannot be made. Medially, the flat contact for metatarsal II is divided into cranial and caudal halves by a shallow, longitudinal groove (Fig. 7L) and is demarcated caudally by a curved, raised rim of bone (Fig. 7L). The proximal part of metatarsal III is unknown in *Megaraptor*; however, neither the raised caudal rim nor the longitudinal groove is present in *Australovenator*, *Fukuiraptor*, or *Neovenator* and are thus considered potential autapomorphies of the new megaraptorid. In proximal view, the articular surface is rounded cranially and mediolaterally expanded, constricted at its midpoint, and mediolaterally expanded caudally, although less so than the cranial half. At the caudal margin of the proximal articular surface, the medial and lateral margins meet to form a right angle in proximal aspect (Fig. 7I). This contrasts with the blunt, roughly square caudal end in *Australovenator*. A prominent anterolateral swelling (in proximal view) continues distally by way of a prominent lateral crest that extends approximately one-quarter the length of the shaft (Fig. 7C,F). The height of this crest diminishes abruptly at its distal end but continues as a low ridge for at least two-thirds the length of the shaft (Fig. 7F,G). This arrangement differs from *Australovenator* in which the transition between the proximal crest and the ridge is gradual rather than abrupt. The distal one-third of the shaft is damaged, so the full extent of this ridge cannot be determined in this specimen. Proximally, this ridge would have braced the medial face of metatarsal IV.

In cross-section, the shaft is teardrop-shaped proximally (the pointed end facing cranially), becoming sub-circular distally. The distal extremity of the metatarsal is weakly expanded both mediolaterally and craniocaudally as in *Fukuiraptor* (Azuma and Currie, 2000) and other megaraptorids for which this element is preserved. The distal articular surface is roughly square in distal view (maximum distal width:maximum craniocaudal length = 1:1) and weakly ginglymoid compared to *Megaraptor* (Novas, 1998) and *Australovenator*, but more so than the megaraptoran *Fukuiraptor* (Azuma and Currie, 2000). The distal part of metatarsal III is missing in *Neovenator*, therefore comparisons are impossible. Deep collateral ligament insertion pits are present on either side of the distal articular surface. The distal articular surface extends proximally onto the cranial face of the metatarsal, which is unusual for theropods but is synapomorphic for Megaraptoridae (Novas et al., 2013). Immediately proximal to the distal articular surface is a broad, arcuate

extensor ligament fossa (Fig 7A, E), which is also a megaraptorid synapomorphy (Novas et al., 2013).

#### **4.6. Ribs and gastralia**

Fragments of several ribs and gastralia were recovered with the holotype. An incomplete rib head (Fig. 8A) comprising the capitulum is craniocaudally compressed with a concave dorsal margin and straight ventral margin (length = 5.5cm). The proximal articular facet is elliptical; the long axis of which forms an acute angle with the dorsal margin of the capitulum in craniocaudal view. A section of rib shaft measuring 12.5cm is nearly straight and tapers distally. The cranial surface is convex. Caudally, the rib is broadly concave medially, convex laterally where it is buttressed by a rounded longitudinal ridge. This ridge diminishes distally such that the distal cross-section is more elliptical. A 10cm section of gastral rib preserves a distinct widening (overtubulation) of the shaft (Fig. 8C). However, surface preservation of this element is poor so it cannot be determined if this widening represents the fusion of two elements (see Sereno et al., 2008), or is pathological or some other artefact. No evidence of pneumaticity was found in any of the gastralia or rib elements.

### **5. Phylogenetic analyses**

#### **5.1. Parsimony analyses**

In order to assess the affinities of the Lightning Ridge theropod, the new Australian taxon was scored using modified versions of the most recent and comprehensive character matrices for megaraptorans, provided by Novas et al. (2013) and Zanno and Makovicky (2013), supporting, alternatively, a tyrannosauroid and carcharodontosaurian placements of Megaraptora. Modifications of the Novas et al. (2013) dataset involved the inclusion of the new specimen, two Jurassic coelurosaurians (*Archaeopteryx* and *Zuolong*) and the recently named megaraptoran *Siats* (Zanno and Makovicky, 2013), and the addition of 26 new morphological characters relevant in resolving the positions of the added taxa, resulting in a data matrix of 313 characters and 49 taxa, with *Ceratosaurus*

used as an outgroup (see Supplementary Information). In both datasets, character scores for *Megaraptor* were updated following Porfiri et al. (2014). Modifications of the Novas et al. (2013) dataset involved the inclusion of the new specimen. Characters 255, 271 and 285 were *a priori* set with weight=0 as they became redundant with other included characters, respectively, characters 35, 78 and 108 (as outlined by Porfiri et al., 2014). Each dataset was analysed under both parsimony analysis and Bayesian inference, the latter integrating morphological and stratigraphic data following the method described by Lee et al. (2014a,b). Parsimony analyses performed heuristic searches with 100 random addition sequence replicates and tree bisection reconnection using the Hennig Society version of TNT (Goloboff et al., 2008). The search using the modified dataset of Novas et al. (2013) retrieved 448 most parsimonious trees with a length of 1031 steps (Consistency Index= 0.36, Retention Index=0.64). Unsurprisingly, the overall results are similar to those of the original analysis by Novas et al. (2013). Megaraptorans were recovered among Coelurosauria in a largely unresolved polytomy due to the uncertain position of *Siats*, found, alternatively, as related to ornithomimosaur, as closer to maniraptorans than tyrannosauroids, as a basal megaraptoran, and as closer to tyrannosaurids than *Xiongguanlong*. When *Siats* is pruned *a posteriori* from the results, the reduced strict consensus of the shortest trees recovered a monophyletic Megaraptora, including the new theropod, as sister-taxon of the clade including Tyrannosauridae, *Appalachiosaurus* and *Xiongguanlong* (Fig. S1). The most parsimonious results of the analysis did not support an allosauroid placement for megaraptorans, as measured by step differences between alternative placement of megaraptorans and our preferred topology: forcing megaraptorans among allosauroids (as per Benson et al., 2010a and Zanno and Makovicky, 2013) produced topologies 8 steps longer than the unforced topologies, with *Neovenator* and *Chilantaisaurus* as successive closest relatives of megaraptorans among the basalmost carcharodontosaurian lineage. Nevertheless, this alternative allosauroid hypothesis is not a statistically worse explanation of the data than the tyrannosauroid placement, based on the Templeton test ( $p>0.7$ ,  $N=88$ ; Templeton, 1983).

We also analysed the placement of the new Australian theropod and megaraptorans using the dataset of Zanno and Makovicky (2013). Modifications to the original dataset of those authors included the addition of the new specimen and the rescoring of several

cranial characters for *Megaraptor* following the findings of Porfiri et al. (2014) (see Supplementary Information). The topologies recovered in the second analysis are largely comparable to the original results by Zanno and Makovicky (2013). In all 20844 shortest trees found (tree length = 1053; CI=0.41; RI=0.69), the Lightning Ridge theropod is recovered among megaraptorans, the latter placed among carcharodontosaurian allosauroids (Fig. S1). Since the ingroup of the second dataset lacks both derived tyrannosauroids and representatives of the other main coelurosaur clades, the quantitative support for the tyrannosauroid/coelurosaurian placement for Megaraptora supported by Novas et al. (2013) cannot be tested with the dataset of Zanno and Makovicky (2013). Therefore, based on re-analysis of the most comprehensive datasets published, we consider premature any placement of Megaraptora beyond Tetanurae *incertae sedis*. We note, however, that wider taxon sampling in the Novas et al. (2013) dataset (compared to that of Zanno and Makovicky [2013]) and the recent discovery of tyrannosauroid features in the skull of *Megaraptor* lend support to the tyrannosauroid hypothesis (Novas et al., 2013; Porfiri et al., 2014). Nevertheless, we discuss the *tempo* and mode of megaraptoran evolution under both the alternative carcharodontosaurian and tyrannosauroid hypotheses.

## 5.2. Bayesian and RASP analyses

Bayesian analysis integrating the morphological data (used in the parsimony analyses) and stratigraphic data was performed with BEAST (Drummond et al., 2012) following the method of Lee et al. (2014b). Stratigraphic data and age constraints for each terminal were obtained primarily from the Paleobiology Database (<http://paleobiodb.org/>) and from the literature, using the known geochronological ages for the formations in which the taxa were found or the mean of the geologic stages associated with those formations. In the modified dataset of Novas et al. (2013), root age prior (i.e., the maximum age of the last common ancestor of *Ceratosaurus* and tetanurans) was set along a uniform range between 167 Mya (the age of the oldest terminal included, *Megalosaurus*) and 201 Mya, the latter considered as a 'loose' hard constraint that consistently pre-dates the age of the oldest potential tetanurans and excluding coelophysids from Ceratosauria (as resulted in the parsimony analysis of the dataset of Zanno and Makovicky, 2013). Relevant for the purpose of this analysis, we remark that less restrictive root age assumptions, based on a

more inclusive Ceratosauria (e.g., Allain et al., 2007) returned results for the neotetanuran nodes similar to the above mentioned, more restrictive, age assumption. Tetanuran monophyly was forced, following outgroup definition in the parsimony analyses, but no age constraint or internal topologies for Tetanurae were enforced. In the modified dataset of Zanno and Makovicky (2013), root age prior (i.e., the maximum age of the last common ancestor of *Eoraptor*, *Herrerasaurus* and neotheropods) was set along a uniform range between 233 Mya (the age of the oldest terminals included, *Eoraptor* and *Herrerasaurus*) and 252 Mya (the Permian-Triassic boundary), the latter considered as a 'loose' hard constraint that consistently pre-dates the age of the oldest potential dinosauromorphs. In both analyses, rate variation across traits was modelled using the gamma parameter, and rate variation across branches was modelled using an uncorrelated relaxed clock. The analyses used four replicate runs of 40 million generations, with sampling every 4000 generations. Burnin was set at 20%, and the Maximum Clade Credibility Tree (MCCT) of the four post-burnin samples was used as framework for phyletic reconstruction.

The analysis of the modified dataset of Novas et al. (2013) produced a topology largely consistent with the parsimony analysis (Fig. S2). Megaraptora was recovered as a tyrannosauroid subclade closer to tyrannosaurids than proceratosaurids. *Fukuiraptor* was placed as basalmost megaraptoran and sister taxon of Megaraptoridae, and the Lightning Ridge theropod as oldest and most basal member of the latter clade. Although some of the included megaraptoran taxa are based on very fragmentary remains, the phyletic placement of the new Australian taxon was robust, with posterior probability (pp) values of Megaraptora, Megaraptoridae, and of the megaraptorid subclade excluding the new Australian taxon that resulted, respectively, 0.78, 0.89 and 0.71. *Siats* was recovered as closer to ornithomimids than other coelurosaurs as in one of the alternative topologies found in the parsimony analysis, although this placement is weakly supported (pp=0.29). Cladogenetic timing inferred by the Bayesian analysis placed the megaraptoran divergence from other tyrannosauroids at about 150 Mya, and the origin of the lineage leading to the Gondwanan megaraptorans (Megaraptoridae) at about 130 Mya.

The BEAST analysis of the modified dataset of Zanno and Makovicky (2013) also produced a topology largely consistent with the parsimony analysis (Fig. S2b). Megaraptorans are placed as a basal carcharodontosaurian lineage, diverging from the

*Neovenator* lineage at about 135 Ma (pp=0.62). Both *Chilantaisaurus* and *Siats* are recovered as megaraptorans more derived than *Fukuiraptor*, although this result is moderately supported (pp=0.50). The new Australian theropod is found as the basalmost member of the Gondwanan megaraptorids, a result weakly supported (pp<0.50) probably due to the fragmentary preservation of both the holotype and other basal megaraptorans. The divergence of the megaraptorid lineage from other megaraptorans is placed at about 121 Ma.

The two alternative topologies recovered by the Bayesian analyses were used as phyletic frameworks for palaeobiogeographic reconstruction, inferring ancestral geographic placement of nodes using RASP (Reconstruct Ancestral State in Phylogenies, Yan et al., 2011). The distribution range of selected theropod taxa was *a priori* divided into six areas: Asia (A), Europe (B), North America (C), Africa (D), South America (E) and Australia (F). Each terminal taxon was scored for the geographic area character state according to the continent(s) it was recovered in (e.g., the new specimen was scored as “F”, whereas *Fukuiraptor* was scored as “A”). Biogeographic inferences on the phylogenetic frameworks were obtained by utilising Statistical Dispersal-Vicariance analysis (S-DIVA) and Bayesian Binary Markov Chain Monte Carlo (BBM) analysis (Yu et al., 2010). S-DIVA and BBM methods suggest possible ancestral ranges at each node and also calculate probabilities of each ancestral range at nodes. The S-DIVA and BBM analyses performed ten Markov Chain Monte Carlo analyses of 50 million generations, sampling every 100 trees. State frequencies were set as fixed and among-site rate variation was set using the gamma parameter. The first 20% of the recovered trees were discarded and the remaining trees were used to infer ancestral range distribution at nodes. In the S-DIVA analyses, direct range dispersal constraints were forced, excluding those routes considered as not plausible based on Jurassic and Cretaceous palaeogeographic reconstructions (Meschede and Frisch, 1998; Viramonte et al., 1999; Macdonald et al., 2003; Case et al., 2000; Fitzgerald, 2002; Jokat et al., 2003; Cook, 2012; Fanti, 2012; Huston et al., 2012).

### 5.3. Results of Palaeobiogeographic analyses

In the following paragraphs, we focus on the results yielded by the palaeogeographic analyses relative to Megaraptora.

#### 5.3.1. *Novas et al. (2013) dataset*

*S-DIVA analysis* (Fig. 9a): S-DIVA analysis indicated that the last common ancestor of megaraptorans and other tyrannosauroids was Asian or, alternatively “Asiamerican”. The analysis was unable to infer the ancestral range of the last common ancestor of *Fukuiraptor* and more derived megaraptorans; however, equally robust support was found for an Australian or “Australia-South America” ancestral range for Megaraptoridae. The analysis found an equal support for a South American or an “Australia-South American” range for the last common ancestor of the megaraptorids more derived than the Lightning Ridge theropod

*BBM analysis* (Fig. 9b): BBM analysis also indicated that the last common ancestor of Megaraptora and other tyrannosauroids was Asian. An Asian ancestral range for Megaraptora is inferred for the earliest Cretaceous phase of megaraptoran evolution. A diffusion event from Laurasia to Gondwana is consequently inferred to occur by no later than the early Aptian, with the most plausible ancestral range of the last common ancestor of the Lightning Ridge theropod and more derived megaraptorids (at ca 113 Ma) placed in Australia. The ancestral range of the last common ancestor of the more derived megaraptorids (at ca 103 Ma) is placed in South America. A single dispersal event from South America to Australia is inferred to have occurred after 96 Ma, leading to *Australovenator*.

#### 5.3.2. *Zanno and Makovicky (2013) dataset*

*S-DIVA analysis* (Fig. 10a): S-DIVA analysis also indicated that the last common ancestor of megaraptorans and other carcharodontosaurians was Eurasian, with an Asia ancestral placement for the megaraptoran node including *Fukuiraptor*. The range of the last common ancestor of the new taxon and more derived megaraptorids is inferred as

Australian, whereas the analysis was unable to determine the ancestral area of more derived megaraptorids (*Australovenator* and the South American taxa).

*BBM analysis* (Fig. 10b): BBM analysis indicated that the last common ancestor of Megaraptora and other carcharodontosaurians was European or, alternatively, Eurasian. An Asian root of Megaraptora is also supported, with *Siats* and Megaraptoridae as results of distinct dispersal episodes out of Asia. The last common ancestor shared by the new specimen with more derived megaraptorids is inferred to be Australian. Similarly, the last common ancestor of *Australovenator* and the South American megaraptorids *Aerosteon* and *Megaraptor* is also inferred to be Australian. Accordingly, the South American megaraptorids are interpreted as descendants from a migration event from Australia that occurred between 102 and 92 Ma.

## 6. Discussion

The Lightning Ridge theropod is assigned to Megaraptoridae based on the possession of a suite of synapomorphies, including: 1. transversely compressed manual ungual I with dorsoventrally elliptical proximal end; 2. metatarsal III with a distal ginglymoid and wide extensor fossa; 3. large, mediolaterally compressed olecranon process (present also in *Baryonyx walkeri* and *Suchomimus tenerensis* [Smith et al., 2008]); 4. lateral ridge on proximal ulna (present in some megalosauroids [Smith et al., 2008]); 5. broad fossa on caudolateral aspect of proximal ulna (present also in *Baryonyx walkeri* and *Suchomimus tenerensis* [Smith et al., 2008]); and 6. sharp caudal crest on proximal ulna. Furthermore, if our identification of the pubic peduncle of the ilium is correct, then an additional synapomorphy may be added to this list: extensive pneumatization of the ilium (present also in *Neovenator* [Benson et al. 2010a]). The association and overall morphology of the preserved bones, as well as the presence of derived megaraptoran features consistently agree in referring all specimens to a single taxon. The discovery of this theropod supplements earlier reports based on isolated Australian material (Smith et al., 2008; Agnolin et al., 2010; Benson et al., 2012) that extends Megaraptoridae into the Albian.

### 6.1. Comparison between Australian megaraptorans

Only one named megaraptoran is currently recognized from Australia:

*Australovenator*, from the upper part of Winton Formation (lower Turonian; Tucker et al., 2013) in central-western Queensland (Fig. 1). A nearly complete left ulna (NMV P186076) from the Albian-aged Eumeralla Formation in Victoria represents an indeterminate megaraptoran similar to *Megaraptor* (Smith et al., 2008; Agnolin et al., 2010). Features listed by Hocknull et al. (2009) and Agnolin et al. (2010) that distinguish NMV P186076 from *Australovenator* (presence of a curved caudal margin of the olecranon process, and absence of a longitudinal groove on the lateral surface of the shaft) cannot be observed in the new specimen due to incompleteness of the latter. However, NMV P186076 differs from the Lightning Ridge theropod in its smaller size (estimated at two-thirds the length of LRF 100-106 based on the assumption LRF 100-106 shares similar proportions to *Australovenator*); a proportionally more slender cranial process, rounded distally in proximal view (Fig. 3). The same features distinguish *Australovenator* from the new specimen, although *Australovenator* is closer in size to the new taxon than NMV P186076 (Fig. 3). Based on comparative measurements of the available material, the Lightning Ridge theropod was approximately 10% larger than *Australovenator* making it the largest theropod yet discovered in Australia. In addition to its smaller size, *Australovenator* can be differentiated from the new theropod on the basis of a set of characters summarised in Table 2. These include: a more robust manual ungual I-2 (Table 1); median ridge that subdivides the proximal articular region on manual ungual I-2 low and rounded; distal articular surface of metatarsal III square in distal view; lateral ridge on metatarsal III less well developed. Furthermore, the ribs of *Australovenator* display strongly dorsoventrally constricted “necks” on the capitulum. This contrasts with the comparatively weakly constricted “neck” on the only known capitulum of the Lightning Ridge theropod; however, we concede that this difference may be due to the incompleteness of the new specimen, variation along the dorsal series, or both.

A third putative megaraptoran is represented by an isolated metacarpal I (NHMUK R3718; holotype of *Rapator ornitholestoides*) from the same locality as the new specimen. However, as discussed earlier, the validity of *Rapator* is not universally accepted (Hocknull et al., 2009; Agnolin et al., 2010; White et al., 2013b). Lack of overlapping material

precludes comparison or unequivocal assignment of NHMUK R3718 relative to the new specimen, although the possibility that the two are congeneric (or conspecific) cannot be dismissed.

## 6.2. Palaeobiogeography of Megaraptora

The fragmentary and still largely debated theropod record of Australia has led to different interpretations on the *tempo* and mode of theropod distribution in the continent. Were these taxa mid-Cretaceous immigrants from adjacent Gondwanan landmasses (i.e. Antarctica and South America) or neoendemic taxa resulted from late Jurassic-earliest Cretaceous forms that were widespread across much of Gondwana and possibly other landmasses? In their recent review, Poropat et al. (2014) remarked on the problematic palaeobiogeographic interpretations of Australia's dinosaurs, which is symptomatic of its highly fragmentary fossil record. Those authors identified two opposing views: one which identifies a fauna of ceratosaurids, dromaeosaurids, neovenatorids, tyrannosauroids, and spinosaurids with Laurasian affinities and an alternative, less-specific interpretation that argues for Gondwanan ties in the Australian fauna. Besides the relatively well-documented affinities between Australian and South American dinosaurs (Molnar and Salisbury, 2005; Smith et al., 2008; Agnolin et al., 2010; Benson et al., 2012; Novas et al., 2013; Poropat et al., 2014), affinities shared by Asian (*Fukuiraptor*) and Australian (the new taxon, *Australovenator*) megaraptorans with other Asian theropods (e.g., *Chilantaisaurus* and several basal tyrannosauroids) play a pivotal role in this debate. Interestingly, similar Asian-South American affinities have been recently identified for the Australian titanosaur *Diamantinasaurus matildae* (Poropat et al., 2014). *Diamantinasaurus* was recovered as closely related to both a roughly coeval South American taxon (*Tapuiasaurus* from Brazil) but also to a latest Cretaceous Asian (*Opisthocoelicaudia* from Mongolia) taxon (Poropat et al., 2014).

In order to properly discuss results presented in this study, it is essential to include data for two important clades, tyrannosauroids and carcharodontosaurids. The fossil record of basal tyrannosauroids predates the oldest known megaraptorans and supports a

Middle-Late Jurassic radiation of tyrannosauroids prior to a Laurasian-Gondwana break-up (Holtz, 1994; Kellner, 1999; Xu et al., 2004, 2006; Hutt et al., 2001; Brusatte and Benson, 2013). The oldest record of carcharodontosaurids is from the Upper Jurassic of western Africa (Rauhut, 2011), which is consistent with the results of the time-calibrated Bayesian analyses proposed here that places the carcharodontosaurid divergence close to the Jurassic-Cretaceous boundary. Independent of the preferred placement of Megaraptora among Tetanurae, the fossil record of putative megaraptoran sister-taxa supports a Late Jurassic origin of the clade. Palaeobiogeographic implications of both the Novas et al. (2013) and Zanno and Makovicky (2013) datasets presented here include the primary divergence of megaraptorans from other theropods in the latest Jurassic-earliest Cretaceous. (Figs. 9, 10). Our analyses also concur in 1) placing the basal part of the megaraptoran evolution in Asia in the latest Jurassic-earliest Cretaceous; 2) supporting an active diffusion of megaraptorans from Laurasia to Gondwana in the earliest Early Cretaceous, and; 3) suggesting an Early Cretaceous radiation of megaraptorids across Gondwana. Furthermore, S-DIVA and BBM analyses of both the Novas et al. (2013) and Zanno and Makovicky (2013) datasets support Australia as the ancestral area of late Early Cretaceous evolution of Megaraptoridae (Figs. 9, 10). Moreover, this interpretation is consistent with the megaraptoran record from the upper Lower Cretaceous of Australia (Smith et al., 2008; Agnolin et al., 2010; Benson et al., 2012; this paper) even excluding the new taxon from the abovementioned analyses. Significantly, this interpretation challenges earlier claims that Australia played a primarily passive role in the evolution and dispersal of various dinosaur groups (Molnar, 1992a, 1997).

Pending further discoveries from continental Africa and Madagascar, data presented here, calibrated with well-documented palaeogeographic reconstructions concur on a latest Jurassic-to-earliest Cretaceous cosmopolitanism of several theropod groups, including megaraptorans. On the contrary, the Hauterivian-Barremian interval can be inferred as a chronological limit for biogeographical connections between southern landmasses and Europe/northern landmasses following widespread continental break up and the appearance of vast epicontinental seas (Crame, 1999; Ezcurra and Agnolin, 2012; Fanti, 2012 and references therein). The survival of theropod taxa in the Australian continent is here interpreted as early dispersal (i.e. Laurasia-Gondwana) followed by

vicariance combined with local faunal turnover (see also Agnolin et al., 2010; Benson et al., 2010b, 2012; Novas et al., 2013). These interpretations are mirrored by an increasing number of formerly Gondwanan clades recently discovered in Laurasia, such as rebbachisaurid sauropods, 'elaphrosaur' and carcharodontosaurian theropods, which argue for similar latest Jurassic-earliest Cretaceous cosmopolitanism of these respective groups (Brusatte et al., 2009; Hocknull et al., 2009; Xu et al., 2009; Benson et al., 2010b; Barrett et al., 2011; Mannion et al., 2011; Torcida Fernández-Baldor et al., 2011). Furthermore, the apparent proliferation of megaraptorid taxa in the Late Cretaceous coincides with the final stages of the total fragmentation of Gondwana, in particular the separation of South America from Africa. Similar trends have also been observed in abelisauroid theropods and titanosaurid sauropods, which suggest vicariance played an important role in the later evolution of these groups (Fanti, 2012). However, we note that the fossil record of basal megaraptorans is limited and that future discoveries from the Early Cretaceous of Australia may alter this view.

Contrary to earlier interpretations, Australia was not an evolutionary cul-de-sac for unidirectional dispersal events within Gondwana, nor was it simply a *refugium* for relict taxa (e.g. Rich and Rich, 1989; Rich and Vickers-Rich, 1994, 2003; Rich, 1996; Rich et al., 2014). Instead, this specimen provides new evidence that Australia played an active role in the evolution and radiation of at least one group of apex theropods. Significantly, the Australian origin of megaraptorid theropods is echoed by eusuchian crocodylomorphs wherein *Isisfordia duncani* from the earliest Upper Cretaceous of Queensland suggests the origin of this clade also has an Australian root (Salisbury et al., 2006). Evidently, faunal interchange involved complex and multidirectional interplay between the Gondwanan landmasses and it is anticipated that future discoveries from the Cretaceous of Australia will contribute to the increasingly complex picture of dinosaur palaeobiogeography (Upchurch, 2008).

## 7. Conclusions

The new Lightning Ridge megaraptoran is the largest and only the second theropod described from Australia based on a partial skeleton. This new taxon supplements and

confirms earlier reports based on isolated Australian material (Smith et al., 2008; Agnolin et al., 2010; Benson et al., 2012; White et al., 2013b) that definitively extends Megaraptoridae into the Albian. Cladogenetic timing inferred by the Bayesian analysis of the two relevant, most recent comprehensive datasets placed the megaraptoran divergence from other theropods close to the Jurassic-Cretaceous boundary (~140 Mya) and the origin of the lineage leading to Gondwanan megaraptorans (Megaraptoridae) at about 130 Mya, approximately 20 Ma prior to the appearance of the Lightning Ridge theropod. Although the phylogenetic position of Megaraptora remains equivocal, these results continue to challenge previous assertions that the Cretaceous of Australia consisted largely of relict fauna derived from elsewhere in Gondwana (e.g. Rich and Rich, 1989; Rich and Vickers-Rich, 1994, 2003; Rich, 1996; Rich et al., 2014). Instead, these findings provide evidence of complex faunal interchange between Australia and the rest of Gondwana leading to the evolution of Megaraptoridae.

## Acknowledgements

LRF 100–106 was discovered, excavated, and generously donated by Rob and Debbie Brogan. PRB is extremely grateful to Jenni Brammall, Liz and Bob Smith, and everyone at the Australian Opal Centre (Lightning Ridge) for their hospitality and diligence in preserving the fossils of Lightning Ridge. We thank Roger Benson for helpful discussions of European Theropoda and providing photos of *Neovenator* and Matt White for the photo of *Australovenator* figure 7. PRB was supported by start-up funding from the University of New England.

## References

Agnolin FL, Ezcurra MD, Pais DF, Salisbury SW. 2010 A reappraisal of the Cretaceous non-avian dinosaur faunas from Australia and New Zealand: evidence for their Gondwanan affinities. *J. Syst. Palaeontol.* **8**, 257–300.

- Allain R, Tykoski R, Aquesbi N., Jalil N-E, Monbaron M, Russell D, Taquet P. 2007 A basal abelisauroid from the late Early Jurassic of the High Atlas Mountains, Morocco, and the radiation of ceratosaurs. *J. Vert. Paleontol.* **27**, 610–624.
- Archer M, Flannery TF, Richie A, Molnar RE. 1985 First Mesozoic mammal from Australia: an Early Cretaceous monotreme. *Nature* **318**, 363–366.
- Azuma Y, Currie PJ. 2000 A new carnosaur (Dinosauria: Theropoda) from the Lower Cretaceous of Japan. *Can. J. Earth Sci.* **37**, 1735–1753.
- Barrett PM, Benson RB, Rich TH, Vickers-Rich P. 2011 First spinosaurid dinosaur from Australia and the cosmopolitanism of Cretaceous dinosaurs faunas. *Biol. Letters* **7**, 933–936
- Benson RB. 2009 A description of *Megalosaurus bucklandii* (Dinosauria: Theropoda) from the Bathonian of the UK and the relationships of Middle Jurassic theropods. *Zool. J. Linn. Soc.* **158**, 882–935.
- Benson RBJ, Carrano MT, Brusatte SL. 2010a A new clade of archaic large-bodied predatory dinosaurs (Theropoda: Allosauroida) that survived to the latest Mesozoic. *Naturwissenschaften* **97**, 71–78. doi:10.1007/s00114-009-0614-x.
- Benson RBJ, Barrett PM, Rich TH, Vickers-Rich P. 2010b A southern tyrant reptile. *Science* **327**, 1613.
- Benson RBJ, Rich TH, Vickers-Rich P, Hall M. 2012 Theropod fauna from southern Australia indicates high polar diversity and climate-driven dinosaur provinciality. *PLoS ONE* **7**, e37122.
- Brusatte SL, Benson RBJ, Hutt S. 2008 The osteology of *Neovenator salerii* (Dinosauria: Theropoda) from the Wealden Group (Barremian) of the Isle of Wight. *Monograph of the Palaeontographical Society* 1–75.
- Brusatte SL, Benson RBJ, Chure DJ, Xu X., Sullivan C, Hone DWE. 2009. The first definitive carcharodontosaurid (Dinosauria: Theropoda) from Asia and the delayed ascent of tyrannosaurids. *Naturwissenschaften* doi: 10.1007/s00114-009-0565-2
- Brusatte SL, Benson RBJ. 2013 The systematics of Late Jurassic tyrannosauroid theropods from Europe and North America. *Acta Palaeontol. Pol.* **58**, 47–54.

- Bryan SE, Cook AG, Allen CM, Siegel C, Purdy DJ, Greentree J, Uysal T. 2012 Early–mid Cretaceous tectonic evolution of eastern Gondwana: from silicic LIP to continental rapture. *Episodes* **35**, 142–152.
- Burger D. 1980 Palynology of the Lower Cretaceous in the Surat Basin. *Bureau of Mineral Resources, Geology and Geophysics, Australia, Bulletin* **189**, 1–106.
- Calvo JO, Porfiri JD, Veralli C, Novas F, Poblete F. 2004 Phylogenetic status of *Megaraptor namunhuaiquii* Novas based on a new specimen from Neuquén, Patagonia, Argentina. *Ameghiniana* **41**, 565–575.
- Carrano MT, Benson RBJ, Sampson SD. 2012 The phylogeny of Tetanurae (Dinosauria: Theropoda). *J. Syst. Palaeontol.* **10**, 211–300.
- Case J, Martin J, Chaney D, Reguero M, Marensi S, Santillana S, Woodburne M. 2000 The first duck-billed dinosaur (family hadrosauridae) from Antarctica. *J. Vertebr. Paleontol* **20**, 612–614.
- Clemens WA, Wilson GP, Molnar RE. 2003 An enigmatic (synapsid?) tooth from the Early Cretaceous of New South Wales. *J. Vertebr. Paleontol.* **23**, 232–237.
- Cook, A. 2012. Cretaceous faunas and events, northern Eromanga Basin, Queensland. *Episodes* **35** (1), 153–159
- Coria R, Currie PJ. 2006 A new carcharodontosaurus (Dinosauria, Theropoda) from the Upper Cretaceous of Argentina. *Geodiversitas* **28**, 71–118.
- Crame J. 1999 An evolutionary perspective on marine faunal connections between southernmost South America and Antarctica. *Sci. Marina* **63**, 1–14.
- Currie PJ, Carpenter K. 2000 A new specimen of *Acrocathosaurus atokensis* (Theropoda, Dinosauria) from the Lower Cretaceous Antlers Formation (Lower Cretaceous, Aptian) of Oklahoma, USA. *Geodiversitas* **22**, 207–246.
- Currie PJ, Zhao X-J. 1993 A new carnosaur (Dinosauria, Theropoda) from the Jurassic of Xinjiang, People's Republic of China. *Can. J. Earth Sci.* **30**, 2037–2081.
- Dettman ME, Molnar RE, Douglas JG, Burger D, Fielding C, Clifford HT, Francis J, Jell P, Rich T, Wade M, Rich PV, Pledge N, Kemp H, Rozefelds A. 1992 Australian Cretaceous terrestrial faunas and floras: biostratigraphic and biogeographic implications. *Cretaceous Research* **13**, 207–262.
- Drummond AJ, Suchard MA, Xie D, Rambaut A. 2012 Bayesian phylogenetics with BEAUti and the BEAST 1.7. *Mol. Biol. Evol.* **29**, 1969–1973.

- Etheridge R. 1917 Reptilian notes: *Megalania prisca*, Owen, and *Notiosaurus dentatus*, Owen; lacertilian dermal armour; opalised remains from Lightning Ridge. *Proceedings of the Royal Society of Victoria* **29**, 127–133.
- Ezcurra MD, Agnolin FL. 2012 A new global palaeobiogeographical model for the Late Mesozoic and Early Tertiary. *Syst. Biol.* **61**, 553–566.
- Fanti F. 2012 Cretaceous continental bridges, insularity, and vicariance in the Southern Hemisphere: which route did dinosaurs take? In *Earth and life* (ed. Talent J), pp. 883–911. Sydney: Springer.
- Fitzgerald P. 2002 Tectonics and landscape evolution of the Antarctic plate since the breakup of Gondwana, with an emphasis on the West Antarctic Rift System and the Transantarctic Mountains. *R Soc N Z Bull* **35**, 453–469.
- Flannery TF, Archer M, Rich TH, Jones R. 1995 A new family of monotremes from the Cretaceous of Australia. *Nature* **377**, 418–420.
- Gauthier J. 1986 Saurischian monophyly and the origin of birds. In *The Origin of Birds and the Evolution of Flight* (ed. Padian K). *Mem. California Acad. Sci.* **8**, 1–55.
- Gray ARG, McKillop M, McKellar JL. 2002 Eromanga Basin Stratigraphy. In *Geology of the Cooper and Eromanga Basins, Queensland* (ed. Draper JJ). Queensland Minerals and Energy Review Series, Queensland Department of Natural Resources and Mines 30–56.
- Green PM, Carmichael DC, Brain TJ, Murray CG, McKellar JL, Beeston JW, Gray ARG. 1997 Lithostratigraphic units in the Bowen and Surat Basins, Queensland. In *The Surat and Bowen Basins south-east Queensland* (ed. Green PM). Queensland Minerals and Energy Review Series 41–108.
- Goloboff P, Farris J, Nixon K. 2008 TNT, a free program for phylogenetic analysis. *Cladistics* **24**, 774–786.
- Haig DW, Lynch DA. 1993 A late early Albian marine transgressive pulse over northeastern Australia, precursor to epeiric basin anoxia: foraminiferal evidence. *Mar. Micropaleontol.* **22**, 311–362.
- Herne MC, Salisbury SW. 2009 The status of *Leallynasaura amicagraphica* (Dinosauria: Ornithischia) from the Early Cretaceous of south-eastern Australia. In Conference

on Australasian Vertebrate Evolution, Palaeontology and Systematics. *Geological Society of Australia Abstracts* **93**, 35.

- Hocknull SA, White MA, Tischler TR, Cook AG, Calleja ND, Sloan T, Elliot DA. 2009 New mid-Cretaceous (latest Albian) dinosaurs from Winton, Queensland, Australia. *PLoS ONE* **4**, e6190. (doi:10.1371/journal.pone.0006190)
- Holtz TR. 1994 The phylogenetic position of Tyrannosauroidae: implications for theropod systematics. *J. Paleontol.* **68**, 1100–1117.
- Von Huene F. 1932 Die fossile Reptil-ordnung Saurischia, ihre Entwicklung und Geschichte. *Monographien zur Geologie und Palaeontologie* **1**, 1–361.
- Huston D, Blewett R, Champion D. 2012. Australia through time: a summary of its tectonic and metallogenic evolution. *Episodes* **35** (1), 23–43.
- Hutchinson JR. 2001 The evolution of pelvic osteology and soft tissues on the line to extant birds (Neornithes). *Zool. J. Linn. Soc.* **131**, 123–168.
- Hutt S, Naish D, Martill DM, Barker MJ, Newbery P. 2001 A preliminary account of a new tyrannosauroid theropod from the Wessex Formation (Early Cretaceous) of southern England. *Cret. Res.* **22**, 227–242.
- Jokat W, Boebel T, Konig M, Meyer U. 2003. Timing and geometry of early Gondwana breakup. *J Geophys Res* **108** (B9), 2428:1–15
- Kear BP. 2006 Plesiosaur remains from Cretaceous high-latitude non-marine deposits in southeastern Australia. *J. Vertebr. Paleontol.* **26**, 196–199.
- Kellner AWA. 1999 Short note on a new dinosaur (Theropoda, Coelurosauria) from the Santana Formation (Romualdo Member, Albian), northeastern Brazil. *Boletim do Museu Nacional* **49**, 1–8.
- Kemp A. 1993 *Ceratodus diutinus*, a new ceratodont from Cretaceous and late Oligocene-medial Miocene deposits in Australia. *J. Paleontol.* **67**, 883–888.
- Kemp A. 1997a A revision of Australian Mesozoic and Cenozoic lungfish of the family Neoceratodontidae (Osteichthyes: Dipnoi), with a description of four new species. *J. Paleontol.* **71**, 713–733.
- Kemp A. 1997b Four species of *Metaceratodus* (Osteichthyes: Dipnoi, Family Ceratodontidae) from Australian Mesozoic and Cenozoic deposits. *J. Vertebr. Paleontol.* **17**, 26–33.

- Korsch RJ, Totterdell JM. 2009 Subsidence history and basin phases of the Bowen, Gunnedah, and Surat Basins, eastern Australia. *Aust. J. Earth Sci.* **55**, 335–353.
- Lee MSY, Cau A, Naish D, Dyke GJ. 2014a Morphological clocks in palaeontology, and a mid-Cretaceous origin of crown Aves. *Systematic Biol.* **63**, 442–449.
- Lee MSY, Cau A, Naish D, Dyke GJ. 2014b Sustained miniaturization and anatomical innovation in the dinosaurian ancestors of birds. *Science* **345**, 562–566.
- Luo Z-X, Kielan-Jaworowska Z, Cifelli RL. 2002. In quest for a phylogeny of Mesozoic mammals. *Acta Pal. Pol.* **47**, 1–78.
- Macdonald D, Gomez-Pereza I, Franzese J, Spalletti L, Lawver L, Gahagan L, Dalziel I, Thomas C, Trewind N, Holed M, Paton D. 2003 Mesozoic break-up of SW Gondwana: implications for regional hydrocarbon potential of the southern South Atlantic. *Mar Petrol Geol* **20**, 287–308.
- Madsen JH Jr. 1976 *Allosaurus fragilis*: a revised osteology. *Utah Geological and Mineral Survey Bulletin* **109**, 1–163.
- Mannion PD, Upchurch P, Carrano MT, Barrett PM. 2011 Testing the effect of the rock record on diversity: a multidisciplinary approach to elucidating the generic richness of sauropodomorph dinosaurs through time. *Biol. Rev.* **86**, 157–181.
- Marsh OC. 1881 Principal characters of American Jurassic dinosaurs. Part V. *Am. J. Sci. ser. 3.* **21**, 417–423.
- Meschede M, Frisch W. 1998 A plate-tectonic model for the Mesozoic and Early Cenozoic history of the Caribbean plate. *Tectonophysics* **296**, 269–291
- Molnar RE. 1980a Australian Late Mesozoic terrestrial tetrapods: some implications. *Memoirs de la Société Géologique de France* **139**, 131–143.
- Molnar RE. 1980b Procoelous crocodile from the Lower Cretaceous of Lightning Ridge, NSW. *Memoirs of the Queensland Museum* **20**, 65–75.
- Molnar RE. 1992a Paleozoogeographic relationships of Australian Mesozoic tetrapods. In *New Concepts in Global Tectonics*. (eds. Chatterjee S, Hotton III N, Williams C), pp 259–266. Lubbock: Texas Tech University Press.

- Molnar RE. 1992b Observations on the Australian ornithopod dinosaur, *Muttaburrasaurus*. *Memoirs of the Queensland Museum* **39**, 639–652.
- Molnar RE. 1997 Australasian dinosaurs. In *Encyclopedia of Dinosaurs* (eds. Currie PJ, Padian K), pp. 27–31. San Diego: Academic Press.
- Molnar RE. 2011 Sauropod (Saurischia: Dinosauria) material from the Early Cretaceous Griman Creek Formation of the Surat Basin, Queensland, Australia. *Alcheringa* **35**, 303–307.
- Molnar RE, Galton PM. 1986 Hypsilophodontid dinosaurs from Lightning Ridge, New South Wales. *Geobios* **19**, 231–239.
- Molnar RE, Salisbury SW. 2005 Observations on Cretaceous sauropods from Australia. In *Thunder-Lizards: the Sauropodomorph Dinosaurs* (eds. Tidwell V, Carpenter K), pp. 454–465. Bloomington: Indiana University Press.
- Molnar RE, Willis PMA. 2001 New crocodyliform material from the Early Cretaceous Griman Creek Formation at Lightning Ridge, New South Wales. In *Crocodylian Biology and Evolution* (eds. Brigg GC, Seebacher F, Franklin CE), pp. 75–82. Sydney: Surrey Beatty and Sons.
- Novas FE. 1998 *Megaraptor namunhuaiquii*, gen. et sp. nov., a large-clawed, Late Cretaceous theropod from Patagonia. *J. Vert. Paleontol.* **18**, 4–9.
- Novas FE, Agnolin FL, Ezcurra MD, Porfiri J, Canale JI. 2013 Evolution of the carnivorous dinosaur during the Cretaceous: the evidence from Patagonia. *Cretaceous Research* **45**, 174–215.
- Ortega F, Escaso F, Sanz JL. 2010 A bizarre, humped Carcharodontosauria (Theropoda) from the Lower Cretaceous of Spain. *Nature* **467**, 203–206.
- Owen R. 1842 Report on British fossil reptiles. Part II. *Rep. Br. Assoc. Adv. Sci.* **1841**, 60–204.
- Porfiri JD, Novas FE, Calvo JO, Agnolin FL, Ezcurra MD, Cerda IA. 2014 Juvenile specimen of *Megaraptor* (Dinosauria, Theropoda) sheds light about tyrannosauroid radiation. *Cretaceous Research* **51**, 35–55.
- Poropat SF, Upchurch P, Mannion PD, Hocknull SA, Kear BP, Sloan T, Sinapius G, Elliott D. 2014 Revision of the sauropod dinosaur *Diamantinasaurus matildae* Hocknull et

- al. 2009 from the mid-Cretaceous of Australia: implications for gondwanan titanosauriform dispersal. *Gondwana Res.* DOI:10.1016/j.gr.2014.03.014
- Price PL. 1997 Permian to Jurassic palynostratigraphic nomenclature of the Bowen and Surat Basins. In *The Surat and Bowen Basins south-east Queensland* (ed. Green PM) Queensland Minerals and Energy Review Series, Queensland Department of Mines and Energy, Brisbane, 137-178.
- Rauhut OWM. 2011 Theropod dinosaurs from the Late Jurassic of Tendaguru (Tanzania). *Special Papers in Palaeontology* **86**, 195–239.
- Raza A, Hill KC, Korsch RJ. 2009 Mid-Cretaceous uplift and denudation of the Bowen and Surat Basins, eastern Australia: relationship to Tasman Sea rifting from apatite fission-track and vitrinite-reflectance data. *Aust. J. Earth Sci.* **56**, 501–531.
- Rey PF. 2013 Opalisation of the Great Artesian Basin (central Australia): an Australian story with a Martian twist. *Aust. J. Earth Sci.* **60**, 291–314.
- Rich TH. 1996 Significance of polar dinosaurs in Gondwana. *Mem. Qld. Mus.*, **39**, 711–717.
- Rich TH, Rich P. 1989 Polar dinosaurs and biotas of the Early Cretaceous of southeastern Australia. *National Geographic Research* **5**, 15–53.
- Rich TH, Vickers-Rich P. 1994 Neoceratopsians and ornithomimosaur: dinosaurs of Gondwanan origin? *National Geographic Research and Exploration* **10**, 129–131.
- Rich TH, Vickers-Rich P. 2003 Protoceratopsian? Ulnae from Australia. *Records of the Queen Victoria Museum* **113**, 1–12.
- Rich TH, Flannery TF, Archer M. 1989 A second Cretaceous mammalian specimen from Lightning Ridge, New South Wales, Australia. *Alcheringa* **13**, 85–88.
- Rich TH, Galton PM, Vickers-Rich P. 2010 The holotype individual of the ornithopod dinosaur *Leallynasaura amicagraphica* Rich and Rich, 1989 (late Early Cretaceous, Victoria, Australia). *Alcheringa* **34**, 385–396.
- Rich TH, Kear BP, Sinclair R, Chinnery B, Carpenter K, McHugh ML, Vickers-Rich P. 2014 *Serendipaceratops arthurclarkei* Rich & Vickers-Rich 2003 is an Australian Early Cretaceous ceratopsian. *Alcheringa* **38**, 456–479.
- Salisbury S, Molnar RE, Frey E, Willis PMA. 2006 The origin of modern crocodyliforms: new evidence from the Cretaceous of Australia. *Proc. Roy. Soc. B-Biol. Sci.* **273**, 2439–2448.

- Sadler R, Barrett PM, Powell HP. 2008 The anatomy and systematics of *Eustreptospondylus oxoniensis*, a theropod dinosaur from the Middle Jurassic of Oxfordshire, England. *Monograph of the Palaeontographical Society, London* **627**, 1–82.
- Seeley HG. 1887 On the classification of the fossil animals commonly called Dinosauria. *Proc. Roy. Soc. London* **43**, 165–171.
- Sereno PC, Martinez RN, Wilson JA, Varricchio DJ, Alcober OA, Larsson HCE. 2008 Evidence of avian intrathoracic air sacs in a new predatory dinosaur from Argentina. *PLoS ONE* **3**, e3303.
- Smith ET. 2010 Early Cretaceous chelids from Lightning Ridge, New South Wales. *Alcheringa* **34**, 375–384.
- Smith ET, Kear BP. 2013 *Spoochelys ormondea* gen. et sp. nov., an archaic meiolanid-like turtle from the Early Cretaceous of Lightning Ridge, Australia. In *Morphology and Evolution of Turtles* (eds. Brinkman DB, Holroyd PA, Gardner JD), pp. 121–146. Netherlands: Springer.
- Smith ND, Makovicky PJ, Agnolin FL, Ezcurra MD, Pais DF, Salisbury SW. 2008 A *Megaraptor*-like theropod (Dinosauria: Tetanurae) in Australia: support for faunal exchange across eastern and western Gondwana in the mid-Cretaceous. *Proc. Roy. Soc. B-Biol. Sci.* **275**, 2085–2093.
- Sterli J, De la Fuente MS, Umazano AM. 2013 New remains and new insights on the Gondwanan meiolaniform turtle *Chubutemys copelloi* from the Lower Cretaceous of Patagonia. *Gondwana Research* (in press)
- Templeton AR. 1983 Phylogenetic inference from restriction endonuclease cleavage site maps with particular reference to the humans and apes. *Evolution* **37**, 221–244.
- Torcida Fernández-Baldor F, Canudo JI, Huerta P, Montero D, Pereda Suberbiola X, Salgado L. 2011 *Demandasaurus darwini*, a new rebbachisaurid sauropod from the Early Cretaceous of the Iberian Peninsula. *Acta Palaeontol. Pol.* **56**, 535–552.
- Totterdell JM, Moloney J, Korsch RJ, Krassay AA. 2009 Sequence stratigraphy of the Bowe-Gunnedah and Surat Basins in New South Wales. *Aust. J. Earth Sci.* **56**, 433–459.

- Tucker RT, Roberts EM, Hu Y, Kemp AIS, Salisbury SW. 2013 Detrital zircon age constraints for the Winton Formation, Queensland: contextualizing Australia's late Cretaceous dinosaur faunas. *Gondwana Res.* **24**, 767–779.
- Upchurch P. 2008 Gondwana break-up: legacies of a lost world? *Trends in Ecology & Evolution* **23**, 229–236.
- Viramonte J, Kay S, Becchio R, Escayola M, Novitski I, 1999 Cretaceous rift related magmatism in central-western South America. *J South Am Earth Sci* **12**, 109–121
- White MA, Cook AG, Hocknull SA, Sloan T, Sinapius GHK, Elliott DA. 2012 New forearm elements discovered of holotype specimen *Australovenator wintonensis* from Winton, Queensland, Australia. *PLoS ONE* **7**, e39364.
- White MA, Benson RBJ, Tischler TR, Hocknull SA, Cook AG, Barnes DG, Poropat SF, Wooldridge SJ, Sloan T, Sinapius GHK, Elliot DA, 2013a New *Australovenator* hind limb elements pertaining to the holotype reveal the most complete neovenatorid leg. *PLoS ONE* **8**, e68649 doi:10.1371/journal.pone.0068649
- White MA, Falkingham PL, Cook AG, Hocknull SA, Elliot DA. 2013b Morphological comparisons of metacarpal I for *Australovenator wintonensis* and *Rapator ornitholestoides*: implications for their taxonomic relationships. *Alcheringa* **37**, 1–7.
- Xu X, Clark JM, Forster CA, Norell MA, Erickson GM, Eberth DA, Jia C, Qi Z. 2006 A basal tyrannosauroid dinosaur from the Late Jurassic of China. *Nature* **439**, 715–718.
- Xu X, Clark JM, Mo J, Choiniere J, Forster CA, Erickson GM, Hone DWE, Sullivan C, Eberth DA, Nesbitt S, Zhao Q, Hernandez R., Jia C-K, Han F-L, Guo Y. 2009 A Jurassic ceratosaur from China helps clarify avian digital homologies. *Nature* **459**, 940–944.
- Xu X, Norell MA, Xeuwen K, Wang X, Qi Z, Jia C. 2004 Basal tyrannosauroids from China and evidence for protofeathers in tyrannosauroids. *Nature* **431**, 680–684.
- Yan Y, Harris AJ, Xingjin H. 2011 RASP (Reconstruct Ancestral State in Phylogenies) 1.1. Available at: <http://mnh.scu.edu.cn/soft/blog/RASP>.
- Yu Y, Harris AJ, He XJ. 2010 S-DIVA (statistical dispersal-vicariance analysis): a tool for inferring biogeographic histories. *Molec. Phylogenet. Evol.* **56**, 848-850.
- Zanno LE, Makovicky PJ. 2013 Neovenatorid theropods are apex predators in the Late Cretaceous of North America. *Nature Comm.* **4**, doi:10.1038/ncomms3827.

## Figures

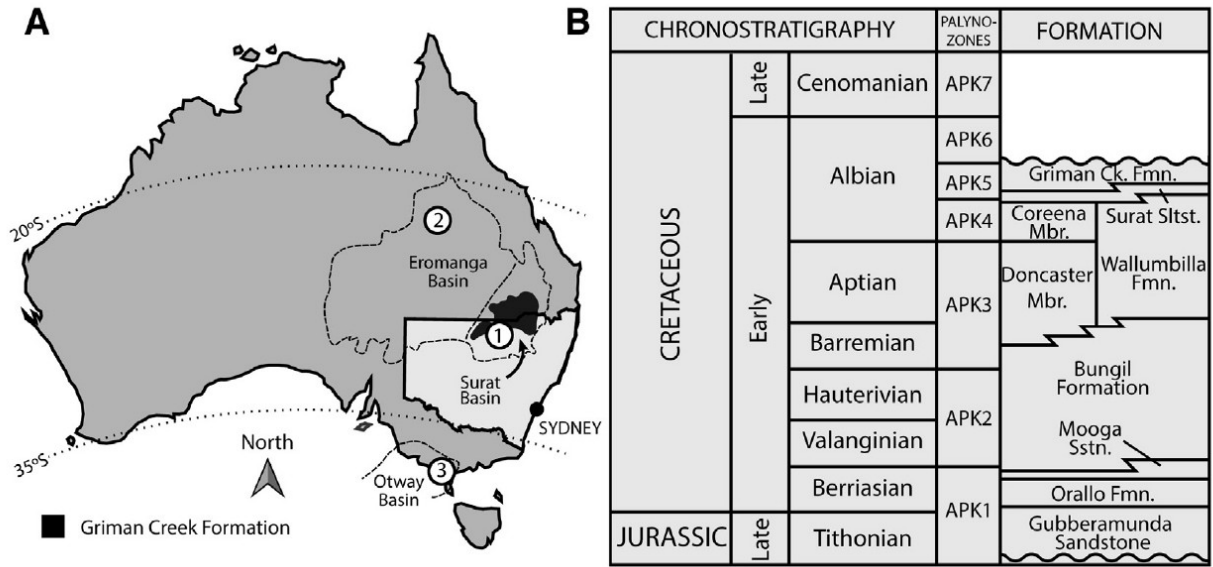


Figure 1. Locality map (A) showing the major sedimentary basins and locations of megaraptoran discoveries in Australia. 1. Lightning Ridge, NSW (Griman Creek Formation, middle Albian); 2. Winton, Queensland (Winton Formation, Cenomanian-Turonian); 3. Otway Basin, Victoria (Eumeralla Formation, late Aptian–early Albian). (B) Chronostratigraphy of the Surat Basin. The Griman Creek Formation has yielded a diverse vertebrate fauna including the remains of the new theropod.

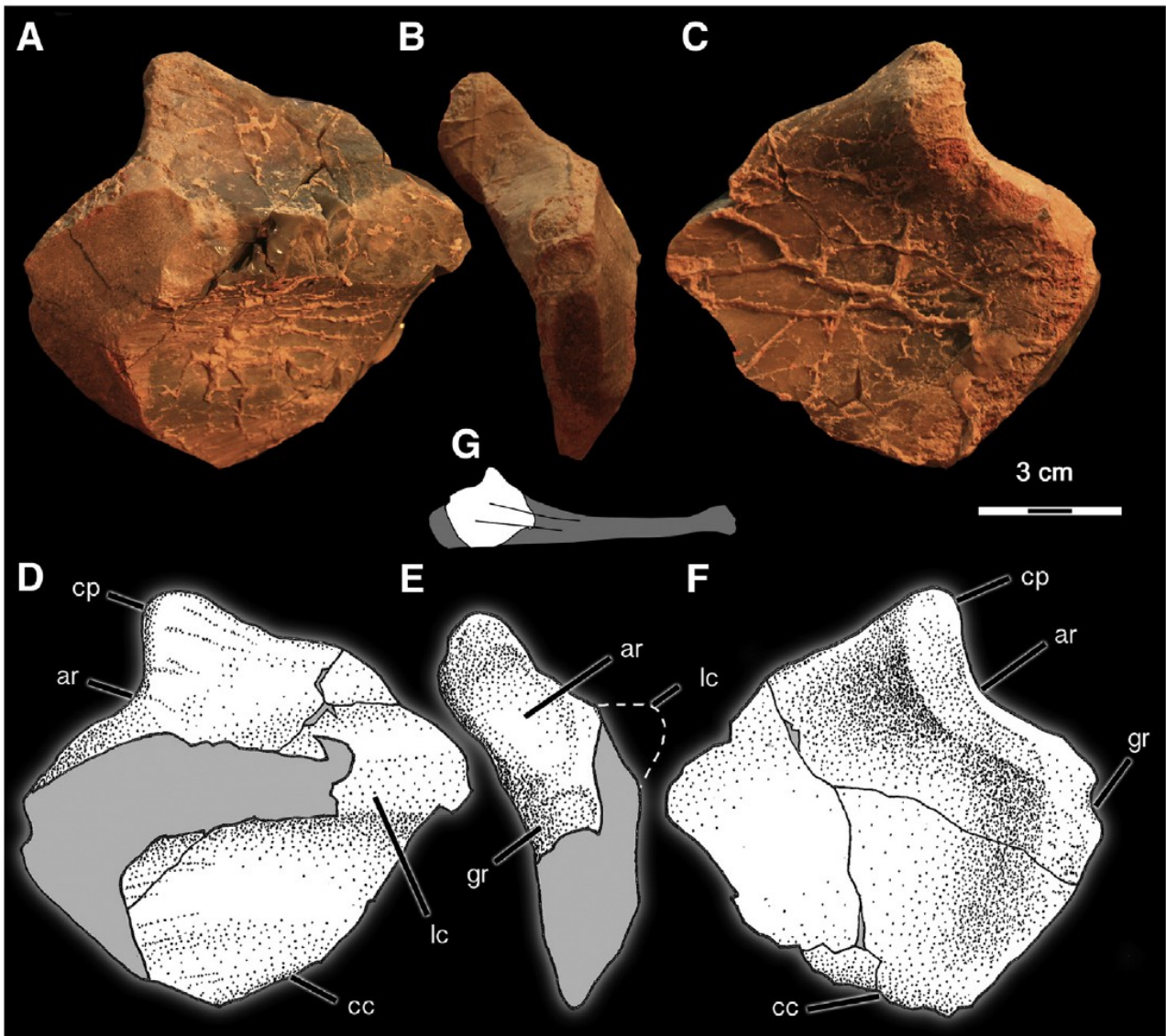


Figure 2. Megaraptoridae right proximal ulna in (A, D) lateral, (B, E) proximal, and (C, F) medial views. (G) reconstruction of right ulna showing known parts in white (not to scale). Outline based on *Australovenator*. Grey in A–F = broken bone surface; Grey in G = reconstructed areas. ar, ulna-humerus articular surface; cp, cranial process; cc, caudal crest; lc, lateral crest; gr, groove.

Lightning Ridge  
megaraptorid  
(LRF 100-106)

*Australovenator*  
*wintonensis*  
(AOD 604)

Megaraptora  
indet.  
(NMV P186076)

*Megaraptor*  
*namunhuaiquii*  
(MCF-PVPH 79)

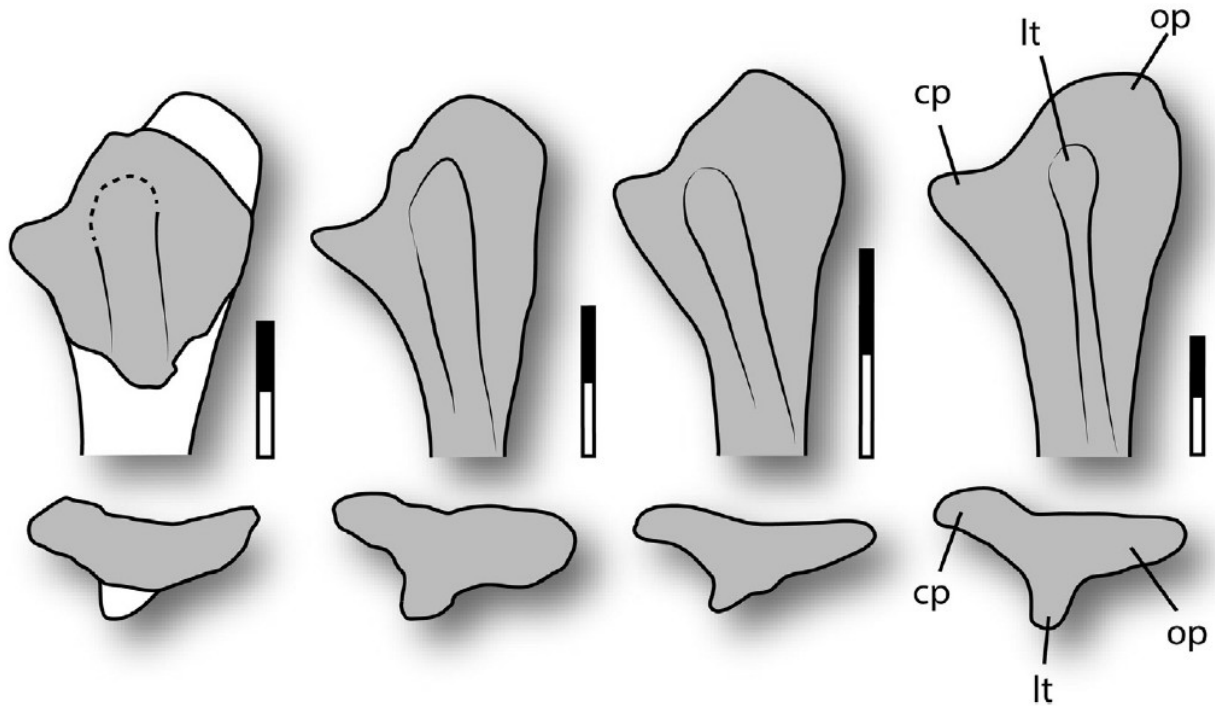


Figure 3. Comparison of megaraptorid proximal left ulnae. Right ulna of the Lightning Ridge theropod reversed for clarity. Scale bars = 5 cm. cp, cranial process; lt, lateral tuberosity; op, olecranon process.

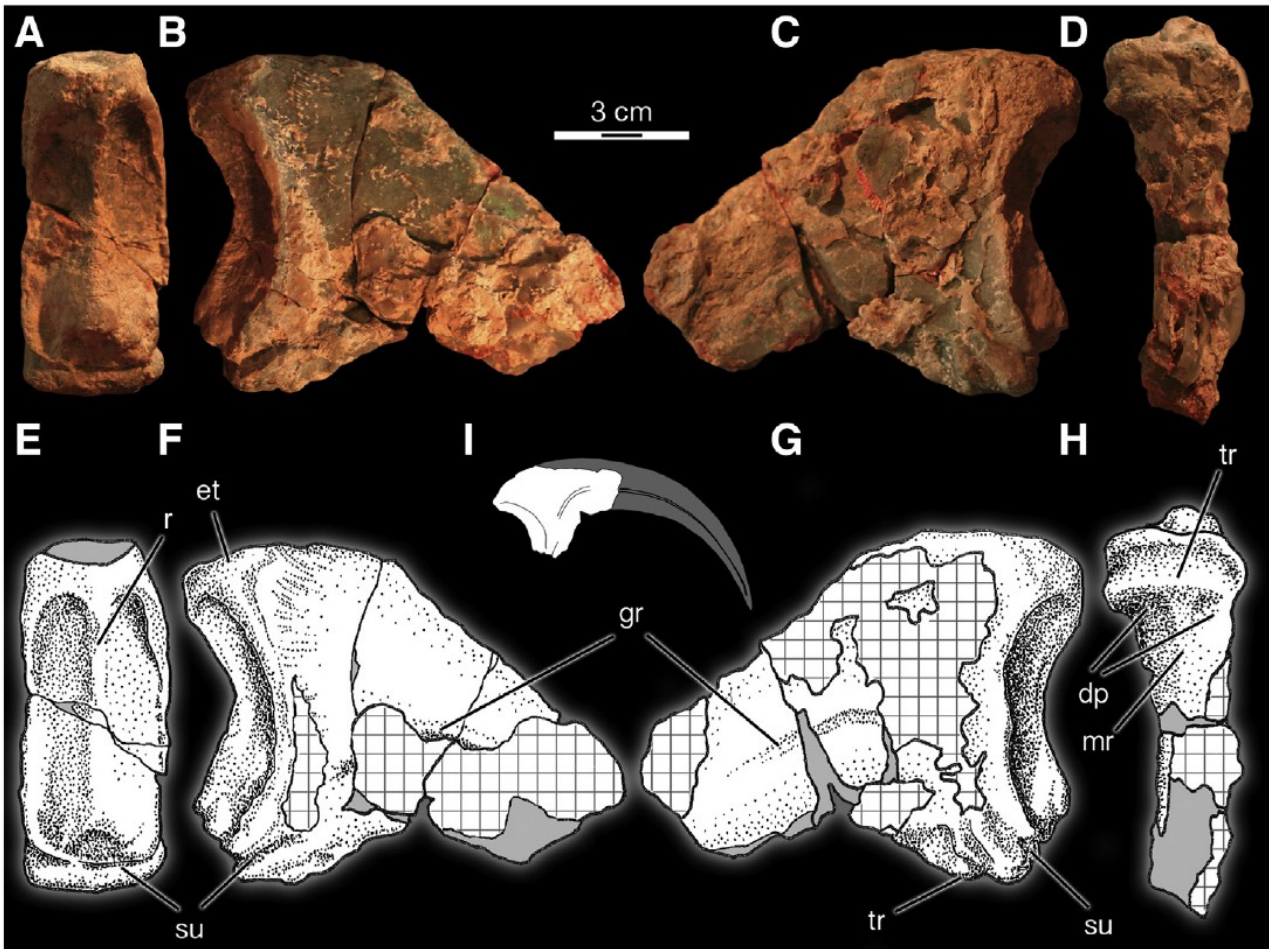


Figure 4. Megaraptoridae left or right manual ungual I-2 in (A, E) proximal; (B, F) right lateral; (C, G) left lateral, and; (D, H) ventral aspects; (I) reconstruction of ungual showing known part in white (not to scale). Outline based on *Megaraptor*. Grey in A–H = broken bone surface; Grey in I = reconstructed areas; cross-hatching = matrix. su, sulcus; dp, depression; et, extensor tubercle; gr, vascular groove; mr, median ridge; r, ridge; tr, transverse ridge.

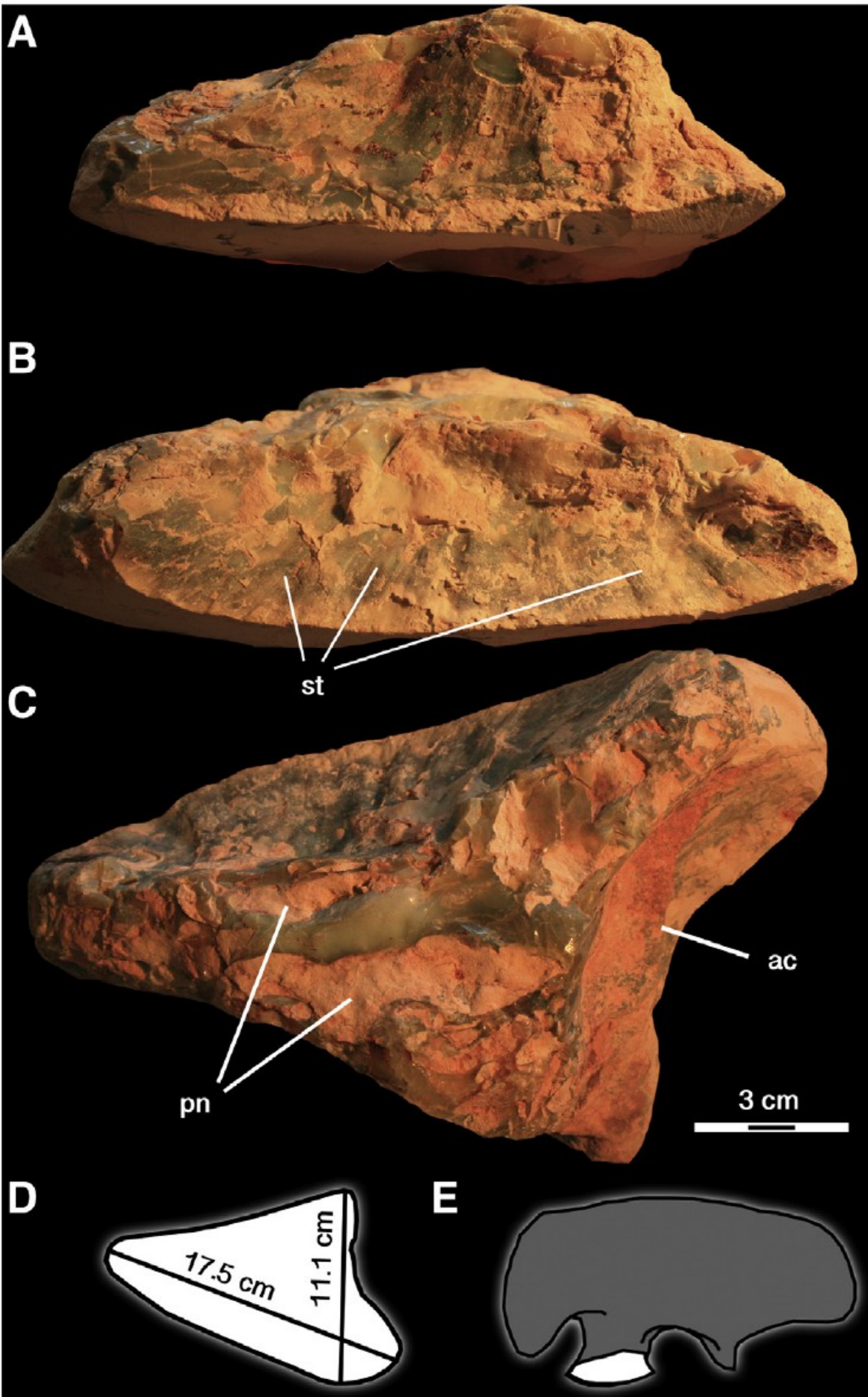


Figure 5. Megaraptoridae pubic peduncle of the left ilium in (A) lateral; (B) medial; (C) dorsal views showing the highly pneumatic interior; (D) ventral view; (E) ventral outline with associated measurements, and; (F) left ilium in lateral view showing known region (white) in the new specimen. ac, acetabulum; pn, pneumatic chamber; st, scars for the attachment of connective ligaments between pubic peduncle and pubis.

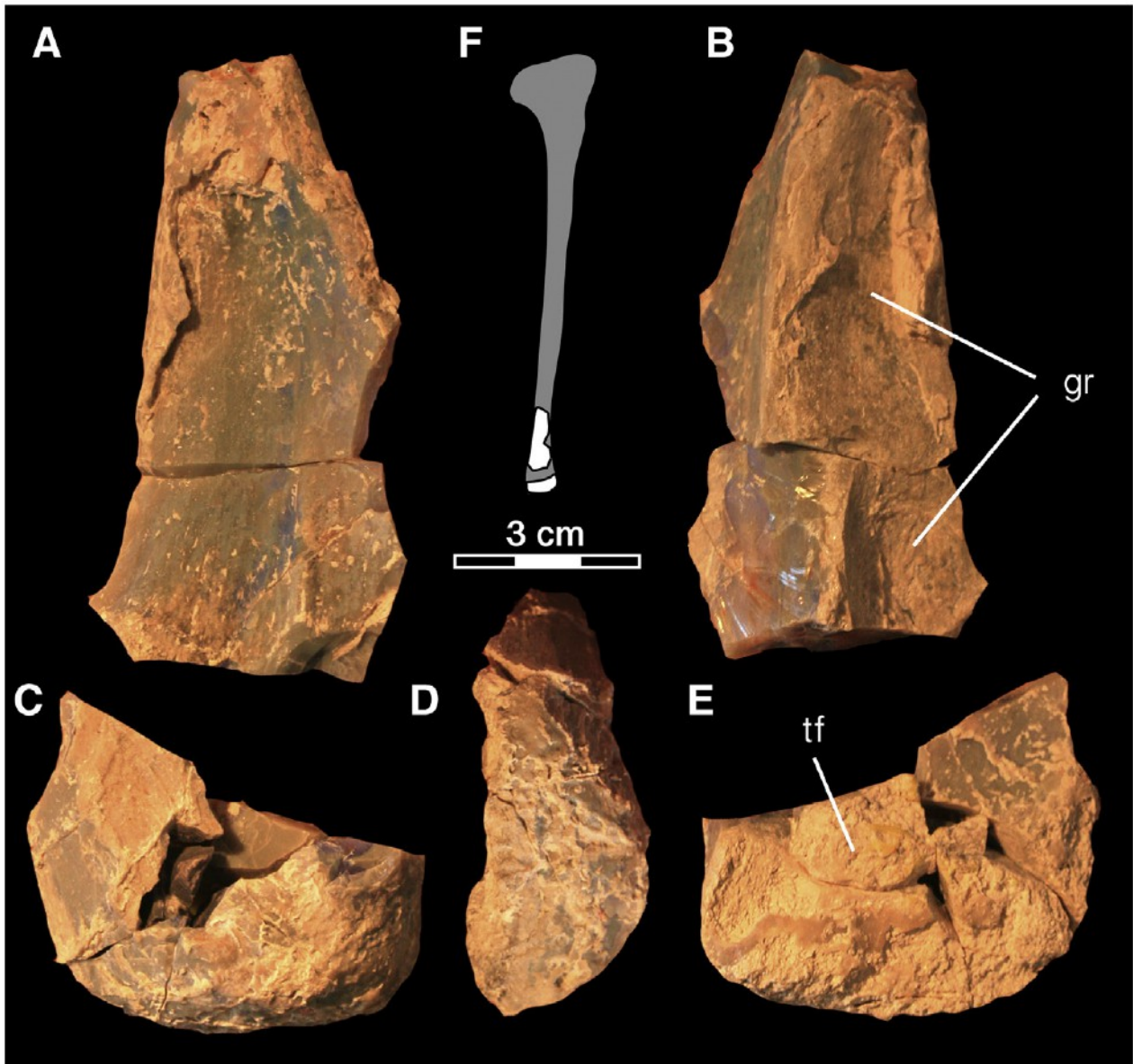


Figure 6. Megaraptoridae partial fibula. Shaft section in (A) lateral and; (B) medial views. Distal end fragment in (C) lateral; (D) distal, and; (E) medial views. (F) Schematic of fibula showing inferred position of present material (white). gr, groove; tf, tibial facet.

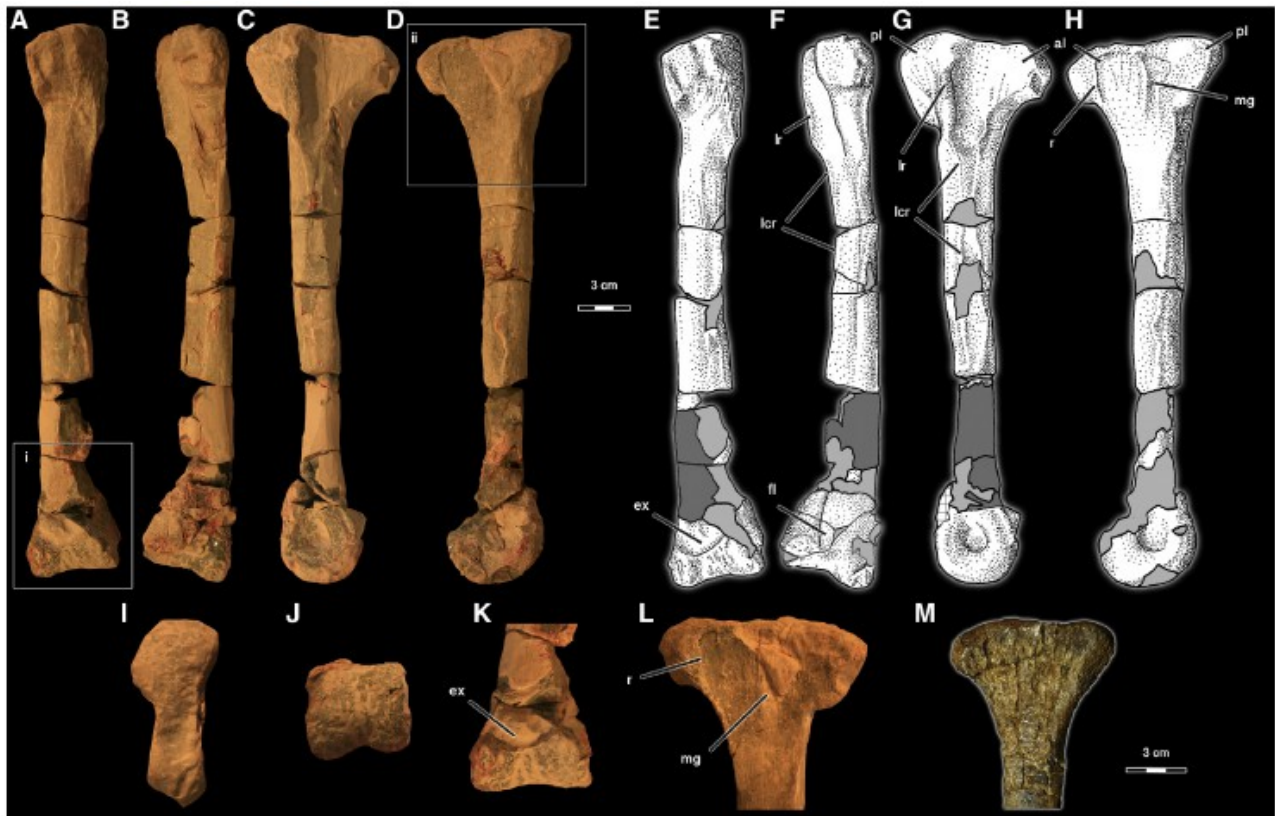


Figure 7. Megaraptoridae left metatarsal III in (A, E) cranial, (B, F) caudal, (C, G) lateral, (D, H) medial, (I) proximal, and (J) distal aspects. (K) Close up of distal cranial surface identified by boxed area (i) in A showing broad extensor fossa. (L, M) Comparison of proximal part of metatarsal III in medial view between (L) Lightning Ridge theropod and (M) *Australovenator* (right element reversed for clarity). Region of close up in L indicated by boxed area (ii). Light grey = broken bone surface; dark grey = plaster; cross-hatching = matrix. al, cranial process of proximal metatarsal; ex, extensor fossa; fl, flexor fossa; lcr, lateral crest; lr, lateral ridge; mg, medial groove; pl, caudal process of proximal metatarsal; r, rim demarcating cranial limit of contact with metatarsal II.



Figure 8. Megaraptoridae (A) thoracic rib head, (B) rib shaft, and (C) gastral fragment. Overtubulation, presumably the result of a healed fracture, indicated by arrowheads.

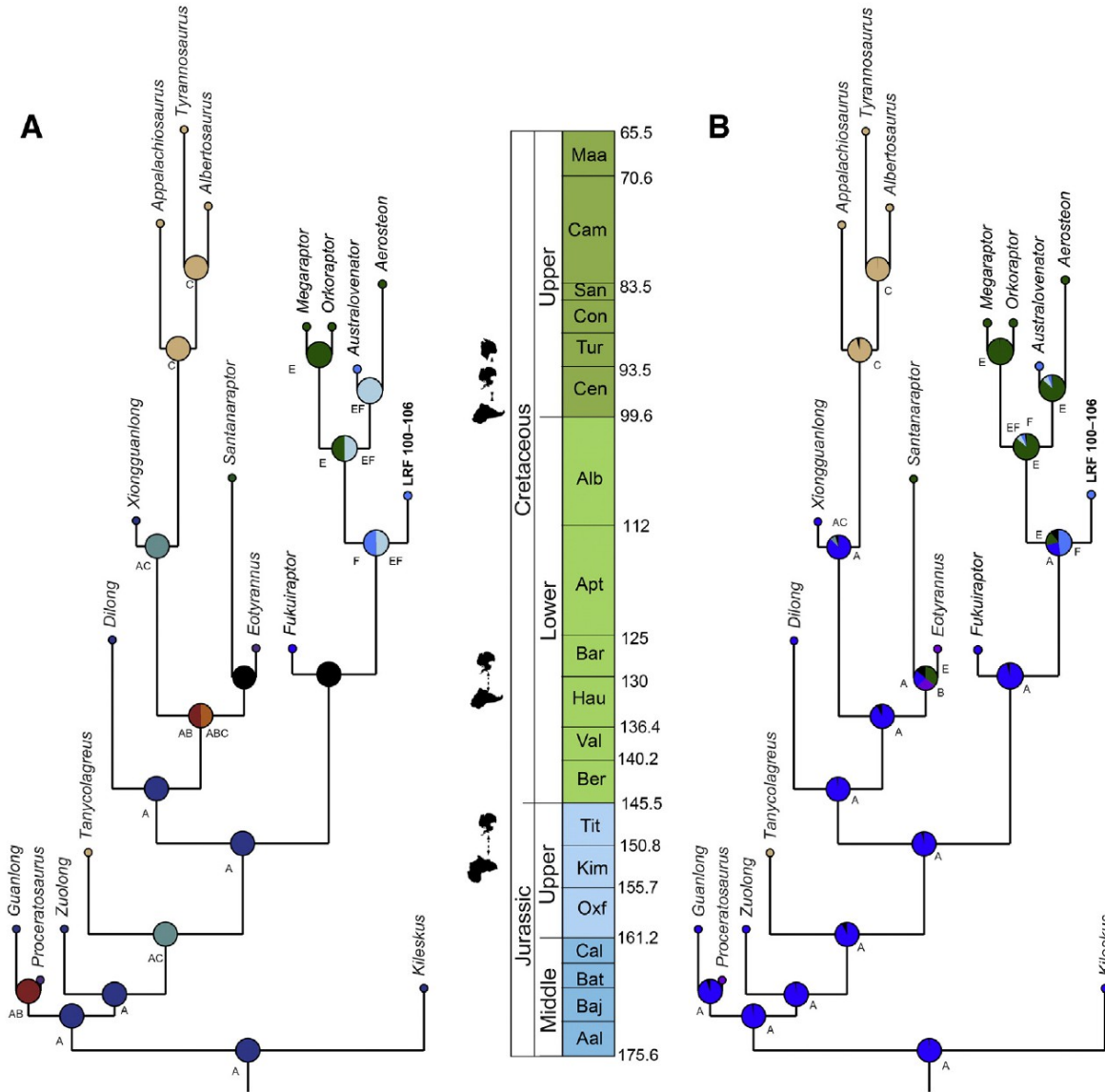


Figure 9. Palaeogeographic ancestral area reconstruction of Tetanurae, from a Bayesian relaxed-clock analysis based on the dataset of Novas et al. (2013). (A) S-DIVA analysis and (B) BBM analysis. Colours and letters at each node represent the geographic areas of origin (A, Asia; B, Europe; C, North America; D, Africa; E, South America; F, Australia) with relative likelihood of alternate hypotheses represented as a pie graph. Ambiguous geographic areas of origin are indicated by black nodes.

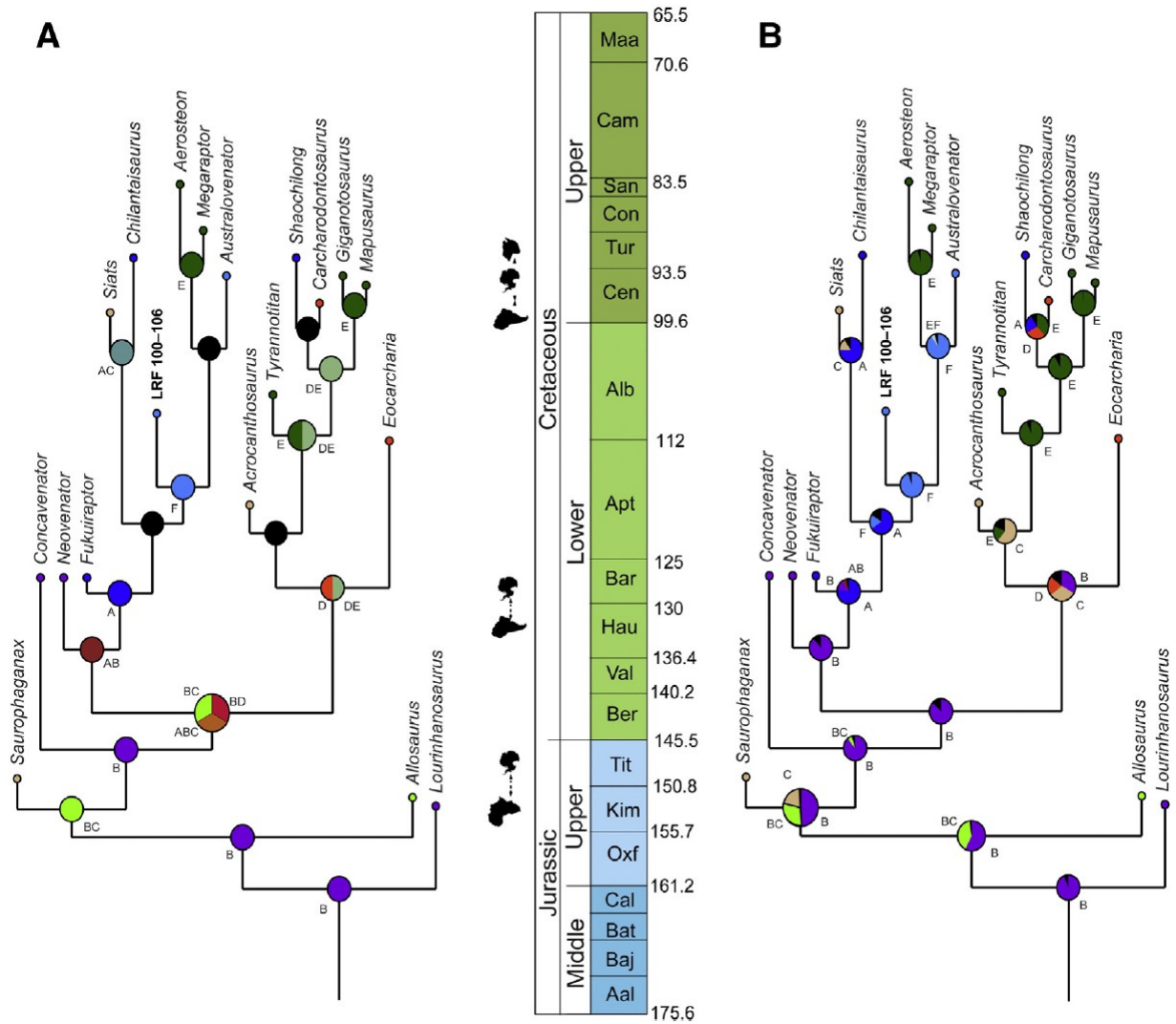


Fig. 10. Palaeogeographic ancestral area reconstruction of Tetanurae, from a Bayesian relaxed-clock analysis based on the dataset of Zanno and Makovicky (2013). (A) S-DIVA analysis and (B) BBM analysis. Colours and letters at nodes represent the geographic areas of origin (A, Asia; B, Europe; C, North America; D, Africa; E, South America; F, Australia) with relative likelihood of alternate hypotheses represented as a pie graph. Ambiguous geographic areas of origin are indicated by black nodes.

		LRF 100-106	<i>Australovenator wintonensis</i>	<i>Megaraptor namunhuaiquii</i>
Manual ungual I-2	Articular facet height	58	44.97	?
	Proximal width	31	26.08	?
	Proximal height	68	59.84	95
Manual ungual II-3	Articular facet height:proximal width	1.87	1.72	?
	Articular facet height	?	45.89	?
	Proximal width	?	24.88	?
	Proximal height	?	55.13	65
	Articular facet height:proximal width	?	1.84	?
Metatarsal III	Length	350	322	450?
	Proximal width	43	36.94	?
	Proximal length (craniocaudally)	94	79.43	?
	Distal width	51.5	53.54	75
	Distal length (medial maleolus)	51	47.45	?

Table 1. Comparative measurements (in mm) of select elements in three megaraptorids. Data from Novas (1998) and Calvo et al. (2004).

Page left blank

## **CHAPTER 6 - High evolutionary rates and the origin of the Rosso Ammonitico Veronese Formation (Middle-Upper Jurassic of Italy) reptiles.**

Submitted: 25<sup>th</sup> March 2015. Published: 01<sup>st</sup> August 2016 in *Historical Biology* vol. 28:952-962.

Andrea Cau, Federico Fanti

### **Abstract**

The fossil record of metriorhynchids and plesiosaurians from the Rosso Ammonitico Veronese Formation (RAVFm, Middle–Upper Jurassic, Italy) is represented by elements collected between the eighteenth and twentieth centuries. All the metriorhynchid material is referred to the genus *Neptunidraco*. The first RAVFm plesiosaurian material was collected in the nineteenth century and referred to *Plesiosaurus*: elements are here described and interpreted as a chimerical association of crocodylomorph and plesiosaurian bones, providing the first co-occurrence of these clades in the RAVFm. The second plesiosaurian is the associated skeleton that we refer to *Anguanax zignoi* gen. et sp. nov. Bayesian phylogenetic analysis confirms the basal geosaurine affinities of *Neptunidraco* resulted by parsimony analysis. Using both methods, *Anguanax* was recovered as a basal pliosaurid, sister group of the clade including *Marmornectes* and *Thalassophonea*. Bayesian inference methods indicate that both Italian lineages diverged from other known lineages between 176 and 171 Mya, also showing divergence rates significantly higher than any other representative of their respective clades. We suggest a phase of rapid evolutionary adaptation to deeper marine environments in the ancestors of the Rosso Ammonitico Veronese reptiles as a response to the latest Liassic regressive regime in Northern Tethys.

**Key words:** Bayesian phylogenetics; Italy; Jurassic; Metriorhynchidae; Pliosauridae; Rosso Ammonitico Veronese Formation.

## 1. Introduction

The Rosso Ammonitico Veronese Formation (RAVFm) (Bajocian-Tithonian) is well documented succession consisting primarily of red, ammonite-bearing, nodular limestones (Martire 1996; Martire et al. 2006 and references therein) largely exposed in the southern Alps of north-eastern Italy. Occasional discoveries of fossil reptiles have been reported since the eighteenth century and include thalattosuchian crocodylomorphs (Bizzarini 1995; Delfino and Dal Sasso 2006; Cau and Fanti 2011; Cau 2014) and plesiosaurs (de Zigno 1883; Dalla Vecchia 1997; Cau and Fanti 2014). The crocodylomorph material from the RAV Formation includes incomplete but articulated skulls, mandibles and cervical vertebrae, all referred to the geosaurine metriorhynchid *Neptunidraco* (Cau and Fanti 2011; Cau 2014; Fig. 1). Similarly, the fossil record of Jurassic plesiosaurs from Italy is currently limited to few Rosso Ammonitico Veronese quarries from the Altopiano di Asiago (Cesuna locality; Fig. 2: De Zigno 1883; Dalla Vecchia 1997; Kaberlaba locality; Fig. 3: Cau and Fanti 2013). De Zigno (1883) mentioned a series of vertebrae that he personally collected in the upper member of the RAV Formation (Upper Jurassic) near Cesuna and putatively referred the material to *Plesiosaurus*. Cau and Fanti (2014) described the first articulated specimen of a plesiosaur from Italy, based on an associated skeleton of a pliosaurid found three decades earlier from the Callovian-Oxfordian beds exposed at the Kaberlaba locality.

In this study, we provide the first detailed description of the material from Cesuna found by De Zigno (1883), and describe additional material of the Kaberlaba specimen not mentioned by Cau and Fanti (2014) that provide new information on the morphology and phylogenetic affinities of the specimen. Furthermore, we apply Bayesian inference methods to reconstruct the phylogenetic affinities and the evolutionary rates of the Rosso Ammonitico Veronese Formation reptiles.

### 1.1. Institutional abbreviations

MGGC, Museo Geologico e Paleontologico 'Giovanni Capellini', Bologna, Italy; MGP-PD, Museo di Geologia e Paleontologia, Padova, Italy; MPPL, Museo Paleontologico e della Preistoria 'P. Leonardi', Ferrara, Italy.

## 2. Material and Methods

The Cesuna material is housed in the collection of the Museo di Geologia e Paleontologia in Padova under the accession number MGP-PD 6752-6757. The Kaberaba material pertains to the collections of the Museo Paleontologico e della Preistoria 'P. Leonardi' in Ferrara under the accession number MPPL 18797. Part of the Kaberlaba material, represented by more than 75 bone and tooth elements from the same individual, was described by Cau and Fanti (2014). Further material referred to the same individual is described here for the first time. Thalattosuchian taxonomy follows Young et al. (2010) and Young (2014). Plesiosaurian taxonomy follows Ketchum and Benson (2010) and Benson and Druckenmiller (2014).

### 2.1. Phylogenetic analyses

To test the phylogenetic affinities of the Kaberlaba plesiosaurian, we scored an operational taxonomic unit (OTU) based on the material housed in the MPPL collection into the modified version of the phylogenetic analysis of Benson and Druckenmiller (2014), updated by Benson et al. (2013). The Cesuna material is too fragmentary to be tested quantitatively by numerical analyses (see below). The phylogenetic affinities of *Neptunidraco* were analysed using a dataset modified from Young (2014), with the Italian taxon score based on direct observation on the holotype and referred specimens (Cau and Fanti 2011; Cau 2014).

Both parsimony analysis of morphological characters and Bayesian inference analysis integrating morphological and stratigraphic information (Lee et al. 2014a, b) were performed. Parsimony analyses were performed with the Hennig Society version of TNT (Goloboff et al. 2008). The data sets were first analysed with the 'New Technology' search strategy, performing 100 replicates, and then with a series of 'Traditional Search' exploring the island found by the first analyses, saving all shortest trees found. Nodal support was calculated performing 1000 'Traditional Search' analyses and saving all trees up to ten steps longer than the shortest trees.

Bayesian inference analyses were performed in BEAST (Drummond et al., 2012) following the method of Lee et al. (2014b). Among the analysed characters, both constant and autapomorphic characters were included, as Bayesian analysis requires the sampling of

not solely synapomorphies (see Lee et al. 2014a, b). The morphological datasets were identical to those used in parsimony analyses. Stratigraphic information for the plesiosaurian and thalattosuchian taxa were based on Young and Andrade (2009), Young et al. (2010), Benson and Druckenmiller (2014) and Benson et al. (2013), and converted to geochronological ages. Stratigraphic data and age constraints for each terminal were also obtained from the Paleobiology Database (<http://paleobiodb.org/>) and from the literature, using published geochronological ages for the formations in which the taxa were found or the mean age of the geologic stages associated with those formations following values provided by the International Commission on Stratigraphy (Cohen et al., 2013). In both datasets, a conservative approach for nodal age prior setting was followed, and we adopted only the tree root age prior (i.e., the age of the last common ancestor of all included taxa). In each analysis, we set tree root age prior along a uniform range between the age of the oldest included taxon (i.e., *Postosuchus* in the thalattosuchian dataset, *Augustasaurus* in the plesiosaurian dataset) and the age of the Permian-Triassic boundary, since the latter event pre-dates the ages of all known immediate sister taxa of these clades and no record of both plesiosauroids and crocodylomorphs has ever been found in Paleozoic strata. In both analyses, rate variation across traits was modelled using the gamma parameter, and rate variation across branches was modelled using an uncorrelated relaxed clock. The analyses used four replicate runs of 40 million generations, with sampling every 4000 generations. Burnin was set at 20%, and the Maximum Clade Credibility Tree (MCCT) of the merged four post-burnin samples was used as framework for phyletic reconstruction.

### **3. Systematic Palaeontology**

#### **Reptilia** Linnaeus, 1758

##### **3.1. Specimens**

MGP-PD 6740, 6741, 6747, 6749, 6750, 6751, 6757, 6758. Isolated presacral centra and neural arches (Fig. 2).

##### **3.2. Locality and horizon**

Cesuna quarry, Altopiano di Asiagno (Vicenza Province, Italy). Tithonian, Upper Jurassic. Rosso Ammonitico Veronese Formation) (de Zigno 1883; Dalla Vecchia 1997; Martire et al., 2006).

### **3.3. Description**

#### **3.3.1. General features**

The vertebral centra are divided into two groups (here named 'Morphotype 1' and 'Morphotype 2', described below), based on the overall proportion of the centrum, the presence/absence of ventral keel and the presence/absence of subcentral foramina and notochordal pits. Based on the absence of both rib facets and chevron facets, all the centra are identified as belonging to dorsal/thoracic vertebrae (Andrews 1913; Ketchum and Benson 2011). All the neural arches share the same morphology and differ each other for the degree of preservation only.

One specimen (MPG 6752) includes an associated centrum and neural arch glued together. De Zigno (1883) did not mention the association of these elements, thus it is unknown whether they were found articulated. The two elements were glued together before their inclusion in the MPG collection (M. Fornasiero, pers. com. to AC, 2013). The association of the neural arch and centrum in MPG 6752 is evidently an artefact, as the anterior end of the left pedicel of the neural arch is glued to the left posterodorsal corner of the centrum; as a consequence, the neural canal runs diagonally along the dorsal surface of the centrum (Fig. 1A-D). Since the neural arch is both narrower and shorter than the corresponding articular surface on the dorsal surface of the centrum (AC, pers. obs., 2013), it is not plausible that they formed a natural articulation. Furthermore, as discussed below, the centrum in MPG 6752 is referred to Morphotype 1, here interpreted as *Crocodylomorpha*, whereas the neural arch is referred to *Pliosauridae*. Accordingly, the centrum-neural arch association in MPG 6752 is considered as a chimaera.

***Crocodylomorpha*** Hay, 1930

?***Thalattosuchia*** Fraas, 1901

#### **3.3.2. Morphotype centrum 1 (MPG 6751, 6752 partim)**

The centra are taller than long. The articular facets describe an inverted teardrop, due to

the medioventrally directed lateral borders, and are deeper than wide in anteroposterior view. The neurocentral sutures are limited to the dorsal surface of the centrum, and describe a gentle concavity facing dorsally. Due to the medioventral inclination of the lateral surfaces, the ventral surfaces are developed as narrow keels. The anterior end of the ventral keels is squared off, but no true hypapophysis is present. No subcentral foramina neither notochordal pits are present.

### **Plesiosauria** de Blainville, 1835

#### Plesiosauria indet.

#### *3.3.3. Morphotype centrum 2 (MPG 6740, 6741, 6747, 6749, 6750; Fig. 1E-G)*

The articular surfaces are ellipses, wider than tall in anteroposterior views, that house small notochordal pits. Dorsally, a slightly developed neurocentral suture is limited to the dorsal surface of the centrum. The lateral surfaces lack rib facets. The ventral surface is transversely concave, with no keel, and bears two small subcentral foramina aligned transversely.

#### *3.3.4. Neural arches (MPG 6752 partim, 6758; Fig. 1H-I)*

The neural arches are partially preserved, lacking most of the dorsal end of the neural spine and the distal end of both transverse processes. No parapophyses are present. The pedicels are low, as wide as long in ventral view. The preserved bases of the diapophyses are elliptical, taller than long in lateral view, and placed at the level of the dorsal half of the neural canal. The small prezygapophyses are poorly preserved, and are placed relatively more ventrally and medially compared to the postzygapophyses. The neural spines are subvertically oriented. The dorsal end of the preserved neural spines are elliptical, longer than wide. Both anterior and posterior surfaces of the neural spines bear a distinct ridge running dorsoventrally along the midline. The anterior spinal ridge is more prominent toward the neural canal, and in its ventral end it expands anteriorly forming a prominent projection that is trapezoidal in lateral view. The posterior spinal ridge is forked ventrally, forming two ridges reaching the postzygapophyses and bounding medially two elliptical fossae above the postzygapophyses.

**Pliosauridae** Seeley, 1874  
***Anguanax zignoi*** gen. et sp. nov.

Pliosauridae gen et sp. indet. Cau and Fanti, 2014

### **3.4. Holotype**

MPPL 18797 (Fig. 3). Partial skull and mandible, 32 isolated teeth, cervical, dorsal and caudal vertebrae, right scapulocoracoid, partial left humerus, left radius, left ulna, three left carpals, partial pelvis, femur, two epipodials, isolated metapodials and phalanges.

### **3.5. Etymology**

“De Zigno’s Anguana Lord”. From *Anguana*, aquatic creature with both fish and reptilian features present in the mythologies from North Eastern Italy; and *-anax*, Greek for 'tribal and military leader'. The species name honours Achille de Zigno (1813-1892), who first found plesiosaurian remains from the Rosso Ammonitico Veronese Formation (de Zigno 1883).

### **3.6. Type locality and horizon**

Kaberlaba quarry, Asiago Municipality, Vicenza Province, Italy. Middle Oxfordian. Lithozone 5, Middle Unit, Rosso Ammonitico Veronese Formation (Pellenard et al., 2013; Cau and Fanti 2014).

### **3.7. Diagnosis**

Pliosaurid plesiosaurian with the following unique combination of features: palpebral with orbital projection placed at mid-height of orbital anterior margin; posterior margin of orbital opening with a stepped posteroventral corner; low coronoid eminence; retroarticular process main axis directed posteriorly; axial neural spine narrow; ventral surface of anterior cervical centra bearing a low and broad midline ridge; rib facets placed dorsally on caudal centra but not extended on neural arch; posteroventral process of coracoid developed as a distinct trapezoid not reaching laterally the glenoid level, and with straight posterior margin directed posterolaterally.

### **3.8. Description**

A description of most of preserved elements of MPPL 18797 was provided by Cau and Fanti (2014). Here, we provide additional information about the skull morphology as additional details of the periorbital region of the skull resulted after re-examination of the specimen. The maxillary posteroventral margin of the external naris is preserved, and shows a distinct anterodorsal projection, that might represent remnant of an incipient bony constriction in the external naris border, as seen in some Cretaceous plesiosaurians (e.g., Bardet et al. 2003). A lip of bone bearing tooth fragments lies ventral to the anterior ramus of the squamosal. Lying along the dorsal oral margin, this element may pertain to the upper tooth row. This element may represent the posteroventral projection of the maxilla along most of the temporal bar, as observed in other plesiosaurians (e.g., Carpenter 1999; Bardet et al. 2003). The orbit is roughly eight-shaped, with the long axis inclined posterodorsally; this shape is due to the presence of a distinct posteroventral projection of the prefrontal into the orbit and a stepped, anteroventral corner of the postorbital bar. The squamosal shows an elongate anteroventral ramus bordering the whole ventral margin of temporal fenestra. A close examination of the mandible revealed a low lip just anterior to the contact between the suspensorium and the posterior half of the mandible. The lip forms the anterodorsal rim of the mandibular glenoid, only marginally exposed laterally. The exposition of the anterior rim of the mandibular glenoid indicates that the latter was placed at the same level as the tooth row.

A discoidal bone with an elliptical outline is interpreted as a partial vertebral centrum, preserved in cross section (Fig. 3D). The bone shows a complex pattern of cancellous bone filling most of the inner volume, an osteoporotic-like condition reported in somatically mature plesiosaurians (Wiffen et al. 1995).

Newly introduced limb elements include the distal end of left humerus, the radius, ulna and carpal elements (Fig. 3C). The humerus distal diaphysis is slightly wider than the femur (18 cm vs 16 cm). The shaft of the humerus shows a moderately concave preaxial margin. Although the distal end of the humerus is partially overlapped by other limb elements, the exposed articular margin shows a gently convex outline. Both radius and ulna are short quadrangular elements articulating with the distal end of the humerus. The radius bears a straight preaxial margin. The postaxial margin of the ulna is straight. Finally, the carpals

are smaller than the antebrachial bones, and show a roughly quadrangular outline.

## 4. Results

### 4.1. Phylogenetic analyses of *Neptunidraco* and *Anguanax*

#### 4.1.1. *Neptunidraco ammoniticus*

The phylogenetic analysis of *Thalattosuchia* modified from Young (2014) produced a result comparable to the topology discussed by Cau (2014). In particular, in the strict consensus of the 27 shortest trees found (tree length = 429 steps; Consistency Index = 0.6527; Retention Index = 0.8484; Fig. 4), *Neptunidraco* was recovered as sister taxon of the clade including “*Metriorhynchus*” *brachyrhynchus*, *Tyrannoneustes* and Geosaurini, as more derived than a basal polytomy including the Patagonian geosaurines.

The result of the Bayesian analysis integrating morphologic and stratigraphic data concurs in overall topology with the parsimony analysis, placing *Neptunidraco* as sister taxon of the clade including “*Metriorhynchus*” *brachyrhynchus*, *Tyrannoneustes* and Geosaurini, and more derived than a clade including the Patagonian geosaurines (Fig. 5). The Bayesian analysis inferred the ages of cladogenetic events and calculated the rates of morphological evolution along branches (divergence, see Lee et al. 2014a, b). Timing of cladogenesis inferred by the Bayesian analysis places the age of the last common ancestor of *Neptunidraco* and more derived geosaurines at about 171 Mya, thus inferring a 3 Myr long ghost lineage for the Italian metriorhynchid. Accordingly, the rate of morphological evolution along the terminal branch leading to *Neptunidraco* is estimated at 8.7% of changes/Myr. This value is the highest estimated for *Thalattosuchia*, being more than one order of magnitude above the background rate of morphological evolution inferred for most of the other branches in all alternative topologies recovered by the Bayesian analysis (Fig. 5).

#### 4.1.2. *Anguanax zignoi*

The inclusion of *Anguanax* in the phylogenetic analysis of Benson and Druckenmiller (2014) placed the taxon among the basal (non-thalassophonean, Benson and Druckenmiller 2014) pliosaurids. The analysis found 5520 shortest trees of 727 steps each (Consistency Index = 0.4649, Retention Index = 0.6473). In the strict consensus topology

of the shortest trees found (Fig. 6), *Anguanax* is placed as sister taxon of the “*Marmornectes* + *Thalassophonea*” node and more derived than the *Hauffiosaurus* species, thus in agreement with the interpretation of this taxon as a member of the “basal longirostrine grade” *sensu* Benson et al. (2011) discussed by Cau and Fanti (2014). *Anguanax* is closer to more derived pliosaurids than *Hauffiosaurus* as it shows a strongly dorsomedially oriented mandibular glenoid almost completely unexposed laterally, anterior cervical centra shorter than high, and the preaxial margin of radius that is straight. Furthermore, it is less derived than *Marmornectes* due to the retention of plesiomorphic features as anterior cervical centra lacking an anteroventral “lip”, caudal vertebrae bearing chevron facets widely spaced and located ventrolaterally and with ventral surface approximately flat, a straight long axis of the femur, and slender phalanges. High nodal support values for the “*Marmornectes* + *Thalassophonea*” and *Thalassophonea* nodes (Fig. 6) suggest that alternative placements of *Anguanax* among more derived pliosaurids are the less parsimonious explanations of the data.

The result of the Bayesian analysis integrating morphological and stratigraphic data agrees in overall topology with the parsimony analysis, with *Anguanax* recovered as sister taxon of the “*Marmornectes* + *Thalassophonea*” node in the Maximum Clade Credibility Tree (MCCT, Fig. 7). The posterior probability value for the least inclusive node containing *Anguanax* is robust (posterior probability: 0.79). Based on the inferred timing of cladogenesis among pliosauroids as resulted by the analysis, the lineage leading to *Anguanax* diverged from other pliosaurids at about 176 Mya, thus a 17 Myr long ghost lineage for the Italian pliosaurid is inferred by the MCCT. Furthermore, the rate of morphological evolution along the branch leading to *Anguanax* is estimated as being the highest among pliosaurids (i.e., 3% of changes/Myr), and significantly higher than almost all of the values estimated for the other lineages among the alternative topologies found (Fig. 7).

## 5. Discussion

### 5.1. Taxonomic revision of the *Cesuna* material

Although all specimens from *Cesuna* were collected from the same locality, de Zigno (1883) did not provide accurate information whether they were found in association or not. He consequently referred all the material to *Plesiosaurus* based on the presence of

subcentral foramina (de Zigno 1883). Nevertheless, Morphotype 1 centra lack any unambiguous plesiosaurian synapomorphy. In particular, the absence of both notochordal pits and subcentral foramina, and the mediolaterally constricted ventral surface of these centra, differ from plesiosaurian dorsal centra, the latter usually unconstricted ventrally, broader than tall and bearing notochordal pits and subcentral foramina (e.g., Andrews 1913; Tarlo 1960; Ketchum and Benson 2011; Knutsen 2012). The combination of features in Morphotype 1 centra is much closely matched by crocodylomorph dorsal vertebrae, in particular, in the mediolateral constriction of the ventral surface (e.g., Andrews 1913; M. Young, pers. com. to AC, 2013). Metriorhynchidae is the only crocodylomorph clade reported in the Rosso Ammonitico Veronese Formation (Cau 2013; Cau and Fanti 2011, 2014). In overall morphology, Morphotype 1 centra do not differ in significant features from the dorsal centra of thalattosuchians (e.g., Andrews 1913; Herrera et al. 2013; M. Young, pers. com. to AC, 2013). Therefore, we refer Morphotype 1 centra to a crocodylomorph, probably a thalattosuchian.

Centra pertaining to Morphotype 2 are referred to Plesiosauria based on the presence of subcentral foramina (Ketchum and Benson 2010), an interpretation in agreement with the overall morphology and proportion of the centra, shared by Jurassic plesiosaurians (e.g., Andrews 1913; Ketchum and Benson 2011). The neural arches show low pedicels with the antero-posteriorly compressed transverse processes placed at the level of the dorsal half of the neural canal, a combination of features present in plesiosaurian dorsal neural arches (e.g., Ketchum and Benson 2011).

The name '*Plesiosaurus italicus*' was mentioned by Dalla Vecchia (1997) in a catalogue of the Cesuna material housed in the MGP-PD collection. That binomial was referred to de Zigno (1883), although the latter author did not erect a new species (de Zigno 1883: 13). Accordingly, '*Plesiosaurus italicus*' is considered as a *nomen nudum*.

Using the width of the atlas-axis complex (55 mm) as a proxy for occipital condyle width, the total skull length of *Anguanax* holotype is estimated to be around 80 cm (following the method in Knutsen et al. 2012). The presence of extensive osteoporosis (Fig. 3D) in the bones indicates that the holotype of *Anguanax zignoi* was somatically mature at the time of death (Wiffen et al. 1995).

## **5.2. Evolution of RAVFm Reptiles**

The results of the Bayesian phylogenetic and palaeobiogeographic analyses for *Anguanax* and *Neptunidraco* produced similar scenarios. The terminal branches leading to both taxa are inferred to: 1) be North-Western European in ancestral range; 2) diverge from their closest relatives during a 5 Myr long interval, close to the Lower-Middle Jurassic boundary (i.e., about 176-171 Ma: corresponding to the late Toarcian-Aalenian interval); 3) have a rate of morphological evolution significantly higher than those of all other members of their clades.

Could such high rates of morphological evolution leading to the Italian reptiles be an artefact of the analyses? Lee et al. (2014a) noted that morphological divergence is highest in youngest terminal taxa, as expected due to anagenesis along longer lineages. This higher divergence may produce artificially inflated rates of divergence for those terminal taxa the age of which are incorrectly overestimated (i.e., when these terminals are placed at an age older than their actual age). We dismiss this interpretation for *Anguanax*, as the age of the type specimen at the Kaberlaba section is well-constrained (note that the Kaberlaba section represents the type section for the RAVFm; Martire et al., 2006; Pellenard et al., 2013; Cau and Fanti 2014, and references therein). We tested the hypothesis that the age of *Neptunidraco* was overestimated and that the type specimen belongs to the Upper Rosso Ammonitico Veronese member instead of the Lower member (see discussion in Cau and Fanti 2011 dismissing an Upper Jurassic placement for *Neptunidraco*), and replicated the Bayesian analysis using a latest Jurassic age (145 Mya) for the Italian metriorhynchid according to this alternative prior. This test inferred the rate of morphological evolution along the terminal lineage leading to *Neptunidraco* as about 2.5 changes/Myr, a value between three and five times higher than those of most other metriorhynchid branches, with only the lineage leading to *Tyrannoneustes* showing a higher value. Therefore, even assuming the youngest possible age for this Rosso Ammonitico Veronese reptile, its rate of divergence remains significantly higher than the background rate of its clade. We conclude that prior age assumptions for the Italian taxa analysed could not explain the high evolutionary rates recovered, and therefore consider the hypothesis that the latter may represent an unusual evolutionary pattern shared by the Rosso Ammonitico reptiles.

As discussed by Cau (2014), *Neptunidraco* shares with later members of Geosaurini a subset of the features interpreted as macrophagous and hypercarnivorous adaptations in

the latter clade. The Bayesian analysis indicates that the evolution of these features in the Italian taxon was a relatively rapid phenomenon, lasting no more than three million years. The lower rates of evolution inferred along the fully hypercarnivorous Geosaurini, compared to values inferred for *Neptunidraco* (and also *Tyrannoneustes*), suggest that this feeding adaptation was not the main factor driving rapid divergence in the Italian taxon, and further supports the interpretation that these features in *Neptunidraco* evolved independently to Geosaurini (Cau 2014). Furthermore, no peculiar feeding adaptations are evident in *Anguanax* when compared with other basal, gracile-longirostrine pliosaurids (e.g., *Hauffiosaurus*, Ketchum and Benson 2011; Benson et al. 2011). Therefore, we do not consider feeding adaptations as thorough explanations for the unusual rates of evolution inferred for the two Italian reptiles.

The Rosso Ammonitico Formation is primarily representative of deep water column deposition (depth >110 m, Martire, 1992; Martire et al., 2006; Cau and Fanti 2011), thus significantly deeper than the epiherc seas deposits where most metriorhynchoids and plesiosaurians are usually recovered (depth <50 m; Hudson and Martill 1991; Young et al. 2010; Massare et al. 2013). The taphonomy of both type specimens of *Anguanax* and *Neptunidraco* suggests that they did not suffer substantial transport neither disarticulation before burial (Cau and Fanti 2011, 2014). It is thus unlikely that these specimens were alloctonous elements transported from shallower marine areas. We therefore consider both taxa as typical inhabitant of open sea environments, and probably more pelagic in lifestyle than most members of their clades. Sea level fluctuation is considered among the main factors in Mesozoic marine reptile diversity trends, an interpretation that assumes that the distribution of these clades was mostly constrained to shallow epiherc seas (Young et al. 2010; Kelley et al. 2014). Tectonics played the principal role in driving high-amplitude sea-level changes during the Mesozoic (Hallam, 1984; Miller et al., 2005), and this is particularly true for the southern Alps region (Winterer and Bosellini, 1981). Kelley et al. (2014) showed that rapid rate of sea-level change, rather than variation in flooded shelf area variation, played an important role in the macroevolutionary trends among Triassic marine reptiles. Furthermore, exploration of new environments and adaptation to new ecologies may be rapidly selected when habitat tracking is not possible due to relatively rapid habitat loss (Eldredge 1995; Pyenson et al. 2011).

Our analyses suggest that both lineages leading to *Anguanax* and *Neptunidraco* during a 5

Myr long interval between the latest Toarcian and the first part of the Aalenian. The most relevant regressive event in Europe before the end of the Jurassic took place during the Aalenian in the North Sea and surrounding areas (Hallam 2001; this region has been included in the 'North Western Europe' area in our analyses). A rapid, tectonic-based, drowning of the Trento Platform (including the type localities of the RAVFm reptiles) is documented during the same interval (Winterer and Bosellini 1981, Martire, 1992; Martire et al., 2006). By the end of the accumulation of the lower RAV, in the early Callovian, the water depth was close to 1000 m. (Winterer and Bosellini, 1981). An hypothesis that we suggest here is whether the significantly higher rates of morphological evolution inferred for the lineages leading to *Anguanax* and *Neptunidraco* could indicate a phase of rapid evolutionary adaptation in the ancestors of the Rosso Ammonitico Veronese reptiles to deeper marine environments as a response to the Aalenian regressive regime in Europe. The novel ecology was eventually inherited by these lineages when they migrated to the deep-sea conditions represented by the RAVFm and more generically by the western Tethyan realm.

## 6. Conclusion

As remarked by Simpson (1944), the *tempo* of evolution provides information on the mode of evolution. The Bayesian inference methods allow to integrate simultaneously different sources of information (i.e., morphologic, stratigraphic) in phylogenetic reconstruction. This "total evidence" approach is relatively novel in palaeontology (see Lee et al. 2014a), although its logical basis follows the Simpson's seminal work on the role of palaeontology in the study of evolution. As shown in this study, this new approach may represent a promising tool in the palaeontological side of evolutionism, as it provides quantitative and testable hypotheses on the *tempo* and mode of evolutionary patterns. Using Bayesian inference methods, we suggest a shared framework for the origin and evolution of the two currently known RAVFm reptiles, the metriorhynchid *Neptunidraco ammoniticus* and the pliosaurid *Anguanax zignoi* gen. et sp. nov. Based on integration of morphological and stratigraphic information, both lineages leading to the RAVFm reptiles diverged from their closest relatives during a relatively short interval between the late Turonian and the Aalenian (176-171 Ma). Along both lineages, the rates of morphological divergence from

their ancestors are inferred to be significantly higher than the background rate of evolution of their clades. We interpret the shared framework in these lineages as due to relatively rapid shift to deeper marine environments, the latter seen as an adaptive response to the regressive phase of the Turonian-Aalenian of Northern Europe and the coeval drowning of the Northern Tethyan margin, that reduced the ancestral shallow marine environments of metriorhynchoids and pliosaurids in Europe. Being both spatially and temporally constrained, this hypothesis on the *tempo* and mode of RAVFm reptile evolution is testable, as it predicts that future members of the Italian lineages could not be found before the late Toarcian-Aalenian regression phase and outside the North Western Europe and Western Tethyan realms.

### Acknowledgments

We thank M. Fornasiero (MGP-PD), R. Pancaldi and B. Sala (both MPPL) who kindly gave permission and access to the studied material. We are grateful to S. Castelli (MGP-PD) and P. Ferrieri (MGGC) for the photographic material provided. Free online version of TNT is available by the sponsorship of the Willi Hennig Society.

### References

- Andrews, C.W. 1913. A Descriptive Catalogue of the Marine Reptiles of the Oxford Clay: Part II. British Museum (Natural History), London.
- Bardet N, Pereda Suberbiola X, Jalil N-E 2003. A new polycotyloid plesiosaur from the Late Cretaceous (Turonian) of Morocco. *C R Palevol*. 2(5):307–315.
- Benson RBJ, Ketchum HF, Noè LF, Gómez-Pérez M. 2011. New information on *Hauffiosaurus* (Reptilia, Plesiosauria) based on a new species from the Alum Shale Member (Lower Toarcian: Lower Jurassic) of Yorkshire, UK. *Palaeontology*. 54: 547–571.
- Benson RBJ, Druckenmiller PS. 2014. Faunal turnover of marine tetrapods during the Jurassic-Cretaceous transition. *Biol Rev* 89:1–23.
- Benson RBJ, Evans M, Smith AS, Sassoon J, Moore-Faye S, Ketchum HF, Forrest R.

2013. A giant pliosaurid skull from the Late Jurassic of England. PLoS ONE 8(5): e65989. doi:10.1371/journal.pone.0065989
- Bizzarini F. 1996. Sui resti di cocodrillo del Rosso Ammonitico Veronese di Sasso di Asiago (Altopiano dei Sette Comuni, Prealpi Venete). Annali del Museo Civico di Rovereto. 11:339–348..
- Carpenter K. 1999. Revision of North American elasmosaurs from the Cretaceous of the western interior. Paludicola. 2(2):148–173.
- Cau A. 2014. The affinities of '*Steneosaurus barettoni*' (Crocodylomorpha, Thalattosuchia), from the Jurassic of Northern Italy, and implications for cranial evolution among geosaurine metriorhynchids. Hist Biol. 26(4):433-440.
- Cau A, Fanti F. 2011. The oldest known metriorhynchid crocodylian from the Middle Jurassic of north-eastern Italy: *Neptunidraco ammoniticus* gen. et sp. nov. Gondwana Res. 19:550–565.
- Cau A, Fanti F. 2014. A pliosaurid plesiosaurian from the Rosso Ammonitico Veronese Formation of Italy. Acta Pal Pol. 59(3):643–650.
- Cohen KM, Finney SC, Gibbard PL, Fan J-X. 2013. The ICS International Chronostratigraphic Chart (Updated). Episodes. 36:199-204.
- Dalla Vecchia FM. 1997. Mesozoic Amphibia and Reptilia stored at the Museum of Paleontology of the University of Padua. Natura Nascosta. 15:34–43.
- Delfino M, Dal Sasso C. 2006. Marine reptiles (Thalattosuchia) from the Early Jurassic of Lombardy (northern Italy). Geobios. 39:346–354.
- De Zigno AV. 1883. Sui Vertebrati fossili dei terreni mesozoici delle Alpi venete. Memorie della Reale Accademia delle Scienze, Lettere e Arti. 2–14.
- Drummond AJ, Suchard MA, Xie D, Rambaut A. 2012 Bayesian phylogenetics with BEAUti and the BEAST 1.7. Mol Biol Evol. 29:1969–1973.
- Eldredge N. 1995. Macroevolutionary Dynamics (McGraw-Hill, New York, 1989); in New Approaches to Speciation in the Fossil Record, D. Erwin and R. Anstey, Eds.

(Columbia Univ. Press, New York, 1995), p. 39; *Reinventing Darwin* (Wiley, New York, 1995), p. 57.

- Goloboff P, Farris J, Nixon K. 2008. TNT, a free program for phylogenetic analysis. *Cladistics*. 24:774–786.
- Hallam A. 1984. Pre-Quaternary sea-level changes. *Annu Rev Earth PI Sc*. 12:205–243.
- Hallam, A. 2001. A review of the broad pattern of Jurassic sea-level changes and their possible causes in the light of current knowledge. *Palaeogeogr Palaeocl*. 167:23–37.
- Herrera Y, Fernández MS, and Gasparini Z. 2013. Postcranial skeleton of *Cricosaurus araucanesis* (Crocodyliformes: Thalattosuchia): morphology and palaeobiological insights. *Alcheringa* 37:1–14.
- Hudson JD, Martill DM. 1991. The Lower Oxford Clay: production and preservation of organic matter in the Callovian (Jurassic) of central England. In *Modern and Ancient Continental Shelf Anoxia*. (eds R. V. Tyson & T. H. Pearson), pp. 363–79. Geological Society of London, Special Publication no. 58.
- Kelley NP, Motani R, Jiang D-Y, Rieppel O, Schmitz L. 2014. Selective extinction of Triassic marine reptiles during long-term sea-level changes illuminated by seawater strontium isotopes. *Palaeogeogr Palaeocl*. 400: 9–16.
- Ketchum HF, Benson RBJ. 2011. A new pliosaurid (Sauropterygia, Plesiosauria) from the Oxford Clay Formation (Middle Jurassic, Callovian) of England: evidence for a gracile, longirostrine grade of Early–Middle Jurassic pliosaurids. *Spec Pap Palaeontol*. 86:109–129.
- Knutsen EM. 2012. A taxonomic revision of the genus *Pliosaurus* (Owen, 1841a) Owen, 1841b. *Norw J Geol*. 92: 259–276.
- Lee MSY, Cau A, Naish D, Dyke GJ. 2014a. Morphological clocks in palaeontology, and a mid-Cretaceous origin of crown Aves. *Systematic Biol*. 63:442–449.
- Lee MSY, Cau A, Naish D, Dyke GJ. 2014b. Sustained miniaturization and anatomical innovation in the dinosaurian ancestors of birds. *Science*. 345:562–566.
- Martire L. 1992. Sequence stratigraphy and condensed pelagic sediments. An example from the Rosso Ammonitico Veronese, northeastern Italy. *Palaeogeogr Palaeocl*. 94:169–191.

- Martire L. 1996. Stratigraphy, facies and synsedimentary tectonics in the Jurassic Rosso Ammonitico Veronese (Altopiano di Asiago, NE Italy). *Facies*. 35:209–236.
- Martire L, Clari P, Lozar F, Pavia G. 2006. The Rosso Ammonitico Veronese (Middle–Upper Jurassic of the Trento Plateau): a proposal of lithostratigraphic ordering and formalization. *Riv Ita Paleontol S*. 112:227–250.
- Massare JA, Wahl WR, Ross M, Connely MV. 2013. Palaeoecology of the marine reptiles of the Redwater Shale Member of the Sundance Formation (Jurassic) of central Wyoming, USA. *Geol Mag*. 151:167–182.
- Miller KG, Kominz MA, Browning JV, Wright JD, Mountain GS, Katz ME, Sugarman PJ, Cramer BS, Christie-Blick N, Pekar SF. 2005. The Phanerozoic record of global sea-level change. *Science*. 310:1293–1298.
- Pellenard P, Nomade S, Martire L, De Oliveira Ramalho F, Monna F, Guillou H. 2013. The first  $^{40}\text{Ar}$ - $^{39}\text{Ar}$  date from Oxfordian ammonite-calibrated volcanic layers (bentonites) as a tie-point for the Late Jurassic. *Geol. Mag*. 150:1136-1142.
- Pyenson ND, Lindberg DR. 2011. What happened to gray whales during the Pleistocene? The ecological impact of sea-level change on benthic feeding areas in the North Pacific Ocean. *PLoS One*. 6:e21295.
- Simpson, G. G. (1944) *Tempo and Mode in Evolution*. New York: Columbia Univ. Press.
- Smith SA. 2009. Taking into account phylogenetic and divergence-time uncertainty in a panameric biogeographic analysis of the Northern Hemisphere plant clade Caprifolieae. *Journal of Biogeography*. 36: 2324–2337.
- Tarlo LB. 1960. A review of Upper Jurassic Pliosaurus. *Bulletin of the British Museum (Natural History)*. *Geology*. 4:145–189.
- Wiffen T, de Buffrénil V, de Ricqlès A, Mazin J. 1995. Ontogenetic evolution of bone structure in Late Cretaceous Plesiosauria from New Zealand. *Geobios*. 28:625–640.

- Wilkinson LE, Young MT, Benton MJ. 2008. A new metriorhynchid crocodile (Mesoeucrocodylia: Thalattosuchia) from the Kimmeridgian (Upper Jurassic) of Wiltshire, UK. *Palaeontology*. 51:1307–1333.
- Winterer EL, Bosellini A. 1981. Subsidence and sedimentation on a Jurassic passive continental margin, Southern Alps, Italy. *AAPG Bul.* 65:394–422.
- Yan Y, Harris AJ, Xingjin H. 2011. RASP (Reconstruct Ancestral State in Phylogenies) 1.1. Available at: <http://mnh.scu.edu.cn/soft/blog/RASP>.
- Young MT. 2014. Filling the ‘Corallian Gap’: re-description of a metriorhynchid crocodylomorph from the Oxfordian (Late Jurassic) of Headington, England. *Hist Biol.* 26(1):80–90.
- Young MT, Andrade MB. 2009. What is *Geosaurus*? Redescription of *Geosaurus giganteus* (Thalattosuchia: Metriorhynchidae) from the Upper Jurassic of Bayern, Germany. *Zool J Linn Soc.* 157:551–585.
- Young MT, Brusatte SL, Ruta M, Andrade MB. 2010. The evolution of Metriorhynchoidea (Mesoeucrocodylia, Thalattosuchia): an integrated approach using geometric morphometrics, analysis of disparity and biomechanics. *Zool J Linn Soc.* 158:801–859.

## Figures

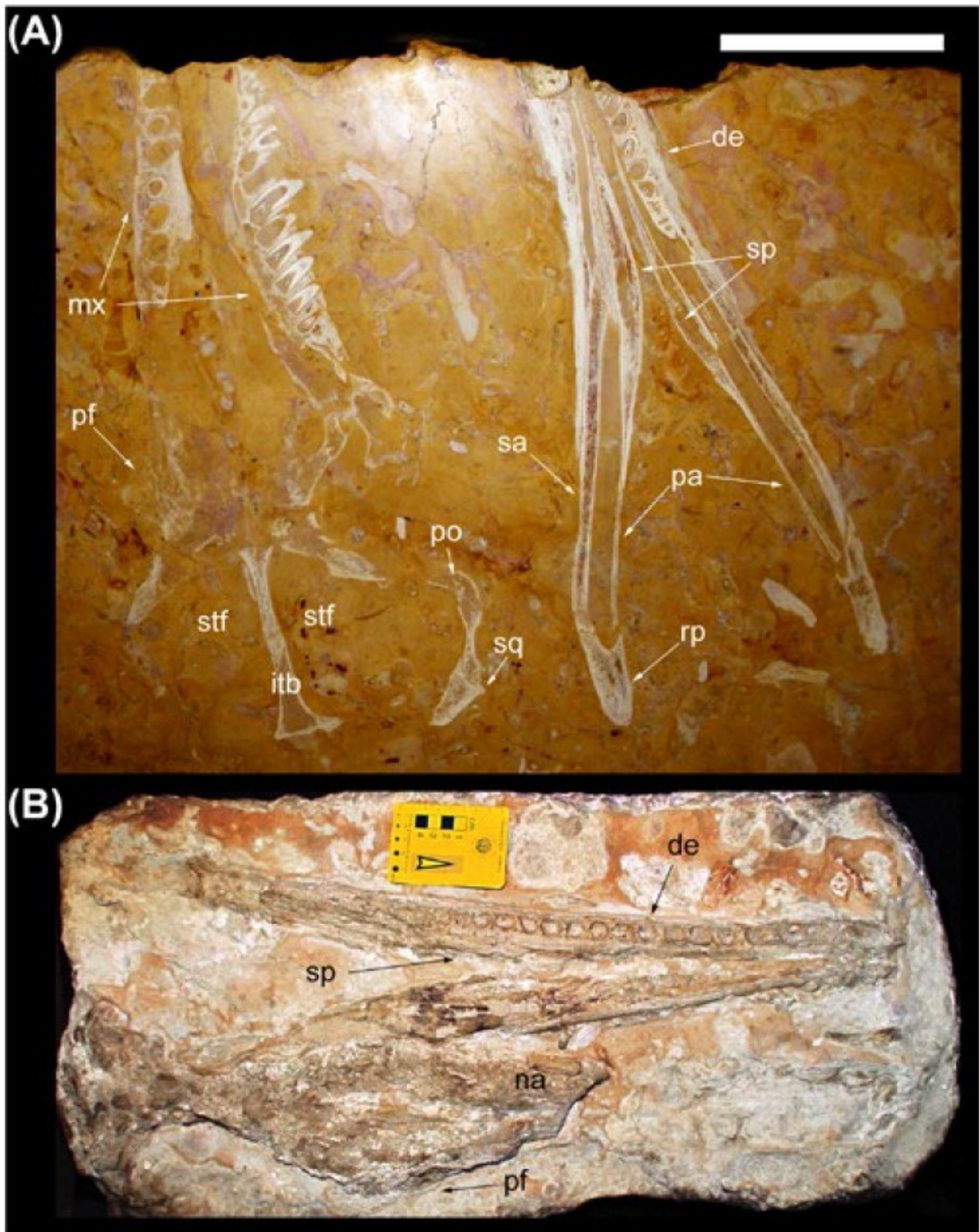


Fig. 1. *Neptunidraco ammoniticus*. (A), part of holotype specimen, MGGC 8846; (B), referred specimen, MGP-PD 6552. Abbreviations: de, dentary; itb, intertemporal bar; mx, maxilla; na, nasal; pa, prearticular; pf, prefrontal; po, postorbital; rp, retroarticular process;

sa, surangular; sp, splenial; sq, squamosal; stf, supratemporal fenestra. Scale bars: (A): 20 cm; (B): 5 cm.

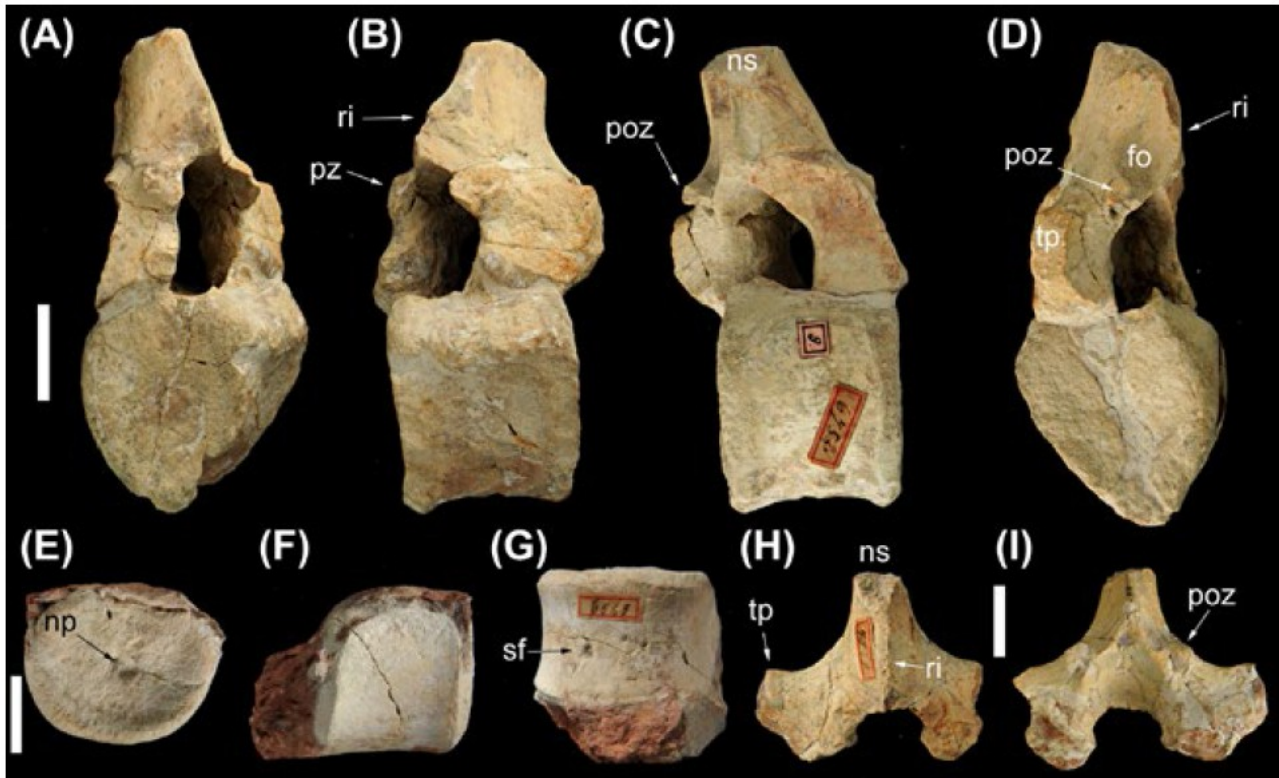


Figure 2. Crocodylomorph and plesiosaurian material from the Rosso Ammonitico Veronese Formation of Cesuna (Veneto, Italy). A-D, MPG 6752, chimaerical association of plesiosaurian neural arch and crocodylomorph centrum in anterior (A), left lateral (B), right lateral (C) and posterior (D) views. E-G, MPG 6549, isolated plesiosaurian centrum in anterior (E.), right lateral (F) and ventral (G) views. H-I, MPG 6752, isolated plesiosaurian neural arch in anterior (H) and posterior (I) views. Scale bars: 2 cm. Abbreviations: fo, fossa; np, notochordal pit; ns, neural spine; poz, postzygapophysis base; pz, prezygapophysis base; ri, ridge; sf, subcentral foramen; tp, transverse process.

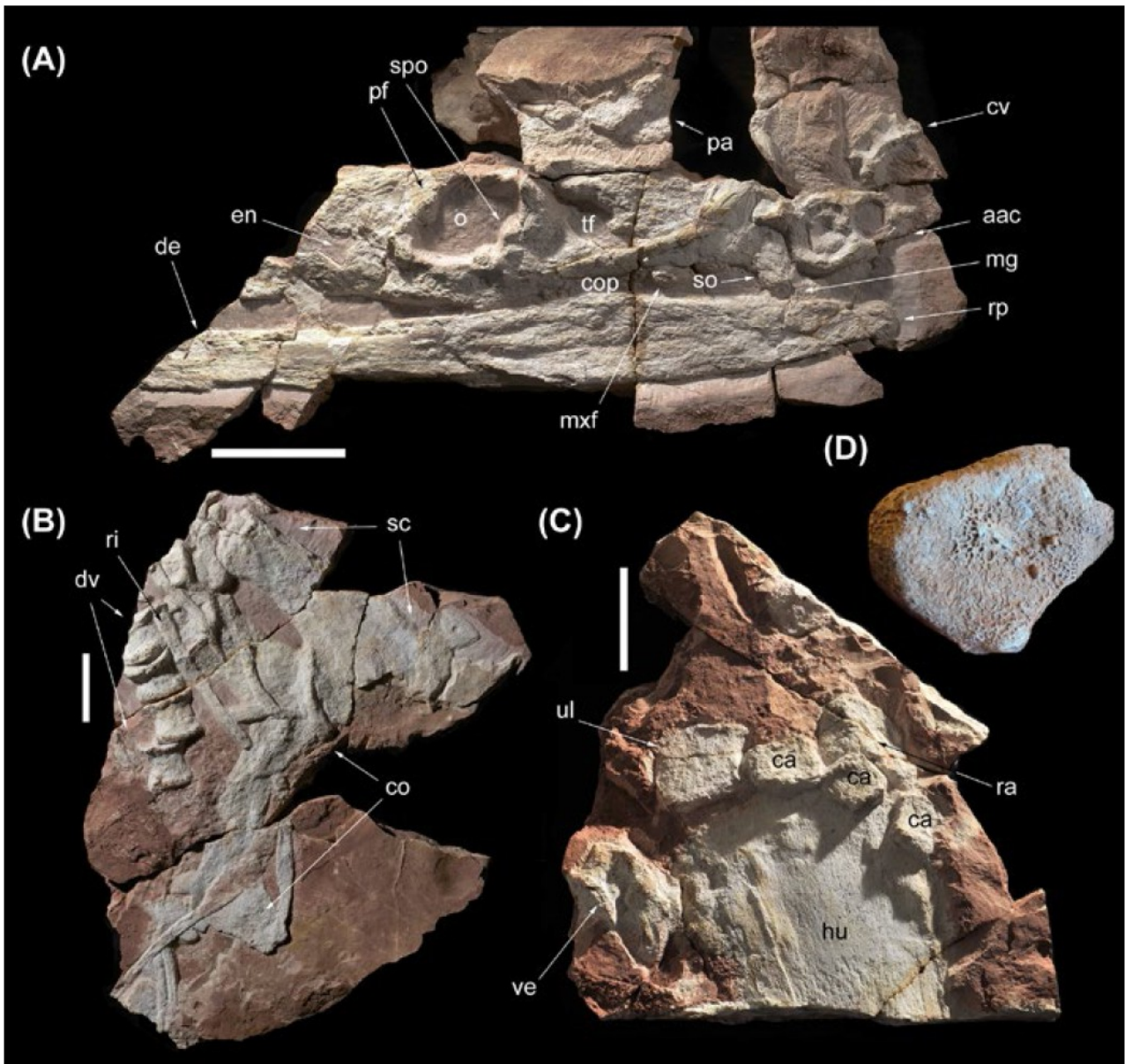


Fig. 3. *Anguanax zignoi* gen. et sp. nov., holotype specimen. Selected elements: (A), skull, left lateral view; (B), dorsal vertebrae and left scapulocoracoid, ventral view; (C), partial left forefin; (D) cross section of unidentified bone (?vertebra) showing cancellous osteoporotic-like texture. Abbreviations: aac, atlas-axis complex; co, coracoid; cop, coronoid process; cv, cervical vertebra; de, dentary; dv, dorsal vertebrae; en, external naris; hu, humerus; mg, mandibular glenoid; mx, maxilla; mf, maxillary fragment; o, orbit; pa, parietal; pf, prefrontal; ra, radius; ri, ribs; rp, retroarticular process; sc, scapula; so, suspensorium; spo, stepped postorbital margin of orbit; tf, temporal fenestra; ul, ulna; ve, vertebra. Scale bars: (A-C): 10 cm; (D): 2 cm.

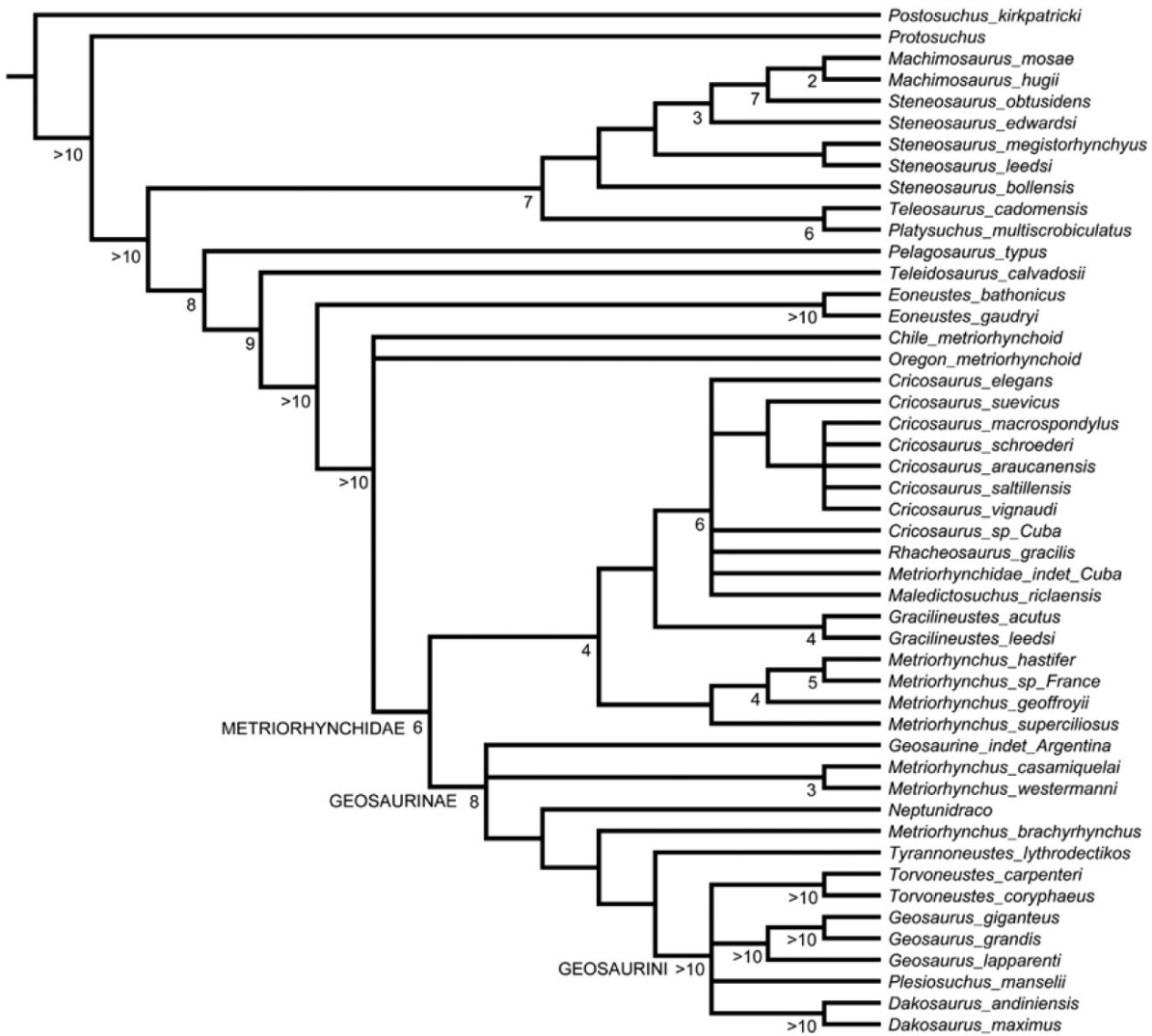


Fig. 4. Strict consensus of the shortest trees found by the parsimony analysis of the thalattosuchian dataset. Number adjacent to nodes indicate Decay Index values >1.

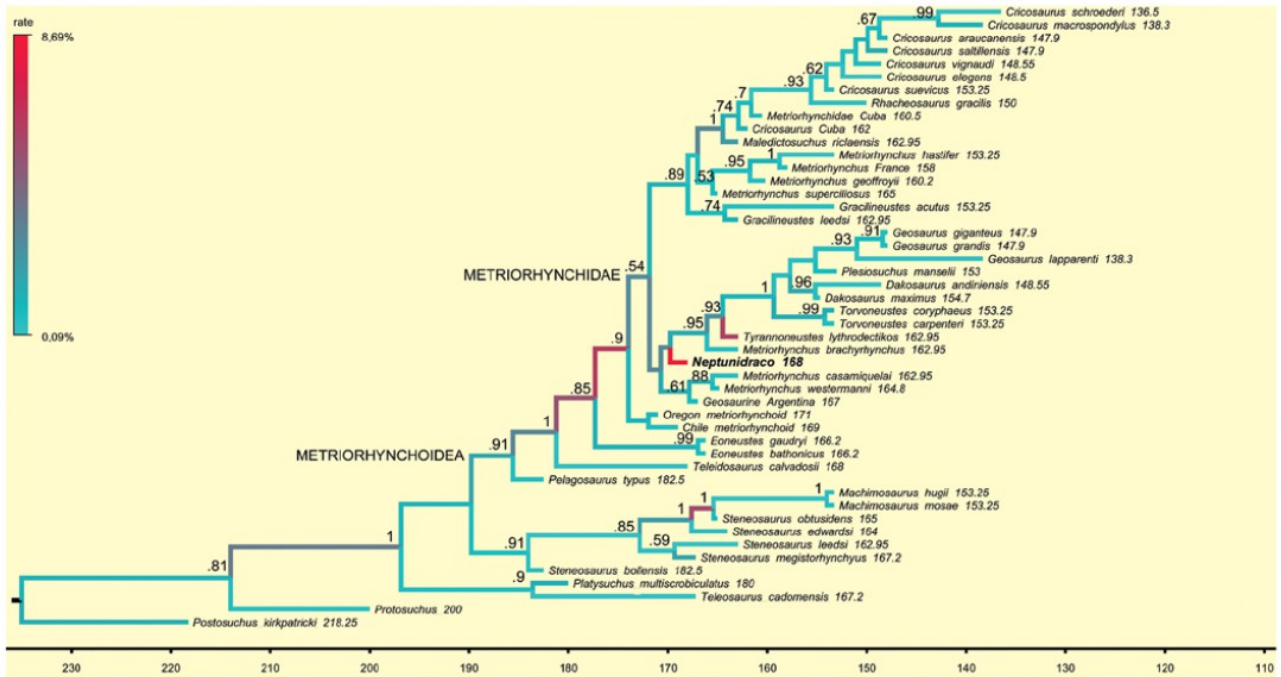


Fig. 5. Maximum Clade Credibility Tree found by the Bayesian analysis of the thalattosuchian dataset. Branches colored according to rate of morphological divergence (Changes/Myr) estimated by analysis. Note the highest value for *Neptunidraco* among metriorhynchids. Number adjacent to nodes indicate posterior probability values >0.5. Scale bar in million years before present.

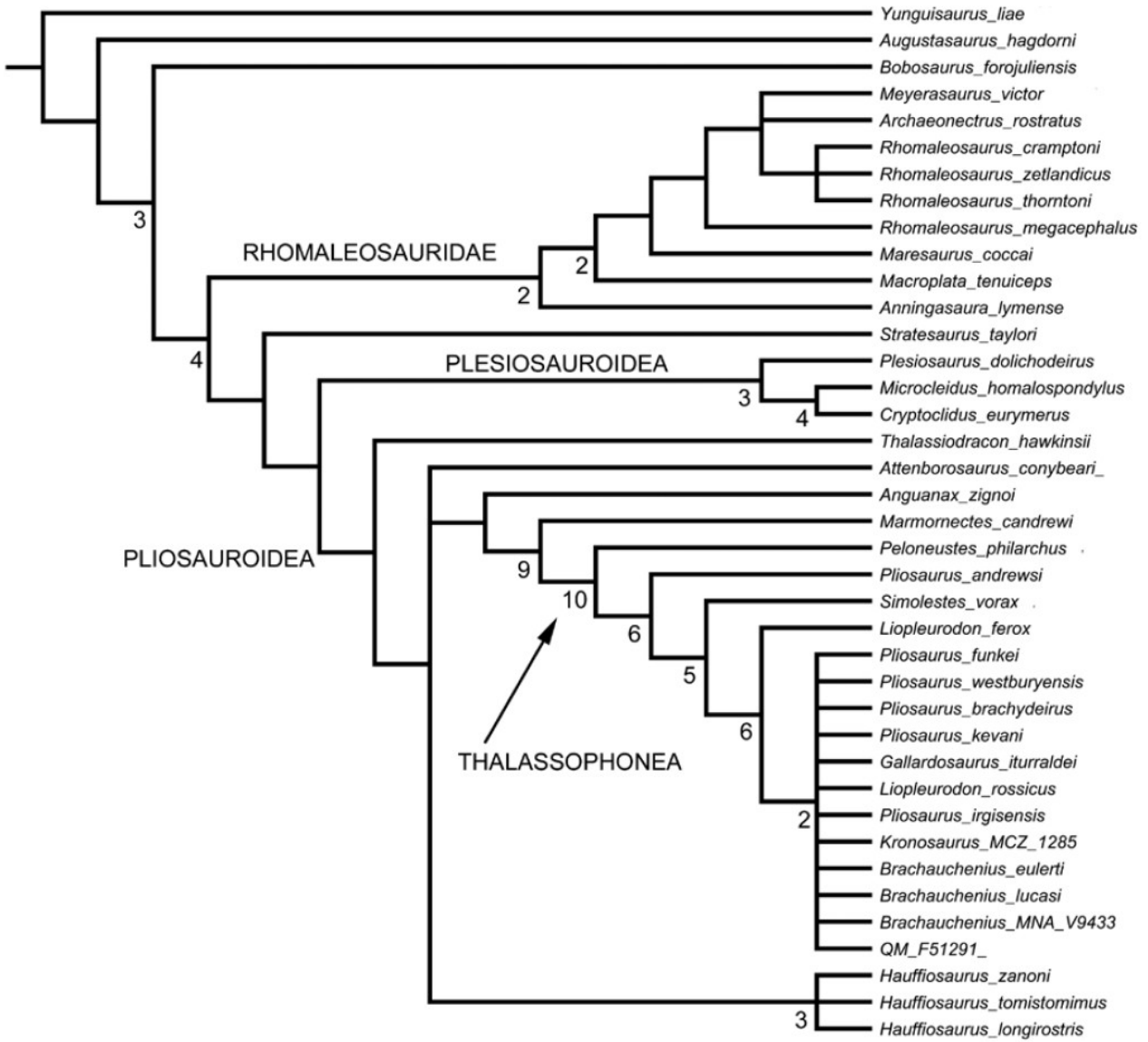


Fig. 6. Strict consensus of the shortest trees found by the parsimony analysis of the plesiosaurian dataset. Number adjacent to nodes indicate Decay Index values >1.

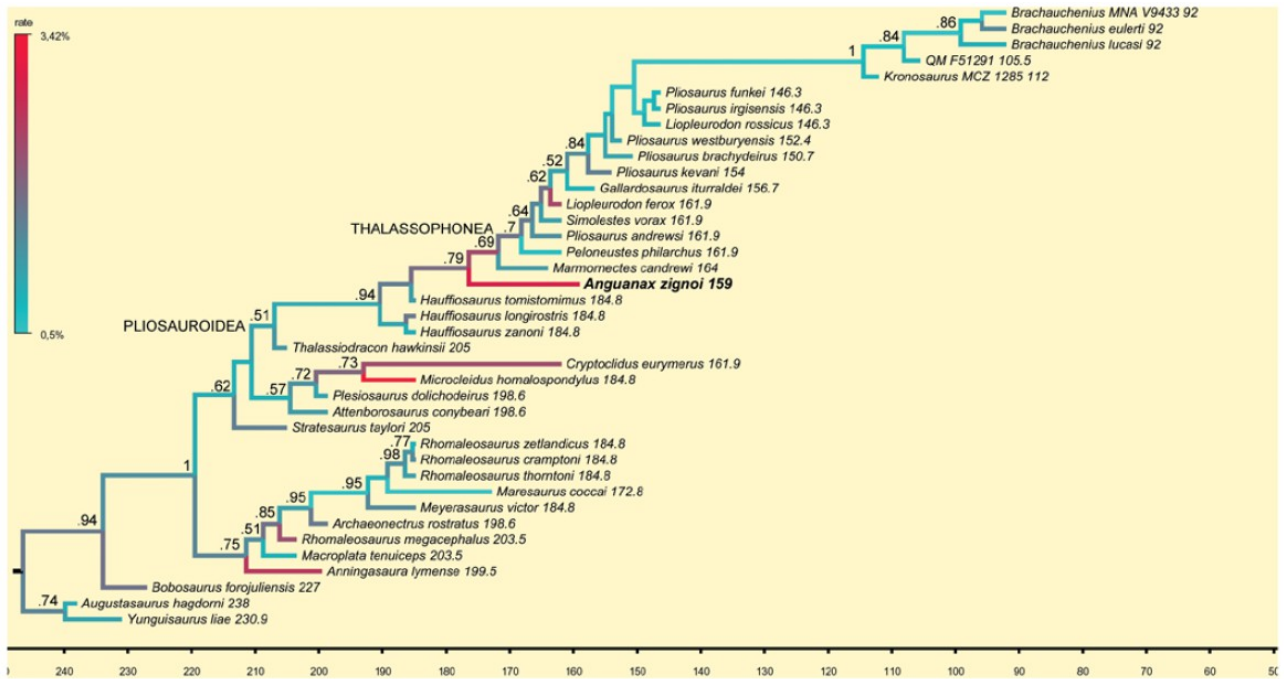


Fig. 7. Maximum Clade Credibility Tree found by the Bayesian analysis of the plesiosaurian dataset. Branches colored according to rate of morphological divergence (Changes/Myr) estimated by analysis. Note the highest value for *Anguanax* among pliosaurids. Number adjacent to nodes indicate posterior probability values >0.5. Scale bar in million years before present.

Page left blank

## **CHAPTER 7 - New information on *Tataouinea hannibalis* from the Early Cretaceous of Tunisia and implications for the *tempo* and mode of rebbachisaurid sauropod evolution**

Submitted: 21<sup>st</sup> October 2014. Published: 29<sup>th</sup> April 2015 in *PLoS ONE* vol.10, issue4:e0123475.

Federico Fanti\*, Andrea Cau\*, Luigi Cantelli, Mohsen Hassine, Marco Auditore

\*FF and AC are Joint Senior Authors.

### **Abstract**

The rebbachisaurid sauropod *Tataouinea hannibalis* represents the first articulated dinosaur skeleton from Tunisia and one of the best preserved in northern Africa. The type specimen was collected from the lower Albian, fluvio-estuarine deposits of the Ain el Guettar Formation (southern Tunisia). We present detailed analyses on the sedimentology and facies distribution at the main quarry and a revision of the vertebrate fauna associated with the skeleton. Data provide information on a complex ecosystem dominated by crocodylian and other brackish water taxa. Taphonomic interpretations indicate a multi-event, pre-burial history with a combination of rapid segregation in high sediment supply conditions and partial subaerial exposure of the carcass. After the collection in 2011 of the articulated sacrum and proximalmost caudal vertebrae, all showing a complex pattern of pneumatization, newly discovered material of the type specimen allows a detailed osteological description of *Tataouinea*. The sacrum, the complete and articulated caudal vertebrae 1-17, both ilia and ischia display asymmetrical pneumatization, with the left side of vertebrae and the left ischium showing a more extensive invasion by pneumatic features than their right counterparts. A pneumatic hiatus is present in caudal centra 7 to 13, whereas caudal centra 14-16 are pneumatised by shallow fossae. Bayesian inference analyses integrating morphological, stratigraphic and paleogeographic data support a flagellicaudatan-rebbachisaurid divergence at about 163 Ma and a South American ancestral range for rebbachisaurids. Results presented here indicate an exclusively South

American Limaysaurinae and a more widely distributed Rebbachisaurinae lineage, the latter including the South American taxon *Katpensaurus* and a clade including African and European taxa, with *Tataouinea* as sister taxon of *Rebbachisaurus*. This scenario would indicate that South America was not affected by the end-Jurassic extinction of diplodocoids, and was most likely the center of the rapid radiation of rebbachisaurids to Africa and Europe between 135 and 130 Ma.

## Introduction

The partial skeleton of a rebbachisaurid sauropod was discovered in the fall of 2011 by Mr. A. Bacchetta during a geological investigation at the Jebel El Mra locality (Tataouine Governorate, Tunisia) led by the University of Bologna. Prospecting activities at the site followed previous discovery of fossil-rich beds and scattered crocodylian and fish remains littering the Aptian-Albian deposits exposed in the area. A first excavation carried out in collaboration with the Office National des Mines resulted in the acquisition of the sacrum and the first five caudal vertebrae, that were consequently transported to the Musée de l'Office National des Mines in Tunis. Unfortunately, these elements were severely vandalized after their transportation to the capital city: the unstable political situation of the recent years resulted in terrible damages at the cultural heritage of this country, including paleontological specimens. Only in the spring of 2012, thanks to the direct involvement of the Tunisian authorities, it was possible to access the specimen and start the difficult preparation of damaged elements. Despite a big investment of time and resources, more than 200 fragments pertaining to the sacrum and proximal caudal vertebrae were not returned to the original conditions. Nevertheless, the restored material allowed to formally instituting *Tataouinea hannibalis* as a new genus and species of rebbachisaurid sauropod (1). The new sauropod is characterized by an extensive pattern of postcranial pneumatization in most of the recovered skeleton. In particular, *Tataouinea* shows, for the first time among non-avian dinosaurs, an ischial pneumatic foramen, further corroborating the presence of a bird-like system of air sacs in sauropods (1). Additional information based on field notes and pictures, measurements, and quarry maps taken during the first excavation are presented in this study in order to carefully reconstruct some of the vandalized skeletal elements. A new field expedition in the spring of 2013 led to the

collection of the fully articulated rest of the tail (caudal vertebrae 6-17) as well as further sedimentological and paleontological investigations at the El Mra locality.

### **Geological setting**

Since the first geological and paleontological reports published more than a century ago by Léon Pervinquière and other French geologists and paleontologists (2-6), the sedimentary beds of the Dahar escarpment in southern Tunisia have been known as a source of pivotal information on the Early Cretaceous ecosystems of northern Africa. The results of geological, paleontological and biogeographic investigations that followed tens of scientific expeditions in the area are largely presented and discussed in the literature (7-16 and references therein). Although the exposed Late Jurassic-Early Cretaceous alternation of shallow-marine, littoral, and non-marine deposits named "*Continental Intercalaire*" by Kilian in 1931 (3) is nowadays documented over much of northern Africa (17-20), the southern Tunisian outcrops provide unequalled stratigraphic and paleontological data (Fig. 1). Several major canyons and gorges as well as numerous minor drainage systems that cut the Dahar Plateau to the pediment that slopes toward the east forming the western margin of the Jeffara plain characterize the study area, located in the Tataouine Governorate. Therefore, the overall geomorphology is characterized by *mesa*-like structures that locally expose up to 150 meters of Jurassic and Cretaceous deposits, historically considered to represent sequential periods of time and different environments. The "*Continental Intercalaire*" exposures in the Tataouine region are represented, in ascending order, by the Oxfordian-lower Aptian Merbah el Asfer Group (Bir Miteur, Boulouha, and Douiret formations) and the overlying lower Albian Ain El Guettar (Chenini, Oum ed Diab and Rhadouane members) and Cenomanian-Turonian Zebbag formations (Kerker and Gattar members) (we refer to (14) for a detailed revision of stratigraphic units and chronostratigraphic framework).

### **The Jebel El Mra section**

The Jebel El Mra site is located approximately 50 km to the south-west of Tataouine, and 5 km to the south of the Bir Amir village (Fig. 1). The carbonate deposits of the Zebbag Formation cap this west-east oriented *mesa*, and substantial erosion has exposed underlying deposits for 120 meters to the uppermost, clay-dominated beds of the

Douiret Formation (Fig. 2). The articulated elements of *Tataouinea hannibalis* were collected in the basal deposits of the Oum ed Diab Member, approximately 1.5 meters above the fossil-rich conglomerate that marks the erosive contact between the Chenini and the overlying Oum ed Diab members (1, 14, 16) (Fig. 2B). This basal marker bed, that crops out with a patchy pattern in the entire Tataouine basin, yielded a rich and diverse vertebrate fauna that include elasmobranchs, actinopterygii, coelacanthiformes, crocodyliforms, rare pterosaurs and dinosaurs. However, as this faunal assemblage occurs within transgressive lag deposits on transgressive erosive surface, part of the preserved taxa may pertain to the underlying Chenini Member. Lacking any direct evidence to detail the age of these beds, (14) assigned an early Albian age to the lower Oum ed Diab Member deposits based on basin-scale paleontological, stratigraphic, and palynological evidence. The skeleton of *T. hannibalis* was preserved in a two meter thick, unconsolidated sandy interval characterized by sizeable, almost unidirectional (to the south-west) cross-bedding structures (Fig. 2C). This interval is capped by meter-thick, carbonate-cemented, horizontally-bedded sandstones: horizontal planes are characterized by extensive hematitic crusts and common, decimeter-scale rhizcretions, both interpreted as pedogenetic features. A significant reduction in flow energy is observed in the overlying deposits that consist in horizontally-bedded, fine- to coarse-grained, largely unconsolidated sandstones. High-angle, cross bedding structures observed in the most basal beds are gradually replaced by fining up sequences of tabular and fine-grained sandstones alternating ripple marks, herringbones cross-bedding and sporadic symmetric, wave-formed ripples.

**Vertebrate remains:** the basal conglomeratic beds of the Oum ed Diab Member sampled at the El Mra locality as well as other localities in the Tataouine basin yielded a rich and diverse vertebrate fauna that include marine elasmobranchs (*Tribodus tunisiensis*, *Lissodus* sp., *Diabodus tataouinensis*, *Retodus semiplicatus*, *Leptostyrax macrorhiza*, *Scaphanorinchus* sp., and *Onchopristis dunklei*), bony fish taxa (*Lepidotes* sp., *Mawsonia* sp., *Ceratodus* sp. and *Neoceratodus* sp.), crocodyliforms (*Sarcosuchus* sp., cf. *Araripesuchus* sp., and cf. *Hamadasuchus* sp.), and dinosaurs (carcharodontosaurids, spinosaurids, abelisaurids, titanosauriforms, and ornithopods) (10, 14-16, 21, 22). At the El Mra locality, the vast majority of identifiable elements pertains to crocodyliforms (a few

notosuchian-like and abundant neosuchian remains), whereas non-sauropod dinosaurs are represented by spinosaurids theropods that may represent two distinct clades, i.e., Baryonychinae and Spinosaurinae (16). The skeletal material of *T. hannibalis* represents the sole articulated dinosaur specimen ever collected from the Oum ed Diab Member and generally from Tunisia.

**Facies analysis and paleoecology:** the sandy deposits of the Oum ed Diab Member at the El Mra locality are interpreted as fluvial sandy bars within a vast, estuarine system characterized by high sediment supply and accommodation rate, as well as relatively high-energy hydraulic regime (Fig. 2C-F). The occurrence of *in situ* plant roots (possibly indicating a patchy, mangrove-like vegetation) are consistent with sub-aerial to low water depth conditions. Furthermore, molds, tubules, and rhizcretions, as well as extensive hematitic hard grounds support the development of thin paleosoils typical of arid to xeric environment (23-25). These lower sandy units gradually shift to shoreface beds interbedded with tidal flat/foreshore deposits, thus interpreted as a vast embayment characterized by tidal influence and dominated by marine taxa (i.e. elasmobranchs).

## Material and methods

In 2012 and 2013, high-resolution digital models of all sacral neural arches, caudal vertebrae, ilia and ischia, as well as of the entire 2013 quarry were acquired in Tunis by combining laser scanner (Next Engine ScanStudio HD Pro®, alignment of the scans) and hi-resolution photogrammetry, and consequently elaborated using Agisoft PhotoScan Professional®, and Meshlab® (Supplementary Material). These data were finally combined in order to obtain photogrammetric virtual reconstruction of the main quarry and scaled replicas (1:3) of the entire caudal series and ischia using a Makerbot 3D printer at the Dipartimento di Scienze Biologiche, Geologiche e Ambientali of the Università di Bologna, Italy (see Supplementary Material). These data were combined with field pictures and measurements and comparison with the sacral region of other sauropods (e.g., *Diplodocus carnegii*, MGGC 8723) in order to reconstruct the damaged section of the sacrum. Field data and replicas of skeletal remains are housed at the Museo Geologico Giovanni Capellini, Bologna. At the time of writing, all elements collected from the Jebel El

Mra locality are housed in the Musée de l'Office National des Mines in Tunis under the accession numbers ONM DT 1-48.

Sacral vertebrae nomenclature follows (26); caudal vertebrae laminae and fossae nomenclatures follow (27) and (28); pneumatic features terminology follows (29, 30).

Phylogenetic taxonomy follows (31) when not emended (see below).

Institutional abbreviations: ONM, Office National des Mines, Tunis; MGGC, Museo Geologico Giovanni Capellini, Bologna

### **Taphonomy of *Tataouinea hannibalis***

The type specimen of *T. hannibalis* represents the first articulated Mesozoic archosaur from Tunisia and one of the best-preserved dinosaur specimens ever collected in northern Africa (Fig. 3A). Unfortunately, a water channel that possibly eroded away the majority of the skeleton delimits the excavated area. However, based on available data it is not possible to determine if the missing parts of the skeleton were: 1. eroded away in recent times, 2. not preserved at the time of the original burial, or 3. buried as disarticulated elements over a wider area. Although preserved elements show no evidence of major post-mortem transportation, flow direction measurements taken on cross-bedding structures at the site suggest that sediment deposited onto the skeleton may have come toward the animal from a posterior to right side direction. The absence of the chevrons of the caudal series that conflicts with the fully articulated and nicely preserved vertebrae and sacral elements also support this interpretation. The sacrum was preserved lying on its ventral surface, a condition that strongly suggests a rapid segregation of this element from hydraulic flows and high sediment supply. In craniodorsal view, the fused neural spines of the sacral vertebrae are vertically oriented with respect to the paleo-ground (Fig. 3B). The overall preservation of skeletal remains was excellent, although sacral neural spines were partially eroded in their dorsal tip. As a possible consequence of relatively short-termed subaerial exposure, the right side of the caudal vertebrae is more deteriorated than the left counterpart. Although the sacral centra were obscured in any view in the field, their preservation indicates they were fully articulated with the neural arches and spines. Similarly, the displacement of both ischia was trivial, although only the proximal end of these elements was preserved. Considering the overall preservation of the skeleton, the

absence of pubis and legs is puzzling as investigation at the site in the sediments surrounding and underlying the sacrum and the tail did not indicate any further skeletal element. The tail curves cranially to the left of the body, lying on the left side, with an angle of almost 90 degrees with respect to the sacrum (Fig. 3C): the complete series of the first seventeen caudal vertebrae was collected at the excavation site. With the exception of the first caudal vertebra that was unexpectedly found detached from the caudal series and laying above the caudal part of the sacrum, all caudal vertebrae were fully articulated. No clear evidence of recent erosive event was noticed at the end of the caudal series, thus the lack of distal caudal vertebrae is interpreted as a displacement of these elements prior to the complete burial. Detailed sedimentological observation at the excavation site supports that skeletal elements were not fully buried in a single event. In particular, the most ventral part of the sacrum was buried by a single, high-energy event (indicated by the high-angle, cross-bedding stratification) that possibly left the dorsal section of the body, at the level of the sacral neural spines, exposed. A second event, represented by the cemented, tabular sand beds exposed in the upper section of the excavation site, finally buried remaining elements. A single, invertebrate feeding trace that did not affect the bony material was found in association with the skeleton. As the effects of invertebrate colonies are well documented in the literature (32-38) a single trace is consistent with a rapid segregation of *T. hannibalis* from the external environment. Lacking evidence of scavenging and deterioration of skeletal elements, the skeleton was most likely fully buried over a restricted period of time.

### **Systematic paleontology**

Dinosauria Owen, 1842  
Saurischia Seeley, 1888  
Sauropoda Marsh, 1878  
Rebbachisauridae Bonaparte, 1997  
Khebbashia clade nov.

**Phylogenetic definition:** The least inclusive clade including *Limaysaurus tessonei*, *Nigersaurus taqueti* and *Rebbachisaurus garasbae*.

**Remarks:** According to Article 36 of the International Code of Zoological Nomenclature, *Rebbachisaurus* is the eponymous genus of the ranked clade Rebbachisaurinae (39). Furthermore, *Limaysaurus* and *Nigersaurus* are the eponymous genera of, respectively, Limaysaurinae (31), and Nigersaurinae (31). Regardless to the relative relationships among these genera and the inclusiveness of the ranked clades anchored to them, we suggest the introduction of the unranked clade name Khebbashia for the least inclusive clade containing all these taxa. Note that Khebbashia cannot be a junior synonym of Rebbachisauridae under any alternative phylogenetic hypothesis, as the latter is a branch-based clade (i.e., the most inclusive clade containing *Rebbachisaurus garasbae* but excluding *Diplodocus longus* (31)) whereas the former is a node-based clade.

**Etymology:** from “Khebbash” or “Khebbache”, a Moroccan seminomadic tribe that inhabited the region where the first rebbachisaurid specimen was found (see 40).

Rebbachisaurinae (Bonaparte, 1997 [Nigersaurinae *sensu* Whitlock, 2011])

**Type genus:** *Rebbachisaurus* Lavocat, 1954.

**Included taxa:** *Rebbachisaurus garasbae* Lavocat, 1954; *Demandasaurus darwini* Fernández-Baldor et al., 2011; *Katepensaurus goicoecheai* Ibiricu et al., 2013; *Nigersaurus taqueti* Sereno et al., 1999; *Tataouinea hannibalis* Fanti et al., 2013.

**Diagnosis:** Middle and caudal dorsal neural arches with caudal centroparapophyseal lamina; proximal caudal vertebrae with a ventral interprezygapophyseal lamina; proximal caudal vertebrae with a lamina bisecting the prezygapophyseal centrodiapophyseal fossa; proximal caudal vertebrae with triangular lateral processes on the neural spine (41-43).

**Phylogenetic definition:** The most inclusive clade including *Rebbachisaurus garasbae* and excluding *Limaysaurus tessonei*.

**Remarks:** Both phylogenetic analyses by (40) and our study (see below), have incorporated information of *Rebbachisaurus* absent in previous phylogenies, and consistently recover the latter closer to *Nigersaurus* than *Limaysaurus*. Therefore, following the taxonomy of (31), *Rebbachisaurus* is a member of the subfamily-ranked clade Nigersaurinae. According to Articles 36 and 63.1 of the International Code of Zoological Nomenclature, the subfamily-ranked clade including *Rebbachisaurus* has to be

Rebbachisaurinae (40). Therefore, we consider Nigersaurinae (31), as a junior synonym of Rebbachisaurinae (39).

*Tataouinea hannibalis* Fanti, Cau, Hassine, Contessi, 2013

**Holotype.** ONM DT 1–48, sacrum, caudal vertebrae 1 to 17, both ilia, both ischia.

**Type locality and horizon.** Ain el Guettar Formation, Oum ed Diab Member, Jebel El Mra, Tataouine Governorate, southern Tunisia; early Albian. Estuarine to shallow marine deposits showing fining-upward sequences of fine-graded sandstones with herringbone cross-bedding, symmetrical wave-formed ripples and discontinuous clay lenses.

**Diagnosis (emended).** Rebbachisaurine sauropod dinosaur with unique combination of: completely fused sacral neural spines 1–3; poorly laminated cranial sacral neural spines, extensively laminated and semicamellate caudal sacral neural spines; elliptical foramen in lateral surface of fourth sacral neural spine penetrating the camerate sector of the spine; proximalmost five caudal vertebrae with elliptical pleurocoel placed at mid-height in the lateral surface of centrum that leads to a camerate internal pneumatisation; proximal caudal prezygapophyses not joined ventrally by a horizontal lamina; pneumatic foramen in the spinoprezygapophyseal fossa of proximal caudal vertebrae; pneumatic foramen in the prezygospinodiapophyseal fossa of proximal caudal vertebrae; “lateral lamina” in proximal caudal neural spines is “inverted Y”-shaped, formed by the spinoprezygapophyseal and spinodiapophyseal laminae, eventually merging dorsally with the spinopostzygapophyseal lamina and bordering a triangular fossa; caudal vertebrae 13-15 with shallow elliptical fossae on lateral surface of centrum; pubic peduncle of ilium hollowed by a large chamber; ischium with large elliptical foramen in the medial surface of the iliac peduncle (autapomorphy).

## Description

### Sacrum

The sacrum (Fig. 4-6) is the part of the preserved skeleton that has suffered the most important damage. The preserved elements include the ventral half of the fused sacral centra 1 to 4 (Fig. 4A-D), part of the ventral half of the isolated fifth sacral centrum (Fig. 4E-J), the ventral half of the completely fused sacral neural spines 1 to 3 (Fig. 4K-N), and

fragments of sacral neural spines 4 and 5 (Fig. 5). Intercentral junctions show a progressive degree of fusion, caudo-cranially directed: intercentral junction s4/5 is open, s3/4 is tightly fused with clearly discernable suture, whereas both s2/3 and s1/2 are completely obliterated with no clear sutures visible. The s1-4 centra form a roughly straight series in both lateral and dorsoventral views. Intercentral junction s3/4 is transversely and dorsoventrally larger than the other junctions. The minimum transversal diameter of all centra is comparable along the series. Consequently, sacral centrum 4 appears as hourglass-shaped in ventral view, sacral centrum 3 appears as a truncated cone, whereas the other centra are more roughly cylindrical. The proximal part of both acetabular rami of the sacral rib 4 are preserved. The costovertebral junction 4 is completely obliterated. The acetabular rami are dorsoventrally expanded and join cranially the intercentral junction s3/4. A large chamber occupies most of the internal space of the fused centra, due to extensive extramural pneumatisation (29, 30). The isolated sacral centrum 5 is partially preserved. The caudal intercentral facet and the dorsal half of the centrum is missing. The cranial intercentral facet is mostly eroded away. The centrum is a truncated cone, with the cranial end wider and deeper than the preserved posterior margin. The lateral surface of the centrum shows shallow elliptical fossae ventral to the costovertebral junctions. Internally, the centrum is extensively pneumatised by a large chamber. The proximal parts of the acetabular rami of sacral ribs are fused to the centrum. The preserved portions of the sacral ribs are projected caudally.

Only a limited part of the sacral neural arches is preserved. The largest element includes the ventral half of co-ossified neural spines 1-3, and the proximodorsal parts of both alar rami of sacral ribs and spinodiapophyseal laminae. In dorsal view, the element describes a cruciate pattern due to the intersection of the joined "neural spines + prespinal laminae" complex (directed axially) and the "ribs + spinodiapophyseal laminae" complex (directed transversely). The neural spines are moderately narrow and laminar. In lateral view, poorly developed ridges, oriented dorsoventrally, mark the interspinal joining between consecutive neural spines. The alar rami of the sacral ribs are directed dorsolaterally, forming an angle of about 60° with the dorsoventral axis of the neural spines. The lateral surfaces of the neural spines are relatively flat, lacking lateral fossae or pneumatic features. The spinodiapophyseal laminae are prominent, and describe a concave curve in cranial/caudal view. The dorsomedial margins of the preserved spinodiapophyseal laminae

expand laterally, suggesting that, when complete, the neural spine was dorsally expanded. The ventral part of sacral neural spine 4 is preserved. It is similar to neural spines 1 to 3 in overall shape and preservation, and differs in showing a more complex pattern of fossae and recesses in the lateral surfaces. Cross section of the neural spine shows a semicamellate internal pneumatisation (Fig. 5I). Both pre- and postspinal laminae are present. The prespinal lamina is thick and gently flares dorsally in cranial view. The cranial surface of the prespinal lamina is scarred by a discontinuous rugose pattern of ossified interspinous ligaments, oriented dorsoventrally. The postspinal lamina is comparable in overall features to the prespinal lamina. The spinodiapophyseal laminae run along mid-length of the lateral surfaces bounding two elliptical fossae (here termed “cranial fossa” and “caudal fossa”). The cranial fossa is excavated on both sides by an accessory fossa, placed at mid-height of the preserved spine (Fig. 5J). This fossa is deeper in its dorsal end, and perforated on both sides by an elliptical foramen with its long axis oriented cranioventrally-caudodorsally. On the left side of the spine, a shallower crescentic fossa is placed caudoventrally to the accessory fossa described above, at the level of the alar ramus of the rib base. No equivalent fossa is present on the right side of the spine (Fig. 5K). The caudal fossae on the lateral surfaces of the neural spine lack accessory pneumatisation. The semicamellate internal pneumatisation of the neural spine includes a cranial camerate sector (formed by a pair of large chambers placed symmetrically) that communicates with the external surface through the elliptical foramina described above, and a caudal camellate sector. Part of the ventral half of the fifth sacral neural spine is preserved. It is similar to the fourth sacral neural spine, in showing prominent pre- and postspinal laminae, and in the presence of the spinodiapophyseal laminae, the latter running dorsoventrally and bordering two elliptical fossae on the lateral surfaces. The pneumatic excavations on the lateral surfaces of the fifth sacral neural spine is less developed than in the previous neural spine, and no accessory fossae or foramina are present (Fig. 5G-H). The most notable feature of the fifth sacral neural spine is the development of a pair of elliptical fossae on both the cranial and caudal surfaces (Fig. 5E-F). These fossae are dorsoventrally oriented, bounded medially by the pre/postspinal laminae and laterally by a couple of ridges that merge ventrally with the pre/postspinal laminae. These ridges are topographically equivalent (and, possibly, serially homologue) to the spinozygapophyseal laminae of the caudal vertebrae (see below).

## Caudal vertebrae

The holotype of *Tataouinea hannibalis* includes the articulated series of the first seventeen caudal vertebrae. Fanti et al. (1) described only the first five proximal caudal vertebrae, the more distally placed vertebrae not yet uncovered at the time of submission of that study. Re-examination of the proximal caudal vertebrae preserved and comparison with photographs of the specimen *in situ* indicate that an additional centrum, although extremely fragmentary and considered part of the sacrum (Fig. 3), is placed between caudal vertebrae 1 and 2 (numeration following (1)). We re-interpret that additional vertebra as the second caudal vertebra; and accordingly, caudal vertebrae 2 to 5 of (1) are reinterpreted here as caudal vertebrae 3 to 6. Caudal vertebrae 1 to 6 suffered important damage after collection (Fig. 7-8), whereas the remaining vertebrae are exquisitely preserved and almost intact (Fig. 9-18). All caudal vertebrae were found lying on the left lateral side, with the right side exposed and usually more weathered than the left one.

### *Caudal 1 (ONM DT 8)*

This vertebra included an almost complete centrum and a partial neural arch, missing most of the right lateral surface. The centrum is taller than long, with a markedly concave lateral surface (on both dorsoventral and proximodistal directions). The proximal intercentral facet was concave, and the distal facet more flattened. The ventral half of the lateral surface had collapsed internally. A large elliptical pneumatic foramen was present in the center of the dorsal half of the lateral surface (Fig. 7B). The neural arch was dorsoventrally elongate. The ribs were almost completely placed on the neural arch but were lost before the discovery of the specimen. Only the proximal part of the centrodiapophyseal laminae was present at the time of discovery. The zygapophyses were poorly preserved. The neural spine was dorsoventrally elongate, slightly dorsodistally inclined. The dorsodistal apex of the neural spine was placed at the level of the distal intercentral surface. The proximal margin of the neural spine was broadly convex and described a gentle curve in lateral view. Both pre- and postspinal laminae were badly preserved. The lateral surface of the neural spine was excavated by a couple of dorsoventrally oriented fossae, separated by a prominent lateral lamina (Fig. 7A).

*Caudal 2 (ONM DT 19-22)*

Only the partially preserved centrum of this vertebra was found. The centrum shows a quadrangular lateral surface pierced by an elliptical pneumatic opening.

*Caudal 3 (ONM DT 9)*

Both the centrum and the neural arch of this vertebra were found. The centrum was taller than long and quadrangular in lateral view. The lateral surface of the centrum was badly preserved and the presence of a pneumatic foramen as in the adjacent vertebrae cannot be confirmed. The neural arch was almost complete. The ribs were placed almost completely on the neural arch, and projected dorsolaterally, exposing the ventral surface in lateral view. The proximal and distal margins of the rib were sub-parallel and inclined mostly laterally and slightly cranially in dorsoventral view. The prezygapophyses and the proximal surface of the neural spine are lost. The right lateral surface of the neural spine is partially preserved and shows a prominent spinoprezygapophyseal lamina directed dorsoventrally and joining the spinodiapophyseal lamina (Fig. 7C-D). This lamina converges dorsally with the spinopostzygapophyseal lamina. The postspinal lamina is well developed and excavated laterally by a dorsoventrally oriented fossa.

*Caudal 4 (ONM DT 10)*

This vertebra was well preserved, missing only the ribs and the dorsal end of the neural spine. The centrum was taller than long in lateral view and taller than wide in proximal/distal view. The intercentral facets were slightly concave. An elliptical foramen pierced the lateral surface of the centrum, at about mid-height. The preserved medial end of the rib was triangular in lateral view, with a broad ventral base. The zygapophyses were badly preserved. The neural spine was dorsoventrally elongate and inclined ventrodistally at about 30° relative to the longitudinal axis of the neural arch. The prezygodiapophyseal lamina was prominent and shelf-like. Both pre- and postspinal laminae were robust and excavated laterally by dorsoventrally oriented fossae. The prominent spinoprezygapophyseal lamina joins ventrally the spinodiapophyseal lamina forming the “lateral lamina” of the neural spine (Fig. 7E). The spinopostzygapophyseal lamina was well developed and projected proximodorsally. Although the spinoprezygapophyseal and spinopostzygapophyseal laminae bounded a lateral triangular fossa, as in caudal 3, the

bad preservation of the dorsal end of the neural spine prevented us for determining whether these laminae merged at their dorsal end.

#### *Caudal 5 (ONM DT 11)*

The centrum is partially preserved (Fig. 8A-D), missing the right dorsal corner of the proximal facet, part of the left ventral corner of the distal surface and the left side of the ventral surface. The centrum is twice taller than long in lateral view, and twice taller than wide in proximal and distal views. The intercentral facets are elliptical, and both distinctly concave, with the proximal facet showing a more marked concavity than the distal. The lateral surfaces are longitudinally concave in dorsal view. The ventral surface shows a prominent ridge running along the ventrolateral margin of the right surface delimiting a central sulcus (the contralateral ridge on the left side is lost). On the left surface of the centrum, an elliptical pneumatic foramen opens just below the mid-height of the centrum. The pleurocoel is longer than tall. No foramen is present in the right surface of the centrum, an asymmetrical pattern of pneumatisation also present in the sacral vertebrae (see above) and in the ischia (see below). No ribs are present on the centrum, the former being entirely placed on the neural arch. Most of the neural arch is preserved: the left side of the pedicels, the left rib and the ventral part of the right rib are lost (Fig. 8A-E). The neural arch pedicels are longer than tall, and the neural canal is suboval in proximal view. The prezygapophyses are prominent and projected well proximal to the intercentral facet level. The postzygapophyses are slightly elevated relative to the prezygapophyses, and supported ventrally by a prominent hyposphenal process. The dorsal surface of the left postzygapophysis shows a “hinge-like” morphology, not present on the right postzygapophysis, and thus interpreted as probably pathological (Fig. 8C, E). Two crests, oriented transversely and subparallel to the dorsodistal corner of the postzygapophysis, and two concavities, one between the two crests and the other between the distal crest and the dorsodistal corner of the postzygapophysis, form this feature. The neural spine is dorsoventrally elongate in lateral view, with straight proximal and distal margins inclined 30° dorsodistally relative to the vertical axis of the centrum, and a complex cross section geometry (Fig. 8F). In proximal view, the neural spine is petal-shaped, with a distinctly lobate dorsal outline. A small lateral projection on the dorsal third of the neural spine is interpreted as homologue to the triangular process present in caudal vertebrae of other

rebbachisaurines (e.g., 42). The left rib is partially preserved, missing the ventral part. The dorsal component of the rib is wing-shaped in dorsal view and inclined laterodorsally at about 45° in proximal/distal view. The spinoprezygodiapophyseal fossae are deep and pierced in their middle by an elliptical foramen (Fig. 8E). The prezygodiapophyseal, centroprezygapophyseal and centrodiapophyseal laminae are prominent and bound a triangular fossa (Fig. 8E). The prespinal lamina is thick and hollowed laterally by drop-shaped depressions oriented dorsoventrally. These depressions are bounded laterally by the spinoprezygapophyseal laminae, the latter contacting the lateroventral end of the prespinal lamina. The floor of the spinoprezygapophyseal fossa is pierced by an elliptical foramen just proximally to the basal end of the prespinal lamina. The spinoprezygapophyseal laminae run laterodorsally and form the prominent lateral laminae of the neural spine. The postspinal lamina is thick and prominent as the prespinal lamina. The spinopostzygapophyseal laminae join the ventrolateral corner of the prespinal lamina and bound a deep interpostzygapophyseal fossa. The postzygodiapophyseal and the distal centrodiapophyseal laminae form the ventrodiscal margin of the neural arch. These laminae and the hyposphenal ridge define a shallow elliptical fossa placed proximovertrally relative to the postzygapophyseal facet.

#### *Caudal 6 (ONM DT 37)*

In this vertebra, both neural arch and centrum are well preserved and tightly sutured together (Fig. 9). The proximal surface and part of the ventral surface of the centrum are mostly eroded away. The centrum is about 130% taller than long, and about 120% taller than wide. The distal intercentral facet is markedly concave, although this seems as partially a preservational artefact. The ventral half of the centrum is mediolaterally narrower than the dorsal, resulting in a trapezoid centrum with ventromedially directed lateral margins in distal view. The neural arch includes relatively low pedicels and a dorsally directed neural spine that is less elongated dorsally than the more proximal vertebrae. The base of the ribs is placed entirely on the neural arch, and extends proximodistally along most of the latter. The rest of the ribs is lost. The neural canal is round and its diameter is less than one fourth of the neural arch width. The prezygapophyses are lost. The postzygapophyses are elevated at about half the combined height of the neural arch and spine. The prespinal lamina is well developed, transversely

robust, and includes the spinoprezygapophyseal laminae in its lateral component. The centrodiapophyseal laminae are poorly preserved. A robust hyposphenal ridge is directed dorsodistally and bifurcates to reach the postzygapophyses. The spinopostzygapophyseal laminae are directed dorsally, and bound a deep postspinal fossa floored by the hyposphenal process. A pair of hyposphenal postzygodiapophyseal fossae are present ventrolaterally to the postzygapophyses. The narrow prezygodiapophyseal lamina is horizontally directed. The postzygodiapophyseal lamina is more robust, and does not extend above the level of the postzygapophysis, neither forms a lateral lamina along the neural spine.

#### *Caudal 7 (ONM DT 38)*

This vertebra is well preserved, lacking only the dorsal half of the neural spine and the lateral end of both ribs (Fig. 10). The anterior half of the vertebra has suffered a more intense transversal compression than the posterior part, producing a partial dislocation of the neural arch, that is shifted onto the proximolateral corner of the right side of the centrum. The centrum is slightly taller than long in lateral view, taller than wide proximal view (in part due to transversal compression) and approximately as tall and wide in distal view. The proximal intercentral facet is flat, whereas the distal facet is distinctly concave. The right lateral surface of the centrum is depressed by a large irregular fossa, the depth of which is probably exaggerated by the vertebra deformation. No lateral fossa is present in the left side of the centrum. The ventral surface of the centrum is transversely narrow, subrectangular in ventral view, with parallel lateral sides that are projected ventrally delimiting a midline sulcus. The neurocentral suture is obliterated. The neural arch extends above the proximal two thirds of the centrum. The bases of the ribs are placed at the level of the neurocentral suture, and are inclined laterodorsally. Prominent distal centrodiapophyseal laminae bound the depressed dorsodistal surface of the centrum, although this may be a taphonomic artefact. The prezygapophyses are projected proximodorsally well beyond the level of the proximal intercentral surface. The prezygapophyses are widely separated and are not joined by a ventral interprezygapophyseal lamina. The postzygapophyses are placed more dorsally than the prezygapophyses. A prominent hyposphenal ridge joins the ventral base of the postzygapophyses and the dorsodistal margin of the neural canal. The preserved base of

the neural spine is placed in the distal end of the neural arch. The neural spine is moderately thick. Both spinoprezygapophyseal and spinopostzygapophyseal laminae are present and well developed. The spinoprezygapophyseal laminae form the sharp lateral margins of the prespinal lamina. The spinopostzygapophyseal laminae bound laterally a deep postspinal fossa, the latter bounded ventrally by the hyposphenal ridge. The prezygodiapophyseal lamina is sharp. The prezygospinodiapophyseal fossae are deep. In the right prezygospinodiapophyseal fossa, an accessory ridge links the middle of the medial margin of the spinodiapophyseal lamina with the floor of the fossa. The prominent postzygodiapophyseal laminae are posteriorly concave and bound the shallow hyposphenal postzygodiapophyseal fossae.

#### *Caudal 8 (ONM DT 39)*

This vertebra and caudal 9 are almost completely preserved, lacking the dorsal end of the neural spines (Fig. 11). The two vertebrae were found tightly connected at the zygapophyses and were not separated after the discovery. In ONM DT 39, only the lateral end of the ribs is missing. The centrum is about as long as tall in lateral view and  $4/3$  taller than wide in proximal view. Both intercentral facets are elliptical in outline and concave, with raised lips along the margins. The ventral surface is hourglass shaped and bears a deep longitudinal pneumatic excavation. The lateral surfaces of the centrum lack pneumatic fossae. The neural arch extends above the proximal three quarters of the centrum. The ribs are entirely on the neural arch. Prominent proximal and distal centrodiapophyseal laminae are present and dorsally bound a distinct fossa. The neural spine is more than twice taller than long, placed above the distal end of the neural arch. The neural spine is quadrangular in lateral view and inclined dorsodistally. The prezygapophyses are widely spaced and project proximally beyond the intercentral facet. The prezygodiapophyseal and centroprezygapophyseal laminae are prominent and bound a shallow triangular fossa. The spinoprezygapophyseal laminae are sharp and run along the proximolateral margins of the neural spine. The prezygospinodiapophyseal fossa is deeply marked proximally, whereas its distal margin is indistinct from the lateral surface of the neural spine. The postzygapophyses are dorsally placed relative to the prezygapophyses, but most of their details are not visible as they are covered by the prezygapophyses of caudal vertebra 9. The postzygodiapophyseal lamina is low and robust. The ventral end of

the spinopostzygapophyseal laminae bound a deep postspinal fossa restricted to just above the postzygapophyses. At mid-height on both lateral surfaces of the neural spine, a pair of short lateral laminae is present. These laminae may be interpreted as serially homologue to the more prominent lateral lamina present in the proximal caudal vertebrae.

*Caudal 9 (ONM DT 40)*

This vertebra is almost completely preserved, lacking only the dorsal end of the neural spine, and is very similar in overall shape and proportions to caudal 8 (Fig. 11). The main differences from the preceding vertebra are the presence of a depressed area on the ventral half of the left lateral surface of the centrum, the less prominent spinozygapophyseal and centrodiapophyseal laminae, and the poor development of the pair of accessory laminae on the lateral surface of the neural spine.

*Caudal 10 (ONM DT 41)*

This vertebra is almost completely preserved, lacking the dorsal end of the neural spine (Fig. 12). The centrum is longer than tall in lateral view and about as wide as tall in proximal view. Both intercentral facets are distinctly concave, with thickened rims. The ventral surface of the centrum is hourglass shaped and excavated by a deep fossa housing a pair of pneumatic openings. The lateral surfaces of the centrum are moderately compressed transversely. The neural arch extend along three fourths of the dorsal surface of the centrum. The neural arch pedicels are proportionally narrower transversely and taller than in the more proximal vertebrae. The neural canal is elliptical, taller than wide. The ribs are reduced to slightly raised tuberosities. The centrodiapophyseal lamination is, accordingly to rib reduction, very poorly developed. The prezygapophyses are short and inclined dorsally, not projected proximally beyond the centrum intercentral facet, and define a "V"-shaped cleft in proximal view. The spinoprezygapophyseal laminae are moderately developed and bound dorsally a shallow prezygospinodiapophyseal fossa, more prominent on the left side. The postzygapophyses are closely placed medially, being less prominent than in more proximal vertebrae, and are supported ventrally by a small hyposphenal ridge. The neural spine is transversely narrower than in more proximal vertebrae, and is slightly inclined dorsodistally. The lateral surfaces of the neural spine

shows a slightly developed lateral lamination oriented dorsoventrally. The anterior end of the left prezygapophysis of caudal 12 is tightly attached to the left postzygapophysis.

*Caudal 11 (ONM DT 42)*

This vertebra is almost completely preserved (Fig. 13), a fragment of the left prezygapophysis is attached to caudal 10 (Fig. 12A, C). The centrum is longer than tall and taller than wide in proximal view. The intercentral facets are elliptical and distinctly concave (the distal concavity is more pronounced than the proximal). The ventral surface is hourglass shaped with a shallow ventral sulcus in the middle. Both lateral surfaces of the centrum are transversely concave and slightly overlapped laterodorsally by the neural arch. The right side of the lateral surface of the centrum has collapsed internally, suggesting a hollow interior of the centrum. The neural arch appears as transversely compressed and long about half of the dorsal surface of the centrum, and displaced slightly proximally relative to the centrum mid-length. The neural arch pedicels are transversely compressed and the neural canal is taller than wide. The prezygapophyses slightly overhang the proximal intercentral surface. The ribs are extremely reduced as small rugosities oriented proximodistally below the level of the prezygapophyses. Most of the neural arch lamination observed in more proximal vertebrae is absent. The subrectangular neural spine is lower than in more proximal vertebrae, placed at the dorsodistal end of the neural arch and poorly inclined distally. The spinoprezygapophyseal laminae are sharply elevated dorsally and bound a deep and narrow sulcus between the neural spine and the prezygapophyseal bases. The postzygapophyses are closely appressed, and projected laterodistally at mid-height of the distal margin of the neural spine. The hyposphenal ridge is less prominent than in more proximal caudal vertebrae.

*Caudal 12 (ONM DT 43)*

The elongate centrum (about 125% longer than tall) of this completely preserved vertebra is taller than wide in proximal view (Fig. 14). The intercentral facets are elliptical and moderately concave. The centrum is markedly compressed transversely with both lateral surfaces collapsed internally just ventral to the neurocentral contact. It is unclear whether the collapsed areas represents pneumatic features, although comparison with the following three vertebrae (see below) suggests that the collapsed areas housed pneumatic

depressions in origins. The ventral surface of the centrum is hourglass-shaped, and bears a shallow mid-line sulcus bearing a distal elliptical fossa. The neural arch pedicels are relatively low and the neural canal elliptical, taller than wide. The ribs are extremely reduced as very low rugosities. No diapophyseal lamination is present. The prezygapophyses are proximally directed and do not project beyond the intercentral surface. The sharp spinoprezygapophyseal laminae bound a distinct fossa on the dorsal surface of the neural arch. The postzygapophyses are placed at about the same dorsoventral level as the prezygapophyses. The hyposphenal ridge is narrow and bounds ventrally a triangular interpostzygapophyseal fossa. The neural spine is quadrangular, taller than ventrally long and slightly inclined dorsodistally.

*Caudal 13 (ONM DT 44)*

This almost completely preserved vertebra is tightly attached to caudal 14 at the level of the postzygapophyses (Fig. 15). The centrum is transversely compressed with the right surface collapsed internally. The centrum is 133% longer than proximally tall, and about as tall as wide in proximal view. The proximal intercentral facet is trapezoidal, wider ventrally. The distal intercentral facet is mostly covered by caudal 14. Both intercentral facets are moderately concave. The ventral surface of the centrum is hourglass-shaped, bearing two proximodistally aligned drop-shaped depressions. The left lateral surface bears an elliptical depression placed in the distal half of the surface. The corresponding area in the right lateral surface lacks a depression. Nevertheless, the collapsed proximal half of the right lateral surface may indicate the presence, in life, of a lateral depression. The low neural arch bears proximally directed prezygapophyses not surpassing the level of the intercentral facet, and postzygapophyses placed at the same level of the prezygapophyses. A deep and narrow spinoprezygapophyseal fossa is bounded by sharp spinoprezygapophyseal laminae. The postzygapophyses are joined medioventrally by a small hyposphene-like projection. The ribs are absent. The neural spine is slightly taller than long and moderately inclined dorsodistally. Neural arch lamination is limited to both spinopre- and spinopostzygapophyseal laminae. Prespinal and postspinal laminae are restricted to the apical half of the spine and scarred by a rugose pattern.

*Caudal 14 (ONM DT 45)*

This vertebra is very similar in overall shape and preservation to caudal 13, differing in the slightly shorter centrum, the better preservation of the centrum lateral surfaces, and the lower neural spine that is longer than tall (Fig. 15). The most interesting feature of vertebra 14 is the presence of distinct fossae in the lateral surfaces of the centrum. The right surface of the centrum bears a narrower and slit-like depression, whereas the fossa on the lateral surface is clearly elliptical, proximodistally elongate, with distinct margins, similar to the pneumatic foramina present in the proximalmost caudal vertebrae. The distal fragment of the right postzygapophysis is attached to the corresponding prezygapophysis of caudal 15.

*Caudal 15 and 16 (ONM DT 46 and 47)*

These completely preserved vertebrae show elongate centra (with the length to proximal height ratio of about 135-140%) with elliptical intercentral facets that are as wide as tall (Fig. 16-17). In overall shape and proportions, these vertebrae are very similar to caudal 14. The ventral surfaces of the centra are hourglass-shaped and house shallow depressions. In both vertebrae, the left lateral surface of the centrum is excavated by a shallow depression, whereas the right lateral surface is collapsed internally and partially crushed. Cracks on the proximal intercentral facet of caudal 16 shows that the internal pneumatisation pattern is camerate. The prominent prezygapophyses are projected proximally beyond the level of the intercentral facet, and are linked to the neural spine by sharp laminae bounding a distinct interprezygapophyseal fossa. The postzygapophyses are reduced and joined ventromedially by hyposphene-like laminae. The neural spines are lower than in more proximal vertebrae and inclined dorsodistally.

*Caudal 17 (ONM DT 48)*

This is the posteriormost preserved caudal vertebra (Fig. 18). The vertebra is almost complete, lacking the right postzygapophysis and the tip of the neural spine. The centrum is elongate (about 150% longer than proximally tall), with roughly rounded intercentral facets that are as wide as tall. The right lateral surface of the centrum is collapsed at the neurocentral junction. The ventral surface of the centrum is transversely constricted but lacks the distinct fossae present in the more proximal vertebrae. The left lateral surface is undeformed and lacks any excavation or depression. Both zygapophyses

and spinoprezygapophyseal laminae are less prominent than in more proximal vertebrae. The hyposphene is poorly preserved, and appears as a shallow lamina below the postzygapophyses.

## **Ilium**

Both iliac blades are partially preserved (ONM DT 3, 4; Fig. 19A-C). The dorsal margin of the bones, the postacetabular processes and most of the ischial peduncles are lost. The preacetabular processes are craniocaudally elongate, and flared laterally. In lateroventral view, the cranioventral corner of the preacetabular blade is gently acuminate, with a rounded craniodorsal margin and a slightly concave ventrolateral margin. The cranioventral corner of the lateral surface is rugose and scarred by an irregular series of low bumps. Most of the lateral surface of the blade is uniformly flat, showing a moderate longitudinal convexity toward the ventral margin, where the lateral surface shifts into the ventral surface. The preacetabular blade is internally hollow. A channel is exposed in the broken region craniodorsal to the pubic peduncle. It leads to an internal chamber on the iliac blade. The large size of the exposed channel and the extensive cavitation of the preacetabular blade suggest a pneumatic origin of the feature. It is unclear whether this channel opened externally through a foramen at the level of the damaged area. The pubic peduncle is massive, projected laterally relative to the ventrolateral surface of the preacetabular process, and describing with the latter a wide concavity. In ventral view, the pubic peduncle is "D"-shaped, with the straight caudal margin oriented mediolaterally and the cranial margin broadly rounded. The ventral end of the pubic peduncle is badly eroded, showing the internal pneumatisation composed of large chambers separated by dorsoventrally narrow septa oriented horizontally.

## **Ischium**

The proximal half of both ischia (ONM DT 1, 2) were found articulated with the iliac blades. The shaft distal to the pubic peduncle is lost in both ischia (Fig. 19D-I, 20). The two bones differ in the preservation of their extremities and in the degree of mediolateral deformation. In the left ischium, the iliac peduncle is almost complete, whereas in the right ischium the same peduncle lacks the cranial part of the proximal surface. In the right ischium, parts of both iliac and pubic peduncles are crushed and have been collapsed

internally. The pubic peduncle in the right ischium is more complete distally than in the left ischium. Nevertheless, combining the information from the two bones, most of the morphology of the ischium, with the exclusion of the distal shaft, is available. The ischia are roughly quadrangular in mediolateral view, with a broadly concave acetabular margin, a dorsoventrally deep pubic facet, a gently concave caudodorsal margin. The acetabular margin is hourglass shaped in proximal view, expanded transversely toward both iliac and pubic peduncles and constricted at mid-length. The ischial body (the preserved part of the bone excluding the iliac peduncle and the pubic facet) is flattened and laminar distal to the acetabular margin. The lateral surface of the ischial body is flat to very gently convex toward the pubic facet. A distinct tuberosity is present on the dorsal margin of the lateral surface just distal to the iliac peduncle base. The medial surface of the ischial body is excavated by a depressed area between the iliac peduncle and the pubic facet. This depression is bounded craniodorsally by the thickened acetabular margin. In cranial view, the pubic facet is triangular, wider dorsally (the acetabular margin) and laminar ventrally. The iliac peduncle is proximodistally elongate and slender in mediolateral view, with the proximodistal axis inclined slightly cranially relative to a line tangential to both acetabular and caudodorsal margins. The iliac peduncle is slightly constricted at mid-height and expanded both craniocaudally and transversely approaching the ilium. The caudal margin of the iliac facet bears a distinct lip that overhangs the shaft of the peduncle. In proximal view, the iliac facet is elliptical, about 170% wider than long. In cranio/caudal view, the medial margin of the iliac peduncle is straight, whereas the lateral margin is gently concave and directed proximomedially. The most interesting feature of the ischia is the pneumatization (1). Both ischial bodies are hollowed internally by a chamber with smooth inner surfaces, each reaching the preserved distal end, although the two bones differ in the degree of preservation of these features. The lateral surface of the left ischium bears a large pneumatic foramen at the level of the distal half of the iliac peduncle. The medial surface of the bone is perforated by a smaller aperture, although it is unclear whether it represents a natural pneumatic foramen or the result of post-mortem collapse of the medial surface of the internal chamber. The lateral foramen in the left ischium is clearly a pneumatic feature, as it shows a defined margin with a regular elliptical outline (damaged on its anteroventral corner) comparable, in shape and proportion, to the pneumatic foramina present in the vertebrae, and leads to the internal chamber of the bone. Although

the medial surface is internally collapsed in the right ischium, the lateral surface of the latter lacks a perforation, indicating that the extent of ischial pneumatization was asymmetrically developed.

### **Phylogenetic and palaeogeographic analyses**

We tested the phylogenetic affinities of *Tataouinea* entering an Operational Taxonomic Unit (OTU) based on the Tunisian taxon in an updated version of the data set of (44) focusing on sauropods. As the diplodocoid affinities of *Tataouinea* are well supported and based on several synapomorphies from both caudal vertebrae and pelvis (1), we removed *a priori* most of the non-diplodocoid OTUs from the original data set, and retained a subset of taxa sampling the morphological diversity among eusauropods. We added five additional characters (listed in the Supplementary Material), to the data set of Carballido et al. (44), and derived from Mannion et al. (41), Ibiricu et al. (43) and Allain and Wilson (40). The characters were set with equal weight and all multistate characters as unordered (non-additive). *Rebbachisaurus* was re-scored based on the recent revision of the taxon by Allain and Wilson (40). We also added the recently named Patagonian rebbachisaurid *Katepensaurus* (43), not included before in a quantitative phylogenetic analysis. Trees were rooted on the basal eusauropod *Shunosaurus*. This dataset (29 OTUs vs 346 characters) was analysed under both parsimony and Bayesian inference, the latter integrating simultaneously morphological and stratigraphic data following the method discussed by Lee et al. (45, 46). Among the 346 included characters, 90 characters are constant, and 55 characters are autapomorphies of the included taxa, as Bayesian analysis requires the sampling of not solely synapomorphies, but also autapomorphies of terminal branches and constant characters (46). Parsimony analyses were performed using the Hennig Society version of TNT (47). The analyses followed two steps: 1) 100 driven searches using the “New Technology analyse” set in TNT with default parameters, followed by 2) a “Traditional Search” analysis exploring the tree islands found by the first run. Nodal support (Decay Index) was calculated performing 1000 “Traditional Search” analyses and saving all trees up to ten steps longer than the shortest topologies. Bayesian analyses were performed using BEAST vers. 1.7 (48) implementing Markov-Chain Monte Carlo Bayesian methods for estimating phylogeny, and using the Lewis’s (49) Markov model for discrete character evolution, as it accommodates variability in rates of evolution

among characters (using the gamma distribution) and across lineages (using relaxed clocks). All characters were treated as a single partition. Stratigraphic data (as mean age value of the known geochronologic range of each OTU, see Supplementary Material) were obtained from the primary literature. Where published ages were given in stratigraphic units (e.g. stage or epoch), the dates for the relevant unit were taken from the ICS/IUGS International Stratigraphic Chart (50). Analyses were conducted using only a single age constraint for the tree, that consisted of the maximum age of the root (Eusauropoda) set at 201 Ma (the Triassic-Jurassic boundary), as this value substantially pre-dates the earliest robust record of eusauropods (51). Accordingly, root ages of the trees were sampled along a uniform range between 168.8 Ma (the age of the oldest known included OTU, i.e., *Omeisaurus*) and 201 Ma. The monophyly of the ingroup (i.e., the clade including all OTUs with the exclusion of *Shunosaurus*) was enforced, but no internal ingroup topologies were constrained. The BEAST analysis involved 4 replicate runs (with different random starting trees and random number seeds). Each of the replicate runs involved 10 million steps with sampling every 1000 generations, with a burning of 2 million steps. Convergence (stationarity) in numerical parameters was identified using Tracer (52). The Maximum Clade Credibility Tree (MCCT) resulted from the Bayesian analysis was used as a temporally calibrated phyletic framework for palaeobiogeographic reconstruction, inferring ancestral geographic placement of nodes using RASP (Reconstruct Ancestral State in Phylogenies, 53). The distribution range of selected sauropod taxa was *a priori* divided into five areas: Asia (A), Europe (B), North America (C), Africa (D), and South America (E). Each terminal taxon was scored for the geographic area character state according to the continent(s) it was recovered in (e.g., *Apatosaurus* was scored as “C”, whereas *Tataouinea* was scored as “D”). Biogeographic inferences on the phylogenetic frameworks were obtained by applying statistical dispersal-vicariance analysis (S-DIVA) and Bayesian Binary Markov Chain Monte Carlo (BBM) analysis (53). S-DIVA and BBM methods suggest possible ancestral ranges at each node and also calculate probabilities of each ancestral range at nodes. The analyses performed ten Markov Chain Monte Carlo chains of 50000 cycles each, sampling every 100 trees. Chain temperature was set at 0.1. State frequencies were set as estimated and among-site rate variation was set using the gamma parameter. The first 20% of the recovered trees were discarded and the remaining trees were used to infer ancestral range distribution at nodes. In the S-DIVA analyses, direct

range dispersal constraints were enforced, excluding those routes considered as not plausible based on Jurassic and Cretaceous palaeogeographic reconstructions (55-62 and references therein; Table S1). In both analyses, time-events algorithm (53) was used to infer the total number of dispersal and vicariance events in rebbachisaurid evolution.

## Results

### Parsimony analyses

The analysis recovered 18 shortest trees of 501 steps each (Consistency Index excluding uninformative characters = 0.5108; Retention index = 0.6941). The strict consensus of the shortest trees (Fig. 21A) supports the monophyly of Rebbachisauridae, and its placement as sister group of Flagellicaudata (the diplodocid-dicraeosaurid clade), as in all previous analyses of the group. The Brazilian rebbachisaurid *Amazonsaurus* was recovered as the basalmost member of the clade. The relationships among the other rebbachisaurids were poorly resolved: *Comahuesaurus*, *Histriasaurus* and *Zapalasaurus* were recovered in an unresolved polytomy with *Khebbashia*. Exploration of the alternative shortest topologies indicates that *Histriasaurus*, *Cathartesaura* and *Rebbachisaurus* acted as “wildcard” OTUs, with several alternative placements among a backbone topology formed by the other taxa. When the “wildcard” OTUs are pruned *a posteriori* from the topologies, the other rebbachisaurids form a pectinate series of progressively closer sister taxa to *Tataouinea*: *Amazonasaurus*, *Zapalasaurus*, *Comahuesaurus*, *Katepensaurus*, *Nigersaurus* and *Demandasaurus*. Among the “wildcard” OTUs, it is noteworthy that all alternative placements of *Rebbachisaurus* place it as closer to *Nigersaurus* than *Limaysaurus*, a result supporting the synonymy between Nigersaurinae and Rebbachisaurinae (see Systematic Palaeontology section above).

Nodal support among Rebbachisauridae was relatively low, due to the inclusion of fragmentary OTUs (Decay Index =2). When the wildcard OTUs were pruned *a posteriori* from calculation, the nodal support of Rebbachisauridae resulted stronger (Decay Index =6).

We tested whether the low resolution among rebbachisaurids was biased by conflict among differently homoplastic characters, performing implied weighting analyses (63, 64). The analyses using TNT followed the same protocol of the first analysis, with the *k* parameter (which determines how strongly homoplasious characters are downweighted;

see 63) set alternatively as =3 (default value in TNT) (47),  $k=1$  (homoplasious characters more strongly downweighted) and  $k=9$  (homoplasious characters less strongly downweighted). The first analysis ( $k=3$ ) found three shortest topologies, the strict consensus of which resolving the relationships among Khebbashia (Fig. 21B). The Limaysaurinae clade, including *Limaysaurus* and *Cathartesaura*, resulted sister taxon of Rebbachisaurinae (Nigersaurinae of (31)), the latter including *Katepensaurus* as basalmost rebbachisaurine, and *Nigersaurus* as sister taxon of a tricotomy including *Demandasaurus*, *Rebbachisaurus* and *Tataouinea*. Setting  $k=1$  and  $k=9$  produced identical results to the analysis with  $k=3$ , indicating that the above discussed relationships are not biased by *a priori* assumptions on character weighting.

### Bayesian analyses

The MCCT found shows a topology overall comparable to the results of parsimony analyses (topology shown in Fig. 22-23). Among non-rebbachisaurid OTUs, the most relevant difference from the parsimony-based analysis was the placement of turiasaurians and *Haplocanthosaurus* among macronarian neosauropods instead of, respectively, as a basal eusauropod branch and the basalmost diplodocimorphs. Nevertheless, the basal macronarian nodes including the above-mentioned taxa showed low posterior probability values, and should be considered as tentative. Since an evaluation of non-diplodocoid relationships was beyond the aims of our analysis, and given the small sample among non-diplodocoids, these conflicting interpretations between parsimony and Bayesian analyses are not further discussed here (see (65) for a discussion of turiasaurian placement among Eusauropoda). The monophyly of both rebbachisaurid-flagellicaudatan node and Rebbachisauridae was well supported by the model (posterior probability values, *pp*, of, respectively, 0.84 and 0.96). Although most of the recovered rebbachisaurid nodes show relatively low *pp*, the topology agrees with the results of the parsimony analysis in placing *Histriasaurus* and *Zapalasaurus* as basal rebbachisaurids not members of Khebbashia, in placing *Cathartesaura* as sister taxon of *Limaysaurus*, in recovering Rebbachisaurinae with the same inclusiveness found in the implied weighting parsimony analyses (above), with *Katepensaurus* as basalmost rebbachisaurine, and *Nigersaurus* as sister taxon of the clade including *Demandasaurus*, *Rebbachisaurus* and *Tataouinea*. The Bayesian and parsimony analyses differ in the placements of *Amazonsaurus* and

*Comahuesaurus* as basal members of Limaysaurinae in the Bayesian topology. It is noteworthy that the results of a parsimony analysis enforcing *Amazonsaurus* and *Comahuesaurus* as basal limaysaurines (as resulted in the Bayesian analysis) produced shortest topologies only four steps longer than the unforced topologies, a step difference not statistically significant ( $p=0.12$ ,  $n=8$ ) (66), suggesting that these taxa act as “wildcard” OTUs with placement biased by the analytical method followed.

Bayesian analysis simultaneously estimated topology and timing of cladogenetic events. The resulted tree (Fig. 22-23) placed the macronarian-diplodocimorph divergence at about 170 Ma, the origin of the rebbachisaurid lineage at about 163 Ma, and the Rebbachisaurinae-Limaysaurinae divergence at about 134 Ma (Hauterivian). Among Rebbachisaurinae, the analysis placed the origin of the lineage leading to African and European taxa at about 130 Ma, the divergence of the lineage leading to *Demandasaurus* at about 127 Ma, and the divergence of the lineages leading to *Rebbachisaurus* and *Tataouinea* at about 116.5 Ma (Aptian).

### Palaeobiogeographic analyses

The BBM analysis (Fig. 22) supports South America as the most plausible ancestral area of both rebbachisaurid origin and early diversification of Khebbashia (support value =0.94). The lineage leading to the Croatian basal rebbachisaurid *Histriasaurus* is therefore interpreted as Gondwanan in origin, with the latter genus resulting from a dispersal event occurred between 134 and 131 Ma. Accordingly, a “Gondwanan – European” range for the last common ancestor of *Histriasaurus* and *Zapalasauros* is poorly supported (support value =0.07). Furthermore, South America is also interpreted as the exclusive range of limaysaurine evolution and the area of rebbachisaurine origin and earliest diversification (support values, respectively =0.99 and =0.91). The most plausible range of the rebbachisaurine subclade including all taxa more derived than *Katepensaurus* is interpreted as African (support value =0.86), with a single dispersal event to Europe between 130 and 127 Ma clarifying the distribution of *Demandasaurus* (support value =0.85). Time-events algorithm for rebbachisaurid evolution inferred a single peak for both dispersal and vicariance events, placed at about 127 Ma (Barremian).

Results of the S-DIVA test (Fig. 23) mostly agree with the BBM analysis, with all area reconstructions having support value =1. South America is once again interpreted as

the ancestral area of both rebbachisaurid origin and for khebbashian early diversification. The range of Limaysaurine evolution is restricted to South America, whereas the ancestral area of early rebbachisaurine evolution includes both South America and Africa. Most of subsequent rebbachisaurine evolution is placed in Africa, with an “Euro-African” range for the last common ancestor of *Demandasaurus*, *Rebbachisaurus* and *Tataouinea*. Accordingly, the evolution of the most derived rebbachisaurines is interpreted by vicariance between an European lineage (leading to *Demandasaurus*) and an African lineage (including *Rebbachisaurus* and *Tataouinea*). Time-events algorithm for rebbachisaurid evolution inferred two peaks for both dispersal and vicariance events, placed, respectively, at about 140 (Barresian-Valanginian) and 127 Ma (Barremian).

## Discussion

### The evolution of pelvic and caudal pneumatisation in Rebbachisauridae

Newly acquired skeletal elements of the type specimen of *Tataouinea hannibalis* shows that some pneumatic features previously considered exclusive of diplodocids among diplodocoids (e.g., deep fossae in the ventral surface of anterior and middle caudal centra, lateral elliptical fossae in middle caudal centra; e.g., *Diplodocus* MGGC 8723) were present also in some rebbachisaurids. *Tataouinea* includes camerate, semicamellate and camellate pneumatisations in distinct parts of the axial skeleton (e.g., camerate sacral and caudal centra, semicamellate and camellate sacral and caudal neural arches). The variation in pneumatisation pattern is not limited to non-homologue elements (e.g., centrum vs neural arch), but is variable also within single bone elements (e.g., the posterior sacral neural arches 4 and 5 show both camerate and camellate patterns). In the sacral neural arches, the pattern of external pneumatisation follows a cranio-caudal direction, with cranialmost three vertebrae showing a less complex pattern than the posterior two. The extent of pneumatic features in *Tataouinea* holotype is asymmetrical, with the left side of the vertebrae and the left ischium usually bearing a more extensive and elaborate pattern of fossae and foramina than their right counterpart. Asymmetry in the expression of postcranial skeletal pneumatisation has been reported in other sauropods (30, 67). The presence of pleurocoels in caudal centra 1 to 6 and of distinct lateral pneumatic excavations in caudal centra 14 to 16, both features absent in caudal vertebrae 7 to 13, represents a pneumatic hiatus as those reported in the tails of

diplodocids and brachiosaurids among neosauropods (67), in some basal sauropodomorphs (68), and in the sacrum of at least one non-avian theropod (*Tyrannotitan*, 69).

Shallow lateral fossae are present in the proximal caudal centra of *Comahuesaurus* (44), a feature that may be homologue to (and may represent an incipient stage of) the deep pneumatic foramina penetrating the centra of *Tataouinea*. Mannion and Barrett (70) report an isolated caudal vertebra of a rebbachisaurid from the Cenomanian of Morocco, sharing with *Tataouinea* the presence of pleurocoel on centrum. Although no direct evidence supports (neither dismisses) the referral of that vertebra to the sympatric *Rebbachisaurus* (40), the sister-taxon relationship between *Tataouinea* and *Rebbachisaurus* in the Bayesian analysis may support the presence of caudal pleurocoels in *Rebbachisaurus*. Pneumatic foramina are also present in isolated rebbachisaurid caudal vertebrae from the Upper Cretaceous of Argentina that may be referred to *Katapultisaurus* (71, see below), a taxon placed among the basal rebbachisaurines in our phylogenetic analyses.

Fanti et al. (1) proposed a “neural arch first” pattern (*sensu* 72) for the evolution of tail pneumatisation in rebbachisaurids, based on character optimization of osteological correlates of pneumatisation among Rebbachisauridae, and considered this pattern as a saurischian synapomorphy. Wedel and Taylor (67) dismissed this pattern for the caudal vertebrae of both diplodocids and brachiosaurids, based on the distribution of pneumatic fossae along well preserved caudal series. The complete middle caudal series of *Tataouinea* shows pneumatic fossae on centra and a reduced, albeit still present, pneumatisation on neural arches. Caudal vertebra 16 is the distalmost showing osteological correlates of pneumaticity, present in both centrum (paired fossae on the ventral surface) and neural arch (spinoprezygapophyseal fossa): it is interesting that lateral pneumatisation on both centrum and neural arch is less developed than in the ventral and dorsal surfaces of the vertebra. Although character optimization among Rebbachisauridae suggests a “neural arch first” pattern for the evolution of tail pneumatisation in that clade (1), the distribution of these features in the tail of *Tataouinea* alone does not support a “neural arch” first neither a “centrum first” pattern of pneumatisation.

Iliac internal chambers are reported in *Amazonsaurus* (73) and *Tataouinea*, and may represent a synapomorphy of Rebbachisauridae. An internal pneumatisation of the

ischium is present in both *Rebbachisaurus* (40) and *Tataouinea*, but only the latter shows a pneumatic foramen perforating the lateral surface of the iliac peduncle, a feature absent in both *Demandasaurus* and *Rebbachisaurus* (40, 74) and thus autapomorphic for the Tunisian taxon (1).

The estimated body length of *Tataouinea hannibalis* type specimen is around 12 meters (see Supplementary Figure 1), comparable to other rebbachisaurids and small-bodied macronarians (40). Although osteological correlates of postcranial pneumatisation may be overlooked, in particular in the tail vertebrae (as evidenced by the recent re-analysis of already known diplodocid and brachiosaurid specimens, 67), pneumatisation seems more extensive among mid- to small-bodied sauropods than in giant forms, challenging the suggested importance of pneumaticity for lightening the skeletons of sauropods (1, 29).

### **Tempo and mode of rebbachisaurid evolution**

Data presented in this study support a Middle-Late Jurassic origin of the rebbachisaurid lineage as well as the presence of this clade in South America from no later than the Berriasian-Valanginian to the Turonian (e.g., 43). Rebbachisaurid teeth from Barremian beds of the La Amarga Formation (75) predating the oldest bone evidence of this clade in South America, also support this scenario. By the Jurassic-Cretaceous boundary, all Laurasian diplodocoids (Flagellicaudata) went extinct (76). Only two flagellicaudatans are known from the earliest Cretaceous (Berriasian-Barremian): the dicraeosaurid *Amargasaurus* (77) and the diplodocine *Leinkupal* (76), both from South America. This geographic pattern may indicate that South American diplodocoids (both rebbachisaurids and flagellicaudatans) were not systematically affected by the Late Jurassic diversity crisis seen in the Northern Hemisphere. All known post-Barremian diplodocoids are rebbachisaurids and analyses presented here indicate that both limaysaurine and rebbachisaurine lineages were present in Patagonia until the Cenomanian-Turonian. Ibiricu et al. (43) describe isolated rebbachisaurid remains from the Cenomanian-Turonian of central Patagonia including an anteriormost caudal vertebra with pleurocoel on centrum, a distinct hyposphenal ridge and a transverse interprezygapophyseal ridge. That combination of features is exclusively present in Rebbachisaurinae (42, this study) and supports the referral of that material to the latter clade, eventually to *Katapsaurus* or to a new taxon (see discussion in 43).

The relatively low support for several nodes recovered by the above mentioned analyses is probably biased by the decision to include extremely fragmentary taxa in the ingroup (e.g., *Histriasaurus*). Nevertheless, for this study we consider taxon sample completeness as more significant in the analysis of macroevolutionary and palaeogeographic patterns than the mere nodal support of the chosen phylogenetic framework. Fragmentary taxa, in fact, may provide both temporal (stratigraphic) and spatial (geographic) information unavailable from the arbitrary subset of the best preserved taxa. Although based on a phylogenetically weak topology, the time-calibrated hypothesis presented here represents a testable scenario constraining the *tempo* and mode of rebbachisaurid origin and evolution within a discrete stratigraphic and geographic range.

## Conclusion

In this paper we present a detailed description of the osteology of the type specimen of *Tataouinea hannibalis*, including newly acquired material. Caudal vertebrae 7-17 were collected as fully articulated elements, are exquisitely preserved and provide additional information on rebbachisaurid tail morphology as well as on the development of pneumatization in the caudosacral region within rebbachisaurid sauropods. Caudal and pelvic synapomorphies support the referral of *Tataouinea* to Rebbachisaurinae, here considered as a senior synonym of Nigersaurinae. Time-calibrated phylogeny of Rebbachisauridae indicates a Middle Jurassic origin of the clade, a South American root of Rebbachisaurid radiation, and an expansion to Africa and Europe of Rebbachisaurinae in the earliest part of the Cretaceous.

The time-calibrated phylogeny presented here suggest a rapid cladogenesis of Rebbachisauridae during the Berriasian-Barremian and at least two independent dispersal phases from South America to Africa and Europe approximately between 135 and 130 Ma, one represented by the lineage leading to *Histriasaurus*, the other represented by the rebbachisaurines. Both vicariance and dispersal rates inferred from the known distribution of rebbachisaurids suggest that the Early Cretaceous was the main phase of their expansion, and that this clade rapidly radiated from South America to Africa and then to Europe during a relatively short time interval. *Nigersaurus* represents a pivotal taxon in this scenario, as it is the best known rebbachisaurid, and the basalmost member of the “Euro-African” subclade of Rebbachisaurinae. According to both Bayesian and S-DIVA

palaeogeographic analyses, the latter subclade originated from a dispersal event from South America to Africa. Furthermore, both models concur in placing the origin of *Nigersaurus* lineage before the dispersal event to Europe leading to *Demandasaurus* (Bayesian scenario) or the establishment of an “Euro-African” bioprovince including the latter taxon and the “*Rebbachisaurus-Tataouinea*” clade (S-DIVA scenario). Both models agree in interpreting the lineage leading to *Tataouinea* as restricted to North Africa. The persistence of both basal forms in South America (i.e., *Katapultisaurus*) and derived forms in Africa (i.e., *Rebbachisaurus*) during the early Late Cretaceous suggests that Rebbachisaurinae was the most successful and widely distributed group of rebbachisaurids.

### Acknowledgements

*T. hannibalis* was found in 2011 by A. Bacchetta, and consequently excavated by a team from the University of Bologna (Italy) and the Office National Des Mines, Tunis, led by the senior author and M.H. in 2013. Described elements were prepared at the Office National Des Mines in Tunis by the senior author, M. Contessi, E. Crescenzi Lanna, M. Riahi and F. M’Nasri. We are grateful to A. Mazzei, E. Crescenzi Lanna, H. Aljane for their support in the field. We are also grateful to R. Allain, J. Wilson and F. Torcida Fernandez-Baldor for the access to unpublished material and constructive discussions. This manuscript greatly benefited from reviews and comments from M. D’Emic, M. Wedel and the Academic Editor P. Dodson. This research was conducted in collaboration with the Office National Des Mines, Tunis, and the Department of Biological, Geological and Environmental Sciences, and Museo Geologico Giovanni Capellini (University of Bologna, Italy).

### References

1. Fanti F, Cau A, Hassine M, Contessi M (2013). A new sauropod dinosaur from the Early Cretaceous of Tunisia with extreme avian-like pneumatization. *Nature Communications* 4:2028, 7 pp. doi: 10.1038/ncomms3038.
2. Pervinquière L (1912) Sur la géologie de l’extrême Sud tunisien et de la Tripolitaine. *Bulletin de la Société Géologique de France* XII(4), 160.

3. Kilian C (1931) Des principaux complexes continentaux du Sahara. Comptes Rendus de la Société Géologique de France 9: 109–111.
4. Kilian C (1937) Esquisse géologique du Sahara français à l'est du 6<sup>ème</sup> degré de longitude, Chronique des Mines et de la Colonisation 58, 21-22 Map 1/4.000.000 Paris.
5. de Lapparent AF (1951) Découverte de Dinosauriens, associés à une faune de Reptiles et de Poissons, dans le Crétacé inférieur de l'extrême Sud tunisien. Comptes Rendus Académie des Sciences, Paris 232: 1430–1432.
6. de Lapparent AF (1960) Les Dinosauriens du "*Continental intercalaire*" du Sahara central. Mémoires de la Société Géologique de France Nouvelle Série 39(88A): 1–58.
7. Bouaziz S, Donze P, Ghanmi M, Zarbout M (1989) La série à dominante continentale (Oxfordien à Cénomanién) de la falaise du Dahar (Sud tunisien); son évolution du Tebaga de Medenine à la frontière tripolitaine. Géologie Méditerranéenne 16: 67–76.
8. Bouaziz S, Barrier E, Soussi M, Turki MM, Zouari H (2002) Tectonic evolution of the northern African margin in Tunisia from paleo stress data and sedimentary record. Tectonophysics 357: 227–253.
9. Ben Ismail MH. (1991) Les bassins mésozoïques (Trias à Aptien) du sud de la Tunisie: stratigraphie intégrée, caractéristiques géophysiques et évolution géodynamique. Ph.D. Thesis, Université de Tunis II, Tunis, 446 p. Accessed at the ONM library, Tunis.
10. Benton MJ, Bouaziz S, Buffetaut E, Martill D, Ouaja M, Soussi M, Trueman C (2000). Dinosaurs and other fossil vertebrates from fluvial deposits in the Lower Cretaceous of southern Tunisia. Palaeogeography, Palaeoclimatology, Palaeoecology 157: 227–246.
11. Barale G, Ouaja M (2002) La biodiversité végétale des gisements d'âge Jurassique supérieur–Crétacé inférieur de Merbah El Asfer (Sud-Tunisien). Cretaceous Research 23: 707–737.
12. Courel L, Ait Salem H, Benaouiss N, Et-Touhami M, Fekirine B, Oujidi M, Soussi M, Tourani A (2003) Mid-Triassic to Early Liassic clastic/evaporitic deposits over the

- Maghreb Platform. *Palaeogeography, Palaeoclimatology, Palaeoecology* 196: 157–176.
13. Ouaja M, Philippe M, Barale G, Ferry S, Ben Youssef M (2004) Mise en évidence d'une flore Oxfordienne dans le Sud-Est de la Tunisie: intérêts stratigraphique et paléocéologique. *Geobios* 37: 89–97.
  14. Fanti F, Contessi M, Franchi F (2012a) The "*Continental Intercalaire*" of southern Tunisia: stratigraphy, paleontology, and paleoecology. *Journal of African Earth Sciences* 73–74:1-23.
  15. Fanti F, Cau A, Hassine M (2014a) Evidence of titanosauriforms and rebbachisaurids (Dinosauria: Sauropoda) from the Early Cretaceous of Tunisia. *Journal of African Earth Sciences* 90: 1–8.
  16. Fanti F, Cau A, Martinelli A, Contessi M (2014b) Integrating palaeoecology and morphology in theropod diversity estimation: A case from the Aptian-Albian of Tunisia. *Palaeogeography, Palaeoclimatology, Palaeoecology* 410: 39–57.
  17. Lefranc JP, Guiraud R (1990) The *Continental Intercalaire* of northwestern Sahara and its equivalents in the neighboring regions. *Journal of African Earth Sciences* 10: 27–77.
  18. Zarbout M, Souquet P, Peybernes B (1994) Séquences de dépôt dans les environnements de transition fluviale-marine de Crétacé inférieur de Dahar (Sud-Tunisien). *Strata* 6: 141–142.
  19. Anderson PE, Benton MJ, Trueman CN, Paterson BA, Cuny G (2007) Paleoenvironments of the vertebrates on the southern shore of the Tethys: the nonmarine Early Cretaceous of Tunisia. *Paleogeography, Paleoclimatology, Paleoecology* 243: 118–131.
  20. Le Loeuff J, Metais E, Dutheil D, Rubinos J, Buffetaut E, Lafont F, Cavin L, Moreau F, Tong H, Blanpied C, Sbeta A (2010) An Early Cretaceous vertebrate assemblage from the Cabao Formation of NW Libya. *Geological Magazine* 147: 750–759.
  21. Cuny G, Ouaja M, Sraf D, Schmitz L, Buffetaut E, Benton MJ (2004) Fossil sharks from the Early Cretaceous of Tunisia. *Revue de Paleobiologie* 9: 127–142.
  22. Cuny G, Cobbett A, Meunier F, Benton M (2010) Vertebrate microremains from the Early Cretaceous of southern Tunisia. *Geobios* 43: 615–628.

23. Harrison EP (1973) Depositional History of Cisco-Wolfcamp Strata, Bend Arch North-Central Texas. Ph.D. Dissertation. Texas Tech University.
24. Lehman T (1989) Upper Cretaceous (Maastrichtian) paleosols in Trans-Pecos Texas. *Geological Society of America Bulletin* 101: 188–203.
25. Kraus M, Hasiotis S (2006) Significance of different modes of rhizolith preservation to interpreting paleoenvironmental and paleohydrologic settings: examples from Paleogene paleosols, Bighorn Basin, Wyoming, U.S.A. *Journal of Sedimentary Research* 76: 633–646.
26. Wilson JA (2011) Anatomical terminology for the sacrum of sauropod dinosaurs. *Contributions from the Museum of Paleontology, University of Michigan* 32: 59–69.
27. Wilson JA (1999) A nomenclature for vertebral laminae in sauropods and other saurischian dinosaurs. *Journal of Vertebrate Paleontology* 19: 639–653.
28. Wilson JA, D’Emic MD, Ikejiri T, Moacdieh EM, Whitlock JA (2011) A nomenclature for vertebral fossae in sauropods and other saurischian dinosaurs. *PLoS One* 6:e17114.
29. Wedel MJ (2005) Postcranial skeletal pneumaticity in sauropods and its implications for mass estimates. In: Wilson JA, Curry-Rogers K, editors. *The Sauropods: Evolution and Paleobiology*. University of California Press, Berkeley. pp 201–228.
30. Wedel MJ (2009) Evidence for bird-like air sacs in saurischian dinosaurs. *Journal of Experimental Zoology* 311A: 611–628.
31. Whitlock JA (2011) A phylogenetic analysis of Diplodocoidea (Saurischia: Sauropoda). *Zoological Journal of the Linnean Society* 161: 872–915.
32. Hasiotis ST, Fiorillo AR (1997) Dermestid beetle boring in sauropod and theropod, dinosaur bones, Dinosaur National Monument, Utah—keys to the taphonomy of a bone bed. Combined Rocky Mountain/South central Geological Society of America Meeting, Abstracts with Program, El Paso, Texas 29(2): 13A
33. Paik IS (2000) Bone chip-filled burrows associated with bored dinosaur bone in floodplain paleosols of the Cretaceous Hasandong Formation, Korea. *Palaeogeography Palaeoclimatology Palaeoecology* 157: 213–225.
34. Campobasso CP, Vella GD, Introna F (2001) Factors affecting decomposition and diptera colonization. *Forensic Science International* 120: 18–27.

35. Roberts E (2003) An experimental approach to identifying and interpreting dermestid (Insecta, Coleoptera) bone modification. *Journal of Vertebrate Paleontology* 23: 89–90.
36. Britt BB, Scheetz RD, Dangerfield A (2008). A suite of dermestid beetle traces on dinosaur bone from the Upper Jurassic Morrison Formation, Wyoming, USA. *Ichnos* 15: 59–71.
37. Saneyoshi M, Watabe M, Suzuki S, Tsogtbaatar K (2011) Trace fossils on dinosaur bones from Upper Cretaceous eolian deposits in Mongolia: taphonomic interpretation of paleoecosystems in ancient desert environments. *Palaeogeography, Palaeoclimatology, Palaeoecology* 311: 38–47.
38. Fanti F, Currie PJ, Badamgarav D (2012b) New Specimens of *Nemegtomaia* from the Baruungoyot and Nemegt Formations (Late Cretaceous) of Mongolia. *PLoS ONE* 7: e31330.
39. Bonaparte JF (1997) *Rayososaurus agrioensis* Bonaparte 1995. *Ameghiniana* 34: 116.
40. Wilson JA, Allain R. Osteology of *Rebbachisaurus garasbae* Lavocat, a diplodocoid (Dinosauria: Sauropoda) from the early Late Cretaceous Kem Kem beds of southeastern Morocco. *Journal of Vertebrate Paleontology*, in press.
41. Mannion PD, Upchurch P, Hutt S (2011) New rebbachisaurid (Dinosauria: Sauropoda) material from the Wessex Formation (Barremian, Early Cretaceous), Isle of Wight, United Kingdom. *Cretaceous Research* 32: 774–780
42. Torcida Fernández-Baldor F, Canudo JI, Huerta P, Montero D, Suberbiola XP, Salgado L (2011) *Demandasaurus darwini*, a new rebbachisaurid sauropod from the Early Cretaceous of the Iberian Peninsula. *Acta Palaeontologica Polonica* 56: 535–552.
43. Ibiricu LM, Casal GA, Martínez RND, Lamanna MC, Luna M, Salgado L (2013) *Katepensaurus goicoecheai*, gen. et sp. nov., a Late Cretaceous rebbachisaurid (Sauropoda, Diplodocoidea) from central Patagonia, Argentina. *Journal of Vertebrate Paleontology* 33: 1351–1366.
44. Carballido JL, Salgado L, Pol D, Canudo JI, Garrido A (2012). A new basal rebbachisaurid (Sauropoda, Diplodocoidea) from the Early Cretaceous of the Neuquén Basin; evolution and biogeography of the group. *Historical Biology* 24: 631–654.

45. Lee MSY, Cau A, Naish D, Dyke GJ (2014a). Morphological clocks in palaeontology, and a Mid-Cretaceous origin of crown Aves. *Systematic Biology* 63: 442–449.
46. Lee MSY, Cau A, Naish D, Dyke GJ (2014b) Sustained miniaturization and anatomical innovation in the dinosaurian ancestors of birds. *Science* 345: 562-566.
47. Goloboff PA, Farris J, Nixon K (2008a) TNT, a free program for phylogenetic analysis. *Cladistics* 24:774–786.
48. Drummond A, Suchard MA, Xie D, Rambaut A (2012) Bayesian phylogenetics with BEAUti and the BEAST 1.7. *Molecular Biology Evolution* 29, 1969.
49. Lewis PO (2001) A likelihood approach to estimating phylogeny from discrete morphological character data. *Systematic Biology* 50: 913-925.
50. Cohen KM, Finney SC, Gibbard PL, Fan J-X (2013) The ICS International Chronostratigraphic Chart. *Episodes* 36: 199–204.
51. Remes K, Ortega F, Fierro I, Joger U, Kosma R, Ferrer JMM (2009) A new basal sauropod dinosaur from the Middle Jurassic of Niger and the early evolution of sauropoda. *PLoS ONE* 4(9): e6924.
52. Rambaut A, Drummond AJ (2009) Tracer: MCMC Trace Analysis Tool v1.5. <http://beast.bio.ed.ac.uk/>
53. Yu Y, Harris AJ, Xingjin H (2011) RASP (Reconstruct Ancestral State in Phylogenies) 1.1. Available at: <http://mnh.scu.edu.cn/soft/blog/RASP>.
54. Yu Y, Harris AJ, He XJ (2010) S-DIVA (statistical dispersal-vicariance analysis): a tool for inferring biogeographic histories. *Molecular Phylogenetics and Evolution* 56: 848–850.
55. Cunningham W, Dalziel I, Lee T, Lawver L (1995) Southernmost South America–Antarctic Peninsula relative plate motions since 84 Ma: implications for the tectonic evolution of the Scotia Arc region. *Journal of Geophysical Research* 100: 8257–8266.
56. Crame J (1999) An evolutionary perspective on marine faunal connections between southernmost South America and Antarctica. *Scientia Marina* 63:1–14
57. Philip J, Floquet M (2000) Early Campanian (83–80.5 Ma). In: Dercourt J, Gaetani M, Vrielynck B, Barrier E, Biju-Duval B, Brunet M, Cadet J, Crasquin S, Sandulescu M, editors. *Atlas Peri-Tethys palaeogeographical maps – explanatory notes*. CCGM/CGMW, Paris, pp 137–144.

58. Macdonald D, Gomez-Pereza I, Franzese J, Spalletti L, Lawver L, Gahagan L, Dalziel I, Thomas D, Trewin N, Hoesly M, Paton D (2003) Mesozoic break-up of SW Gondwana: implications for regional hydrocarbon potential of the southern South Atlantic. *Marine and Petroleum Geology* 20: 287–308.
59. Jokat W, Boebel T, König M, Meyer U (2003) Timing and geometry of early Gondwana breakup. *Journal of Geophysical Research* 108: 1–15.
60. Guedes E, Heilbron M, Vasconcelos P, Valeriano C, de Almeida J, Teixeira W, Filho A (2005) K-Ar and  $^{40}\text{Ar}/^{39}\text{Ar}$  ages of dikes emplaced in the onshore basement of the Santos Basin, Resende Area, SE Brazil: implications for the south Atlantic opening and the Tertiary reactivation. *Journal of South American Earth Sciences* 18: 371–382.
61. Gheerbrant E, Rage J (2006) Paleobiogeography of Africa: how distinct from Gondwana and Laurasia. *Palaeogeography, Palaeoclimatology, Palaeoecology* 212: 224–246.
62. Fanti F. 2012. Cretaceous continental bridges, insularity, and vicariance in the southern hemisphere: which route did dinosaurs take? In: Talent J, editor. *Earth and Life: Global biodiversity, extinction intervals and biogeographic perturbation through time*. Springer. pp. 883-911.
63. Goloboff PA (1993) Estimating character weights during tree search. *Cladistics* 9: 83–91.
64. Goloboff PA, Carpenter JM, Arias JS, Esquivel DFM (2008b) Weighting against homoplasy improves phylogenetic analysis of morphological datasets. *Cladistics* 24: 758–773.
65. Mateus O, Mannion PD, Upchurch P (2014) *Zby atlanticus*, a new turiasaurian sauropod (Dinosauria, Eusauropoda) from the Late Jurassic of Portugal. *Journal of Vertebrate Paleontology* 34: 618–634.
66. Templeton AR (1983) Phylogenetic inference from restriction endonuclease cleavage site maps with particular reference to the evolution of humans and the apes. *Evolution* 37: 221–244.
67. Wedel MJ, Taylor MP (2013) Caudal pneumaticity and pneumatic hiatuses in the sauropod dinosaurs *Giraffatitan* and *Apatosaurus*. *PLoS ONE* 8: e78213.

68. Yates AM, Wedel MJ, Bonnan MF (2012) The early evolution of postcranial skeletal pneumaticity in sauropodomorph dinosaurs. *Acta Palaeontologica Polonica* 57: 85–100.
69. Canale JI, Novas FE, Pol D (2014). Osteology and phylogenetic relationships of *Tyrannotitan chubutensis* Novas, de Valais, Vickers-Rich and Rich, 2005 (Theropoda: Carcharodontosauridae) from the Lower Cretaceous of Patagonia, Argentina. *Historical Biology* (advance online publication) DOI:10.1080/08912963.2013.861830
70. Mannion PD, Barrett PM (2013) Additions to the sauropod dinosaur fauna of the Cenomanian (early Late Cretaceous) Kem Kem beds of Morocco: Palaeobiogeographical implications of the mid-Cretaceous African sauropod fossil record. *Cretaceous Research* 45: 49-59.
71. Ibiricu LM, Casal GA, Lamanna MC, Martínez RND, Harris JD, Lacovara KJ (2011) The southernmost records of Rebbachisauridae (Sauropoda: Diplodocoidea), from early Late Cretaceous deposits in central Patagonia. *Cretaceous Research* 34: 220–232.
72. Benson RB, Butler RJ, Carrano MT, O’Connor PM (2012) Air-filled postcranial bones in theropod dinosaurs: physiological implications and the “reptile”–bird transition. *Biological Reviews* 87: 168–193.
73. Carvalho IS, Avilla LS, Salgado L (2003) *Amazonsaurus maranhensis* gen. et sp. nov. (Sauropoda, Diplodocoidea) from the Lower Cretaceous (Aptian–Albian) of Brazil. *Cretaceous Research* 24: 697–713.
74. Torcida Fernández-Baldor F (2012) Sistemática, filogenia y análisis paleobiogeográfico de *Demandasaurus darwini* (Sauropoda, Rebbachisauridae) del Barremiense superior-Aptiense de Burgos (España). Ph.D. thesis, Universidad Zaragoza, 390 pp.
75. Apesteguía S (2007) The sauropod diversity of the La Amarga Formation (Barremian), Neuquén (Argentina). *Cretaceous Research* 12: 533–546.
76. Gallina PA, Apesteguía S, Haluza A, Canale JI (2014) A diplodocid sauropod survivor from the Early Cretaceous of South America. *PLoS One* 9: e97128

77. Salgado L, Bonaparte JF (1991) Un nuevo saurópodo Dicraeosauridae, *Amargasaurus cazai* gen. et sp. nov., de la Formación La Amarga, Neocomiano de la provincia del Neuquén, Argentina. *Ameghiniana* 28: 333–346.
78. Upchurch P, Barrett PM, Dodson P (2004) Sauropoda. In: Weishampel DB, Dodson P, Osmólska H, Hilton RP, editors. *The Dinosauria*. University of California Press. pp. 259–322.
79. Royo-Torres R, Cobos A, Alcalá L (2006) A Giant European Dinosaur and a New Sauropod Clade. *Science* 314: 1925-1927.
80. Sander PM, Mateus OV, Laven T, Knötschke N (2006) Bone histology indicates insular dwarfism in a new Late Jurassic sauropod dinosaur. *Nature* 441: 739–741.

## Figures

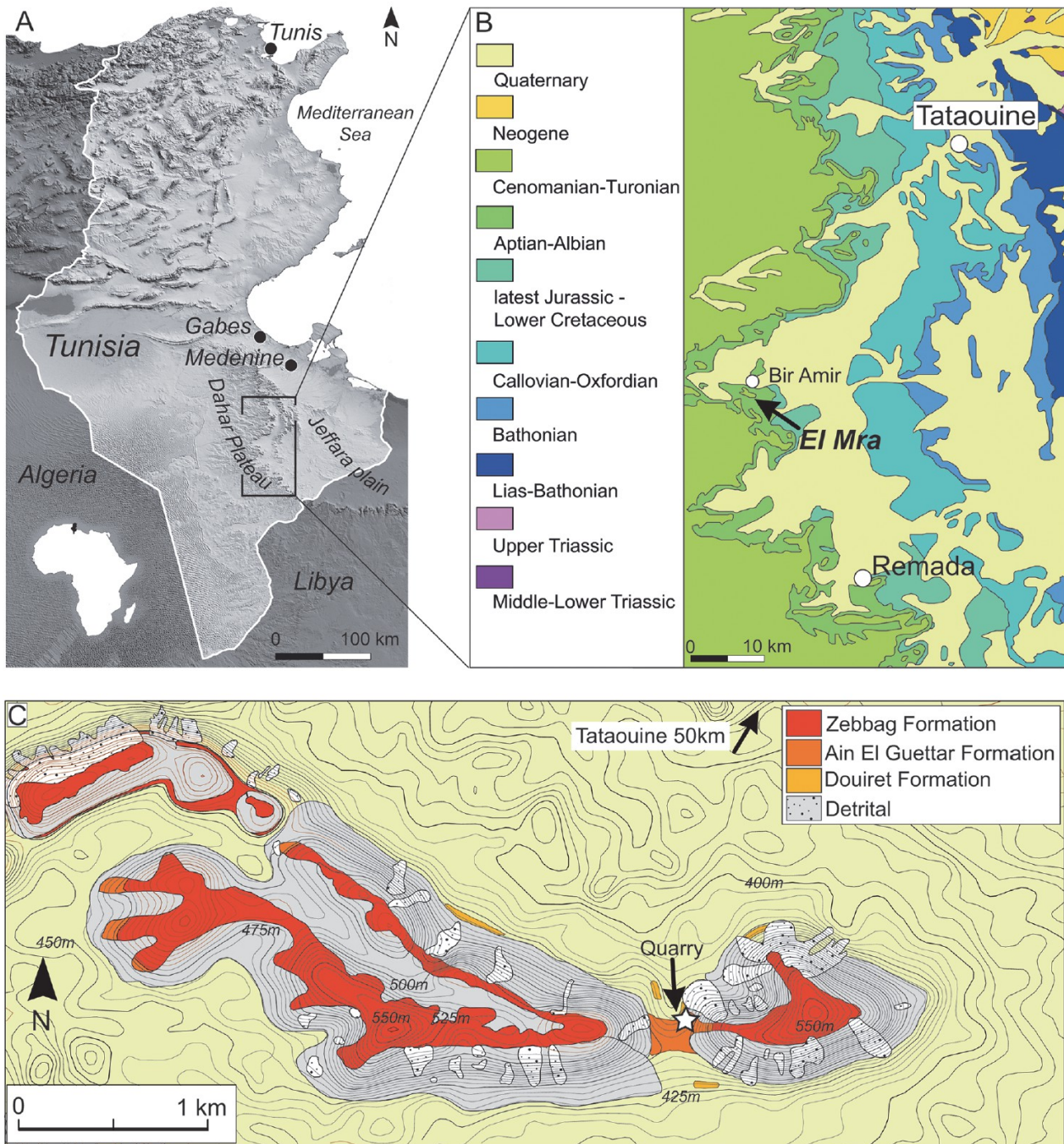


Figure 1: **The Tataouine basin in southern Tunisia.** A, reference map of the Tataouine region in southern Tunisia; B, simplified geological map of the study area showing the distribution of Mesozoic deposits and the El Mra locality near the village of Bir Amir. C, - detailed topographic and geological map of the El Mra locality.

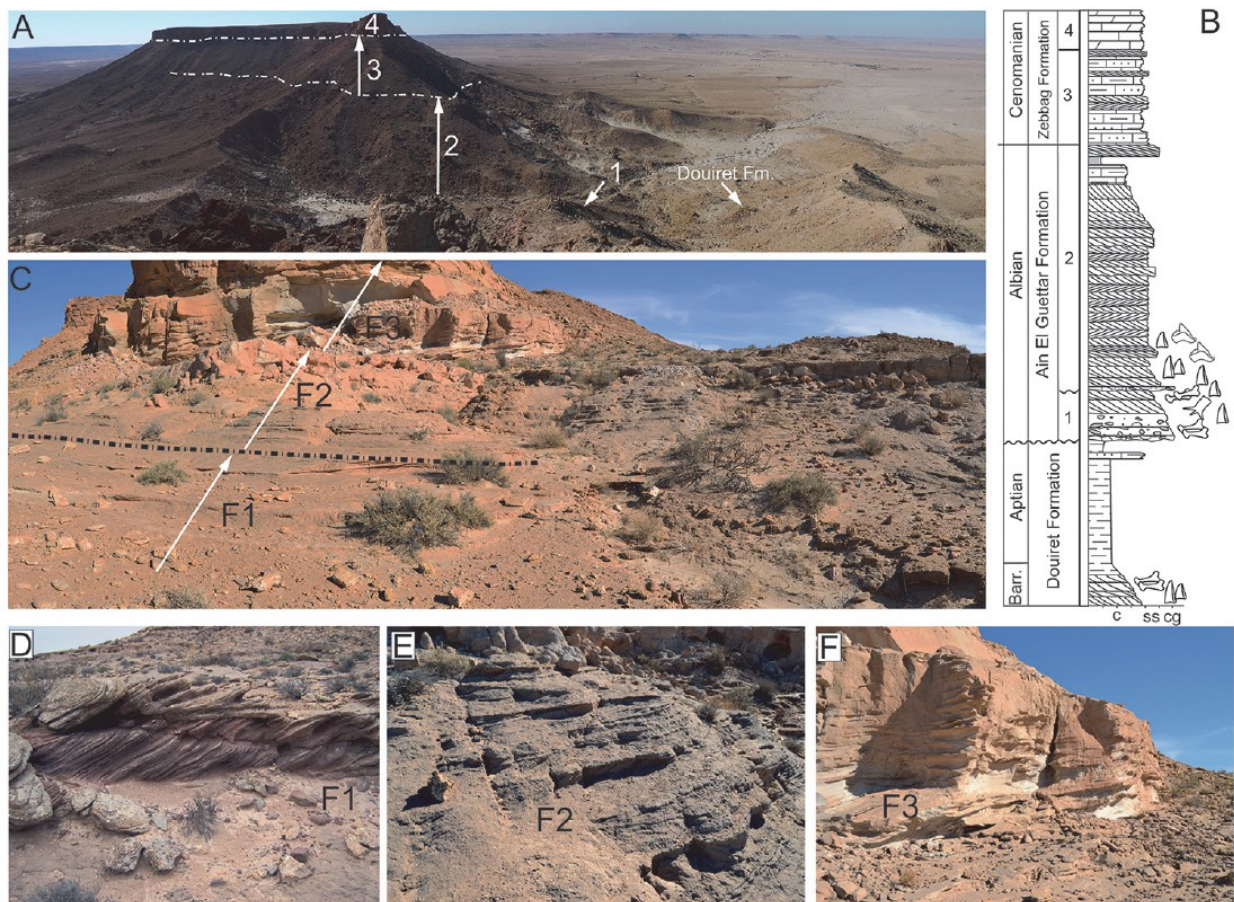


Figure 2: **Stratigraphy at the El Mra locality.** A, panoramic view of the El Mra mesa-like morphology. 1. Chenini Mbr., 2. Oum Ed Diab Mbr., 3. Keker Mbr., 4. Gattar Mbr. B, simplified field-log of the El Mra section showing the stratigraphic occurrence of vertebrate and plant remains. C, facies distribution in the Chenini-Oum Ed Diab transition. F1, high-energy, fluvial sandy bar deposits; F2, low-angle shoreface deposits; F3, fine-grained tidal deposits with flaser-like structures. D, E, F, field photographs of the different deposits exposed at the El Mra locality. *T. hannibalis* was recovered from the F1 beds.

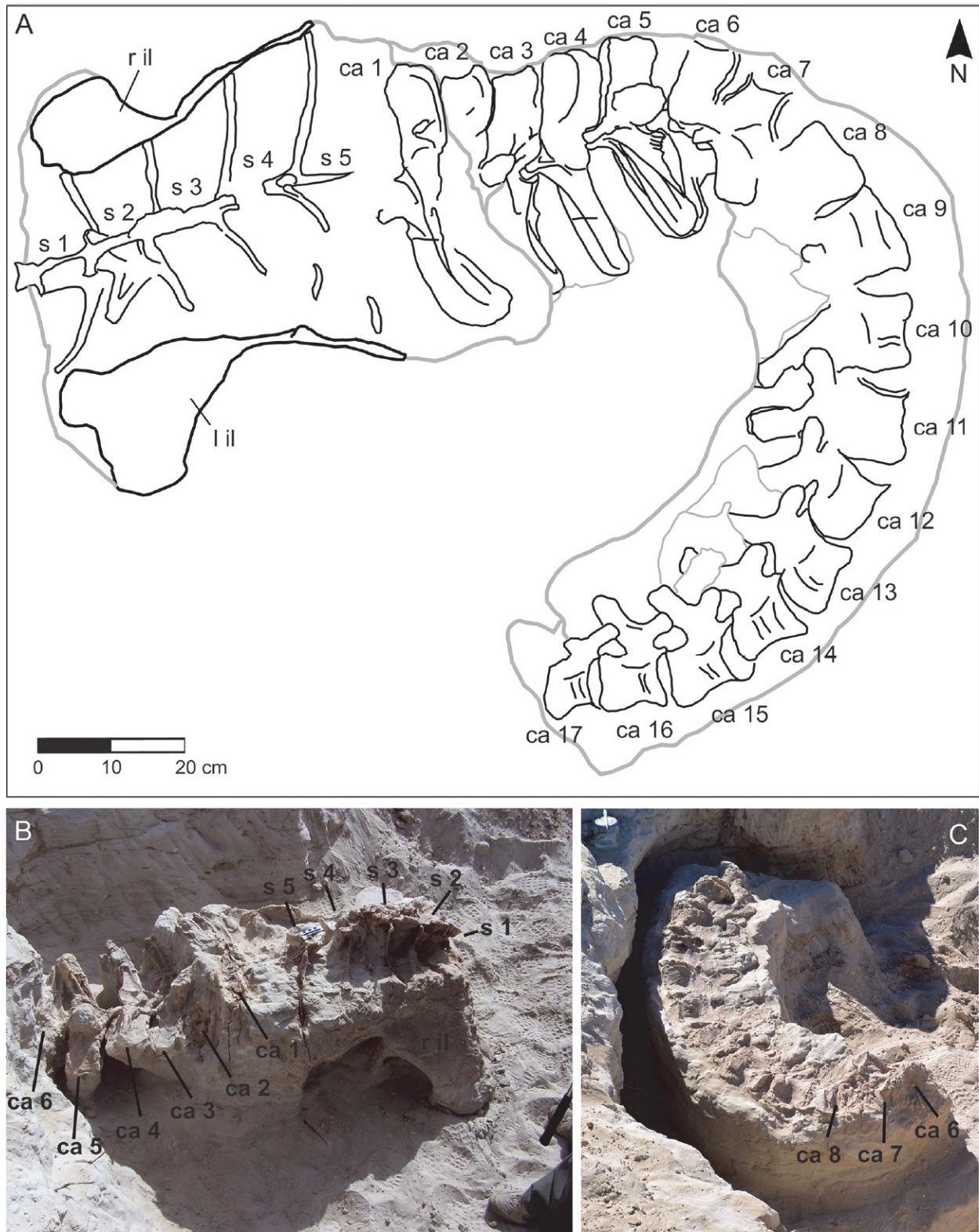


Figure 3. **Preserved elements of *Tataouinea hannibalis* (ONM DT 1-48).** A, quarry map showing the orientation of collected elements. B, field photograph of the elements collected at the end of 2011, and C, of elements collected in 2013. Ca, caudal vertebra 1-17; S, sacral vertebra 1-5; r il, right ilium; l il, left ilium.

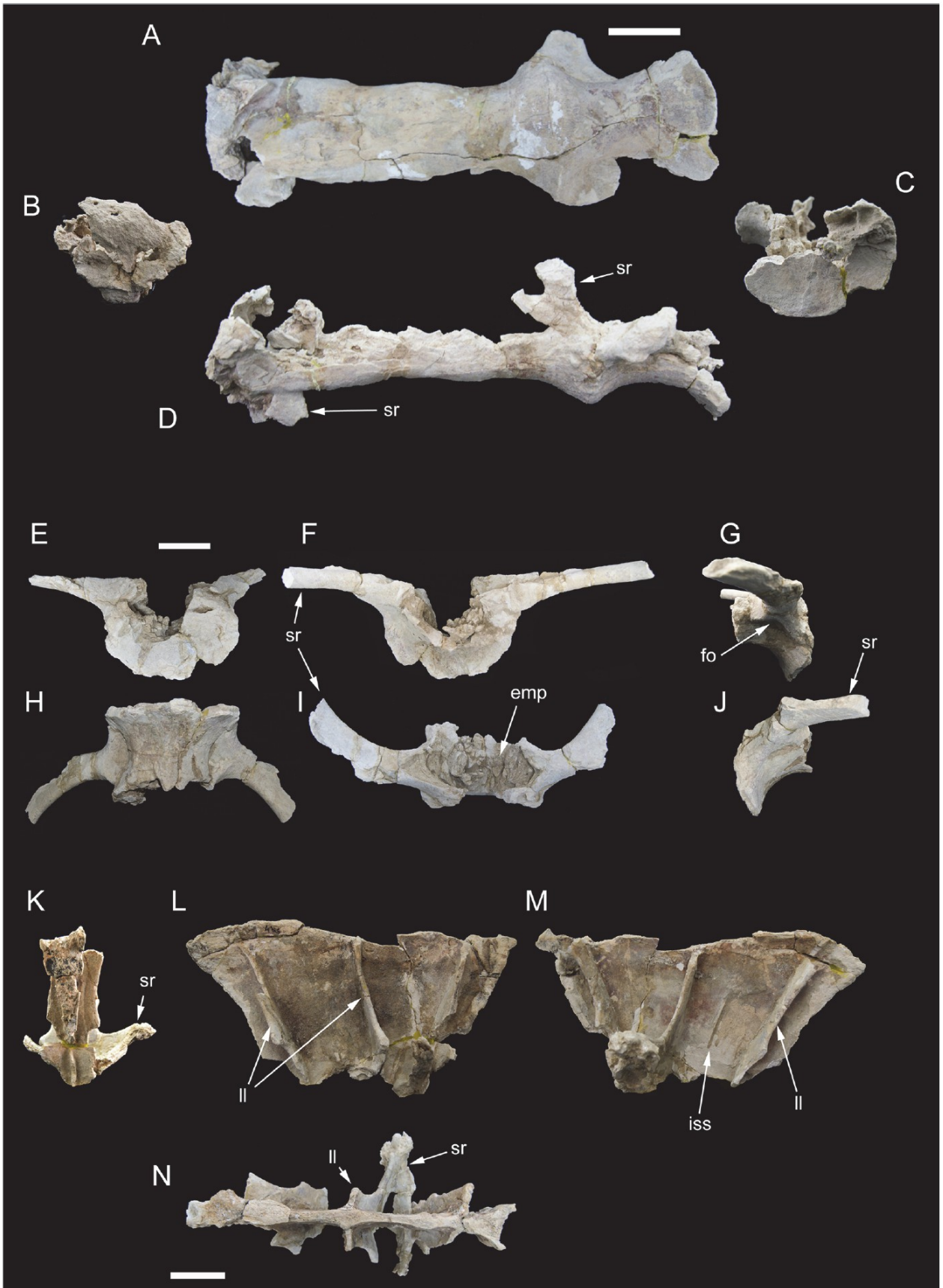


Figure 4. **Partial sacrum of *Tataouinea hannibalis***. Partial sacral centra 1-4 in ventral (A), cranial (B), caudal (C) and left lateral (D) views. Partial sacral centrum 5 in caudal (E), cranial (F), right lateral (G), ventral (H), dorsal (I) and left lateral (J) views. Scale bars: 10 cm. Abbreviations: emp, extramural pneumatization; fo, fossa; iss, interspinous suture scar; ll, lateral lamina; sr, sacral ribs.

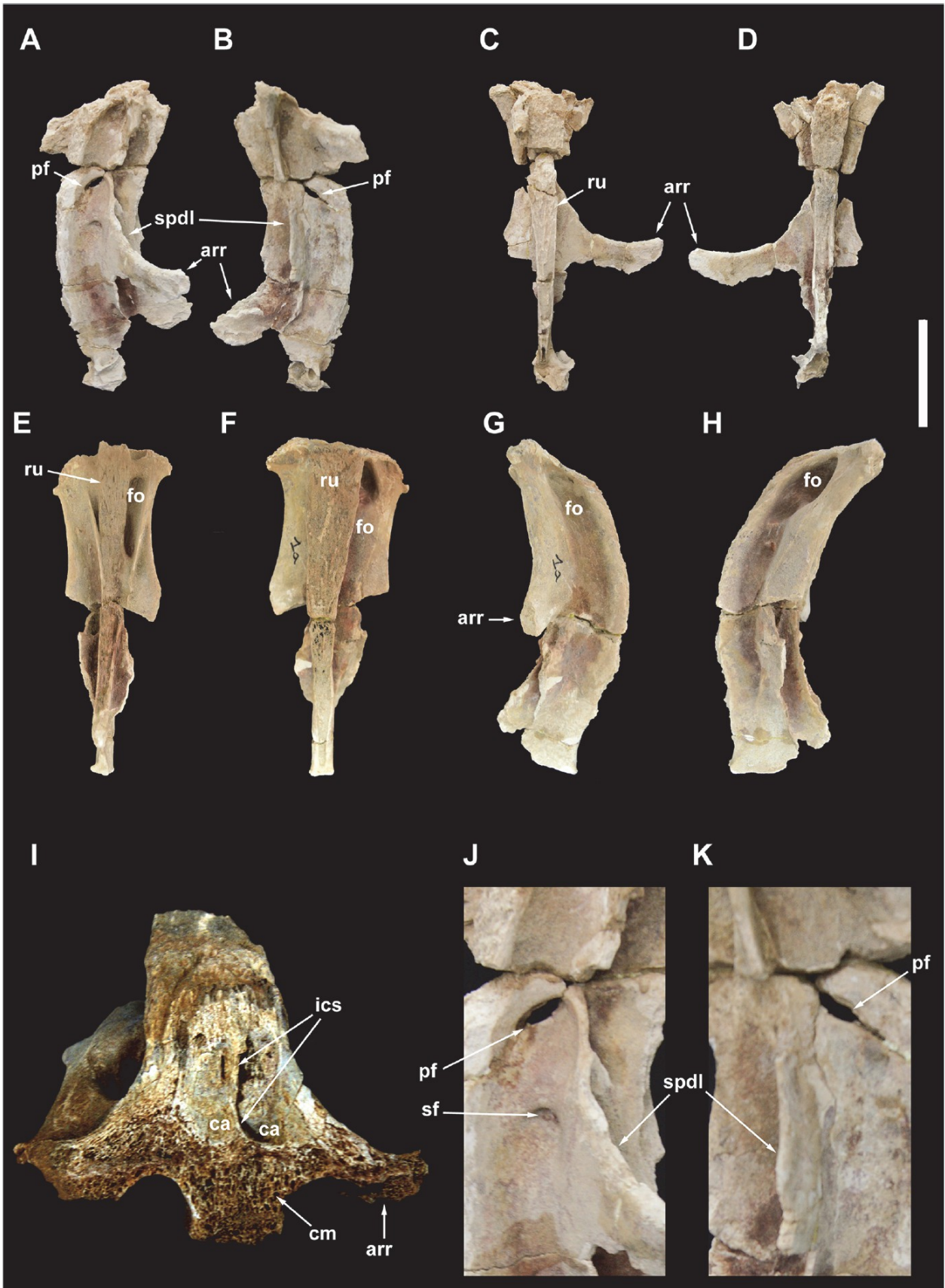


Figure 5. **Sacral neural spines 4 and 5 of *Tataouinea hannibalis*.** Sacral neural spine 4 in left lateral (A), right lateral (B), cranial (C) and caudal (D) views. Sacral neural spine 5 in caudal (E), cranial (F), right lateral (G) and left lateral (H) views. Cross section of sacral neural spine 4 (I). Details of sacral neural spine 4 pneumatization in left lateral (J) and right lateral (K) views. Scale bar: 10 cm. Abbreviation: arr, alar ramus of rib; ca, camera; cm, camellae; fo, fossa; ics, intercamerate septum; pf, pneumatic foramen; ru, rugosities; sf, semilunate fossa; spdl, spinodiapophyseal lamina.

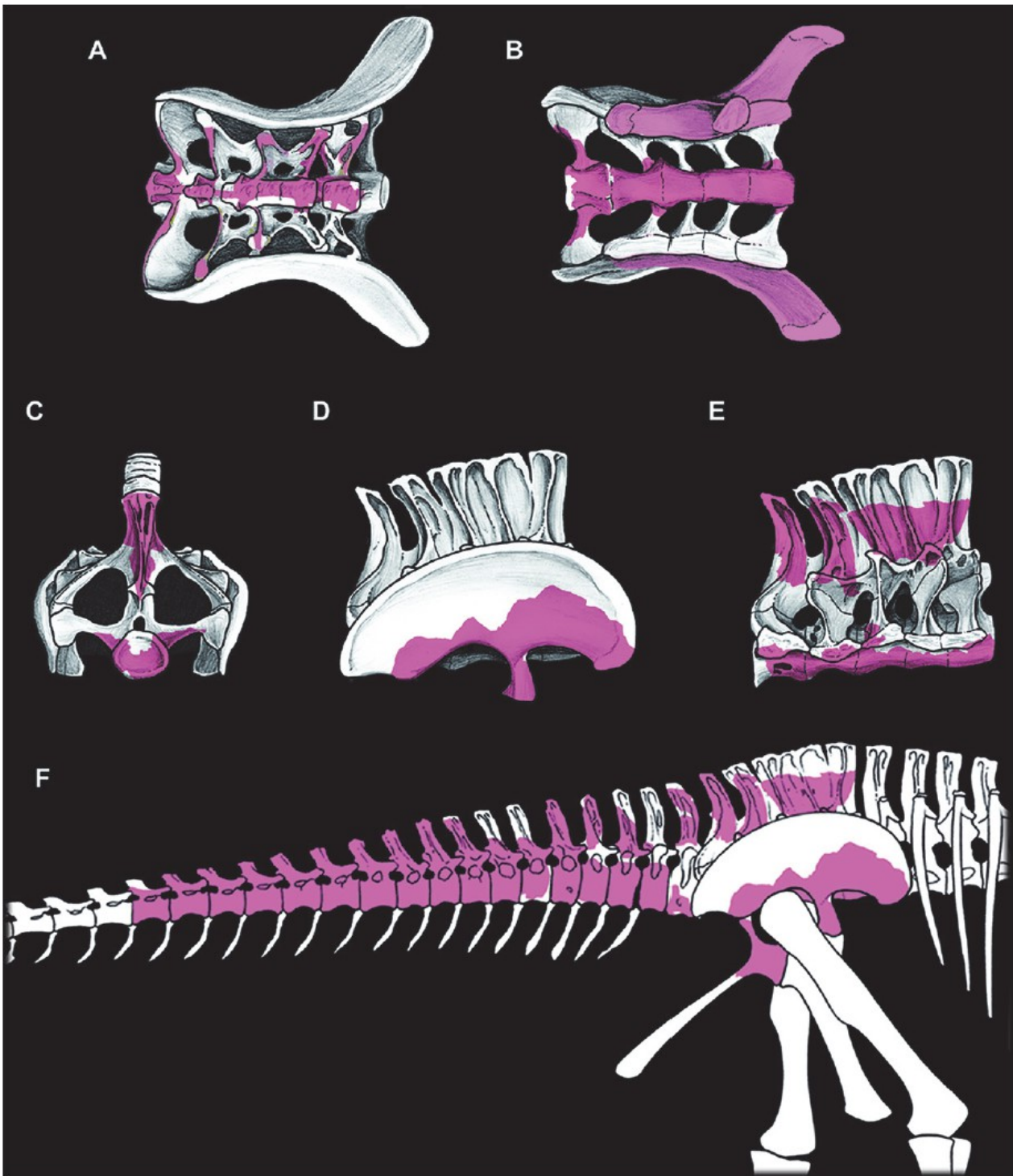


Figure 6. **Sacrum with associated ilia, and reconstruction of known elements of *Tataouinea hannibalis*.** Sacrum in dorsal view (A), ventral view (B), caudal view (C), right lateral view with ilium associated (D) and with ilium removed (E). In (B), the peduncles of the right ilium are removed. Skeletal reconstruction of caudosacral region of *Tataouinea hannibalis* (F). Recovered elements in color. A full skeletal reconstruction is shown in Supplementary Material (S1, Fig.1).

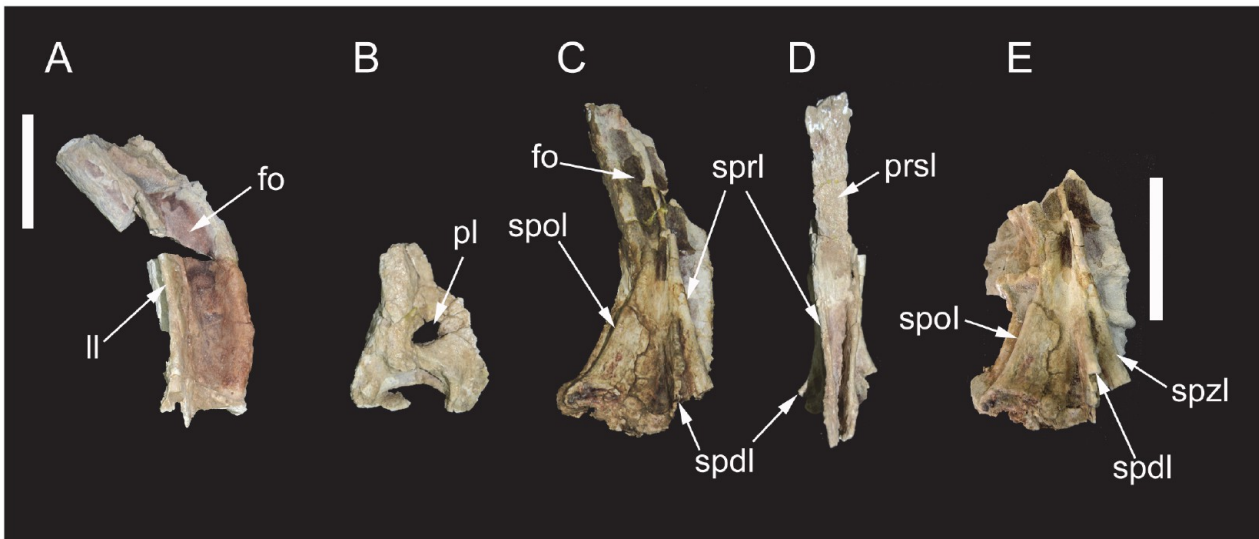


Figure 7. **Partial proximal caudal vertebrae of *Tataouinea hannibalis*.** Partial caudal neural spine 1 in right lateral view (A). Partial caudal centrum 1 in right lateral view (B). Partial neural arch 3 in right lateral (C) and proximal (D) views. Partial caudal neural arch 4 in right lateral view (E). Scale bars: A-D: 10 cm, E: 10 cm. Abbreviations: fo, fossa; ll, lateral lamina; pl, pleurocoel; prsl, prespinal lamina; spdl, spinodiapophyseal lamina; spol, spinopostzygapophyseal lamina; sprl, spinoprezygapophyseal lamina.



Figure 8. **Caudal vertebra 5 of *Tataouinea hannibalis*.** Vertebra in proximal (A), left lateral (B), distal (C), right lateral (D) views. Detail of neural arch in right proximodorsal view (E). Cross section shapes of neural arch (shown in proximal view) in six points indicated by arrows (proximal is bottom). Scale bar: 10 cm. Abbreviations: fo, fossa; hr, hyposphenal ridge; ll, lateral lamina; nc, neural canal; pl, pleurocoel; pozp, postzygapophysis pathology; psl, prespinal lamina; pz, prezygapophysis; pzdl, prezygodiapophyseal lamina; ri, rib; spol, spinopostzygapophyseal lamina; sprl, spinoprezygapophyseal lamina.

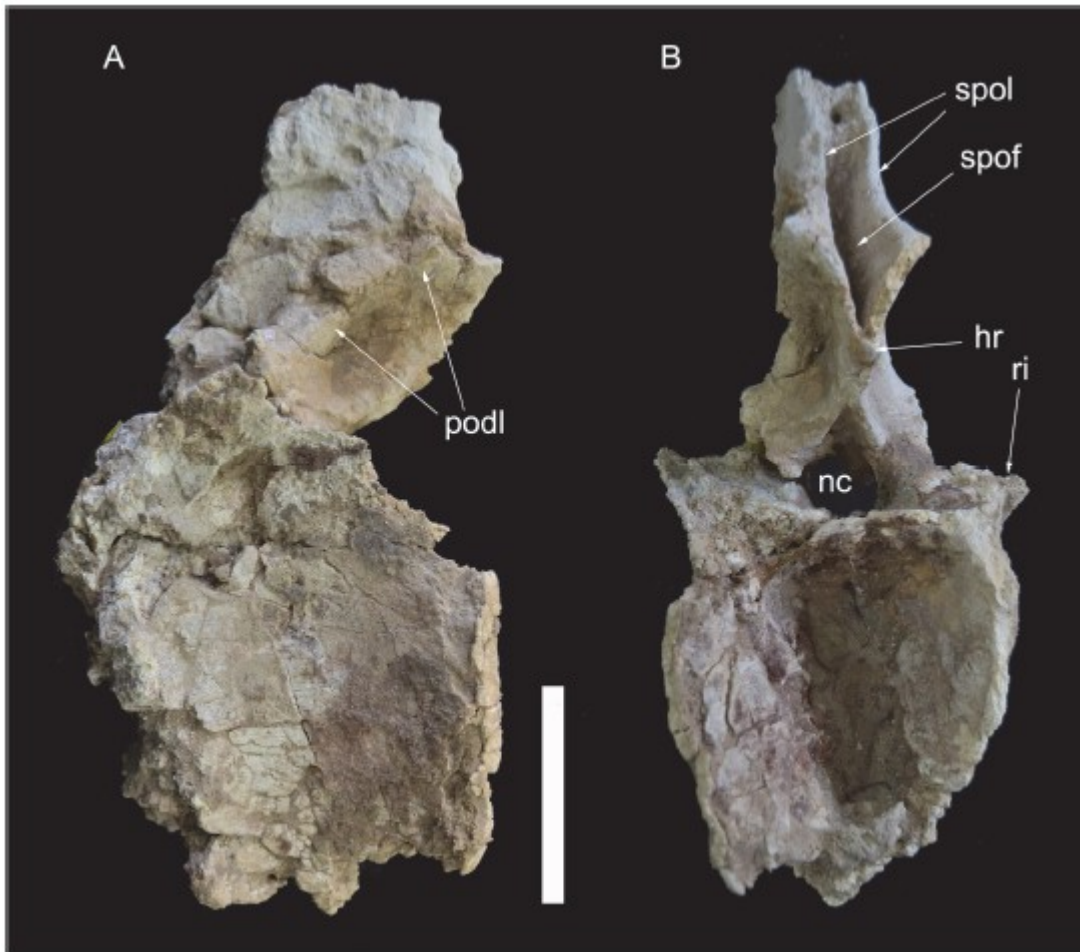


Figure 9. **Caudal vertebra 6 of *Tataouinea hannibalis***. Vertebra in left lateral (A) and distal (B) views. Scale bar: 10 cm. Abbreviations: hr, hyposphenal ridge; nc, neural canal; podl, postzygodiapophyseal lamina; ri, rib; spo spinopostzygapophyseal fossa; spol, spinopostzygapophyseal lamina.

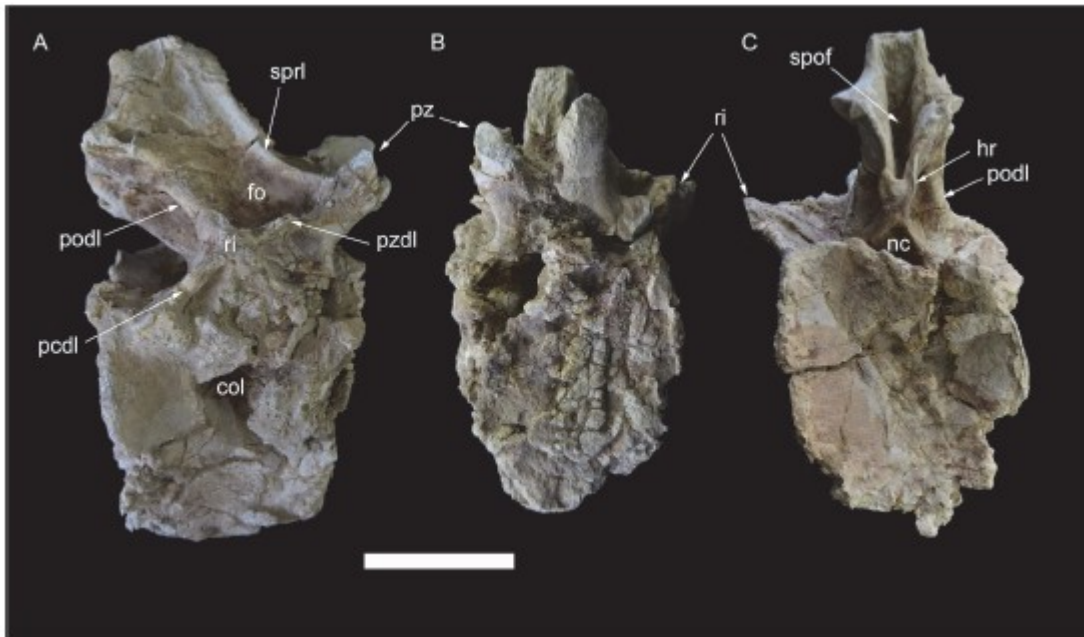


Figure 10. **Caudal vertebra 7 of *Tataouinea hannibalis*.** Vertebra in right lateral (A), proximal (B) and distal (C) views. Scale bar: 10 cm. Abbreviations: col, collapsed area; fo, fossa; hr, hyposphenal ridge; nc, neural canal; pcdl, posterior centrodiapophyseal lamina; podl, postzygodiapophyseal lamina; pz, prezygapophysis; pzd, prezygodiapophyseal lamina; ri, rib; spof, spinopostzygapophyseal fossa; sprl, spinoprezygapophyseal lamina.

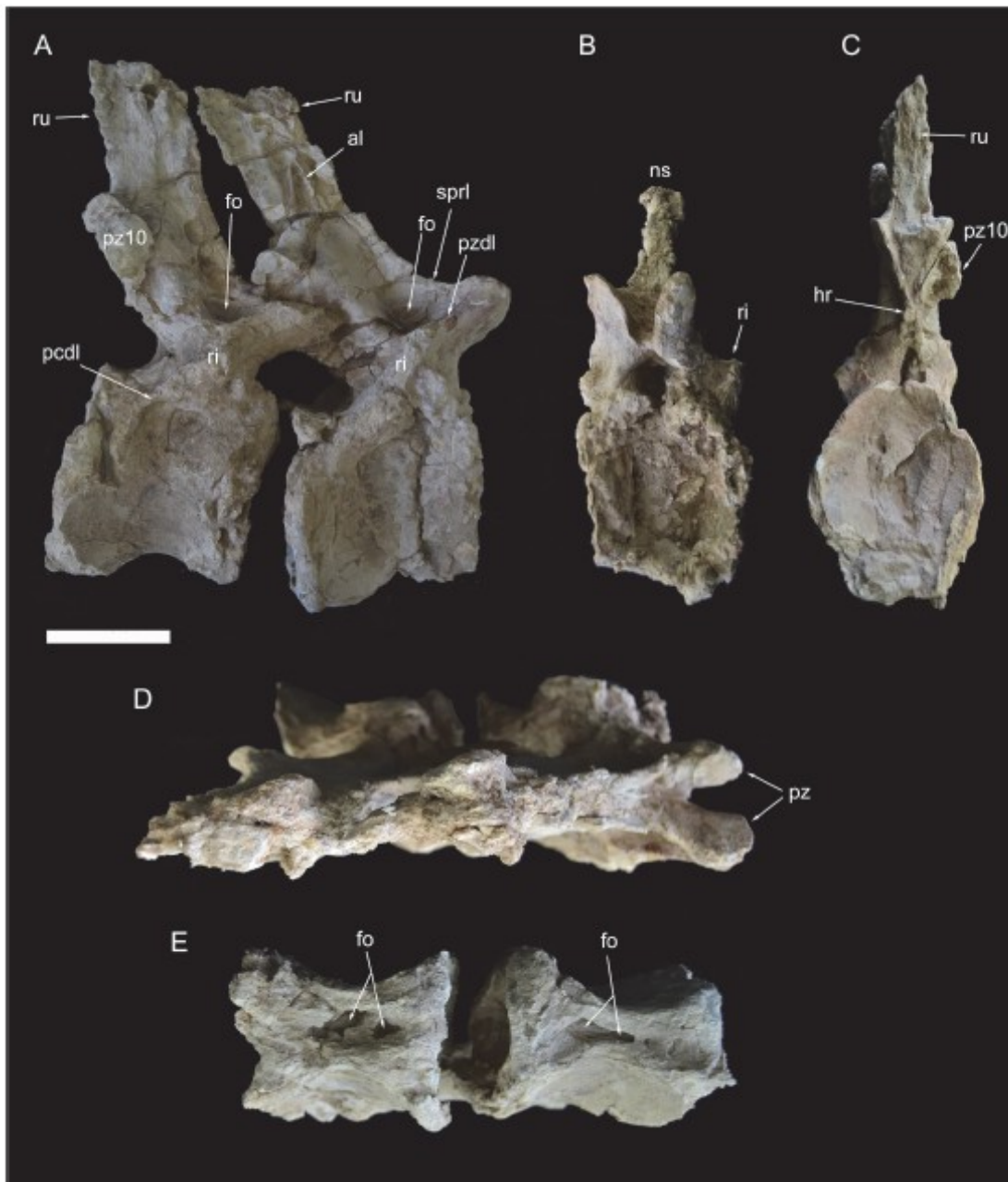


Figure 11. **Caudal vertebrae 8 and 9 of *Tataouinea hannibalis*.** Vertebrae in right lateral (A), proximal (B), distal (C), dorsal (D) and ventral (E) views. Scale bar: 10 cm. Abbreviations: al, accessory laminae; fo, fossa; hr, hyposphenal ridge; ns, neural spine; pcdl, posterior centrodiapophyseal lamina; pz, prezygapophysis; pz10, fragment of caudal 10 right prezygapophysis; pzdl, prezygodiapophyseal lamina; ri, ribs; ru, interspinal rugosity; sprl, spinoprezygapophyseal lamina.

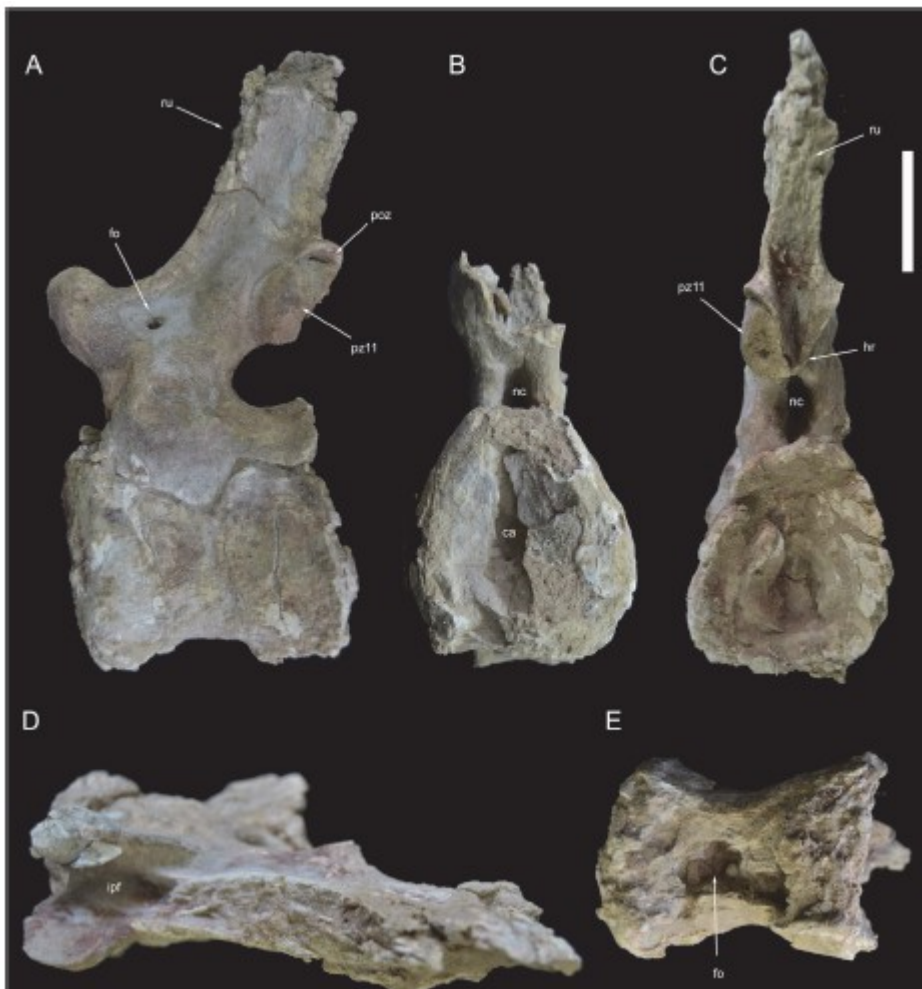


Figure 12. **Caudal vertebra 10 of *Tataouinea hannibalis***. Vertebra in left lateral (A), proximal (B), distal (C), dorsal (D) and ventral (E) views. Scale bar: 10 cm. Abbreviations: fo, fossa; hr, hyposphenal ridge; ipf, interprezygapophyseal fossa; nc, neural canal; poz, postzygapophysis; pz11, fragment of caudal 11 left prezygapophysis; ru, rugosities.

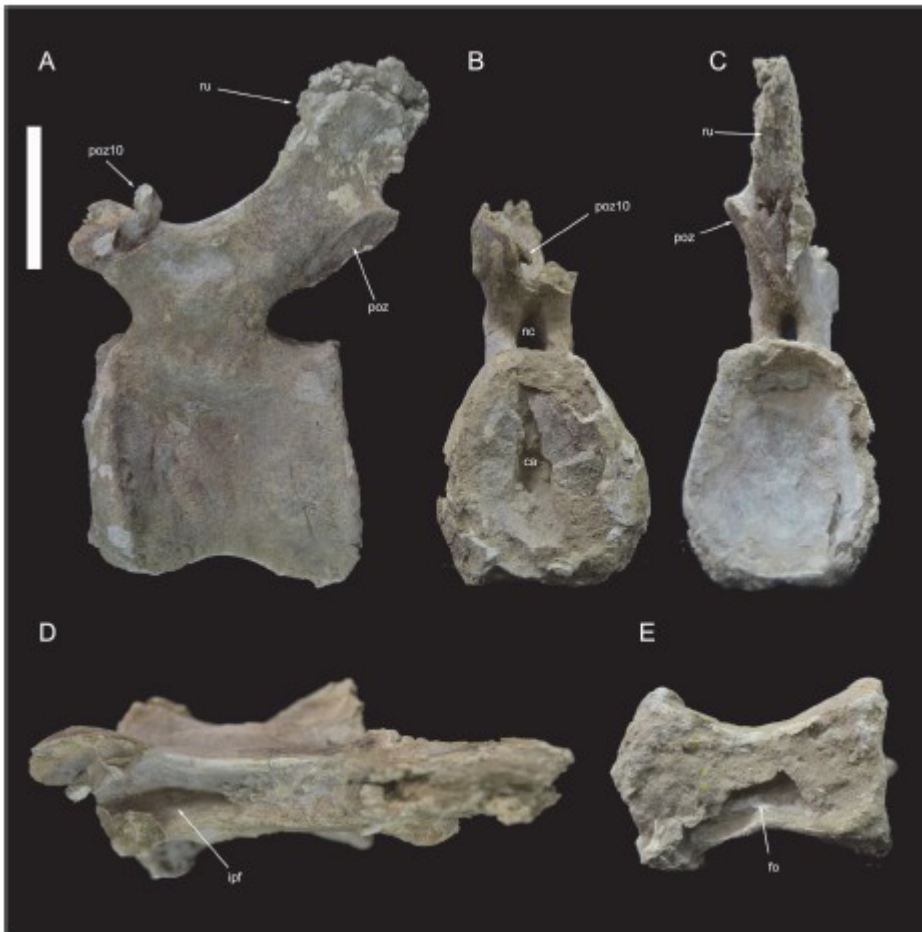


Figure 13. **Caudal vertebra 11 of *Tataouinea hannibalis***. Vertebra in left lateral (A), proximal (B), distal (C), dorsal (D) and ventral (E) views. Scale bar: 10 cm. Abbreviation: ca, camerae; fo, fossa; ipf, interprezygapophyseal fossa; nc, neural canal; poz, postzygapophysis; poz10, fragment of caudal 10 right postzygapophysis; ru, rugosities.

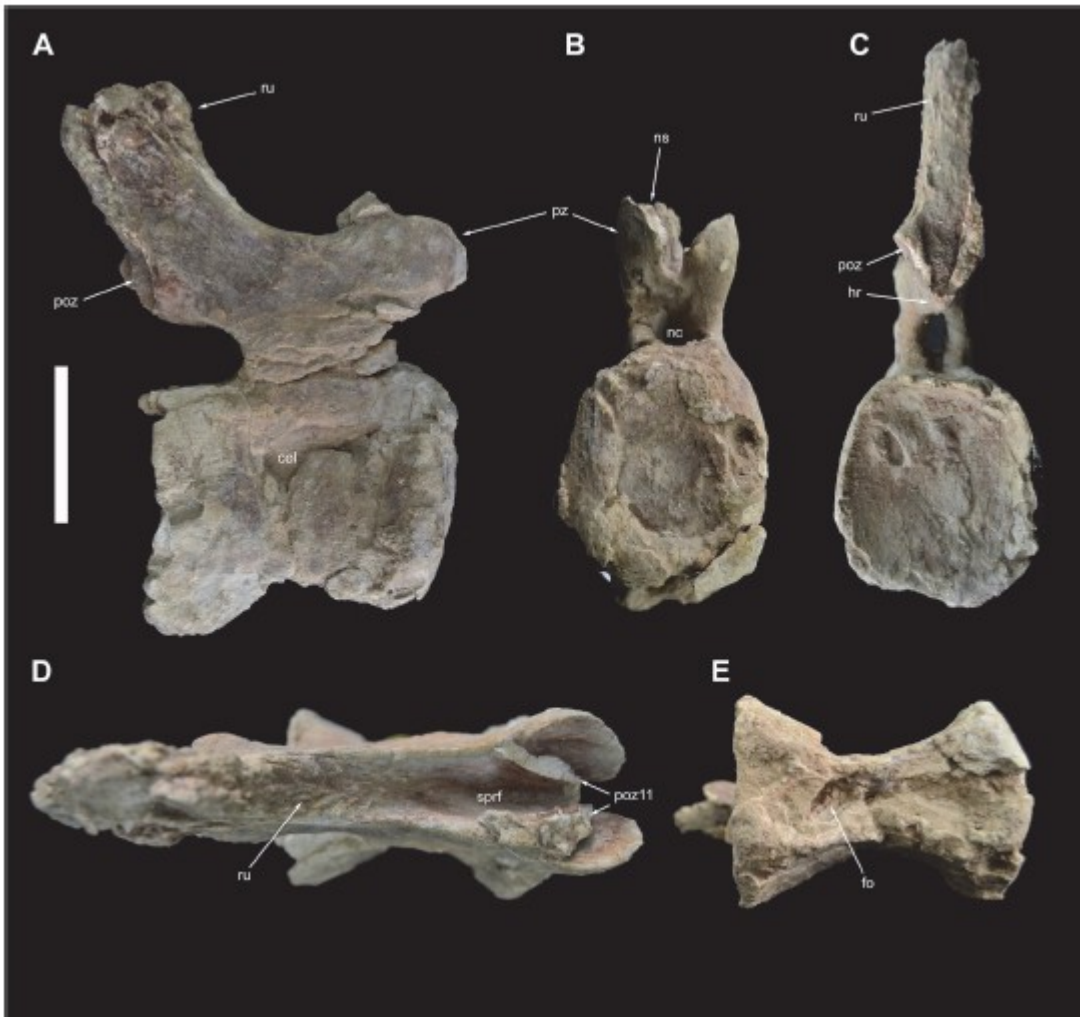


Figure 14. **Caudal vertebra 12 of *Tataouinea hannibalis***. Vertebra in right lateral (A), proximal (B), distal (C), dorsal (D) and ventral (E) views. Scale bar: 10 cm. Abbreviation: fo, fossa; hr, hyposphenal ridge; nc, neural canal; ns, neural spine; poz, postzygapophysis; poz11, fragment of caudal 11 postzygapophysis; pz, prezygapophysis; ru, rugosities; sprf, spinoprezygapophyseal fossa.



Figure 15. **Caudal vertebrae 13 and 14 of *Tataouinea hannibalis***. Vertebrae in right lateral (A), proximal (B), distal (C), dorsal (D) and ventral (E) views. Scale bar: 10 cm. Abbreviations: fo, fossa; hr, hyposphenal ridge; ns, neural spine; poz, postzygapophysis; pz, prezygapophysis; ru, rugosities; sprf, spinoprezygapophyseal fossa.

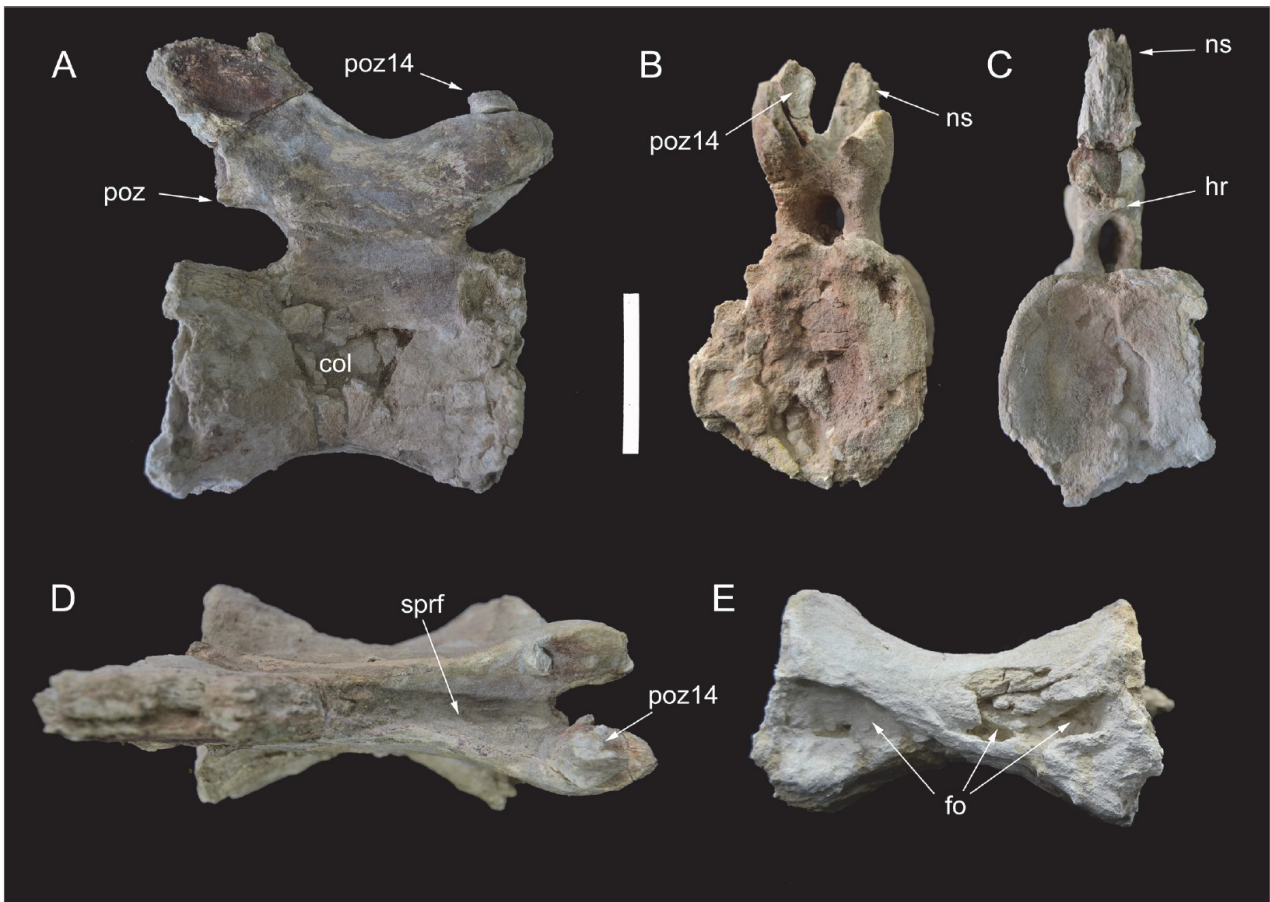


Figure 16. **Caudal vertebra 15 of *Tataouionea hannibalis***. Vertebra in right lateral (A), proximal (B), distal (C), dorsal (D) and ventral (E) views. Scale bar: 10 cm. Abbreviations: col, collapsed area; fo, fossa; hr, hyposphenal ridge; ns, neural spine; poz, postzygapophysis; poz14, right caudal 14 postzygapophysis fragment; sprf, spinoprezygapophyseal fossa;

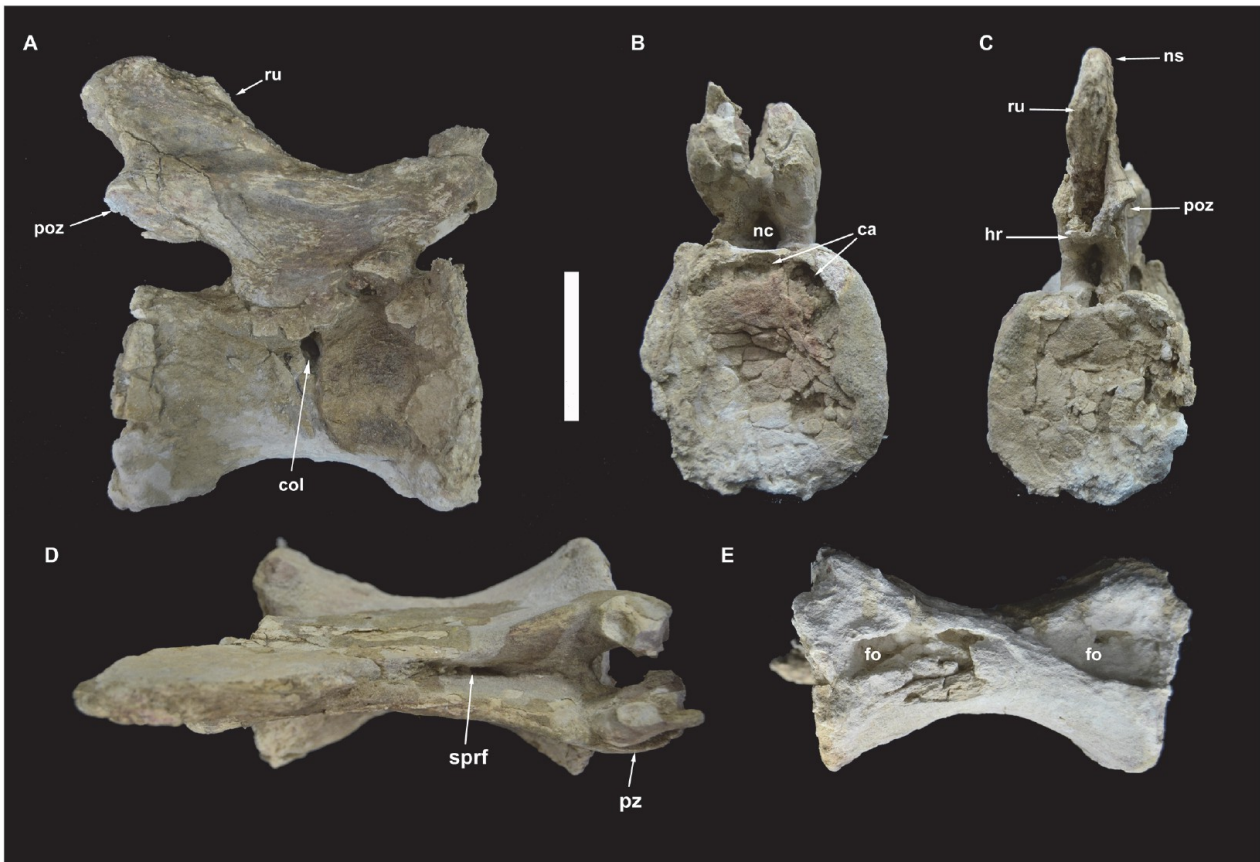


Figure 17. **Caudal vertebra 16 of *Tataouinea hannibalis***. Vertebra in right lateral (A), proximal (B), distal (C), dorsal (D) and ventral (E) views. Scale bar: 10 cm. Abbreviations: ca, camerae; col, collapsed area; fo, fossae; hr, hyposphenal ridge; nc, neural canal; ns, neural spine; poz, postzygapophysis; pz, prezygapophysis; ru, rugosities.

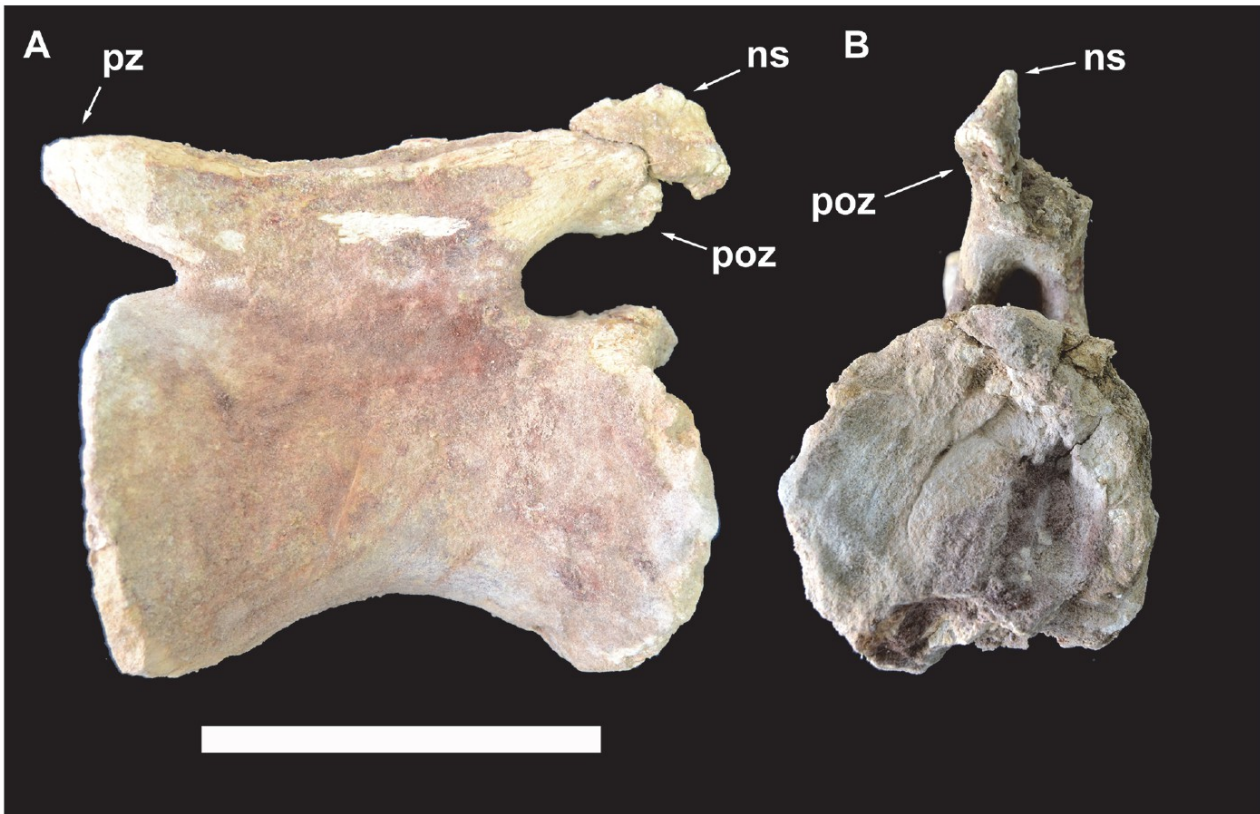


Figure 18. **Caudal vertebra 17 of *Tataouinea hannibalis***. Vertebra in left lateral (A) and distal (B) views. Scale bar: 10 cm. Abbreviations: ns, neural spine; poz, postzygapophysis; pz, prezygapophysis.

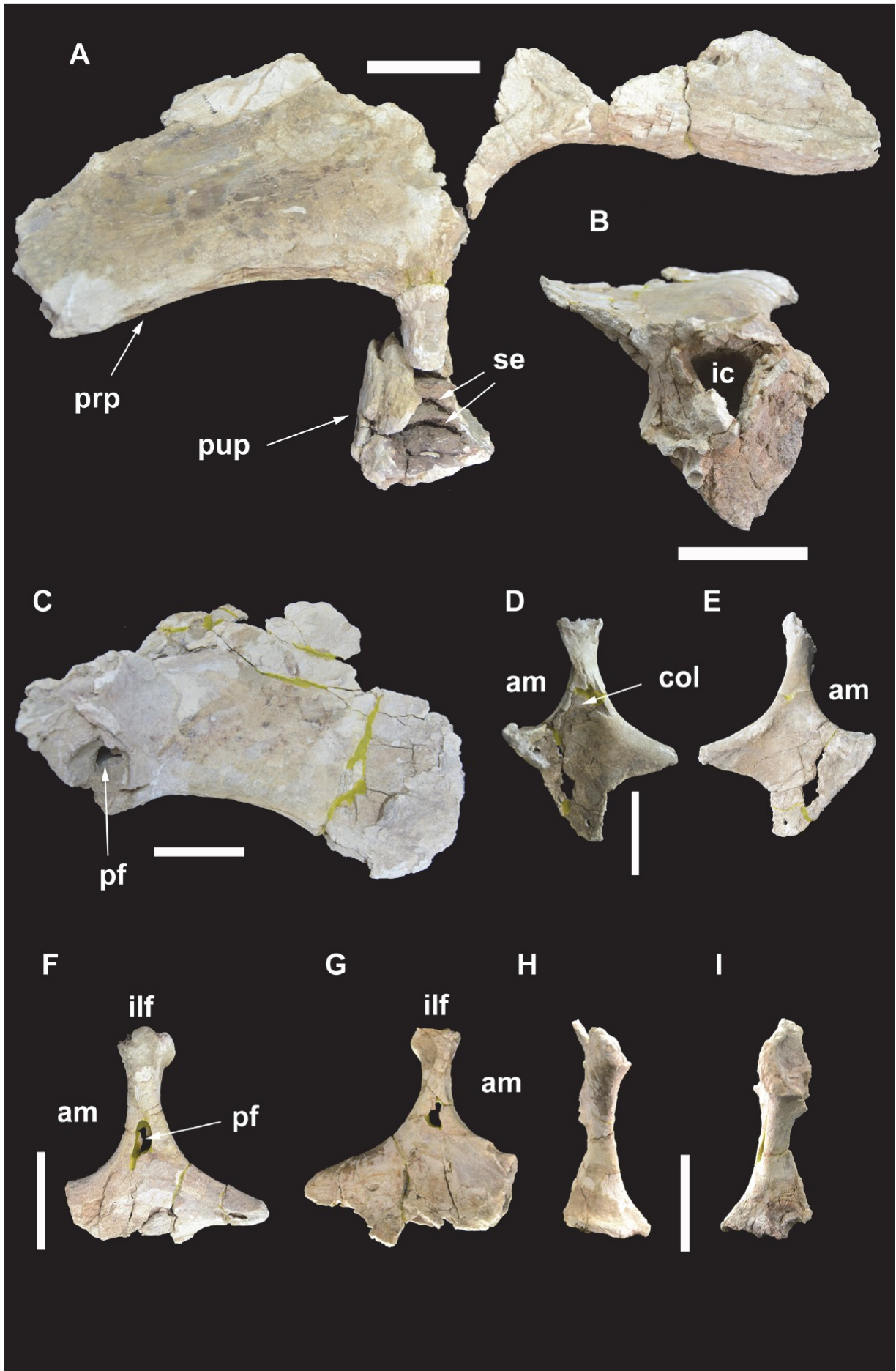


Figure 19. **Pelvic elements of *Tataouinea hannibalis***. Left ilium in lateral view (A). Left pubic peduncle in distal/ventral view (B). Right preacetabular process of ilium in lateral view (C). Right ischium in medial (D) and lateral (E) views. Left ischium in lateral (F) and medial (G) views. Right ischium in proximal (acetabular) view (H). Left ischium in proximal (acetabular) view (I). Scale bar: 10 cm. Abbreviations: am, acetabular margin; col, collapsed area; ic, internal chamber; ilf, iliac facet; pf, pneumatic foramen; prp, preacetabular process; pup, pubic peduncle; se, septa.

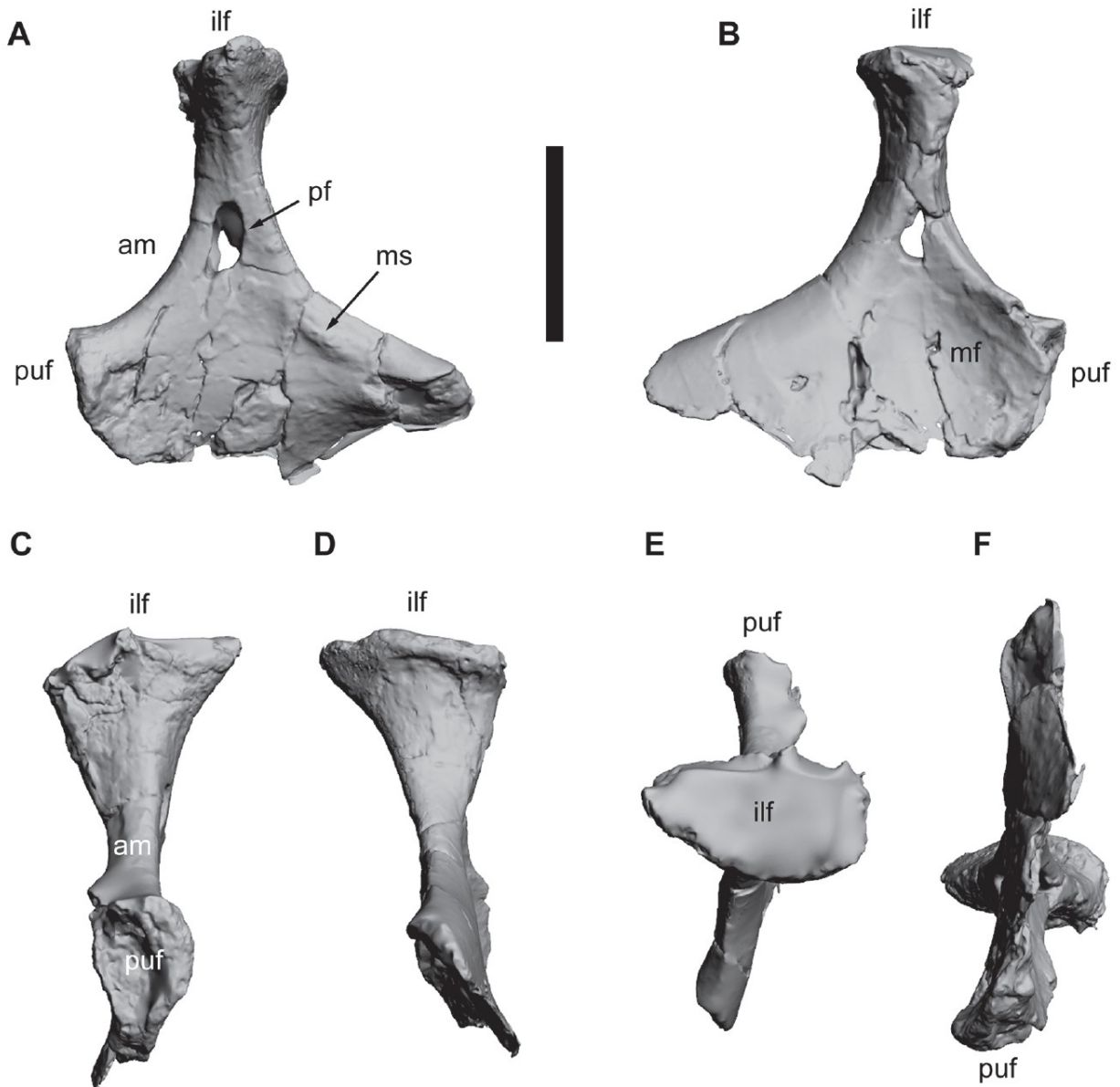


Figure 20. **Left ischium of *Tataouinea hannibalis***. Ischium in lateral (A), medial (B), cranial (C), caudal (D), proximal/dorsal (E), distal/ventral (F) views. Scale bar: 10 cm. Abbreviations: am, acetabular margin; ilf, iliac facet; mf, medial fossa; ms, muscle scar; pf, pneumatic foramen; puf, pubic facet.



Figure 21. **Phylogenetic relationships among rebbachisaurids.** Strict consensus topology under equal weighting (A) and under implied weighting (B) of the shortest trees recovered by the parsimony analyses of the dataset. Numbers adjacent to nodes in the equally weighted analysis tree indicate Decay Index values >1.

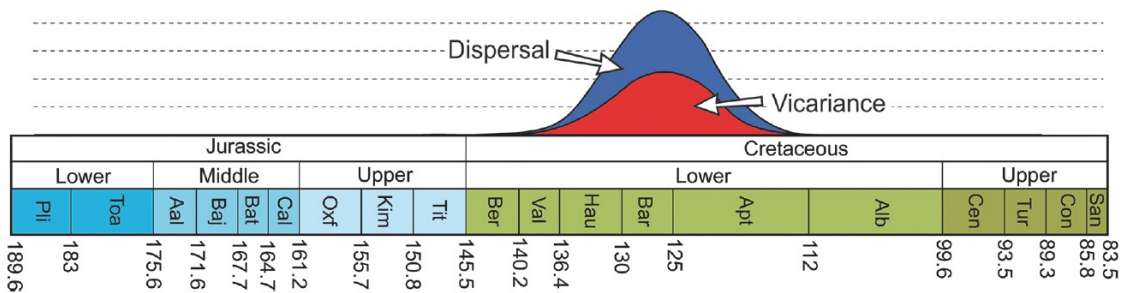
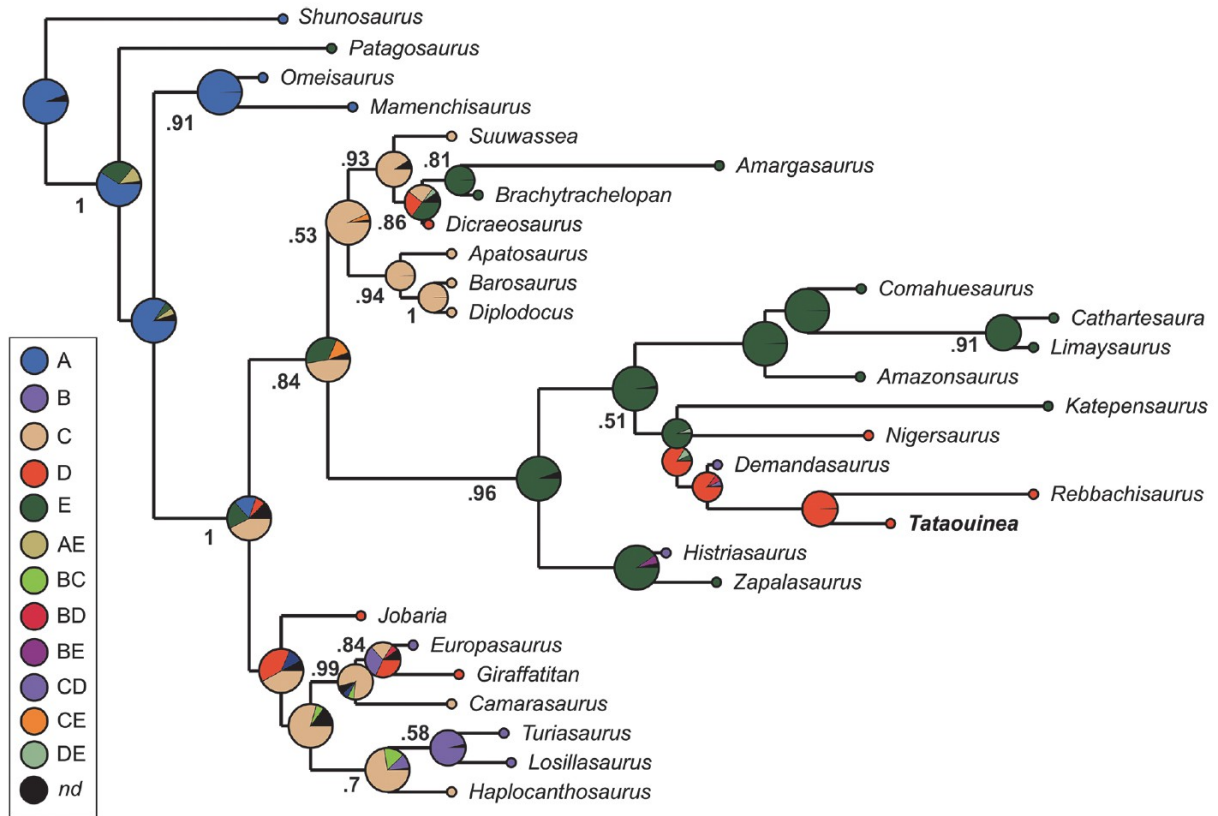


Figure 22. **BBM palaeogeographic analysis of Rebbachisauridae.** Time-calibrated palaeobiogeography of eusauropods focusing on rebbachisaurids (above) and result of the time-event algorithm test on Rebbachisauridae (below), based on the BBM analysis of the MCCT recovered by Bayesian inference. Values at nodes indicate posterior probability values >0.5. Abbreviations: A, Asia; B, Europe; C, North America; D, Africa; E, South America. Black circles indicate uncertain optimization.

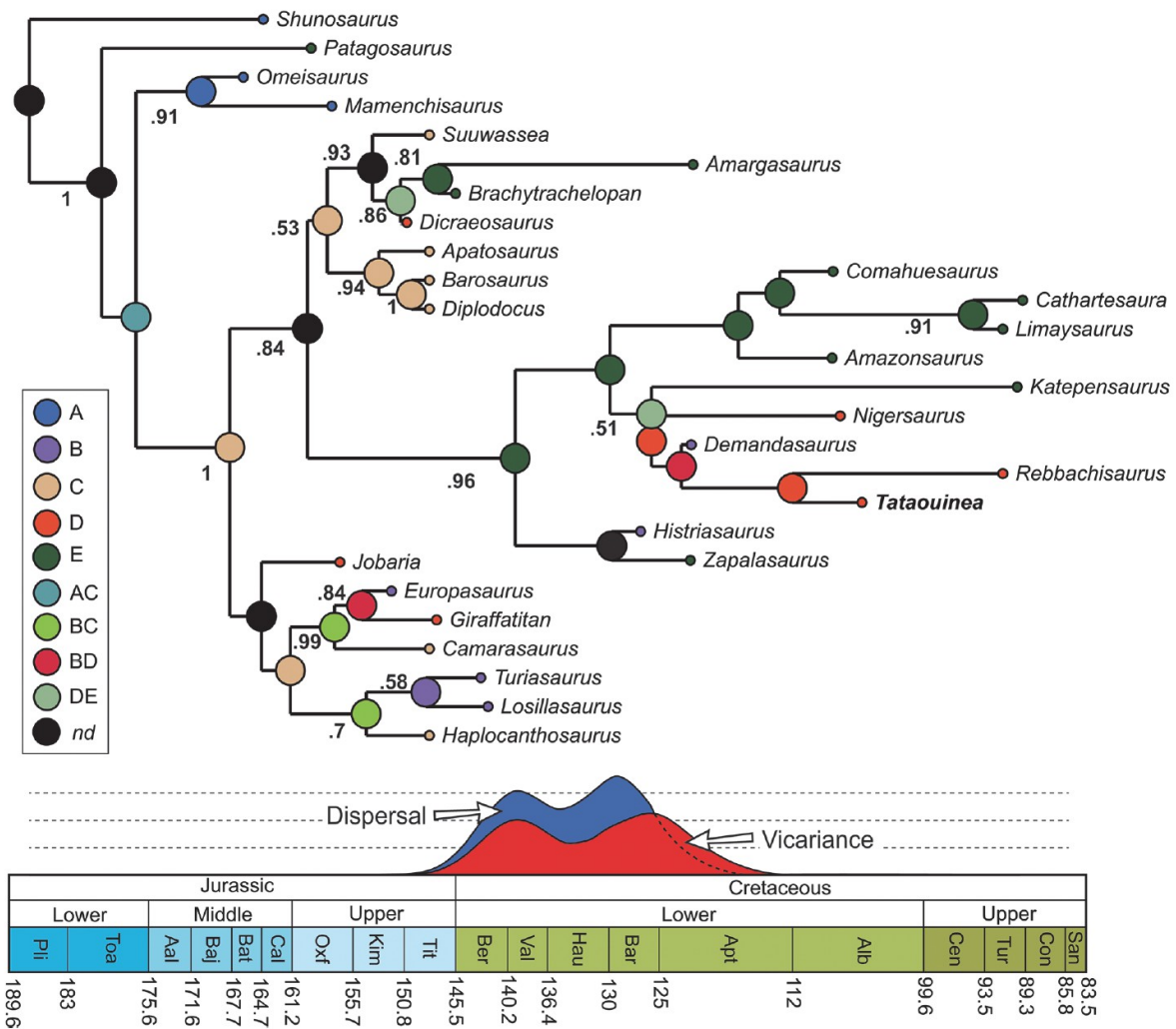


Figure 23. **S-DIVA palaeogeographic analysis of Rebbachisauridae.** Time-calibrated palaeobiogeography of eusauropods focusing on rebbachisaurids (above) and result of the time-event algorithm test on Rebbachisauridae (below), based on the S-DIVA analysis of the MCCT recovered by Bayesian inference. Values at nodes indicate posterior probability values >0.5. Abbreviations: A, Asia; B, Europe; C, North America; D, Africa; E, South America. Black circles indicate uncertain optimization.

Page left blank

## **CHAPTER 8 - The largest thalattosuchian (Crocodylomorpha) supports teleosaurid survival across the Jurassic-Cretaceous boundary**

Submitted: 18<sup>th</sup> July 2015. Published: 10<sup>th</sup> January 2016 in *Cretaceous Research* vol. 61:263-274.

Federico Fanti, Tetsuto Miyashita, Luigi Cantelli, Fawsi Mnasri, Jihed Dridi, Michela Contessi, Andrea Cau\*

\*Corresponding author

### **Abstract**

A new teleosaurid from the Lower Cretaceous of Tataouine (Tunisia), *Machimosaurus rex* sp. nov., definitively falsifies that these crocodylomorphs faced extinction at the end of the Jurassic. Phylogenetic analysis supports its placement closer to *M. hugii* and *M. mosae* than *M. buffetauti*. With the skull length up to 160 cm and an estimated body length of 10 m, *M. rex* results the largest known thalattosuchian, and the largest known crocodylomorph at its time. This giant crocodylomorph probably was an ambush predator in the lagoonal environments that characterized the Tethyan margin of Africa during the earliest Cretaceous. Whether the Jurassic-Cretaceous mass extinction was real or artefact is debated. The discovery of *M. rex* supports that the end-Jurassic crisis affected primarily Laurasian biota and its purported magnitude is most likely biased by the incomplete Gondwanan fossil record. The faunal turnovers during the J-K transition are likely interpreted as local extinction events, triggered by regional ecological factors, and survival of widely-distributed and eurytypic forms by means of habitat tracking.

**Keywords:** Lower Cretaceous; *Machimosaurus*; Teleosauridae; Thalattosuchia; Tunisia

### **1. Introduction**

The Jurassic-Cretaceous (J-K) transition has been considered a complex phase of global extinctions in both terrestrial and marine faunas, which affected rates of lineage diversification and morphological evolution during the Early Cretaceous (Bakker, 1978, 1998; Sepkoski, 1984; Bardet, 1994; Benton, 2001; Upchurch, 2005; Lu et al., 2006; Benson et al., 2010). Whether this event was real (i.e., a complex combination of clade-specific extinction patterns driven by physical and biotic factors) or represents an artefact remains unresolved (Gasparini et al., 2004; Bambach, 2006; Benson et al., 2010; Ruban, 2012; Newham et al., 2014). Among speciose clades of Jurassic marine reptiles, teleosauroid crocodylomorphs stand as the sole that supposedly went extinct at the Jurassic-Cretaceous boundary (Young et al., 2014a), with all purported Cretaceous remains re-interpreted as belonging to other reptilian clades, in particular, to the other thalattosuchian clade, Metriorhynchoidea (Young et al., 2014a,b). From a palaeogeographic perspective, Teleosauroidea is known largely from Europe (Vignaud, 1995), with Gondwanan remains rare, often limited to problematic or extremely fragmentary specimens (e.g., Martin et al., *in press*; Young et al., 2014a).

In December 2014, the articulated remains of a giant crocodylomorph were found during prospecting activities at the Touil el Mhahir locality, Tataouine Governorate, Tunisia (Figs. 1, 2). In this study, we describe this new specimen and determine its affinities and stratigraphic placement. The results of our analyses support the erection of a new species of thalattosuchian teleosaurid, *Machimosaurus rex*. Furthermore, we discuss the implications of this new African taxon in the debate on the end-Jurassic biotic crisis.

## 2. Material and Methods

Specimens collected at the Touil el Mhahir locality in 2014 are housed in the Musée de l'Office National Des Mines (Ministère de l'Industrie et de la Technologie, Tunis), under the accession numbers ONM NG 1–25, 80, 81, and 83–87. Microvertebrate fossils, field notes and locality coordinates, and the 3D data are housed at the Museo Geologico Giovanni Capellini (MGGC, Bologna, Italy). Assemblage data were interpreted from the final quarry map as well as from field notes: all elements were mapped using a 1m<sup>2</sup> grid box. Following the discovery of small elements from the surface of the outcrop, a total of 2.5 kg of sandy and clayish sediments were collected from both the excavation site and

the matrix surrounding the skull for screen washing. Samples were soaked with water and H<sub>2</sub>O<sub>2</sub> (5%) and screened using progressive sieves of 1mm, 200 µm, and 63 µm. With 100% of collected matrix screened and sorted, a total of 231 specimens were identified. The collected specimens were primarily identified and compared with those described and illustrated by Cuny (2004), Cuny et al. (2010) (Early Cretaceous of southern Tunisia), and Pouech et al. (2015) (Berriasian of France). Furthermore, during the preparation of the skull, four displaced osteoderms lying slightly imbricated on the snout were recovered and prepared (ONM NG 14-17).

## 2.1 Taxonomy

The taxonomic content of the genus-level ranked clade *Machimosaurus* von Meyer, 1837, is controversial. Young et al. (2014a, b) recognised four species of *Machimosaurus*: *M. buffetauti* Young et al., 2014b, *M. hugii* von Meyer, 1837, *M. mosae* Sauvage and Liénard, 1879, (all from Europe) and *M. nowackianus* (von Huene, 1938) (from Ethiopia). Martin et al. (*in press*) challenged the distinction among the first three species suggested by Young et al. (2014a, b), referring all European *Machimosaurus* to *M. hugii*, and considered *M. nowackianus* as a *nomen dubium*. We follow the distinction among the species of *Machimosaurus* as suggested by Young et al. (2014b) since both morphological and stratigraphic disparities among the three European morphotypes support a species-level distinction among them, and tested whether the inclusion of the new Tunisian material in a phylogenetic analysis of Teleosauroidea further supports or challenges a taxonomic distinction among the European *Machimosaurus*.

## 2.2 Phylogenetic analysis of *Thalattosuchia*

In order to analyse the evolutionary affinities of the Tunisian thalattosuchian, we performed Bayesian inference methods integrating the morphological and stratigraphic data with BEAST (Drummond et al., 2012; Rambaut and Drummond, 2009) following the method of Lee et al. (2014). The morphological dataset is based on Young (2014) and modified by Cau (2014) after the *a priori* exclusion of all non-thalattosuchian taxa. As branch duration estimation and cladogenesis timing using Bayesian inference requires sampling among both constant characters and autapomorphies of terminal taxa – not solely among synapomorphies of internodes (Lee et al., 2014) – we retained all characters

of the dataset of Young (2014), including those resulted phylogenetically uninformative by the *a priori* removal of most crocodyliform taxa from the ingroup. The ingroup was consequently expanded by the inclusion of *Machimosaurus buffetauti* (based on Martin and Vincent, 2013, and Young et al., 2014b) and the new Tunisian thalattosuchian. One Triassic pseudosuchian closely related to Crocodylomorpha (*Postosuchus* Chatterjee, 1985) and one basal crocodyliform (*Protosuchus* Brown, 1934) were used as outgroups – with the former set as root of the trees – according to the recent revision of thalattosuchian affinities by Wilberg (*in press*) indicating a non-crocodyliform placement for Thalattosuchia. Stratigraphic data and age constraints for each terminal were obtained primarily from the Paleobiology Database (<http://paleobiodb.org/>) and from the literature, using provided geochronological ages for the formations in which the taxa were found or the mean of the geologic stages associated with those formations. The root age prior (i.e., the maximum age of the last common ancestor of all included taxa) was set along a uniform range between 218 Mya (the age of the oldest terminal included, *Postosuchus*) and 252 Mya (the Permian-Triassic boundary). The latter was considered as a 'loose' hard constraint that consistently pre-dates the age of the oldest potential crocodylomorphs and basal loricatans. In the analysis, rate variation across traits was modelled using the gamma parameter, and rate variation across branches was modelled using an uncorrelated relaxed clock. The analyses used four replicate runs of 40 million generations, with sampling every 4000 generations. Burnin was set at 20%, and the Maximum Clade Credibility Tree (MCCT) of the merged four post-burnin samples was used as framework for phyletic reconstruction.

### 2.3 3D photogrammetry and modelling

During the last decade, the development of Structure from Motion (SFM) techniques has been dramatically improved allowing accurate reconstruction of 3D structures processing 2D images (Trucco, 1998; Koenderink, 1991; Beardsley, 1996; Dellaert, 2000; Haming, 2010; Fanti et al., 2013; Engel, 2014; Fanti et al., 2015). We acquired digital models of the *Machimosaurus* quarry, the skull (both dorsal and ventral views), and the prepared dorsal vertebrae, using high-resolution photogrammetry. We used Agisoft PhotoScan Professional, and Meshlab for this technique. The models were built as in the

following procedure: 1. positioning of coded targets so that 70% of photos frame at least one target (actual distances between targets will serve to include accurate measurement tools in the model); 2. proper preparation of the light so that variations in the enlightenment are minimal; 3. prearrangement of a photo-shooting path. In order to properly perform the metric reconstruction in the 3D model, it was mandatory to work with a camera with a fixed focal length lens. The lens profile for Agisoft Photoscan was set using the software Agisoft lens. Automatic check of images verified the complete coverage of selected objects before proceeding with the alignment of frames that originated the first point cloud based on corresponding points recognized in different photos. Once the consistency of the generated surface were verified, a photographic texture was generated.

### 3. Stratigraphy and age

The Touil el Mhahir locality (the exact locality data can be obtained upon request) is located less than 50 km to the south-west of the city of Tataouine and about 25 km to the north-west of Remada (Fig. 1). Substantial erosion resulted in a badland-like morphology that exposed the basal beds of the Douiret Formation, and in particular of the Douiret Sand Member. In the Tataouine Basin, the Douiret Formation uncoformably overlays the Boulouha Formation which has been assessed a Barremian age based on the occurrence of the Cretaceous brachiopod *Loriolithyris russillensis* (De Loriol, 1866), in the upper beds of the unit (Peybernes et al., 1996; Ouaja et al., 2004; Bodin et al., 2010). However, recent re-evaluation of stratigraphic and biostratigraphic data in southern Tunisia and western Lybia (Cuny, 2010; Le Loeuff et al., 2010; Fanti et al., 2012) placed the lower, sandy deposits of the Douiret Formation in the Barremian. Specifically, the age of the Douiret Formation has been assessed primarily through a detailed, basin-scale revision of the stratigraphic occurrence and lateral variability of fossil-bearing strata (Fanti et al., 2012). The occurrence of the hibodontid *Egertenodus* Maisey, 1987, and *Gyrodus* Agassiz, 1833, in the Douiret Formation supports an Hauterivian-Barremian age for this unit. In fact, Rees and Underwood (2008) indicate the latest ascertain record of *Egertenodus* in the Barremian of Spain, and Kriwet and Schmitz (2005) note the youngest record of *Gyrodus* in the Hauterivian of Germany. Therefore, although a pre-Hauterivian age of the lower Douiret beds cannot be excluded, based on 1) the Early Cretaceous age of the Boulouha

Formation, and 2) stratigraphic and biostratigraphic data provided by Cuny et al. (2010), Le Loeuff et al. (2012), and Fanti et al. (2012), we conservatively consider the age of the Touil el Mhahir locality as Hauterivian-Barremian.

The deposits are characterized by repeating, fining-up sequences of fine-grained sand and clay, capped by an alternating sequence of clay and dolostone or dolomitized sandstone. The *M. rex* quarry is located approximately 20 meters above the fossil-rich conglomerate that, on a basin scale, marks the base of the Douiret Formation (Fanti et al., 2012). Furthermore, we report isolated teeth of *Machimosaurus* sp. occurring in several localities from the Douiret Formation deposits along the Dahar Escarpment (i.e. El Hmama, Jebel Haddada, Boulouha localities; Fanti et al., 2012) of southern Tunisia, supporting that this genus is a representative of this formation.

#### 4. Taphonomy and Paleoecology

The type specimen of *Machimosaurus rex* represents the first articulated vertebrate from the Douiret Formation and the second Mesozoic archosaur skeleton collected in Tunisia (Fanti et al., 2012, 2013, 2015). The skeleton lies on its ventral side with the head rotated clockwise toward the right side of the body (Figs. 2-4). Only three teeth were found preserved in the alveoli (Fig. 5), whereas seven were shed along the snout. Although preserved elements show no evidence of major pre-burial transportation (Figs. 2-8A), the overall posture (i.e. the body lying on its ventral side and the head curved on the right side of the body) combined with displacement of osteoderms and the missing anterior end of the snout strongly suggest that there was some influence from paleocurrents (paleoflow from the south-east). In addition, the right side of the skull is laterally compressed (see also the taphonomic model of Syme and Salisbury, 2014). The dorsal part of the skeleton was found partially eroded with the exception of the skull, which lay slightly below ground level. Large turtle plastron elements were collected near the skull (Fig. 7E). The skull, two dorsal vertebrae, several dorsal rib and gastralia fragments, a partial humerus and osteoderms were collected during the excavation. The remaining part of the quarry was mapped and isolated elements littering the ground were collected.

The *M. rex* holotype was collected in association with abundant, disarticulated elements from large turtle carapaces, plastrons and vertebrae. The largest turtle elements,

including a 25 cm long hyoplastron associated with the skeleton (Fig. 7E), suggest an individual close to one meter in body length. Because most of the turtle elements were slightly above the type skeleton of *M. rex*, these elements can be attributed to a subsequent depositional event. Microvertebrate remains are representative of brackish and marine taxa and include elasmobranchs, actinopterygians, dipnoans and rare pterosaur teeth. Bivalves, gastropods, fragmentary echinoids shell and spines, and scaphopods are also abundant.

In terms of relative percentage, fish elements (teeth, scales and centra) represent 71% of the isolated elements; crocodylian (teeth and osteoderms) 10%; invertebrates (gastropods, bivalves, and echinoderms) 4%; elasmobranchs 3%; and the remaining 12% consists of unidentifiable bony elements and teeth. Significantly, several teeth less than 5 mm in apicobasal length and a 4 mm wide osteoderm are otherwise morphologically similar to those described for *Machimosaurus*; the teeth are referred to the latter taxon based on shared presence of blunt apex and anastomosing apicobasal ridges on tooth crown. In addition, a partial dentary with *in situ* teeth referable to a juvenile individual of *Machimosaurus* was recovered in association with the type skull of *M. rex*. Prospecting activities in the area revealed the presence of four additional crocodylomorph individuals comparable in size and overall preservation to the *M. rex* holotype within 200 m from the main quarry.

The lower beds of the Douiret Formation are also rich in megaplant remains, including large gypsified and sporadic hematized trunks reaching 8 meters in length. Remarkable fossil abundance in the area and recurrent tree trunks indicate high rates of sediment supply and accumulation: however, the lack of *in situ* plant roots and organic components in the sediments combined with gypsified fossils and dolomitized sandstones indicate arid to xeric environments subject to evaporitic conditions. Overall, *facies* analysis and faunal assemblage are interpreted as a vast lagoonal system with both marine and terrestrial influences.

## 5. Systematic Paleontology

Crocodylomorpha Hay, 1930

Thalattosuchia Fraas, 1901

Teleosauridae Geoffroy, 1831

*Machimosaurus* von Meyer, 1837

*Machimosaurus rex* sp. nov.

(ZooBank code: LSID urn:lsid:zoobank.org:act:1A11E9B9-0B1C-4557-92B7-165168658C17)

### 5.1. Etymology

The species name *rex*, Latin for “king”, refers to its majestic size among known *Machimosaurus* and all thalattosuchians.

### 5.2. Holotype

ONM NG NG 1–25, 80, 81, and 83-87 (Figs. 2-7D; Table 1).

### 5.3. Locality and Horizon

Touil el Mhahir, Tataouine Governorate, Tunisia; Douiret Sand Member, Douiret Formation, Hauterivian, Lower Cretaceous.

### 5.4. Diagnosis

Teleosaurid differing from other species by unique combination of: adult basicranial length >155 cm (Fig. 5); rostrum ornamented by densely arranged, parallel longitudinal ridges; orbit elliptical; interorbital space narrow (one fifth length of skull posterior to orbit); anteromedial margin of supratemporal fossae round; frontal not extended anteriorly to orbit and with reduced orbital margin; relatively large maxillary alveoli; anterior dorsal neural spine height less than centrum height; dorsal osteoderms with tightly packed pits that are round centrally and ellipsoid peripherally.

### 5.5 Differential diagnosis

Among the genus *Machimosaurus* (Fig. 8), *M. rex* differs from *M. buffetauti* (Fig. 8A) in having relatively larger and more closely spaced alveoli, and in bearing apicobasally aligned enamel ridges immediately adjacent to the apical anastomosed region of crown teeth that are closely packed on both labial and lingual sides; from *M. hugii* (Fig. 8C) in showing more developed ornamentation on maxillae and nasals, elliptical orbits, narrower interorbital space, and dorsal osteoderms with more closely spaced pits that become more

elongate peripherally; from *M. mosae* (Fig. 8B) in bearing elliptical orbits and shallower and unkeeled ventral osteoderms. There is currently no overlapping material between *M. nowackianus* and *M. rex* for a direct morphological comparison. Although stratigraphic placement alone cannot be used as a taxonomic criterion, based on stratigraphic separation between the two type localities of *M. nowackianus* and *M. rex* (the former is Oxfordian-Kimmeridgian in age, see Young et al., 2014b), we consider likely these two African species as distinct.

## 6. Description of *Machimosaurus rex* type specimen

### 6.1 Skull and mandible (Figs. 3-7A)

The anterior end of the snout is missing. Based on comparison with other specimens of *Machimosaurus* (Hua, 1999; Martin and Vincent, 2013; Young et al., 2014a, b), we estimate that approximately posterior two thirds of the maxillae are intact. The preserved parts are ornamented with a dense pattern of lightly developed longitudinal ridges (Fig. 5A). Eight alveoli are preserved in the right maxilla (Fig. 5C). They are relatively large, their diameter being up to one sixth of snout width, and are closely spaced (Martin and Vincent, 2013; Young et al., 2014b). The interalveolar space is regular, as in the mid- and posterior part of the maxilla of *M. hugii* and *M. mosae*. The nasal is subtriangular in dorsal view and ornamented by a finely developed pattern of longitudinal ridges. It does not reach the narial region anteriorly. The periorbital region is poorly preserved, with only fragmentary prefrontals and lacrimals present. Nevertheless, the preserved outline indicates elliptical orbits, more like that in *M. buffetauti*, differing from the more quadrangular shape observed in both *M. hugii* and *M. mosae* (Young et al., 2014b). The lateral margins of the orbits are at the level of the anteromedial corners of the supratemporal fossae, relatively much closely placed than in *M. hugii* (Young et al., 2014b, fig. 41). The nasofrontal suture is at the level of the anterior margin of the orbit. The anterior end of the dorsal interfenestral bar is preserved, but most of the bar, including the parietal, is lost. The anterior margin of the supratemporal fossa is gently rounded. The posterior floor of the supratemporal fossae is partially preserved. The postorbital is robust and elongate posteriorly. Only the lateral part of both squamosals is preserved. The

occipital region of the skull is preserved in numerous fragments. Nevertheless, the occipital condyle was preserved *in situ*, allowing an accurate estimation of the preserved basicranial length. The occipital condyle (Fig. 7A) consists exclusively of the basioccipital, as in other species of *Machimosaurus* (Young et al., 2014b). The posterior ends of both dentaries are preserved in articulation with the postdentary bones. The external mandibular fenestra is elongate anteroposteriorly. Both the left and right surangulars are articulated with the glenoid region. The angulars are in fragments. The retroarticular processes are elongate posteriorly and triangular in dorsal view. The teeth (Fig. 6) have several diagnostic features for *Machimosaurus* (Young et al., 2014c). The relatively low crowns are blunt apically and slightly curved apicodistally. No carinae are present, suggesting that all preserved teeth belong to the posterior half of the tooth row. The crowns are ornamented with tightly packed ridges oriented apicobasally. As in *M. hugii*, and differing from *M. buffetauti* (Young et al., 2014c), these ridges are closely packed on both labial and lingual sides of the crown. The ridges are irregularly undulated, but not producing distinct pseudo-tubercles as in *M. hugii* (Young et al., 2014a, b). The ridges are anastomosed in the apical third of the crowns, forming a complex network as in other species of *Machimosaurus*. Most teeth show a distinct (macroscopical) apical wear.

## 6.2 Postcranial skeleton (Figs. 2, 7B-D)

The cervical series is poorly preserved. Few fragments of the atlas-axis complex were recovered adjacent to the occipital region of the skull. Two well-preserved anterior dorsal vertebrae have massive centra that are as wide as tall in anterior view (Fig. 7B). The articular facet of the centra are subcircular and moderately concave. The lateral surfaces of the centra are both dorsoventrally and anteroposteriorly concave, due to the marked lateral rims of the articular facets. The neural arch is transversely wide and low dorsoventrally and has closely joined diapophyses and parapophyses that are oriented subhorizontally. The parapophyses extend laterally to half the extent of the diapophyses, with their articular surfaces facing posterolaterally. The dorsal surface of the transverse process is anteroposteriorly convex. The ventrolateral surfaces of the neural arches are moderately concave centrally. The neurocentral suture is obliterated, suggesting a mature individual. The zygapophyses are stout and moderately projected anteroposteriorly, being placed lateral to the neural canal and medial to the centrum outline in anterior/posterior

views. The neural spine is robust, lower dorsoventrally than the height of the centrum and moderately expanded transversally at its apex. Several dorsal ribs and gastralia were found in articulation, although extremely fragmented.

Appendicular elements include fragments of the left forelimb, interpreted as the humeral shaft, and worn elements that, based on *in situ* placement posterior to the dorsal ribs series, are interpreted as belonging to the hindlimb.

### 6.3 Osteoderms (Figs. 7C, D)

Isolated osteoderms were found adjacent to the lower jaws. As the skull is turned backward relative to the presacral vertebral column, the osteoderms are interpreted as pertaining to the dorsal region. The osteoderms are quadrangular, with poorly developed anterolateral processes. Osteoderm ornamentation includes a tightly packed pattern of rounded pits in the central part of the dorsal surface, surrounded peripherally by radially elongate pits that reach the margin of the osteoderm; this pitting pattern differs from the more irregular pattern reported by Young et al. (2014b) for *Machimosaurus hugii*. Furthermore, none of the recovered osteoderms bears the marked thickening and the distinct keel both diagnostic of *Machimosaurus mosae* (Hua, 1999).

## 7. Results

### 7.1 Phylogenetic analysis

The MCCT of Thalattosuchia resulted by the Bayesian phylogenetic analysis (Fig. 9) agrees in overall topology with previous analyses of the same dataset using parsimony as tree search strategy (e.g., Young 2014). The analysis strongly supports the monophyly of *Machimosaurus* (posterior probability: 97%) and the inclusion of the new Tunisian taxon in that genus. *Machimosaurus buffetauti* resulted the basalmost member of the genus, excluded from the clade including *M. rex* and the other European species (posterior probability: 63%). The analysis therefore supports the distinction of *M. buffetauti* from other *Machimosaurus* suggested by Young et al. (2014a). Cladogenetic timing estimated by the Bayesian analysis places the divergence of the lineage leading to *M. rex* from the other *Machimosaurus* lineages at about 155 Mya.

## 8. Size of *Machimosaurus rex*

### 8.1 Skull length

The skull of the type specimen of *M. rex* lacks the anterior end of maxillae and the premaxillae. The basicranial length of the preserved skull is 114 cm, the length of the preserved skull from the anterior end to the left mandibular glenoid is 134 cm. The length of the skull from occiput to the anterior end of the orbits ('post-snout' length) is 65 cm. In a complete skull of *M. buffetauti* with a basicranial length of 93.5 cm (Kimmeridgian, Germany; Martin and Vincent, 2013; Fig. 8A), the equivalent part of the skull is 39 cm long (42% of basicranial length). In other specimens of *Machimosaurus*, the snout length of the skull is approximately 58% of the basicranial length, a value that is considered as an autapomorphy of *Machimosaurus* by (Hua, 1999; Young et al., 2014b; Fig. 8B). That implies a 'post-snout' length of about 42% of the skull length in this taxon (see also Martin and Vincent (2013), table 6). Assuming that the proportions of the complete skull of *M. rex* holotype were comparable to those observed in other *Machimosaurus* species, we estimate a minimum total basicranial length for the Tunisian taxon of 155 cm. Prior to this discovery, the largest size of *Machimosaurus* was based on a fragmentary skull of *M. hugii* (the "Leira specimen" of Young et al. 2014b, see Krebs (1967), Fig. 8C) with the basicranial length estimated between 141 cm (Hua, 1999) and 149 cm (Young et al., 2014b). Nevertheless, the "Leira specimen" lacks most of the orbital and temporal regions, and no measurements of the preserved elements are available, thus preventing any testable estimation of its actual size (see Krebs, 1967).

A comparison between the size of the alveoli in *M. rex* type specimen and other *Machimosaurus* individuals further supports the giant size of the Tunisian taxon. In the skull of *M. buffetauti* type specimen (Martin and Vincent, 2013), the mesiodistal diameter of the alveoli at mid-length of the maxilla is between 15 and 18 mm. In the neotype of *M. mosae*, the middle maxillary alveoli diameter ranges between 18 and 25 mm (Hua, 1999). In the type specimen of *M. rex*, the mesiodistal diameter of the middle maxillary alveoli ranges between 30 and 43 mm, a value 200% or more than those of *M. buffetauti* holotype, and about 166-173% larger than those in the *M. mosae* neotype. The latter range confirms that the basicranial length of the Tunisian specimen is at least 166% larger than that of the *M. mosae* neotype. Since the type skull of *M. rex* is also estimated about

165-170% the size of the *M. buffetauti* type skull (Martin and Vincent, 2013), the Tunisian species shows proportionally larger alveoli than in *M. buffetauti*.

## 8.2 Total body length

Young et al. (2014b) used the well-preserved neotype specimen of *M. mosae* to estimate the total body length of various specimens of *Machimosaurus* from their basicranial lengths, assuming a body length to basicranial length ratio of about 6.22. Assuming isometry among the various *Machimosaurus* individuals, and using the same relationships of Young et al. (2014b), the total body length of *M. rex* type is estimated at least as 9.6 m. Compared to the neotype of *M. mosae*, the alveoli in *M. rex* holotype are about 166% larger than the same element in the French specimen (Hua, 1999). Therefore, assuming isometry in body proportions, based on both cranial and dental comparisons with the best preserved specimen of *Machimosaurus mosae* (Hua, 1999) the total body length of the Tunisian individual is estimated at about 10 meters (166% of 6 meters, see Young et al., 2014b; Fig. 8E).

## 9. Discussion

### 9.1 Hypothetical lifestyle

The skull of *M. rex* bears a platyrostral snout, longitudinally oriented ornamentations on the skull roof, elongate subrectangular supratemporal fossae and blunt-crowned teeth with anastomosed apical enamel ornamentation (Figs. 1, 2), all synapomorphies of derived teleosaurids (Young et al., 2014b). With the skull length up to 160 cm and an estimated body length around 10 meters (Fig. 8E), the new Tunisian species is the largest known thalattosuchian, and was the largest known crocodylomorph from the Triassic until the Aptian-Albian (see Young et al., 2014b, Johnson et al., 2015). As in other *Machimosaurus* (in particular, *M. hugii*, Young et al., 2014b, c), the low-crowned, sub-globidont dentition of *M. rex* supports a generalist-durophagous feeding ecology. The abundance of turtle remains in the *M. rex* quarry, including large-bodied forms with length approaching one meter, suggests that chelonians were a significant part of the diet also in the Tunisian taxon.

Krebs (1969) and Hua (1999) discussed the hypothetical lifestyles of *M. hugii* and *M. mosae* respectively (see also the review by Young et al., 2014b). The former was interpreted as well-adapted to an open sea environment, whereas the latter resulted better adapted to high-energy, coastal conditions. Based on extant analogues among crocodylians showing an inverse relationships between dermal ornamentation and aquatic adaptation, the relatively reduced ornamentation in both skull roof and osteoderms of *Machimosaurus hugii* has been suggested as additional functional adaptation to a pelagic lifestyle (Young et al., 2014b). Similarly, the thick and keeled ventral osteoderms of *M. mosae* are interpreted as adaptations to a high-energy/turbulent environment (Hua, 1999; Young et al., 2014b). In *M. rex*, both skull roof ornamentation and extent of pitting on the osteoderms are more developed than in *M. hugii*. The relatively shallower osteoderms lacking a keel suggest that the Tunisian species was not adapted to a high-energy environment as that inferred for *M. mosae*. This interpretation is consistent with the paleoecology of the *M. rex* type locality (see above) indicating a lagoonal environment with significant terrestrial influences.

In analogy with modern semi-aquatic crocodylians, we suggest that *M. rex* was an ambush predator that preyed on both aquatic and terrestrial vertebrates. Since *Machimosaurus* bite marks on a sauropod dinosaur bone are already known (Young et al., 2014b), we predict that *M. rex* included mid- to large-bodied dinosaurs in its diet.

### 9.2. Implications for teleosaurid extinction

Unlike their survival into the Cretaceous of southern Tethys, teleosaurids did not cross the J-K boundary in the northern realm (Young et al., 2014a, b). The Late Jurassic species of *Machimosaurus* occur from Portugal to Germany to Ethiopia in lagoonal to shallow marine settings (Young et al., 2014b). These environmental conditions existed well into Cretaceous times in southern Tunisia, where lagoonal to tidal flats deposits straddle the J-K transition and dominate the Lower Cretaceous sedimentary successions (Benton, 2000; Barale and Ouaja, 2002; Ouaja et al., 2004; Anderson et al., 2007; Ouaja et al., 2011; Fanti et al., 2012). Conversely, the end-Jurassic transition in Europe is characterized by rapid climatic oscillations (alternation of 'greenhouse' conditions and cooling events) and concomitant extension of pelagic environments with dramatic loss of shallow marine and coastal ecosystems (Adatte, 1996; Cecca, 1999, 2001; Dromart et al.,

2003; Lécuyer, 2003; Cecca et al., 2005; Husinec and Jelaska, 2006; Ruban, 2011; Martin-Garin et al., 2012;). Reduction of these habitats most likely resulted in local extinction of teleosauroids across the J-K boundary of Europe. Among macropredatory marine reptiles, as many as nine ichthyosaurian, three plesiosaurian and at least four metriorhynchoid lineages crossed the J-K boundary, and morphological disparity of these clades maintained the pre-boundary levels through Early Cretaceous (Fischer et al., 2012, 2013, 2014; Benson and Druckenmiller, 2014; Young et al., 2014a; Chiarenza et al., 2015). Our study adds teleosauroids to the list of the reptilian lineages that crossed the Jurassic-Cretaceous boundary.

## 10. Conclusion

*Machimosaurus rex* sp. nov. is based on the articulated skeleton of a giant crocodylomorph from the Hauterivian of Tunisia. This taxon represents the first indisputable Cretaceous teleosauroid, and the first member of this clade from Africa based on well preserved remains. With a basicranial length approaching 160 cm (and a partial skeleton indicating a total body length around 10 m), *M. rex* is the largest known thalattosuchian. Both paleoecological data and morphological features suggest that this species was an ambush generalist predator with an ecology comparable to extant semi-aquatic crocodylians. The discovery of *M. rex* falsifies a global mass extinction event at the J-K transition (i.e., teleosauroid extinction), thereby highlighting the problem of sampling bias in the reconstruction of large-scale patterns in the geological record. The new Tunisian teleosaurid points to a conservative interpretation of faunal turnovers during the J-K transition: local extinction events triggered by regional ecological factors and survival of widely-distributed and eurytypic forms by means of habitat tracking.

## Acknowledgements

This research was supported by the National Geographic Society (grant 9586-14), Museo Geologico G. Capellini (Bologna) and Office National des Mines (Tunis). This manuscript benefited from discussion with A.R. Fiorillo (Perot Museum of Nature and

Science, Dallas, U.S.A.). We thank S. Hua, M. Young and Editor in Chief E. Koutsoukos for detailed revisions that improved the quality of the manuscript. The *Machimosaurus rex* holotype was discovered by FM during prospecting activities led by FF, and excavated by a team including FF, JD, LC, AC and FM. The specimen was prepared in Tunis by FF, FM, JD, LC, TM, and MC. AC and FF conceived and wrote the manuscript, performed the analyses and prepared the figures. TM, LC, MC, JD and FM helped draft the manuscript and prepare the figures. Skeletal reconstructions of *M. rex* are by M. Auditore. We thank the other members of the 2014 Italian-Tunisian palaeontological expedition in the Tataouine Governorate, in particular, H. Aljane, M. Hassine, L. Angelicola, A. Bacchetta, S. Cafaggi, J. Carlet and G. Mignani.

### Supplementary Materials

Data matrix for Bayesian phylogenetic analyses.

**Table 1. Selected measurements of *Machimosaurus rex* type specimen**

	<b>Measurements (cm)</b>
<i>Skull</i>	
Preserved basicranial length	114
Left side, from preserved anterior end to mandibular glenoid	134
Right side, distance from mandibular glenoid to anterior orbit	64
Width of snout anterior to orbits	25
Internal supratemporal fenestra length	33
Distance between five maxillary alveoli	22
Estimated total length of maxillary tooth row (range)	80-97
Preserved snout length	49
Postorbital skull length	65
Interorbital width	11.5
Occipital condyle width	6.2

*Postcranial*

Anterior dorsal centrum height	8.5
Anterior dorsal vertebra total height	17.6
Anterior dorsal vertebra width across diapophyses	24.3

<b>Maxillary Alveoli*</b> (MD, mesiodistal diameter; LL, labiolingual diameter, in mm)	<b>MD</b>	<b>LL</b>
1	29.6	35.2
2	29.5	28.8
3	34.4	28.2
4	32.6	26.1
5	33.6	29.9
6	43.4	34.7
7	38.9	29.9
8	n.d.	32.4

\* Numeration refers to position along the preserved maxilla and not to the inferred position in the complete tooth row.

**Figures**

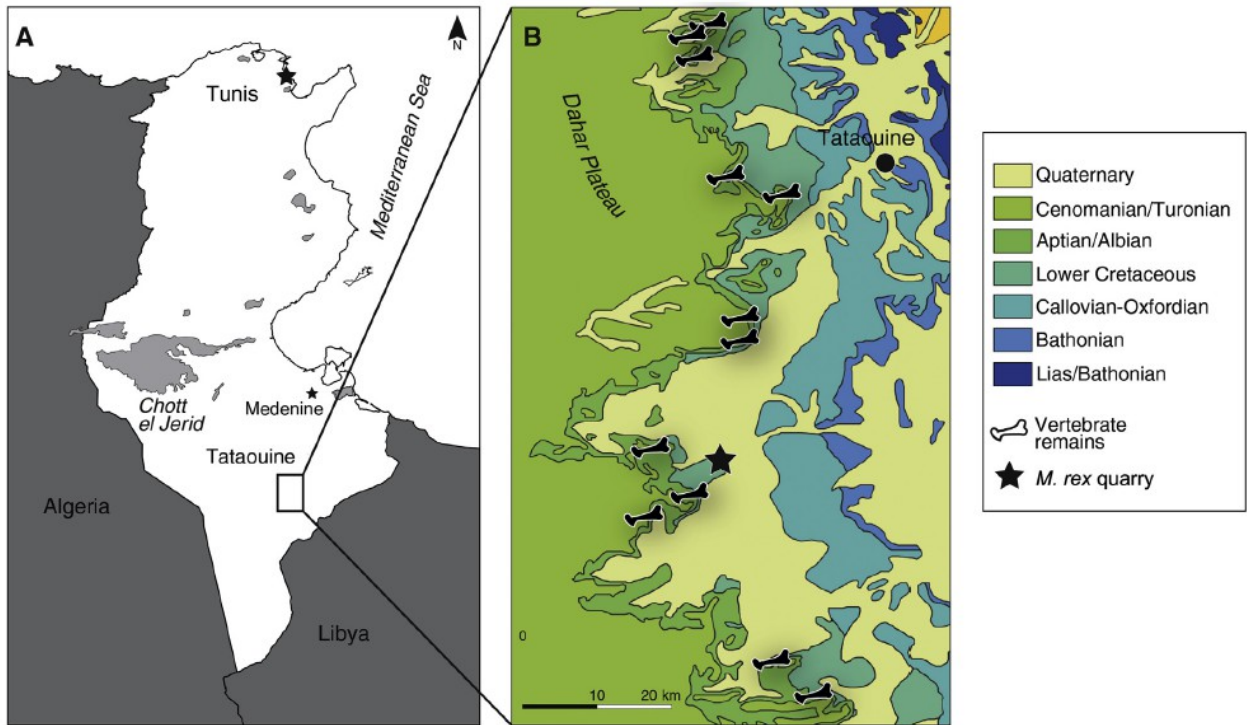


**Fig. 1.** (A) Geographic location and type locality of *M. rex*. (B) Simplified geological map of the Tataouine basin of southern Tunisia showing the Touil el Mhahir locality.

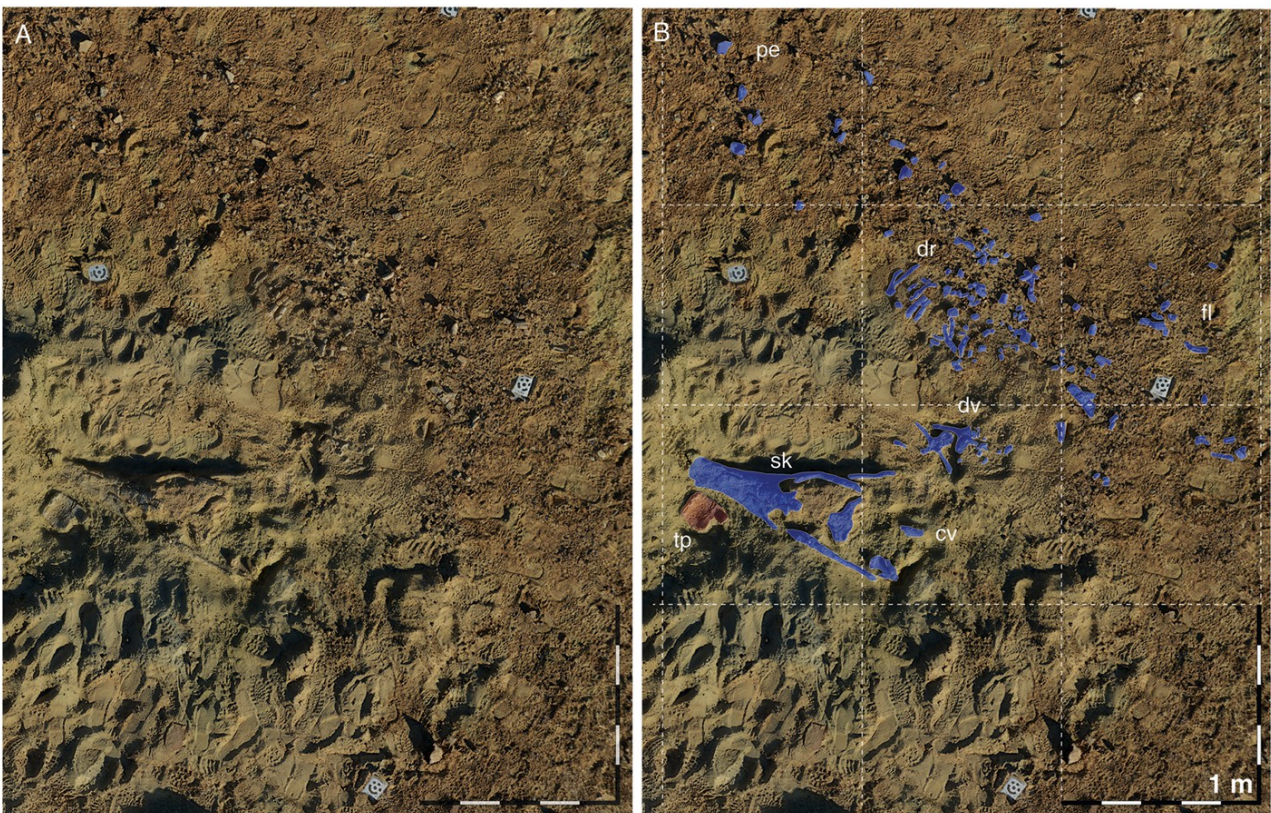


**Fig. 2.** *Machimosaurus rex* quarry map. Ortographic images of the 3D photogrammetry-based model of the main quarry in natural light (A) and with superimposed collected elements (B). Abbreviations: cv, cervical vertebrae; dr, dorsal ribs; dv, dorsal vertebrae; fl, forelimb bones; pe, pelvic elements; sk, skull; tp, turtle hyoplastron.

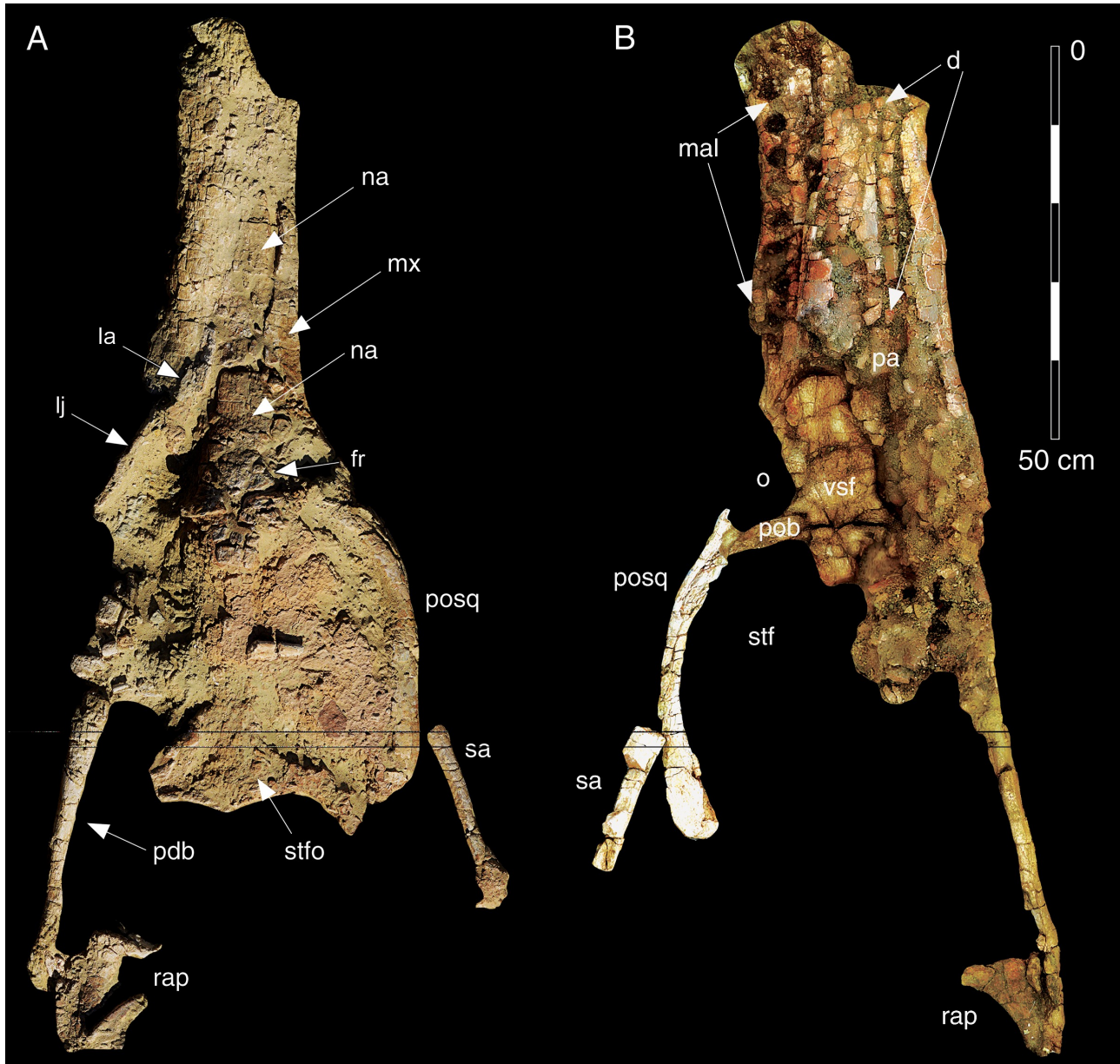


**Fig. 3.** *Machimosaurus rex* type skull, (A) dorsal view, (B) ventral view. Abbreviations: d, dentary; fr, frontal; lj, left jugal; la, lacrimal; mal, maxillary alveoli; mx, maxilla; na, nasal; pa, palatal element; pdb, postdentary bones; posq, postorbital-squamosal bar; rap, retroarticular process; sa, surangular; stfo, floor of supratemporal fossa. Scale bar 50 cm.

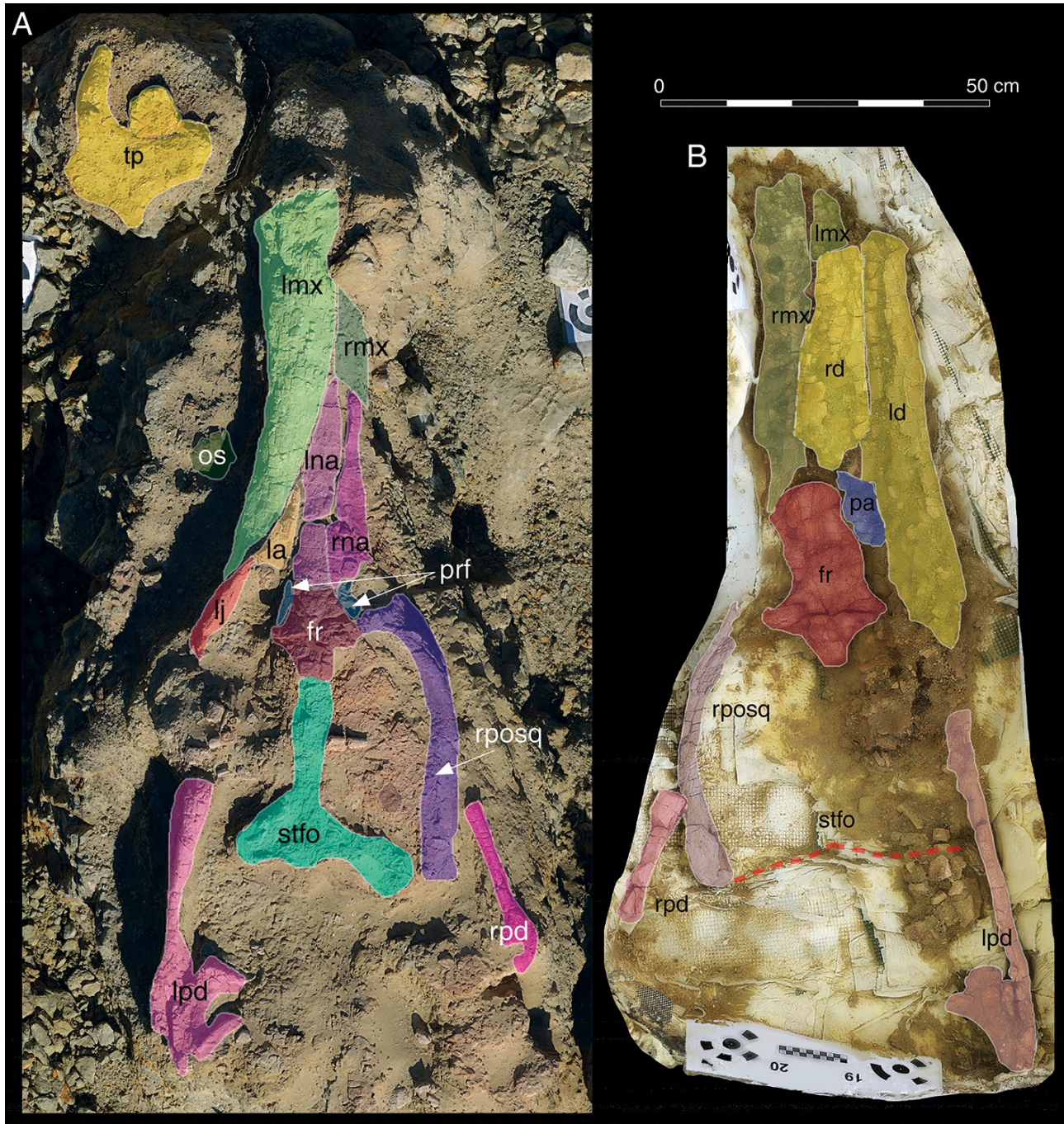


**Fig. 4.** *Machimosaurus rex* type skull, (A) *in situ* photograph showing dorsally exposed preserved bones, (B) prepared ventral surface. Abbreviations: fr, frontal; lj, left jugal; la, lacrimal; ld, left dentary; lmx, left maxilla; ina, left nasal; lpd, left postdentary elements; lposq, left postorbitalsquamosal bar; os, osteoderm; pa, palatal element; rd, right dentary; rmx, right maxilla; rna, right nasal; rpd, right postdentary elements; rposq, right postorbitalsquamosal bar; stfo, floor of supratemporal fossa; tp, turtle plastron element. Scale bar = 50 cm.

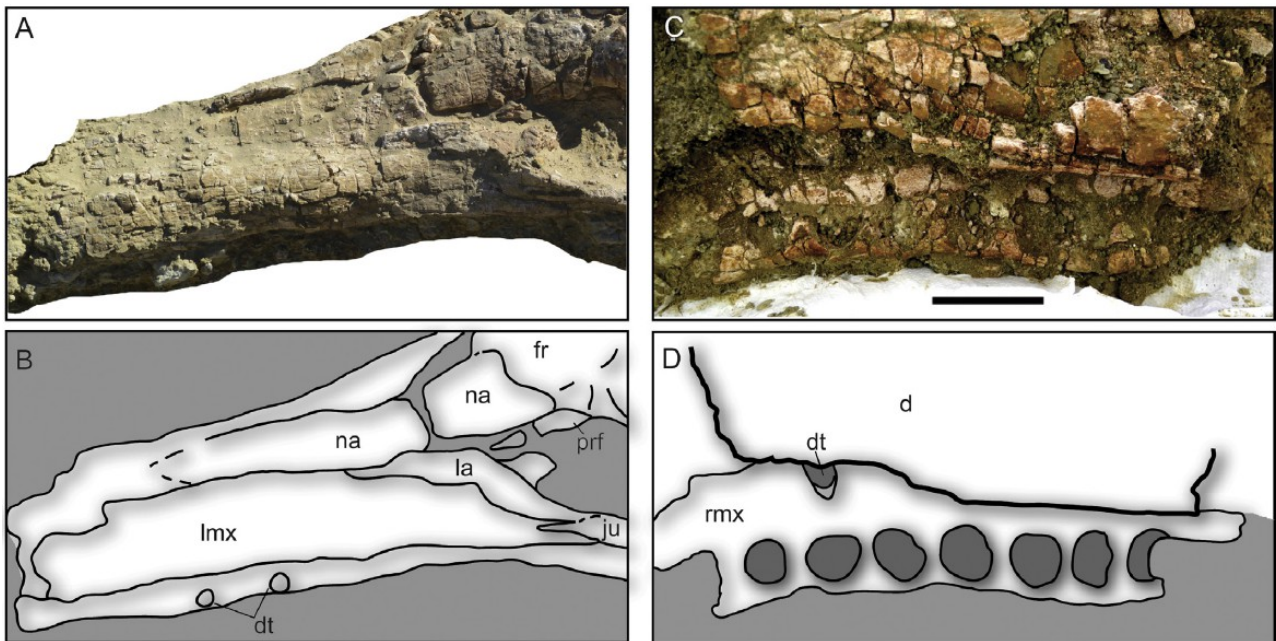


**Fig. 5.** Detail of *M. rex* type snout in dorsal (A, B) and ventral (C, D) views. Abbreviations: d, dentary; dt, dentary tooth; fr, frontal; ju, jugal; la, lacrimal; lmx, left maxilla; na, nasal; prf, prefrontal; rmx, right maxilla. Scale bar in C = 5 cm.

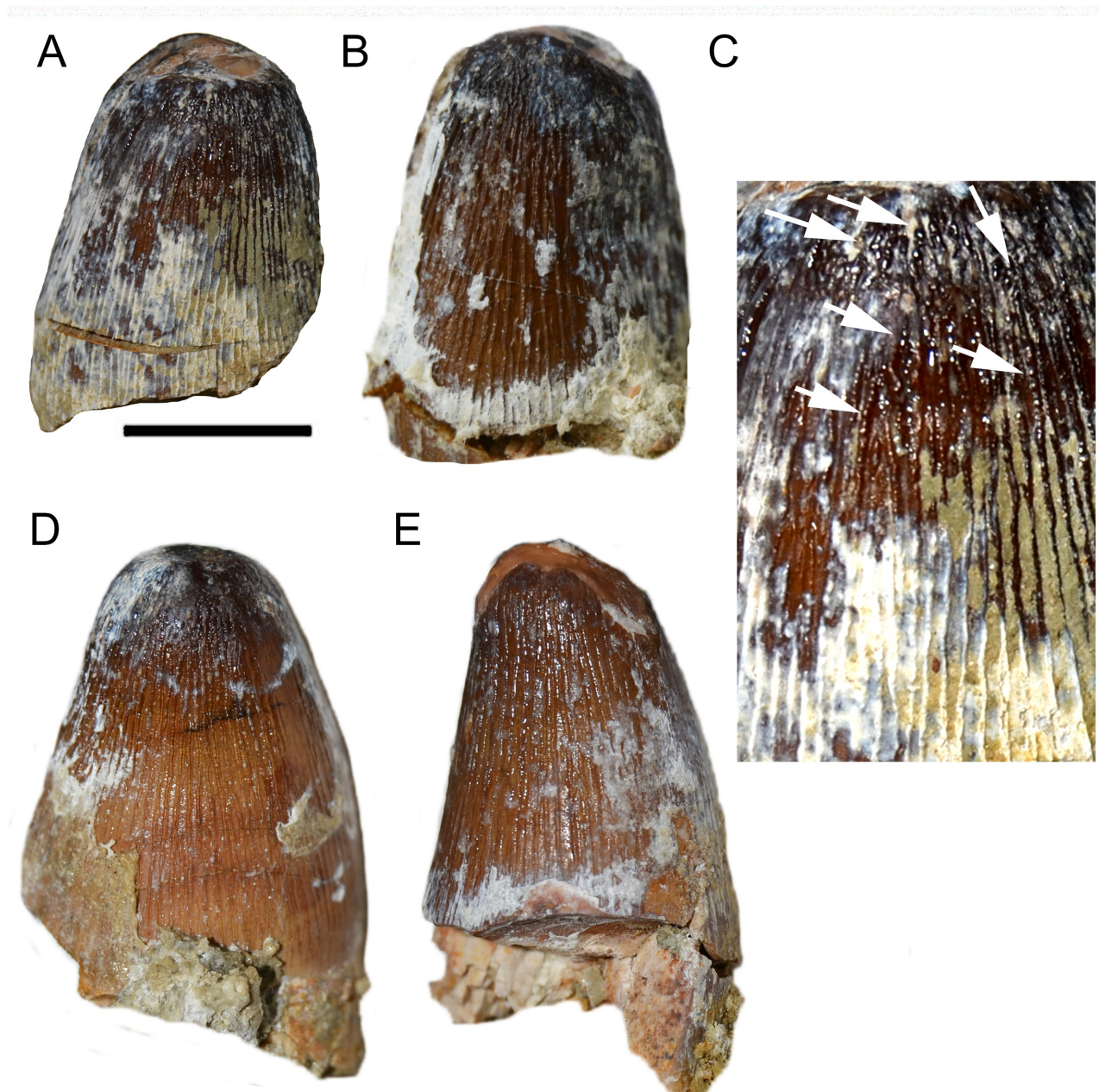


**Fig. 6.** Dentition of *M. rex* type. Isolated tooth crowns in labial (A, D) and lingual (B, E) views; (C) detail of enamel close to apex. Arrows indicate tubercle-like ornamentation of ridges. Scale bar = 5 cm.

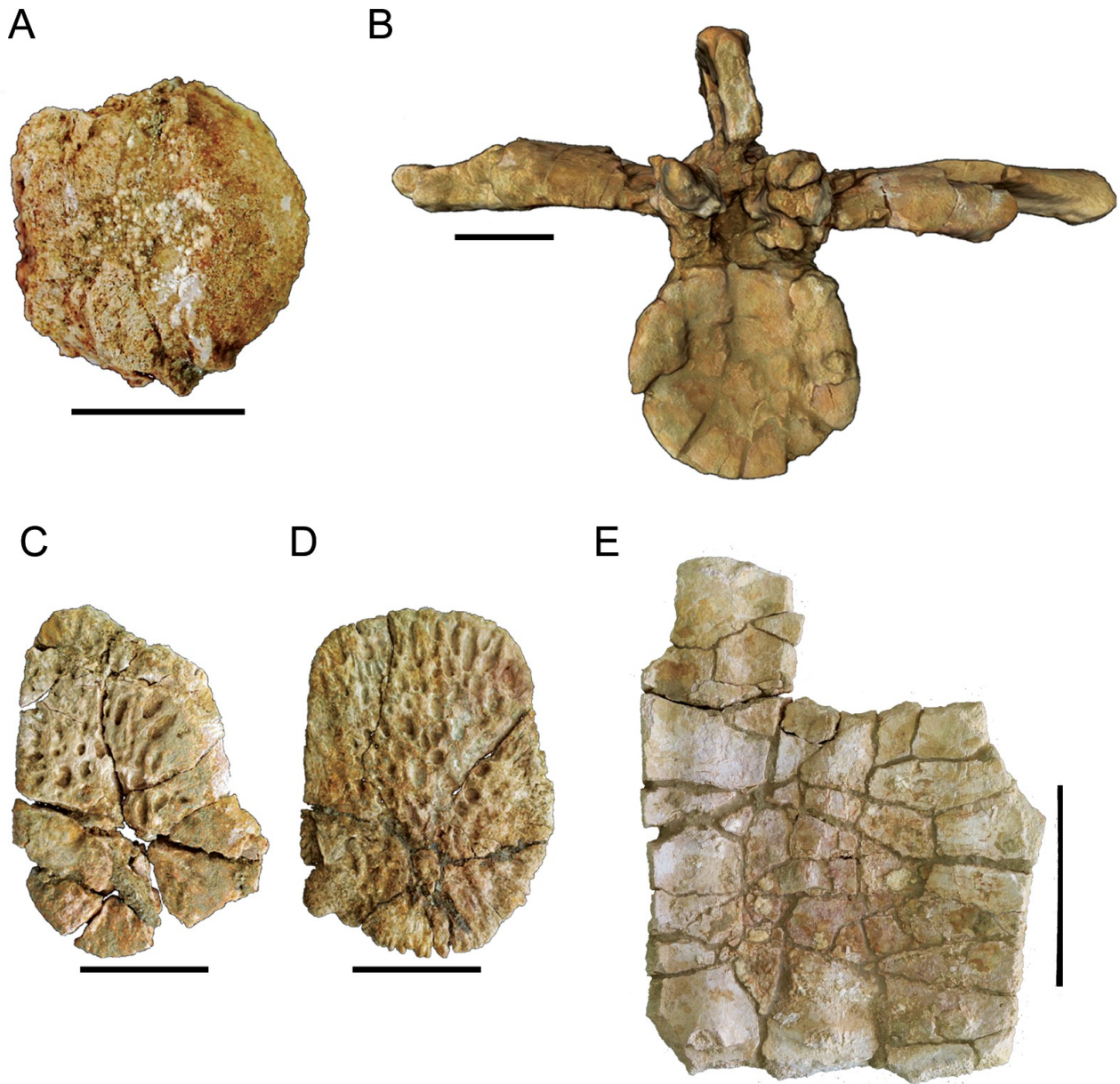


**Fig. 7.** Skeletal anatomy of *M. rex* sp. nov. type specimen and associated turtle remains. (A) Occipital condyle in dorsal view. (B) Anterior dorsal vertebra in anterior view. (C-D) Osteoderms in dorsal views. (E) Turtle hyoplastron in visceral view. Scale bars A-D = 5 cm; E = 10 cm.

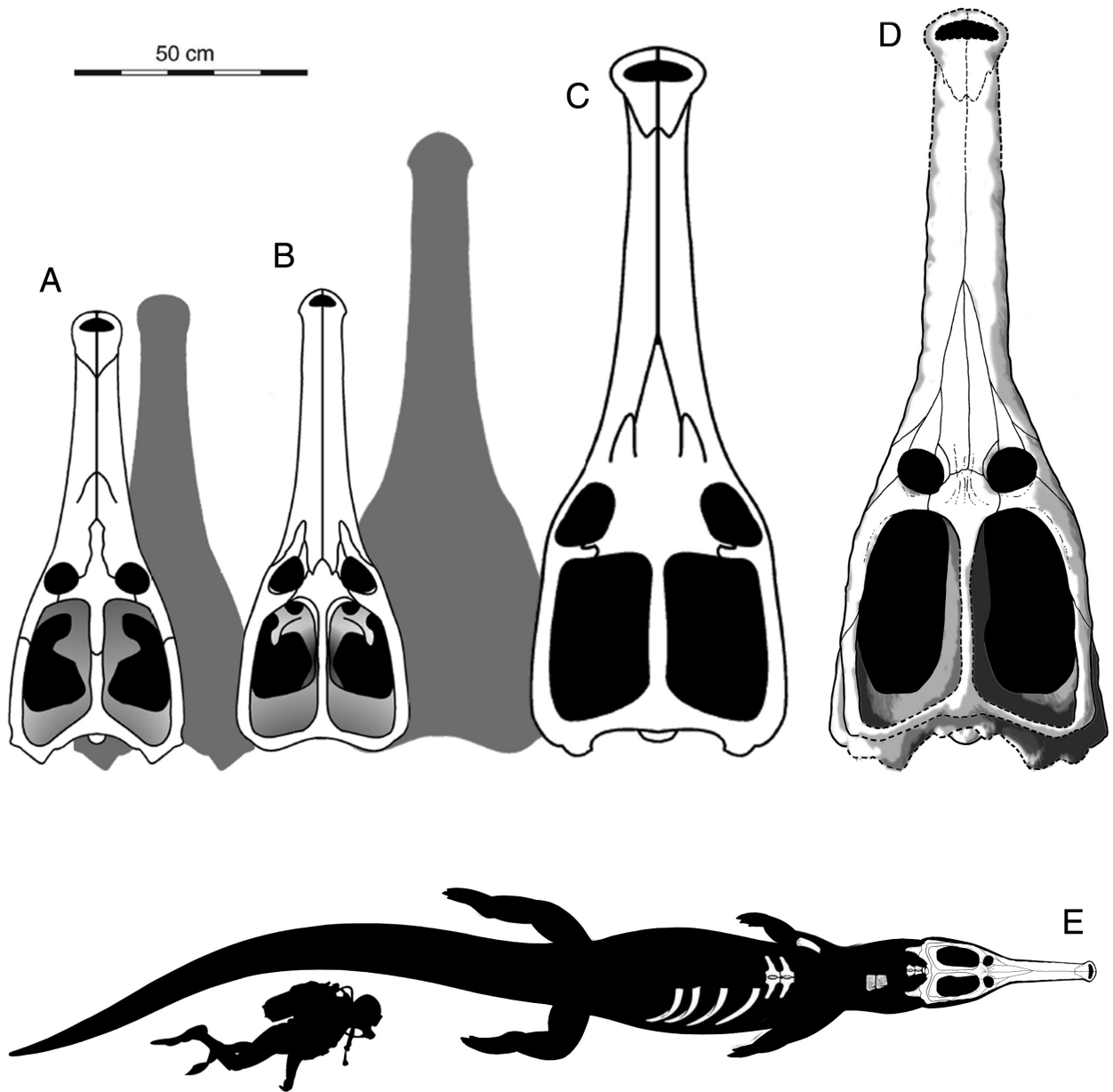


**Fig. 8.** Comparison among skulls of *Machimosaurus*. (A) holotype of *M. buffetauti*, (B) neotype of *M. mosae*, (C) estimated size of the 'Leira specimen' of *M. hugii*, (D) holotype of *M. rex*. Dashed areas in (A) and (B) indicate size of largest known individuals of those species. (E) Reconstruction of *M. rex* body based on preserved elements. Figures (A)-(C) modified from Young et al. (2014b).

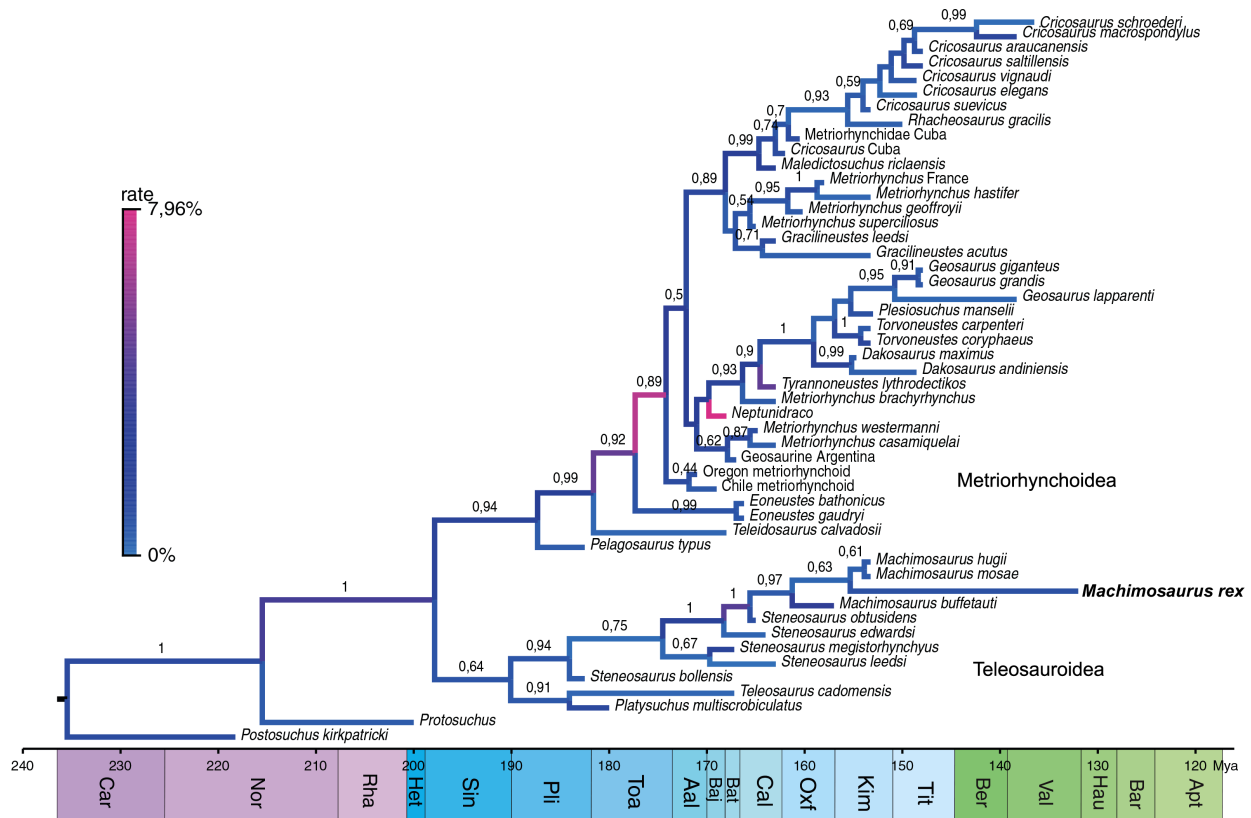


**Fig. 9.** Maximum Clade Credibility Tree of thalattosuchian evolution with divergence rates indicated by colored branches. Values at nodes indicate posterior probability values  $>0.5$ .

## References

- Adatte, T., Stinnesbeck, W., Remane, J., Hubberten, H., 1996. Paleoceanographic changes at the Jurassic–Cretaceous boundary in the Western Tethys, northeastern Mexico. *Cretaceous Research* 17, 671-689.
- Agassiz, L. 1833. *Recherches sur les poissons fossiles*. Petitpierre, Neuchâtel et Soleure.
- Anderson, P.E., Benton, M.J., Trueman, C.N., Paterson, B.A., Cuny, G., 2007. Palaeoenvironments of vertebrates on the southern shore of Tethys: The nonmarine Early Cretaceous of Tunisia. *Palaeogeography, Palaeoclimatology, Palaeoecology* 243, 118-131.
- Bakker, R.T., 1978. Dinosaur feeding behaviour and the origin of flowering plants. *Nature* 274, 661-663.
- Bakker, R.T., 1998. Dinosaur mid-life crisis: the Jurassic-Cretaceous transition in Wyoming and Colorado, In: *Bulletin, N.M.M.o.N.H.a.S.* (Ed.), Lower and Middle Cretaceous terrestrial ecosystems, pp. 67-78.

- Bambach, R.K., 2006. Phanerozoic Biodiversity Mass Extinctions. *Annual Review of Earth and Planetary Science Letters* 34, 127-155.
- Barale, G., Ouaja, M., 2002. La biodiversité végétale des gisements d'âge Jurassique supérieur–Crétacé inférieur de Merbah El Asfer (Sud-Tunisien). *Cretaceous Research* 23, 707-737.
- Bardet, N., 1994. Extinction events among Mesozoic marine reptiles. *Historical Biology* 7, 313-324.
- Beardsley, P., Torr, P., Zisserman, A., 1996. 3D model acquisition from extended image sequences. *Computer Vision ECCV 96*, 683-695.
- Benson, R.B., Butler, R.J., Lindgren, J., Smith, A.S., 2010. Mesozoic marine tetrapod diversity: mass extinctions and temporal heterogeneity in geological megabiases affecting vertebrates. *Proc Biol Sci* 277, 829-834.
- Benson, R.B., Druckenmiller, P.S., 2014. Faunal turnover of marine tetrapods during the Jurassic-Cretaceous transition. *Biol Rev Camb Philos Soc* 89, 1-23.
- Benton, M.J., 2001. Biodiversity on land and in the sea. *Geological Journal* 36, 211-230.
- Benton, M.J., Bouaziz, S., Buffetaut, E., Martill, D., Ouaja, M., Soussi, M., Trueman, C., 2000. Dinosaurs and other fossil vertebrates from fluvial deposits in the Lower Cretaceous of southern Tunisia. *Palaeogeography, Palaeoclimatology, Palaeoecology* 157, 227-246.
- Brown, B. 1934. A change of names. *Science* 79, 80.
- Cau, A., 2014. The affinities of '*Steneosaurus barettoni*' (Crocodylomorpha, Thalattosuchia), from the Jurassic of Northern Italy, and implications for cranial evolution among geosaurine metriorhynchids. *Historical Biology* 26, 433-440.
- Cecca, F., 1999. Palaeobiogeography of Tethyan ammonites during the Tithonian (latest Jurassic). *Palaeogeography, Palaeoclimatology, Palaeoecology* 147, 1-37.
- Cecca, F., Martin Garin, B., Marchand, D., Lathuiliere, B., Bartolini, A., 2005. Paleoclimatic control of biogeographic and sedimentary events in Tethyan and peri-Tethyan areas during the Oxfordian (Late Jurassic). *Palaeogeography, Palaeoclimatology, Palaeoecology* 222, 10-32.
- Cecca, F., Savary, B., Bartolini, A., Remane, J., Cordey, F., 2001. The Middle Jurassic-Lower Cretaceous Rosso Ammonitico succession of Monte Inici (Trapanese

- domain, western Sicily): sedimentology, biostratigraphy and isotope stratigraphy. *Bulletin De La Soci t  G ologique De France* 172, 647-660.
- Chatterjee, S. 1985. *Postosuchus*, a new thecodontian reptile from the Triassic of Texas and the origin of Tyrannosaurs. *Philosophical Transaction of the Royal Society B: Biological Sciences* 309(1139), 395-460.
- Chiarenza, A.A., Foffa, D., Young, M.T., Insacco, G., Cau, A., Carnevale, G., Catanzariti, R. 2015. The youngest record of metriorhynchid crocodylomorphs, with implications for the extinction of Thalattosuchia. *Cretaceous Research* 56, 608-616.
- Cuny, G., Cobbett, A.M., Meunier, F.J., Benton, M.J., 2010. Vertebrate microremains from the Early Cretaceous of southern Tunisia. *Geobios* 43, 615-628.
- Cuny, G., Ouaja, M., Srarfi, D., Schmitz, Buffetaut, E., Benton, M., 2004. Fossil shark from the Early Cretaceous of Tunisia. *Revue de Pal obiologie, Geneve* 9, 127-142.
- Dellaert, F., Seitz, S., Thorpe, C., Thrun, S., 2000. Structure from motion without correspondence, Conference on IEEE Hilton head Island, pp. 557-564.
- Dromart, G., Garcia, J.P., Picard, S., Atrops, F., L cuyer, C., Sheppard, S.M.F., 2003. Ice age at the Middle–Late Jurassic transition? *Earth and Planetary Science Letters* 213, 205-220.
- Drummond, A.J., Suchard, M.A., Xie, D., Rambaut, A., 2012. Bayesian phylogenetics with BEAUti and the BEAST 1.7. *Mol Biol Evol* 29, 1969-1973.
- Engel, J., Schops, T., Cremers, D., 2014. LSD-SLAM: large-scale direct monocular SLAM. *Computer Vision – ECCV 2014* 8690, 834-849.
- Fanti, F., Cau, A., Cantelli, L., Hassine, M., Auditore, M., 2015. New Information on *Tataouinea hannibalis* from the Early Cretaceous of Tunisia and Implications for the Tempo and Mode of Rebbachisaurid Sauropod Evolution. *PLoS One* 10, e0123475.
- Fanti, F., Cau, A., Hassine, M., Contessi, M., 2013. A new sauropod dinosaur from the Early Cretaceous of Tunisia with extreme avian-like pneumatization. *Nat Commun* 4, 2080.
- Fanti, F., Contessi, M., Franchi, F., 2012. The “Continental Intercalaire” of southern Tunisia: Stratigraphy, paleontology, and paleoecology. *Journal of African Earth Sciences* 73-74, 1-23.

- Fischer, V., Appleby, R.M., Naish, D., Liston, J., Riding, J.B., Brindley, S., Godefroit, P., 2013. A basal thunnosaurian from Iraq reveals disparate phylogenetic origins for Cretaceous ichthyosaurs. *Biol Lett* 9, 20130021.
- Fischer, V., Bardet, N., Guiomar, M., Godefroit, P., 2014. High diversity in cretaceous ichthyosaurs from Europe prior to their extinction. *PLoS One* 9, e84709.
- Fischer, V., Maisch, M.W., Naish, D., Kosma, R., Liston, J., Joger, U., Kruger, F.J., Perez, J.P., Tainsh, J., Appleby, R.M., 2012. New ophthalmosaurid ichthyosaurs from the European Lower Cretaceous demonstrate extensive ichthyosaur survival across the Jurassic-Cretaceous boundary. *PLoS One* 7, e29234.
- Fitzinger, L.J.F.J., 1843. *Systema reptilium*. Braumüller et Seidel, Wien.
- Fraas, E., 1901. Die Meerkrokodile (*Thalattosuchia* n. g.) eine neue sauriergruppe der Juraformation. *Jahreshefte des Vereins für vaterländische Naturkunde in Württemberg* 57, 409-418.
- Gasparini, Z., Fernandez, M., Spalletti, L., Matheos, S., Cocca, S., 2004. Reptiles marinos neuquinos en la transición Jurásico-Cretácico. *Ameghiniana* 41, 69R.
- Geoffroy Saint-Hilaire, É. 1831. Recherches sur de grands sauriens trouvés à l'état fossile aux confins maritimes de la Basse-Normandie, attribués d'abord au crocodile, puis déterminés sous les noms de *Teleosaurus* et *Steneosaurus*. *Mémoire de l'Académie des Science* 12, 1-138.
- Haming, K., Peters, G., 2010. The structure-from-motion reconstruction pipeline – a survey with focus on short image sequences. *Kybernetika* 46, 926-937.
- Hay, O.P., 1930. *Second Bibliography and Catalogue of the Fossil Vertebrata of North America*, vol. 2. Carnegie Institute Washington, Washington DC.
- Hua, S. 1999. Le Crocodilien *Machimosaurus mosae* (*Thalattosuchia*, *Teleosauridae*) du Kimmeridgien du Boulonnais (Pas de Calais, France). *Palaeontographica Abt. A*. 252(4-6), 141-170.
- Huene, F. von, 1938. Ein Pliosauride aus Abessinien. *Zentralblatt für Mineralogie, Geologie und Paläontologie*, B 1938 (10), 370-376.
- Husinec, A., Jelaska, V., 2006. Relative Sea-Level Changes Recorded on an Isolated Carbonate Platform: Tithonian to Cenomanian Succession, Southern Croatia. *Journal of Sedimentary Research* 76, 1120-1136.

- Johnson, M.M., Young, M.T., Steel, L., Lepage, Y. 2015. *Steneosaurus edwardsi* (Thalattosuchia: Teleosauridae), the largest known crocodylomorph of the Middle Jurassic. *Biological Journal of the Linnean Society* 115(4): 911-918.
- Koenderink, J., Doorn, J.J., 1991. Affine structure from motion. *Journal of the Optical Society of America* 8, 377-385.
- Kriwet, J., Schmitz, L., 2005. New insight into the distribution and palaeobiology of the pycnodont fish *Gyrodus*. *Acta Palaeontologica Polonica* 50, 49-56.
- Krebs, B., 1967. Der Jura-Krokodilier *Machimosaurus* H. v. Meyer. *Paläontologische Zeitschrift* 41, 46-59.
- Le Loeuff, J., Lang, E., Cavin, L., Buffetaut, E., 2012. Between Tendaguru and Baharia: on the age of the Early Cretaceous dinosaur sites from the Continental Intercalaire and other african formations. *Journal of Stratigraphy* 36, 486-502.
- Lécuyer, C., Bogey, C., Garcia, J-P., Grandjean, P., Barrat, J-A., Floquet, M., Bardet, N., Pereda-Superbiola, X., 2003. Thermal evolution of Tethyan surface waters during the Middle-Late Jurassic: Evidence from  $\delta^{18}\text{O}$  values of marine fish teeth. *Paleoceanography* 18.
- Lee, M.S., Cau, A., Naish, D., Dyke, G.J., 2014. Dinosaur evolution. Sustained miniaturization and anatomical innovation in the dinosaurian ancestors of birds. *Science* 345, 562-566.
- Loriol, P.de, 1866. Description des fossiles de l'Oolite Corallienne de l'etage Valanginien et de l'etage Urgonien du Mont-Saleve. In: E. Favre (Ed), *Recherches geologiques dans les parties de la Savoie, du Piemont et de la Suisse voisines du mont Blanc*. pp. 310-405.
- Lu, P.J., Yogo, M., Marshall, C.R., 2006. Phanerozoic marine biodiversity dynamics in light of the incompleteness of the fossil record. *Proc Natl Acad Sci U S A* 103, 2736-2739.
- Maisey, J.G. 1987. Cranial anatomy of the Lower Jurassic shark *Hybodus reticulatus* (Chondrichthyes: Elasmobranchii), with comments on Hybodontid systematics. *American Museum Novitates* 2878, 1-39.
- Martin-Garin, B., Lathuilière, B., Geister, J., 2012. The shifting biogeography of reef corals during the Oxfordian (Late Jurassic). A climatic control? *Palaeogeography, Palaeoclimatology, Palaeoecology* 365-366, 136-153.

- Martin, J.E., Vincent, P., 2013. New remains of *Machimosaurus hugii* von Meyer, 1837 (Crocodylia, Thalattosuchia) from the Kimmeridgian of Germany. *Fossil Record* 16, 179-196.
- Martin, J.E., Vincent, P., Falconnet, J., *in press*. The taxonomic content of *Machimosaurus* (Crocodylomorpha, Thalattosuchia). *Comptes Rendus Palevol*.
- Meyer, C.E.H., von. 1837. Mitteilungen, an Professor Bronn gerichtet. *Neues Jahrbuch für Mineralogie, Geologie, Geognosie und Petrefaktenkunde* 4, 413-418.
- Newham, E., Benson, R., Upchurch, P., Goswami, A., 2014. Mesozoic mammaliaform diversity: The effect of sampling corrections on reconstructions of evolutionary dynamics. *Palaeogeography, Palaeoclimatology, Palaeoecology* 412, 32-44.
- Ouaja, M., Barale, G., Philippe, M., Ferry, S., 2011. Occurrence of an in situ fern grove in the Aptian Douiret Formation, Tataouine area, South-Tunisia. *Geobios* 44, 473-479.
- Ouaja, M., Philippe, M., Barale, G., Ferry, S., Ben Youssef, M., 2004. Mise en évidence d'une flore oxfordienne dans le Sud-Est de la Tunisie : intérêts stratigraphique et paléoécologique. *Geobios* 37, 89-97.
- Peybernes, B., Vila, J.M., Souquet, P., Charriere, A., Ben Youssef, M., Zarout, M., Calzada, S., 1996. Trois gisements de brachiopodes dans le Cretace inferieur tunisien. *Batalleria* 6, 45-58.
- Pouech, J., Mazin, J.-M., Cavin, L., Poyato-Ariza, F.J., 2015. A Berriasian actinopterygian fauna from Cherves-de-Cognac, France: Biodiversity and palaeoenvironmental implications. *Cretaceous Research* 55, 32-43.
- Rambaut, A., Drummond, A.J., 2009. Tracer: MCMC Trace Analysis Tool v1.5, <http://beast.bio.ed.ac.uk/>
- Rees, J., Underwood, C., 2008. Hybodont sharks of the English Bathonian and Callovian (Middle Jurassic). *Palaeontology* 51, 117–147.
- Ruban, D., 2012. Mesozoic mass extinctions and angiosperm radiation: does the molecular clock tell something new? *Geologos* 18.
- Ruban, D.A., 2011. Diversity Dynamics of Callovian-Albian Brachiopods in the Northern Caucasus (Northern Neo-Tethys) and a Jurassic/Cretaceous Mass Extinction. *Paleontological Research* 15, 154-167.
- Sauvage, H.-E., Liénard, F. 1879. Mémoire sur le genre *Machimosaurus*. *Mémoires de la Société géologique de France*, 3ème série 4, 1-31.

- Sepkoski, J.J., 1984. A Kinetic Model of Phanerozoic Taxonomic Diversity. III. Post-Paleozoic Families and Mass Extinctions. *Paleobiology* 10, 246-267.
- Syme, C.E., Salisbury, S.W., 2014. Patterns of aquatic decay and disarticulation in juvenile Indo-Pacific crocodiles (*Crocodylus porosus*), and implications for the taphonomic interpretation of fossil crocodyliform material. *Palaeogeography, Palaeoclimatology, Palaeoecology* 412, 108-123.
- Trucco, E., Verri, A., 1998. Introductory techniques for 3-D computer vision. Englewood Cliffs: Prentice Hall 201, 178-194.
- Upchurch, P., Barrett, P.M., 2005. Sauropodomorph diversity through time. In: Curry Rogers, K., Wilson, J. (Ed.), *The sauropods: evolution and paleobiology*. University of California Press, Berkeley, CA, pp. 104–124.
- Vignaud, P., 1995. Les Thalattosuchia, crocodiles marins du Mésozoïque: Systématique, phylogénie, paléoécologie, biochronologie et implications paléogéographiques. University of Bristol, p. 350.
- Wilberg, E.W., *in press*. What's in an Outgroup? The Impact of Outgroup Choice on the Phylogenetic Position of Thalattosuchia (Crocodylomorpha) and the Origin of Crocodyliformes. *Systematic Biology*.
- Young, M.T., 2014. Filling the 'Corallian Gap': re-description of a metriorhynchid crocodylomorph from the Oxfordian (Late Jurassic) of Headington, England. *Historical Biology*, 80-90.
- Young, M.T., Brandalise de Andrade, M., Cornée, J.-J., Steel, L., Foffa, D., 2014a. Re-description of a putative Early Cretaceous "teleosaurid" from France, with implications for the survival of metriorhynchids and teleosaurids across the Jurassic-Cretaceous Boundary. *Annales de Paléontologie* 100, 165-174.
- Young, M.T., Brusatte, S.L., Ruta, M., De Andrade, M.B., 2010. The evolution of Metriorhynchoidea (mesoeucrocodylia, thalattosuchia): an integrated approach using geometric morphometrics, analysis of disparity, and biomechanics. *Zoological Journal of the Linnean Society* 158, 801-859.
- Young, M.T., Hua, S., Steel, L., Foffa, D., Brusatte, S.L., Thuring, S., Mateus, O., Ruiz-Omenaca, J.I., Havlik, P., Lepage, Y., De Andrade, M.B., 2014b. Revision of the Late Jurassic teleosaurid genus *Machimosaurus* (Crocodylomorpha, Thalattosuchia). *Royal Society Open Science* 1, 140222.

Young, M.T., Steel, L., Brusatte, S.L., Foffa, D., Lapage, Y. 2014c. Tooth serration morphologies in the genus *Machimosaurus* (Crocodylomorpha, Thalattosuchia) from the Late Jurassic of Europe. *Royal Society Open Science* 1, 140269.

Page left blank

## CHAPTER 9 - Specimen-level phylogenetics in palaeontology using the Fossilized Birth-Death model with Sampled Ancestors

Submitted: 14<sup>th</sup> September 2016. Published: 01<sup>st</sup> March 2017 in *PeerJ* vol. 5:e3055:1-19.

Andrea Cau

### ABSTRACT

Bayesian phylogenetic methods integrating simultaneously morphological and stratigraphic information have been applied increasingly among palaeontologists. Most of these studies have used Bayesian methods as an alternative to the widely-used parsimony analysis, to infer macroevolutionary patterns and relationships among species-level or higher taxa. Among recently introduced Bayesian methodologies, the Fossilized Birth-Death (FBD) model allows incorporation of hypotheses on ancestor-descendant relationships in phylogenetic analyses including fossil taxa. Here, the FBD model is used to infer the relationships among an ingroup formed exclusively by fossil individuals, i.e., dipnoan tooth plates from four localities in the Ain el Guettar Formation of Tunisia. Previous analyses of this sample compared the results of phylogenetic analysis using parsimony with stratigraphic methods, inferred a high diversity (five or more genera) in the Ain el Guettar Formation, and interpreted it as an artefact inflated by depositional factors. In the analysis performed here, the uncertainty on the chronostratigraphic relationships among the specimens was included among the prior settings. The results of the analysis confirm the referral of most of the specimens to the taxa *Asiatoceratodus*, *Equinoxiodus*, *Lavocatodus* and *Neoceratodus*, but reject those to *Ceratodus* and *Ferganoceratodus*. The resulted phylogeny constrained the evolution of the Tunisian sample exclusively in the Early Cretaceous, contrasting with the longer scenario inferred by the stratigraphically-calibrated topology resulted using parsimony analysis. The phylogenetic framework also suggests that 1) the sampled localities are laterally equivalent, 2) but three localities are restricted to the youngest part of the section; both results in agreement with previous stratigraphic analyses of these localities. The FBD model of specimen-level units provides a novel tool

for phylogenetic inference among fossils but also for independent tests of stratigraphic scenarios.

## INTRODUCTION

The use of Bayesian inference methods in phylogenetic analysis of morphological features (Lewis 2001, Nylander *et al.* 2004, see Lee and Palci 2015) is a relatively novel approach in palaeontology (Pyron 2011, Lee *et al.* 2014a, Wright and Hillis 2014, O'Reilly *et al.* 2016). In particular, co-estimation of topology and divergence times using morphology, including tip-dating methods (Ronquist *et al.* 2012), has become more popular in recent years, and it may represent a promising area for the integration of the two main sides of palaeontology: the biostratigraphic (focusing on the distribution of the fossil record along the Geological Time) and the systematic (focusing on the inclusion of the fossil record in the Tree of Life). Stadler (2010) and Heath *et al.* (2014) introduced a method for fossil calibration in phylogenetic analysis that integrates extinct and extant species with a single macroevolutionary model, named the "Fossilized Birth-Death (FBD) process" (Heath *et al.* 2014). Another significant area of application for Bayesian phylogenetic analyses is the reconstruction of evolutionary patterns among a set of taxa where both sister-taxon (cladogenetic) and ancestor-descendant (anagenetic) relationships are involved. In most of the studies mentioned above, the tree search strategies used were based on a strictly cladogenetic approach, which assumes that the analysed ingroup does not include potential ancestors of other members of the same ingroup. Gavryushkina *et al.* (2014) introduced a Bayesian phylogenetic model that allows one sampled member of the analysed ingroup to be a direct ancestor of another sampled taxon. This method, initially developed for analysis of molecular data, was implemented by Gavryushkina *et al.* (2016) allowing the inclusion of morphological data. As outlined by Gavryushkina *et al.* (2014) and Gavryushkina *et al.* (2016), failing to account for sampled ancestors may lead to significant bias in parameter estimation, in particular in nodal age inference, in the quantification of cladogenetic events and in the estimation of the fossil diversity.

The majority of the palaeontological studies applying Bayesian phylogenetic methods and integrating the morphological and stratigraphic information of the terminal units included

have focused on analysis of species-level taxa in order to reconstruct macroevolutionary patterns (e.g., Lee *et al.* 2014b, Close *et al.* 2015, Dembo *et al.* 2015, Fanti *et al.* 2015, Cau and Fanti 2015, Bell *et al.* 2016, Fanti *et al.* 2016b). Specimen-level analysis (i.e., analysis using exclusively individual specimens as terminal tips) has been a poorly explored area of application of these new methodologies, compared to recent results that used parsimony as tree search strategy (e.g., Upchurch *et al.* 2004, Scannella *et al.* 2014, Mounier and Caparros 2015, Tschopp *et al.* 2015). Here, the FBD model implemented by Gavryushkina *et al.* (2016) is applied to the study on the affinities among specimen-level taxonomic operational units, specifically, dipnoan sarcopterygian specimens from the Lower Cretaceous Ain el Guettar Formation of southern Tunisia (Fanti *et al.* 2016a). Recently, these specimens were analysed integrating “traditional” stratigraphic, palaeoecological and taphonomic methods with phylogenetic analysis of morphological features that used parsimony as tree search strategy (Fanti *et al.* 2016a). In that study, Fanti *et al.* (2016a) documented an unusually high diversity among the sample of isolated tooth plates, referable to five or more lineages (at genus-level, using Linnean-rank taxonomy) of dipnoans. The authors concluded that the high diversity of dipnoans in the Ain el Guettar Formation was a taphonomic artefact. In particular, Fanti *et al.* (2016a) suggested that a series of depositional factors significantly inflated observed lungfish diversity in the estuarine and marginal-marine deposits of the Oum ed Diab Member of the Ain el Guettar Formation, and concluded that the sampled fauna was representative of a larger, inland palaeo-hydrographic system. Here, the data of Fanti *et al.* (2016a) is re-analysed using Bayesian tip-dating approach for a discussion on the distribution of the dipnoan taxa across the four Tunisian localities sampled.

The aims of this study are to test 1) the application of the FBD model with sampled ancestors to a set of exclusively fossil taxa, 2) the use of Bayesian phylogenetic methods in specimen-level phylogenetics, 3) the incorporation of age uncertainty in phylogenetic models integrating both anagenetic and cladogenetic patterns, and 4) the application of phylogenetic models using both morphological and chronological data as auxiliary tool for stratigraphic inference.

## **ABBREVIATIONS**

CPHNAMA, Centro de Pesquisa de História Natural e Arqueologia do Maranhão, Praia Grande, São Luís, Brazil; HGN, Museum National d'Histoire Naturelle, Paris, Nord du Hoggar; MGGC, Museo Geologico Giovanni Capellini, Bologna, Italy; MGCT, Museo de Geociencias, Tacuarembó, Uruguay; ONM, Office National des Mines, Tunis; QM, Queensland Museum, Brisbane, Australia; ROM, Royal Ontario Museum, Toronto, Canada; UFMA, Coleção Paleontológica da Universidade Federal do Maranhão, Bacanga, São Luís, Brazil; ZPAL, Institute of Paleobiology, Polish Academy of Sciences, Warsaw, Poland.

## MATERIAL AND METHODS

A discussion on the taxonomy and phylogenetic nomenclature of Mesozoic dipnoans is beyond the aims of this study. Furthermore, it is controversial whether Linnean ranks could be conciliated with phylogenetic-based taxonomies (Kuntner and Agnarsson 2006). For simplicity, in the discussion of the topologies found here, I follow the convention to name informal lineages, defined topologically and anchored to the genus names of the non-Tunisian taxonomic units included in the analysis. Accordingly, for “*Genus name A*” *lineage* it is meant the most inclusive lineage including the non-Tunisian taxonomic unit(s) referred in literature to Genus *A* and excluding all other taxonomic units referred in literature to other genus-level Linnean ranks. These lineages are meant exclusively as clades and even if mention “genus-level” taxa, they do not refer to particular Linnean ranks. For example, the term “*Asiatoceratodus* lineage” refers to the most inclusive lineage resulted by the analyses performed here that includes the two non-Tunisian specimens HGS 64 and UFMA 1 40 454 (both referred in literature to *Asiatoceratodus*, see Fanti *et al.* 2016 and references therein) and excludes all other non-Tunisian specimens analysed.

I performed Bayesian phylogenetic analysis to a modified version of the character-taxon matrix of Fanti *et al.* (2016a), integrating the morphological data with chronostratigraphic information, following the methods discussed by Lee *et al.* (2014a), Lee *et al.* (2014b) and Gavryushkina *et al.* (2016) (see model settings below). Modifications of the original character-taxon matrix involved:

1) the removal of one of the two outgroup taxa included in the parsimony analysis of Fanti *et al.* (2016a), QMF 2108, referred to the Lower Cretaceous ceratodontid *Metaceratodus*

*wollastoni*, and the use of a single taxonomic unit, ZPAL ABbIII 2393, referred to *Ptychoceratodus roemeri*, as outgroup. This operational taxonomic unit is Late Triassic in age and is considered as a more appropriate representative of the ancestral morphology for the ingroup than QMF 2108, from both phylogenetic and stratigraphic reasons, because it consistently pre-dates all other included taxonomic units. The Early Cretaceous age of QMF 2108 implies a >50 Mys long branch for this terminal unit relative to the root of the tree (the latter must be older than the Triassic terminal ZPAL ABbIII 2393): as outlined by Lee *et al.* (2014a), younger terminal units may have undergone more morphological anagenesis than older units, with the consequence that it cannot be dismissed that the character state combination in QMF 2108 had significantly diverged from the ancestral combination at the root relative to ZPAL ABbIII 2393.

2) the multistate character statement #3 was split into two binary character statements (i.e., the redefined character #3 and the new character #43; see Appendix).

3) the character statement #8 was defined as binary instead of multistate: the previous state “2” in character #8 in Fanti *et al.* (2016a) is clearly redundant with state “1” of character #9 (i.e., an angled mesial margin defines two distinct mesio-buccal and mesio-internal margins). Accordingly, the previous states “1” and “2” of character #8 were merged into a single state “1” as both describe the same condition, i.e., a convex mesial margin (see Appendix).

4) *a priori* removal of characters #2, #7 and #10 as they refer to measurement values of tooth plate margins. Exploration of the character scores in the original matrix shows that these three characters co-vary consistently. Thus, these character statements are redundant, referring to the same phenomenon (the absolute size of the plate).

Furthermore, size-based characters are individually- and ontogenetically-variable features with poor phylogenetic signal.

Modifications 2) and 3) have removed all the redundant character statements present in the parsimony analysis (Fanti *et al.* 2016a) and have replaced the non-redundant multistate characters with a series of analogous binary character statements. In particular, this modification results in the included character #3 as being split into two binary characters (the new #3 and the #46). One reason for splitting multistate character

statements into a series of simpler binary characters is to allow the Bayesian analysis to test whether different state transitions evolved at different rates. In parsimony analysis, different state transitions along the evolution of a feature occur at the same rate regardless of being all states of the same character or being them split into distinct character statements. On the contrary, in likelihood analyses using the rate variability gamma parameter, different state transitions can evolve at different rates if they are defined as distinct characters. Thus, splitting a multistate character included in a Bayesian inference phylogenetic analysis into a series of non-redundant binary characters allows to investigate the effect of among-state variation heterogeneity in the evolution of that character.

Bayesian analyses were performed using BEAST (Bayesian Evolutionary Analysis Sampling Trees) vers. 2.4.4 (version updated in November 2016, Drummond *et al.* 2012, Bouckaert *et al.* 2014). Usually, in phylogenetic analyses based on morphological characters and using parsimony as tree search strategy, only variable characters (potential synapomorphies) are sampled (Lewis 2001, Lee *et al.* 2014a). Being all the terminal units used in this analysis represented by single individuals, the term “autapomorphy” for those character states present exclusively in a single terminal unit is probably misleading: features that are autapomorphies at the species-level are recorded as synapomorphies at the specimen-level among conspecific individuals. Thus, “terminal” feature is here preferred over “autapomorphy” when referring to a character state change optimised along a specimen-level tip. The original character statements used in the analysis of Fanti *et al.* (2016a) were based on a series of phylogenetically significant features, mostly derived from the literature and suggested to diagnose “genus/species-level” taxa, including characters with a high level of homoplasy (in particular, characters that may not result synapomorphic at any node but may result as terminal features in two or more distinct terminal branches). It is here assumed that the terminal features may provide information on the length of the terminal branches in an analogous way as autapomorphies for species-level tips. In the analysis performed here, the Markov-Chain Monte Carlo Bayesian method for estimating phylogeny used the Lewis’s (2001) Markov model for the evolution of discrete morphological characters. Variability in rates of evolution among characters was accommodated using the gamma distribution, and variability across

lineages was accommodated using the relaxed clock model (Lee *et al.* 2014b, supplementary material; Dembo *et al.* 2015). All characters were treated as a single partition, and the Lewis's (2001) model was conditioned to variable characters only using the implementation included in BEAST vers. 2.4.4. The Fossilized Birth-Death model with Sampled Ancestors implemented by Gavryushkina *et al.* (2016) was used as tree prior. In this study, the only notable difference from the method used by Gavryushkina *et al.* (2016) was the setting of the rho parameter, that defines the probability of sampling at the present: being the analysed sample formed exclusively by fossil individuals, rho was set as =0.

A significant application of Bayesian inference in phylogenetic analysis of fossil taxa compared to parsimony analysis is the integration of morphological and stratigraphic (age) information during tree search (Lee *et al.* 2014a, Lee *et al.* 2014b). Absolute age ranges were determined for each terminal unit (based on Fanti *et al.* 2016a) according to the ages reported in the International Chronostratigraphic Chart (International Commission on Stratigraphy, vers. 2016; [www.stratigraphy.org](http://www.stratigraphy.org)). In absence of direct dating from radiometric analysis, the absolute age of fossil taxa is usually inferred from the age of the boundaries of the stratigraphic series including those taxa (Lee *et al.* 2014a), which implies a variable amount of uncertainty on the age of the tip. In order to incorporate age uncertainty in the analysis, the ages of each terminal tip included in this study were defined as uniform range priors instead of using single (mean) values. In particular, the ages of all Tunisian specimens were conservatively set along an uniform range sampling the whole Albian stage (~113-100 Mya). The age of the two most recent operational taxonomic units included (ROM 47626 and ROM 47627, both referred to *Lavocatodus humei*, see Fanti *et al.* 2016a) were both fixed at 83 Mya (the mean value between the lower and upper boundary ages of the Late Cretaceous, see Fanti *et al.* 2016a, supplementary material), because BEAST vers.2 requires at least the age of the most recent terminals to be fixed.

The BEAST analysis involved 5 replicate runs (with different random starting trees and random number seeds). Each of the replicate runs involved 50 million steps with sampling every 5000 generations, with a burn-in set at the first 20% sampled. The Log and Tree output files of the five replicates were merged using LogCombiner (Drummond *et al.* 2012,

Rambaut and Drummond 2009). Convergence (stationarity) in numerical parameters was identified using Tracer vers. 1.5 (Rambaut and Drummond 2009). The Maximum Clade Credibility Tree (MCCT) resulted from the Bayesian analysis was used as a temporally-calibrated phyletic framework for phylogenetic and taxonomic discussion.

In order to test whether the clades including the Tunisian specimens are locality-specific, the four Tunisian localities where the specimens have been collected (i.e., El Hmaïma, El Kambout, El Mra, Oum ed Diab; see Fanti *et al.* 2016a, supplementary information) were plotted on the resulted phylogenetic framework. The MCCT resulted from the Bayesian analysis was used as a temporally calibrated phyletic framework for palaeobiogeographic reconstruction, inferring ancestral geographic placement of nodes using RASP (Reconstruct Ancestral State in Phylogenies, Yu *et al.* 2015). The distribution range of the taxonomic units was *a priori* divided into five areas: "Non-Tunisia" (all non-Tunisian specimens were scored for this area, used as palaeogeographic outgroup for the analysis), El Mra, Oum ed Diab, El Kambout, and El Hmaïma. Each terminal taxon was scored for the area character state according to the location where it was recovered. Locality inferences on the phylogenetic frameworks were obtained in RASP by applying Bayesian Binary Markov Chain Monte Carlo (BBM) analysis (Yu *et al.* 2015). The BBM method suggests possible ancestral ranges at each node and also calculates probabilities of each ancestral range at nodes according to both tip scores and branch lengths. The BBM analyses performed ten Markov Chain Monte Carlo chains of 50000 cycles each, sampling every 100 trees. Chain temperature was set at 0.1. State frequencies were set as estimated and among-site rate variation was set using the gamma parameter. The first 20% of the recovered trees were discarded and the remaining trees were used to infer ancestral range distribution at nodes. The time-events algorithm implemented in RASP (Yu *et al.* 2015) was used to infer the total distribution of cladogenetic events at the El Mra and Oum ed Diab localities (where the majority of the Tunisian specimens has been collected) along the chronologic interval estimated by the BEAST analysis.

## RESULTS

The MCCT of the combined tree samples supports the monophyly of the non-Tunisian species included in the analysis (Figure 1): each least inclusive node containing the representatives of these species does not include any member of the other species. Convergence (stationarity) in parameters identified using Tracer vers. 1.5 (Rambaut and Drummond 2009) is supported by effective sample size (ESS) of every parameter being >200. Focusing on the MCCT topology, the analysis found *Ferganoceratodus jurassicus* as the basalmost lineage of the ingroup (posterior probability, *pp*, value is 0.75), as sister-taxon of the node containing the specimen of *Ceratodus africanus* and a clade including all other specimens (*pp*: 0.86). The latter clade (*pp*: 0.82) is formed by two main lineages: the most inclusive, leading to the specimens of *Asiatoceratodus cf. tiguidentis*, and the other including the specimens referred to *Neoceratodus africanus*, *Lavocatodus humei* and *Equinoxiodus schultzei*. The robustness of the higher-level relationships among the main lineages including the Tunisian specimens is very low (*pp*<0.5) for the majority of nodes, and most of these nodes are recovered in less than half of the sampled trees (Figure 2). Nevertheless, this is expected because the evaluation of ceratodontid higher-level relationships was beyond the aims of this study, and the data matrix was assembled to test lower-level relationships using exclusively tooth plate features. Among the main lineages recovered in the MCCT, the analysis found support for the referral of specimen MGGC 21920 and MGGC 21922 to the *Lavocatodus* lineage (*pp*: 0.87). A subset of the Tunisian specimens is recovered among a lineage that is sister taxon of the clade including the *Equinoxiodus*, *Lavocatodus* and *Neoceratodus* lineages, but does not lead to non-Tunisian specimens.

Bayesian analysis integrating morphological and stratigraphic information simultaneously estimates relationships among clades and the timing of cladogenesis (Lee *et al.* 2014a, Lee *et al.* 2014b). Based on the median age of the nodes in the MCCT, the lineage leading to all ingroup specimens diverged from the lineage leading to *Ptychoceratodus roemeri* in the Late Triassic (mean age: ~206 Mya). The mean age of divergence of the lineage leading to the specimen referred to *Ferganoceratodus* from its sister lineage is ~172 Mya, and the divergence of the lineage leading to *Ceratodus africanus* specimen from the lineage including all other specimens is inferred at ~155 Mya. The mean age of the last common ancestor of all Tunisian specimens included in the analysis is inferred at ~130

Mya. In the MCCT, all the terminal branches leading to the Tunisian specimens have been inferred to originate between 121 and 106 Mya.

The use of the FBD model in tree reconstruction allows to test whether one or more members of the analysed ingroup can be ancestor(s) of other sampled taxa and formed anagenetic series. Exploration of the relationships found among the post-burnin trees saved indicates that the median number of sampled ancestors *per* topology sampled is 7 (95% confidence interval: 0-14).

When the sampled localities are plotted on the MCCT diagram (Figure 3), all the four main lineages including the Tunisian specimens are represented at the El Mra locality. The two specimens from El Hmima (MGGC 21919 and 21920) resulted, respectively, one among the *Asiatoceratodus* lineage as sister taxon of one of the two specimens from El Kambout, and the other as sister taxon of the lineage leading to the two non-Tunisian specimens of *Lavocatodus humei*. The other specimen collected at El Kambout resulted a member of the *Asiatoceratodus* lineage. Among the specimens collected at the Oum ed Diab locality, four formed a clade that is nested among the *Asiatoceratodus* lineage. The other three specimens from Oum ed Diab resulted, respectively, each among the *Equinoxiodus*, *Lavocatodus* and *Neoceratodus* lineages. All the other specimens were collected from El Mra and are referable to the four main lineages. The BBM analysis of the locality distributions relative to the phyletic framework inferred El Mra as the ancestral area for the last common ancestor of the Tunisian sample and for most of the lineages of the sample, and Oum ed Diab as the ancestral area for a subclade of the *Asiatoceratodus* lineage (the sample from the other localities is too small to be analysed). The time-events algorithm implemented in RASP was used to estimate the number of cladogenetic events inferred to be recorded at the two localities according to the phylogenetic framework. This test is used to compare the richness of the fossil record from El Mra relative to that from Oum ed Diab, assuming that, given the relative geographic proximity and lateral continuity between the two series (Fanti et al. 2016a) the difference in their taxonomic disparity is mostly due to depositional and taphonomic factors than a genuine evolutionary signal, and the more inclusive the stratigraphic series is the larger number of cladogenetic events are documented there. The time-events algorithm test for the two localities suggests that the currently known fossil record from Oum ed Diab is stratigraphically less inclusive than the

record from El Mra and overlaps only the youngest part of the record from the latter locality (Figure 3A). The BBM analysis also revealed a shared pattern among the Tunisian specimens relative to the localities where they were sampled: all the specimens from El Hmima, El Kambout and Oum ed Diab are nested among clades formed by the specimens from El Mra. Although this result may be partly a sampling artefact, biased by the richer sample from El Mra relative to the other localities, it is noteworthy that the inferred relationships among the localities, according to the MCCT topology, is described by a relatively simple scenario that requires seven migration events, all starting from El Mra (Figure 3B): three migration events from El Mra to Oum ed Diab, two events from El Mra to El Kambout, two events from El Mra to El Hmima. None of the specimens from El Mra is interpreted as being the result of migration events started from the other localities.

## DISCUSSION

Fanti et al. (2016a) identified the majority of the specimens included in this sample at the genus- or species-level based on the shared presence of diagnostic features reported in the literature. About 60% of the taxonomic identifications provided by Fanti et al. (2016a) are confirmed by the result of the Bayesian analysis (Table 1). In particular, the identification of all but one specimen of *Asiatoceratodus*, and of all specimens of *Equinoxiodus* and *Lavocatodus* suggested by Fanti et al. (2016a) is confirmed by the result of the Bayesian analysis. All the specimens identified as belonging to *Ceratodus* or *Ferganoceratodus* by Fanti et al. (2016a) have been re-interpreted as belonging to the three above mentioned taxa or to a yet-unnamed lineage. These results suggest that the combinations of tooth plate features used in literature to diagnose the taxa *Asiatoceratodus*, *Equinoxiodus* and *Lavocatodus* are phylogenetically significant and allow an accurate identification of these taxa even using isolated dental elements. On the contrary, the results of the Bayesian analysis do not support the identification of the isolated tooth plates to *Ceratodus* and *Ferganoceratodus*: this suggests that the two taxa cannot be identified from isolated tooth plates, or, alternatively, that the features used in literature to diagnose them define non-monophyletic assemblages. The second interpretation is indirectly supported by the topology of the MCCT (Figure 1):

*Ferganoceratodus* and *Ceratodus* form a paraphyletic series along the basal branch leading to the clade containing the other genus-level taxa and the Tunisian specimens.

The majority of the nodes recovered by the Bayesian analysis of the modified data set of Fanti *et al.* (2016a) using the FBD model show low posterior probability values ( $pp < 0.5$ ). This result is not unexpected, and is due to the low number of phylogenetically significant features obtained from the tooth plate morphology relative to the number of included specimens (43 characters vs. 53 taxonomic units) and the high level of homoplasy among the specimens (Fanti *et al.* 2016a). Nevertheless, the Bayesian analysis performed here integrated stratigraphic information, not included in the previous analysis using parsimony as tree search strategy (Fanti *et al.* 2016a), and obtained some relationships with a relatively robust support. In particular, the analysis indicates that the last common ancestor of the sampled specimens from Tunisia was Early Cretaceous in age (~130 Mya). This topology constraints the origin and evolution of the dipnoan taxa sampled in the Ain el Guettar Formation to a 20-30 Myrs long interval. This result markedly differs from that discussed by Fanti *et al.* (2016a: figure 10) based on parsimony analysis, that estimated at least four lineages leading to the Tunisian specimens that had to be extended back to the Middle Jurassic in order to re-conciliate the phyletic pattern with the stratigraphic placement of some of the non-Tunisian specimens included in the analysis.

In summary, the Bayesian analysis of the dipnoan specimens from the Ain el Guettar Formation does not support the faunal diversity reported by Fanti *et al.* (2016). As stated above, *Ferganoceratodus* is found to be outside the least inclusive clade containing all Tunisian specimens. Furthermore, none of the specimens sampled has been referred to *Ceratodus* (*contra* the results in Fanti *et al.* 2016a): the specimens referred by Fanti *et al.* (2016a) to that genus have been placed by the Bayesian analysis among the basalmost branch of the *Asiatoceratodus* lineage (Table 1). The Bayesian analysis confirms that *Asiatoceratodus* is the most abundant clade, being it found in all localities (Fanti *et al.* 2016a). The *Equinoxiodus* lineage is found in two localities (El Mra and Oum ed Diab). The *Lavocatodus* lineage is also recorded in two localities, respectively, at El Hmaima (where *Equinoxiodus* is not found) and Oum ed Diab. The *Neoceratodus* lineage is found at El Mra and Oum ed Diab. The 95% confidence ranges of the ages of the terminal tips from the four Tunisian localities inferred by the Bayesian analysis broadly overlap, a result

that confirms the lateral equivalence among the series from the four localities (Fanti *et al.* 2016a). The RASP analysis was used to compare the richness of the fossil record from the El Mra locality relative to that from the Oum ed Diab locality, following the hypothesis that the sections exposed at the two localities were laterally equivalent (Fanti *et al.* 2016a). Focusing on the MCCT framework and the distribution of the specimens in the localities, the scenario resulted by the RASP analysis suggests that the dipnoan lineages sampled from the El Kambout, El Hmaima and Oum ed Diab localities descended from migration events originated from the El Mra locality. Apparently, the relationships among the sampled localities (i.e., El Mra resulting the ancestral locality for the Tunisian sample inferred by the RASP analysis) and the asymmetrical relationships in the polarity of the migration events among the four localities inferred by the RASP analysis of the MCCT topology (i.e., all migration events started from El Mra) challenge the hypothesis that these localities were laterally equivalent, and may indicate diachrony among these sections. The migration episodes inferred by the RASP analysis could be considered as spurious events, analytical artefacts due to poor sampling from the sections at the El Hmaima, El Kambout, and Oum ed Diab localities. Although artefacts in specimen collection and the non-homogeneous sampling among the localities may explain this pattern (in particular, about 74% of the whole sample was collected at the El Mra locality), the difference in the time-algorithm profiles of the two most sampled localities (Figure 3A) may also be explained assuming that the stratigraphic sequence sampled at the Oum ed Diab locality is equivalent to only the upper part of the series that is more extensively recorded at El Mra. This alternative interpretation is confirmed by stratigraphic analyses at regional scale: although the El Mra and Oum ed Diab beds represent partially lateral equivalent deposits, the latter locality is representative only of the youngest history of the section (Fanti *et al.* 2016a and references therein). The lower beds of this unit (mostly recorded at El Mra) are interpreted as fluvial sand bars that deposited in a vast estuarine system, whereas the overlying deposits (recorded at Oum ed Diab) gradually shift to shoreface, tidal flat, and foreshore deposits.

In this study, the FBD model with sampled ancestors (Gavryushkina *et al.* 2016) has been applied for the first time to a set of exclusively extinct taxa sampled at the specimen level (thus, avoiding *a priori* assumptions on species-level definitions, diagnosis and

inclusiveness). One advantage of the FBD model relative to previously developed models for phylogenetic inference is that it allows to test ancestor-descendant relationships among a sample of fossils. The failed recognition of ancestors among a sample of taxonomic units may lead to the inference of spurious cladogenetic events, and to overestimation of the number of co-existing lineages along a particular time interval. Furthermore, overestimation of cladogenetic events significantly bias the parameter estimation at branches, in particular the estimation of lineage extent and duration (Gavryushkina *et al.* 2014, Gavryushkina *et al.* 2016).

The Triassic or Jurassic origins for some of the Tunisian lineages that were inferred by the stratigraphic calibration of the topology resulted by the parsimony analysis in Fanti *et al.* (2016a), compared to the exclusively Cretaceous ages recovered by the Bayesian analysis using the FBD model here, is probably biased by methodological artefacts, in particular, the use of tree search strategies, like parsimony, that are unable to incorporate stratigraphic information in tree reconstruction. Although the use of the FBD model with sampled ancestors represents a more realistic reconstruction of the evolutionary history of the Ain el Guettar Formation dipnoan specimens compared to the strictly cladogenetic pattern resulted by parsimony analysis (which does not incorporate stratigraphic information during the tree search), it should be remarked that the FBD model assumes uniform rate of sampling for the fossil specimens over time. Nevertheless, the sample analysed here does not adequately met such assumption, because it is not uniformly distributed over time (i.e., although the whole sample spans from the Late Triassic to the Late Cretaceous, the large majority of the specimens is distributed exclusively in the Albian-Cenomanian stage). Future implementations of the FBD model with sampled ancestors may incorporate heterogeneity in the rate of fossil sampling over time (see Stadler *et al.* 2013, for an epidemiological application of this approach).

The use of specimens as terminal units instead of species means that the topological pattern recovered in the MCCT may include both intraspecific and interspecific relationships. In particular, intraspecific relationships may indicate genealogical sequences among populations of the same species, or anagenetic sequences along a phyletic lineage without splitting events (Gould 2002). In this study, the character list was based on morphological features previously used for species/genus-level identifications among

Mesozoic ceratodontids, and it is not unexpected that the most robust relationships found by the Bayesian analysis are among the nodes that support supraspecific relationships, whereas the intraspecific relationships result relatively weakly supported. The incorporation of age uncertainty (tip priors) in the FBD model allows the analysis to simulate anagenetic series among the specimens from the same stratigraphic series because tip-dates were treated as random variables with uniform prior distributions, with bounds based on the shortest chronostratigraphic range including the Ain el Guettar Formation. These anagenetic series are retained in the saved trees if they fit the data (in particular, the morphological information) better than a strictly cladogenetic pattern.

## CONCLUSIONS

Phylogenetic analysis integrating morphological and stratigraphic information and using the Fossilized Birth-Death model implemented by Gavryushkina *et al.* (2016) was applied to investigate the diversity among a sample of isolated specimens referred to dipnoan sarcopterygians from the Ain el Guettar Formation. The analysis estimated an earliest Cretaceous age for the last common ancestor of the Tunisian sample and provided a framework for comparing the taxonomic composition of the samples from distinct localities at the Ain el Guettar Formation. Previous analyses using parsimony suggested five or more genus-level lineages included in this Tunisian sample (Fanti *et al.* 2016a). In particular, Fanti *et al.* (2016a) included *Ceratodus* and eventually *Ferganoceratodus* among the lineages represented in the sample, a result not supported by the Bayesian analysis performed here. The taxonomic content of the four Tunisian localities sampled is not homogeneous. Although sampling artefacts cannot be dismissed among the factors producing this taxonomic heterogeneity, comparison between the phylogenetic pattern resulted and the geographic distribution of the specimens among the sampled localities supports the hypothesis that the El Mra locality represents a stratigraphic sequence more inclusive than the other localities. This interpretation is in agreement with the stratigraphic analysis of the sampled localities along the Oum ed Diab Member, which indicates that the largest part of the series is recorded at El Mra (Fanti *et al.* 2016a). In the previous analysis of the sample, Fanti *et al.* (2016a) suggested that the high taxonomic diversity among the Ain el Guettar dipnoans was inflated by taphonomic artefacts. Although this study does not

dismiss some role for taphonomic factors in inflating the diversity recovered in the Ain el Guettar Formation (Fanti *et al.* 2016a), it is suggested that the taxonomic diversity of fossil assemblages may be inflated by analytical approaches not taking into account the stratigraphic information or the presence of anagenetic lineages (see Fanti *et al.* 2014).

The FBD model with sampled ancestors and incorporating tip priors for the analysis of fossil taxa may constitute a novel approach not only because it integrates morphological and stratigraphic information in macroevolutionary and systematic analysis of higher-level clades, but also as a methodology for lower-level taxonomic analysis using specimens and individuals as terminal units instead of species. As a method discriminating anagenetic lineages from cladogenetic patterns, the FBD model, and in particular the approach used here incorporating tip age uncertainty, may improve our knowledge of those phenomena at the boundary between micro- and macroevolution (Gould 2002). The recognition of ancestor-descendant relationships in fossils is debated (Szalay 1977, Bretsky 1979, Dayrat 2005, Scannella *et al.* 2015). In this study, 95% of the sampled trees include a number of sampled ancestors ranging between 0 and 14 (median value, 7; Figure 4). This value suggests that up to 23% of the specimens collected in the sample may represent members of populations that are anagenetic ancestors of the other individuals included. As noted above, failed recognition of potential ancestors may led to overestimate the number of lineages represented in a fossil assemblage. The application of the FBD model with sampled ancestors and incorporating tip age uncertainty to a broad series of fossil clades may help in estimating the frequency of ancestor-descendant relationships in the fossil record. Furthermore, this method may also represent an auxiliary tool for testing hypotheses on the taxonomic diversity among stratigraphically related localities.

## **Acknowledgments**

I thank Federico Fanti and the MGGC direction for access to the studied material, and Mike Lee for discussions on application of Bayesian phylogenetics in palaeontology. Alexandra Gavryushkina is thanked for the help in the use of BEAST2. Detailed comments and suggestions by Editor Kenneth De Baets, Paul Z. Barrett and two anonymous reviewers significantly improved the quality of this manuscript.

Figures

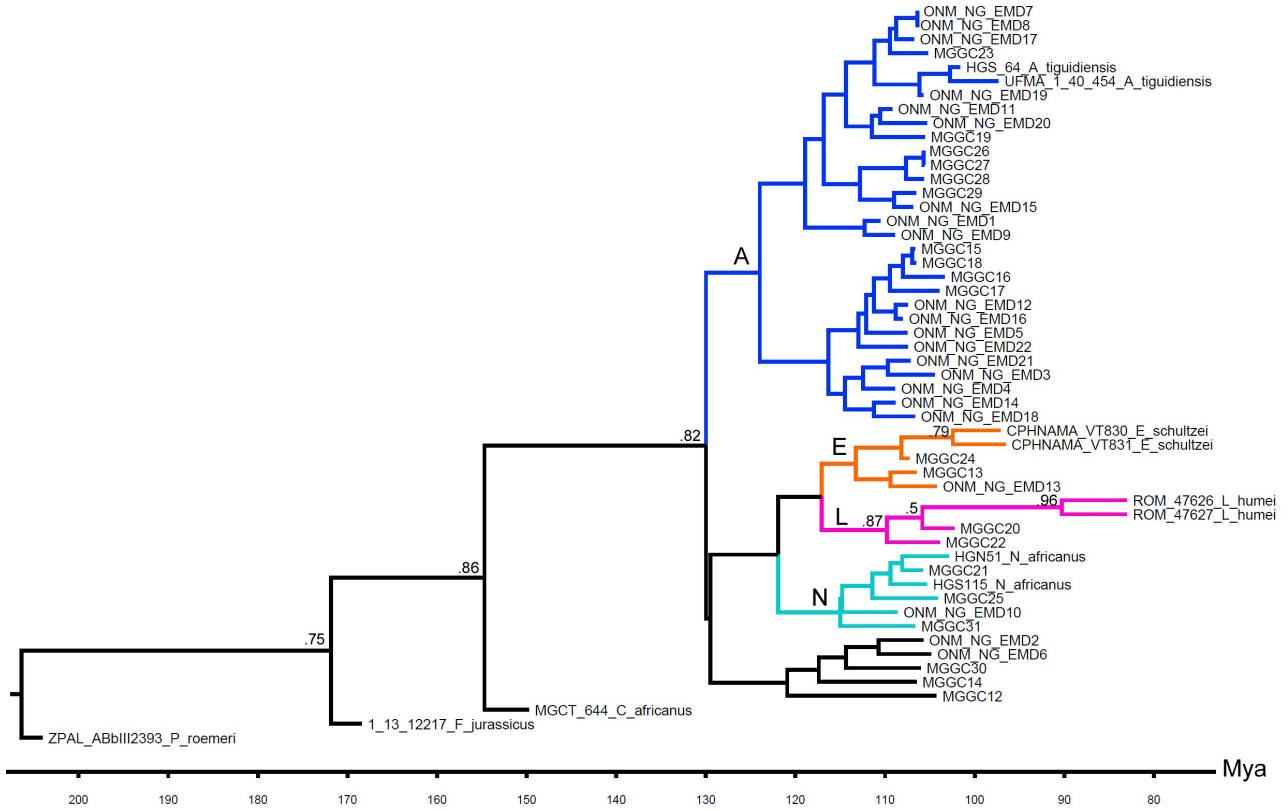


**Figure 1: MCCT resulted by Bayesian phylogenetic analysis of the dipnoan specimens discussed in this study.** Numbers adjacent to nodes indicate posterior probability value greater than or equal to 0.5. Abbreviations: A, *Asiatoceratodus* lineage; E, *Equinoxiodus* lineage; L, *Lavocatodus* lineage; N, *Neoceratodus* lineage.

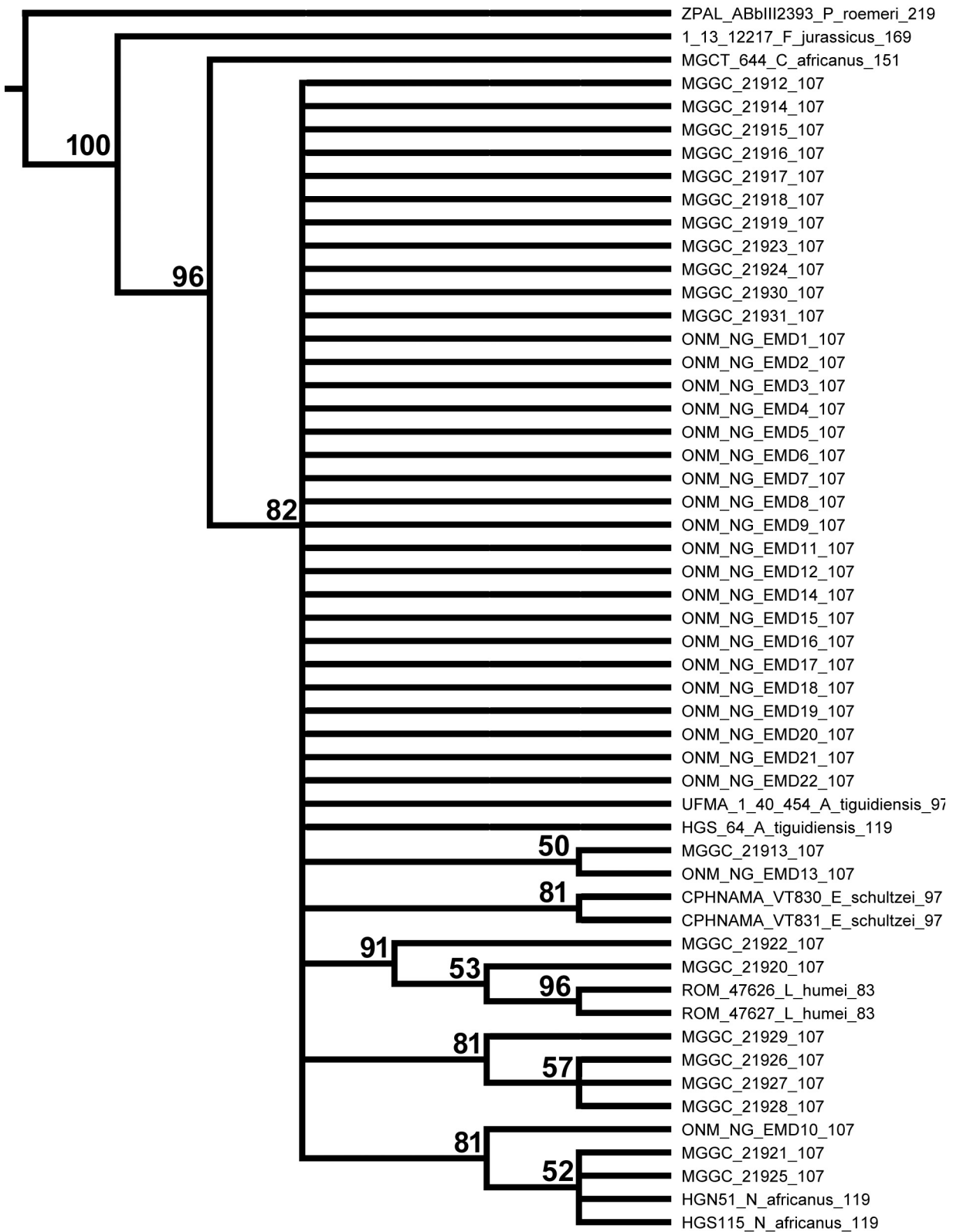


**Figure 2: Half compact (majority rule) consensus of the topologies found among the post-burnin trees saved.** Branch lengths not to scale. Numbers at end of terminal unit names indicate mean value of tip priors (in Mya).

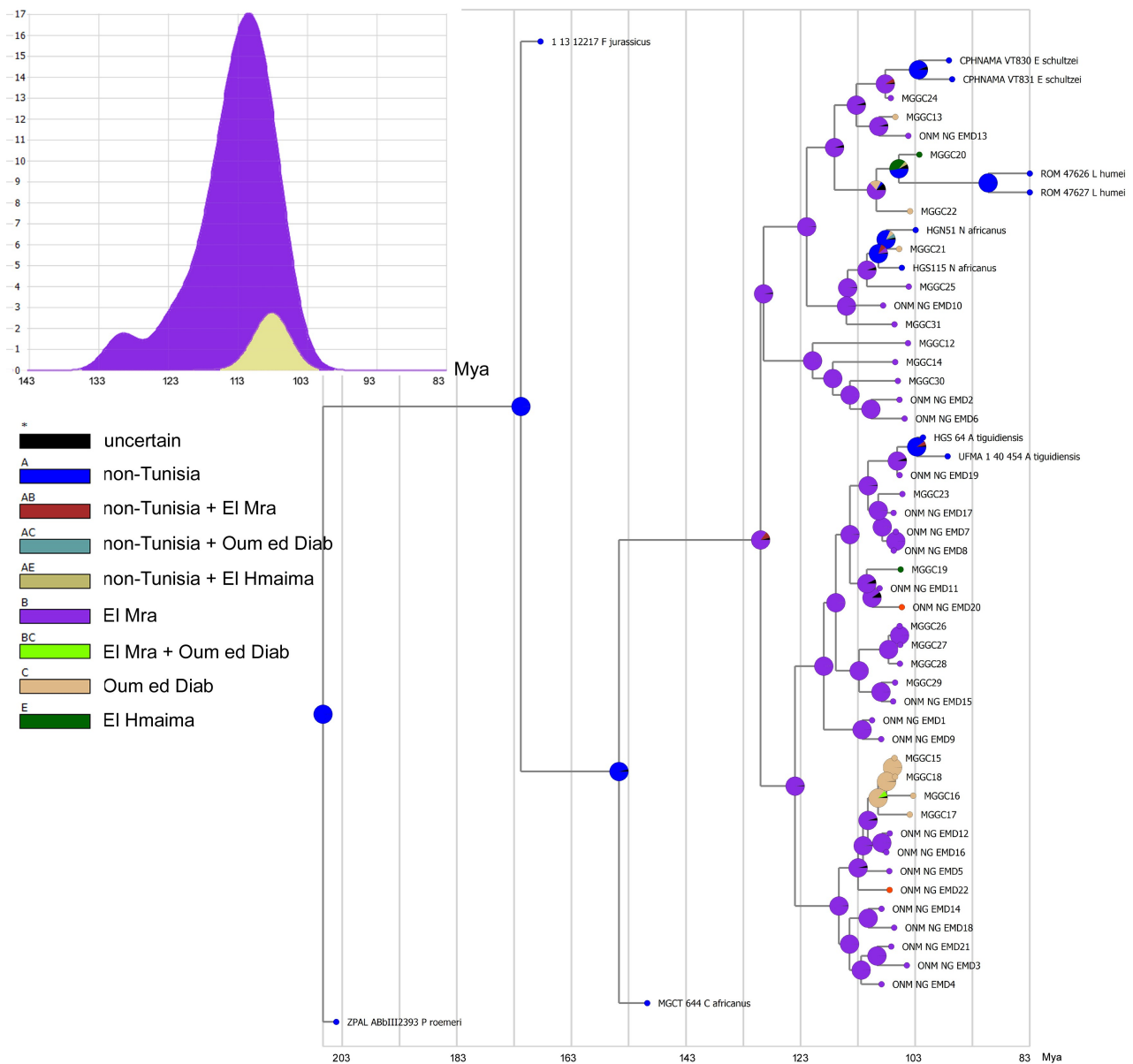


**Figure 3: Stratigraphic inference from the MCCT framework.** A, result of the time-events algorithm analysis using RASP for the El Mra and Oum ed Diab localities, showing the number of cladogenetic events inferred at El Mra and Oum ed Diab. B, Ancestral Area Reconstruction at the locality-scale using the framework obtained by the phylogenetic analysis using the BBM method in RASP.

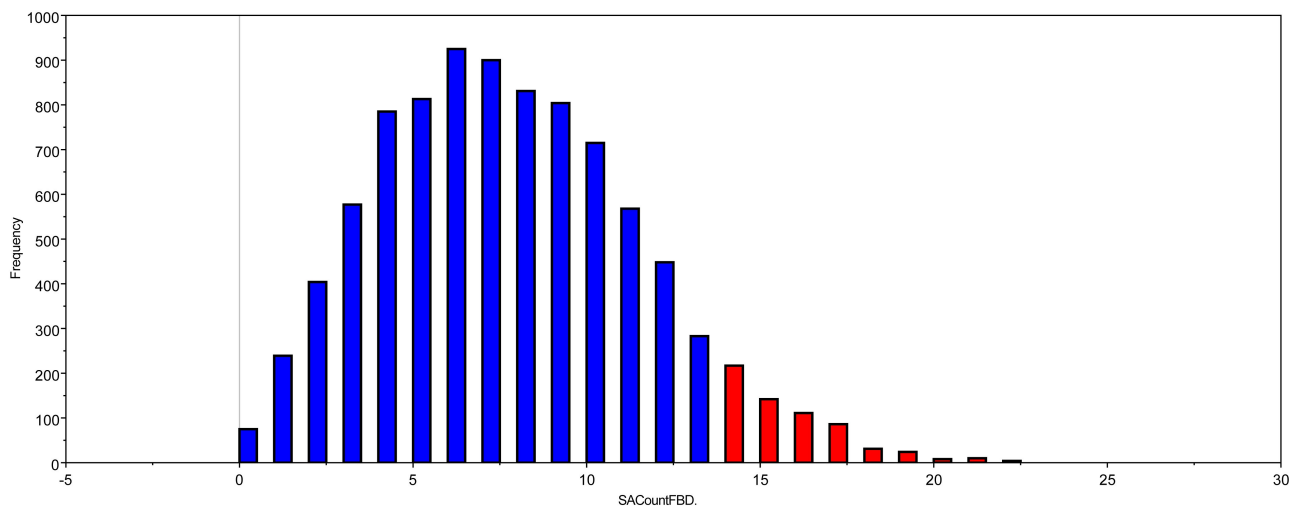


**Figure 4. Frequency of sampled ancestors counted (SACountFBD) in the post-burnin trees recovered.** The 95% confidence interval is indicated in blue.

## References

- Bell P.B., Cau A., Fanti F., Smith E. 2016. A large-clawed theropod (Dinosauria: Tetanurae) from the Lower Cretaceous of Australia and the Gondwanan origin of megaraptorid theropods. *Gondwana Research* 36:473-487.
- Berg L.S. 1940. Classification of fishes, both recent and fossil. Reprint of *Akademiia nauk SSSR Zoologicheskii Institut Trudy* 5:1-517.
- Bouckaert R.R., Heled J., Kuehnert D., Vaughan T.G., Wu C.-H., Xie D., Suchard M.A., Rambaut A., Drummond A.J. 2014. BEAST 2: A software platform for Bayesian evolutionary analysis. *PLoS Computational Biology* 10(4): e1003537
- Bretsky S.S. 1979. Recognition of ancestor–descendant relationships in invertebrate paleontology. In *Phylogenetic analysis and paleontology* (eds Cracraft J, Eldredge N), pp. 113-163. New York, NY: Columbia University Press.
- Cau A., Fanti F. 2016. High evolutionary rates and the origin for the Rosso Ammonitico Veronese Formation (Middle-Upper Jurassic of Italy) reptiles. *Historical Biology* 28(7):952-962.
- Close R.A., Friedman M., Lloyd G.T., Benson R.B.J. 2015. Evidence for a Mid-Jurassic Adaptive Radiation in Mammals. *Current Biology* 25:2137-2142.
- Dayrat B. 2005. Ancestor–descendant relationships and the reconstruction of the Tree of Life. *Paleobiology* 31, 347-353.

- Dembo M., Matzke N.J., Mooers A.O., Collard M. 2015 Bayesian analysis of a morphological supermatrix sheds light on controversial fossil hominin relationships. *Proceedings of the Royal Society B* 282:20150943.
- Drummond A.J., Suchard M.A., Xie D., Rambaut A. 2012. Bayesian phylogenetics with BEAUti and the BEAST 1.7. *Molecular Biology and Evolution* 29:1969-1973.
- Fanti F., Cau A., Cantelli L., Hassine M., Auditore M. 2015. New Information on *Tataouinea hannibalis* from the Early Cretaceous of Tunisia and implications for the tempo and mode of rebbachisaurid sauropod evolution. *PLoS One* 10 (4): e0123475.
- Fanti F., Cau A., Martinelli A., Contessi M. 2014. Integrating paleoecology and morphology in theropod diversity estimation: a case study from the Aptian–Albian of Tunisia. *Paleogeography Paleoclimatology Paleoecology* 410:39-57.
- Fanti F., Larocca Conte G., Angelicola L., Cau A. 2016a. Why so many dipnoans? A multidisciplinary approach on the Lower Cretaceous lungfish record from Tunisia. *Paleogeography Paleoclimatology Paleoecology* 449:255-265.
- Fanti F., Miyashita T., Cantelli L., Mnasri F., Dridi J., Contessi M. and Cau A. 2016b. The largest Thalattosuchian (Crocodylomorpha) supports Teleosaurid survival across the Jurassic-Cretaceous boundary. *Cretaceous Research* 61:263-274.
- Gavryushkina A., Heath T.A., Ksepka D.T., Stadler T., Welch D., Drummond A.J. 2016. Bayesian total evidence dating reveals the recent crown radiation of penguins. *Systematic Biology* doi: 10.1093/sysbio/syw060.
- Gavryushkina A., Welch D., Stadler T., Drummond A.J. 2014. Bayesian inference of sampled ancestor trees for epidemiology and fossil calibration. *PLoS Computational Biology* 10(12): e1003919.
- Gould S.J. 2002. *The Structure of Evolutionary Theory*, Cambridge MA: Belknap Press of Harvard University Press, ISBN 978-0-674-00613-3.
- Kuntner M., Agnarsson I. 2006. Are the Linnean and Phylogenetic Nomenclatural Systems Combinable? Recommendations for Biological Nomenclature. *Systematic Biology* 55:774-784.
- Lee M.S.Y., Cau A., Naish D., Dyke G.J. 2014a Morphological clocks in paleontology, and a mid-Cretaceous origin of crown Aves. *Systematic Biology* 63:442-449.
- Lee M.S.Y., Cau A., Naish, D., Dyke G.J. 2014b. Sustained miniaturization and anatomical innovation in the dinosaurian ancestors of birds. *Science* 345:562-566.

- Lee M.S.Y., Palci A. 2015. Morphological phylogenetics in the genomic age. *Current Biology* 25:R922–R929.
- Lewis P.O. 2001 A likelihood approach to estimating phylogeny from discrete morphological character data. *Systematic Biology* 50:913-925.
- Mounier A., Caparros M. 2015. The phylogenetic status of *Homo heidelbergensis* – a cladistic study of Middle Pleistocene hominins. *Bulletins et mémoires de la Société d'anthropologie de Paris* 27:110-134.
- Müller J. 1844. Ueber den Bau und die Grenzen der Ganoiden und über das natürliche System der Fische. *Abhandlungen der Königlich Preussischen Akademie der Wissenschaften*, Berlin: 117-126.
- O'Reilly J.E., Puttick M.N., Parry L., Tanner A.R., Tarver J.E., Fleming J., Pisani D., Donoghue P.C.J. 2016. Bayesian methods outperform parsimony but at the expense of precision in the estimation of phylogeny from discrete morphological data. *Biology Letters* 12: 20160081.
- Pyron RA. 2011. Divergence time estimation using fossils as terminal taxa and the origins of Lissamphibia. *Systematic Biology* 60:466481 DOI 10.1093/sysbio/syr047
- Rambaut A., Drummond A.J. 2009. Tracer: MCMC Trace Analysis Tool v1.5. <http://beast.bio.ed.ac.uk/>
- Ronquist F., Kloppstein S., Vilhelmsen L, Schulmeister S., Murray D.L., Rasnitsyn A.P. 2012. A Total-Evidence Approach to Dating with Fossils, Applied to the Early Radiation of the Hymenoptera. *Systematic Biology* 61 (6): 973-999.
- Scannella J.B., Fowler D.W., Goodwin M.B., Horner J.R. 2014. Evolutionary trends in *Triceratops* from the Hell Creek Formation, Montana. *Proceedings of the National Academy of Sciences of the United States of America* 111:10245-10250. doi: 10.1073/pnas.1313334111
- Stadler T. 2010. Sampling-through-time in birth-death trees. *Journal of Theoretical Biology* 267(3):396-404.
- Stadler T., Kühnert D., Bonhoeffer S., Drummond A.J. 2013. Birth–death skyline plot reveals temporal changes of epidemic spread in HIV and hepatitis C virus (HCV). *Proceedings of the National Academy of Sciences of the United States of America* 110:228-233.

- Szalay F.S. 1977. Ancestors, descendants, sister groups and testing of phylogenetic hypotheses. *Syst. Biol.* 26, 12-18.
- Tschopp E., Mateus O.V., Benson R.B.J. 2015. A specimen-level phylogenetic analysis and taxonomic revision of Diplodocidae (Dinosauria, Sauropoda). *PeerJ.* 3:e857.
- Upchurch P, Tomida Y, Barrett PM. 2004. A new specimen of *Apatosaurus ajax* (Sauropoda: Diplodocidae) from the Morrison Formation (Upper Jurassic) of Wyoming, USA. *National Science Museum Monographs* 26:1-118.
- Vorobiyeva E.I. 1967. Triassic ceratod from South Fergana and remarks on the systematics and phylogeny of ceratodontids. *Paleontological Journal* 4:1-87.
- Wright A.M., Hillis D.M. 2014. Bayesian analysis using a simple likelihood model outperforms parsimony for estimation of phylogeny from discrete morphological data. *PLoS ONE* 9:e109210.
- Yu Y., Harris A.J., Blair C., He X.J. 2015. RASP (Reconstruct Ancestral State in Phylogenies): a tool for historical biogeography. *Molecular Phylogenetics and Evolution* 87:46-49.

Page left blank

## GENERAL CONCLUSIONS

The stratigraphic occurrence of a fossil and its phylogenetic affinities are often analysed independently from each other. Although the stratigraphic position and the phylogenetic placement of a fossil taxon are implicitly recognized as two related and complementary phenomena stemming from evolutionary history, they are commonly analysed using methods and aims that are distinct into two disciplines, well separated in the two branches of the Natural Sciences: a geological approach (Stratigraphy) and a biological approach (Systematics). In this thesis, it is documented how these two types of information provided from the Fossil Record can be integrated, not only qualitatively or *a posteriori*, but also quantitatively and simultaneously, by applying a methodology that incorporates both data sets.

Here, the various studies and analyses performed in the nine chapters of the thesis are summarised, focusing on the methods and conclusions they share. In Chapters 1, 2 and 3 of this thesis, a series of case studies on material collected from the Ain el Guettar Formation of southern Tunisia has shown that the analysis of the morphological diversity recovered in fossil localities may lead to erroneous interpretations (in particular, taxonomic overestimations) if the biological information is not adequately integrated with stratigraphic and taphonomic analyses. The application of phylogenetic analysis using parsimony indicated that the eight tooth morphotypes identified among the theropod dinosaur sample (Chapter 1) can be interpreted as different ontogenetic and/or the positional variability among three lineages. Both taphonomic and depositional analyses of this sample, once combined with the phylogenetic interpretations, suggest that the three theropod clades recovered in the Ain el Guettar Formation were partitioned into two ecologically - and environmentally - segregated groups. The parsimony analysis of a sample of tooth plates recovered from the Ain el Guettar Formation and referable to dipnoans sarcopterygians (Chapter 2) suggests at least five distinct lineages. This result was integrated with taphonomic and stratigraphic analyses, in order to determine whether the high diversity in the sample could be explained by non-biological factors. These analyses suggest that the taxonomic diversity in the sample is probably inflated by taphonomic and depositional factors. The combination of morphological and taphonomic analyses on the ornithischian

remains from the Ain el Guettar Formation (Chapter 3) suggests that the record of this clade is biased by a marked taphonomic filter: the group is represented exclusively by isolated teeth from large-bodied iguanodontians collected exclusively from the Oum ed Diab Member. The results of the three studies summarized above, even if focusing on clades relatively disparate both phylogenetically and ecologically, converge to a common conclusion: the evolutionary history of these Cretaceous clades in Tunisia (and, eventually, in the rest of North Africa) cannot be adequately understood, leading to misinterpretations (in particular, taxonomic diversity overestimation), if the biological information is not integrated with the stratigraphic and taphonomic analyses of the samples.

Lee et al. (2014a) introduced a novel phylogenetic method for the analysis of the relationships among a set of fossils taxa, which integrated simultaneously the morphological diversity and the stratigraphic distribution of the analysed taxonomic units. Compared to the tree search strategy most widely used in palaeontology (i.e., parsimony analysis of discrete morphological characters), the Bayesian method of Lee et al. (2014a) extends the phylogenetic analysis beyond the mere reconstruction of topologies since it can directly infer dated phylogenies where the terminal taxa differ in stratigraphic age, by estimating the optimal phylogeny and lineage durations that best explain the stratigraphic distribution and the characters exhibited by the terminal taxa.

In the conclusion of their study, Lee et al. (2014a: 447) wished their analysis “*may spur further empirical analyses*” to investigate the range of applications and improve the methodological basis of this new approach. This thesis aims to add a contribution to that hope by providing a series of case studies exploring novel areas of application for this method. In particular, an updated version of the protocol described by Lee et al. (2014a) has been introduced here (Chapter 4). This modified version used for the first time the BEAST package (Drummond et al. 2012) as analytical tool for the phylogenetic analyses of fossil taxa instead of the MrBayes software used in previous analyses incorporating morphological information from fossils (e.g., Lee et al. 2014a, Ronquist et al. 2012a). This new approach allowed to implement a series of methods (listed in the Supplementary material of Chapter 4) previously limited or unavailable. The tree search algorithms used in BEAST can simultaneously infer tree topology, divergence dates (lineage durations), and ancestral states for both discrete and continuous traits. This allows to implement

likelihood-based models of evolution for all quantitatively-defined morphological features. In addition to calibrating trees *via* tip ages, the novel method can also enforce node calibrations analogous to those enforced in molecular phylogenetic analyses, with the relevant novelty that the last common ancestor of a particular set of taxa could be constrained to have a defined age (or stratigraphic range) even without topological constraints (i.e., the *a priori* assumption that such node defines a monophyletic group formed exclusively by that set of taxa). This implementation allows to incorporate stratigraphic information relative to a set of taxa even when the phylogenetic status of that set (i.e., its monophyly relative to other taxa included in the analysis) is uncertain. In the analysis performed in Chapter 4, a continuously-variable trait (i.e., a measurement used as proxy of body size) was incorporated in the analysis of discrete morphological characters (an approach not tested in the analysis by Lee et al. 2014a), and the evolution of this trait was determined by estimating the ancestral value at nodes according to the relationships among the taxa and the duration of the branches, both inferred by the analysis. In Chapters 5, 6, 7, 8 and 9, this novel methodology was used as main tool for phylogenetic inference, and as auxiliary tool for analyses focusing on palaeoecological inference, for large-scale palaeobiogeographic reconstruction, and for biostratigraphic analysis at the regional scale.

In Chapters 5 and 7, the ultrametric topologies inferred using the method discussed in Chapter 4 have been used as phyletic frameworks for testing palaeobiogeographic hypotheses. Both studies used the software RASP (Reconstruct Ancestral State in Phylogeny), in particular the palaeogeographic models Statistical Dispersal-Vicariance Analysis (S-DIVA) and Bayesian Binary Markov (BBM) Chain Monte Carlo analysis (Yan et al., 2010). As discussed in those studies, the use of ultrametric topologies as frameworks (i.e., topologies where both nodes and branches are time-calibrated) for the palaeogeographic analyses allows to incorporate chronological information (in particular, divergence time from the common ancestry) in the inference of the ancestral state at nodes. In analogy with the Bayesian inference analyses of morphological characters, where the stratigraphic distribution is integrated with morphological diversity to infer tree topology, the length of the branches (a by-product of tree topology inference) is integrated with geographic distribution to infer the palaeobiogeographic pattern. In both approaches,

ancestral state reconstruction in the nodes of the topology is inferred according to the significance of the states (both morphological and geographic) present among the taxa: this significance is itself inferred according to the stratigraphic distribution of the taxa.

A promising area of application of the method introduced in this thesis is the use of Bayesian tip-dating methods as tool for independent test of stratigraphic hypotheses. This application was tested in Chapter 9, where the data set used in Chapter 2 (where parsimony analysis was used as tree search strategy) was re-analysed and the phylogenetic framework resulted was used for inferring the relative stratigraphy among the sampled localities. In Chapter 9, the tip-dating approach that was widely used in the previous chapters for the analysis of macroevolutionary patterns (i.e., phenomena at or above the species level), was used in the analysis of microevolutionary patterns (i.e., phenomena involving the single individuals as evolutionary units). In that study, the “Fossilized Birth-Death with Sampled Ancestors” (FBDSA) model of Gavryushkina et al. (2016), a recently-introduced method that discriminates anagenesis from cladogenesis in evolutionary reconstruction, was applied to a sample formed exclusively by fossil specimens. The application of the FBDSA model to data sets formed by specimen-level terminals follows recent implementations of the BEAST package that allow to incorporate the stratigraphic uncertainty in the age of the fossil specimens among the priors used in the settings of the tree search strategy. This implementation further improves the accuracy of the models used to estimate the combination of biological and geological processes (the evolutionary pattern and the preservational filter) that generated the fossil record.

In conclusion, the Bayesian phylogenetic methods focusing on fossil taxa and the particular analytical protocol introduced in this thesis represent an innovative multidisciplinary tool in the following research areas, all of which expand the original aims of application for this method (i.e., the reconstruction of phylogenetic relationships among fossil taxa and a quantitative and testable inference of cladogenetic timing):

1. *Quantitative estimation of the rates of phenotypic evolution among fossil lineages.*

The inclusion of age priors in the reconstruction of phyletic relationships allows to estimate the rate of morphological evolution *per* branch. Thus, this approach maps on the phylogenetic framework any heterogeneity in the process of morphological

divergence. Once the amount of divergence is mapped, it provides a visual representation of the “hot spots” in phenotype evolution.

2. *Creation of ultrametric frameworks for palaeobiogeographic inference, in particular for analyses requiring branch lengths in ancestral area reconstruction.* A phylogenetic diagram may provide a framework for testing alternative scenarios on palaeogeography, since it constraints the possible geographic connections to that subset of routes compatible with the divergence pattern described by the phylogeny. Nevertheless, a phyletic pattern not calibrated stratigraphically is a weak basis for inferring palaeogeographic constraints, because it is unable to associate the timing of evolutionary divergences with the evolution of the geographic system. Furthermore, in absence of quantitative estimation of branch duration, it is unclear how alternative scenarios (in particular, those that support the same geographic network but differ in the duration of the geographic routes) can be discriminated. This novel method provides a quantitatively-defined base for the integration of palaeogeographic models in the reconstruction of clade history, and allows to compare alternative biogeographic scenarios according to their fit with the stratigraphic record.
3. *Comparison between the phylogenetic patterns among distinct lineages sharing the same palaeogeographic and stratigraphic ranges.* Distinct lineages may co-evolve or may be constrained to similar evolutionary trajectories if subjected to a similar adaptive regime. This novel approach allows to test whether a common environmental context constrained the evolution of distinct lineages along shared trajectories.
4. *Inference on the taxonomic diversity among a sample of individuals collected from the same stratigraphic unit.* Any palaeontological species (and, in general, any species) is a systematic hypothesis, a statement on the genealogical relationships among a set of individuals. Thus, the single individuals can properly be considered as unambiguous taxonomic units, whereas the species is a testable model on the causal patterns linking the individuals. An analysis of the biological diversity at the individual level of organization may lead to different interpretations if the morphological diversity in the sample is stable or directionally variable along the chronological axis (Gould 2002). This implies that the inclusion of stratigraphic

information in a model that reconstructs the phyletic patterns among the individuals may be used as a test on the robustness of the hypotheses called “fossil species”. The Bayesian method implemented here introduces a novel approach for testing the alpha-taxonomy in the fossil record.

5. *Auxiliary and independent test of stratigraphic relationships among fossil localities sharing the same fossil groups.* The method for the taxonomic discrimination mentioned in the last point may also be used to test alternative scenarios in biostratigraphy. Using a set of individuals that belong to the same clade, but were collected from different localities, the Bayesian approach discussed here can test the stratigraphic relationships among the sampled localities according to the phyletic pattern obtained by the morphological analysis of the fossil sample. This novel application estimates the stratigraphic placement of each individual according to the phyletic framework derived from the analysis of their morphological diversity. This approach stems from the biostratigraphic concept that the chronological distribution of the fossil forms is causally ordered, and, thus, it implies that such order, once reconstructed (for example, by phylogenetic analysis) may inform on the stratigraphic position of these fossils. The Bayesian method discussed here allows to estimate quantitatively the relationships between morphological divergence and stratigraphic distance, thus providing a quantitative estimation of the age of the fossils (and the age of their localities).

Following the Darwinian paradigm, the evolution is conceived as descent with modifications. The Evolutionary Palaeontology is thus meant as a multidisciplinary discipline integrating the analysis of descent (seeking for the causal patterns that link diachronous taxa) and the analysis of modifications (expressed in the Fossil Record by the morphological diversity). Combining and integrating quantitative information obtained from the geological history and the biological diversity, the method implemented here aims to contribute to the naturalistic revolution that so radically has shaped our view of Life over 150 years ago, when it was stated that “*from so simple a beginning endless forms most beautiful and most wonderful have been, and are being, evolved*”.

## **References listed in *Introduction, Material and Methods, General Aims of this Thesis, and General Conclusions***

- Benson R.B., Evans M., Smith A.S., Sassoon J., Moore-Faye S., Ketchum H.F., Forrest R. 2013. A giant pliosaurid skull from the late Jurassic of England. *PLoS One* 8(5):e65989. doi: 10.1371/journal.pone.0065989.
- Bell P.B., Cau A., Fanti F., Smith E. 2016. A large-clawed theropod (Dinosauria: Tetanurae) from the Lower Cretaceous of Australia and the Gondwanan origin of megaraptorid theropods. *Gondwana Research* 36:473–487.
- Carballido J.L., Salgado L., Pol D., Canudo J.I., Garrido A. 2012. A new basal rebbachisaurid (Sauropoda, Diplodocoidea) from the Early Cretaceous of the Neuquén Basin; evolution and biogeography of the group. *Historical Biology* 24:631–654.
- Cau A. 2014. The affinities of '*Steneosaurus barettoni*' (Crocodylomorpha, Thalattosuchia), from the Jurassic of Northern Italy, and implications for cranial evolution among geosaurine metriorhynchids. *Historical Biology* 26:433–440.
- Cau A., Dalla Vecchia F.M., Fabbri M. 2013. A thick-skulled theropod (Dinosauria, Saurischia) from the Upper Cretaceous of Morocco with implications for carcharodontosaurid cranial evolution. *Cretaceous Research* 40:251–260.
- Cau A., Dyke G.J., Lee M.S.Y., Naish D. 2014. Data from: Sustained miniaturization and anatomical innovation in the dinosaurian ancestors of birds. *Science* <http://dx.doi.org/10.5061/dryad.jm6pj>
- Cau A., Fanti F. 2016. High evolutionary rates and the origin for the Rosso Ammonitico Veronese Formation (Middle-Upper Jurassic of Italy) reptiles. *Historical Biology* 28(7):952–962.
- Darwin C.R. 1859. *On the Origin of Species by Means of Natural Selection, or the Preservation of Favoured Races in the Struggle for Life*. First Edition. London: John Murray, Albemarle Street.
- Dembo M., Matzke N.J., Mooers A.Ø., Collard M. 2015. Bayesian analysis of a morphological supermatrix sheds light on controversial fossil hominin relationships. *Proceedings of the Royal Society B* 282:20150943. <http://dx.doi.org/10.1098/rspb.2015.0943>

- Drummond A., Suchard M.A., Xie D., Rambaut A. 2012. Bayesian phylogenetics with BEAUti and the BEAST 1.7. *Molecular Biology and Evolution* 29:1969–1973.
- Fanti F., Cau A., Cantelli L., Hassine M., Auditore M. 2015. New Information On *Tataouinea hannibalis* From The Early Cretaceous of Tunisia And Implications For The Tempo And Mode Of Rebbachisaurid Sauropod Evolution. *Plos One* 10(4): e0123475:1–46.
- Fanti F., Cau A., Martinelli A., and Contessi M. 2014. Integrating palaeoecology and morphology in theropod diversity estimation: a case from the Aptian-Albian of Tunisia. *Palaeogeography, Palaeoclimatology, Palaeoecology* 410:39–87.
- Fanti F., Cau A., Panzarin L., Cantelli L. 2016b. Evidence of iguanodontian dinosaurs from the Lower Cretaceous of Tunisia. *Cretaceous Research* 60:267–274.
- Fanti F., Larocca Conte G., Angelicola L., Cau A. 2016a. Why so many dipnoans? A multidisciplinary approach on the Lower Cretaceous lungfish record from Tunisia. *Palaeogeography, Palaeoclimatology, Palaeoecology* 449:255–265.
- Fanti F., Miyashita T., Cantelli L., Mnasri F., Dridi J., Contessi M. and Cau A. 2016c. The largest Thalattosuchian (Crocodylomorpha) supports Teleosaurid survival across the Jurassic-Cretaceous boundary. *Cretaceous Research* 61:263–274.
- Farris J.S. 1976. Phylogenetic classification of fossils with Recent groups. *Systematic Zoology* 25:271–282.
- Gavryushkina A., Heath T.A., Ksepka D.T., Stadler T., Welch D., Drummond A.J. 2016. Bayesian total evidence dating reveals the recent crown radiation of penguins. *Systematic Biology* doi: 10.1093/sysbio/syw060.
- Gould S.J. 2002. *The Structure of Evolutionary Theory*, Cambridge MA: Belknap Press of Harvard University Press, ISBN 978-0-674-00613-3.
- Hendrickx C., Mateus O., 2014. Abelisauridae (Dinosauria: Theropoda) from the Late Jurassic of Portugal and dentition-based phylogeny as a contribution for the identification of isolated theropod teeth. *Zootaxa* 3759:1–174.
- Hennig W. 1965. Phylogenetic Systematics. *Annual Review of Entomology* 10:97–116.
- Hennig W. 1975. Cladistic Analysis or Cladistic Classification?: A Reply to Ernst Mayr. *Systematic Zoology* 24:244–256.

- Lee M.S.Y., Cau, A., Naish, D., Dyke, G.J. 2014a. Morphological clocks in palaeontology, and a Mid-Cretaceous origin of crown Aves. *Systematic Biology* 63:442–449. doi: 10.1093/sysbio/syt110.
- Lee M.S.Y., Cau A., Naish, D., Dyke G.J. 2014b. Sustained miniaturization and anatomical innovation in the dinosaurian ancestors of birds. *Science* 345:562–566.
- Lee M.S.Y., Palci A. 2015. Morphological phylogenetics in the genomic age. *Current Biology*. 25:R922–R929. doi:10.1016/j.cub.2015.07.009
- Lewis P.O. 2001. A likelihood approach to estimating phylogeny from discrete morphological character data. *Systematic Biology*. 50:913–925. doi:10.1080/106351501753462876
- Novas F.E., Agnolin F.L., Ezcurra M.D., Porfiri J., Canale J.I. 2013. Evolution of the carnivorous dinosaur during the Cretaceous: the evidence from Patagonia. *Cretaceous Research* 45, 174–215.
- O'Reilly J.E., Puttick M.N., Parry L., Tanner A.R., Tarver J.E., Fleming J., Pisani D., Donoghue P.C. J. 2016. Bayesian methods outperform parsimony but at the expense of precision in the estimation of phylogeny from discrete morphological data. *Biology Letters* 12(4):20160081. doi:10.1098/rsbl.2016.0081.
- Porfiri J.D., Novas F.E., Calvo J.O., Agnolin F.L., Ezcurra M.D., Cerda I.A. 2014 Juvenile specimen of *Megaraptor* (Dinosauria, Theropoda) sheds light about tyrannosauroid radiation. *Cretaceous Research* 51:35–55.
- Ronquist F., Kloppstein S., Vilhelmsen L., Schulmeister S., Murray D.L., Rasnitsyn A.P. 2012b. A total-evidence approach to dating with fossils, applied to the early radiation of the Hymenoptera. *Systematic Biology* 61:973–999.
- Ronquist F., Teslenko M., van der Mark P., Ayres D.L., Darling A., Höhna S., Larget B., Liu L., Suchard M.A., Huelsenbeck J.P. 2012a. MrBayes 3.2: Efficient Bayesian phylogenetic inference and model choice across a large model space. *Systematic Biology* 61:539–542.
- Simpson G.G. 1944. *Tempo and Mode in Evolution*. New York: Columbia University Press.
- Szalay F.S. 1977. Ancestors, descendants, sister groups and testing of phylogenetic hypotheses. *Systematic Biology* 26(1):12–18.

- Tschopp E., Mateus, O.V., Benson, R.B.J. 2015. A specimen-level phylogenetic analysis and taxonomic revision of Diplodocidae (Dinosauria, Sauropoda). PeerJ. 3: e857. doi:10.7717/peerj.857.
- Wilson JA, Allain R. In press. Osteology of *Rebbachisaurus garasbae* Lavocat, a diplodocoid (Dinosauria: Sauropoda) from the early Late Cretaceous Kem Kem beds of southeastern Morocco. Journal of Vertebrate Paleontology  
<http://dx.doi.org/10.1080/02724634.2014.1000701>
- Wright A.M., Hillis D.M. 2014. Bayesian Analysis Using a Simple Likelihood Model Outperforms Parsimony for Estimation of Phylogeny from Discrete Morphological Data. PLoS ONE 9(10): e109210. doi:10.1371/journal.pone.0109210
- Yan Y., Harris A.J., Xingjin H. 2011. RASP (Reconstruct Ancestral State in Phylogenies) 1.1. Available at: <http://mnh.scu.edu.cn/soft/blog/RASP>.
- Yang Z., Rannala B. 1997. Bayesian Phylogenetic Inference Using DNA Sequences: A Markov Chain Monte Carlo Method. Molecular Biology and Evolution 14:717–724.
- Young M.T. 2014. Filling the ‘Corallian Gap’: re-description of a metriorhynchid crocodylomorph from the Oxfordian (Late Jurassic) of Headington, England. Historical Biology. 26(1):80–90.
- Zanno L.E., Makovicky P.J. 2013 Neovenatorid theropods are apex predators in the Late Cretaceous of North America. Nature Communications. 4. doi:10.1038/ncomms3827.

Page left blank

## ACKNOWLEDGMENTS

Federico Fanti is thanked for the wide freedom he left to my idiosyncratic way to develop this project.

I thank Mike Lee, who contacted me in 2012 for a collaboration aiming to use what was later defined (literal quote) “a McGywer approach” combining Bayesian phylogenetics and fossils. That collaboration produced two papers: one preceding and inspiring this project, the other has formed the core of this thesis (Chapter 4).

Pascal Godefroit is thanked for all the assistance during my research period in Brussels, in particular, for the unique opportunity to study some of the most exquisitely-preserved paravian dinosaurs ever found. I would like to thank all the people at the Royal Belgian Institute of Natural Sciences, in particular, Ulysse Lefevre and Justine Jacquemin.

Pascal Godefroit and Pasquale Raia provided constructive comments on the first draft of this thesis.

I thank all the members of the 2014 team in southern Tunisia: Federico Fanti, Luigi Cantelli, Aldo Bacchetta, “*il mitico*” Germano Mignani, Luana Angelicola, Sara Cafaggi and Jacopo Carlet.

I thank Prof. Gian Battista Vai, former director of the Geological Museum “Capellini”, for the support on all my activities with the museum. Gigliola Bacci and Paolo Ferrieri are thanked for the help during the various activities in the museum.

I congratulate to all the other students of the 29<sup>th</sup> *curriculum* at the Earth Science Department in Bologna, with particular thank to Serena Giacomelli for her nice friendship.

I thank Massimo Delfino and Emanuel Tschopp who invited me to co-organize the workshop on novel phylogenetic methods in palaeontology (Turin, 12-13 April, 2016), and all the international group of students that joined it.

For the various help during the development of this thesis, I also thank S. Maganuco, M. Auditore, L. Panzarin, D. Bonadonna, E. Troco., P. Bell, M. Bon, M. Casarin, A. Chiarenza, M. Contessi, C. Dal Sasso, F. Dalla Vecchia, G. Dyke, B. Favaretto, M. Fornasiero, G. Larocca Conte, S. Hua, F. M’Nasri, T. Miyashita, D. Naish, R. Pancaldi, B. Sala, G. Savio and M. Young.

*Questa tesi è dedicata a Miriam Cau, che non era quando questo progetto partì, ed ora è.*

Page left blank

## APPENDIX

### Peer-reviewed studies published during this Ph.D. project but not included in this thesis

1. **Cau A., Brougham T., Naish D. 2015 - The phylogenetic affinities of the bizarre Late Cretaceous Romanian theropod *Balaur bondoc* (Dinosauria, Maniraptora): dromaeosaurid or flightless bird? *PeerJ* 3:e1032. [DOI:10.7717/peerj.1032](https://doi.org/10.7717/peerj.1032).**

*Abstract:* The exceptionally well-preserved Romanian dinosaur *Balaur bondoc* is the most complete theropod known to date from the Upper Cretaceous of Europe. Previous studies of this remarkable taxon have included its phylogenetic interpretation as an aberrant dromaeosaurid with velociraptorine affinities. However, *Balaur* displays a combination of both apparently plesiomorphic and derived bird-like characters. Here, we analyse those features in a phylogenetic revision and show how they challenge its referral to Dromaeosauridae. Our reanalysis of two distinct phylogenetic datasets focusing on basal paravian taxa supports the reinterpretation of *Balaur* as an avialan more crownward than *Archaeopteryx* but outside of Pygostylia, and as a flightless taxon within a paraphyletic assemblage of long-tailed birds. Our placement of *Balaur* within Avialae is not biased by character weighting. The placement among dromaeosaurids resulted in a suboptimal alternative that cannot be rejected based on the data to hand. Interpreted as a dromaeosaurid, *Balaur* has been assumed to be hypercarnivorous and predatory, exhibiting a peculiar morphology influenced by island endemism. However, a dromaeosaurid-like ecology is contradicted by several details of *Balaur*'s morphology, including the loss of a third functional manual digit, the non-ginglymoid distal end of metatarsal II, and a non-falciform ungual on the second pedal digit that lacks a prominent flexor tubercle. Conversely, an omnivorous ecology is better supported by *Balaur*'s morphology and is consistent with its phylogenetic placement within Avialae. Our reinterpretation of *Balaur* implies that a superficially dromaeosaurid-like taxon represents the enlarged, terrestrialised descendant of smaller and probably volant ancestors.

2. **Chiarenza A.A., Cau A. 2016 - A large abelisaurid (Dinosauria, Theropoda) from Morocco and comments on the Cenomanian theropods from North Africa. *PeerJ* 4:e1754; [DOI 10.7717/peerj.1754](https://doi.org/10.7717/peerj.1754)**

*Abstract:* We describe the partially preserved femur of a large-bodied theropod dinosaur from the Cenomanian "Kem Kem Compound Assemblage" (KKCA) of Morocco. The fossil is housed in the Museo Geologico e Paleontologico "Gaetano Giorgio Gemmellaro" in Palermo (Italy). The specimen is compared with the theropod fossil record from the KKCA and coeval assemblages from North Africa. The combination of a distally reclined head, a not prominent trochanteric shelf, distally placed

lesser trochanter of stout, alariform shape, a stocky shaft with the fourth trochanter placed proximally, and rugose muscular insertion areas in the specimen distinguishes it from *Carcharodontosaurus*, *Deltadromeus* and *Spinosaurus* and supports referral to an abelisaurid. The estimated body size for the individual from which this femur was derived is comparable to *Carnotaurus* and *Ekrixinatosaurus* (up to 9 meters in length and 2 tons in body mass). This find confirms that abelisaurids had reached their largest body size in the “middle Cretaceous,” and that large abelisaurids coexisted with other giant theropods in Africa. We review the taxonomic status of the theropods from the Cenomanian of North Africa, and provisionally restrict the Linnean binomina *Carcharodontosaurus iguidensis* and *Spinosaurus aegyptiacus* to the type specimens. Based on comparisons among the theropod records from the Aptian-Cenomanian of South America and Africa, a partial explanation for the so-called “Stromer’s riddle” (namely, the coexistence of many large predatory dinosaurs in the “middle Cretaceous” record from North Africa) is offered in term of taphonomic artifacts among lineage records that were ecologically and environmentally non-overlapping. Although morphofunctional and stratigraphic evidence supports an ecological segregation between spinosaurids and the other lineages, the co-occurrence of abelisaurids and carcharodontosaurids, two groups showing several craniodental convergences that suggest direct resource competition, remains to be explained.

3. **Chiarenza A.A., Foffa D., Young M.T., Insacco G., Cau A., Carnevale G., Catanzariti R. 2015 - The youngest record of metriorhynchid crocodylomorphs, with implications for the extinction of Thalattosuchia. *Cretaceous Research* 56: 608-616. [doi:10.1016/j.cretres.2015.07.001](https://doi.org/10.1016/j.cretres.2015.07.001)**

*Abstract:* Here we describe an isolated tooth of a metriorhynchid crocodylomorph from the Hybla Formation (Aptian, Lower Cretaceous) of Rocca Chi Parra quarry (Montagna Grande, Calatafimi, Trapani Province), Sicily, Italy. The specimen shares with the Upper Jurassic taxon *Plesiosuchus manselii* a mediolaterally compressed conical tooth crown, noticeable lingual curvature, mesial and distal carinae with microscopic, rectangular contiguous denticles, strong distal curvature of the mesial margin, and the presence of weak 'carinal flanges' on the labial and lingual surfaces (which are preeminent at the mid-crown). This suite of morphologies is also present in an unnamed Valanginian (Lower Cretaceous) plesiosuchinan from France. However, the Sicilian tooth differs from these taxa in having more pronounced carinae, and faint apicobasally aligned enamel ridges. It also differs from *P. manselii* in having more extensive 'carinal flanges' on the labial surface. The specimen extends the known geological range of Metriorhynchidae and Thalattosuchia by approximately 7–8 million years. This overturns previous hypotheses of Metriorhynchidae becoming extinct early in the Early Cretaceous.

4. **Dal Sasso C., Pierangelini G., Famiani F., Cau A., Nicosia U. 2016 - First sauropod bones from Italy offer new insights on the radiation of Titanosauria between Africa and Europe. *Cretaceous Research* 64:88-109.**  
[doi:10.1016/j.cretres.2016.03.008](https://doi.org/10.1016/j.cretres.2016.03.008)

*Abstract:* Here we describe the first sauropod skeletal remains from the Italian peninsula that also represent the earliest record of titanosaurs in Southern Europe. Scattered bones, including an almost complete anterior caudal vertebra, were found in Cretaceous (Aptian–Albian) marine deposits, some 50 km East of Rome. The vertebra shows a bizarre and perhaps unique orientation of the zygapophyseal articular facets that renders their interpretation problematic. Phylogenetic retrofitting tests support the placement of the Italian titanosaur among basal lithostrotians. Palaeobiogeographic analysis based on the resulting phyletic relationships suggests an Afro-Eurasian route for the ancestors of the Italian titanosaur, a scenario compatible with the palaeogeographic evolution of the Italian microplates during the Cretaceous. Together with previously recorded titanosaurian-like ichnites from a Cenomanian locality in Latium, this new find suggests a quite long emersion for the Apenninic carbonate platform. We suggest that the Italian titanosaur was member of a population that crossed the western Tethys Sea through a “filtering bridge” composed of a chain of ephemeral islands and peninsulae, known as Periadriatic (Adria) carbonate platforms, that connected sporadically Africa and Europe since the Early Cretaceous.

5. **Dalla Vecchia F.M., and Cau A. 2014 - Reexamination of the purported pterosaur wing metacarpals from the Upper Triassic of England. *Historical Biology* 27(6):684-696.** doi:[10.1080/08912963.2014.933826](https://doi.org/10.1080/08912963.2014.933826).

*Abstract:* Two small bones from the Upper Triassic of Cromhall Quarry (Gloucestershire, England), which are referred in the literature to pterosaurian wing metacarpals, are compared with wing metacarpals of unequivocal pterosaur specimens from the Upper Triassic of Italy and Greenland as well as those of the Liassic *Dimorphodon macronyx* from England. The two are morphologically distinct from the unequivocal wing metacarpals. Comparison with the phalanges of drepanosauromorphs suggests that they are probably penultimate phalanges of those bizarre diapsids. Drepanosauromorphs are now known from Cromhall Quarry, but they were not in 1990 when the two presumed wing metacarpals were described. There is no definitive evidence of the presence of pterosaurs in the Triassic of the UK.

6. **Insacco G., Chiarenza A.A., Cau A. 2015 - *Temnodontosaurus* and *Stenopterygius* (Diapsida: Ichthyosauria) specimens in the Comiso Natural History Museum (Sicily, Italy). *Natura Rerum* 3: 812-824.**  
[\[http://www.edizionibelvedere.it/images/pdf/volume3/1.%20Insacco%20et%20al.pdf\]](http://www.edizionibelvedere.it/images/pdf/volume3/1.%20Insacco%20et%20al.pdf)

*Abstract:* The paleontological collection of the Comiso Natural History Museum (Sicily, Italy) includes two ichthyosaurian specimens from the Lower Jurassic Posidonia Shale (southwestern Germany). Based on comparative morphology, we refer them to *Temnodontosaurus* and *Stenopterygius* both common genera in the Toarcian of Southern Germany.

### International Meeting Abstracts and Posters published during this Ph.D. project

1. **Cau A.**, Baiano M.A., and Raia P. 2014 - A new sphenodontian (Reptilia, Lepidosauria) from the Lower Cretaceous of Southern Italy and the phylogenetic affinities of the Pietraroia Plattenkalk rhynchocephalians. *XII Meeting of Young Researchers in Paleontology, Sobarbe Geopark, Spain, 10-12 April 2014.*
2. Chiarenza A.A., **Cau A.**, Fanti F. 2015 - "Cetiosaur" strikes back: morphometric and comparative analysis of the tail of *Tataouinea hannibalis* (Dinosauria: Sauropoda). *XV Edizione delle "Giornate di Paleontologia" Paleodays2015 – Palermo 27-29 Maggio 2015.*
3. Dyke G., **Cau A.**, Naish D., Brougham T., Godefroit P. 2014 - *Archaeopteryx* and paravian phylogeny: the enigma of *Balaur*. 74th Annual Meeting of the Society of Vertebrate Paleontology, Berlin. *Journal of Vertebrate Paleontology, Program and Abstracts, 2014:* 123.
4. Lefevre U., **Cau A.**, Cincotta A., Dongyu H., Wenhao W., Escuillié F., Godefroit P. 2015 - A Jurassic avialan from China challenges the flight abilities in the earliest birds. *The 12th Symposium on Mesozoic Terrestrial Ecosystems, Shenyang, China: August 16-20, 2015.*
5. Lefevre U., **Cau A.**, Hu D., Wu W., Escuillié F., Godefroit P. 2014 - New basal Avialae from the Jurassic of China. 74th Annual Meeting of the Society of Vertebrate Paleontology, Berlin. *Journal of Vertebrate Paleontology, Program and Abstracts, 2014:* 167.
6. Madzia D., **Cau A.** 2015 - Insights into the evolutionary history of Mosasauroidae (Squamata) using parsimony and Bayesian inference. *XIII Annual Meeting of the European Association of Vertebrate Palaeontologists. Opole, Poland, 8-12 July 2015.*